Vol. 171, May 1, 1985
Complete in one issue

ISSN 0003-2670

ANALYTICA CHIMICA ACTA

International journal devoted to all branches of analytical chemistry

ELSEVIER

ANALYTICA CHIMICA ACTA

International journal devoted to all branches of analytical chemistry
Revue internationale consacrée à tous les domaines de la chimie analytique
Internationale Zeitschrift für alle Gebiete der analytischen Chemie

PUBLICATION SCHEDULE FOR 1985

	J	F	M	A	M	J	J	A	S	O	N	D
Analytica Chimica Acta	167	168	169	170/1 170/2	171	172	173	174	175	176	177	178

Scope. *Analytica Chimica Acta* publishes original papers, short communications, and reviews dealing with every aspect of modern chemical analysis both fundamental and applied.

Submission of Papers. Manuscripts (three copies) should be submitted as designated below for rapid and efficient handling:

Papers from the Americas to: Professor Harry L. Pardue, Department of Chemistry, Purdue University, West Lafayette IN 47907, U.S.A.

Papers from all other countries to: Dr. A. M. G. Macdonald, Department of Chemistry, The University, P.O. Box 363 Birmingham B15 2TT, England. Papers dealing particularly with computer techniques to: Professor J. T. Clerc Universität Bern, Pharmazeutisches Institut, Baltzerstrasse 5, CH-3012 Bern, Switzerland.

Submission of an article is understood to imply that the article is original and unpublished and is not being considered for publication elsewhere. Upon acceptance of an article by the journal, authors will be asked to transfer the copyright of the article to the publisher. This transfer will ensure the widest possible dissemination of information.

Information for Authors. Papers in English, French and German are published. There are no page charges Manuscripts should conform in layout and style to the papers published in this Volume. Authors should consult Vol. 170 for detailed information. Reprints of this information are available from the Editors or from: Elsevier Editorial Services Ltd., Mayfield House, 256 Banbury Road, Oxford OX2 7DH (Great Britain).

Reprints. Fifty reprints will be supplied free of charge. Additional reprints (minimum 100) can be ordered. An order form containing price quotations will be sent to the authors together with the proofs of their article.

Advertisements. Advertisement rates are available from the publisher.

Subscriptions. Subscriptions should be sent to: Elsevier Science Publishers B.V., Journals Department, P.O. Box 211, 1000 AE Amsterdam, The Netherlands. Tel: 5803 911, Telex: 18582.

Publication. *Analytica Chimica Acta* appears in 12 volumes in 1985. The subscription for 1985 (Vols. 167–178) is Dfl. 2400.00 plus Dfl. 264.00 (p.p.h.) (total approx. US $986.70). All earlier volumes (Vols. 1–166) except Vols. 2 and 28 are available at Dfl. 215.00 (US $79.60), plus Dfl. 15.00 (US $5.60) p.p.h., per volume.

Our p.p.h. (postage, packing and handling) charge includes surface delivery of all issues, except to subscribers in the U.S.A., Canada, Japan, Australia, New Zealand, P.R. China, India, Israel, South Africa, Malaysia, Singapore, South Korea, Taiwan, Pakistan, Hong Kong and Brazil who receive all issues by air delivery (S.A.L. — Surface Air Lifted) at no extra cost. For the rest of the world, airmail and S.A.L. charges are available upon request.

Claims for issues not received should be made within three months of publication of the issues. If not they cannot be honoured free of charge.

For further information, or a free sample copy of this or any other Elsevier Science Publishers journal, readers in the U.S.A. and Canada can contact the following address: Elsevier Science Publishing Co. Inc., Journal Information Center, 52 Vanderbilt Avenue, New York, NY 10017, U.S.A., Tel: (212) 916-1250.

FIRST ANNOUNCEMENT

International Symposium on Coal Characterisation for Conversion Processes
Rolduc, The Netherlands, 28th April - 1st May 1986

Scope
The past decade has been characterized by a renewed interest in coal as an energy source and as a basic material for the chemical industry. This has induced a revival in coal research activities both from a fundamental and an applied point of view. Due to changing economics, however, the large scale introduction of new coal conversion processes has been postponed and, as a consequence, more time is available for research to gain fundamental insights into coal structure and to obtain a better understanding of its impact on conversion processes. In view of this, the initiative has been taken to organize the international "**Rolduc Symposia on Coal Science**". These are intended to fill the need for small-scale working symposia on specific subjects and with a limited number of participants (about 150), as a supplement to the large-scale Coal Science Conferences. The opportunity for in-depth discussions and maximum profit from exchange of knowledge and ideas can thereby be assured.

The first symposium of the series will be devoted to "Coal Characterisation for Conversion Processes". Its aim is to build a bridge between the techniques and methods nowadays available for coal characterisation and the need for relevant parameters to operate and design coal conversion processes.

Scientific Program
The scientific program will cover Coal Characterisation in relation to Gasification, Combustion, Pyrolysis, and Liquefaction. A full symposium day will be devoted to each of the four processes and each day's session will commence with a plenary lecture by an invited expert:
Gasification: **K.H. van Heek** (Bergbau-Forschung GmbH, Germany)
Combustion: **P.A. Roberts** (Int. Flame Research Foundation, The Netherlands)
Pyrolysis: **R. Cyprès** (Free University Brussels, Belgium)
Liquefaction: **C. Snape** (British Gas, U.K.)
Poster sessions and discussions on selected topics will be organized. There are no parallel sessions. The congress language will be English.

Proceedings
The participants will receive a hard-bound edition of the proceedings. This will be a reprint of a special issue of the journal *Fuel Processing Technology*, published by Elsevier.

Fee
A special symposium package, including registration, accommodation for four nights, all meals, and a copy of the proceedings will be available at approximately Dfl. 1050 per participant (about US $ 350).

Further Information
Further information can be obtained from
F. Kapteijn,
Secretary First International Rolduc Symposium on Coal Science,
Institute for Chemical Technology of the University of Amsterdam,
Nieuwe Achtergracht 166,
1018 WV Amsterdam,
The Netherlands.
Telephone 31 - (0) 20-522 3490/2265.
Telex FACWN 16460.

ANATECH'86

An International Symposium on Applications of Analytical Chemical Techniques to Industrial Process Control

Noordwijkerhout, The Netherlands **22 - 24 April, 1986**

Organised under the sponsorship of
- **Royal Netherlands Chemical Society (KNCV) section for Analytical Chemistry**
- **Federation of European Chemical Societies (FECS)**

SCOPE

The importance of analytical techniques for the control of industrial processes is steadily increasing.

The development of process analysers has taken place to a great extent outside the analytical laboratory. This has led to a distinct gap between experts in the field of process analysis and analytical chemists. Bridging this gulf is one of the main objectives of this symposium which is aimed at an interdisciplinary audience of industrial and academic analytical scientists and those involved in process control and process analysis.

The scientific programme will consist of invited plenary lectures, keynote lectures and submitted research papers dealing with

- ★ State of the art of analytical techniques already successfully applied in process analysis
- ★ Sampling procedures and sampling strategy
- ★ Selection of analytical procedures and instruments with regard to optimum process control
- ★ New analytical techniques of possible interest for process control.

An exhibition of instruments within the scope of the symposium will be held.

Those wishing to present a paper or who would like to receive full details, please write to:

Professor Dr. W.E. van der Linden
Laboratory for Chemical Analysis
Dept. of Chemical Technology
Twente University of Technology
P.O. Box 217
NL - 7500 AE Enschede, The Netherlands
Telephone: (53) 892436

7322

BALANCE

A Program to Compare the Means of Two Series of Measurements

Authors: D.L. Massart et al.

- requires no profound knowledge of statistics
- guides user with playful ease to the correct statistical test
- incorporates:
  - paired t-test (parametric)
  - Wilcoxon test (non-parametric)
  - Student's t- and Cochran's tests (parametric)
  - Mann-Whitney's U-test (non-parametric)
  - tests for small and large numbers of measurements
  - one/two tailed (sided) tests
- full source code listings
- clear, fully descriptive manual with worked examples
- US $ 150.00

AVAILABLE FROM

Elsevier Scientific Software (JIC)
52 Vanderbilt Avenue
New York, NY 10017 USA
Phone: (212) 370 5520
Telex: 420643

or
Elsevier Scientific Software
P.O. Box 330
1000 AH Amsterdam
THE NETHERLANDS
Phone: (020) 5803 911
Telex: 18582

Write to us for further information on our other programs.

No shipping charge if paid in advance

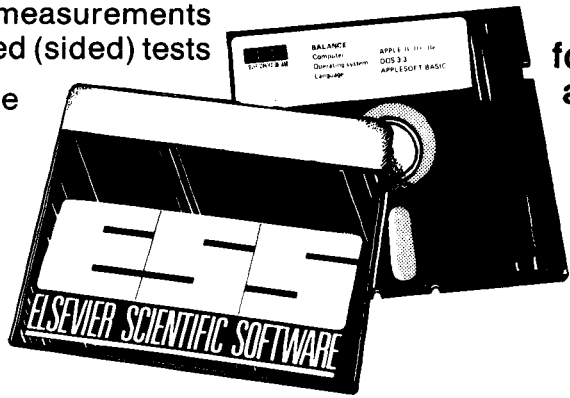

for: IBM-PC and Apple II series

ESS
ELSEVIER SCIENTIFIC SOFTWARE

ANALYTICA CHIMICA ACTA
VOL. 171 (1985)

ANALYTICA CHIMICA ACTA

International journal devoted to all branches of analytical chemistry

ELSEVIER Amsterdam–Oxford–New York–Tokyo

Anal. Chim. Acta, Vol. 171 (1985)

0003-2670/85/$03.30

Printed in The Netherlands

Analytica Chimica Acta, 171 (1985) 1—11
Elsevier Science Publishers B.V., Amsterdam — Printed in The Netherlands

DETERMINATION OF THE PROTEINS IN MIXTURES OF MEAT, SOYMEAL AND RIND FROM THEIR CHROMATOGRAPHIC AMINO-ACID PATTERN BY THE PARTIAL LEAST-SQUARES METHOD

WALTER LINDBERG*, JERKER ÖHMAN and SVANTE WOLD

Department of Analytical Chemistry and Research Group for Chemometrics, Institute of Chemistry, University of Umeå, S-90187 Umeå (Sweden)

HARALD MARTENS

Norwegian Food Research Institute, P.O. Box 50, N-1432 Ås-NLH (Norway)

(Received 27th August 1984)

SUMMARY

The simultaneous determination of muscle protein and rind protein in mixtures of muscle, soymeal and rind is described. Hydrolysates are derivatized with dansyl chloride and separated by reversed-phase liquid chromatography. The chromatographic pattern is subjected to multivariate evaluation. An indirect calibration method, partial least-squares modelling in latent variables (p.l.s.), is used. The rind protein is determined accurately regardless of sample composition. The accuracy of muscle protein determinations is lower when high concentrations of soymeal are present in the samples, because of the similarity in amino acid composition between soy protein and muscle. The method not only predicts the concentrations of the constituents but also calculates a measure of the similarity between the calibration set and each unknown sample. This gives an indication of the reliability of the predicted concentrations.

Various methods for quantifying proteins in food products have been proposed. None of them is sufficiently accurate and reliable to be accepted as a general standard method. Difficulties originate from the chemical complexity of the samples, containing different kinds of proteins, as well as from the physical and chemical changes occurring in manufacturing processes that can affect protein solubility, for example. The analytical problem is to find properties which are unaffected by the manufacturing process and which are sufficiently unique for each protein.

Within the framework of determining the protein composition of meat products, three different approaches are possible. In the first, the amount of non-meat proteins, e.g., soy protein of different kinds (isolates, texturates), is determined in order to detect possible illegal types or levels of protein additions. Similarly, cheap meat protein sources such as collagen or blood protein may be determined. In the second, the concentration of the really expensive protein component, namely the non-collagen meat protein (muscle

0003-2670/85/$03.30

protein), is determined. In the third, the concentrations of all the major protein species, i.e., both non-meat and meat proteins, are determined.

Many papers have been devoted to the first approach; electrophoresis has been the major technique. Two major problems have been met, namely, the difficulty in quantifying electrophoretic bands and the variability in solubility of some proteins, such as isolates and texturates containing soy protein. A chromatographic method based on the determination of a pentapeptide (SP-1) has been proposed by Llewellyn et al. [1]. This peptide is obtained by enzymatic cleavage of the denaturated protein by trypsin and is quantified by using ion-exchange chromatography. Morrissey et al. [2] recently determined soy protein by measuring galactose and arabinose with an enzymatic method. These sugars show great selectivity for soymeal and even soy isolate. However, because the difference in concentrations of these sugars in meal and isolate is large, the method seems to be uncertain for real samples. Collagen-containing tissue such as rind is usually estimated by measuring hydroxyproline. This is accepted as a rather reliable method because hydroxyproline is present at a fairly high concentration and is very selective for collagen.

Some papers have been devoted to the second approach. Most of these are based on the determination of a single compound supposed to be specific for that particular protein. Meat protein is usually determined by the content of 3-methylhistidine from actin and myosin in muscle tissue. The drawback with this method is that the determination is based on a single compound present at comparatively low concentration. An interesting approach is that of Jones et al. [3] who used a derivatization procedure claimed to be selective for *N*-methylhistidine, histidine and histidyl peptides. Unfortunately, this idea has not yet been thoroughly tested.

A separation by liquid chromatography gives data for a large number of compounds in a sample, which are all more or less carriers of information. For example, amino acid analysis of meat products yields quantitative data for the about 16 different amino acids in the proteins. Different protein species have different amino acid compositions and they therefore can be used for quantifying the protein species in the meat product.

However, analogies to the simple relationship between collagen and hydroxyproline do not exist for other protein species. All the protein species in the product contain all the normal amino acids, although in different amounts. Thus the amino acid data interfere mutually and no single amino acid can yield the concentration of, e.g., soy protein or muscle protein. However, multivariate data analysis makes it possible to convert nonspecific measurements to specific chemical concentrations of the individual constituents in mixtures such as meat products. Therefore it should be possible to determine the concentrations of all relevant types of proteins in the sample from one chromatographic run.

If the amino acid composition of a set of different protein species is known, their concentration in an unknown mixture can be estimated by a

least-squares fit of its amino acid composition to the compositions of the pure proteins. This approach has been used in several papers for analyzing protein mixtures; Sheldrick [4] was probably the first to use it. Lindquist et al. [5] used it to quantify protein sources in milk products; Martens [6] used it to quantify protein groups in cereal samples. Olsman [7] and Martens et al. [8] used this approach to quantify proteins in meat products. The method is very similar to direct multicomponent evaluation used in certain types of spectroscopy.

This method of eliminating chemical interferences requires that the mathematical model of the amino acid composition of the meat product is complete, i.e., that all the major protein species in the meat product are included in the amino acid model. Moreover, it requires that these amino acid data for the pure protein species are accurately known, because no allowance for analytical uncertainties is made in the model data. The direct multicomponent evaluation also requires that the amino acid compositions of the proteins measured in the pure state correspond to the contribution which these proteins make to the total amino acid composition in the sample in situ, i.e., that no other physical phenomena interfere with the measured signal. This restriction is difficult to fulfil in the chromatography of amino acids. The overall composition of the sample (e.g., its carbohydrate content) probably affects the hydrolysis process, and the relative amino acid composition of the sample affects the chromatographic separation and the peak integration. Therefore, pure proteins cannot be expected to yield results completely representative of how proteins appear in the total amino acid data of a meat product. If such physical interferences can be modelled quantitatively, they can be included in the direct multicomponent evaluation as if they were additional chemical interferences, as was done by Martens et al. [9] for fatty acid data in the determination of fat sources in margarines. In most cases, however, the physical interferences cannot be modelled in advance, and therefore the direct multicomponent evaluation cannot be justified.

In order to account for both known and unknown interferences, an indirect multivariate method [10] can be used. In the present case, this implies an analysis of amino acid data from a representative set of calibration samples which have protein compositions similar to those of samples, thus allowing the modelling of possible interferences. This approach is used extensively in modern near-infrared (n.i.r.) reflectance spectrometry of foods and feeds, and provides a general tool for diminishing interferences from quantitative analytical data.

However, certain mathematical problems exist with the conventional statistical method most often used for indirect multivariate calibration, the multiple linear regression (m.l.r.) and many of its derived methods, such as the stepwise multiple linear regression (s.m.l.r.) [10]. Therefore a new regression technique was applied, the partial least-squares (p.l.s.) regression. This method allows for multicollinearity and errors in both regressors and regressands and therefore corresponds well to the situation in real

chromatographic data. The method is based on the work of H. Wold [12, 13] and was recently developed further for calibration applications [14, 15].

In the present report, hydrolysates of meat, rind and soymeal were derivatized with dansyl chloride and the amino acids were separated by reversed-phase high performance liquid chromatography (h.p.l.c.). The two animal protein sources, muscle and collagen, were calibrated for simultaneously, while soy protein was treated as an unknown interference during the calibration process. After calibration, the calibration coefficients were used to predict muscle protein and collagen in a number of other meat samples with different levels of soy protein and the accuracy of the results was related to the level of this unknown interference.

MATHEMATICAL METHOD

The details of the p.l.s. method in connection with an analytical problem have been presented elsewhere [15, 16], thus only a brief description will be given. A chromatogram of a protein hydrolysate contains signals for each amino acid in the sample. Proteins having different amino acid composition thus give patterns which are specific. A mixture of proteins gives a mixture of these patterns in which the intensity of a pattern is proportional to the concentration of the corresponding protein. Multivariate calibration can be used to resolve the chromatograms into the concentrations of the different protein species in the samples.

The calibration set of n samples of known composition is analyzed to give a number of signals (p) for each sample. Thus a matrix is obtained with one block (Y) containing the known concentrations of the q different protein species and one block (X) containing the corresponding p amino acids (Fig. 1). This matrix can be subjected to a number of data processing techniques to give a calibration model relating X to Y.

The commonest method is multiple regression. In this method, parameters of the x-variables (signals) are determined so as to fit each y-variable as well

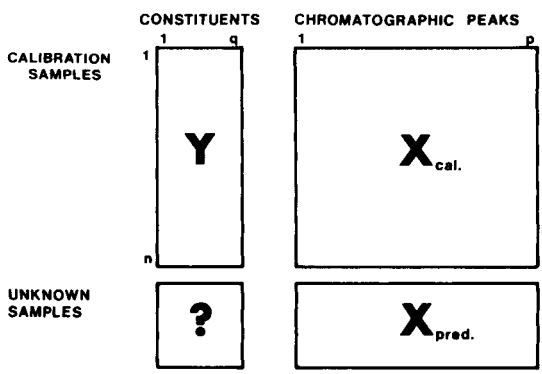

Fig. 1. Organization of data in multivariate calibration.

as possible in some statistical sense. One of the prerequisites of multiple regression is that each x-variable is sampled independently of the others. This condition is usually not met in the present kind of data, because when the concentration of a protein rises, all amino acid concentrations increase simultaneously, i.e., the x-variables are highly correlated.

One way to get around this problem is to construct a set of orthogonal x-variables, here called t, before the regression is done. This is the philosophy of principal component regression (p.c.r.). This calculation can be seen as a projection of the variables in x-space to the t-subspace containing the independently sampled variables. Its dimension is thus equal to the number of orthogonal vectors in the data set.

The same idea is adopted in the p.l.s. method which, however, besides modelling the X-matrix also simultaneously correlates the signals with the concentrations of each substance. The p.l.s. method has somewhat better predictive properties than p.c.r. and multiple regression for compounds connected to smaller eigenvalues, i.e., those for which the information is scarce [17]. The p.l.s. is computationally faster than p.c.a. and multiple regression and is easy to program for microcomputers.

After the calibration model has been generated, it can be used to predict concentrations of constituents (Y) in unknown samples from their chromatographic pattern (X).

EXPERIMENTAL

Apparatus and reagents

The chromatographic system consisted of two Constametric III pumps, a gradient controller and a Spectromonitor III u.v. detector (Laboratory Data Control). The detector was operated at 250 nm. The column (150 × 4 mm) was packed in the laboratory with Hypersil ODS (5 μm particle size; Shandon). The chromatograms were recorded and integrated with an HP-3388 integrator. For data evaluation, the SIMCA-3B BASIC program package for 8-bit CP/M microcomputers was used. (The package is available from Sepanova AB, Östrandsvägen 14, S-12243 Enskede, Sweden or Principal Data Components, 2505 Shepard Blvd. Columbia, Missouri 65201, U.S.A.)

Acetonitrile (h.p.l.c. grade) was obtained from Rathburns. Dansyl chloride and dansyl amino acids were from Sigma. All other chemicals were of analytical-reagent quality and were used as received.

Procedure

Freeze-dried samples were hydrolyzed with 6 M hydrochloric acid for 22 h at 383 K at a concentration of 2 mg of protein per ml of acid. The samples were subsequently filtered and evaporated under nitrogen. Finally the residues were diluted to appropriate concentrations with lithium carbonate buffer (0.04 M, pH 9.5, with acid). The derivatization was done as described by Tapuhi et al. [18]. Chromatographic conditions were as follows: pump A,

acetonitrile/water, 20/80 (v/v) with 0.03 M phosphate buffer pH 6.5; pump B, acetonitrile/water 40/60 (v/v); gradient, 0—100% B in 15 min, 4 min delay; gradient curvature, slightly exponential (exp. 2).

For data evaluation, the areas of every peak were used as x-variables in the p.l.s. calibration. Each variable was scaled to unit variance. After preliminary calculations, those variables giving poor descriptions in the calibration equation were omitted and a final relation was established.

RESULTS AND DISCUSSION

The proposed method based on the multivariate characterization of proteins in terms of their amino acid composition followed by multivariate data processing allows the determination of food proteins such as rind and muscle to a precision of about 2 and 8%, respectively. These results are comparable or better than previously published methods based on single marker amino acid analysis. In addition, the present method is advantageous in that samples dissimilar from those used in the calibration are identified. This method can be useful for protein determinations, particularly because it gives rather accurate results in a short time.

In the determination of proteins in food it is necessary to find a quality on the molecular level which can represent the macroscopic foodstuff. This quality must also be preserved during treatments such as cooking which the raw material undergoes in a manufacturing process. For this purpose, amino acids can be used as markers for different foodstuffs. Advantages of this approach are that it measures the protein itself and not an indirect property correlated with protein content and that amino acids are also relatively unaffected by heat treatments. The difficulty is that amino acid compositions originating from different foods are very similar in some cases. In Table 1 an example is shown where the percentage signal of the common amino acids for pork and soy have been calculated. It is seen that the differences in composition are of the same magnitude as the standard deviations of the measurements. The imprecision is due to variance from the derivatization step and the variance from the chromatographic system. The signal composition of rind protein is not shown because it has a more characteristic pattern particularly rich in hydroxyproline, glycine and proline.

The chromatographic conditions were developed so as to be a reasonable compromise between accuracy and time requirement (Fig. 2). Each peak was assigned with standard dansyl amino acids. Dansyl chloride was chosen as the derivatization agent mainly because its reaction products are stable, which facilitates some time flexibility in the chromatographic step and because it reacts with the secondary amino acids, proline and hydroxyproline. In the hydrolysis, asparagine and glutamine are converted to their corresponding acids, cysteine is oxidized to cysteic acid, thus eluting in the solvent front whereas tryptophan is destroyed. The unidentified peaks in the chromatogram had low informatory power in the model and therefore no attempts were

TABLE 1

Chromatographically determined percentage signal composition of the common amino acids of muscle and soy protein (the compositions are mean values of five measurements)

Amino acid	Composition (%)		Difference	St. dev. of difference[a]
	Soy	Muscle		
Asp	7.96	6.65	1.31	0.117
Glu	14.3	13.7	0.6	0.16
Ser	5.30	5.54	−0.24	0.137
Thr	4.77	5.08	−0.31	0.074
Gly	6.54	6.68	−0.14	0.076
Ala	6.83	7.05	−0.22	0.073
Pro	6.46	6.89	−0.43	0.053
Arg	5.60	5.83	−0.23	0.059
Val	4.20	4.07	0.13	0.043
Met	1.48	1.63	−0.15	0.101
Ile	4.86	4.81	0.05	0.090
Leu	8.27	8.40	−0.13	0.223
Phe	3.63	3.43	0.20	0.096
Lys	11.2	12.3	−1.1	0.190
His	5.45	5.21	0.24	0.359
Tyr	2.92	2.71	0.21	0.389

[a]Calculated as $(s_1^2/n_1 + s_2^2/n_2)^{1/2}$; $n_1 = n_2 = 5$.

made to identify these. Arginine, alanine, lysine and histidine eluted in pairs and thus gave only two peaks.

Calibration sets were prepared which were composed of protein hydrolysates of eight known mixtures of pork, rind and soy protein. This comparatively small size of the calibration set benefits the speed and ease of calibration somewhat, at the cost of lower precision in the estimated parameters. The concentration levels of each protein were chosen so that they would give an approximately equal contribution to the signal and would span the concentration range found in the test set. However, no calibration sample containing very high soy concentration and low meat concentration was included, because such a combination would not occur in a real sample. After a preliminary calibration, aspartic acid, glutamic acid and tyrosine were omitted from the data set because they gave low explanatory power to the model, and then a final model was calculated. These experiments and the data processing were repeated in order to confirm the results. The composition of the calibration sets is listed in Table 2. The concentration units shown are the concentrations of the proteins in the solutions which were subjected to chromatography. The object was to determine pork protein and rind protein and to study the degree of interference caused by soy protein in these mixtures.

In the calibration phase, cross-validation is used as a criterion for the number of significant components in the model, i.e., the dimensionality of

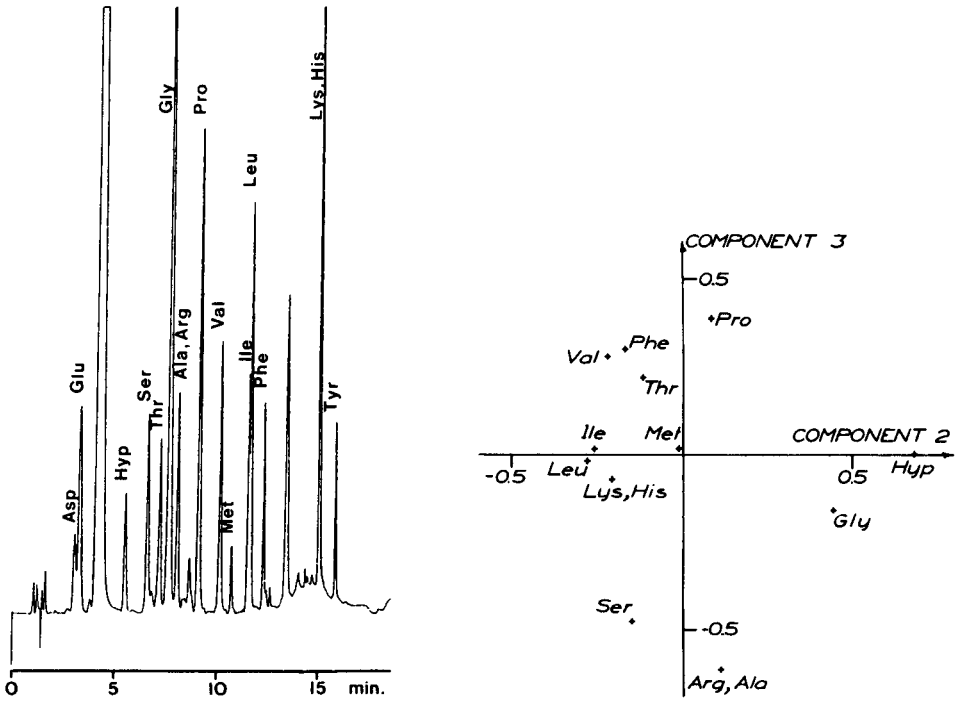

Fig. 2. Separation of dansyl amino acids of a protein hydrolysate. For chromatographic conditions, see Experimental.

Fig. 3. The p.l.s.-component loadings for components two and three.

TABLE 2

Compositions of the two calibration sets (μg protein/ml)

Sample no.	Muscle	Rind	Soy	Sample no.	Muscle	Rind	Soy
Calibration set I				*Calibration set II*			
1	38.8	30.8	33.4	1	44.6	31.7	31.1
2	31.8	90.8	83.6	2	44.1	101	76.8
3	29.2	28.6	80.4	3	107	84.0	24.8
4	89.1	99.3	31.3	4	156	140	128
5	89.9	136	27.9	5	88.0	153	25.2
6	145	174	23.0	6	168	153	108
7	130	132	89.8	7	155	155	31.8
8	128	129	109	8	157	40.0	104

the t-space. In this case, three p.l.s. components were found to be significant and were therefore used in the prediction phase. The first had almost equal loadings for all variables and corresponded to the general increase in signal for all amino acids when the concentrations of the constituents increased.

The second and third modelled the variation in rind and meat, respectively. In Fig. 3 the loadings for these components are plotted against each other. In the second component, hydroxyproline and glycine have the highest loadings, which is in agreement with the composition of rind, whereas for the third component more amino acids, in particular proline, valine and phenylalanine, are involved in describing the meat pattern from the chromatogram. Methionine has very little influence, probably because of its comparatively low signal-to-noise ratio.

The test sets consisted of similar mixtures of known concentrations in order to check the predictive power of the model. Both calibrations gave consistent results, and in the further discussion all samples are treated as one class. In Table 3, the predicted concentrations are shown together with a reliability measurement that reflects the similarity between the sample and the calibration set. This dissimilarity factor is the residual variance of the

TABLE 3

Comparison between true concentrations and predicted concentrations for muscle and rind (μg protein/ml)

Sample no.	Muscle		Rind		Soy	Dissimilarity factor[a]
	Actual	Pred.	Actual	Pred.	Actual	
1	86.2	70.0	94.4	29.7	122	10.5
2	126	112	74.8	107	126	4.73
3	132	86.2	29.6	38.4	94.6	5.61
4	133	81.8	29.6	35.8	94.6	6.02
5	40.1	61.6	114	123	40.9	3.49
6	93.2	96.5	84.7	84.6	27.2	0.88
7	44.6	51.2	31.7	32.6	31.1	0.64
8	88.0	97.3	153	158	25.2	0.76
9	44.6	50.4	31.7	36.1	31.1	0.48
10	38.8	21.7	30.8	32.6	33.4	0.59
11	142	149	37.7	37.9	36.5	2.42
12	168	184	153	147	108	1.01
13	157	176	40.0	34.9	104	1.80
14	142	152	37.7	36.4	36.5	2.86
15	156	172	140	141	129	1.09
16	98.8	71.0	52.0	35.6	55.0	2.81
17	42.1	57.6	45.6	49.5	115	2.24
18	36.0	52.3	89.6	74.7	109	2.00
19	139	76.5	55.7	63.3	42.2	2.42
20	93.2	96.5	84.7	87.2	27.2	0.99
21	155	143	155	154	31.8	1.03
22	63.2	53.2	63.3	68.8	63.6	1.37
$[(\Sigma y - y_{pred.})^2/17]^{1/2}$		20.2		6.5		
$(\Sigma y - y_{pred.})/17$		0.1		0.7		

[a]See text for explanation.

sample divided by the residual variance within the calibration set and thus its significance can be approximately tested by a F-distribution. The degree of freedom for the sample are the number of variables (p = 12) minus the number of extracted components (a = 3). For the calibration set, the degrees of freedom are $(n - a - 1)(p - a)$, where n is the number of samples (n = 8, Table 2). For this set, the F-statistic is 2.2 on the 95% confidence level; in practice, this means that samples with dissimilarity factors far below 2.2 can be regarded as having reliable predictions, those around 2.2 must be handled with some caution in the interpretation of the results, and for dissimilarity factors far above 2.2, the predictions are unreliable.

From the dissimilarity factors, it can be seen that samples 1—4, and perhaps sample 5, do not fit the calibration model and the predictions are unreliable. A possible explanation is that the derivatization may have been unsuccessful. This kind of information may be especially valuable when the samples have been subjected to extensive pretreatment such as preconcentration or derivatization. The probability that something goes out of control is then increased. Another situation in which this reliability warning is valuable is if an unknown sample contains an unexpected type of protein or some other unknown factor violates the calibration assumption.

The lowest dissimilarity factors and also good predictions are obtained for samples 6—10. In those samples, the concentration of the interfering compound is rather low. Still, the interfering signal contributes from 30% to 90% of the pork protein signal. The worst prediction of these samples is given for sample 10, in which the soy protein concentration was of the same magnitude as the pork protein concentration. Some samples (11—15) have somewhat higher dissimilarity factors but acceptable predictions; these lie in the outer regions of the calibration space which are always more uncertain than those in the center.

The results for samples 16—18 show lower accuracies and also higher dissimilarity factors. These values indicate a possibility that the samples do not belong to the class. In the test set, only the results for sample 19, for which the dissimilarity factor does not fully reflect the bad prediction of muscle protein, seem likely to mislead an experienced analyst.

Conclusion

It is shown that the goodness of prediction is governed by the uniqueness of the chromatogram and the precision of the experimental results. This is illustrated by the fact that the rind protein concentrations are correctly predicted whereas the pork protein predictions are better for those samples in which the pork/soy protein ratio is high. Useful information is obtained from the dissimilarity factor, which justifies the use of a calibration set in the determination of a sample. To improve these results, future work should be directed towards measuring compounds with better selectivity. This would reduce the multicollinearity and diminish the demands made on the precision of the experiments as well as the matching between the calibration set and the samples.

REFERENCES

1 J. W. Llewellyn, A. C. Dean, R. Sawyer, F. J. Bailey and C. H. S. Hitchcock, J. Food Technol., 13 (1978) 249.
2 P. A. Morrissey, K. Olbrantz and M. L. Greaser, Meat Science, 7 (1982) 109.
3 D. Jones, D. Shorley and C. Hitchcock, J. Sci. Food Agric., 33 (1982) 677.
4 B. Sheldrick, Biochem. J., 123 (1971) 966.
5 B. Lindquist, J. Östgren and I. Lindberg, Z. Lebensm. Unters.-Forsch., 159 (1975) 15.
6 H. Martens, Anal. Chim. Acta, 112 (1979) 423.
7 W. J. Olsman, J. Am. Oil Chemists Soc., 56 (1979) 285.
8 H. Martens, K. I. Hildrum, A. Bakker, S. Å. Jensen, P. Lea, B. Eskeland, E. Vold and H. Russwurm, in 26th Eur. Meeting of Meat Research Workers, Colorado Springs, 1980, Vol. 1, 1980, p. 146.
9 H. Martens, F. Paulson, E. Spjötvoll and R. Volden, in E. Diday et al. (Eds.), Data Analysis and Informatics, North-Holland, Amsterdam, 1980.
10 H. Martens and T. Naes, in O. H. J. Christie (Ed.), Nordic Symposium on Applied Statistics, Stokkland Forlag, Stavanger, Norway, 1983.
11 N. R. Draper and H. Smith, Applied Regression Analysis, 2nd edn., Wiley, New York, 1981.
12 S. Wold, H. Wold, W. J. Dunn III and A. Ruhe, Report UMINF-83, Department of Chemistry, University of Umeå, Sweden, 1980; published in SIAM J. Sci. Stat. Comput., 5 (1984) 735.
13 H. Wold, in K. G. Jöreskog and H. Wold (Eds.), Systems under Indirect Observations, Part II, North-Holland, Amsterdam, 1982.
14 S. Wold, H. Martens and H. Wold, in A. Ruhe and B. Kågström (Eds.), Proc. Symp. Matrix Pencils, Piteå 1982 Lecture Notes in Mathematics, Springer-Verlag, Heidelberg, 1983.
15 H. Martens and S. Å. Jensen, in J. Holas and J. Kratchovil (Eds.), 7th World Cereal and Bread Congress, Prague, June 1982, Elsevier, Amsterdam, 1983.
16 W. Lindberg, J.-Å. Persson and S. Wold, Anal. Chem., 55 (1983) 643.
17 M. Sjöström, S. Wold, W. Lindberg, J.-Å. Persson and H. Martens, Anal. Chim. Acta, 150 (1983) 61.
18 Y. Tapuhi, D. E. Schmidt, W. Lindner and B. L. Karger, Anal. Biochem., 115 (1981) 123.

Analytica Chimica Acta, 171 (1985) 13—31
Elsevier Science Publishers B.V., Amsterdam — Printed in The Netherlands

SINGLE- AND MULTI-CHANNEL DETECTION FOR GENERALIZED QUANTITATIVE ANALYSIS IN CASES OF UNRESOLVED CHROMATOGRAPHIC PEAKS

MATTHIAS OTTO

Department of Chemistry, Bergakademie Freiberg, 9200 Freiberg (German Democratic Republic)

WOLFHARD WEGSCHEIDER* and ERNST P. LANKMAYR

Institute for Analytical Chemistry, Micro- and Radio-chemistry, Technical University of Graz, Technikerstrasse 4, A-8010 Graz (Austria)

(Received 7th September 1984)

SUMMARY

Computerized quantification of components under overlapping chromatographic peaks is done by calibration of chromatograms against component mixtures. For conventional (single-channel) detectors, the limitations of earlier methods based on ordinary multiple regression, can be circumvented by data reduction with the aid of principal component analysis with the partial least-squares approach. Simulation studies show that the method can be applied even when there is severe peak overlap, unstable baseline, noisy chromatograms or non-linear detector response. Advantages in the quantification of fused peaks by means of multichannel detectors are outlined. Present limitations on the quantitative evaluation of several overlapping component peaks from a single spectro-chromatogram by means of the partial least-squares method combined with multiple regression on the pure component spectra, are discussed with respect to practical high-performance liquid chromatography.

Chromatographic analysis of complex samples regularly produces fused peaks because of the limited peak capacity of chromatographic columns [1]. One solution to the problem is multi-column chromatography. Another possibility, considered here, is mathematical deconvolution of fused peaks as a preliminary to quantifying the components. This approach is also of interest in process control as it enables overlapped peaks to be resolved mathematically during analysis of further samples and, hence, high sample throughput is feasible with short columns.

Separation of overlapping peaks has been achieved by rather limited graphic methods [2] and later by curve-fitting methods based on gaussian and other peak models [3—5]. These methods are advantageous in the sense that curve resolution is possible from one chromatogram without calibration. Essential assumptions, however, are constant peak shapes and selection of the right peak model. In order to overcome these limitations, multiple linear-regression methods have been proposed that are based on shape information

0003-2670/85/$03.30

from pure component or component mixture chromatograms [6—8]. From chromatograms of the pure components or of component mixtures, the response factors (sensitivities) at preselected retention times (volumes) are estimated by relating the intensities to pure component or to mixture concentrations, respectively, by multiple linear regression.

Application of ordinary multiple linear regression is hampered if there are deviations from linear relationships between signal and concentration. These difficulties have been circumvented by applying a second-order polynomial in concentrations [6] or by use of a linear correction matrix [7]. Such approaches, however, solve only one of the problems encountered with ordinary multiple regression, as this technique fails if unidentified components are present under the fused peak, if the random noise is high, or when severe overlap is operative (i.e., in case of poor conditioning of the response matrix [9]).

Resolution of overlapping components under the mentioned conditions is best done by means of principal component analysis (p.c.a.) or factor analysis as has been demonstrated for resolution of chemical equilibria [10], or spectroscopic bands [11—13] or chromatographic peaks [14—16]. With these methods, the intensity matrix is decomposed into principal components or abstract factors and quantification of concentrations is achieved by rotating the principal components under certain restrictive assumptions [14] or by relating them to a parametric model [15, 16]. Limitations of such approaches arise from the fact that the use of a parametric model [15] introduces all the disadvantages of curve-fitting methods into the p.c.a.; the rotation under restrictive assumptions has been worked out for two-component systems only [14, 17].

In the work described here, overlapping peaks are quantified by techniques which preserve the advantages of p.c.a. and which are applicable to more than two overlapping components. The techniques are based on decomposition of the intensities, measured with a single-channel or a multichannel detector, into principal components which are then regressed on spectra from standard mixtures of the components or from standard pure components. The method extends a recently described approach for qualitative analysis of fused components by liquid chromatography/u.v. spectrometry based on target-factor analysis [18]. In order to reduce the data efficiently, p.c.a./multiple linear regression was done with the so-called partial least-squares (p.l.s.) method [19—23].

The practical usefulness of the method is demonstrated by analysis of a priority pollutant standard of polycyclic aromatic hydrocarbons (PAH) by means of high-performance liquid chromatography (h.p.l.c.) and detection with a photodiode-array detector.

THEORY

Single-channel detector

In principle, resolution of fused chromatographic peaks with a single-channel detector is possible if the pure components are chromatographed and the response factors, sampled at several retention times (volumes), are used as the proportionality matrix between signals and concentrations. Thus

$$\mathbf{S} = \mathbf{C}\,\mathbf{R} \tag{1}$$

where the signal intensity matrix S contains n rows, the number of mixtures, and p columns, the number of retention times sampled, the matrix of concentrations C is a $n \times m$ matrix with n mixture rows and m components under the peak, and the response factor matrix R consists of m components times p sensor columns.

In the case of calibration against pure components, the response factors are obtained directly from the chromatograms. The concentrations sought in an unresolved peak are obtained from the measured signal intensity vector by solving for $\mathbf{c}_{oj}$

$$\mathbf{c}_{oj}' = \mathbf{s}_{ok}'\,\mathbf{R}'\,(\mathbf{R}\,\mathbf{R}')^{-1} \tag{2}$$

where subscript o indicates the prediction phase, the vector $\mathbf{c}_{oj}$ contains the jth component of m components present, $\mathbf{s}_{ok}$ characterizes the kth retention time of the p points measured in the chromatogram and dashes indicate the transpose of a matrix or a vector. Equation 2 represents the classical calibration solution [14] for the unknown concentration $\mathbf{c}_{oj}$. As the inverse of $\mathbf{RR}'$ is almost singular, a generalized inverse solution is preferable with a numerically stable algorithm like that of Householder [24]. This algorithm was used throughout the work, in the present case to solve the least-squares problem for $\mathbf{c}_{oj}$ from

$$\mathbf{R}'\,\mathbf{c}_{oj} = \mathbf{s}_{ok} \tag{3}$$

Although some methods have been based on evaluating the response factors from chromatograms of pure components [7], it is more realistic to calibrate the response factors from chromatograms of component mixtures by multiple linear regression. Thus, from the chromatograms obtained, the signal matrix has to be fitted to the mixture concentration matrix C as follows

$$\mathbf{R} = (\mathbf{C}'\,\mathbf{C})^{-1}\,\mathbf{C}'\,\mathbf{S} \tag{4}$$

This calibration method is known as the inverse calibration solution.

To overcome the limitations inherent in the ordinary multiple regression approach, p.c.a. was done through partial least squares. In p.c.a., the signal intensity matrix is decomposed into latent variables (or abstract factors) that are fitted to the concentrations by multiple regression techniques. In the p.l.s. approach, additionally, the concentration matrix is decomposed

into latent variables and the resultant latent variables from both the signal and concentration matrices are related by regression.

Decomposition of the signal and concentration matrix reveals the following latent variables F (factor scores) and L (factor loadings):

$$\mathbf{S} = \mathbf{F}_s \mathbf{L}_s + \mathbf{E}_s \tag{5}$$

$$\mathbf{C} = \mathbf{F}_c \mathbf{L}_c + \mathbf{E}_c \tag{6}$$

where $\mathbf{F}_s$ is the signal score matrix and $\mathbf{F}_c$ the concentration score matrix consisting of n rows, the number of mixtures, and d columns, the number of estimated factors; $\mathbf{L}_s$ represents signal loadings with d rows (factors) and p columns (the number of sensors) and $\mathbf{L}_c$ are the concentration loadings with d rows and m columns (number of components); $\mathbf{E}_s$ and $\mathbf{E}_c$ are error matrices for the signal and concentration matrices having the same dimensions as the original signal matrix (n mixtures times p sensors) and the original concentration matrix (n mixtures times m components), respectively.

Regression of the signal score matrix on the concentration score matrix gives a diagonal matrix V that contains d latent components (dimensions)

$$\mathbf{F}_s \mathbf{V} = \mathbf{F}_c + \mathbf{E}_d \tag{7}$$

where $\mathbf{E}_d$ is an error matrix. To predict the sought concentrations $\mathbf{c}_{oj}$ in an unknown sample, the signal vector of this sample is introduced into the equation

$$\mathbf{c}'_{oj} = \mathbf{s}'_{ok} (\mathbf{F}'_c \mathbf{S})' \mathbf{V} \mathbf{L}_c \tag{8}$$

where the matrices $\mathbf{F}_c$, S and $\mathbf{L}_c$ as well as the regression matrix V are already known from calibration. Details of the derivation of Eqn. 8 have been published [20].

Multichannel detection

By monitoring the chromatogram with several channels, the possibilities for separation of overlapping peaks can be enhanced; an array detector offers a new dimension in selectivity.

Calibration based on standard mixtures. Multiple channel detection can be applied for resolution of fused peaks according to the same principles as demonstrated for single-channel detection if the calibration is based on standard mixtures of the components. The only difference lies in the structure of the signal intensity matrix, as this matrix consists now of n standard mixtures (rows) and p columns obtained from all detector channels at all retention times selected. For example, the signal matrix constructed from sampling at three retention times (t_1, t_2, t_3) and at several (here: $p/3$) channels is as follows:

$$\mathbf{S} = \begin{bmatrix} \overbrace{s_{11}^{t_1} \quad s_{12}^{t_2} \quad s_{13}^{t_3}}^{\text{channel 1}} & \overbrace{s_{14}^{t_1} \quad s_{15}^{t_2} \quad s_{16}^{t_3} \ldots s_{1p}^{t_3}}^{\text{channel 2} \ldots} \\ s_{21}^{t_1} \quad s_{22}^{t_2} \quad s_{23}^{t_3} & \vdots \quad \vdots \quad \vdots \quad \vdots \\ \vdots \quad \vdots \quad \vdots & \\ s_{n1}^{t_1} \quad s_{n2}^{t_2} \quad s_{n3}^{t_3} \ldots\ldots\ldots\ldots & s_{np}^{t_3} \end{bmatrix}$$

It is essential to understand that the physical difference between retention times and wavelength channels is not reflected in the mathematical formulae: channels and retention times can be written in arbitrary numbers and arbitrary order into matrix S as long as the number and order are constant for all rows. As seen from the dimension of the matrix, ordinary multiple regression based on mixture calibration can be done according to Eqns. 1—4 and p.l.s. evaluation by means of Eqns. 5—8, in the same way as for single-channel detection.

Quantification based on standard spectra. Another approach to quantifying components with multichannel detectors is based on data reduction of the spectro-chromatogram of the sample by matching it to the pure spectra of the components. Here, the signal matrix, which consists of the spectro-chromatogram having n retention times (rows) and p sensors (columns) is decomposed into principal components according to Eqn. 5. In contrast to the p.l.s. method, however, the principal components are estimated without regard to a second matrix, giving a score matrix $\mathbf{F}_s$ and a loading matrix $\mathbf{L}_s$ which can be interpreted as the abstract or rotated response and concentration matrix, respectively. For this purpose the decomposition of the signal matrix is rewritten as follows:

$$\mathbf{S} = \mathbf{R}^* \mathbf{C}^* \tag{9}$$

where $\mathbf{R}^*$ is the $n \times m$ (number of retention times multiplied by number of components) abstract response matrix and $\mathbf{C}^*$ is the abstract concentration matrix of dimension $m \times p$ (i.e., m components times p sensors). The abstract response factors $\mathbf{R}^*$ are related to the response factors of the m pure components (pure spectra) $\mathbf{R}$ by regression to a transformation matrix $\mathbf{T}$

$$\mathbf{R} = \mathbf{R}^* \mathbf{T} + \mathbf{E}_R \tag{10}$$

Insertion of $\mathbf{T}$ into Eqn. 9 gives

$$\mathbf{S} = \mathbf{R}^* \mathbf{T} \mathbf{T}^{-1} \mathbf{C}^* \tag{11}$$

Now, $\mathbf{R}^* \mathbf{T}$ represents the pure spectra and the product $\mathbf{T}^{-1} \mathbf{C}^*$ represents the required concentrations from the equation $\mathbf{C} = \mathbf{T}^{-1} \mathbf{C}^*$, where $\mathbf{C}$ consists of m rows (the components) and p columns corresponding to the concentrations at the retention times measured. The concentrations in the columns

are actually the elution profiles of the resolved components. The total concentration of each component is then obtained by integrating over its profile.

EXPERIMENTAL

Apparatus and reagents

Chromatographic experiments were done with mixtures of benzo(b)-fluoranthene, benzo(k)fluoranthene and perylene on a 5-μm Spherisorb ODS-2 stationary phase (Phase Separation). A slurry-packed 150 × 4.6 mm column was used with a Waters model 6000A pump, a Hewlett-Packard 3390A integrator and a Waters 710A WISP automated sample injector. The mobile phase was water/methanol (15/85, v/v) at a flow rate of 1 ml min^{-1}. Injection volumes were 20 or 40 μl. The absorbances were monitored with a photodiode-array detector (HP 1040) at 245 nm (single channel) or at five wavelengths (245, 265, 285, 305, 325 nm) simultaneously connected to a HP-85 desk computer and a dual floppy-disk drive.

For practical application, a certified PAH standard from the National Bureau of Standards (SRM 1647) was examined.

Procedures and computation

Mixtures of the pure components were prepared from standard solutions of benzo(k)fluoranthene (B(k)F; 175 μg ml^{-1}), benzo(b)fluoranthene (B(b)F; 500 μg ml^{-1}) and perylene (140 μg ml^{-1}). Typically, to aliquots of a three-component mixture of 50 μl of B(k)F, 50 μl of B(b)F and 300 μl of perylene, diluted to a total volume of 1400 μl, increments of 25 μl to 200 μl of the standard solutions were added, giving the final concentrations shown in Table 1. For analysis of the PAH standard, three aliquots of the sample solution were spiked with standard mixtures 2—7 (Table 1) as sample-to-standard volume ratios of 1:1 (20 μl/20 μl).

TABLE 1

Concentrations of mixtures for calibrating a three-component system of unresolvec chromatographic patterns

Sample no.	Additions (μl)			Concentrations injected (μg ml^{-1})		
	B(k)F	B(b)F	Perylene	B(k)F	B(b)F	Perylene
1	50	50	300	6.25	17.90	30.0
2	75	50	300	9.21	17.50	29.5
3	100	50	300	12.10	17.20	29.0
4	50	75	300	6.14	26.30	29.5
5	50	100	300	6.03	34.5	29.0
6	50	50	400	5.83	16.7	37.3
7	50	50	600	5.15	14.7	49.4

All programs were written in FORTRAN IV and the computations were run on an UNIVAC 1100 computer. For conventional multiple linear regression, the Householder algorithm given by Lawson and Hanson [24] was implemented and executed in double precision. The p.c.a. and p.l.s. procedure was based on the NIPALS algorithm [25] (cf. [19—21]). The number of principal components in the model was estimated by cross-validation [25].

RESULTS AND DISCUSSION

Single-channel detection

Three-component sample. The advantages of the proposed solution for resolving fused chromatographic peaks compared to ordinary multiple regression techniques is demonstrated for h.p.l.c. of the polyaromatic hydrocarbons B(k)F, B(b)F and perylene monitored at 245 nm. Separation of the fluoranthenes by h.p.l.c. is, in principle, possible with the polymeric stationary phase commercially available as Vydac ODS. When monomeric reversed-phase materials are used and perylene is present, however, severe overlap is observed (Fig. 1) for wide ranges of mobile-phase compositions. This makes curve resolution obligatory.

Calibration for the three-component system was done by means of the standard mixtures shown in Table 1. In the chromatography of every mixture, signal intensities (absorbances at 245 nm) were sampled every 3.2 s. Thus, the signal calibration matrix consisted of 6 rows (mixtures 2—7, Table 1) and 14 columns (retention times). In the prediction step, mixture 1 (Table 1) with all three components was processed, the chromatogram being fitted to Eqn. 8. Results obtained with conventional multiple regression and the p.l.s. approach are shown in Table 2. The prediction standard error is expressed as the square root of percentage unexplained variance, i.e., the sum of squares of differences between predicted ($\hat{c}_j$) and actual (c_j)

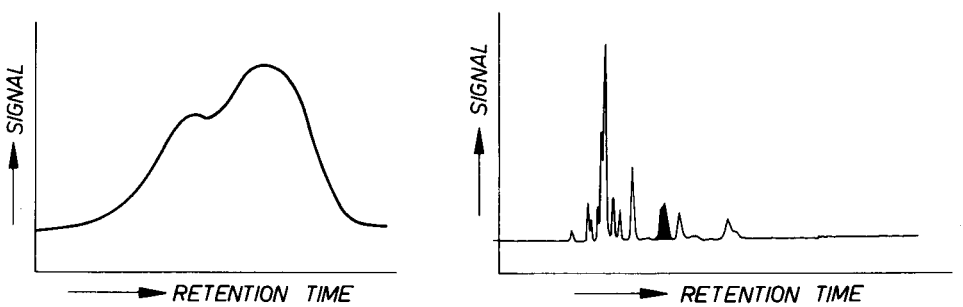

Fig. 1. Three-component overlap in the h.p.l.c. of benzo(k) fluoranthene, benzo(b)-fluoranthene and perylene on Spherisorb ODS-2.

Fig. 2. H.p.l.c. of a priority pollutant polycyclic aromatic hydrocarbon standard (NBS 1647) on Spherisorb ODS-2 monitored at 245 nm.

TABLE 2

Results for quantitative h.p.l.c. of three components under an unresolved peak by the multiple regression and p.l.s. methods

	B(k)F	B(b)F	Perylene	Prediction error (%)
Theoretical (μg ml^{-1})	6.25	17.90	30.0	
Found by multiple regression (μg ml^{-1})[a]	5.65	24.82	20.03	34.2
Relative deviation (%)	−9.6	+38.63	−33.23	
Found by p.l.s. (μg ml^{-1})	6.10	14.88	27.11	11.8
Relative deviation (%)	−2.40	−16.87	−9.63	

[a] See text for explanation.

concentrations divided by the sum of squares of actual concentrations: $[\Sigma_m(\hat{c}_j - c_j)^2/\Sigma_m c_j^2]^{1/2}$.

Table 2 shows that predictions by use of the p.l.s. method provide up to three times better results than those found with multiple regression. The worst results obtained with multiple regression are mainly due to non-linearity in detector response, caused by the low spectral resolution (4.0 nm) of the photodiode-array detector. For the p.l.s. algorithm, non-linearity is less of a problem than in multiple linear regression [20]. The difference between the two methods is less pronounced than expected because all components present under the peak were calibrated before the analysis, because there is no unknown base-line, and because some bias in the time shift between different chromatographic runs interferes with the mathematical analysis in both cases.

The PAH standard. The resolution method was applied to the PAH standard (SRM 1647), for which two of the components, B(k)F and B(b)F, are certified. A chromatogram of this standard material is shown in Fig. 2. The unresolved peak of interest (blackened on the figure) occurs at a retention time of 6.65 min. To account for matrix effects from other constituents of the sample [22], standard mixtures 2—7 (Table 1) were added to three aliquots of the SRM solution in equal ratios, to give the final incremental concentrations shown in Table 3. From the chromatograms monitored at 245 nm, absorbances were measured at 13 retention times and the differences in absorbances between the total and the absorbances from the SRM alone were fitted to the concentration matrix listed in Table 3. The results obtained for the three-component analysis (Table 4) are all discouraging at first glance; the absent component perylene is calculated to be at negative concentrations by both multiple regression and p.l.s. although p.l.s. gives the better results for the other components. The negative prediction for perylene concentrations by the p.l.s. method has to be attributed to some noise pattern in the real matrix that is estimated by cross-validation as a component and related to the absent perylene. Matching the SRM chromatogram only to the com-

TABLE 3

Standard additions of three components to the SRM 1647

Mixture	Added concentrations in the injected sample (μg ml^{-1})		
	B(k)F	B(b)F	Perylene
1	0.0	0.0	0.0
2	4.61	8.75	14.75
3	6.05	8.60	14.50
4	3.07	13.15	14.50
5	3.02	17.25	14.25
6	2.92	8.35	18.65
7	2.58	7.35	23.7

TABLE 4

Analysis of SRM 1647 for benzo(k)fluoranthene and benzo(b)fluoranthene by multiple regression and p.l.s. monitored at 254 nm

	B(k)F	B(b)F	Perylene	Prediction error (%)
Certified (μg ml^{-1})	2.56	2.51	(0.0)	
Three-component analysis				
Found by multiple regression (μg ml^{-1})	2.04	2.47	−2.14	62.9
Relative deviation (%)	−20.31	−4.00		
Found by p.l.s. (μg ml^{-1})	2.42	2.34	−2.37	66.5
Relative deviation (%)	−5.47	−6.77		
Two-component analysis				
Found by multiple regression (μg ml^{-1})	1.22	1.04		55.4
Relative deviation (%)	−52.24	−58.56		
Found by p.l.s. (μg ml^{-1})	2.42	2.34		6.1
Relative deviation (%)	−5.47	−6.77		
Simulated analysis for 3 components				
Found by p.l.s. (μg ml^{-1})	3.17	2.65	−1.07	34.7
Relative deviation (%)	−23.83	−5.58		
Simulated analysis for 2 components				
Found by p.l.s. (μg ml^{-1})	2.86	2.39		8.92
Relative deviation (%)	−11.72	−4.78		

ponents of interest with the use of p.l.s. makes the certified values reproducible within a total relative error of 6% whereas ordinary multiple regression produces a mean prediction error of >50% (Table 4). Data reduction by the p.l.s. method based on fewer components than are actually present in the sample demonstrates another feature of p.c.a. This method can also be applied if unidentified components appear. However, unidentified components are only modelled as principal components if their concentrations vary in the mixtures used for calibration, as is the case when the method of standard additions is applied.

This practical example illustrates some of the advantages of the p.l.s. program compared to multiple regression. In order to stress the performance of the p.l.s. method in a more general sense, simulated data were analyzed in relation to the most important variables that affect the separability of overlapping chromatographic peaks.

Simulation studies. As a first approximation, gaussian peaks for 2—5 components were generated in dependence on peak separation ($\Delta\sigma$, where σ is the standard deviation of the gaussian peak), superimposed noise, intensity ratios of the peaks, number of retention times sampled, number of calibration mixtures, base-line drift and noise, non-linearity effects, and bias in the position of the chromatogram on the time axis.

In typical experiments, two-component systems were calibrated by use of ten mixtures, each containing both components at levels ranging from 0.1 to 1.0 concentration units at 0.1 increments. The sequence of concentration data was randomized. The peaks were separated by 1.0 σ and intensity values, that had been superimposed by 1% noise relative to the signal, were read equally spaced at twenty retention times. To obtain an averaged measure for the quality of prediction with different sets of variables, the concentrations of ten mixtures were predicted with randomized compositions, again between 0.1 and 1.0 concentration units at 0.1 increment units. The final prediction errors expressed as percentage unexplained variances [23] or its square root (standard prediction errors as in Table 4) were obtained by averaging five complete calibration/prediction runs: $100\ \Sigma_j\ \Sigma_i\ (\hat{\mathbf{c}}_{ij} - \mathbf{c}_{ij})^2/\Sigma_j\ \Sigma_i\ \mathbf{c}_{ij}{}^2$, where the $\hat{\mathbf{c}}_{ij}$ are the predicted concentrations from the ith run and the jth component, and the $\mathbf{c}_{ij}$ represent the actual concentrations in the mixtures.

The dependences of peak separations on prediction error are shown in Fig. 3 for two- and five-component systems. The peaks in the 5-component system are equally spaced by $\Delta\sigma$, giving rise to multicomponent overlap. As expected, the prediction errors increase by decreasing the peak separation more seriously in the 5-component system than in the 2-component system.

At fixed levels of other variables, a simple relationship can be found between the prediction error normalized to the square root of component number and the so-called condition number, that is defined as a measure of the quality of a system of linear equations [9, 22, 26]. The condition number of the response factor matrix, Cond(**R**), is calculated from $\mathrm{Cond}(\mathbf{R}) = \|\mathbf{R}\|\ \|\mathbf{R}^{-1}\|$, where $\|\mathbf{R}\|$ and $\|\mathbf{R}^{-1}\|$ are the norms of the response factor matrix and the inverse response matrix, respectively, calculated from the square roots of the largest and the reciprocal smallest eigenvalues of the response matrix.

This relationship between prediction error and condition number is illustrated in Fig. 4 where additional simulations with 3 and 4 components at equally and differently spaced peak separations are included. Under the simulation conditions, the normalized prediction error increased 10-fold if

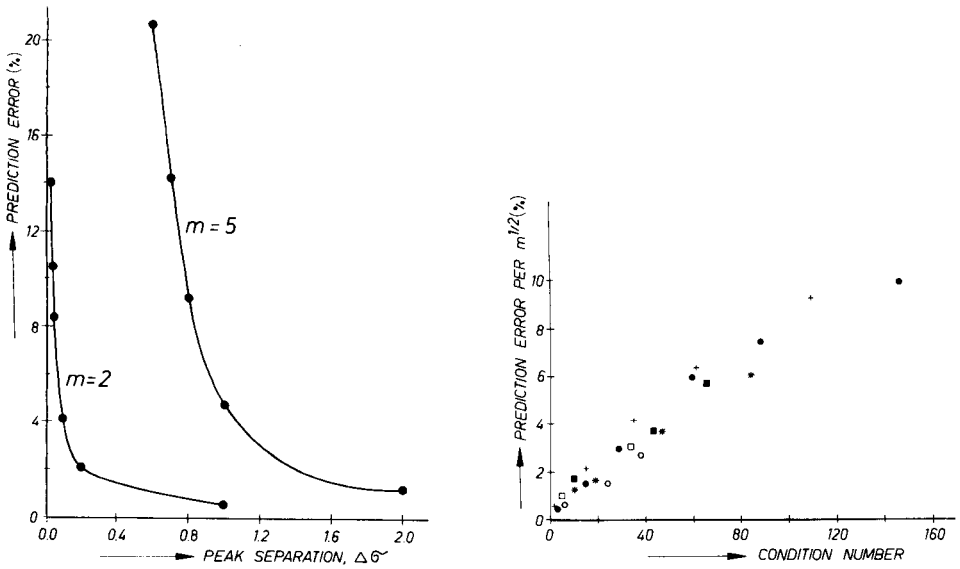

Fig. 3. Prediction error in relation to peak separation for 2 or 5 components (10 calibration mixtures, 20 retention times, 1% signal noise).

Fig. 4. Relation between prediction error normalized to the square root of component number (m) and conditioning of the linear system (conditions as in Fig. 3). Number of components at equally spaced peak separation: (•)2; (○)3; (*)4; (+)5. Number of components at differently spaced peak separations: (▪)3; (□)4.

the condition number rises roughly 100-fold, regardless of the number of components under the chromatographic peak.

Noise levels other than 1% superimposed on the signal intensities were studied under the conditions given in Fig. 3. If the signal noise changes from 1% to 10%, the mean prediction error increases linearly from 0.54% to 5.2%. Additional noise superimposed on the initial concentrations at a signal noise level of 1% gave prediction errors between 1.3 and 11.7% at a concentration noise ranging between 1% and 10% (i.e., concentration noise is more critical than signal noise in this system). Of course, the prediction error depends on the actual degree of peak overlap. A decrease of peak separation from 1 σ to 0.2 σ at a signal noise of 10% raises this error from 5.2% to 21.8%.

The number of sensors (retention times) along the chromatographic axis is important if severe overlap occurs. This conclusion follows from simulations at peak separations of 1 σ and 0.05 σ changing the number of sensors from 5 to 41. Figure 5 shows the dependence of the prediction error at 0.05 σ peak separation for a two-component system. As long as the number of sensors exceeds 10 (i.e., 5 times the component number), only minor changes in the prediction error are to be expected, in contrast to the noticeable increase in error when fewer are used.

Similarly, the number of calibration mixtures becomes critical if it equals the number of components to be separated. For a 5-component case at 0.7 σ peak separation with 5, 10 and 15 calibration mixtures, prediction errors of 58%, 14 and 7.9% were obtained, respectively.

Changing the ratios of peak intensities from 1:1 to 1:100 increases the prediction error at typical variable levels (cf. Fig. 3) from 0.56% to 4.8%. This increase in error also correlates with linear enhancement of the condition number in the two-component case but not if more components are measured.

The effect of the different variables (peak separation, noise of signal, number of calibration mixtures and ratio of peak intensities) on prediction error follows qualitatively the error propagation scheme as used in linear algebra and shown for multivariate analytical calibration by Jochum et al. [26]. Thus, the upper limit of relative error in prediction of the sought concentrations depends on the condition number of the response matrix, the relative signal noise ($\|\delta \mathbf{s}_0\|/\|\mathbf{s}_0\|$) and the calibration error ($\|\delta \mathbf{R}\|/\|\mathbf{R}\|$)

$$\|\delta \mathbf{c}_0\|/\|\mathbf{c}_0\| \leqslant \mathrm{Cond}(\mathbf{R})\,[(\|\delta \mathbf{s}_0\|/\|\mathbf{s}_0\|) + (\|\delta \mathbf{R}\|/\|\mathbf{R}\|)] \qquad (12)$$

where the parallel bars characterize the norm of a vector, i.e., $\|\mathbf{x}\| = (\Sigma\, \mathbf{x}^2)^{1/2}$

If one calculates the upper error limit for the practical analysis of the PAH

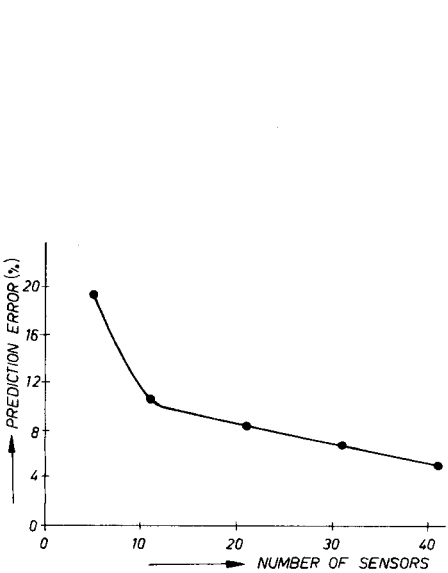

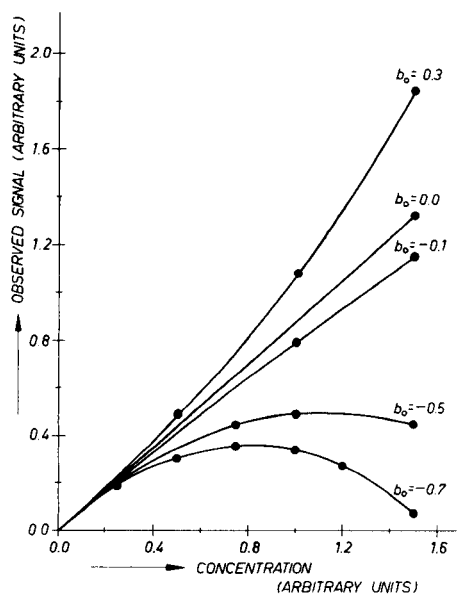

Fig. 5. Dependence of prediction error on the number of sensors at severe peak overlap (0.05 σ peak separation, other conditions as in Fig. 3 for two components).

Fig. 6. Non-linear detector response in relation to concentration. Other conditions as in Fig. 3 at 1 σ peak separation and two components. See text for explanation.

SRM (Table 4) according to Eqn. 12 from the actual condition number of the three-component system to be about 8, at 1% relative signal noise and a calibration error of 1%, the solution of the linear equation system should be possible at relative errors lower than 16% even with ordinary multiple linear regression. Comparison of this upper error limit with the 55% relative error found in the 2-component analysis (Table 4), however, demonstrates the limitations of this error propagation scheme when applied to real systems that do not fulfil the propositions stated for deducing Eqn. 12 [9], i.e., that are not linear systems.

In order to approximate the conditions of chromatography more closely, non-linear effects, base-line drift and noise, and bias in the start of the chromatographic run were included in the simulation studies. Non-linear effects that may arise from non-linear detector response or from non-ideal distribution isotherms were approached by a quadratic model in the form

$$S_q = S + b_o S^2 \qquad (13)$$

where S is the original signal expected under linear conditions, S_q is the resulting signal, and b_o is an appropriate constant. Typical calibration curves in the case of non-linear detector response are shown in Fig. 6. The results of predictions when there are deviations from linearity for a two-component system are given in Table 5. It can be concluded that weak non-linear effects have little influence on prediction errors by use of the p.l.s. algorithm. Surprisingly, even calibration curves showing a maximum (cf. Fig. 6) gave errors less than 10%; this may be explained by the fact that always mixtures of both components were calibrated and predicted so that the poor calibration dependences may still be usable. For single-component samples, the method will not provide a unique result as the concentration will be predicted on either side of the curve maximum.

A drifting base-line was programmed by superimposing a time-dependent constant a on the chromatographic signals, where the observed signal equals the theoretical signal plus the drift: $S_{obs.} = S_{theor.} + a\ t$ (t is time). The drift was assumed to range over all ten calibration and ten prediction measurements where the duration of a single chromatogram was 10 time units and the signal of the overlapping peak was sampled between the 4th and 5th time unit. Table 6 presents the results at a total base-line drift up to 4% based on the maximum signal measured in calibration. If the total drift of the base-line exceeds 2%, a marked increase in the prediction error is observed.

TABLE 5

Prediction of concentrations by p.l.s. at different degrees of deviation from linear signal/concentration dependences (cf. Eqn. 13), for conditions, see Fig. 6

Quadratic deviation, b_o	0.0	−0.1	−0.5	−0.7	+0.3
Prediction error (%)	0.56	1.14	1.62	9.90	1.86

TABLE 6

Effect of different levels of base-line drift over the calibration and prediction experiments (conditions as in Fig. 3 at 1 σ peak separation for two components)

Drift constant[a] a	Percentage of drift based on maximum signal (%)	Prediction error (%)
0.0	0.0	0.56
−0.0001	1.4	2.7
−0.0002	2.8	5.5
−0.0003	4.0	8.3

[a]The drift constant a represents a linear time drift according to the model: $S_{obs.} = S_{theor.} + a\,t$ (cf. text).

Superimposing moderate noise on the drifting base-line simulated for the total drift of 2.8% (cf. Table 6) gave no significant error changes; instead of a prediction error of 5.5% without noise (Table 6), errors of 4.6% and 6.6% were found when constant base-line noise of 1% and 3% of the maximum signal, respectively, was added.

As the last variable, bias in the time shift between chromatographic runs was generated; this is concerned with non-reproducible starts of the chromatograms or by migration of peaks along the time axis. For these cases, the first retention time at the beginning of the fused peak (sampled at 2 σ distance in front of the mean of the first peak) was varied randomly by 10—30% of the relative standard deviations within the calibration and prediction measurements. The actual intensity values were then calculated by use of these retention times shifted along the time axis. Under the conditions given in Fig. 3 at 1 σ peak separation, an increase in the relative prediction error from 0.5% without bias to 2 or 3% with added bias was found, regardless of the level of the deviation imposed between 10 and 30%.

To estimate the contributions of all the variables on the error in chromatographic quantification of unresolved peaks, the variables for the h.p.l.c. of the PAH standard were adjusted in the simulation process and the results were compared to the data obtained by the practical h.p.l.c. From the experiments, a set of possible variable levels was deduced: peak separations 1.0 σ for B(k)F vs. B(b)F and 1.25 for B(b)F vs. perylene, (Cond(R) = 8), 0.1% signal noise, 1% error in concentration of additions, detector non-linearity of 67%, 1% base-line noise, 1.4% base-line drift, and reproducibility of about 1.6% for retention times between chromatographic runs. The results in predicting the simulated certified standard contents are given in Table 4; they were close to the errors made in practical analysis of the sample.

Multichannel detection

To demonstrate the detection at several channels, chromatograms of three-component PAH mixtures were monitored with the aid of a

photodiode-array detector at five wavelengths. A typical spectro-chromatogram is given in Fig. 7.

Standard calibration mixtures. In the first step, data processing was based on standard calibration mixtures according to the same data reduction scheme as for single-channel detectors. The method was applied to the mixtures in Table 1; again mixtures 2 to 7 were used for calibration of the system and mixture 1 was treated as the unknown. Spectro-chromatograms were recorded at 7 retention times and 5 wavelengths giving 35 signal-intensity values for each mixture. Then the procedure was used for analyzing the NBS standard by means of standard addition mixtures as given in Table 3. The spectro-chromatograms were monitored in the same way as described

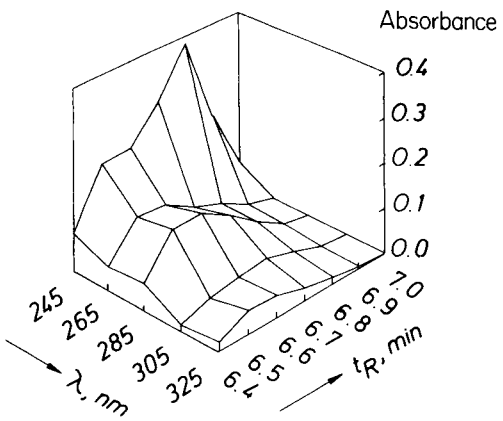

Fig. 7. Spectro-chromatogram of an unresolved peak from the h.p.l.c. (Spherisorb) of the PAH with a photodiode-array detector.

TABLE 7

Analysis of the PAHs in model and standard samples by use of photodiode-array detection at five wavelengths

	B(k)F	B(b)F	Perylene	Prediction error (%)
Model solution				
Theoretical (μg ml^{-1})	6.25	17.90	30.00	
Found by multiple regression (μg ml^{-1})	4.86	13.29	46.11	47.40
Relative deviation (%)	−28.68	−25.77	53.71	
Found by p.l.s. (μg ml^{-1})	5.98	14.35	29.09	10.34
Relative deviation (%)	−4.34	−19.83	−3.03	
NBS standard				
Certified (μg ml^{-1})	2.56	2.51	(0.0)	
Found by multiple regression (μg ml^{-1})	3.56	2.98	−7.29	205.8
Relative deviation (%)	39.06	18.76		
Found by p.l.s. (μg ml^{-1})	2.89	2.56	0.0062	9.55
Relative deviation (%)	13.2	2.15		

for the mixtures in Table 1. The results for both the model and the NBS standard are summarized in Table 7. As expected, the performance of the p.l.s. algorithm is superior to the ordinary multiple regression approach.

The main feature of the multichannel system, however, is the finding that the absent perylene in the NBS standard is correctly estimated (Table 7) in contrast to the single-channel system where with the p.l.s. algorithm too many components were cross-validated, indicating a negative concentration of perylene (cf. Table 4). The higher numerical stability of the p.l.s. method when used with multichannel detection is attributed to the increased selectivity of the system, obtained by spectral resolution between the three components [28]. In this context, it is of interest to know what chromatographic resolution is necessary to resolve peaks mathematically at a given spectral overlap of the single components. To judge this, simulations with a two-component system were undertaken based on closely related gaussian spectra with a band separation of 0.05 σ. When the separation of the chromatographic peaks was varied between (0.0 σ and 0.5 σ, the prediction error decreased from 10.31% to 1.12% (Table 8).

In general, it was found with the 2-component sample that the error is determined mainly by that pair of chromatographic peaks or spectral bands which is best separated (i.e., by the most selective pair of peaks or bands). To underline this, systems of two components, each component having 5 gaussian spectral bands, were investigated with 0.05 σ separation of the chromatographic peaks and different spectral band separations. (The other conditions were the same as in Table 8.) Band separations of 0.1, 0.2 and 0.3 and 0.4 σ were adjusted for the first system and compared to those of a system with worse spectral band separations within the primary 4 bands but the same for the last band, namely 0.05, 0.05, 0.05, 0.4 σ.

The prediction error increased from 2.32% to 2.98% only, as was expected from the similar condition numbers of 11.64 and 14.33, respectively. The error was similar to that obtained for single spectral bands, as shown in Table 8 in which the prediction error at 0.4 σ peak separation is 1.28% at a

TABLE 8

Influence of chromatographic peak separation of two components on the error in multichannel detection with closely related component spectra (band separation of spectra is 0.05 σ, 10 retention times at 11 wavelengths each; other conditions as in Fig. 3)

Peak separation [$\Delta\sigma$]	Condition number	Prediction error (%)
0.0	58.54	10.31
0.05	58.54	9.15
0.1	36.23	5.98
0.2	19.59	2.91
0.3	13.30	1.72
0.4	10.06	1.28
0.5	8.09	1.12

condition number of 10.06. The practical conclusion is, that additional sensors improve the accuracy and precision of the results if they improve the selectivity of the system. Sensors positioned at channels which do not contribute to discrimination among the components affect the overall error only slightly.

Of course, if more than two components are to be quantified under the peak, the quality of the p.l.s. results is not determined simply by the best separated bands or peaks. A median peak separation value would be the actual criterion; that is reflected, however, quantitatively by the condition number of the rotated p.l.s.-derived response factor matrix.

Standard component spectra. In the second step of the study of the multichannel system, overlapping component peaks were quantified on the basis of the known pure component spectra. In this approach, the spectrochromatogram of the sample was matched to the known spectra of the expected components, giving the resolved concentration profiles (peaks) of the components from which the concentrations were evaluated by integrating over those profiles (Eqn. 9 et seq.). The method was tested with simulated data assuming a three-component system with chromatographic peak separations of 1.0 and 1.25 σ and measuring spectral data at 5 wavelengths taken as the spectra of B(k)F, B(b)F and perylene. The signal matrix obtained from 7 retention times at 5 wavelengths was superimposed by 0.1% relative signal noise and was similar to that of Fig. 7.

With the synthetic data, the concentration profiles may be reproduced within computational and random error; an example for one component is given in Table 9. Next, simulations were produced for conditions more relevant to practical work: apart from the 0.1% signal noise, the simulation also included relative concentration noise of 1%, 1% baseline noise and 1% base-line drift (the last two based on the signal maximum), 67% of detector non-linearity and 1.6% standard deviation in the start of the chromatogram. Under such conditions, however, the decomposition of the signal matrix failed; only one component instead of three was evaluated by cross-validation. This can be explained by the high degree of similarity between the spectro-chromatograms of the three components, i.e., the collinearity of the underlying three components is more severe in a spectro-chromatogram from one mixture than in the case of a data matrix that is obtained from

TABLE 9

Quantitative evaluation of a hypothetical spectrochromatogram by matching pure component spectra to the data

	Component concentrations at seven retention times (arbitrary units)						
	A	B	C	D	E	F	G
Expected	0.1358	0.6340	1.000	0.532	0.096	0.006	0.0001
Predicted	0.1368	0.6393	1.011	0.543	0.100	0.006	0.0002

spectro-chromatograms of different mixtures of the three components. As a consequence the pure spectra could not be predicted accurately even by use of three principal components. Logically, the estimated concentrations were quite wrong. This failed analysis was not caused solely by the collinearity problem but also by the assumed non-linearity in the detector response that spoils the definition of pure component spectra. As expected, the decomposition of the experimentally obtained spectro-chromatograms (cf. Fig. 7) gave poor estimates of concentrations that could not be used for practical quantification.

CONCLUSIONS

Overlapping peaks monitored at a single channel can be quantified by the p.l.s. method based on calibration against standard mixtures of the components. Compared to ordinary multiple linear regression, the p.l.s. approach provides resolution of the components with good accuracy and precision even in cases of severe overlap, high noise level, drifting base-line, non-linear effects, biased chromatograms. If standard additions are used, the approach can be applied in the presence of unidentified components.

Multichannel detectors, such as mass spectrometers in gas chromatography or photodiode-array detectors in h.p.l.c., enhance the applicability of the technique if the selectivity in the spectral dimension exceeds that in the chromatographic direction. Quantitative multichannel analysis based on knowledge of the pure component spectra is presently limited to data without error. Under practical conditions, as demonstrated for h.p.l.c./u.v. spectrometry, deviations from linearity and poor resolution in the spectra of the components gave poor quantitative results.

Permission to use the Hewlett-Packard computer-plotter system (Projekt 2098, Fonds zur Förderung der wissenschaftlichen Forschung, Wien) was kindly granted by M. Ramek and H. P. Fritzer (Institute for Physical and Theoretical Chemistry, Technical University, Graz). The u.v./visible array detection system was generously provided by Hewlett-Packard Austria. One of the authors (M. Otto) gratefully acknowledges the Bundesministerium für Wissenschaft und Forschung, Austria, for a visiting fellowship.

REFERENCES

1 J. M. Davis and J. C. Giddings, Anal. Chem., 55 (1983) 418.
2 L. R. Snyder and J. J. Kirkland, Introduction to Modern Liquid Chromatography, Wiley, New York, 1979.
3 A. H. Anderson, T. C. Gibb and A. B. Littlewood, Anal. Chem., 41 (1970) 434.
4 H. M. Gladney, B. F. Dowden and J. D. Swalen, Anal. Chem., 41 (1969) 883.
5 E. Grushka, M. N. Meyers and J. C. Giddings, Anal. Chem., 42 (1970) 21.
6 J. T. Lundeen and R. S. Juvets, Anal. Chem., 53 (1981) 1369.
7 J. P. Gourlia and J. Bordet, J. Chromatogr. Sci., 19 (1981) 35.
8 B. Goldberg, J. Chromatogr. Sci., 9 (1971) 287.

9 J. Stoer, Einführung in die Numerische Mathematik I, 2. Auflage, Springer, Heidelberg, 1976.
10 E. A. Sylvestre, W. H. Lawton and M. S. Maggio, Technometrics, 16 (1974) 353.
11 E. R. Malinowski and M. McCue, Anal. Chem., 49 (1977) 284.
12 F. J. Knorr and J. H. Futrell, Anal. Chem., 51 (1979) 1236.
13 M. McCue and E. R. Malinowski, Anal. Chim. Acta, 133 (1981) 125.
14 M. A. Sharaf and B. Kowalski, Anal. Chem., 54 (1982) 1291.
15 F. J. Knorr, H. R. Thorsheim and J. M. Harris, Anal. Chem., 53 (1981) 821.
16 T. Naes, Unpublished results, Norwegian Food Research Institute, 1983.
17 E. Spjøtvoll, H. Martens and R. Volden, Technometrics, 24 (1982) 173.
18 M. McCue and E. R. Malinowski, Appl. Spectrosc., 37 (1983) 463.
19 S. Wold, H. Martens and H. Wold, Proc. Conf. Matrix Pencils, in A. Ruhe and B. Kågström (Eds.), Lecture Notes in Mathematics, Springer, Heidelberg, 1982.
20 W. Lindberg, J.-Å. Persson and S. Wold, Anal. Chem., 55 (1983) 643.
21 M. Sjöström, S. Wold, W. Lindberg, J.-Å. Persson and H. Martens, Anal. Chim. Acta, 150 (1983) 61.
22 S. A. Jensen and H. Martens, in H. Martens and J. Russwurm, Jr. (Eds.), Food Research and Data Analysis, Applied Science Publishers, Essex, 1983, p. 253.
23 H. Martens, O. Vangen and E. Sandberg, in O. H. J. Christie (Ed.), Nordic Symposium on Applied Statistics, Stokkand Forlag, Stavanger, 1983, p. 235.
24 L. Lawson and R. Hanson, Solving Least Squares Problems, Hall, Englewood Cliffs, New York, 1974.
25 S. Wold, Technometrics, 20 (1978) 397.
26 C. Jochum, P. Jochum and B. Kowalski, Anal. Chem., 53 (1981) 85.
27 P. J. Brown, J.R. Stat. Soc. B, 44 (1982) 287.
28 R. A. Friedel and M. Orchin, Ultraviolet Spectra of Aromatic Compounds, Wiley, New York, 1970.

Analytica Chimica Acta, 171 (1985) 33—43
Elsevier Science Publishers B.V., Amsterdam — Printed in The Netherlands

THE USEFULNESS OF THE DECONVOLUTION OF CHROMATOGRAMS INTO ORTHOGONAL POLYNOMIALS FOR CHARACTERIZING THE QUALITY OF SEPARATION

H. J. G. DEBETS*, A. W. WIJNSMA[a] and D. A. DOORNBOS

Optimization Research Group, Department of Pharmaceutical and Analytical Chemistry, State University, Ant. Deusinglaan 2, NL-9713 AW Groningen (The Netherlands)

H. C. SMIT

Laboratory for Analytical Chemistry, University of Amsterdam, Nieuwe Achtergracht 166, NL-1018 WV Amsterdam (The Netherlands)

(Received 24th April 1984)

SUMMARY

Simulated chromatograms are deconvoluted into series of orthogonal polynomials. The number of terms necessary to achieve a preset goodness of fit, the reproducibility of coefficients in the presence of noise and the effects of signal-to-noise ratio, peak-height ratio and peak asymmetry on the value of coefficients from the deconvolution are investigated. A convenient method for the deconvolution of real chromatograms is described in order to characterize the quality of separation in the chromatogram. A known quality criterion is modified by using coefficients from the deconvolution in order to enhance its performance. Performance is tested on a simulated separation of five sulfa drugs on a reversed-phase column.

Several mathematical functions that can be used to describe a chromatographic peak are available. The Gauss function is useful for symmetric peaks [1—8]; modified Gauss-functions [2, 9, 10], Poisson functions [11, 12], bigaussian functions [3, 8, 11, 12] as well as others generated by multiplication or linear combination of Gauss and Cauchy functions [2] are useful to describe asymmetric peaks. A Gauss function convoluted with an exponential decay has also often been used for asymmetric peaks [6, 10, 14—21].

In this paper, the usefulness of the deconvolution of chromatograms into series of orthogonal polynomials, as suggested by Klous [22] and Scheeren et al. [23] is investigated. Coefficients from the deconvolution are tested for their usefulness in the characterization of the quality of separation in patterns of (strongly) overlapping peaks. A convenient method for the handling of real chromatograms is developed. A new quality criterion is proposed, in which coefficients from a deconvolution are used. The performance of the criterion is tested on the optimization of the reversed-phase high-performance liquid chromatographic (h.p.l.c.) separation of five sulfa drugs.

[a]Present address: Gerechtelijk Laboratorium, Rijswijk, The Netherlands.

0003-2670/85/$03.30

THEORY

Chromatographic peaks were generated by a modified Gauss function as described by Fraser and Suzuki [2]

$$F_k(t) = h_k \exp \{-\ln (2) A_k^{-2}[\ln (1 + (2 \ln 2)^{-1/2} A_k(t - t_k)\sigma_k^{-1})]^2\} \quad (1)$$

where h_k is the height of peak k, A_k its asymmetry, t_k the time at its maximum, and σ_k the standard deviation of the symmetric peak. The factor A denotes the asymmetry of the peak on the right-hand side. A large value of A means strongly asymmetric peaks; the peak becomes symmetric again when A tends to zero, because $[\ln (1 + Ax)]/A$ tends to x. In most cases, the value of A lies between 0 and 1.

Chromatographic profiles can be described by orthogonal polynomials. Series of orthogonal polynomials can be written as

$$F(t) = P_0(t) + P_1(t) + \sum_{n=1}^{\infty} [P_{n+1}(t) - P_n(t)] \quad (2)$$

These polynomials can be made orthogonal with respect to certain weighting functions, resulting in the new representation [22, 23]:

$$G(t) = F(t)[w(t)]^{1/2} \quad (3)$$

These polynomials, and their advantages and disadvantages for the purpose described here, have been thoroughly discussed by Scheeren et al. [23]. In this study only Hermite polynomials are used, according to the formulae

$$P_0(t) = 1, P_1(t) = 2t, P_{n+1}(t) = 2t.\ P_n(t) - 2n.\ P_{n-1}(t) \quad (4)$$

with the weighting function $w(t) = \exp(-t^2)$ and the norm $\pi^{1/2}2^n n!$ Hermite polynomials are very useful when chromatographic profiles with three peaks or fewer in a cluster have to be fitted, while very complex chromatograms with many peaks or clusters of peaks can be described much better by Chebyshev polynomials [23]. In the first part of this study, only simulated chromatograms with less than three peaks were considered, thus deconvolution of the chromatograms into Hermite polynomials was used.

EXPERIMENTAL

The simulation of chromatographic peaks and the development of chromatograms into orthogonal polynomials were done by using the RACE program package [23]. The Cyber 170/760 computer (Control Data Corporation) at the Universitair Rekencentrum, State University Groningen, was used. Plots were made on an electrostatic plotter (Versatec V80) with routines from the Komplot package.

The data necessary for calculating the equations expressing the retention behaviour of twenty sulfa drugs in reversed-phase liquid chromatographic

separations, as described by Weyland et al. [24], where obtained by separating the sulfa drugs with an eluent consisting of deionized water and Micropore-filtered acetonitrile, methanol or tetrahydrofuran (all from Merck) on a stainless steel column (150 × 4.6 mm i.d.) packed with Nucleosil 5RP8 (Machery and Nagel).

The RACE program package used in this study has been described in detail [23]. Some modifications were made for applications to real chromatograms and the investigation of the reproducibility of the coefficients.

RESULTS AND DISCUSSION

Simulated chromatograms

First, the number of terms necessary to achieve a preset goodness of fit in the approximation of a chromatographic peak was examined. The value of the asymmetry factor of a simulated peak (h = 1.0, σ = 1.0) was varied from 0.0 to 1.0 at several values of the multiplication factor of the noise for both white noise and $1/f$ noise. The deviation in area between the simulated peak and its approximation was plotted against the number of terms used, with a maximum of thirty terms. The results are collected in Table 1. It can be seen that chromatographic profiles observed with $1/f$ noise need more terms to achieve the preset goodness of fit than those obscured with white noise. This happens because calculation of the coefficients during the deconvolution is mathematically identical to putting the chromatographic signal through a low-pass filter [23]. Thus the added $1/f$ noise is hardly affected by the deconvolution procedure, whereas the white noise will be filtered. The reason why $1/f$ noise was investigated anyhow, is that a frequency analysis of

TABLE 1

The number of terms needed to achieve a preset goodness of fit by using a Hermite deconvolution of a chromatographic peak at several combinations of asymmetry and noise (white and $1/f$)

Asymmetry	Number of terms								
	Noise-free	White 0.001	$1/f$	White 0.005	$1/f$	White 0.01	$1/f$	White 0.05	$1/f$
0.0	7	7	9	9	10	12	15	20	21
0.1	7	7	10	9	10	14	10	23	19
0.2	8	9	10	12	13	15	13	24	22
0.3	9	9	11	14	11	15	12	22	23
0.4	10	10	11	12	11	15	12	>30	>30
0.5	10	10	9	13	12	16	13	>30	>30
0.6	14	14	10	14	19	24	>30	24	>30
0.7	16	16	25	23	18	27	15	23	>30
0.8	16	16	19	15	>30	15	>30	23	>30
0.9	22	22	>30	>30	>30	28	>30	>30	>30
1.0	18	18	15	16	23	18	25	>30	28

the detector signal from the h.p.l.c. apparatus used indicated that low frequency signals are the most powerful in the spectrum. From the autocovariance function of the detector signal, a noise file was created as described by Laeven et al. [25]. Samples from this noise file were taken every time $1/f$ noise was needed.

Another criterion for the goodness of fit is the standard deviation between the fitted and the original profile [23]. In the calculation of that criterion, the difference between the value of the simulated profile and the value of its approximation at every point on the time axis is taken into account. A cluster of two identical symmetric peaks, time-shifted with respect to each other, was generated and deconvoluted into Hermite polynomials. The number of terms used was varied from one to twenty, and the standard deviation was calculated and plotted against the number of terms used. Figure 1 shows that an approximation with nine terms gives excellent results.

When noise is added to a chromatographic profile, the value of the standard deviation increases. If more terms are added in the deconvolution of the noisy chromatogram, the value of the standard deviation decreases again, but the added higher-order terms in the polynomial only try to describe the noise that is superimposed on the chromatographic profile. As shown in Fig. 1, a nine-term Hermite deconvolution gives an exact description of the underlying chromatographic profile, so that adding more terms to the deconvolution is not necessary. The effect of changes in the peak-height ratio of two partial overlapping peaks on the number of terms necessary was shown to be insignificant.

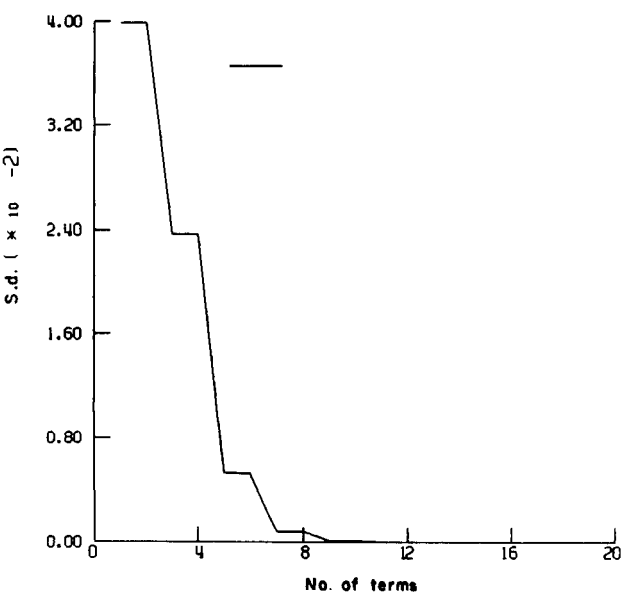

Fig. 1. Plot of the standard deviation, as described in the text, against the number of terms used in a Hermite deconvolution of a chromatogram with two symmetric peaks.

When deconvolution of chromatographic profiles into orthogonal polynomial series is used to achieve coefficients which characterize the quality of separation in a chromatogram, the reproducibility of the coefficients in the presence of noise must be investigated first. A standard peak, as in Eqn. 1 with $h = 1.0$, $\sigma = 1.0$ and $A = 0.4$, was tested with superimposed noise resulting in a signal/noise (S/N) ratio of 1000. Deconvolutions were done in different circumstances, with 10 terms or 20 terms and with white noise or $1/f$ noise. To avoid bias in the noise sequences used, the starting points for reading from the noise file were established by using a random generator. The results are collected in Table 2 for the first six coefficients. Fifty measurements were used to calculate the mean and standard deviation of a coefficient ($n = 50$). From Table 2 it can be seen that all the coefficients show excellent reproducibilities. However, the reproducibility of a coefficient can be affected by the signal/noise ratio of the measured signal. The influence of the signal/noise ratio on the values of the first six coefficients was investigated. Because the detector signal in this application had S/N ratios of about 1000, the multiplication factor of the noise was varied from 0.0 to 0.005. This resulted in a standard peak (Eqn. 1) with a S/N ratio varying from infinity down to 200. The changes in the values of the first two coefficients are shown in Fig. 2. The variations caused by a decreasing S/N ratio are clearly much smaller than the standard deviations from Table 2. Thus even when there are changes in the signal/noise ratio, in the range specified, the coefficients offer a reproducible description of the chromatographic profile that is deconvoluted.

TABLE 2

The mean, standard deviation (SD) and relative standard deviation (RSD, %) of the first six coefficients from a deconvolution of a standard peak into Hermite polynomials[a]

	Coeff. 1	Coeff. 2	Coeff. 3	Coeff. 4	Coeff. 5	Coeff. 6
1/f noise, 10 terms						
Mean	1.013	-0.1516	0.5914×10^{-1}	0.1254×10^{-1}	-0.1233×10^{-2}	0.8238×10^{-3}
SD	0.5472×10^{-3}	0.1175×10^{-3}	0.1285×10^{-3}	0.1923×10^{-4}	0.1574×10^{-4}	0.2050×10^{-5}
RSD	0.054	0.078	0.217	0.153	1.28	0.249
1/f noise, 20 terms						
Mean	1.013	-0.1516	0.5911×10^{-1}	0.1253×10^{-1}	-0.1237×10^{-2}	0.8233×10^{-3}
SD	0.3976×10^{-3}	0.1275×10^{-3}	0.1082×10^{-3}	0.2519×10^{-4}	0.1314×10^{-4}	0.2686×10^{-5}
RSD	0.039	0.084	0.183	0.201	1.06	0.326
White noise, 10 terms						
Mean	1.013	-0.1516	0.5921×10^{-1}	0.1252×10^{-1}	-0.1225×10^{-2}	0.8227×10^{-3}
SD	0.2579×10^{-3}	0.1392×10^{-3}	0.8777×10^{-4}	0.3374×10^{-4}	0.1253×10^{-4}	0.3518×10^{-5}
RSD	0.025	0.092	0.148	0.269	1.02	0.428
White noise, 20 terms						
Mean	1.013	-0.1516	0.5918×10^{-1}	0.1254×10^{-1}	-0.1225×10^{-2}	0.8232×10^{-3}
SD	0.2006×10^{-3}	0.1490×10^{-3}	0.6127×10^{-4}	0.2973×10^{-4}	0.9716×10^{-5}	0.4174×10^{-5}
RSD	0.020	0.098	0.104	0.237	0.793	0.507

[a]In all cases, $n = 50$ and S/N = 1000.

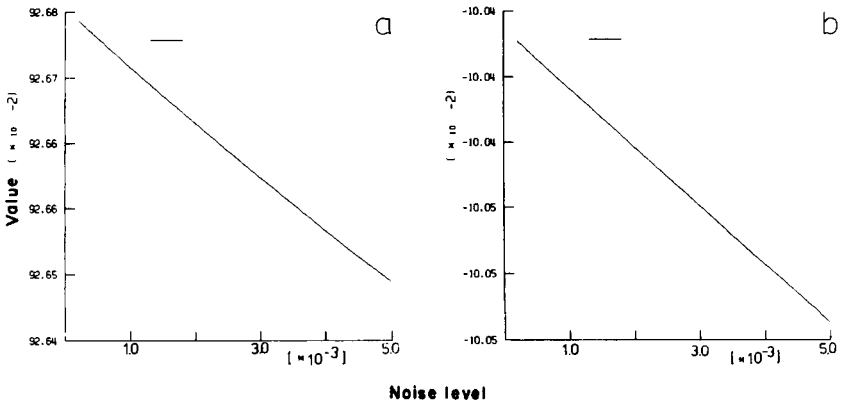

Fig. 2. The decrease in the value of the first coefficient (a) and the second coefficient (b) with increasing noise level. Coefficients from a deconvolution of a standard peak into Hermite polynomials.

Another problem is the behaviour of the coefficients when chromatographic peaks become more or less symmetric. The dependency of the first six coefficients on the asymmetry factor in Eqn. 1 was therefore investigated. The same standard peak as before was used, but the asymmetry factor was varied from 0.0 to 1.0 in 20 steps. As would be expected from theoretical considerations, the even-numbered coefficients tended to decrease when the asymmetry factor was increased. This happens because the scaling is done around the mathematical mean of the profile and the even-numbered terms are the symmetric ones. The odd-numbered coefficients behave differently. Plots of the values of the first two coefficients with increasing asymmetry factor are shown in Fig. 3. The changes in the coefficients when peaks become more or less symmetric are rather large relative to their standard deviations in Table 2. Fortunately, this will be less important in the optimization studies, because the asymmetry of chromatographic peaks is mainly determined by column quality and sample-specific effects. As only chromatographic profiles from a single sample had to be compared, which were all measured on the same chromatographic column, dramatic changes in peak asymmetry were not expected.

To express the quality of separation in a chromatogram by using coefficients from a deconvolution, the relation of the coefficients to chromatographic resolution must be investigated. Therefore, two symmetric peaks (Eqn. 1) were simulated; the first had a constant retention time of 90 units and the second a retention time changing from 30 units to 150 units in 5-unit steps. The peak width was chosen as 10 units and the S/N ratio was 1000. The value of the first coefficient showed a symmetric profile when it was plotted against the retention time of the second peak (Fig. 4a). This could be expected because the deconvoluted profile changes from non-gaussian to gaussian and back to non-gaussian when the peak cross-over takes place. The

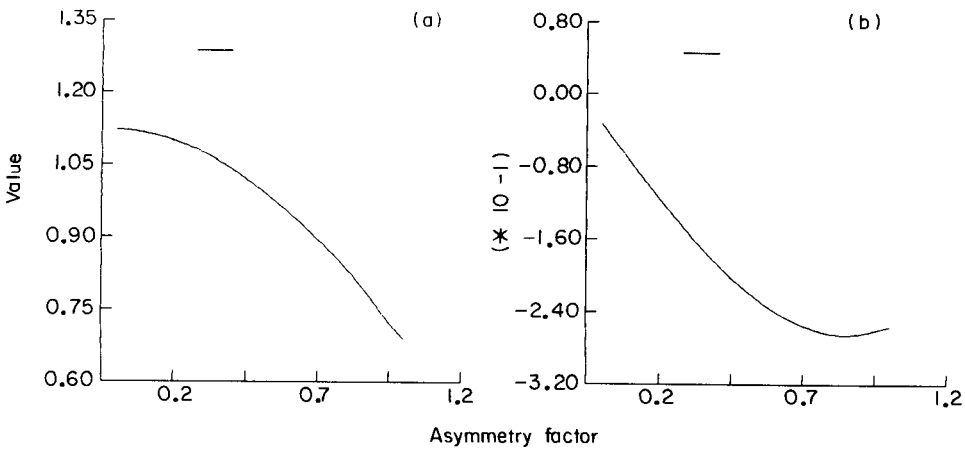

Fig. 3. The change in the value of the first coefficient (a) and the second coefficient (b) with increasing asymmetry factor. Coefficients from a deconvolution of an asymmetric peak into Hermite polynomials.

value of the second coefficient shows a similar behaviour, but in the opposite direction (Fig. 4b). The other coefficients showed no unequivocal relation with chromatographic resolution, except the fifth coefficient in some particular situations. Combination of all results, described above, shows that only the first two coefficients can be used to express the quality of separation in a chromatogram.

Real chromatograms

As mentioned above, the deconvolution of chromatographic profiles into Hermite polynomials is only appropriate when a few peaks are present in a cluster. The appearance of baseline between peaks is inconvenient when a Hermite deconvolution is used. Therefore it is not useful to apply a Hermite deconvolution to a whole chromatogram. The most convenient way of handling any chromatogram is to split it up into peak patterns without baseline. In this application, a simple peak-search routine, developed in this laboratory, was used to obtain all the information necessary to split up the chromatogram. After that the peak patterns were fed into the deconvolution subroutines. This procedure is indicated in Fig. 5.

The output of the deconvolution subroutines consists of series of coefficients for each peak pattern. To characterize the quality of separation in the whole chromatogram, the results from the separate deconvolutions have to be combined. This can be achieved by using utility functions as described by Debets et al. [26]. Such use of deconvolution data can be valuable in the more detailed characterization of the quality of separation in patterns of strongly overlapping chromatographic peaks which is still a difficult problem in the automatic optimization of chromatographic separations. To illustrate

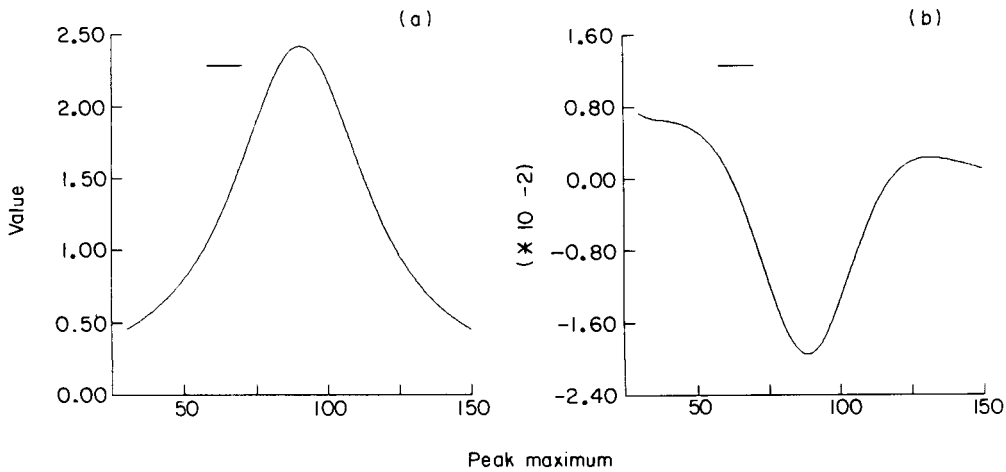

Fig. 4. The change in the value of the first coefficient (a) and the second coefficient (b) plotted against the position of the peak maximum of the second peak in a chromatogram with two symmetric peaks. Coefficients from a deconvolution into Hermite polynomials.

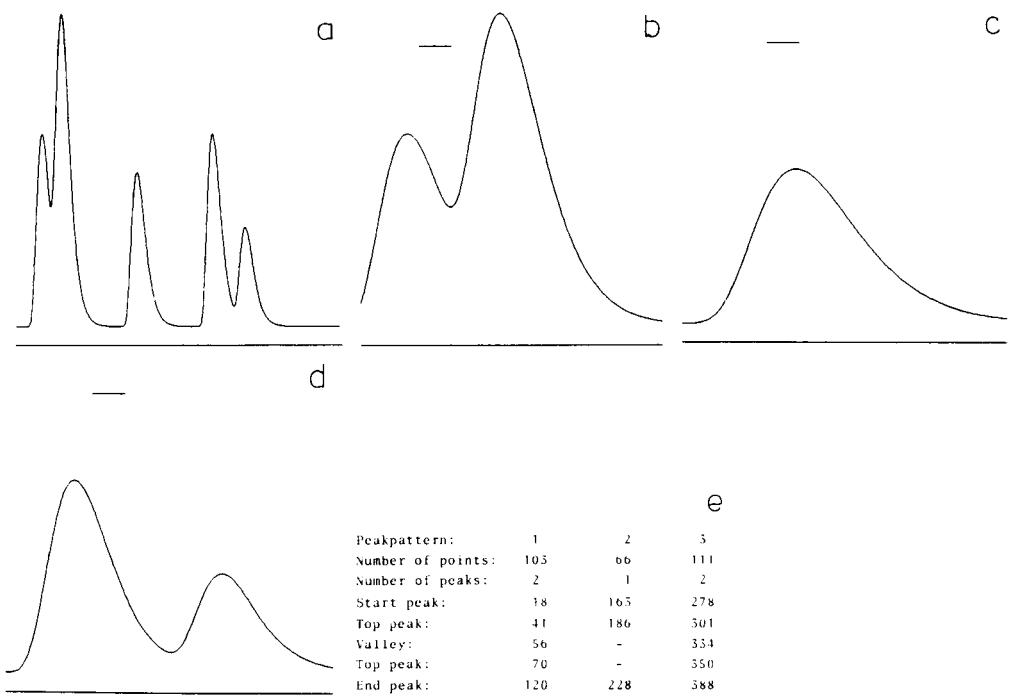

Fig. 5. (a) A chromatogram with five peaks; (b—d) the three peak patterns into which the chromatogram is split; (e) the data from the peak-search routine according to which the chromatogram is split.

this, a data set from Weyland et al. [24] was used to simulate reversed-phase h.p.l.c. separations of five sulfa drugs. The Fraser-Suzuki model [2] was used to simulate chromatograms at all possible solvent compositions of a ternary mixture of water, methanol and acetonitrile within the constraints that the water fraction was between 40% and 80% and the acetonitrile fraction between 0% and 60%. The step width between two ternary compositions was 2% in either direction. Each chromatogram, available in digital form, was fed into the peak-search routine, which gave the results shown in Fig. 5. These results were used to calculate the coefficients for every peak pattern in the chromatogram and then to calculate the new quality criterion, which is given by

$$\mathrm{CRF} = \left\{ \sum_{i=1}^{k} \left[\left(\sum_{j=1}^{n_i - 1} f/g \right)_i - cf_i(1) - |cf_i(2)| \right] k^{-1} + \mathrm{NPEAK}^{1.5} \right. \tag{5}$$

where k is the number of peak patterns in the chromatogram, n_i the number of peaks in peak pattern i, f/g the peak separation of a peak pair as defined by Kaiser [27], NPEAK the number of peaks in the chromatogram, $cf_i(1)$ the first coefficient from the deconvolution of peak pattern i, and $cf_i(2)$ the second coefficient from the same deconvolution.

The response surface of this criterion for the separation of the five sulfa drugs is shown in Fig. 6A. To judge the effect of adding coefficients from a deconvolution, a response surface of the quality criterion without coefficients was also calculated (Fig. 6B). It is clear that the addition of coefficients gives more information about the changes in the quality of separation when peaks overlap strongly. This is indicated by the differences between values of the quality criterion when there is no (or almost no) visible change in the chromatogram (these are the flat parts of the response surface in Fig. 6B). The overall performance of the new quality criterion is comparable to the

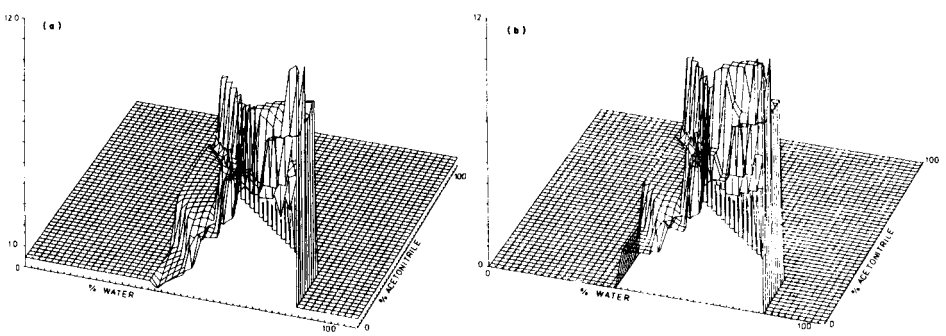

Fig. 6. (A) A three-dimensional response surface of the value of the CRF criterion (Eqn. 5), calculated for chromatograms obtained from sulfanilamide, sulfacetamide, sulfadiazine, sulfisomidine and sulfathiazole with eluents consisting of water, methanol and acetonitrile. (B) As for (A) but calculated without the cf_i coefficients.

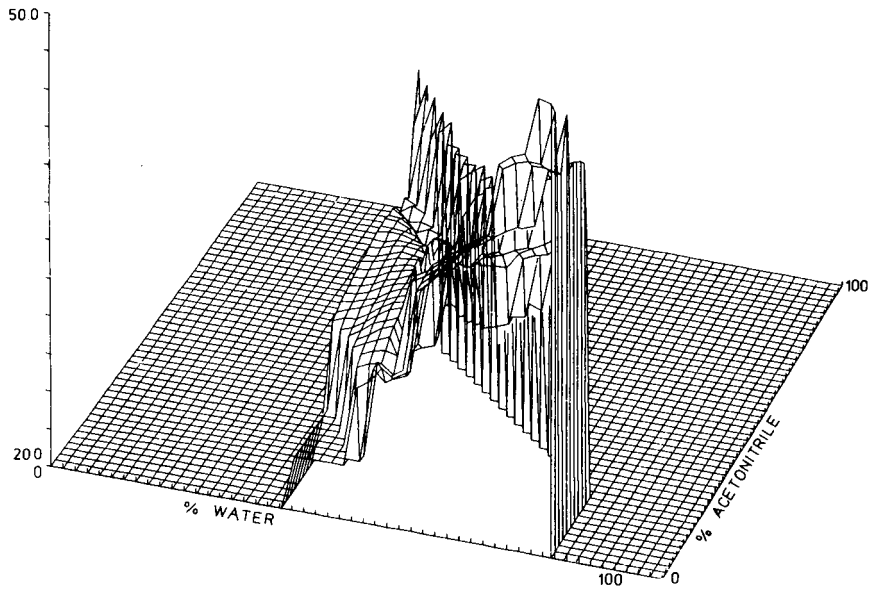

Fig. 7. A three-dimensional response surface of the value of the criterion from Berridge [28], calculated for the separations mentioned in Fig. 6. Formula: CRF = $\Sigma_{i=1}^{L-1} 2R_i + L^{1.5} - 0.05(600 - T_1) - 0.05[T_1 - (T_0 + 120)]$.

performance of (for example) the quality criterion defined by Berridge [28] (Fig. 7). To formulate better quality criteria, further research must be done on the formulation of new criteria wherein the contribution of coefficients from a deconvolution is more important.

Conclusion

The deconvolution of chromatograms into orthogonal polynomials can be useful in several applications. When the quality of separation in a chromatogram or in a pattern of strongly overlapping peaks has to be expressed in one numerical value (for optimization purposes), the coefficients from a Hermite deconvolution give valuable information. The coefficients are little influenced by the signal/noise ratio and the peak-height ratio. Changes in the asymmetry of peaks cause rather large variations in the coefficients, but this is not important in the application to optimization problems. The performance of a criterion for the quality of separation in the automatic optimization of h.p.l.c. separations is improved by adding coefficients from a deconvolution of the chromatogram that is to be judged.

The authors thank Dick Velders for his computational efforts and Ir. P. J. H. Scheeren for valuable discussions about the manuscript.

REFERENCES

1 J. C. Bartlet and D. M. Smith, Can. J. Chem., 38 (1960) 2057.
2 R. D. B. Fraser and E. Suzuki, Anal. Chem., 41 (1969) 37.
3 F. Hock, Chromatographia, 2 (1969) 334.
4 S. Polezza and M. Tamarasso, Chim. Ind. (Milan), 44 (1962) 33.
5 S. M. Roberts, Anal. Chem., 44 (1972) 502.
6 S. M. Roberts, D. H. Wilkinson and L. R. Walker, Anal. Chem., 42 (1970) 886.
7 B. Sen, Anal. Chim. Acta, 22 (1960) 130.
8 A. W. Westerberg, Anal. Chem., 41 (1969) 1770.
9 A. B. Littlewood, T. C. Gibbs and A. H. Anderson, in C. L. A. Harbourn (Ed.), Proc. 7th Int. Symp. Gas Chromatography 1968, Institute of Petroleum, London, 1969, p. 297.
10 J. C. Sternberg, Adv. Chromatogr., 6 (1968) 173.
11 T. S. Buys and K. de Clerk, Anal. Chem., 44 (1972) 1273.
12 E. Grushka, M. N. Myers and J. C. Giddings, Anal. Chem., 42 (1970) 21.
13 M. Abramowitz and I. A. Stegun, Handbook of Mathematical Functions, Dover Publications, New York, 1968, pp. 771—802.
14 A. H. Anderson, T. C. Gibbs and A. B. Littlewood, J. Chromatogr. Sci., 8 (1970) 640.
15 E. Cuso, X. Guardino, J. M. Riera and M. Gassiot, J. Chromatogr., 95 (1974) 147.
16 H. M. Gladney, B. F. Dowden and J. D. Swalen, Anal. Chem., 41 (1969) 883.
17 E. Grushka, Anal. Chem., 44 (1972) 1733.
18 L. G. McWilliam and H. C. Bolton, Anal. Chem., 41 (1969) 1755; 43 (1971) 883.
19 R. E. Pauls and L. B. Rogers, Anal. Chem., 49 (1977) 625.
20 W. W. Yau, Anal. Chem., 49 (1977) 395.
21 S. N. Chesler and S. P. Cram, Anal. Chem., 43 (1971) 1943.
22 Z. Klous, Hoofdvak Stageverslag, University of Amsterdam, 1982.
23 P. J. H. Scheeren, Z. Klous, H. C. Smit and D. A. Doornbos, Anal. Chim. Acta, 171 (1985) 45.
24 J. W. Weyland, C. H. P. Bruins and D. A. Doornbos, J. Chromatogr. Sci., 22(1) (1984) 31.
25 J. M. Laeven, H. C. Smit and J. V. Lankelma, Anal. Chim. Acta, 157 (1984) 273.
26 H. J. G. Debets, B. L. Bajema and D. A. Doornbos, Anal. Chim. Acta, 151 (1983) 131.
27 R. Kaiser, Gas-Chromatografie, Geest und Portig, Leipzig, 1960, p. 33.
28 J. C. Berridge, J. Chromatogr., 244 (1982) 1.

Analytica Chimica Acta, 171 (1985) 45—60
Elsevier Science Publishers B.V., Amsterdam — Printed in The Netherlands

A SOFTWARE PACKAGE FOR THE ORTHOGONAL POLYNOMIAL APPROXIMATION OF ANALYTICAL SIGNALS, INCLUDING A SIMULATION PROGRAM FOR CHROMATOGRAMS AND SPECTRA

P. J. H. SCHEEREN, Z. KLOUS and H. C. SMIT*

Laboratorium voor Analytische Scheikunde, Universiteit van Amsterdam, Nieuwe Achtergracht 166, 1018 WV Amsterdam (The Netherlands)

D. A. DOORNBOS

Vakgroep Farmaceutische en Analytische Chemie, Ant. Deusinglaan 2, 9713 AW Groningen (The Netherlands)

(Received 11th May 1984)

SUMMARY

The computer package calculates the coefficients of the terms of orthogonal polynomial series used to approximate the analytical signal. Two different polynomial series (Hermite and Chebyshev) are used, depending on the number of peaks and spreading of the error of the approximation over the interval. The package is applied for data reduction and filtering of the analytical signal. Part of the package facilitates optimization in chromatography, by calculating the effect of varying chromatogram parameters on polynomial terms. Some scaling methods for the analytical signal are discussed. For testing purposes, a program that generates chromatograms is added to the computer package. The program simulates chromatographic peaks with user-defined peak parameters; noise can be added. The theoretical background is described and some results are presented.

Much attention has been paid to the automatic extraction of relevant parameters from peak-shaped analytical signals. In general, the peak shape is described in rudimentary terms by peak height, retention time (position of the peak maximum), and sometimes moments and related quantities like skewness and kurtosis. The accurate measurement of these parameters can be disturbed by noise, baseline drift and bad resolution. Most of the methods developed for automatic data handling use a sequence of different procedures: noise is smoothed by means of low-pass digital filters [1—3], the problem of bad resolution is handled with the perpendicular drop method [4—6] or triangulation [7] and baseline drift is corrected for, interpolating between the start and end of a peak [8].

A more general method of dealing with analytical signals is to describe the complete signal by a mathematical model. Non-linear regression methods can be used to fit a well defined model to analytical data [9—16]. The usefulness of these methods depends on the model. Models proposed to describe a peak-shaped function are, e.g., the Gauss function, Cauchy function, Poisson function and different modified Gauss functions.

0003-2670/85/$03.30

Some disadvantages of non-linear regression methods are as follows [17, 18]: the chosen mathematical model can cause systematic errors; the method may need much computer time to fit a complete analytical signal; the starting values of the parameters have to be estimated; and in many cases the approximation is not unique.

A computer package for describing peak-shaped functions by means of orthogonal polynomials is described here. Advantages in using orthogonal polynomials are as follows [19, 20]. Instead of a non-linear regression a convolution is used to calculate the coefficients of the polynomial terms; this method is faster, and the solution is unique. Further, starting values of parameters are not needed, and the peak model can be changed at any moment by adding more polynomial terms; because of the orthogonality of the terms only the added terms need to be calculated. The terms of a polynomial do not usually have a direct relationship with conventional analytical parameters; however, it is sometimes possible to calculate height, area and retention time of a peak from known polynomial terms. For this reason, the orthogonal polynomial model was expected to be more useful in other applications such as efficient storage of the information in a signal by means of coefficients of polynomial terms, which means significant data reduction, or in simultaneous filtering of a signal (see below), or in studies of the change in a signal by monitoring the values of the coefficients. This last application is useful in the field of optimization and can be used to describe non-linear effects in chromatography [21].

In this paper, the theory and layout of the computer package built on different orthogonal polynomial models are described. Simulation of chromatograms is discussed. Some results are given to illustrate applications of the package.

THEORY

In order to explain the advantages of the models chosen for the computer package, some common properties of polynomials may be outlined. (Symbols are defined in Table 1.) An nth order polynomial is defined by

$$p_n(t) = a_0 + a_1 t + a_2 t^2 + \ldots\ldots + a_k t^k \qquad (1)$$

where $n \geqslant 0$, and $a_k \neq 0$ are the coefficients of the polynomial. If the set of polynomials is complete, then, according to the Weierstrass theorem, for every function $f(t)$ which is continuous in a closed interval $[a, b]$, it is possible to choose $\epsilon > 0$ and a polynomial $p_n(t)$ such that $P[f(t), p_n(t)] < \epsilon$, where P is defined as the risk function of the polynomial $p_n(t)$ and the function $f(t)$

$$P[f(t), p_n(t)] = ||f(t) - p_n(t)||^2 = \int_a^b [f(t) - p_n(t)]^2 w(t) dt \qquad (2)$$

TABLE 1

List of symbols and definitions

$p_n(t)$	=	nth order polynomial
$w(t)$	=	weighting function of polynomial terms
a_n	=	coefficient of polynomial term n
$H_n(t)$	=	nth order Hermite polynomial
$He_n(t)$	=	nth order modified Hermite polynomial
H	=	peak-maximum amplitude
A	=	asymmetry factor
t_R	=	retention time
σ	=	Gaussian standard deviation of a peak
CM2	=	second central moment
NPTS	=	number of data
S/N	=	signal/noise ratio, defined as maximum amplitude/square root of variance of baseline noise
$F(\omega)$	=	Fourier transform of $f(t)$
$G(\omega)$	=	Gauss function in frequency domain
T_m	=	maximum sampling time
f_m	=	maximum frequency
ω_m	=	maximum angular frequency
I_∞	=	integral of a function on $[-\infty, \infty]$
I_L, I_R	=	integral of a function on $[-\infty, t_R]$ or $[t_R, \infty]$ respectively
$\mathrm{erf}(z)$	=	error function on interval $[0, z]$

where $w(t)$ is a weighting function; $w(t) \geqslant 0$ for $a \leqslant t \leqslant b$ and $w(t)$ is continuous in $[a, b]$. Furthermore, $\lim_{n \to \infty} P(f(t), p_n(t)) = 0$, which means that every function $f(t)$ can be approximated with any desired precision. As the order of the polynomial $p_n(t)$ is increased, the two functions converge if no error of estimation is introduced.

A series of polynomials is called independent if it is not possible to express a term $f_i(t)$ as a linear combination of the other terms $f_n(t)(n \neq i)$. A series of orthogonal polynomials is the set $[p_n(t)]$ satisfying the condition that the convolution of different polynomial terms is zero

$$\langle p_n(t), p_m(t) \rangle = \int_a^b p_n(t) p_m(t) w(t) dt = 0 \qquad \text{for } n \neq m \tag{3}$$

If $\langle p_n(t), p_n(t) \rangle = 1$ the series is called orthonormal. According to Gram—Schmidt theory [19, 20], for every independent series of functions $f_n(t)$, there exists an orthogonal series, $p_n(t)$, such that every function $g(t)$ expressed by a linear combination of terms, $f_n(t)$, can also be given by a linear combination of orthonormal polynomials, $p_n(t)$. It is possible to form an orthonormal series, $p_n(t)$, from an independent series $f_n(t)$ by taking:

$$p_1(t) = f_1(t)/||f_1(t)||$$

$$h_2(t) = f_2(t) - [f_2(t), g_1(t)]\, g_1;\ p_2(t) = h_2(t)/||h_2(t)||$$

$$h_3(t) = f_3(t) - [f_3(t), p_2(t)]\,p_2(t);\ p_3(t) = h_3(t)/\|h_3(t)\|$$

$$h_n(t) = f_n(t) - \sum_{k=1}^{n-1} [f_n(t), p_k(t)]\,p_k(t);\ p_n(t) = h_n(t)/\|h_n(t)\|$$

Furthermore, if $[p_n(t)]_{n=0}^{k}$ is a base of the k-dimensional space, which is a part of space V, and the function $g(t)$ is an element of V, then the value of $\|g(t) - \Sigma_{n=0}^{k} a_n p_n(t)\|^2$ is minimal if $a_n = \langle g(t), p_n(t)\rangle$. Thus a function $g(t)$ on the interval $[a, b]$ can be expressed as a converging series of orthogonal polynomials $[p_n(t)]_{n=0}^{\infty}$ by taking $g(t) = \Sigma_{n=0}^{\infty} a_n p_n(t)$ with $a_n = \langle g(t), p_n(t)\rangle / \|p_n(t)\|^2$. The coefficients a_n are independent. In this aspect, orthogonal polynomials are superior to other polynomials: calculation of the coefficients is simple and fast and, because every function $g(t)$ can be expressed as a series of orthogonal polynomials, they can be widely applied.

A series of orthogonal polynomials satisfies the recurrent mathematical relation:

$$p_{n+1}(t) = [a_n t + b_n]\,p_n(t) - c_n p_{n-1}(t) \qquad (n = 1, 2, 3, \ldots.)$$

with $p_0(t) = p_0$ and $p_1(t) = a_1 t + b_1$. Thus it is possible to develop special series of orthogonal polynomials. Well-known classical orthogonal polynomial series are the Jacobi, Laguerre and Hermite series. One particular Jacobi series is called the Chebyshev polynomial series [20]. In the computer package described here, modified Hermite and Chebyshev series are used. Classical orthogonal polynomial series have maximum values at the limits of the defined interval. In instrumental analytical practice, peak-shaped functions are usually involved. In Appendix 1 it is shown that 7 polynomial terms are sufficient to fit a peak-shaped function. However, it is possible to use prior knowledge about the shape of a signal to define a new set of orthogonal polynomials. The result will be optimal for describing the signal; moreover, a minimum number of terms is used for a defined imprecision. This modification is shown below for Hermite polynomials. The new set $He_n(t)$ is defined by

$$He_n(t) = H_n(t)[w(t)]^{1/2} = H_n(t) \exp(-t^2/2) \qquad (4)$$

This new set is orthogonal to the new weighting function $w_e(t) = 1$ [20]; the values decrease towards the limits of the interval. To check the orthogonality of the new set [22, 23], the term

$$[He_m, He_n] = \int_{-\infty}^{\infty} He_m He_n dt = \int_{-\infty}^{\infty} H_m H_n \exp(-t^2) dt = \pi^{1/2} 2^n n! \qquad n = m$$
$$= 0 \qquad n \neq m$$

for $n = m$ or is zero for $n \neq m$. It is possible to describe the series by a recurrent relationship:

$$He_{n+1}(t) = H_{n+1}(t) \exp(-t^2/2) = 2t \exp(-t^2/2) H_n(t)$$
$$- 2n \exp(-t^2/2) H_{n-1}(t) = 2t\, He_n(t) - 2n\, He_{n-1}(t) \qquad (5)$$

If $g(t)$ is defined as $\Sigma_{k=0}^{\infty} a_k \mathrm{He}_k(t)$ then

$$a_k = (2^k k! \pi^{1/2})^{-1} \int_{-\infty}^{\infty} g(t)\mathrm{He}_k(t)\mathrm{d}t \qquad (6)$$

where the norm $||\mathrm{He}_k(t)||$ is $(2^k k! \pi^{1/2})^{-1}$ and no weighting function is applied.

For the computer package presented here, the sets are defined as follows:

Name	$p_0(t)$	$p_1(t)$	$p_{n+1}(t)$	$\|\|p_n(t)\|\|^2$
Hermite	1	$2t$	$2t\,p_n(t) - 2n\,p_{n-1}(t)$	$\pi^{1/2} 2^n n!$
Chebyshev	1	$2t$	$2t\,p_n(t) - p_{n-1}(t)$	$\pi/2$

A closer look at Eqn. 6 shows that calculating the coefficients a_k is the same as taking one point of the cross-correlation function of the analytical signal and the kth term of the polynomial series. For example, for the first coefficient a_0, the cross-correlation of the analytical signal with a Gauss function is calculated. This is exactly equivalent to putting the analytical signal through a Gaussian filter. Thus, expressing a peak-shaped function as an orthogonal polynomial series means simultaneous filtering with a low-pass filter. According to Appendix I, this statement is valid if no more than seven polynomial terms are used; otherwise the (optimal) low-pass filter effect will be degraded. For an asymmetric function, more terms are needed to fit the peak.

Scaling of the analytical signal

Hermite polynomial series are orthogonal in the interval $[-\infty, \infty]$, so that in theory no scaling is needed. However, the terms decrease rapidly with increasing distance from zero. This implies that Hermite polynomials are best suited to fit a signal with an approximate peak shape (i.e., one peak or a cluster of badly separated peaks) and that it is necessary to scale the signal for a fast convergence. Two different ways of scaling were used here: (1) if the peak maximum is placed in the middle of the interval, convergence will be fast, but this advantage will disappear as the peak becomes asymmetric; (2) the first moment of the peak is placed at the centre of the interval. The next step in scaling is the multiplication of the distance between the data points to contract the peak around the zero point.

All Hermite polynomials are symmetric; the even terms are symmetric to the vertical axis and the odd terms to the origin. To describe a symmetric peak, only the even terms are needed (the odd terms will be zero). For this reason, the computer package has an option to split an asymmetric peak at the position of the maximum and then calculate the coefficients of two symmetric peaks and recombine the polynomial series to the original peak.

Chebyshev polynomial series are orthogonal in the interval $[-1, +1]$, so all analytical signals are scaled to this interval, by multiplying the distance between the data points by an appropriate factor.

Errors in the fitted polynomial series

Putting the Gaussian weighting function into the Hermite polynomial terms changed the spread of error in the interval. As explained above, calculating the coefficients is the same as cross-correlating the analytical signal with the exponential function. This means that the error will be maximal in the middle of the interval and will decrease towards the ends of the peak. When the Chebyshev series is used, the error will be spread evenly over the whole interval; this special feature of the Chebyshev series may be advantageous in analytical practice. The natural order of the polynomial terms is not necessarily the best order for a fast convergence [20].

Testing with a simulated chromatogram

To test the properties of the sets of orthogonal polynomials, a computer program was developed to simulate chromatographic signals. The Fraser–Suzuki function [12] was chosen as the mathematical model to simulate peaks because it gives a good approximation of practical signals. The function is

$$f(t) = H \exp \{(-\ln 2/A^2)[\ln \{1 + [A(t - t_R)/\sigma(2 \ln 2)^{1/2}]\}]^2\}$$

where H is the height of the peak, σ the standard deviation, t_R the time at the peak maximum, and A the asymmetry factor.

The function is continuous: for $A \neq 0$, if $A > 0$ then $t > t_R - (2 \ln 2)^{1/2}\sigma/A$, and if $A < 0$ then $t < t_R - (2 \ln 2)^{1/2}\sigma/A$. Then

$$\lim_{A \to 0} f(t) = \lim_{A \to 0} H \exp \left\{-\ln 2 \left[\frac{\ln \{1 + [A(t - t_R)/\sigma(2 \ln 2)^{1/2}]\}}{A}\right]^2\right\}$$

$$= H \exp \{-\ln 2[(t - t_R)/\sigma(2 \ln 2)^{1/2}]^2\} = H \exp [-(t - t_R)^2/2\sigma^2]$$

because $\lim_{A \to 0} \{[\ln(1 + Ax)]/A\} = x$. Thus the limit for $A \to 0$ is the well known Gaussian function.

The area of the Fraser–Suzuki function is derived as shown in Appendix 2. The results from Appendix 2 were used to calculate the area deviation between the simulated chromatogram and the polynomial. The area of the polynomial approximation is calculated with a trapezium integration for the Hermite polynomials and with Simpson for the Chebyshev polynomials according to the precision needed [24]. The implementation of the theory in a computer package is described below.

COMPUTER PACKAGE HRMT, RACE

The complete computer package is divided into two main programs, HRMT and RACE. A Hewlett-Packard HP 1000 minicomputer was used; the operating system was RTE 6 VM. The language is Fortran IV, compatible with Fortran 77. A graphics terminal is needed. The package uses HP-VIS routines, a firmware Vector Instruction Set that speeds up vector calculations

4–10 times. Both the HRMT and RACE programs are written in an overlay structure, every overlay performing a specific task. The basic principles of both programs are the same: HRMT describes a simulated chromatogram as coefficients of Hermite or Chebyshev polynomials; RACE allows the study of variations of parameters in a simulated chromatogram.

HRMT

Segment HRMT. The program starts with the generation of a simulated chromatogram, using the Fraser–Suzuki function to generate the peaks. Up to 50 peaks can be introduced into a chromatogram of at most 1000 data points. For each peak, the program asks for the retention time (position of the peak maximum), the standard deviation, the peak height, and the value of the asymmetry factor. For each peak, the program calculates the peak area and the interval limits of an interval containing 99% of the area. Negative values of the asymmetry factor will result in fronting of the peak.

Segment ANOIS. The overlay ANOIS adds noise to the simulated chromatogram. The measured noise from some chromatographic detector or the simulated noise (a program for generating simulated noise is available [25]) can be multiplied by any factor to define the signal-to-noise (S/N) ratio of a peak.

Segment APROX. APROX performs the approximation of the chromatogram with an orthogonal polynomial series. Possible options are: (a) Hermite polynomials with different scaling possibilities as is explained in the theory (top on centre of the interval, mean on centre of the interval, splitting of the peak); and (b) Chebyshev polynomials. The segment performs the scaling of the distance between the data points in a Hermite approximation, multiplying the distance by $(1/CM2)^{1/2}$, where CM2 is the second central moment of the signal. In fact, the scaling is a normalization of the peak width. Scaling dependent on the number of terms was tested and appeared to give fast convergence of asymmetric peaks. However, the value of the coefficients of the polynomial terms will depend on the number of terms calculated and the orthogonality principle is disturbed. For this reason, the simple scaling formula is preferred. After the coefficients have been calculated, the chromatogram and approximation are back-scaled.

Segment POWSP. POWSP applies a fast Fourier transform to the chromatographic signal, so that the user can get an impression of the number of terms needed (see Appendix 1).

Segment WRHRM. The last part of program HRMT calculates the approximation determined by the values of the polynomial terms and the coefficients of segment APROX, the area deviation between the chromatogram and the approximation as [(Area approximation − Area chromatogram)/Area chromatogram] × 100, and finally the estimated variance of the data points of the chromatogram and the approximation as: $(1/NDF)\,\Sigma_{i=1}^{NDF}\{f(t_i) - p(t_i)\}^2$, where $f(t_i)$ is the chromatogram value at point t_i, $p(t_i)$ the approximation value at point t_i, and NDF the number of degrees of freedom.

Race

The RACE program was developed to study the effect of changes in the chromatogram on the values of the coefficients of the polynomial terms. The program varies one or two parameters in the simulated chromatogram to user-defined values, calculates the coefficients of the polynomial terms at each parameter value and shows graphs of the variations. Parameters that can be varied are: (1) height of a peak in the chromatogram; (2) retention time of a peak; (3) peak area by changing the peak height; (4) asymmetry factor of a peak; (5) peak width; (6) signal/noise ratio of the chromatogram. The user chooses one or two parameters to vary and defines the values for them. The program checks for independency of the parameters and for values that are allowed. Results are shown in the form of a graph or a table.

Test programs TESTH and TESTC. These programs test the accuracy of the calculated Hermite or Chebyshev coefficients. The input is the values of coefficients of the first thirteen polynomial terms. With these values, a signal is generated using the polynomial series. Next, the coefficients are calculated according to the theory used. Output is a list of chosen and calculated coefficients (Figs. 1 and 2).

RESULTS

Some results obtained with the HRMT and RACE programs are shown in Figs. 3—8. Only a few applications were examined, mainly to test the programs. Some practical applications are shown in Figs. 9—11.

As expected, Hermite polynomial series are suitable for fitting one or two peaks. Chebyshev series are suitable for fitting a bunch of reasonably separated peaks. To fit one peak, the Hermite polynomial needs less than the theoretical

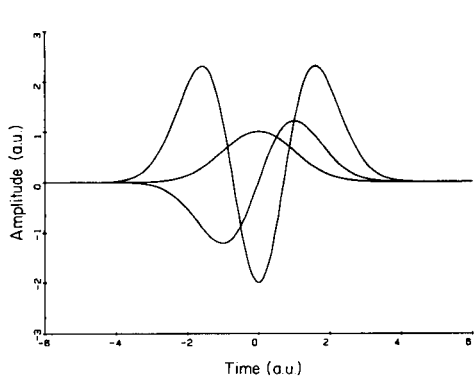

Fig. 1. Hermite polynomial terms 0, 1 and 2. The number of zero-crossings is equal to the number of the term. Values shown are in arbitrary units (a.u.).

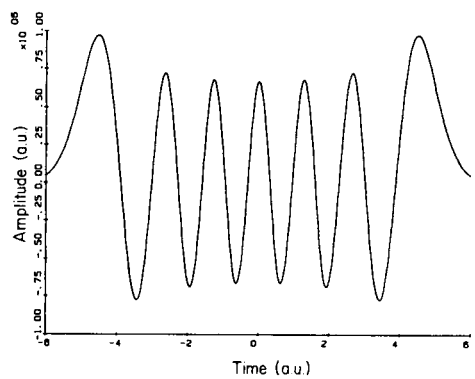

Fig. 2. Hermite polynomial term 12. The amplitude is in the order of 1.000.000; the value of the coefficient will be small in most applications.

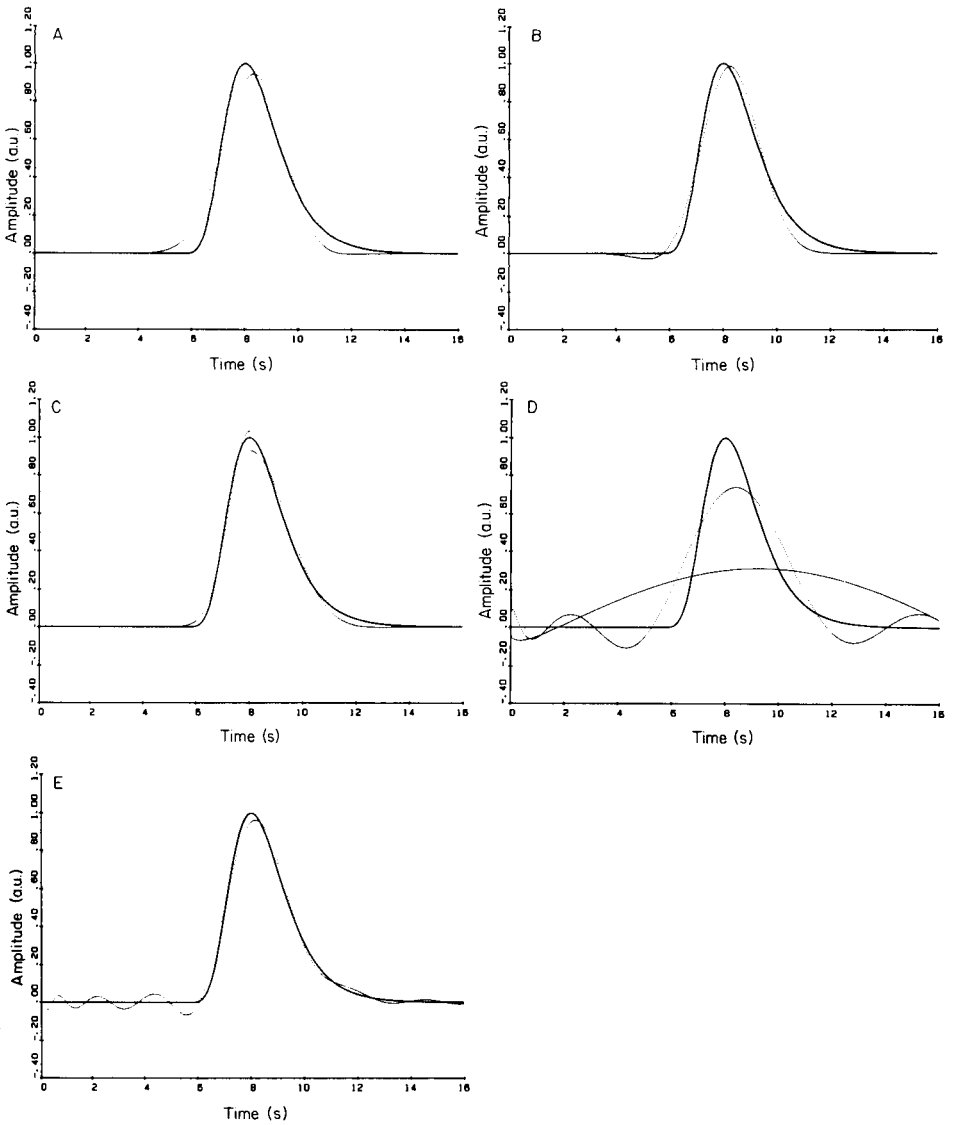

Fig. 3. Peak simulated with the Fraser—Suzuki model is shown as the solid line. Approximations are shown as dotted lines. (A) Approximation with 3 Hermite polynomial terms; the scaling method involves placing the first moment in the middle of the interval; the area duration is 0.253×10^{-2}. (B) As for A, but the scaling method involves placing the top in the middle of the interval; the area duration is 0.137×10^{-2}. (C) As for A, but for scaling the peak is split at the top, the half peaks are completed to symmetric peaks; these peaks are approximated and an approximation to the original peak is reconstructed; the width of the two peaks is different, which means a different scaling of the time axis; the effect is seen at the top of the approximation; the area duration is 0.4×10^{-3}. (D) Approximation with 3 and 10 terms of the Chebyshev polynomial series. (E) Approximation with 20 Chebyshev polynomial terms.

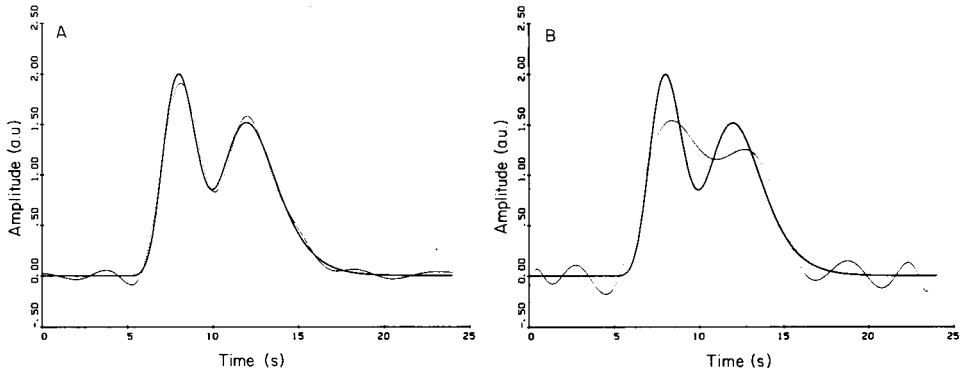

Fig. 4. Two poorly separated peaks, simulated with the Fraser—Suzuki model, are shown as solid lines. (···) Approximations: (A) with 14 Hermite polynomial terms; (B) with 14 Chebyshev polynomial terms.

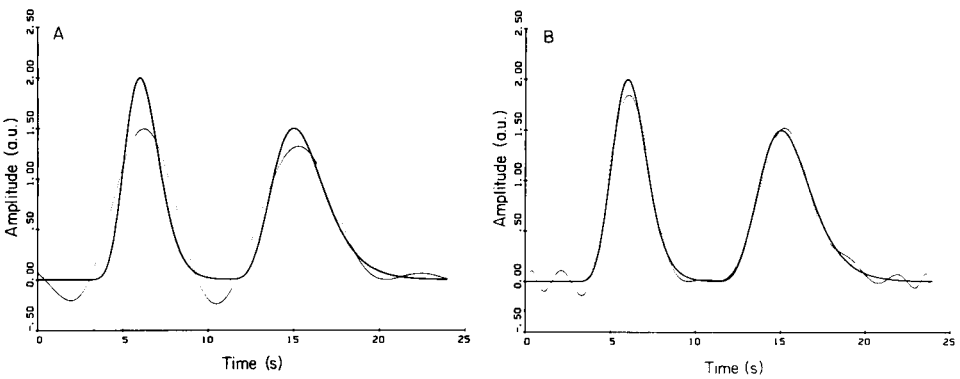

Fig. 5. Two well separated peaks, simulated with the Fraser—Suzuki model, are shown as solid lines. (···) Approximations: (A) with 18 Hermite polynomial terms; (B) with 18 Chebyshev polynomial terms.

number of terms (a Gaussian function needs only one term because the weighting function is placed in this term) but the Chebyshev series needs more terms. An increased number of peaks shows the opposite effect. To calculate more than 25 Hermite terms is not useful because the values of the terms increase very quickly and thus the values of the coefficients become very small; the machine precision places the limit on the number of terms. Chebyshev series do not have this problem.

In tests of the accuracy of the coefficients, it appeared that the Hermite approximation has an error in the order of 0.005% whereas the error can be up to 3% for the Chebyshev series. The overall conclusion is that the Chebyshev approximation is less precise but keeps its precision when the number of terms is increased; the Hermite approximation starts with a small

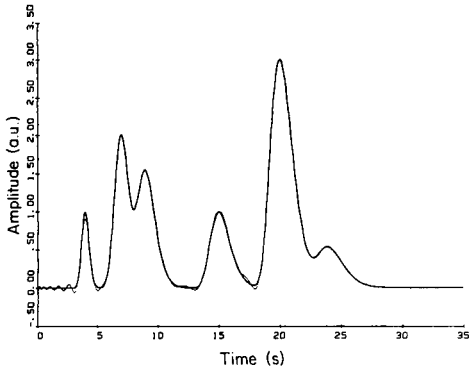

Fig. 6. (——) Simulated chromatogram; (· · ·) Chebyshev polynomial approximation, 60 terms.

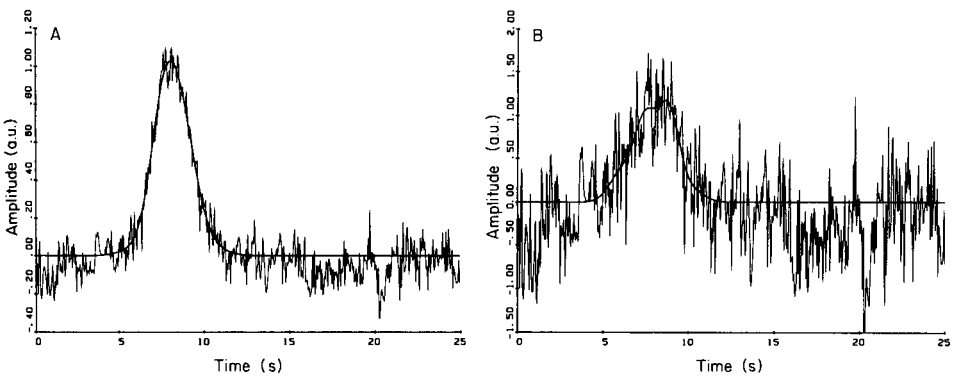

Fig. 7. Simulated peaks with $1/f$ noise added. (A) S/N = 10 and a 7-term Hermite polynomial approximation. (B) S/N = 2; to calculate the moments of the peak, peak start and peak end were detected by zero-crossings, thus the moments are underestimated and the 7-term Hermite approximation shows a double peak.

error but the error increases with increasing number of terms. With the simulated peaks, there was no significant difference between the scaling methods for Hermite series, with regard to precision of the approximation (Fig. 8B).

When the RACE program was used to study the influence of varying peak parameters, calculating the same number of terms, it was found that the area deviation between a simulated chromatogram and the polynomial approximation varied with different features. Thus, the area deviation increased with increasing standard deviations of the peaks using Hermite series, but the effect was the opposite for Chebyshev polynomials. The area deviation increased rapidly with increasing asymmetry factor of the Fraser—Suzuki model when Hermite polynomials were used; with the Chebyshev series there

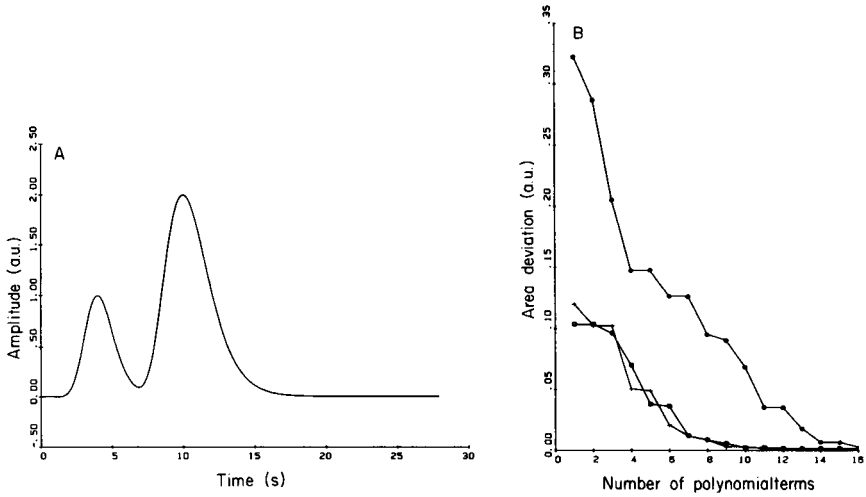

Fig. 8. (A) Two peaks simulated with the Fraser—Suzuki model. (B) Plot of the area deviation against the number of terms used for approximation of the peaks in A: (○) Hermite, scaling "mean on top"; (+) Hermite, scaling "top on top"; (*) Chebyshev.

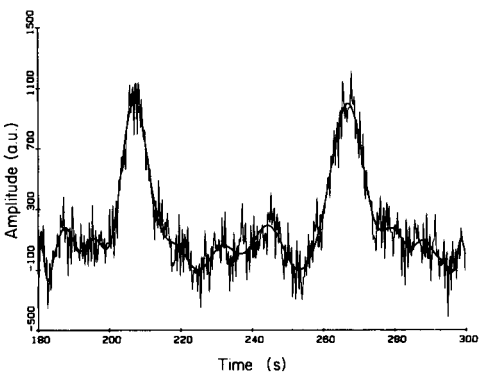

Fig. 9. Chebyshev approximation used as a filter on part of a chromatogram (0.1 μg l^{-1} anthracene, 0.5 μg l^{-1} benzanthracene, reversed-phase h.p.l.c., Supelco LC-8DB (5 μm), column length 15 cm (i.d. 4.6 mm), mobile phase methanol/water 70/30 v/v, detector SP-83000, 254 nm; 40 terms Chebyshev polynomial approximation).

was an approximately linear dependence. The area deviation also increased as the S/N ratio decreased, as was shown with Hermite polynomials (Table 2). As the low-pass filtering theory predicts, the effect of $1/f$ noise is more pronounced than that of white noise. Finally, the area deviation increased with increasing length of baseline pieces when Chebyshev polynomials were used.

In general, it can be concluded that the information present in a chromatographic signal is reflected in the values of polynomial coefficients. For Hermite approximations, the limiting factor is the machine precision. It is

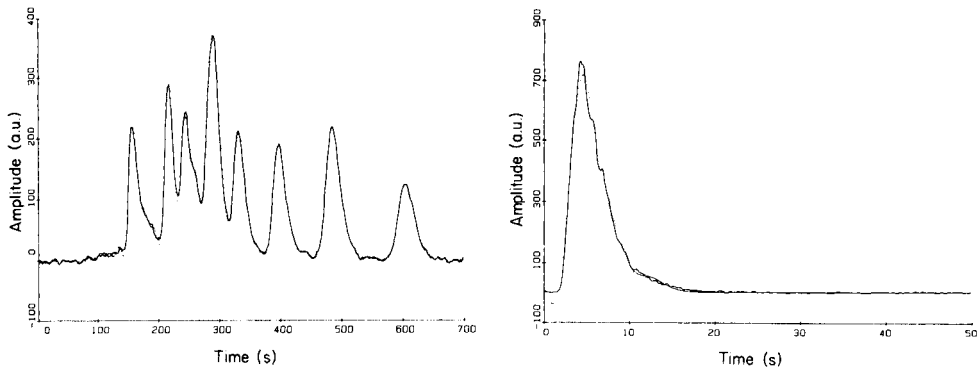

Fig. 10. (——) Chromatogram of alkylbenzenes (reversed-phase h.p.l.c., RP-18 Zorbax ODS, column length 15 cm (i.d. 4.6 mm), mobile phase methanol/water 70/30 v/v. (···) 100-term Chebyshev approximation.

Fig. 11. Approximation of a peak shape in i.c.p. emission spectroscopy with discrete sampling. (——) Peak obtained for 100 μl of 1 mg l^{-1} zinc solution (cross-flow nebulizer, 213.856-nm line, incident power 1.1 kW, observation height 17 mm). (···) 12-term Hermite approximation; the asymmetric form of the peak causes a fluctuation just before the peak.

TABLE 2

Influence of white noise on the area of a Hermite polynomial approximation (Calculation of the area of a simulated peak disturbed by white noise (S/N = 10). The approximation used is a Hermite polynomial series, (scaling with mean on top). This is done ten times with different noise samples. The relative error is the difference between the area of the peak without noise and the mean value of the area of the approximation.)

Number of terms	Mean area (arbitrary units)		Standard deviation (arbitrary units)		Relative error (%)	
	(1)[a]	(2)[b]	(1)[a]	(2)[b]	(1)[a]	(2)[b]
1	2.550	2.393	0.034	0.065	0.7	5.9
3	2.520	2.503	0.045	0.047	0.8	1.5
5	2.518	2.514	0.054	0.050	0.9	1.1

[a]Moments of the peak without noise used. [b]Moments calculated from peak start to peak end, both detected by zero-crossing of the signal.

possible to use the coefficients of Hermite polynomial terms to describe changes in the parameters of the chromatogram. However, more research is needed to decide on possible applications. It is important to establish which polynomial term gives the best indication of a change in a specific peak parameter, and if the relationship is reproducible for different peaks. Some of the research is reported in another paper [21].

DISCUSSION

Chebyshev polynomials are suitable for approximation of a complete chromatogram, but the number of terms needed increases very quickly if baseline separation is present. This difficulty can be avoided by cutting the chromatogram in pieces after a peak-finding procedure and removing the baseline pieces. After the coefficients of the different parts of the chromatogram have been calculated, the approximation is reconstructed by returning the baseline pieces between the back-scaled parts. When this procedure is used, it is also possible to describe only a few peaks with Chebyshev series instead of Hermite series.

The performance of the Hermite polynomial approximation is poor in the presence of noise. It is clear that this is caused by the scaling method. In calculating the second moment, the chromatogram, including the noise, is multiplied by t^2, which causes a rapidly increasing difference from the real value of the moment with increasing value of t. For this reason, the scaling method has to be changed if Hermite polynomials are used as low-pass filters. In chromatography, it is possible to calculate the moments of the signal from a chromatogram with very high S/N ratio. The program offers the possibility of using these moments for a chromatogram with low S/N ratio. Another option in the program makes it possible to use a different method in calculating an approximation of the moments. Research on the application of the method to a variety of chromatograms is in progress.

APPENDIX 1

Theoretical approximation of the number of independent terms needed to describe a peak-shaped function

The Fourier transform of a Gaussian function $f(t) = \exp(-t^2/2\sigma_t^2)$ is $F(\omega) = \int_{-\infty}^{\infty} f(t) \exp(-j\omega t)d\omega$. As given by Deutsch [20], $F(\omega) = \sigma_t(\pi/2)^{1/2} \exp(-\omega^2\sigma_t^2/2)$. A Gaussian function in the frequency domain is defined as $G(\omega) = H_\omega \exp(-\omega^2/2\sigma_\omega^2)$, where H_ω is the peak height. Thus $G(\omega) = F(\omega)$ if $H_\omega = \sigma_t(\pi/2)^{1/2}$ and $\sigma_\omega = 1/\sigma_t$. If the maximal angular frequency, ω_{max}, is defined as $\omega_{max} = 3.5\sigma_\omega = 7/2\sigma_t = 2\pi f_m$, where f_m is the maximal frequency, then the error in the area of the spectrum is $<0.1\%$.

According to Shannon, the maximal sampling time $T_m = 1/2f_m$ is $T_m = 4\sigma_t\pi/14 \approx \sigma_t$ (12.5/14). To approximate the area of the Gaussian function in the time domain with $<0.1\%$ error, the interval $[-3.5\ \sigma_t, 3.5\ \sigma_t]$ is used, thus a minimum of $7 \times 12.5/14$ samples is needed; this means that a bell-shaped function can be described with 7 independent samples. For an asymmetric bell-shaped function, the value of f_m still holds (only the amplitudes of the lower frequencies increase) but more terms (points) are needed because the peak width in the time domain increases.

APPENDIX 2 [22, 23]

Derivation of the area formula of the Fraser–Suzuki function

To calculate the area I of the function:

$$f(t) = \frac{I_\infty}{\sigma(2\pi)^{1/2} \exp(A^2/4 \ln 2)} \exp\left[-\frac{\ln 2}{A^2}\left\{\ln\left(1 + \frac{A(t - t_R)}{\sigma(2 \ln 2)^{1/2}}\right)\right\}^2\right]$$

where I_∞ is the integral over the interval $[-\infty, \infty]$. If $I_L(T_L)$ is defined as the integral of the left part of the peak over interval $[T_L, t_R]$ then $I_L(T_L) = \int_{t_R - T_L}^{t_R} f(t)dt$.

Let $\alpha = I_\infty/\sigma(2\pi)^{1/2} \exp(A^2/4 \ln 2)$, $\beta = \ln 2/A^2$, $\gamma = -AT_L/\sigma(2 \ln 2)^{1/2}$, $\delta = \sigma(2 \ln 2)^{1/2}/A$, and $x = A(t - t_R)/\sigma(2 \ln 2)^{1/2} \rightarrow dx/dt = A/\sigma(2 \ln 2)^{1/2} = 1/\delta$.

Then

$$I_L(T_L) = \alpha\delta \int_\gamma^0 \exp[-\beta \ln^2(1 + x)]dx$$

Substituting $y = \ln(1 + x)$, $\gamma = -T_L/\delta$ and $dx/dy = \exp y$:

$$I_L(T_L) = \alpha\delta \int_{\ln(1-T_L/\delta)}^0 \exp[-(\beta y^2 - y)]dy$$

$$= \alpha\delta \int_{\ln(1-T_L/\delta)}^0 \exp[-(\beta y^2 - y + 1/4\beta) + 1/4\beta]dy$$

$$= \alpha\delta e^{1/4\beta} \int_{\ln(1-T_L/\delta)}^0 \exp[-(y\beta^{1/2} - 1/2\beta^{1/2})^2]dy$$

$$= \alpha\delta \exp(1/4\beta)\beta^{-1/2} \int_{\ln(1-T_L/\delta)}^0 \exp[-(y\beta^{1/2} - 1/2\beta^{1/2})^2 d(y\beta^{1/2} - 1/2\beta^{1/2})$$

Substituting $t = y\beta^{1/2} - 1/2\beta^{1/2}$,

$$I_L(T_L) = \alpha\delta \exp(1/4\beta)\beta^{-1/2} \int_{\beta^{1/2}\ln(1-T_L/\delta)-1/2\beta^{1/2}}^{-1/2\beta^{1/2}} \exp(-t^2)dt$$

$$\int_0^z \exp(-t^2)dt = 0.5\pi^{1/2} \operatorname{erf}(z)$$

hence:

$$I_L(T_L) = \frac{\alpha\delta}{2} (\pi/\beta)^{1/2} \exp(1/4\beta)[-\operatorname{erf}(1/2\beta^{1/2}) + \operatorname{erf}\{1/2\beta^{1/2} - \beta^{1/2} \ln(1 - T_L/\delta)\}]$$

Back-substituting the definitions of α, β, γ, δ and x, and setting $p = A/2(\ln 2)^{1/2}$ yields

$$I_L(T_L) = \frac{1}{2}[\operatorname{erf}\{p - (1/2p) \ln(1 - p2^{1/2} T_L/\sigma)\} - \operatorname{erf}(p)]$$

For the right integral of the peak, the analogous expression is

$$I_R(T_R) = \frac{1}{2}[\operatorname{erf}(p) - \operatorname{erf}\{p - (1/2p) \ln(1 + p2^{1/2} T_R/\sigma)\}]$$

and $I_L(-\infty) = 1/2[1 - \operatorname{erf}(p)]$ and $I_R(\infty) = 1/2[1 + \operatorname{erf}(p)]$. These formulae make it possible to calculate the exact area of the simulated peaks and also the 99% interval.

REFERENCES

1 A. Savitzky and M. J. E. Golay, Anal. Chem., 36 (1964) 1627.
2 A. B. Littlewood, A. H. Anderson and T. C. Gibb, Gas Chromatography 1968, Proc. 7th Int. Symp. Gas Chromatography, Inst. of Petroleum, London, 1969, p. 297.

3 S. P. Cram, S. N. Chesler and A. C. Brown, J. Chromatogr., 126 (1969) 279.
4 R. Kaiser and M. Klier, Chromatographia, 2 (1969) 559.
5 E. Proksch, H. Bruneder and V. Granzner, J. Chrom. Sci., 7 (1969) 473.
6 J. Novak, K. Petrovic and S. Wicar, J. Chromatogr., 55 (1971) 221.
7 A. W. Westerberg, Anal. Chem., 41 (1969) 1770.
8 J. D. Hettinger, J. R. Hubbard, J. M. Gill and L. A. Miller, J. Chrom. Sci., 9 (1971) 710.
9 T. S. Buys and K. de Clerk, Anal. Chem., 44 (1972) 1273.
10 E. Grushka, M. N. Myers and J. C. Giddings, Anal. Chem., 42 (1970) 21.
11 A. H. Anderson, T. C. Gibbs and A. B. Littlewood, J. Chrom. Sci., 8 (1970) 640.
12 R. D. B. Fraser and E. Suzuki, Anal. Chem., 41 (1969) 37.
13 O. Grubner, Anal. Chem., 43 (1971) 1934.
14 E. Grushka, M. N. Myers, P. O. Schettler and J. C. Giddings, Anal. Chem., 41 (1969) 889.
15 E. Cusó, X. Guardino, J. M. Riera and M. Gassiot, J. Chromatogr., 95 (1974) 147.
16 R. O. Butterfield, E. B. Lancaster and H. J. Dutton, Sep. Sci., 1 (1966) 329.
17 G. C. Allen and R. F. McMeeking, Anal. Chim. Acta, 103 (1978) 73.
18 P. R. Bevington, Data Reduction and Error Analysis for the Physical Sciences, McGraw-Hill, New York, 1969, p. 204.
19 C. Vidal-Madjar and G. Guiochon, J. Chromatogr., 142 (1977) 61.
20 R. Deutsch, System Analysis Techniques, Prentice-Hall, New Jersey, 1969, p. 279.
21 H. J. G. Debets, A. W. Wijnsma, D. A. Doornbos and H. C. Smit, Anal. Chim. Acta, 170 (1985) 33.
22 M. Abramowitz and I. A. Segun, Handbook of Mathematical Functions, Dover, New York, 1968, p. 771.
23 M. R. Spiegel, Mathematical Handbook, Schaum's Outline Series, McGraw-Hill, New York, 1968, p. 146.
24 Ph. J. Davis and Ph. Rabinowitz, Numerical Integration, Blaisdell, Waltham, MA, 1967.
25 J. M. Laeven, H. C. Smit and J. V. Lankelma, Anal. Chim. Acta, 157 (1984) 273.

Analytica Chimica Acta, 171 (1985) 61—76
Elsevier Science Publishers B.V., Amsterdam — Printed in The Netherlands

PRIMA: A NEW PATTERN RECOGNITION METHOD

ISTVÁN JURICSKAY
Medical University of Pécs (Hungary)
GÁBOR E. VERESS
Institute of General and Analytical Chemistry, Technical University of Budapest (Hungary)
(Received 17th August 1984)

SUMMARY

PRIMA, a new supervised classification method is based on the concept of class distance (Euclidean distance). For each class, a separate class distance is defined on the basis of the centre of gravity and inhomogeneity for the class; this class distance is then used to produce the classification. The PRIMA classifier based on class distance can be applied in different, complex cases. The conditions of applicability are less strict than those of other methods. The algorithm is simple; efficiency and stability are good. The simplicity of the method even for complex cases, e.g., with very many variables or multicategory classification, or with noisy or incomplete data processing, is noteworthy when compared with other effective pattern recognition methods.

In this paper, the PRIMA method of pattern recognition (Pattern Recognition by Independent Multicategory Analysis) is introduced. The fundamentals of pattern recognition and their chemical applications have been discussed in several monographs and reviews [1—5], thus only a brief outline is given here. Pattern recognition involves the classification of objects (e.g., materials) into classes (categories, groups). Classes are defined on the basis of some property of the objects included in the class. In chemistry, the property can be chemical (e.g., the presence or absence of an aromatic ring in a compound) or a users' property (e.g., the origin of an archaeological artefact or the quality of a product).

The class-defining property cannot generally be measured directly, or only with difficulty or at great expense. However, the objects will have other properties that can easily be measured or observed. If the easily measurable properties, known as features, can be related to the class-defining property, then it is expedient to classify the objects indirectly on the basis of these features. The principle of pattern recognition is to achieve classification based on easily measurable quantitative features instead of the class-defining properties that are only qualitative or are difficult to quantify. Obviously, the measured properties must be characteristic for the classes. Pattern recognition methods are, therefore, based on the assumption that the distance between objects belonging to one class in the pattern space is

0003-2670/85/$03.30

small, whereas the distance between objects from different classes is large. This means that the points corresponding to objects from different classes appear in separate subspaces of the pattern space. In pattern recognition, objects are assigned to the class corresponding to the subspace that contains the datum point(s) of the object.

THE PRINCIPLE OF METHOD PRIMA

Basic concepts

The objects are indicated by $i = 1, \ldots, I$. The objects may belong to known or unknown classes indexed as $k = 1, \ldots, K$; in some cases l is used. The notations used are summarized in Table 1. The objects are described by properties. A J-dimensional property or pattern space X is defined; x_{ij}^k is used to denote the value of the jth property of the ith object belonging to the kth class. The k superscript is omitted if the class is unknown or arbitrary; an asterisk is used to indicate an unknown class. The property values form a pattern vector $\mathbf{x}_i = x_{i1} \ldots, x_{ij}$, where $\mathbf{x}_i \in X$. Each object is a point in pattern space given by the pattern vector.

Objects can be grouped into two groups, one of known class membership giving the training set or test set, and one of unknown class membership, i.e., the objects to the classified. Correspondingly, a training data matrix $\mathbf{X}^L$ on the training set can be defined

$$\mathbf{X}^L = \begin{bmatrix} \begin{bmatrix} x_{11}^1 & \ldots & x_{1J}^1 \\ \vdots & & \vdots \\ x_{I^1 1}^1 & \ldots & x_{I^1 J}^1 \end{bmatrix} \\ \vdots \\ \begin{bmatrix} x_{11}^k & \ldots & x_{1J}^k \\ \vdots & & \vdots \\ x_{I^k 1}^k & \ldots & x_{I^k J}^K \end{bmatrix} \\ \vdots \\ \begin{bmatrix} x_{11}^K & \ldots & x_{1J}^K \\ \vdots & & \vdots \\ X_I^K K_1 & \ldots & X_I^K K_J \end{bmatrix} \end{bmatrix}$$

where I^k for $k = 1, \ldots, K$ is the number of objects in the kth class. In a completely analogous way, the test data matrix $\mathbf{X}^T$ can be defined. The

TABLE 1

Notation used

d	threshold of class distance
$d^k = d^k(\mathbf{x}_i, \bar{\mathbf{x}}^k)$	the kth class distance of ith object
$d_j^k(x_{ij}, \bar{x}_j^k)$	the jth property component of the kth class distance
$d^{kl} = d^{kl}(\bar{x}^k, \bar{x}^l)$	distance between classes k and l
$d_j^{kl}(\bar{x}_j^k, \bar{x}_j^l)$	the jth property component of the between-class distance k and l
$\mathbf{D}_j$	matrix of the jth property component of between-class distances
$\mathbf{D}$	between-class distance matrix
F_j^{kl}	Fischer quotient of jth property for classes k and l
i	index of object
I	number of objects
I^k	number of objects belonging to class k in the training set
$\hat{I}^k$	number of objects classified to class k in the training set
I^{kT}	number of objects belonging to class k in the test set
$\hat{I}^{kT}$	number of objects classified to class k in the test set
I^*	number of objects to be classified
j	index of properties
J	number of properties
k	index of classes
K	number of classes
l	index of classes
r	recognition ability
r^k	recognition ability for class k
p	prediction ability
p^k	prediction ability for class k
s_j^k	inhomogeneity of the jth property for class k
$\mathbf{s}^k$	inhomogeneity vector of class k
$\mathbf{s}_j^{kl}$	average inhomogeneity of the jth property for classes k and l
w_j^k	weight of jth property for class k
$\mathbf{w}^k$	weight vector for class k
x_{ij}	jth property of the ith object
x_{ij}^k	jth property of the ith object in class k
x_{ij}^*	jth property of the ith object of unknown class
$\mathbf{x}$	property or pattern vector of an object
$\mathbf{x}_i$	property or pattern vector of the ith object
$\bar{x}_j^k$	average of property j in class k
$\bar{\mathbf{x}}^k$	centre of gravity for class k
$\mathbf{X}^L$	training data matrix
$\mathbf{X}^T$	test data matrix
$\mathbf{X}^*$	recognition data matrix
X	J-dimensional pattern space
z_{ij}^k	standard value of the jth property for object i of class k

recognition data matrix $\mathbf{X}^*$ is given in the form

$$\mathbf{X}^* = \begin{bmatrix} x_{11}^* & \dots & x_{1J}^* \\ \vdots & & \vdots \\ x_{I^*1}^* & \dots & x_{I^*J}^* \end{bmatrix}$$

where I^* is the number of objects to be classified.

The centre of gravity and inhomogeneity of classes

In learning, the classes are characterized by two parameters, the centre of gravity and inhomogeneity. The average of a given property j in a class k can be calculated simply by formula

$$\bar{x}_j^k = \left(\sum_{i=1}^{I^k} x_{ij}^k \right) I^k \quad (j = 1, \ldots, J, \text{ and } k = 1, \ldots, K)$$

The value of $\bar{x}_j^k$ is calculated by summing the appropriate column in the submatrix of the training data matrix corresponding to the given class. The centre of gravity of the given class k is the vector formed from the property averages

$$\bar{\mathbf{x}}^k = (\bar{x}_1^k \ \ldots \ \bar{x}_J^k)(k = 1, \ldots, K)$$

The spread of the classes in pattern space can be characterized by the inhomogeneity or dispersion of the properties. The inhomogeneity of a property j in class k, s_j^k, is the dispersion of the property

$$s_j^k = \left\{ \left[\sum_{i=1}^{I^k} (x_{ij}^k - \bar{x}_j^k)^2 \right] \Big/ (I^k - 1) \right\}^{1/2} \quad (j = 1, \ldots, J \text{ and } k = 1 \ldots, K)$$

An equivalent concept is the weight of a given property in a given class, w_j^k, which is the reciprocal of the square of the inhomogeneity: $w_j^k = 1/(s_j^k)^2$. The inhomogeneity vector of a given class $\mathbf{s}^k$ is a vector formed from the property inhomogeneities, i.e., $\mathbf{s}^k = (s_1^k \ldots s_j^k)$ for $k = 1, \ldots, K$. The class weight vector $\mathbf{W}^k$ can be defined in an analogous way as a vector of the property weights, i.e., $\mathbf{W}^k = (w_1^k \ldots w_J^k)$ for $k = 1, \ldots, K$.

It should be noted that the above concepts can also be calculated independently for incomplete data sets. The actual number of data I^k must then be taken into account in the formulae.

Class distance

Very many distances can be defined between the points of pattern space. Here, the Euclidean distance is used as a class distance; other distance definitions could also be used. Before a definition of the class distance is given, the concept of a property component of the class distance must be introduced. The jth property component of the class distance with respect to the kth class is

$$d_j^k (x_{ij}, \bar{x}_j^k) = (1/s_j^k)(x_{ij} - \bar{x}_j^k) \quad (i = 1, \ldots, I, j = 1, \ldots, J, k = 1, \ldots K)$$

On the basis of property components, the basic idea of this method, the class distance, can be defined as

$$d^k (\mathbf{x}_i, \bar{\mathbf{x}}^k) = \left\{ (1/J) \sum_{j=1}^{J} [d_j^k (x_{ij}, \bar{x}_j^k)]^2 \right\}^{1/2} \quad (i = 1, \ldots, I, k = 1, \ldots, K)$$

which means that the square of the class distance is the average of the squares of the property components. If the property component definition is applied, the class distance can take the form

$$d^k(\mathbf{x}_i, \bar{\mathbf{x}}^k) = \left\{(1/J) \sum_{j=1}^{J} [1/(s_j^k)^2] (x_{ij} - \bar{x}_j^k)^2\right\}^{1/2}$$

or

$$d^k(\mathbf{x}_i, \bar{\mathbf{x}}^k) = \left\{(1/J) \sum_{j=1}^{J} w_j^k (x_{ij} - \bar{x}_j^k)^2\right\}^{1/2} \quad (i = 1, \ldots, I, k = 1, \ldots, K)$$

The class distance of a given point is the average distance for a single property of the point measured from the centre of gravity of the class weighted by the class weight vector.

The above concept of distance as an average distance [6] can be applied to incomplete data where the value of J must be decreased accordingly. The normalizing factor, $1/J$, is included in the formula in order to ensure proper comparison of the distances regardless of the dimension. It should be noted that for $s_j^k = 0$ an arbitrary value depending on the nature of the problem (e.g., measurement error) must be used.

The class distance can be interpreted by spanning the pattern space of each class with a coordinate system having its origin at the centre of gravity of the class and a unit of property inhomogeneity. In such interpretation, the class distance can be given by a z transformation [6] or by autoscaling according to each class

$$d^k(\mathbf{x}_i, \bar{\mathbf{x}}^k) = \left[(1/J) \sum_{j=1}^{J} (z_{ij}^k)^2\right]^{1/2} \quad (i = 1, \ldots, I, k = 1, \ldots, K)$$

where $z_{ij}^k = (x_{ij} - \bar{x}_j^k)/s_j^k$ for $i = 1, \ldots, I$, $j = 1, \ldots, J$, and $k = 1, \ldots, K$, is the z transform or standardized value for the kth class of the property value x_{ij}.

It should be noted that SIMCA [7] is based on similar transformations in principal component space and that the axes of the plot discussed by Derde et al. [8] also correspond to special class distances.

Statistical interpretation of the PRIMA method

In order to achieve the best classification from the point of view of decision theory (Bayesian decision), it is necessary to know not only the probabilities of the classes based on prior knowledge, but also the conditional probabilities of the classes according to each property. In point methods (e.g., k-nearest neighbours), this is approached by considering the information obtainable from the training samples with the same weights. It can be proved that this approach is limited only by the memory capacity and computational time need. In methods based on the centre of gravity, the probability distribution is characterized only by a single point, the centre of gravity of the class.

In the PRIMA method the true distributions are approximated by also considering the inhomogeneity. The averages can be regarded as estimates of the expected value of the properties, and the measures of inhomogeneity (standard deviation) as estimates of the second central moments. The justification and accuracy of these estimates are given by the well-known criteria of single-variable statistical methods. The expected value of variables of the transformed pattern space are zero if the object belongs to the class in question. The class distance thus defined makes a good estimate possible. If further moments were taken into consideration in characterizing the distributions, better approximations for the Bayesian decision could be achieved. This would mean a bias transformation where the class distance is anisotropic; which is the main point in feature extraction.

CLASSIFICATION WITH THE PRIMA METHOD

Training and recognition

Training with the PRIMA method means the determination of class centres of gravity $\mathbf{x}^1, \ldots, \mathbf{x}^K$ and class inhomogeneity vectors $\mathbf{s}^1, \ldots, \mathbf{s}^K$ or class weight vectors $\mathbf{w}^1, \ldots, \mathbf{w}^K$ from the training data matrix $\mathbf{X}^L$.

Recognition consists of two steps. First, the class distances of the object $\mathbf{x}^*$ to be recognized, i.e., $d^1(\mathbf{x}^*, \bar{\mathbf{x}}^1), \ldots, d^K(\mathbf{x}^*, \bar{\mathbf{x}}^K)$ are evaluated. In the second step, the class or classes to which the unknown object belongs must be decided. There are several possible ways of evaluating the class membership. Classification can be done by assigning the object to the class for which the class distance is minimal, i.e., $\min_k \{d^1, \ldots, d^K\}$. A more practical solution is achieved if the class membership is determined by the condition $d^k(\mathbf{x}^*, \bar{\mathbf{x}}^k) \leqslant d$, which means that object $\mathbf{x}^*$ belongs to the kth class if the above condition is satisfied, where d is a suitably selected limit value, the so-called class distance threshold. In this case, an object can belong naturally to more than one class or even be an outlier. In this sense, PRIMA is similar to SIMCA [7]. The threshold value d depends on the problem and is best evaluated iteratively (see below).

The PRIMA algorithm

A block diagram of the algorithm is shown in Fig. 1. The algorithm consists of two steps like other supervised classification methods. In the first step (training), the class centres of gravity and class inhomogeneities are evaluated. The second step is recognition or classification. The pattern vector of the unknown object is transformed to the standardized pattern spaces of the classes and the class distances are calculated. Then the object is classified. The algorithm is supplemented by characterization of the classes and classification.

The algorithm of the PRIMA method was programmed in FORTRAN for a VIDEOTON 1010 minicomputer and is also available in BASIC for ROSY 80 microcomputer.

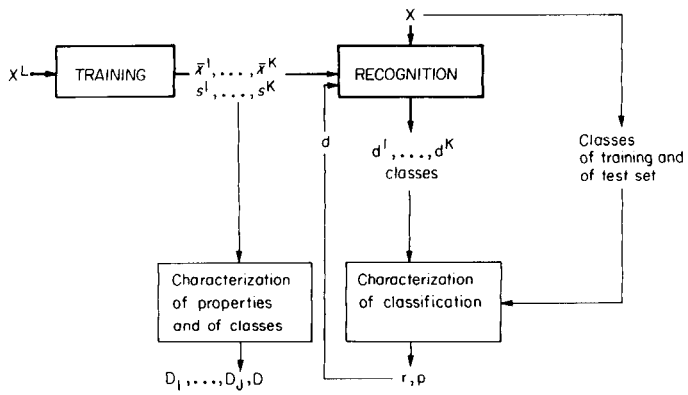

Fig. 1. Block diagram for the PRIMA algorithm.

Between-class distance

From the definitions given above, it follows that the distance between the centres of gravity of two classes depends on the class weight vector, thus the distances generally do not coincide.

$$d^k(\bar{\mathbf{x}}^l, \bar{\mathbf{x}}^k) = \left\{(1/J) \sum_{j=1}^{J} [1/(s_j^k)^2]\ (\bar{x}_j^l - \bar{x}_j^k)^2\right\}^{1/2}$$

and $$d^l(\bar{\mathbf{x}}^k, \bar{\mathbf{x}}^l) = \left\{(1/J) \sum_{j=1}^{J} [1/(s_j^l)^2]\ (\bar{x}_j^l - \bar{x}_j^k)^2\right\}^{1/2}$$

Various between-class distances can be defined for the centres of gravity of the classes. The between-class distance can be interpreted as

$$d^{kl}(\bar{\mathbf{x}}^l, \bar{\mathbf{x}}^k) = \left\{(1/J) \sum_{j=1}^{J} [1/(s_j^{kl})^2]\ (\bar{x}_j^l - \bar{x}_j^k)^2\right\}^{1/2} \quad (k, l = 1, \ldots, K)$$

where $1/(s_j^{kl})^2 = 1/2\,\{[1/(s_j^k)^2] + [1/(s_j^l)^2]\}$ ($j = 1, \ldots, J$, and $k, l = 1, \ldots, K$), i.e., $(s_j^{kl})^2 = 2(s_j^k)^2\,(s_j^l)^2/[(s_j^k)^2 + (s_j^l)^2]$ ($j = 1, \ldots, J$ and $k, l = 1, \ldots, K$); s_j^{kl} means the average inhomogeneity of the two classes for property j.

Similarly to the case of the class distance, the property components of between-class distance can also be defined

$$d_j^{kl}(\bar{x}_j^l, \bar{x}_j^k) = [1/2\,\{[1/(s_j^k)^2] + [1/(s_j^l)^2]\}]^{1/2}\ (\bar{x}_j^l - \bar{x}_j^k)\ (j = 1, \ldots, J \text{ and } k, l = 1, \ldots, K)$$

or by applying the average inhomogeneity

$$d_j^{kl}(\bar{x}_j^l, \bar{x}_j^k) = (1/s_j^{kl})\ (\bar{x}_j^l - \bar{x}_j^k)\ (j = 1, \ldots, J \text{ and } k, l = 1, \ldots, K).$$

It should be noted that the Fisher quotient $F_j^{kl} = [1/(s_j^k + s_j^l)]\ (\bar{x}_j^l - \bar{x}_j^k)$ ($j = 1, \ldots, J$ and $k, l = 1, \ldots, K$) can be regarded as a special property component of the between-class distance.

Characterization of properties

The property component of the between-class distance characterizes the importance of the given property. When all property components are considered, the matrix of the property component of the between-class distance is given by

$$\mathbf{D}_j = \begin{pmatrix} d_j^{11} & \dots & d_j^{1K} \\ \vdots & & \vdots \\ d_j^{K1} & \dots & d_j^{KK} \end{pmatrix} \quad (j = 1, \dots, J)$$

where the diagonal elements are all zero. The matrix can be used to characterize the importance of a given property from the point of view of classification. Thus, if the absolute value of d_j^{kl} is large, then the jth property discriminates well between classes k and l; if its value is small, the discriminating power of property j between classes k and l is small or negligible.

Characterization of classes

The location of classes from the training set can also be characterized on the basis of the between-class distance. The matrix D for the between-class distances is:

$$\mathbf{D} = \begin{pmatrix} d^{11} & \dots & d^{1K} \\ \vdots & & \vdots \\ d^{K1} & \dots & d^{KK} \end{pmatrix}$$

The matrix is symmetric, its diagonal elements being zero. If the value of d^{kl} is large, then the classes can be separated in pattern space, and the probability of misclassification is small. If d^{kl} is small, then the classes are not well separated in pattern space.

Characterization of classification by the training set

The recognition ability corresponds to the fraction of objects from the training set that are classified correctly, i.e., $r^k = \hat{I}^k / I^k \quad (k = 1, \dots, K)$, where $\hat{I}^k$ is the number of objects classified into class k, and I^k is the number of objects belonging to that class in the training set [3]. The recognition ability for the total training set is given by $r = \sum_{k=1}^{K} \hat{I}^k / \sum_{k=1}^{K} I^k$. The recognition ability is thus a suitable coefficient for the iterative evaluation of the class-distance threshold value (see Fig. 1).

Characterization of classification by the test data set

Besides the recognition ability, the efficiency of classification can also be characterized by the prediction ability [3]. Prediction ability expresses the fraction of test objects that are classified correctly, i.e., $p^k = \hat{I}^{kT} / I^{kT} \quad (k = 1, \dots, K)$, where $\hat{I}^{kT}$ is the number of test objects classified into class k and I^{kT} is the number of test objects belonging to class k. The prediction ability

can also be defined for the complete test set and not only for the separate classes by $p = \Sigma_{k=1}^{K} \hat{I}^{kT} / \Sigma_{k=1}^{K} I^{kT}$. Classification is characterized in the PRIMA algorithm as shown in Fig. 1.

APPLICATIONS OF THE PRIMA METHOD

The IRIS data

For validation, the PRIMA method was tested for problems which have been already solved by other methods. The classical IRIS example [9] was selected. Wold [7] dealt with this problem in detail, comparing the linear discriminant methods kNN and SIMCA. The measured data consist of four features of *Iris setosa* (class I), *Iris versicolor* (class II) and *Iris virginica* (class III), the length and breadth of the sepal and the petal. Each class had 50 samples; 25 of these made up the training set, 25 the test set.

In the training phase, the PRIMA method was used to determine the class characteristics, i.e., centres of gravity and inhomogeneities; these are shown in Table 2. The data characterizing classification, i.e., the feature components of class distance and between-class distance are shown in Table 3. As can be seen, the class distances between I and II, and I and III are large, thus these classes are easily separated. Classes II and III, however, are very close. It was found that features 3 and 4 were effective in separating all class

TABLE 2

Property averages and property inhomogeneities of classes with respect to the sepal and petal features

Class	Property average				Property inhomogeneities			
	Sepal		Petal		Sepal		Petal	
	length	breadth	length	breadth	length	breadth	length	breadth
I *Iris setosa*	5.03	3.48	1.46	0.25	0.39	0.36	0.19	0.10
II *Iris versicolor*	5.89	2.78	4.31	1.34	0.81	0.35	0.43	0.20
III *Iris virginica*	6.58	2.93	5.64	2.04	0.71	0.35	0.63	0.25

TABLE 3

Property components of class distance, and between-class distances for the sepal and petal features

Class	Property component				Between-class distance
	Sepal		Petal		
	length	breadth	length	breadth	
I–II	−0.96	1.41	−5.99	−4.84	3.94
I–III	−1.91	1.09	−6.31	−6.65	4.72
III–III	−0.63	−0.31	−1.73	−2.18	1.43

pairs while features 1 and 2, especially between classes II and III, did not display significant discriminating power. Class distances evaluated by the PRIMA method are shown in Fig. 2.

The solutions of the IRIS data obtained by the PRIMA method are given in Table 4. The following inequality was found to be true for each sample $d(\mathbf{x}, \mathbf{x}^k) \leqslant 1.9$ ($k = 1, \ldots, K$), if the sample actually belonged to class k, though not necessarily only to class k. The inequality was found to be true for 83% of the samples for one class, and 17% for two classes, i.e., for a given $\mathbf{x}$, two inequalities were found to be true: $d(\mathbf{x}, \mathbf{x}^k) \leqslant 1.9$ and $d(\mathbf{x}, \mathbf{x}^l) \leqslant 1.9$. Even in 80% of these cases, the two distances were not equivalent and $d(\mathbf{x}, \mathbf{x}^k) < d(\mathbf{x}, \mathbf{x}^l)$, i.e., the actual class was k.

There was no misclassification in the solution of the problem. In 17% of the cases giving dual classes, the correct class was always present; in 80% of these cases, the correct class was given first (smallest distance). For comparison, 9 samples were misclassified by the 3-NN method and by the SIMCA method 5 samples were misclassified with a one-dimensional model and

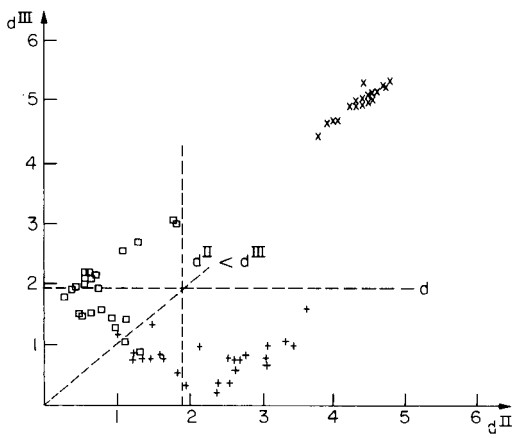

Fig. 2. Class distances: (×) I; (□) II; (+) III.

TABLE 4

Efficiency of IRIS classification of the IRIS data (no misclassifications were found)

Classes	Correct classification	Dual classification	
		nearer[a]	farther[b]
I *Iris setosa*	42	8	—
II *Iris versicolor*	43	5	2
III *Iris virginica*	40	7	3
Total	125	20	5

[a] Nearer to true class. [b] Farther from true class.

3 samples with a two-dimensional model. The samples assigned to two classes by the PRIMA method agreed precisely with the results of the SIMCA method.

Conformational analysis

Wold [10] discussed the following example: 7 parameters of infrared and ultraviolet spectra for sixteen compounds with α- and β-unsaturated carbonyl groups were measured. The primary data were taken from the work of Mecke and Noack [11]. The problem is to decide if the data are appropriate for discriminating between *trans*- and *cis*-isomers. The first six samples were known to be *trans*-isomers (class I) and the last three *cis*-isomers (class III). It was uncertain whether the remaining samples formed a cluster of their own ("skew" conformation, class II) or belonged to class I or III. Because the *cis* group was too small for principal components analysis, SIMCA was trained by only classes I and II. The SIMCA results showed that classes I and II (*trans* and skew) could be distinguished, and that the *cis* class was similar to class II.

PRIMA was applied to solve the same problem. Here, the three groups were used for training. The class property averages and class inhomogeneity data are listed in Table 5. The discrimination power of the properties between classes and the between-class distances are included in Tables 6 and 7.

TABLE 5

Property averages and property inhomogeneities of classes

Class	Features						
	1	2	3	4	5	6	7
Property averages							
I. *trans*	1687	8.58	12.3	1632	1.09	2212	12780
II. skew	1694	4.27	10.6	1622	3.39	2311	8728
III. *cis*	1690	4.63	13.0	1618	3.88	2410	8033
Property inhomogeneities							
I. *trans*	13.1	0.75	7.22	9.51	0.77	90.1	2270
II. skew	4.65	0.51	3.87	3.63	1.70	66.9	2904
III. *cis*	4.36	0.31	3.04	5.86	0.32	36.1	709

TABLE 6

Property components of class distance and between-class distances for features 1—7

Classes	Property component							Between-class distance
	1	2	3	4	5	6	7	
I—II	−0.53	4.75	0.22	1.00	−1.23	−0.88	1.10	1.98
I—III	−0.23	4.87	−0.09	1.28	−3.35	−2.03	2.00	2.53
II—III	0.70	−0.60	−0.49	0.61	−0.28	−1.30	0.23	0.69

TABLE 7

Class distances and classification

Compound	Class distances			True class	Estimated class
	I	II	III		
1	1.36	2.84	6.60	I	I
2	0.80	4.08	7.29	I	I
3	0.78	3.60	7.57	I	I
4	0.94	4.63	7.97	I	I
5	0.61	4.46	7.24	I	I
6	0.78	4.09	6.31	I	I
7	2.72	1.03	3.20	II	II
8	2.62	0.90	2.66	II	II
9	3.54	0.99	4.01	II	II
10	3.08	0.73	2.96	II	II
11	2.45	0.76	3.27	II	II
12	2.39	1.02	1.73	II	II
13	2.50	1.04	2.16	II	II
14	2.83	0.47	0.74	III	II—III
15	2.75	0.62	0.57	III	III—II
16	2.66	1.84	1.06	III	III

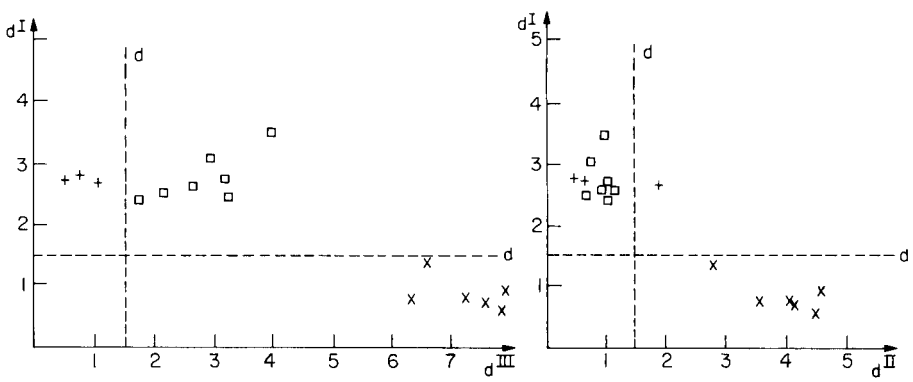

Fig.3. Class distances: (×) I; (□) II; (+) III.

Figure 3 shows the class distances between samples. If classification follows the minimal distance criterion, then the method gives a correct classification of all samples except compound 14. If a threshold value of 1.5 is applied as a classification criterion, then compounds 14 and 15 become borderline cases between classes II and III.

It can be seen that results obtained by PRIMA are in agreement with those from SIMCA but more information can be extracted.

Other applications

PRIMA was also applied to some medical diagnosis problems. Twelve steroid components of urine were determined by gas chromatography and used as features to discriminate between eight groups of sick children. A recognition ability of 94% was achieved [12].

The applicability of PRIMA was also illustrated in a study of maturity of asphaltine materials, where 17 features were used to assign materials to five classes [13]. The recognition ability was 90%.

It may be noted here that PRIMA is also suitable for image recognition; results obtained in solving a letter recognition problem described by 35 binary features will be reported elsewhere.

DISCUSSION

The application of pattern recognition offers the user numerous options even for one given problem. The user must select not only the most appropriate pattern recognition method but also the applied features to be used. The user must also decide on the transformation of variables, the applied similarity measure or distance, the class model, and on how to fill in missing data. In actual applications, this confusingly large variety of mathematical methods necessitates categorization of criteria of applicability and validity of the methods. Some technical facts must also be considered, e.g., the memory capacity of the computer available, program, and computation time. Experience so far indicates that the applicability of the PRIMA method is less strict than that of other supervised pattern recognition methods. In the following paragraphs, some problems likely to occur in applications are discussed.

Outliers and objects belonging to more than one class

Decisions by binary classifiers are relatively simple: calculation of the sign of the scalar product of the pattern vector and of a suitably selected weight vector suffices to decide to which class the object belongs. There are no borderline cases and no outliers. When binary classifiers are applied and the separating function is used successively, multicategory classification can be achieved, of course, but an object cannot be an outlier even in this case.

Multicategory methods based on the object distance (kNN or the potential function method) will indicate a possible outlier only if the value of the distance (or potential) is considered. Methods based on the class-distance concept (SIMCA, PRIMA) make it possible to map the objects into the class-distance space so that an object can unambiguously be assigned to a single class, or to several classes simultaneously, or be qualified as an outlier. If the classes are not mutually exclusive and are not exhaustive, only PRIMA and SIMCA are likely to be successful.

Continuous and discrete variables

In many problems, difficulties arise from the fact that some components of the pattern vector are continuous while others are discrete (in special cases, of the binary encoded type). Though the PRIMA method has been developed mainly for continuous variables, some experience with applications to binary variables show that the method is also very effective even if the data are noisy or incomplete. In this case, it is necessary to ensure that the inhomogeneity values differ from zero.

The simultaneous treatment of mixed variables seems to be an important merit of PRIMA. Lack of experience with such applications makes it necessary to judge each case independently for the ratio of continuous and discrete components.

Incomplete data

In various applications, the completeness of the data matrix cannot be secured. Obviously, overcoming this difficulty by omitting objects or properties from the training set leads to loss of information. Methods based on matrix calculus are the most sensitive to incomplete data sets (e.g., discriminant or principal component analysis), because the matrix operations involved require complete matrices. Missing data may be replaced by averages or interpolated data but this is sensible only if the missing data do not exceed 5% of the total data set. Great care is needed in filling in missing data in this way, because concepts such as correlation and variance can become meaningless. If the pattern vector of the unknown contains missing components, then methods based on the joint transformation of variables (e.g., discriminant or principal component analysis) cannot be used without arbitrarily filling in the absent data.

The class-distance concept of PRIMA makes it possible to map the class distance into a lower-dimensional space without repeating the training process. Because class distances are normalized, they can be compared with results obtained from the whole data set. Classifications with incomplete data are especially important because the preliminary classification could determine whether or not other time-consuming, costly measurements are necessary. This special ability is very important in diagnostic filtering, image recognition, etc.

Additional data

A special case leading to missing data is when the measurements used are changed or new properties are added. In most pattern recognition methods, this case can only be handled by removing all information collected up to that point and preparing a new training set containing the new variables. Most methods are stiff in the sense that neither the columns (properties) nor the rows (samples) can be expanded in the original data matrix.

The use of PRIMA for new properties requires only knowledge of some new training samples so that the class averages and inhomogeneities of the

new property can be determined. Unknown objects can be classified by using the new class characteristics and the prior knowledge. The training algorithm permits extension of the training set with an object after classification and confirmation by a supervisor. In this way, a continuously training, adaptive algorithm can be constructed, and the rows of the data matrix can be extended without repeating the training process from the start. From the above, it follows that outlier objects can indicate the existence of a new class, and so the number of classes can also be extended. This particular feature of PRIMA is utilized in applications with relatively small data sets or process control.

Characteristics of the computation technique

The optimal solution of classification problems is often made difficult by practical factors such as computer memory capacity and computation time. In point methods, the memory requirement is roughly $I \times J$, where I is the number of objects and J is the number of features. Because I distances must be calculated and examined for minimum search the computation time is also large, proportional to I.

For methods based on the joint transformation of variables, the memory requirement is even larger because the matrix operations also need memory capacity. SIMCA is an exception, because the principal component analysis is done separately for each class, thus not all training samples have to be accessible. The computation time mainly depends on the convergence rate of training and on matrix operations. The time required for recognition is negligible relative to this.

The memory requirement for the PRIMA method is a multiple value of $J \times K$ where K is the number of classes; this value is generally much smaller than the memory requirement for other methods. The computation time for training and recognition are nearly equivalent and proportional to $J \times K$. Classification by PRIMA can thus be done even with microcomputers. The diagnostic applications mentioned above, for example, were solved on a 16-kbyte Sinclair ZX-81 computer.

Comparison of SIMCA and PRIMA

The essential feature of both SIMCA and PRIMA is that a coordinate system, the class distance, is defined for each class. The main difference between the two is that SIMCA defines class distance in the principal component space, PRIMA in the pattern space. Consequently, SIMCA considers the correlation between properties whereas PRIMA builds only on their deviation. SIMCA, therefore, reduces the dimension of pattern space whereas PRIMA does not. PRIMA can be applied successfully to incomplete data. The memory and computation requirement of SIMCA is larger; PRIMA can be implemented more simply.

On the basis of these features, the application of PRIMA is proposed when the training set or the available computer is small or the data set is

incomplete. If a sufficiently large training set and computer capacity are available and strong correlation is assumed between the properties then it is expedient to apply SIMCA. PRIMA is more useful when negligible correlation is presumed between properties.

REFERENCES

1 P. C. Jurs and T. L. Isenhour, Chemical Applications of Pattern Recognition, Wiley, New York, 1975.
2 A. J. Stuper, W. E. Brugger and P. C. Jurs, Computer-Assisted Studies of Chemical Structure and Biological Function, Wiley, New York, 1979.
3 K. Varmuza, Pattern Recognition in Chemistry, Springer, Berlin, 1980.
4 L. Kryger, Talanta, 28 (1981) 871.
5 G. E. Veress, Trac, 1 (1982) 374.
6 D. L. Massart and L. Kaufman, The Interpretation of Analytical Chemical Data by the Use of Cluster Analysis, Wiley, New York, 1983, pp. 14—18.
7 S. Wold, Pattern Recognition, 8 (1976) 127.
8 M. P. Derde, D. Coomans and D. L. Massart, Anal. Chim. Acta, 141 (1982) 187.
9 R. A. Fisher, Ann. Eugenics, 7 (1936) 179.
10 S. Wold, Analysis of Chemical Data in Terms of Analogy and Similarity, First International Symposium on Data Analysis and Informatics, Sept. 1977, Textes des Communications, Vol. 2., 683—712.
11 R. Mecke and K. Noack, Chem. Ber., 93 (1960) 210.
12 I. Juricskay Ms., I. Juricskay and G. E. Veress, Paper presented at the Budapest Chromatography Conference, Budapest, 1983.
13 A. Bruckner-Wein and G. E. Veress, Paper presented at the "Chemometrics '83" Conference, Csopak, Hungary, 1983.

Analytica Chimica Acta, 171 (1985) 77—87
Elsevier Science Publishers B.V., Amsterdam — Printed in The Netherlands

MINICOMPUTER CONTROL OF MEASUREMENTS OF SPECTROELECTROCHEMICAL PROCESSES
Part 2. A New Measurement System for Simultaneous Coulometric and Spectrophotometric Investigations

M. ŁAPKOWSKI and J. W. STROJEK*

Institute of Inorganic Chemistry and Technology, Silesian Technical University, 44-100 Gliwice (Poland)

M. NEMETH and J. MOCAK

Department of Analytical Chemistry, Slovak Technical University, 88-039 Bratislava (Czechoslovakia)

(Received 13th August 1984)

SUMMARY

The design of a system for simultaneous coulometric and spectrophotometric measurements is described. A special fiber optic cell is coupled to a rapid scanning spectrophotometer. The assembly is controlled by a Nova-2 minicomputer which simultaneously acquires and processes the data. The programmed measurement procedures enable spectrophotometric and coulometric curves to be recorded for linear or stepped sweep of the electrode potential, and kinetic relations to be found for a constant electrode potential. Test measurements on chlorpromazine and trifluoroperazine showed that the system is useful for studies of kinetics and mechanisms of electrode processes. The advantages and disadvantages of the method are discussed.

Spectroscopic methods have been widely used in electrochemistry since the early 1960s [1]. The first studies were based on the application of optically transparent electrodes [1—5]; this allows spectrophotometric analysis of the solution in the cell during the electrode process, providing additional data about the mechanism and kinetics of the system under investigation. Also thin-layer spectroelectrochemistry [6—9] has rapidly developed as a powerful method for studying reactions in which colored compounds [10—20] or various substances of importance in biology [21—29] are involved. The thin-layer method is especially useful when the number of electrons in an electrode reaction or the molar absorptivity for the electrode reagents is being determined [10—29]. The latest achievements in this field facilitate measurements of the adsorption of the original substances or the products of the electrode process deposited on the electrode surface [30—33]. Determination of the structure of the adsorption layer is also possible [34, 35].

0003-2670/85/$03.30

The method has many advantages; its main disadvantage is the complex mathematical description of the process being investigated. In the case of complicated mechanisms, the partial differential equations which describe diffusion in the semi-infinite layer are so complicated that they cannot be solved by the usual mathematical procedures. Therefore, numerical analysis and computer simulation of the process investigated may be helpful [36—41]. Even in these cases, however, the time-consuming numerical methods are not always effective because the results obtained are subject to numerical error [42]. When there is intensive mixing, the solution in the cell can be regarded as homogeneous and normal differential equations then apply. It would be interesting in this case to apply a combination of standard coulometric and spectrophotometric techniques. Elimination of diffusion from the process investigated can increase the accuracy of the kinetic data obtained, and the proposed kind of mechanism of the consecutive reactions taking place in the solution can be established more easily. Coulometric techniques have frequently been applied in studies of the mechanisms of electrode processes [43]. Additional spectral information collected from the solution under investigation should enable further development of the method and thus increase its use.

In this paper, computer-controlled spectrocoulometric equipment for versatile studies of electrode processes in aqueous solution is described. A spectrocoulometric cell is situated outside the spectrophotometer and is optically coupled to it by two fiber-optic probes. The working electrode may be polarized with a step voltage or linear sweep. In the first case, a normal coulometric measurement is combined with spectral analysis; this may be called spectrocoulometry. In the second case, because of the slow sweep (a few mV s^{-1}) and the intensive mixing of the solution, the current curve is similar in shape to a voltammetric curve; this is called potential-sweep spectrocoulometry.

EXPERIMENTAL

The spectrocoulometric cell

The spectrocoulometric cell is presented in Fig. 1. It consists of two main parts: a cylindrical body (4) and a cylindrical housing (9). In the teflon body there are several holes: the central electrochemical chamber is connected to the spectrophotometric cell (10); an opening (11) for inert gas, which enters just above the solution in the electrochemical chamber; an opening (12) for a reference electrode, connected to the electrochemical chamber by non-impregnated porous graphite; and a set of six symmetrical channels, each equipped with a fixed frit (5), to provide electrochemical connection with the auxiliary electrode. Six graphite rods connected by platinum wire are inserted as the auxiliary electrode (8), which is situated in the space between the body and housing. A three-way stopcock (13) is placed in the central channel at the bottom of the cell (7); this serves as a gas inlet or an outlet for the

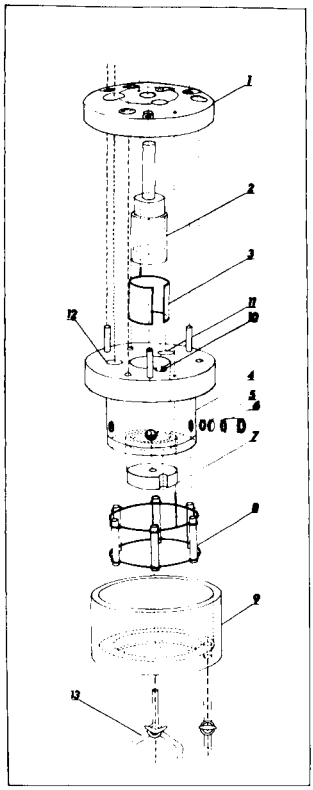

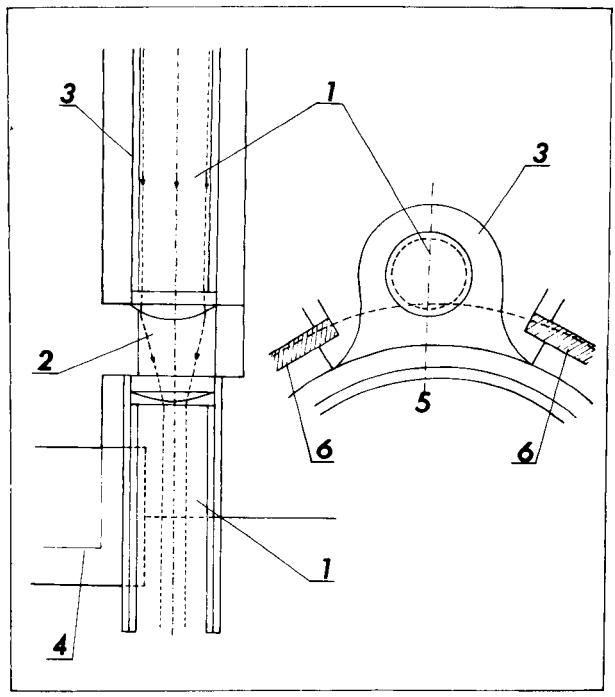

Fig. 1. Spectrocoulometric cell design: (1) cover, (2) stirrer, (3) working electrode, (4) body of cell, (5) frits, (6) threaded bush, (7) bottom of the cell, (8) auxiliary electrode, (9) external housing, (10) opening for optical probe, (11) opening for inert gas, (12) opening for reference electrode, (13) three-way stopcock.

Fig. 2. Cross-section of the spectrophotometric cell: (1) fiber optics of optical probe, (2) measurement chamber, (3) opening for optical probe, (4) bottom of the electrochemical chamber, (5) stirrer, (6) frit.

solution. A cylindrical platinum grid is used as the working electrode (3). Inside it, a round glass stirrer (2) is situated.

A cross-section of the spectrophotometric cell is shown in Fig. 2. The ends of both fiber optic probes (Carl Zeiss Jena; type 2N 2242, 100-cm length) are pressed into teflon tubes terminated with a lens. One of the probes is fixed into the bottom of the spectrophotometric cell but the position of the second can be varied, so that the measurement chamber thickness can be adjusted to the required absorbance of the solution.

This cell design reduces the volume of solution needed to less than 8 ml, ensures uniform potential distribution at the working electrode, and makes it possible to mix the solution vigorously.

Other apparatus and reagents

A schematic diagram of the main electrical connections and optical couplings is given in Fig. 3. The ends of the two optical fiber probes fixed in the spectrocoulometric cell, are placed in the measuring chamber of the rapid scanning spectrophotometer (RSS). To obtain the maximum intensity of radiation, it is necessary to position the fibers correctly. The three electrodes of the cell are connected to a potentiostat (Tacussel; type PRT-100-1X), equipped with a TP-PRT programmed generator and an X-Y recorder (Yokogawa, Japan). A DGC Nova-2 minicomputer, equipped with a MERA-5962 CRT display (MERA-ELZAB, Poland), a PK-1 cassette memory unit (MERAMAT, Poland) and a home-made plotter, controls the potentiostat and RSS and collects analog data from them (i.e., the values of absorbance and current). The computer program for the Nova-2, developed for spectro-electrochemical measurements, has already been described in detail [44]. Solutions in the spectrocoulometric cell were mixed by using a variable-speed laboratory stirrer (model ML-3; W.A.T. Horyzont, Poland).

The spectral characteristics of the fiber optics and the assembled optical system were measured with a Specord u.v.-visible spectrophotometer (Carl Zeiss Jena).

Chlorpromazine and trifluorperazine (Drug Institute, Warsaw) were used without further purification. Buffer solutions were prepared from redistilled water (in quartz apparatus), citric acid, disodium hydrogenphosphate, and potassium chloride (all analytical grade; POCh, Gliwice, Poland).

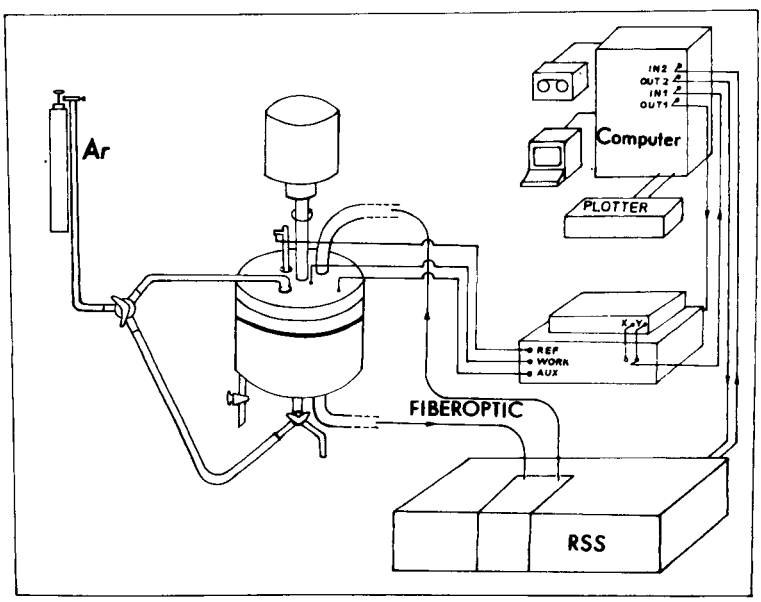

Fig. 3. Assembly for spectrocoulometric measurement; RSS is the rapid scanning spectrophotometer.

Procedures

Before each measurement, the RSS was calibrated by using interference filters and then the spectrocoulometric cell was filled. The solution was then stirred and argon was passed through it. After removal of oxygen, the three-way stopcock was switched and argon was directed above the solution.

The following spectrocoulometric methods of measurement were developed and programmed.

Method 1. Spectral response after a potential step is applied to the working electrode. Each spectrum for a programmed wavelength range (up to 250 nm) is recorded during 8 ms. Then during a 6-s period, it is re-recorded onto the cassette and the measurement cycle can be repeated. It is possible to record the average results from several (N) spectra (up to 256) onto the cassette. In this case, the time unit of a single measurement is $6 + N \times 0.008$ s. With this method of measurement, it is possible to establish the mechanism of the process.

Method 2. Absorbance changes when a potential step is applied to the working electrode. The computer records the current flowing through the working electrode and the absorbance at a programmed constant wavelength, at a programmed number of points (up to 2048). This measurement is used for rate constant calculations.

Method 3. Absorbance changes when a potential step is applied to the working electrode and during relaxation. The same recordings as in Method 2 are used, with the possibility of disconnecting the working electrode after a programmed period of time. This is known as open-circuit relaxation measurement [45—49] and is used to evaluate a rate constant. In this case, only a homogeneous chemical reaction, unaffected by a heterogeneous electrode reaction, can be monitored.

Method 4. Spectral response during a linear potential sweep of the working electrode. The same measurements as in Method 1 are taken, with the possibility of recording the current flowing through the electrode. It is possible also to change the potential of the electrode from a linear sweep to a stepped (staircase) sweep. The profile of the sweep is programmed. This method makes it possible to observe consecutive reactions, monitor the formation of intermediates, and measure a standard potential of the electrode process, as well as to conduct a complete spectral analysis of the whole electrochemical process.

RESULTS AND DISCUSSION

Before electrochemical measurements were made, the transmission of the optical system with the empty spectrophotometric cell was recorded. The results are shown in Fig. 4. It can be seen that with the glass fiber optics, a transmittance of about 60% for visible light (above 420 nm) was obtained. Application of recently manufactured quartz fiber optics would extend the spectral range.

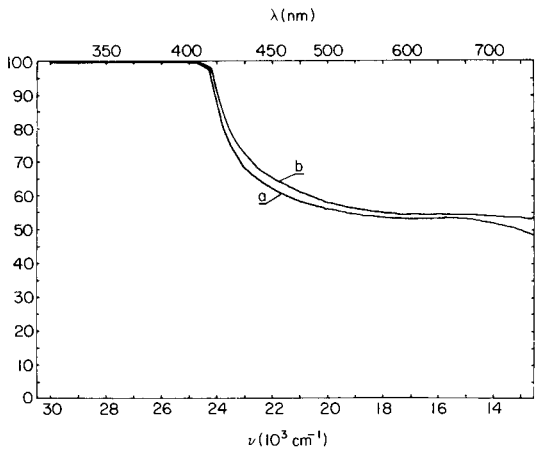

Fig. 4. Transmittance spectra for the optical system with the empty spectrocoulometric cell: (a) optical probes without glass lenses; (b) probes with glass lenses.

The water-soluble phenothiazine derivatives chlorpromazine (CPZ) and trifluoroperazine (TFPZ), previously investigated by coulometric [50—52], electrochemical [53, 54] and spectroelectrochemical [55—58] methods, were chosen for the electrochemical studies. They are suitable test compounds because their electrode reaction mechanism has been described and electrochemically or spectrochemically proved [51, 52, 58]. According to the coulometric data [51, 52], the electro-oxidation mechanism for CPZ and TFPZ in water can be expressed by the following simple equations

$$A \xrightarrow{p} B^{+\cdot} + e^- \qquad (1)$$

$$2B^{+\cdot} \xrightarrow[H_2O]{k} A + C + 2H^+ \qquad (2)$$

where A is CPZ or TFPZ, $B^{+\cdot}$ is $CPZ^{+\cdot}$ or $TFPZ^{+\cdot}$, and C is the final product of electro-oxidation. Equation 1 refers to a first-order electrode reaction (p is its rate constant) and Eqn. 2 describes a second-order disproportionation reaction with rate constant k. A colored radical-cation $B^{+\cdot}$ [58], formed in the electrode reaction, makes it possible to conduct spectrocoulometric measurements. The disproportionation rate constant k depends on the pH of the solution [51, 52].

However, Feldberg [59] has proposed three other mechanisms for the oxidation of these compounds and has proved that it is not possible to distinguish any difference between them when only electrochemical data are used. Therefore, the methods proposed above were used for experimental verification of Feldberg's considerations.

The results of potential-sweep spectrocoulometric measurements for electro-oxidation of TFPZ, in solutions of different pH values, obtained by

Method 4, are presented in Fig. 5. Both electrochemical and spectrophotometric results indicate the following features. First, there is only one current peak of oxidation, which appears at a potential of >0.6 V (depending a little on the pH). The area of the peak increases with pH; at pH 5, it is nearly doubled with respect to that for 0.1 M hydrochloric acid. Secondly, the height of the reduction current peak decreases with pH (especially for pH > 2). Thirdly, there is only one absorbance peak (at 460 nm) in the wavelength range 300–600 nm; the height of this peak increases with time of oxidation and its wavelength is constant throughout the reaction. These results show that the intermediate $B^{+\cdot}$ is observed spectrophotometrically and thus proves the mechanism (reactions 1 and 2) presented above.

Method 2 was also applied to study the electro-oxidation of TFPZ. The results of these measurements are presented in Fig. 6 for three different solutions. These experimental results are in agreement with the theoretical values calculated numerically by Mocak et al. [51, 52]. However, more precise comparison indicates that only the shapes of these curves are similar. Accurate calculations show that there is no unique value of k which would enable both the coulometric and spectrophotometric data to be fitted. This confirms Feldberg's considerations and indicates that the mechanism proposed by Mocak et al. [51, 52] should be replaced by one of the more detailed variants described by Feldberg [59].

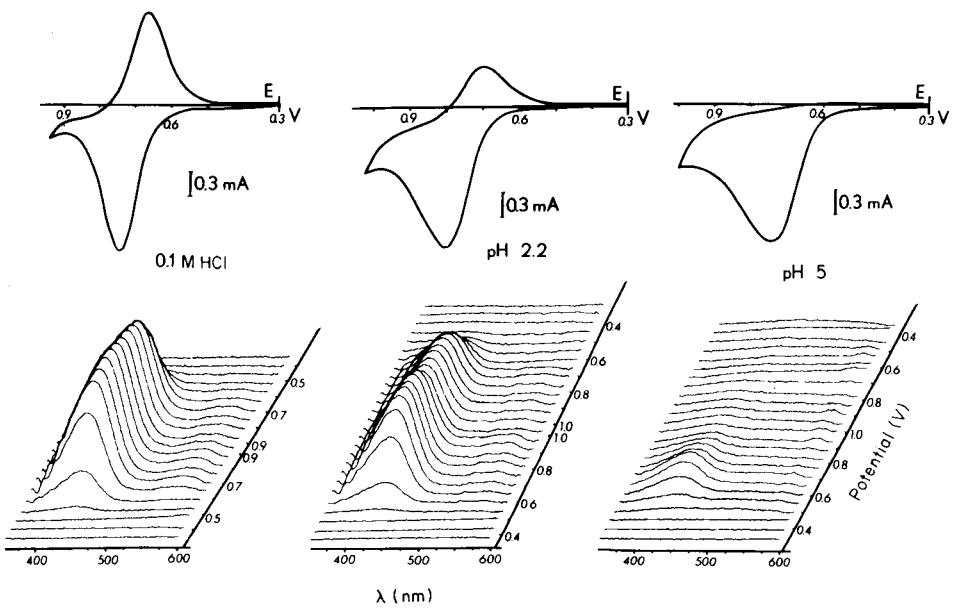

Fig. 5. Spectral response of the TFPZ electro-oxidation product recorded during measurements of cyclic coulometric curves for various pH values of the test solution. Scan rate, 3 mV s^{-1}.

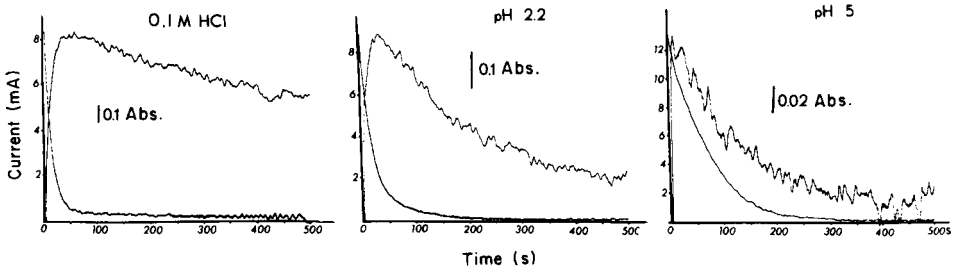

Fig. 6. Coulometric lower traces) and spectrophotometric (upper traces) curves of TFPZ electro-oxidation in solution at different pH value. The potentials applied were: —0.75 V for 0.1 M HCl, and —0.80 V for pH 2.2 and pH 5.

Spectrocoulometric measurements on CPZ obtained by Method 1 are presented in Fig. 7. These results confirm the conclusions of the mechanism proved with the results obtained by Method 4. The only difference is that the CPZ reactions are slower.

Figure 8 shows the results of the CPZ electro-oxidation measurements obtained by Method 3. These results have not yet been used for further calculations on kinetics.

The measurements presented above illustrate the various possibilities of the methods proposed and provide examples of measurement procedures for obtaining data necessary for calculating physicochemical constants. Further results will be reported later.

CONCLUSIONS

The proposed design of the spectrocoulometric cell has shown its usefulness for investigating the mechanism and kinetics of electrode reactions. The cell has various advantages. Replacement of a solution and adjustment of the optical pathlength is very easy and fast because the cell is situated outside the spectrophotometer; measurements can therefore be produced very quickly. The spectral sensitivity is high because of the relatively long optical path; $CPZ^{+\bullet}$ spectra can be recorded for concentrations of CPZ greater than 3×10^{-6} M without any process averaging. It is possible to analyze solutions of different concentrations and absorptivities because the optical pathlength can be adjusted easily. The time taken to electrolyze completely all the electroactive material is relatively short (60—200 s depending on the rate constant k of reaction 2), because of the intensive mixing as well as the high ratio between the electrode surface area and the volume of the test solution. Further, it is possible to obtain precise results for calculations of physicochemical constants because the information about the process investigated is enhanced; apart from the electric data about current and potential of the peak, spectral information (peak wavelength and absorbance vs. time) is easily obtained. Physicochemical data can be achieved even for processes

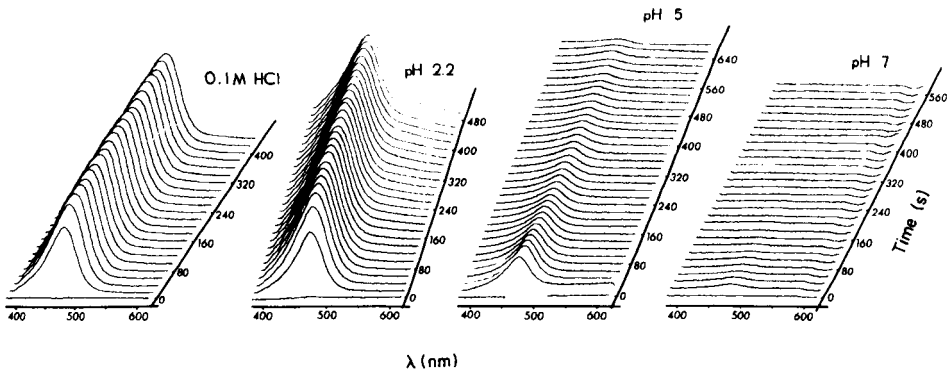

Fig. 7. Spectra of CPZ electro-oxidation recorded during coulometric measurement at constant potential of the working electrode for various pH values of the test solution. The potentials applied were 0.75 V for 0.1 M HCl, 0.80 V for pH 2.2 and pH 5, and 0.85 for pH 7.

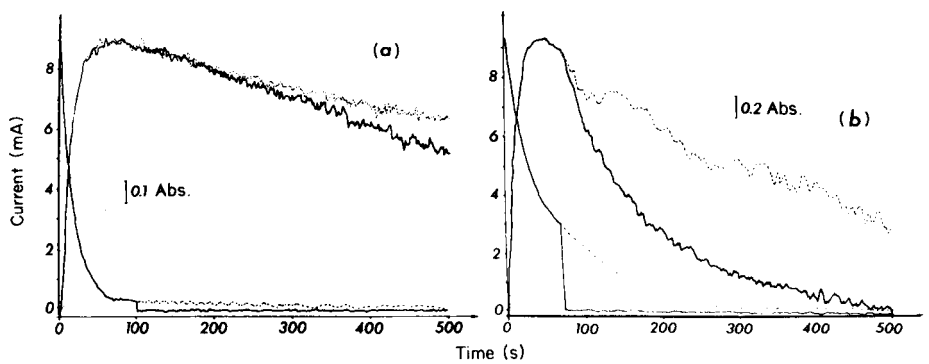

Fig. 8. Coulometric and spectrophotometric curves for CPZ electro-oxidation in different solutions: (a) pH 2.2; (b) pH 5. (—) Open-circuit relaxation method; (• • •) potential-step method. Measurements were made at a working electrode potential of 0.80 V.

that do not influence the recorded current curves because it is possible to record an absorbance vs. time relationship for substances that undergo further homogeneous chemical reactions. Because the spectral measurement is done away from the electrode, products or deposits of the process (e.g., polymeric material) cannot interfere with the optical signal. Finally, the possibility of using normal differential equations enables results to be calculated more easily, quickly and precisely.

However, there are also some disadvantages which should be stated explicitly. The spectral range of the fiber optics used in the system is narrow. There is attenuation of the spectral signal by the long fiber optics (>2 m). Spectral information may be affected by gas bubbles because of the vigorous mixing of the solution. Further, the system cannot be used for measurements

of very fast consecutive reactions because the spectral measurements are made at a certain distance from the electrode; some dead-time is therefore involved.

Nevertheless, it seems that the advantages of the system significantly outweigh the disadvantages. The system has fulfilled expectations and can be applied to investigations of the kinetics and mechanism of various physicochemical processes.

The authors are grateful to Dr. Jerzy Żak for helpful discussion, and thank Mrs. Walicka, Drug Institute in Warsaw, for supplies of chlorpromazine and trifluoroperazine.

REFERENCES

1 T. Kuwana, R. K. Darlington and D. W. Leedy, Anal. Chem., 36 (1964) 2023.
2 T. Kuwana and N. Winograd, in A. J. Bard (Ed.), Electroanalytical Chemistry, Vol. 7, M. Dekker, New York, 1974, p. 1.
3 T. Kuwana, Ber. Bunsenges. Phys. Chem., 77 (1973) 868.
4 T. Kuwana and W. R. Heineman, Acc. Chem. Res., 9 (1976) 241.
5 W. R. Heineman, Anal. Chem., 50 (1978) 390A.
6 T. P. DeAngelis and W. R. Heineman, J. Chem. Educ., 53 (1974) 594.
7 R. W. Murray, W. R. Heineman and G. W. O'Dom, Anal. Chem., 39 (1967) 1666.
8 W. R. Heineman, J. N. Burnett and R. W. Murray, Anal. Chem., 40 (1968) 1970.
9 I. Piliac and R. W. Murray, J. Electrochem. Soc., 118 (1971) 1758.
10 G. Peychal-Heiling and G. S. Wilson, Anal. Chem., 43 (1971) 545, 550.
11 B. P. Neri and G. S. Wilson, Anal. Chem., 44 (1972) 1002; 45 (1973) 442.
12 V. S. Srinivasan and F. C. Anson, J. Electrochem. Soc., 120 (1973) 1359.
13 T. M. Kenyhercz, T. P. DeAngelis, B. J. Norris, W. R. Heineman and H. B. Mark Jr., J. Am. Chem. Soc., 98 (1976) 2469.
14 E. A. Blubaugh, A. M. Yacynych and W. R. Heineman, Anal. Chem., 51 (1979) 561.
15 D. F. Rohrbach, W. R. Heineman and E. Deutsch, Inorg. Chem., 18 (1979) 2536.
16 P. Bugnon and R. E. Hester, Chem. Phys. Lett., 102 (1983) 537.
17 L. M. Charney, H. O. Finklea and P. A. Schultz, Inorg. Chem., 21 (1982) 549.
18 D. Lancon and K. M. Kadish, J. Am. Chem. Soc., 105 (1983) 5610.
19 K. M. Kadish, D. Chang, T. Malinski and H. Ledon, Inorg. Chem., 22 (1983) 3490.
20 J. L. Bear, T. P. Zhu, T. Malinski, A. M. Dennis and K. M. Kadish, Inorg. Chem., 23 (1984) 674.
21 W. R. Heineman, T. Kuwana and C. R. Hartzel, Biochem. Biophys. Res. Commun., 49 (1972) 1.
22 T. Kuwana and W. R. Heineman, Bioelectrochem. Bioenerg., 1 (1974) 389.
23 W. R. Heineman, B. J. Norris and J. F. Goelz, Anal. Chem., 47 (1975) 79.
24 B. J. Norris, M. L. Meckstroth and W. R. Heineman, Anal. Chem., 48 (1976) 630.
25 W. R. Heineman, M. L. Meckstroth, B. J. Norris and G.-H. Su, Bioelectrochem. Bioenerg., 6 (1979) 577.
26 C. W. Anderson, H. B. Halsal and W. R. Heineman, Anal. Biochem., 93 (1979) 366.
27 M. L. Meckstroth, B. J. Norris and W. R. Heineman, Bioelectrochem. Bioenerg., 8 (1981) 63.
28 W. R. Heineman, Denki Kagaku, 50 (1982) 142.
29 W. R. Heineman, W. C. Anderson, H. B. Halsal, M. M. Hurst, J. M. Johnson, G. P. Kreishman, B. J. Norris, M. J. Simone and C.-H. Su, in K. M. Kadish (Ed.), Advances in Chemistry Series, No. 201, Electrochemical and Spectrochemical Studies of Biological Redox Components, Am. Chem. Soc., Washington, DC, 1982.

30 L. Meites, in A. Weissberger and B. Rossiter (Eds.), Techniques of Chemistry, Vol. 1, Part IIA, Wiley-Interscience, New York, 1971, Ch. 9.
31 Z. Galus, in Fundamentals of Electrochemical Analysis, Horwood, Chichester, 1976.
32 A. J. Bard and L. R. Faulkner, in Electrochemical Methods: Fundamentals and Applications, Wiley, New York, 1980.
33 L. R. Faulkner, in T. Kuwana (Ed.), Physical Methods in Modern Chemical Analysis, Vol. 3, Academic Press, New York, 1983, p. 137.
34 J. Zak, M. D. Porter and T. Kuwana, Anal. Chem., 55 (1983) 2219.
35 W. T. Yap, E. A. Blubaugh, R. A. Durst and R. T. Burke, J. Electroanal. Chem., 160 (1984) 73.
36 S. W. Feldberg and C. Auerbach, Anal. Chem., 36 (1964) 505.
37 S. W. Feldberg, in A. J. Bard (Ed.), Electroanalytical Chemistry, Vol. 3, M. Dekker, New York, 1969, p. 199.
38 S. W. Feldberg, in J. S. Mattson, H. B. Mark Jr. and H. C. MacDonald (Eds.), Electrochemistry, M. Dekker, New York, 1972, p. 185.
39 D. Britz, Lecture Notes Chem., 23 (1981) 1.
40 L. F. Whitting and P. W. Carr, J. Electroanal. Chem., 81 (1977) 1.
41 B. S. Pons, in A. J. Bard (Ed.), Electroanalytical Chemistry, Vol. 13, M. Dekker, New York, 1984, p. 115.
42 M. Łapkowski and J. W. Strojek, J. Electroanal. Chem., 182 (1985) 315.
43 A. J. Bard and K. S. V. Santhanam, in A. J. Bard (Ed.), Electroanalytical Chemistry, Vol. 4, M. Dekker, New York, 1969.
44 J. Krawczyk, M. Łapkowski and J. W. Strojek, Anal. Chim. Acta, 152 (1983) 45.
45 G. C. Grant and T. Kuwana, J. Electroanal. Chem., 24 (1970) 11.
46 H. N. Blount and T. Kuwana, J. Electroanal. Chem., 27 (1970) 464.
47 H. N. Blount, N. Winograd and T. Kuwana, J. Phys. Chem., 74 (1970) 3231.
48 J. F. Evans and H. N. Blount, J. Phys. Chem., 80 (1976) 1011; 102 (1979) 289.
49 E. Steckhan, J. Am. Chem. Soc., 100 (1978) 3526.
50 F. H. Merkle and C. A. Discher, Anal. Chem., 36 (1964) 1639.
51 J. Mocak, D. I. Bustin and V. Pencak, Chem. Zvesti, 31 (1977) 153.
52 J. Mocak and D. I. Bustin, J. Electroanal. Chem., 79 (1977) 307.
53 H.-Y. Chang, P. H. Sackett and R. L. McCreery, J. Med. Chem., 21 (1978) 948.
54 P. H. Sackett and R. L. McCreery, J. Med. Chem., 22 (1979) 1447.
55 M. Neptune and R. L. McCreery, J. Org. Chem., 43 (1978) 5006.
56 J. S. Mayausky and R. L. McCreery, J. Electroanal. Chem., 145 (1983) 117.
57 J. S. Mayausky and R. L. McCreery, Anal. Chem., 55 (1983) 308.
58 T. B. Jarbawi and W. R. Heineman, J. Electroanal. Chem., 132 (1982) 323.
59 S. W. Feldberg, J. Phys. Chem., 73 (1969) 1238.

Analytica Chimica Acta, 171 (1985) 89—100
Elsevier Science Publishers B.V., Amsterdam — Printed in The Netherlands

COMPUTER-ASSISTED LIBRARY SEARCH SYSTEM FOR IDENTIFICATION OF UNKNOWN MASS SPECTRA

AKIO YASUHARA*, JUNKO SHINDO, HIROYASU ITO, TSUGUO MIZOGUCHI and KEIICHIRO FUWA

National Institute for Environmental Studies, 16-2, Onogawa, Yatabe, Tsukuba, Ibaraki 305 (Japan)

(Received 3rd October 1984)

SUMMARY

The library search system described identifies a single component or two components in the unknown pure or mixture mass spectra by comparing them with a large data base of reference spectra. A preliminary search is based on the spectral interpretation and the main search is based on the probability of peak appearance. The performance of this system was tested on 254 pure spectra and 88 mixture spectra. The percentages of successful search by using the NIH/EPA/MSDC data base were 75% for the pure spectra, and 63% for both the first and second components in mixture spectra. The percentages of successful search improved to 94% for the first components of the mixture spectra and 77% for both first and second components of the mixture spectra, when conditions for measurement of reference spectra were the same as those for the unknown spectra.

Gas chromatography/mass spectrometry (g.c./m.s.) is one of the most effective methods for identification of many components in mixture. Recent gas chromatograph/mass spectrometer combinations are capable of producing numerous mass spectra every run by automatic data acquisition and reduction. Therefore, a rapid and reliable search based on a computer and a large data base of reference spectra is needed in order to identify numerous unknown spectra. Several search systems of mass spectra have already been used. Biemann and coworkers [1, 2] have developed the well-known method which encodes the two most intense peaks in every 14-mass unit interval and compares peak intensities between abbreviated reference and unknown spectra. The "peak and intensity" search by Heller et al. [3, 4] is a conversational retrieval system and is used with successive input of mass number and intensity of significant peaks in unknown spectra. Reverse-search methods have been developed by Abramson [5] and Grönneberg et al. [6]. McLafferty and coworkers [7, 8] developed an important reverse-search method which is called probability-based matching (PBM). In the PBM method, a K value is calculated as a confidence index, based on the probability of occurrence of a peak with a certain intensity at a particular mass number. This PBM method has been improved considerably so that impurities do not affect the search for major component significantly [8, 9]. Some other interesting retrieval

0003-2670/85/$03.30

methods such as the multidimensional vector space method [10], the combined forward/reverse method [11], the SISCOM system [12], and Dromey's method [13, 14] have been reported. Rapid search is one of the most important factors in routine identification of unknown mass spectra. Some techniques for rapid search have been used in several methods [2, 6, 13, 15].

Because complete gas-chromatographic resolution is difficult in the analysis of complex mixtures such as environmental and biological samples, two or more components are often included in one mass spectrum. Recently, the theoretical limit for the effectiveness of g.c./m.s. of multicomponent mixture has been studied [16]. Some techniques for resolving the mixture spectra into single spectra have been reported [17—19]. But these techniques are not always effective. Therefore, new methods for the identification of several components in mixture spectra by computer-assisted search are needed. It has already been shown that reverse-search procedures are very valuable for mixture spectra [5, 7, 8] and some algorithms for extraction of each spectrum from mixture spectra have been reported [17, 20—22].

A new library-search system called the NIES/MSLS (National Institute for Environmental Studies/Mass Spectral Library Search) system has been developed by the authors and studied over a period of several years. The preliminary system was outlined earlier [23]. This system can identify a main component in an unknown spectrum through seven steps of presearch and a main search. It is also able to retrieve the first and second components in mixture spectra simultaneously. In the intervening years of use, the system has been continuously improved and become more efficient. This paper describes the details of the improved system and search results.

THE LIBRARY SEARCH SYSTEM

The computer used for the NIES/MSLS system was a HITAC M-180.

Encoding of reference mass spectra

The NIH/EPA/MSDC data base published in 1982 was used as the original data. The mass numbers and the intensities of the selected peaks of 38198 spectra were encoded along with some additional information to characterize the spectra, through the procedure of data checking, peak selection and editing. This data base is called Data Base I. Another data base, Data Base II, was constructed in order to evaluate the performance of the system when the reference spectra and the unknown spectra were measured under the same experimental conditions. In addition to the NIH/EPA/MSDC mass spectral data, 614 mass spectra measured with a JEOL-DX300 mass spectrometer by the authors were encoded in Data Base II. Of the 614 compounds, mass spectra of 272 compounds were already included in the NIH/EPA/MSDC data. All components of which mass spectra were used as unknown spectra for evaluating the system were selected from among these 272 compounds.

The data bases were composed of two files named Spectrum data file and Name data file. The contents of these files are shown in Table 1, where asterisked terms are the additional information which is extracted or created from the mass-spectral data. The 800 peaks with relative intensity $\lt 1\%$ for every spectrum can be used as the input data. For each peak, U, A, C and KSORT values are assigned; U and A (Table 2) are the contributions to the probability of the uniqueness of the m/z value and the abundance value of the peak, and were calculated in advance using all peaks over 1% relative intensity in all spectra as described by Pesyna et al. [8]. The special parameter C is set at 100 for the base peak, the most intense molecular ion peak (relative intensity $\geqslant 5\%$), and peaks (relative intensity $\geqslant 20\%$) corresponding to the loss of an even-numbered mass, but is set at 30 for peaks over 2% relative intensity. KSORT is the priority order according to the decreasing

TABLE 1

Contents of the Spectrum data file and the Name data file in the data base[a]

Symbol or term	Content
Spectrum data file	
KEY*	Record accession number
*MW**	Integral molecular weight
m/z, Int.	Mass numbers and relative intensities of peaks to the number of 100
*U**, *A**	*U* value and *A* value as defined by McLafferty et al.
KSORT*	The priority order of each peak (1 to 100)
*BP**	Mass number of base peak(s)
MME*	Maximum mass number allowed for an existence of peaks in mass spectrum (MME = $MW + 2N_{Cl} + 2N_{Br} + N_{Si} + N_S + 3$, where N_{Cl}, N_{Br}, N_{Si}, and N_S denote the number of Cl, Br, Si, and S atoms, respectively)
NIS*	Number of isotopic peaks at maximum mass range
ISOTOP*	Maximum mass number among the isotopic peaks
ISOPK*	Abundance ratio of each isotopic peak to the most intense peak
NRAP*	Number of rearrangement peaks over 20% relative intensity at mass number $\lt 60$ (10 peaks at the most)
MRAP*	Mass number of the rearrangement peaks
IRAP*	Intensity of the rearrangement peaks
MOLION*	The mass number of a molecular ion with $>5\%$ relative intensity
Name data file	
KEY*	Record accession number
NAME	Name of the compound
MFORM	Molecular formula
MWAC*	Accurate molecular weight
CAS	CAS registry number
TPRI	Retention index in temperature-programmed gas chromatography
COMMENT	Origin of the spectrum data, measurement conditions, etc.

[a]Asterisked terms are calculated or treated by computer automatically.

TABLE 2

U and *A* values used in the data base

Value	Range of peak occurrence corresponding to *U* value (%)	Range of relative intensity corresponding to *A* value (%)
0	100—70.71	0.0—2.1
1	70.70—35.35	2.2—6.9
2	35.34—17.68	7.0—15.9
3	17.67—8.84	16.0—30.9
4	8.83—4.42	31.0—54.9
5	4.41—2.21	55.0—100
6	2.20—1.11	
7	1.10—0.00	

order of the $(U + A + C)$ value. For example, the KSORT value of the peak having largest $(U + A + C)$ is assigned as 1. When more than one peak has the same $(U + A + C)$ value, the peak with higher mass number has the smaller KSORT value. Peaks having KSORT values of $\leqslant 100$ were selected and encoded into the data base. Most of the additional terms in the Spectrum data file are relevant to the important peaks for spectral interpretation, i.e., base peaks, isotopic peaks, rearrangement peaks, molecular ion peaks, etc. A series of peaks at the alternate mass numbers around the maximum mass area is regarded as the isotopic pattern, when the compound contains Cl, Br, Si or S atoms. Because the peaks that occur by rearrangement fragmentation often show the loss of an even-numbered mass from the molecular ion, these peaks were defined as rearrangement peaks for the sake of convenience.

Algorithm of the library search system

This system has four modes of search (S-1, S-2, M-1, and M-2) and users should select one of them according to their purposes and the characteristics of the unknown spectra. The S-1 mode is suitable for identification of pure mass spectra. The S-2 mode is for mass spectra contaminated with column bleed, for mass spectra with less reliable intensities, and for the identification of the first components in the mixture spectra. The M-1 mode is for search of only the second components in mixture spectra by specifying the first component which has been established by the S-2 mode or some other analytical technique. The M-2 mode is for the simultaneous identification of the first and second components in mixture spectra. A similar idea was reported by Atwater et al. [21]. In this mode, the first component is retrieved by the same procedure as the S-2 mode at the first stage. The spectrum of the first component is then subtracted from the mixed spectrum to yield the residual spectrum at the second stage. At the final stage, the residual spectrum is submitted to the search to identify the second component. The five candidates for the first component selected at the first stage are used to prepare five residual spectra and these spectra are identified successively.

The identification process for unknown spectra is composed of the presearch and main search. In the presearch, the characteristic peaks of the reference spectra on the basis of mass-spectral interpretation and fragmentation are compared with the unknown spectra in order to eliminate grossly dissimilar spectra. The comparison in the each step of the presearch is applied by using the additional information in the Spectrum data file described above. In the case of the S-1 mode, seven steps of presearch called Presearch A are applied. For other modes, another presearch (Presearch B) is applied; the criteria for this are less severe than those for Presearch A. The details of each step are as follows: M_{max}, M_{base}, M_{mol}, and MW denote the maximum mass number, mass number of the base peak, mass number of the molecular ion peak, and molecular weight, respectively. Superscripts U and R indicate the unknown and reference spectra, respectively.

Step 1: Molecular weight range. The molecular weight for searching ranges from the larger value between $[M^R_{max} - 18]$ and $[M^R_{base} - 10]$ to the value of $[M^R_{max} \times 2]$ for Presearch A. For Presearch B, it ranges from the value of $[M^R_{base} - 10]$ to $[M^R_{max} \times 3]$. Optionally, users can assign the range of molecular weight for search.

Step 2: Molecular ion check. When reference spectra have a molecular ion peak with a relative intensity exceeding 5%, the relative intensity of the corresponding peak in the unknown spectra should be greater than 2.5% for Presearch A and greater than 1% for Presearch B.

Step 3: Maximum mass limitation for reference spectra. Reference spectra should not have peaks with relative intensity exceeding 5% at a mass number higher than $[M^U_{max} + 5]$ for both the Presearches A and B.

Step 4: Maximum mass limitation for unknown spectra. Unknown spectra should not have peaks with relative intensity exceeding 5% at a mass number higher than $[M^R_{max} + 3]$ for Presearch A. This step is not applied in Presearch B.

Step 5: Base peak check. Unknown spectra should have a peak with a relative intensity over 50% for Presearch A or over 30% for Presearch B at $[M^R_{base}]$. In Presearch A, reference spectra should also have a peak of relative intensity over 50% at $[M^U_{base}]$.

Step 6: Rearrangement peak check. The definition of the rearrangement peak was described above. When reference spectra have rearrangement peaks with a relative intensity over 20% at a mass number $\lessdot 60$, the relative intensity of the corresponding peak in the unknown spectra should be greater than the smaller value between a half of the peak intensity of reference spectra and 20% for Presearch A. For Presearch B, it should be greater than the smaller value between three tenths of the intensity of the reference spectra and 20%.

Step 7: Isotopic peak check. If reference spectra containing Cl, Br, Si or S atoms show isotopic patterns at a mass area near the maximum mass peak, the unknown spectra should show a similar pattern at the corresponding mass area for Presearches A and B.

The reference spectra satisfying all steps of presearch are given a "value" indicating the reliability of identification by the main search, in which fifteen peaks with the smallest KSORT values of the reference spectrum are used.

Two criteria, *KS* and *PC*, are used in the main search as measures of matching between the reference and unknown spectra. *KS* indicates the confidence for existence of the reference spectrum in the unknown spectrum and is defined on the basis of reverse search

$$KS = \sum_{j}^{k} (U_j^R + A_j^R) \sum_{j}^{15} (U_j^R + A_j^R)$$

where U_j^R and A_j^R are the U and A values of the peak of the reference spectra, respectively, and k is the number of matched peaks among the 15 peaks used. A "matched peak" as defined here means that the ratio of the peak intensity in the unknown spectrum to the peak intensity in the reference spectrum, $\rho_j = I_j^U/I_j^R$, is greater than 0.15. A bad mark is given to the unmatched peaks, and the reference spectrum is eliminated as dissimilar if the sum of the bad mark exceeds a fixed threshold value. The bad marks are set to the following values depending on the relative intensity of the reference spectra: 1 ($I_j^R <$ 10%), 2 (10% $\leqslant I_j^R <$ 20%), 3 (20% $\leqslant I_j^R <$ 30%), 5 (30% $\leqslant I_j^R <$ 40%), 7 (40% $\leqslant I_j^R <$ 50%), 9 (50% $\leqslant I_j^R <$ 70%), and 11 (70% $\leqslant I_j^R$). The threshold value is set at 10 for the S-1 mode and 15 for the others if other values are not specified by users.

The other measure, *PC*, indicates the proportion of contamination by other substances and is calculated by using the ten peaks having the largest ($U + A$) values in the unknown spectra

$$PC = \left\{ \sum_{j}^{h} I_j^U + \sum_{j}^{k} [I_j^U - \alpha_j I_j^R \rho_{\min}] \right\} \Big/ \sum_{j}^{h+k} I_j^U$$

where h denotes the number of peaks that are present only in the unknown spectrum. The term in square brackets [X] is defined as follows: if $X > 0$, [X] = X, and if $X \leqslant 0$, [X] = 0. Also, $\rho_{\min}$ is the smallest one among the ρ_j ($j = 1 \cdots k$) values, and α_j denotes the allowance parameter regarding the fluctuation of intensities. When the intensity (I_j^U) of unknown spectrum exceeds $\alpha_j I_j^R \rho_{\min}$, the peak is considered to be contaminated by other components. The value of α_j is set as follows, depending on the relative intensity of the peak in the reference spectrum: 4.0 ($I_j^R <$ 10%), 3.5 (10% $\leqslant I_j^R <$ 30%), 3.0 (30% $\leqslant I_j^R <$ 50%), 2.5 (50% $\leqslant I_j^R <$ 70%), and 1.5 (70% $\leqslant I_j^R$). Both the *KS* and *PC* values range between 0.0 and 1.00. If all the reference peaks are contained in the unknown spectrum with reasonable intensities, *KS* has a maximum of 1.00, regardless of contamination by other spectra. The reference spectra having a *KS* value greater than 0.4 and a *PC* value less than 0.5 are stored as possible candidates. The candidates selected by this method are arranged in decreasing order of *KS* values. If there are more than one reference spectra with the same *KS* value, the one having the smaller *PC* value is superior to the others.

Residual spectra are generated from mixture spectra as follows

$$I_j^D = f_N[I_j^U - \beta I_j^R]$$

where I_j^D denotes the intensity of residual spectra at mass number j. All peaks of reference spectra encoded in the data base are subtracted from the mixture spectra to produce the residual spectra. If abbreviated reference spectra are used in this procedure, a considerable fraction of the first component would remain in the residual spectra. The β indicates the proportion of the reference component in the unknown spectra and f_N is the normalization factor which stands for the reciprocal of a proportion of the second component in the unknown mixture spectrum. The estimation of β is done either by the least-squares method, or by applying the value of ρ_{min}. Moreover, in the M-1 mode, an arbitrary β value can be specified, if necessary. These residual spectra are submitted automatically to Presearch B and the main search.

In each mode, a maximum of fifteen candidates with the best match in the main search are printed out.

Unknown spectra for testing the library search system

Mass spectra of 254 pure compounds shown in Table 3 were measured with JEOL JMS-DX300 gas chromatograph/mass spectrometer and used as unknown spectra to test the search system. Mass spectrometric conditions were as follows: ion-source pressure, 2×10^{-6} torr; ion-source temperature, 180°C; ionizing current, 300 μA; electron energy, 70 eV; scan range, m/z 10—500; scan speed, 2.1 s/scan; repetition time, 2.5 s; accelerating voltage, 3 kV. All procedures of scanning control, data acquisition, and background subtraction were done automatically with the JEOL JMA-3500 mass data-analysis system. Also, 88 mixture spectra were generated by the same system. All these spectra were sent from the JMA-3500 system to a host computer via a Texas Instruments Model 771 Intelligent Terminal System through a telephone cricuit for the library search.

RESULTS AND DISCUSSION

Presearch aims at elimination of grossly dissimilar reference spectra before performance of main search so that the search time can be shortened.

TABLE 3

Compounds used for testing the library search system

Group of compound	Number	Group of compound	Number
Hydrocarbon	16	Halogenated compound	26
Alcohol	21	Phenol	17
Carbonyl compound	15	Amine	5
Carboxylic acid	27	Nitro compound	8
Ester	58	S-containing compound	3
Terpene hydrocarbon	9	P-containing compound	6
Terpene alcohol	14	Heterocyclic compound	10
Terpene aldehyde	4	Others	11
Terpene ketone	4	Total	254

Contents of the presearch in this system are on the basis of interpretation of mass spectra. Whether mass spectra are pure or not should be judged preliminarily by users before the search is started. When the judgment is difficult, it is recommended that searches by both the S-1 and S-2 modes be done. In order to obtain the shortest calculation time in presearch, the seven steps must be arranged in the most appropriate order. The "elimination rate (r_i)" is defined as the ratio of the number of spectra eliminated in Step "i" to the number of reference spectra searched in the step. Also, t_i is defined as the time required to perform Step "i" for each reference spectrum. The steps should be arranged in the decreasing order of filtering efficiency, defined as r_i/t_i, if r_i and t_i are independent of the order of steps. However, this supposition is generally incorrect. Accordingly, the order of steps was established by the following procedure. The first step was chosen as the one which had the largest r_i/t_i determined by the search using all reference data (38812 data). The r_i and t_i were measured experimentally by averaging the results obtained with the 254 samples shown in Table 3. The elimination rates of Step 5 (base peak check) and Step 6 (rearrangement peak check) were extremely high (0.984 and 0.818, respectively). But another filter was chosen as the first step because these two steps required a very long time for the search. In order to decide on the second step, the r_i and t_i for each of the remaining six steps were measured again by using the reference spectra which survived the first step and the step of largest r_i/t_i was chosen. The order of the following steps was decided in a similar manner. Table 4 shows the filtering efficiency and the number of reference spectra remaining after each step and used subsequently. In Step 1, the molecular weight of a certain component is set automatically according to the mass number of the maximum mass peak and base peak. It is noteworthy that base peaks sometimes appear over molecular ion peaks in mass spectra of compounds containing several atoms as Cl and Br, which have isotopes with fairly high abundances. Step 6

TABLE 4

Filtering efficiency and the number of reference spectra remaining after each step in Presearch A[a]

Step	Filtering efficiency (s^{-1})	Number of spectra remaining
1	9.91×10^4	17398
2	8.70×10^4	5913
3	2.60×10^4	3311
4	2.51×10^4	2183
5	1.22×10^4	81
6	1.97×10^3	43
7	6.87×10	42

[a]All these data are average values when 254 spectra were tested. The total number of reference spectra was 38 812.

is a very important and effective filter. Loss of an even-numbered mass from the molecular ion provides important information on molecular structure. For example, some fatty acids and esters show McLafferty rearrangement peaks in their mass spectra that correspond to this concept. Also, peaks arising from α-elimination reactions or retro Diels—Alder reactions are in accordance with this notion. But it should be noted that this step is not always effective for nitrogen-containing compounds, because a loss of odd-numbered mass from the molecular ion sometimes occurs in these reactions.

When 254 unknown mass spectra were submitted to the NIES/MSLS system, the times consumed for search in the S-1 mode were 493.41 s (1.94 s/spectrum), whereas 6549.52 s (25.79 s/spectrum) was required when only Step 1 of the Presearch A was applied. The search speed in the former case is around 13 times faster. The application of the presearch is thus very effective in reducing the search time significantly. When the correct candidate is ranked between the first and fifth positions, the search is considered to be successful. There was no significant difference in the percentages of successful search between searches with and without the presearch.

The percentage of successful searches of 254 mass spectra was 75% in the S-1 mode for Data Base I. Reference spectra in Data Base I are sometimes very different from spectra measured with a JMS-DX300 mass spectrometer. An example is shown in Fig. 1. The differences in these spectra might be due to different instruments, different measurement conditions or inadequate quality of the mass spectra. In such a case, a correct answer could not be obtained. The percentage of successful searches was over 99% in searches of Data Base II.

The number of peaks in the reference spectrum to be used for identification has been discussed by some workers. Rasmussen and Isenhour [24] reported that a search system based on all peaks is the best. In contrast,

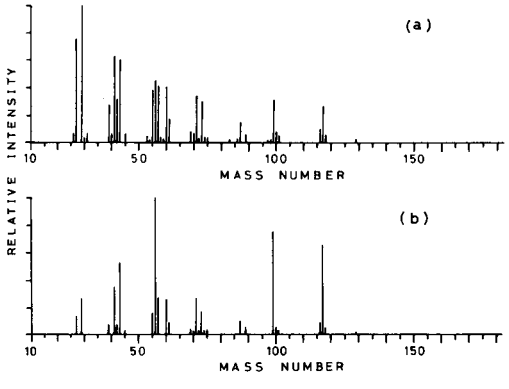

Fig. 1. Mass spectra of butyl hexanoate: (a) reference spectrum in NIH/EPA/MSDC data base (Data Base I); (b) spectrum measured with the JEOL JMS-DX300 mass spectrometer (Data Base II).

Pesyna et al. [8] indicated that reducing the number of peaks is necessary to achieve high reliability. A search based on all peaks exceeding 2% relative intensity was tested in this investigation, in addition to the normal procedure in which 15 peaks were used. The percentage of successful searches when all peaks were used (67%) was worse than that when 15 peaks were used. It is concluded that the selected small number of peaks produces a better result than the use of all peaks.

Search results of 88 mixture spectra by all modes are shown in Table 5. The results suggest that the S-2 mode is superior to the S-1 mode for mixture spectra for both Data Bases I and II. The percentage of successful searches with Data Base II was higher than that with Data Base I. Search by the M-1 mode was done under the condition that the first components were known in advance. In the M-2 mode, the search was considered to be successful when both correct candidates of the first and second components were ranked between the first and fifth positions. In the case of Data Base II, satisfactory results were obtained. The percentages of successful searches ranged between 67 and 80%, depending on the method used to determine the value of β, which is the proportion of the first component in the mixture spectrum. The least-squares method often yielded erroneous residual spectra, when the spectra of the first and second components were significantly similar to each other; it gave too high a β value so that too many fractions were subtracted as the first component. The mixture spectrum of decane and undecane is shown in Fig. 2; the spectra of these two components are almost identical except for the peaks of mass number 142 and 156. By the least-squares method, the β value was 0.97 which produced an erroneous residual spectrum, whereas a reasonable residual spectrum was obtained by the other

TABLE 5

Percentage of successful searches on 88 mixture spectra[a]

Search mode	Successful searches (%)	
	Data Base I	Date Base II
S-1	55	73
S-2	63	94
M-1		
Method 1	44	68
Method 2	31	80
M-2		
Method 1	35	67
Method 2	29	77

[a]S-1, S-2, M-1, and M-2 modes are searches for clear single spectra, for unreliable single spectra or the first component of mixture spectra, for the second component of mixture spectra, and for both first and second components of mixture spectra, respectively. Methods 1 and 2 represent the least-squares method and the method based on ρ_{min}, respectively.

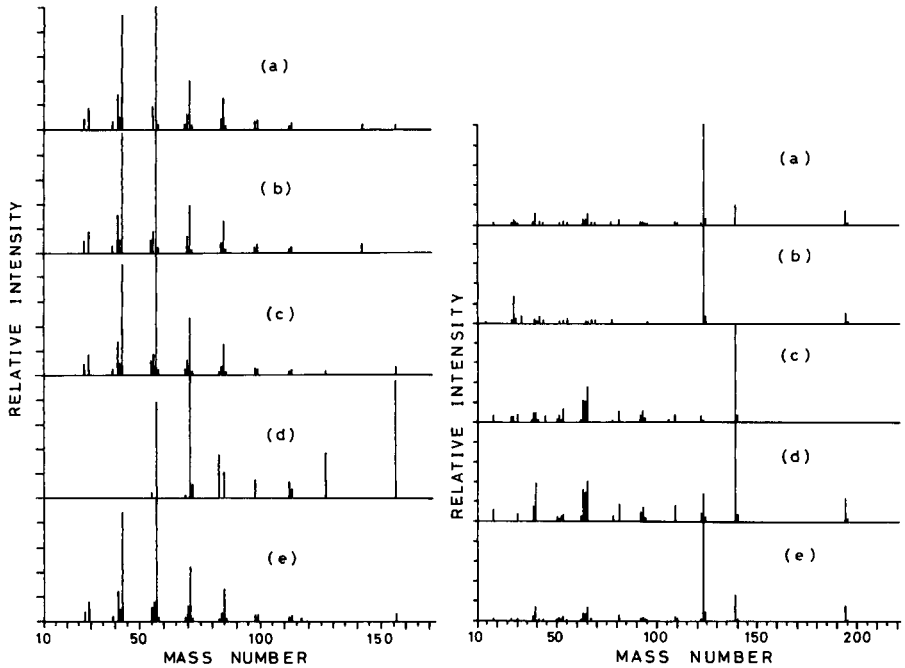

Fig. 2. An example of a mixture spectrum from two components with very similar spectra: (a) mixture spectrum; (b) reference spectrum of the first component (decane); (c) reference spectrum of the second component (undecane); (d) residual spectrum (β = 0.971 by the least-squares method); (e) residual spectrum (β = 0.494 by the method based on ρ_{min}).

Fig. 3. An example of a mixture spectrum from two components with less similar spectra: (a) mixture spectrum; (b) reference spectrum of the first component (4-hexylresorcinol); (c) reference spectrum of the second component (2-nitrophenol); (d) residual spectrum by the least-squares method (β = 0.945); (e) residual spectrum by using ρ_{min} (β = 0.226).

method. When Data Base I was used, the least-squares method was better than the other one, although the percentage of successful searches was low. When the reference spectra and the unknown spectra are less similar, the β value in the method based on ρ_{min} is too small. As a result, the residual spectra still contain the spectrum of the first component. When the first component is retrieved again in the search for the second component, it is recommended to try the search by the least-squares method. A typical example of this case is shown in Fig. 3. There were large differences in the percentage of successful searches between Data Base I and Data Base II. These results indicate that the reliability of reference spectra greatly affects the result for the identification of the second component from the mixture spectra.

There are clearly limitations in library search applied to mixture spectra. For example, if the mass spectra of the components are fully identical, e.g., *m*-cresol and *p*-cresol, the situation is impossible. Another limitation occurs when the reference spectra in the data base are very different from the sample

spectra because of different conditions of measurement or unreliability of the reference spectra. The drawback in the latter case may be overcome by standardization of measurement and establishment of criteria on the quality of mass spectra [25, 26].

REFERENCES

1 R. A. Hites and K. Biemann, Adv. Mass Spectrom., 4 (1968) 37.
2 H. S. Hertz, R. A. Hites and K. Biemann, Anal. Chem., 43 (1971) 681.
3 S. R. Heller, Anal. Chem., 44 (1972) 1951.
4 S. R. Heller, D. A. Koniver, H. M. Fales and G. W. A. Milne, Anal. Chem., 46 (1974) 947.
5 F. P. Abramson, Anal. Chem., 47 (1975) 45.
6 T. O. Grönneberg, N. A. B. Gray and G. Eglinton, Anal. Chem., 47 (1975) 415.
7 F. W. McLafferty, R. H. Hertel and R. D. Villwock, Org. Mass Spectrom., 9 (1974) 690.
8 G. M. Pesyna, R. Venkataraghavan, H. E. Dayringer and F. W. McLafferty, Anal. Chem., 48 (1976) 1362.
9 R. Venkataraghavan, H. E. Dayringer, B. L. Atwater, G. M. Pesyna and F. W. McLafferty, Adv. Mass Spectrom., 7B (1978) 989.
10 G. T. Rasmussen, B. A. Hohne, R. C. Wieboldt and T. L. Isenhour, Anal. Chim. Acta, 112 (1979) 151.
11 J. Kwiatkowski and W. Riepe, Adv. Mass Spectrom., 8B (1980) 1582.
12 H. Damen, D. Henneberg and B. Weimann, Anal. Chim. Acta, 103 (1978) 289.
13 R. G. Dromey, Anal. Chem., 48 (1976) 1464.
14 R. G. Dromey, Anal. Chim. Acta, 112 (1979) 133.
15 R. B. Lam, S. J. Foulk and T. L. Isenhour, Anal. Chem., 53 (1981) 1679.
16 D. Rosenthal, Anal. Chem., 54 (1982) 63.
17 R. G. Dromey, M. J. Stefik, T. C. Rindfleisch and A. M. Duffield, Anal. Chem., 48 (1976) 1368.
18 M. A. Sharaf and B. R. Kowalski, Anal. Chem., 54 (1982) 1291.
19 J. M. Halket, Anal. Chem. Symp. Ser., 4 (1979) 413.
20 J. E. Biller and K. Biemann, Anal. Lett., 7 (1974) 515.
21 B. L. Atwater, R. Venkataraghavan and F. W. McLafferty, Anal. Chem., 51 (1979) 1945.
22 B. E. Blaisdell and C. C. Sweeley, Anal. Chim. Acta, 117 (1980) 17.
23 J. Shindo, A. Yasuhara, H. Ito and T. Mizoguchi, Chem. Lett., (1982) 521.
24 G. T. Rasmussen and T. L. Isenhour, J. Chem. Inf. Comput. Sci., 19 (1979) 179.
25 G. W. A. Milne, W. L. Budde, S. R. Heller, D. P. Martinsen and R. G. Oldham, Org. Mass Spectrom., 17 (1982) 547.
26 B. E. Blaisdell, Anal. Chem., 49 (1977) 180.

Analytica Chimica Acta, 171 (1985) 101—110
Elsevier Science Publishers B.V., Amsterdam — Printed in The Netherlands

MEASUREMENT OF PEAK AREAS IN ENERGY-DISPERSIVE X-RAY FLUORESCENCE SPECTROMETRY

BJARNE BO JENSEN and NIELS PIND*

Department of Chemistry, Aarhus University, Langelandsgade 140, DK-8000 Aarhus C (Denmark)

(Received 2nd November 1984)

SUMMARY

An algorithm is outlined for the measurement of peak areas in spectra obtained by energy-dispersive x-ray fluorescence techniques. Each fluorescence line is assumed to be a pure Gaussian function. Initially, a calibration equation relating the full width at half maximum (FWHM) to the centre of the peak is set up. Then, in an unknown spectrum, the Gauss function parameters are found by a stepwise procedure making a non-linear minimization procedure redundant. First, the background is estimated and subtracted; then the peak centres are found, and the FWHM is given by the calibration equation, which relates FWHM to the position of the peak centre. Finally, the amplitudes are estimated from a set of linear equations. The reliability of the proposed algorithm was proved for a variety of samples. The method was compared with a non-linear χ^2 minimization routine. Quantitative analysis of two standard reference alloys was accurate. Below 20 keV, a suitable FWHM calibration is obtained from a set of K_α lines. Above 20 keV, a set of $K_{\beta_{1,3}}$ lines is recommended.

Peak overlaps are the rule rather than the exception in energy-dispersive x-ray fluorescence (x.r.f.) spectrometry. Normally, spectra are resolved by using an appropriate deconvolution routine. Some commonly used deconvolution routines are based on iterative non-linear least-squares procedures [1—8]. Because the response function for energy-dispersive x.r.f. spectra is nearly Gaussian, all descriptions of the response function include a Gaussian. Although the SAMPO and SAMPO80 programs [1—3] were written for γ-ray spectral analysis, they are also applicable to x-ray spectra. These programs describe a peak by means of seven parameters. The peak is characterized by three Gaussian parameters; one tail on each side of the Gaussian is assumed to be exponential, which gives two more parameters. Finally, there are three background parameters, which describe a parabolic shape. The exponential parameters and width parameters of the Gaussian are found to vary smoothly with energy and are calculated in advance by a calibration procedure, and the minimization is done by an iterative gradient method. In the QUEST [4] program for energy-dispersive x.r.f. spectra, the peak response function is a pure Gaussian characterized by three parameters. Again a non-linear least-squares procedure is used, but in this case in conjunction with an iterative

0003-2670/85/$03.30

SIMPLEX procedure [5]. Van Espen et al. [6] also used a Gaussian in conjunction with some prior information: (1) K and L x-ray peaks are known to be present at specific energies; (2) the variation of energy resolution as a function of the energy is known; and (3) ratios of the spectral intensities of an analyte for a given series (K_β/K_α, $L_\gamma/L_\beta/L_\alpha$) are known for thin samples. This approach decreased considerably the number of peak-shape parameters to be calculated. In another paper by Van Espen et al. [7], the deviation from the pure Gaussian was described by the introduction of a numerical correction term, which did not change the number of peak-shape parameters. In both papers by Van Espen et al., the parameters were found by a non-linear iterative least-squares procedure. Marageter et al. [8] gave the energy response function as a pure Gaussian with a low-energy asymmetry function, and the background description included changes caused by the elemental absorption edges. Marageter et al. also used the energy calibration and the known relation between spectral width and energy. All these approaches require quite complex programming, and the necessary CPU times may not be available with small computers.

In the present paper, a simple stepwise non-iterative deconvolution procedure is described. The procedure is based on a pure Gaussian description of the fluorescence lines. First, the background is estimated and subtracted from the spectrum, then line positions and line widths are found, and finally, in a pure Gaussian description, the amplitudes are found by simple linear least-squares procedure. The line widths are found from a relationship between peak centres and spectral widths. This calibration relationship is obtained prior to the execution of the procedure.

The proposed procedure was investigated for different sample types. Reliable results were obtained by using a set of K_α lines for full width at half maximum (FWHM) calibration in the region below 20 keV. At higher fluorescence energies, the $K_{\alpha_{1,2}}$ separation is appreciable, and a FWHM calibration based on a set of $K_{\beta_{1,3}}$ lines is recommended. The method was compared with a non-linear χ^2 minimization, PROFIT [9]. In PROFIT, the background is estimated again and subtracted before evaluation, but peak centres, widths and amplitudes for several peaks are found simultaneously by an iterative procedure. Peak areas obtained by both procedures were used for quantitative analysis of two NBS standard alloys. The concentrations found with both procedures agreed well with the certified concentrations.

THEORY

The counts, I, in each channel, x, are assumed to consist of a background function, $B(x)$, and a sum of N Gaussians, one for each fluorescence line:

$$I(x) = B(x) + \sum_{i=1}^{N} P_i \exp\{-[1.665(C_i - x)/F_i]^2\} \qquad (1)$$

where P is the amplitude, C is the line centre and F is the FWHM. $B(x)$ is not a simple function, but a simple expression for $B(x)$ can be used (e.g., linear, parabolic or exponential) at suitable chosen intervals. The integrated peak area of each Gaussian is proportional to $P_i F_i$.

In the present study, $B(x)$ is estimated from those parts of the spectra where no peaks appear. Hence, the background-corrected intensities, $I'(x)$, are given by the sum of Gaussians in Eqn. 1. Then the parameters in Eqn. 1 are found stepwise, which makes a non-linear minimization routine redundant.

Initially, a calibration equation relating FWHM and peak centre is set up

$$\log F_i = a_0 + a_1 C_i \tag{2}$$

where a_0 and a_1 are calibration constants. This relation is purely empirical. The theoretical relation requires that log (F) be replaced by F^2 [10]. Because of the better linearity given by Eqn. 2, this equation was chosen for the FWHM calibration here.

The calibration is done by using non-overlapping peaks either in a calibration spectrum or if possible in the spectrum to be evaluated. Each of these peaks is treated successively as single peaks, and the following procedure is applied: (1) the background is estimated and subtracted from intervals on each side of the peak; (2) an automatic peak-search routine [11] calculates the centre of the peak; (3) the Gaussian is then rewritten, and F and P are found from the background-corrected intensities by using the expression

$$\log [I'(x)] = \log (P) - [1.665(C - x)]^2 / F^2 \tag{3}$$

The channels chosen and the corresponding corrected intensities are used for establishing a set of simultaneous equations similar to Eqn. 3 with the previously measured C value. Finally, log (P) and $1/F^2$ are found by a linear least-squares procedure.

Once all the lines chosen for the FWHM calibration have been treated, a set of C and corresponding F values is obtained. For each of these sets, an equation similar to Eqn. 2 is established, and a_0 and a_1 are found by a linear least-squares procedure. The FWHM calibration (Eqn. 2) is then used in the evaluation of the unknown spectrum. After subtraction of the background, the peak centres are found. Once the peak centres are known, the FWHM values are related to the peak centres and calculated from the calibration equation. Finally, the amplitudes are estimated from the normal equations for a set of simultaneous equations of type $Y(x) = \Sigma_{i=1}^{N} P_i f_i(x)$, where $Y(x) = I(x) - B(x)$ and the functions f_i are calculated, by using the previously determined C_i and F_i values.

The measurement of peak positions is essential to the described approach, and in the program used, several ways of evaluating peak positions are possible. In one, an automatic peak-search routine [11] finds and calculates accurate peak centres; this routine is available in the library of the central computer at this institute, but it can only find a peak centre which is given by a maximum in the spectrum and so highly overlapped peaks are not found.

In another method, the operator finds the centres by visual inspection on a graphic display, which gives the possibility of finding overlapped peaks. In a third method, the lines used for the FWHM calibration are identified, and the previously calculated centres are used for energy calibration of the spectrum; this calibration is used for qualitative analysis of the spectrum, which in turn is used for defining peak centres. This approach gives the operator the possibility of using the centres of highly overlapped peaks. In a fourth method, visual inspection of the residuals, $(I_{obs} - I_{calc})/(I^2_{obs})$, may indicate undetected overlapping peaks; though the positions of such peaks may be difficult to establish, the residuals indicate their approximate positions. Finally, a combination of these four methods may be used. It was found that residuals should always be investigated in the case of a complex spectrum. Thus, the procedure for finding peak centres may be time-consuming.

Quantitative calculations

In the case of mono-energetic excitation, the basic equation for the fluorescence line area, I, of an analyte line, i, is

$$I_i = GK_iA_i(1 + H_i)W_i \qquad (4)$$

where G is an absolute calibration constant, depending on the generator settings, kV and mA, the secondary target and the geometry of the excitation chamber; K is the relative calibration constant and includes the excitation and detection efficiency for the fluorescence line; A corrects for self-absorption of both exciting and fluorescent radiation, and H corrects for enhancement effects (both A and H depend on the excitation energy and the specimen composition); W is the concentration of the analyte expressed as a weight fraction. The values of K, A and H are calculated from tabulated physical parameters [12—14], as described earlier [15].

When all the elements in a given sample are amenable to x-ray fluorescence spectrometry and can all be determined by means of one secondary target, the absolute calibration constant may be interpreted as a weight-fraction scaling factor; G is scaled such that the sum of all weight fractions equals unity.

For cases in which peak overlap could not be resolved by the programs, a numerical procedure in the quantitative calculation was employed. In the case of the Cr K_α and the Mn K_β lines, the intensities were fitted as one line. Hence, only the sum of their intensities, I(Mn K_α + Cr K_β), was calculated. The intensity for the Mn K_α line, I(Mn K_α) was estimated by the following iterative procedure: (1) initially I(Mn K_α) was set equal to I(Mn K_α + Cr K_β); (2) the calculated intensities were then used for calculating the weight fractions as described above; (3) for these weight fractions, theoretical intensities were calculated from Eqn. 4; (4) the calculated Cr K_β intensity was used to estimate a new Mn K_α intensity value: I(Mn K_α, estimated) = I(Mn K_α + Cr K_β, experimental) — I(Cr K_β, calculated); (5) the corrected Mn K_α intensity was used in a new calculation of weight fractions; (6) if a convergence

criterion was fulfilled, the iterative procedure was stopped, otherwise, the iteration returned to step (3).

EXPERIMENTAL

Apparatus

The energy-dispersive x-ray spectrometer consisted of a laboratory-built excitation chamber with secondary target excitation, a Philips PW-1732/10 high-voltage generator, a Philips PW-2181/00 spectrometer tube with a gold anode, a DTG Si(Li) detector (160 eV at 5.9 keV), a Canberra model 2000 Bin power supply, a Canberra model 3102 high-voltage power supply, a Canberra model 2020 amplifier with pulse pile-up rejection, a Canberra model 2070 analog/digital converter and a dedicated Motorola 68000 computer, which provided on-line control of the spectrometer. For data evaluation, the spectra were transferred to a time-shared VAX 11/780 via a teletype line. The excitation chamber and the software for the spectrometer have been described in detail [9, 16].

Materials, preparation of samples and measurements

For the measurements, the following single-element discs were used: Ti, Fe, Ni, Cu, Zn, Zr, Mo, Sn and Pb (Goodfellow Metals, Cambridge, England) and Cr, Mn, Co, Ge, Se, Y, Nb, Ag, Cd, In, Ta, W, Gd, Au and Bi (prepared from analytical-grade chemicals in the laboratory). When single-element samples were not available, pressed pellets of analytical-grade chemicals were used: CsCl, $BaCl_2 2H_2O$ and LaF_3.

For FWHM and energy calibration, a pellet containing Ti, Zn, Sr and Mo was prepared. Finally, for investigation of complex spectra and for quantitative analysis, two standard reference materials, SRM 1198 (Incoloy 901) and SRM 1201 (Hastelloy X), both from the U.S. National Bureau of Standards, were examined.

For a general investigation of FWHM values, a silver secondary target and a spectrometer setting of 5 mA and 50 kV were used to excite samples of Ti, Cr, Mn, Fe, Co, Ni, Cu, Zn, Ge, Se, Y, Zr, Nb, Mo, $BaCl_2 2H_2O$, LaF_3, Gd, Ta, W, Au, Pb and Bi, and the acquisition time was varied between 100 and 5400 s, depending on the count rate.

For the analysis of complex spectra and spectra with L lines, the Ti/Zn/Sr/Mo pellet, the two SRM alloys and the Ta, W and Pb samples were used. Spectra were recorded at 10 mA and 45 kV with the silver secondary target for 300 s for the pellet and the pure-element samples and for 2000 s for the SRM samples. The SRM samples and the Ti/Zn/Sr/Mo pellet were measured four times. To investigate cases with a marked separation of the $K_{\alpha_{1,2}}$ lines, the samples of Ag, Cd, In, Sn, CsCl and $BaCl_2 2H_2O$ were analyzed. A gadolinium secondary target was used, and the spectrometer setting was 20 mA and 60 kV. For each of these spectra, the acquisition time was 300 s.

Programs

Two computer programs, FWHMCAL and PROFIT [9], were used for peak-area calculations. The stepwise procedure outlined above was used in FWHMCAL. In PROFIT, the parameters are found by a non-linear χ^2 minimization procedure. The selected background function in FWHMCAL can be either linear or exponential. PROFIT uses either a linear or a parabolic background. In both programs, several points chosen at the limits of the selected interval are assumed to be pure background points, from which $B(x)$ is estimated by a linear least-squares procedure.

A computer program, VAP [9], which exploits the fundamental parameter technique was used for quantitative evaluation. In the case of Cr K_β + Mn K_α, severe peak overlaps occurred in both PROFIT and FWHMCAL. Furthermore, the Ni K_α + Co K_β overlap could be resolved by FWHMCAL but not by PROFIT. In these cases, the numerical procedure for severe peak overlap was included in VAP.

All three programs are coded in VAX-11 FORTRAN and were executed on the VAX 11/780.

RESULTS AND DISCUSSION

The FWHM values for the K_α, K_β, L_α and L_β lines were calculated by PROFIT from the spectra obtained by using the silver secondary target for Ti, Cr, Mn, Fe, Co, Ni, Cu, Zn, Ge, Se, Y, Zr, Nb, Mo, Ba, La, Gd, Ta, W, Au, Pb and Bi. The results are shown in Fig. 1. For the K_α, L_α and K_β lines below 13 keV, the results are satisfactory. For the K_β lines above 13 keV and the L_β lines, the results diverge, mainly because the former are doublets and the latter are multiplets.

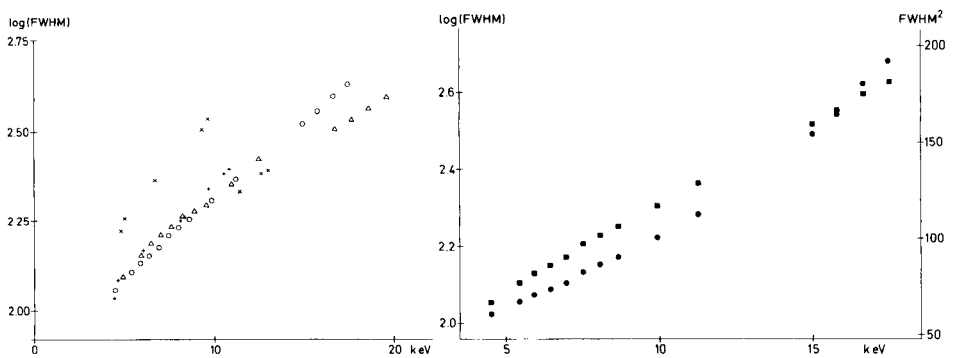

Fig. 1. Logarithmic FWHM values found by fitting Gaussian functions to experimental x-ray fluorescence lines. The unit for FWHM is the number of channels. (○) K_α lines; (△) K_β lines; (+) L_α lines; (×) L_β lines.

Fig. 2. Logarithm and square of FWHM values found by fitting Gaussian functions to experimental x-ray fluorescence lines. The unit for FWHM is number of channels. (▪) Log (FWHM); (•) FWHM².

Theoretically, log F in Eqn. 2 should be replaced by F^2 [10]. Both log (FWHM) and FWHM^2 from the previous K_α results are shown in Fig. 2. Better linearity is observed for the log (FWHM) than for FWHM^2. The deviation from theory is caused by the increasing separation of the K_{α_1} and K_{α_2} lines, which in the FWHM calculation with PROFIT are treated as a single line. Thus, because of the better linearity, the use of log F in Eqn. 2 is preferred.

The spectra of SRM 1198 and SRM 1201 were evaluated by both the PROFIT and FWHMCAL programs, and the results were compared. The K_α lines in the spectra of the Ti/Zn/Sr/Mo pellet were used for the FWHM calibration. For SRM 1198, Fig. 3 shows that the FWHMCAL procedure was able to fit all fourteen lines to the experimental data, whereas with the PROFIT routine, it was necessary to omit all the escape lines and the K_α lines from cobalt and copper. FWHMCAL coped well with any number of lines tried, the present limit being fourteen. However, the residuals obtained

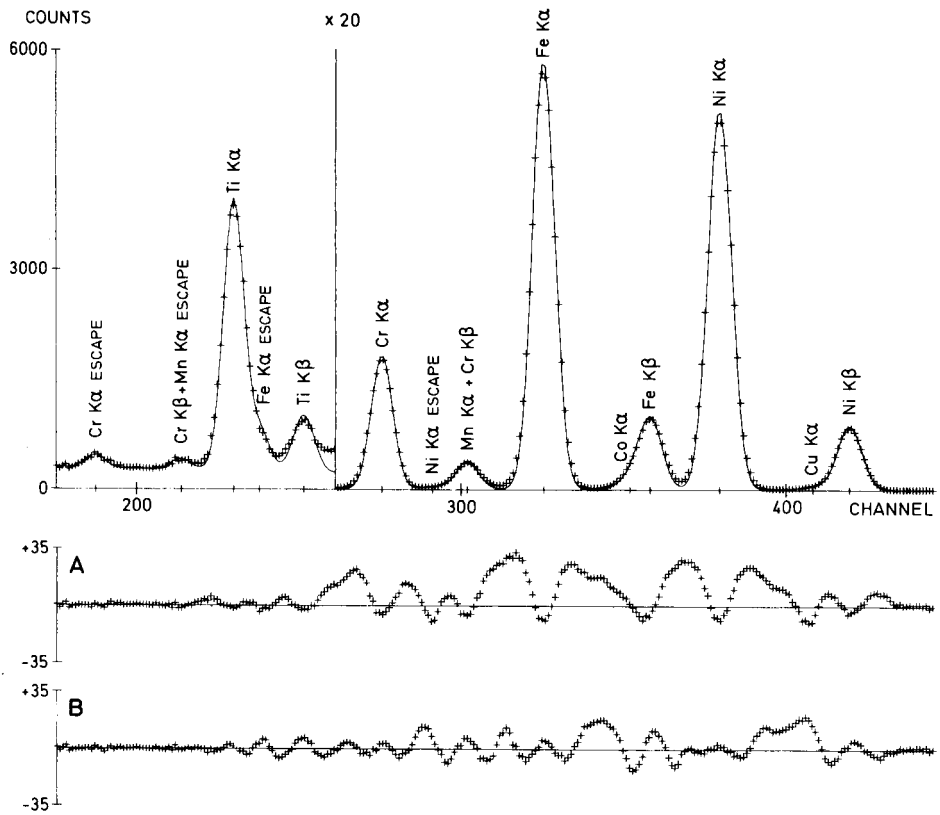

Fig. 3. Comparison of the two procedures used for fitting x-ray fluorescence lines to the spectrum of NBS SRM 1198: (+) experimental points; (—) the fitted curve calculated by FWHMCAL. The residuals, given by $(I_{obs} - I_{calc})/(I^2_{obs})$, for the two procedures are shown below the spectrum: (A) for the FWHMCAL procedure; (B) for the PROFIT procedure.

by PROFIT were slightly lower than those obtained by FWHMCAL. In the vicinity of the large peaks (e.g., the K_α line of iron), the latter residuals indicated too small FWHM values obtained by the calibration procedure. Further, the mean value of the ratios for the peak areas calculated by PROFIT to those obtained by FWHMCAL was found to be 1.09 with a sample standard deviation of 0.02. However, a change of the intensities by a constant factor should not affect the quantitative results. Table 1 gives the quantitative results obtained for SRM 1198 and 1201. The relative standard deviations were usually about 1% are obtained by both calculation procedures. Thus, in both cases, the precision is considered satisfactory, and, for most major elements, the results obtained by both procedures are in reasonable agreement with the certified values.

The FWHM calibration obtained by using parameters for the K_α lines from Ti, Zn, Sr and Mo was used to evaluate the peak areas of L lines. The validity of this approach was investigated by examining the spectra of Ta, W and Pb. In all three cases, satisfactory results were obtained. Figure 4 shows the L spectrum of lead, with two sets (B and C) of fitted spectra and their residuals. In fit C, an energy calibration was used to calculate the exact position for fourteen lead L lines. In fit B, the automatic peak-search routine assigned seven peaks (l, α, η, β, γ_5, $\gamma_{2,3,6}$ and $\gamma_{4,4'}$) initially, and the remaining seven

TABLE 1

Quantitative analysis of NBS SRM 1198 and SRM 1201 (mean values and standard deviations of four replicate measurements are given)

Element	Element concentration (% w/w)		
	Peak-area algorithm PROFIT	FWHMCAL	Certified
SRM 1198			
Ti	2.84 (0.07)	2.811 (0.018)	2.59 (0.01)
Cr	13.10 (0.02)	13.26 (0.02)	12.9 (0.1)
Mn	1.07 (0.02)	0.813 (0.013)	0.49[a]
Fe	36.54 (0.04)	36.92 (0.05)	36.2 (0.1)
Co	1.655 (0.016)	0.80 (0.09)	0.70 (0.01)
Ni	39.19 (0.07)	39.68 (0.05)	40.1 (0.1)
Zr	0.0201 (0.0013)	0.0203 (0.0008)	0.014[a]
Mo	5.584 (0.017)	5.71 (0.08)	6.08 (0.05)
SRM 1201			
Cr	20.93 (0.02)	21.11 (0.06)	20.7 (0.1)
Mn	0.637 (0.019)	0.469 (0.013)	—
Fe	23.66 (0.01)	23.88 (0.04)	23.2 (0.1)
Co	1.409 (0.014)	0.62 (0.01)	0.56 (0.01)
Ni	45.00 (0.02)	45.38 (0.04)	45.7 (0.1)
Mo	8.371 (0.014)	8.55 (0.10)	9.18 (0.05)

[a]Not certified; additional information.

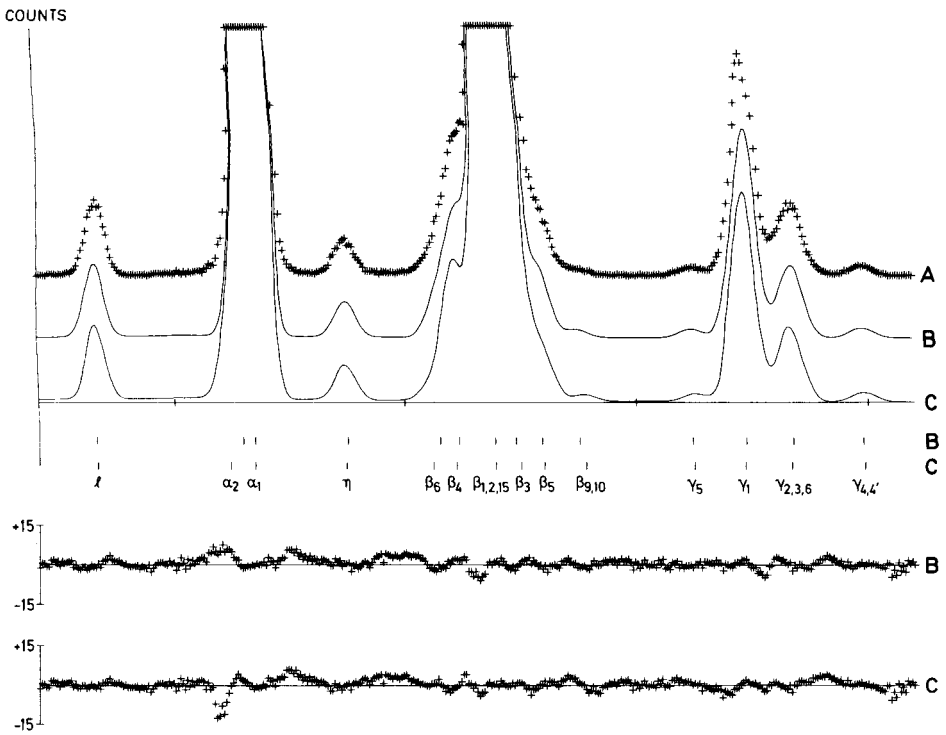

Fig. 4. The FWHMCAL procedure used for fitting the L lines in the spectrum of pure lead. Experimental points, fitted curves (linear scale on the energy axis) and residuals for two different calculations are shown. (A) Experimental data points; (B) line positions found by the automatic peak-search routine and by visual investigation of residuals in the cases of severe line overlap; (C) the use of an energy calibration defines the exact L line positions. Residuals are given by $(I_{obs} - I_{calc})/(I^2_{obs})$.

line positions were found by visual inspection of the residuals. The best results were obtained in fit C, but both methods produced usable descriptions of the L spectra.

For energies above 20 keV, there is a marked separation of the K_{α_1} and K_{α_2} lines. However, the use of $K_{\beta_{1,3}}$ lines for the FWHM calibration solves the calibration problems in this range. Figure 5 shows the experimental data, fitted results and residuals for the silver and barium lines.

The authors are grateful to the Danish Technical Research Council for financial support (grant 16-1866), and to S. E. Rasmussen and L. Kryger for their advice on the preparation of the paper.

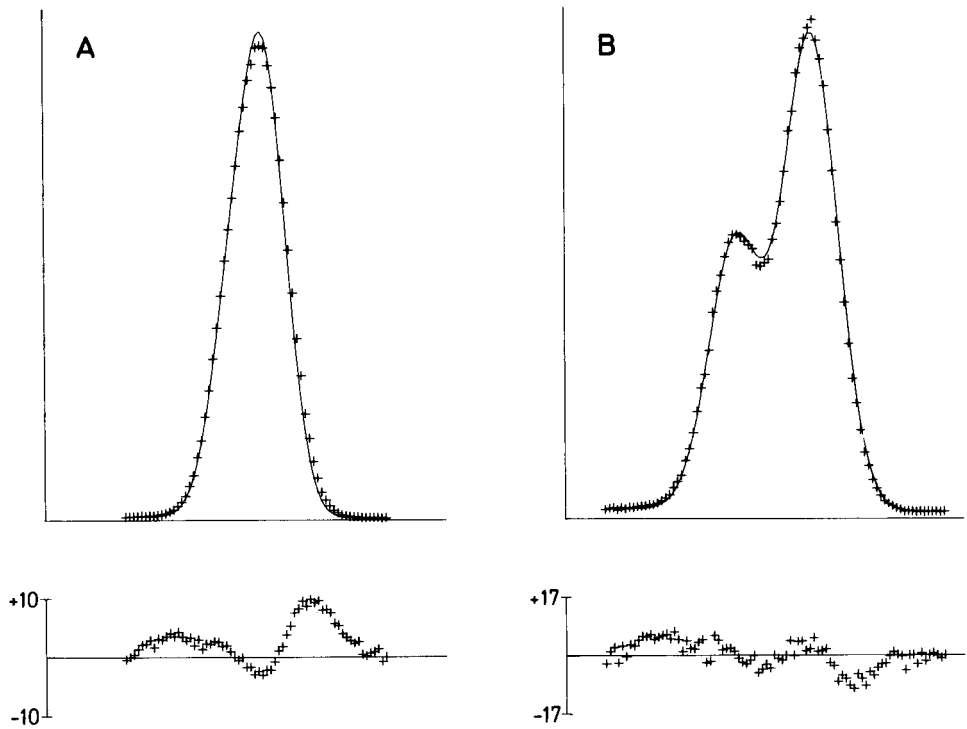

Fig. 5. The FWHMCAL procedure used for fitting the K_{α_1} and K_{α_2} lines in the spectra of silver (A) and barium (B). FWHM calibration was done by using the $K_{\beta_{1,3}}$ lines from samples of Ag, Cd, In, Sn, Cs and Ba. Experimental points (+) and fitted curves (—) are shown on a linear scale on an energy axis. Residuals are given by $(I_{obs} - I_{calc})/(I^2_{obs})$.

REFERENCES

1 J. T. Routti and S. G. Prussin, Nucl. Instrum. Methods, 72 (1969) 125.
2 M. J. Koskelo, P. A. Aarnio and J. T. Routti, Nucl. Instrum. Methods, 190 (1981) 89.
3 M. J. Koskelo, P. A. Aarnio and J. T. Routti, Comput. Phys. Commun., 24 (1981) 11.
4 H. L. Bank, A. J. Forst and C. F. Lam, Ultramicroscopy, 5 (1980) 153.
5 C. F. Lam, A. Forst and H. Bank, Appl. Spectrosc., 33 (1979) 273.
6 P. Van Espen, H. Nullens and F. C. Adams, Z. Anal. Chem., 285 (1977) 215.
7 P. Van Espen, H. Nullens and F. Adams, Nucl. Instrum. Methods, 145 (1977) 579.
8 E. Marageter, W. Wegscheider and K. Müller, Nucl. Instrum. Methods, Phys. Res., B1 (1984) 137.
9 B. B. Jensen, J. N. Marcussen and N. Pind, Anal. Chim. Acta, 161 (1984) 175.
10 S. J. B. Reed, in V. D. Scott and G. Love (Eds.), Quantitative Electron-Probe Microanalysis, Ellis Horwood, Chichester, England, 1983, p. 90.
11 S. Brodersen, Procedure TOP in MATBIB at VAX 11/780 at the Department of Chemistry, Aarhus University, Denmark, 1984 (available on request).
12 W. H. McMaster, N. Kerr Del Grande, J. H. Mallett and J. H. Hubbell, Compilation of X-ray Cross Sections, Sect. 2, Rev. 1, 1969, UCRL-50174.
13 M. O. Krause, J. Phys. Ref. Data, 8 (1979) 307.
14 J. H. Scofield, At. Data Nucl. Data Tables, 14 (1974) 121.
15 B. B. Jensen, J. N. Marcussen and N. Pind, Anal. Chim. Acta, 167 (1985) 305.
16 L. H. Christensen, S. E. Rasmussen, N. Pind and K. Henriksen, Anal. Chim. Acta, 116 (1980) 7.

Analytica Chimica Acta, 171 (1985) 111—118
Elsevier Science Publishers B.V., Amsterdam — Printed in The Netherlands

MATHEMATICAL DESCRIPTION OF CONCENTRATION PROFILES AND ANODIC CURRENTS FOR AMPEROMETRIC TWO-ENZYME ELECTRODES

THOMAS SCHULMEISTER* and FRIEDER SCHELLER

Central Institute of Molecular Biology, Academy of Sciences, Robert-Rössle-Str. 10, 1115 Berlin-Buch (German Democratic Republic)

(Received 9th October 1984)

SUMMARY

Formulae are presented for explicit solutions of partial differential equations describing the transient behaviour of concentration profiles and the anodic current in amperometric two-enzyme electrodes. The mathematical treatment is based on reaction-diffusion models with irreversible first-order catalytic reactions. Numerical results are presented to demonstrate the practical use of the derived formulae.

Since the concept of enzyme electrodes was described [1, 2], various mathematical models and numerical simulations of these sensors have been published [3—8]. Single-enzyme models have been investigated for the stationary operational mode and for kinetic measurements [9—12]. However, an increasing number of sensors based on two-enzyme membranes have been designed [13—24]. The present paper deals with mathematical models for two basically two-enzyme sensors, the enzyme sequence electrode and the enzyme competition electrode.

THEORY

An amperometric one-layer enzyme electrode with two co-immobilized enzymes homogeneously distributed in the layer is assumed. The irreversible enzyme reactions are assumed to depend linearly on the corresponding substrate concentrations. For an enzyme sequence electrode,

$$S_1 + A_1 \xrightarrow{k_1} S_2 + A_2;\ S_2 + A_3 \xrightarrow{k_2} \alpha P_1 + A_4 \qquad (1)$$

and for the enzyme competition electrode

$$S_3 + S_4 \xrightarrow{k_3} A_5 + A_6;\ S_4 + A_7 \xrightarrow{k_4} \alpha P_2 + A_8 \qquad (2)$$

where A_i ($i = 1 \ldots 8$) denote substances that have no influence on the reaction rates, $k_j S_j$ ($j = 1 \ldots 4$), or on the measuring principle; α represents the stoichiometric factor of the product-forming reaction.

0003-2670/85/$03.30

If a one-dimensional diffusion model is used and excesses of A_1 and A_3 are assumed in the first-order reactions (1), the transient behaviour of the sequence electrode can be described by a system of three reaction-diffusion equations [18]

$$\partial S_1/\partial t = D_{S_1}\,\partial^2 S_1/\partial r^2 - k_1 S_1 \tag{3}$$

$$\partial S_2/\partial t = D_{S_2}\partial^2 S_2/\partial r^2 + k_1 S_1 - k_2 S_2 \tag{4}$$

$$\partial P_1/\partial t = D_{P_1}\partial^2 P_1/\partial r^2 + \alpha k_2 S_2 \tag{5}$$

where $S_1(r, t)$, $S_2(r, t)$ and $P_1(r, t)$ denote the concentrations of substrate, intermediate product and product at point r ($0 \leqslant r \leqslant d$) and time t ($t \geqslant 0$), respectively; d is the thickness of the enzyme layer. The diffusion coefficients and kinetic parameters are denoted by D_{S_1}, D_{S_2}, D_{P_1}, k_1 and k_2, respectively. At the start of the measurement ($t = 0$), substrate, intermediate product and product are assumed to be absent in the enzyme membrane. Further, perfect stirring is assumed [8, 10—13]. Maximal sensitivity will be obtained when the electrode potential is set to oxidize or reduce the product completely [10]. Therefore the boundary and initial conditions of the model can be written [20]

$S_1(0, t) = S^{10}$; $\partial S_1/\partial r(d, t) = 0$ for $t > 0$; $S_1(r, 0) = 0$ for $0 \leqslant r \leqslant d$

$S_2(0, t) = 0$; $\partial S_2/\partial r(d, t) = 0$ for $t > 0$; $S_2(r, 0) = 0$ for $0 \leqslant r \leqslant d$

$P_1(0, t) = 0$; $P_1(d, t) = 0$ for $t > 0$; $P_1(r, 0) = 0$ for $0 \leqslant r \leqslant d$

where S^{10} denotes the bulk concentration of S_1.

Analogously for the enzyme competition electrode

$$\partial S_3/\partial t = D_{S_3}\partial^2 S_3/\partial r^2 - k_3 S_3 \tag{6}$$

$$\partial S_4/\partial t = D_{S_4}\partial^2 S_4/\partial r^2 - k_3 S_3 - k_4 S_4 \tag{7}$$

$$\partial P_2/\partial t = D_{P_2}\partial^2 P_2/\partial r^2 + \alpha k_4 S_4 \tag{8}$$

For the enzyme competition electrodes described [16, 23] stationary initial conditions can be assumed for the product-forming reaction (2). The corresponding stationary solutions of Eqns. 7 and 8 (without S_3) may be derived by using the formulae for single-enzyme membranes [12]. Thus

$S_3(0, t) = S^{30}$; $\partial S_3/\partial r(d, t) = 0$ for $t > 0$; $S_3(r, 0) = 0$ for $0 \leqslant r \leqslant d$

$S_4(0, t) = S^{40}$; $\partial S_4/\partial r(d, t) = 0$ for $t > 0$; $S_4(r, 0)$

$= S^{40} \cosh[\alpha_4(d - r)]/\cosh(\alpha_4 d)$ for $0 \leqslant r \leqslant d$

$P_2(0, t) = P^0$; $P_2(d, t) = 0$ for $t > 0$

$P_2(r, 0) = \alpha(D_{S_4}/D_{P_2})S^{40}\{1 - \cosh[\alpha_4(d - r)]/\cosh(\alpha_4 d)$

$+ (r/d)\{[1/\cosh(\alpha_4 d)] - 1\}\} + P^0(1 - r/d)r$ for $0 \leqslant r \leqslant d$

where $\alpha_i = (k_i/D_{S_i})^{1/2}$ $(i = 1 \ldots 4)$ and S^{30}, S^{40} and P^0 denote the bulk concentrations of S_3, S_4 and P_2, respectively.

In both systems, the first differential equation can be solved separately [26]. The solutions can be inserted into Eqns. 4 and 7, respectively. The arising linear inhomogeneous parabolic equation can be solved by using the integral-transform technique [27]. Insertion of the resulting expressions into Eqns. 5 and 8, respectively, again gives linear differential equations that can be solved with the same formulae. For the enzyme sequence electrode,

$$S_1(r, t) = S^{10} \left\{1 - \frac{4}{\pi} \sum_{m=0}^{\infty} \frac{\sin[(2m+1)\pi r/(2d)]}{2m+1} \frac{k_1 + u\exp[-(u+k_1)t]}{k_1 + u}\right\} \quad (9)$$

$$S_2(r, t) = \frac{4}{\pi} k_1 S^{10} \sum_{m=0}^{\infty} \frac{\sin[(2m+1)\pi r/(2d)]}{2m+1} \frac{u}{k_1 + u}$$

$$\left\{\frac{1 - \exp[-(k_2 + w)t]}{k_2 + w} \frac{\exp[-(k_1 + u)t] - \exp[-(k_2 + w)t]}{w + k_2 - u - k_1}\right\} \quad (10)$$

with $u = D_{S_1}(2m+1)^2\pi^2/(4d^2)$ and $w = D_{S_2}(2m+1)^2\pi^2/(4d^2)$

$$P_1(r, t) = \frac{8}{\pi^2} \alpha k_1 k_2 S^{10} \sum_{n=1}^{\infty} (-1)^n \sin(n\pi r/d) \sum_{m=0}^{\infty} \frac{(-1)^{m+1}}{2m+1} \frac{n}{n^2 - (2m+1)^2/4}$$

$$\frac{u}{k_1 + u} \left\{\frac{1}{w + k_2} \left[\frac{1 - \exp(-yt)}{y} - \frac{\exp[-(k_2 + w)t] - \exp(-yt)}{y - k_2 - w}\right]\right.$$

$$\left. - \frac{1}{w + k_2 - u - k_1} \left[\frac{\exp[-(k_1 + u)t] - \exp(-yt)}{y - k_1 - u}\right.\right.$$

$$\left.\left. - \frac{\exp[-(k_2 + w)t] - \exp(-yt)}{y - k_2 - w}\right]\right\} \quad (11)$$

with $y = D_{P_1} n^2\pi^2/d^2$.

For the enzyme competition electrode,

$$S_3(r, t) = S^{30} \left\{1 - \frac{4}{\pi} \sum_{m=0}^{\infty} \frac{\sin[(2m+1)\pi r/(2d)]}{2m+1} \frac{k_3 + v\exp[-(k_3 + v)t]}{k_3 + v}\right\} \quad (12)$$

$$S_4(r, t) = S^{40} \frac{\cosh[\alpha_4(d - r)]}{\cosh(\alpha_4 d)} - k_3 S^{30} \frac{4}{\pi} \sum_{m=0}^{\infty} \frac{\sin[(2m+1)\pi r/(2d)]}{2m+1} \frac{v}{v + k_3}$$

$$\left\{\frac{1 - \exp[-(k_4 + z)t]}{k_4 + z} - \frac{\exp[-(k_3 + v)t] - \exp[-(k_4 + z)t]}{k_4 + z - k_3 - v}\right\} \quad (13)$$

with $v = D_{S_3}(2m+1)^2\pi^2/(4d^2)$ and $z = D_{S_4}(2m+1)^2\pi^2/(4d^2)$

$$P_2(r,t) = S^{40}\alpha \frac{D_{S_4}}{D_{P_2}} \left\{ \frac{r}{d} \left[\frac{1}{\cosh(\alpha_4 d)} - 1 \right] - \frac{\cosh[\alpha_4(d-r)]}{\cosh(\alpha_4 d)} + 1 \right\}$$

$$- S^{30}\alpha k_3 k_4 \frac{8}{\pi^2} \sum_{n=1}^{\infty} \sin(n\pi r/d)(-1)^n \sum_{m=0}^{\infty} \frac{(-1)^{m+1}}{2m+1} \frac{n}{n^2 - (2m+1)^2/4}$$

$$\times \frac{v}{k_3+v} \left\{ \frac{1}{k_4+z} \left[\frac{1-\exp(-xt)}{x} - \frac{\exp[-(k_4+z)t] - \exp(-xt)}{x-k_4-z} \right] \right.$$

$$\left. - \frac{1}{k_4+z-k_3-v} \left[\frac{\exp[-(k_3+v)t] - \exp(-xt)}{x-k_3-v} \right. \right.$$

$$\left. \left. - \frac{\exp[-(k_4+z)t] - \exp(-xt)}{x-k_4-z} \right] \right\} + P^0(1-r/d) \tag{14}$$

with $x = D_{P_2} n^2\pi^2/d^2$.

If it is assumed that, at the start of the enzyme competition electrode measurement, the substrate S_4 is not present in the enzyme membrane, i.e., the non-stationary initial conditions of reaction (2), then $S_4(r, 0) = 0$, and the first term of Eqn. 13 must be replaced by

$$S^{40}(4/\pi) \sum_{m=0}^{\infty} \{\sin[(2m+1)\pi r/(2d)]/(2m+1)\} [z/(k_4+z)]$$

$$\times \{1 - \exp[-(k_4+z)t]\} \tag{15}$$

and the first term of Eqn. 14 by

$$S^{40}\alpha k_4 \frac{8}{\pi^2} \sum_{n=1}^{\infty} \sin(n\pi r/d)(-1)^n \sum_{m=0}^{\infty} \frac{(-1)^{m+1}}{2m+1} \frac{n}{n^2 - (m+1)^2/4} \frac{z}{k_4+z}$$

$$\times \left[\frac{1-\exp(-xt)}{x} - \frac{\exp(-(k_4+z)t) - \exp(-xt)}{x-k_4-z} \right] \tag{16}$$

The stationary solutions may be derived in the same order by using the formulae for undamped inhomogeneous oscillations [25, 20]

$$S_1(r) = S^{10} \frac{\cosh[\alpha_1(d-r)]}{\cosh(\alpha_1 d)} \tag{17}$$

$$S_2(r) = \frac{S^{10} k_1}{D_{S_2}(\alpha_2^2 - \alpha_1^2)} \left\{ \frac{\cosh[\alpha_1(d-r)]}{\cosh(\alpha_1 d)} - \frac{\cosh[\alpha_2(d-r)]}{\cosh(\alpha_2 d)} \right\} \tag{18}$$

$$P_1(r) = \frac{\alpha k_1 k_2 S^{10}}{D_{S_2} D_{P_1}(\alpha_1^2 - \alpha_2^2)} \left[\frac{1}{\alpha_1^2} - \frac{1}{\alpha_2^2}\right] (r/d - 1) + \frac{\cosh[\alpha_1(d-r)] - r/d}{\alpha_1^2 \cosh(\alpha_1 d)}$$
$$- \frac{\cosh[\alpha_2(d-r)] - r/d}{\alpha_2^2 \cosh(\alpha_2 d)} \tag{19}$$

$$S_3(r) = S^{30} \frac{\cosh[\alpha_3(d-r)]}{\cosh(\alpha_3 d)} \tag{20}$$

$$S_4(r) = \frac{S^{30} k_3}{D_{S_3}(\alpha_3^2 - \alpha_4^2)} \left\{\frac{\cosh[\alpha_3(d-r)]}{\cosh(\alpha_3 d)} - \frac{\cosh[\alpha_4(d-r)]}{\cosh(\alpha_4 d)}\right\}$$
$$+ S^{40} \frac{\cosh[\alpha_4(d-r)]}{\cosh(\alpha_4 d)} \tag{21}$$

$$P_2(r) = -\frac{\alpha k_4}{D_{P_2}} \left\{\frac{S^{40}}{\alpha_4^2} \left[\frac{\cosh[\alpha_4(d-r)]}{\cosh(\alpha_4 d)} + [1 - 1/\cosh(\alpha_4 d)] r/d - 1\right]\right.$$
$$+ \frac{k_3 S^{30}}{D_{S_4}(\alpha_3^2 - \alpha_4^2)} \left[\frac{\cosh[\alpha_3(d-r)]}{\alpha_3^2 \cosh(\alpha_3 d)} - \frac{\cosh[\alpha_4(d-r)]}{\alpha_4^2 \cosh(\alpha_4 d)}\right]$$
$$\left. + \frac{r}{d}\left[\frac{\cosh(\alpha_3 d) - 1}{\alpha_3^2 \cosh(\alpha_3 d)} - \frac{\cosh(\alpha_4 d) - 1}{\alpha_4^2 \cosh(\alpha_4 d)}\right] - \left(\frac{1}{\alpha_3^2} - \frac{1}{\alpha_4^2}\right)\right\} \tag{22}$$

The anodic current may be obtained explicitly from Faraday's Law and Fick's First Law with the flux of product at the electrode surface [10]:

$$i(t) = \pm nFAD_Q \, (\partial Q/\partial r)(d, t) \tag{23}$$

where n, F and A denote the number of electrons involved in the electrochemical reaction of substance Q, the Faraday constant and the electrode surface area, respectively.

RESULTS AND DISCUSSION

Equations 11 and 23 reflect the linear concentration dependence of the enzyme sequence electrode. In the case of the enzyme competition electrode, the change in the anodic current depends linearly on the concentration of the added substrate, S^{30}. The models are valid only in the linear range of the corresponding enzyme reactions. Furthermore, it is assumed for the enzyme competition electrode that the reaction rate constant, k_3, and the bulk concentration value, S^{30}, are sufficiently small to avoid total degradation of the substrate S_4. Examples of the enzyme sequence electrode are systems of glucose oxidase with invertase [15], glucoamylase [23] or maltase [15]. Competition electrodes are the glucose oxidase/hexokinase system [15, 16, 18], the glucose oxidase/glucose dehydrogenase system [16, 23] and the catalase/peroxidase system [16, 23].

With given current/time data and with knowledge of some of the enzyme electrode parameters, the remaining parameters can be calculated by least-squares fits. The method was applied to data obtained from a maltose sequence electrode [23]

$$\text{maltose} + H_2O \xrightarrow[\text{D-glucoamylase}]{k_1} 2\beta\text{-D-glucose}$$

$$2\beta\text{-D-glucose} + 2O_2 + 2H_2O \xrightarrow[\text{glucose oxidase}]{k_2} 2\text{D-gluconic acid} + 2H_2O_2$$

$$2H_2O_2 \rightarrow 2O_2 + 4H^+ + 4e^-$$

The values of the diffusion coefficients of hydrogen peroxide and glucose in hydrophilic gel membranes are known [12]: $D_{\text{glucose}} = 1.53 \times 10^{-4}$ mm^2 s^{-1}, $D_{H_2O_2} = 2.46\, D_{\text{glucose}}$. Further, $k_2 = 0.95$ s^{-1} and $\alpha = 2$. Thus, from the current/time data given in Table 1, $D_{\text{maltose}} = 7.52 \times 10^{-5}$ mm^2 s, $k_1 = 0.06$ s^{-1} and $d = 0.141$ mm. The sum of least squares is less than 0.4 (nA)^2. The current/time data used and the calculated transient behaviour of the anodic current are represented in Fig. 1. Figure 2 shows concentration profiles calculated from Eqns. 9—11 and 17—19 for the values given above for the three diffusion coefficients, k_1, k_2 and d.

Conclusions

Theoretical investigations of models of two-enzyme electrodes usually require tedious numerical procedures. Therefore it seemed to be useful to seek explicit expressions of concentration profiles and the anodic current. In the case of first-order reaction rates, the proposed formulae allow application of this approach. Extensive theoretical investigations as well as the characterization of commercial two-enzyme electrodes become possible. In the development described here, the effects of the concentration boundary and the dialysis membranes were ignored. There are further types of amperometric

TABLE 1

Current/time dependence of a maltose enzyme sequence electrode[a]

Time (s)	Current (nA) for variable S^{10}			Time (s)	Current (nA) for variable S^{10}		
	0.071 mM	0.142 mM	0.285 mM		0.071 mM	0.142 mM	0.285 mM
5	0.1	0.1	0.1	35	2.35	4.7	9.05
10	0.45	0.8	1.75	40	2.45	5.0	9.7
15	0.9	1.95	4.0	45	2.65	5.2	10.05
20	1.35	2.95	5.9	50	2.75	5.35	10.25
25	1.85	3.75	7.65	55	2.75	5.5	10.45
30	2.1	4.25	8.4	60	2.75	5.6	10.65

[a]Specific activity of glucose oxidase and D-glucoamylase are 23 and 50 units mg^{-1}, respectively; electrode surface area 0.2 mm^2; gelatine 1 mg cm^{-2}.

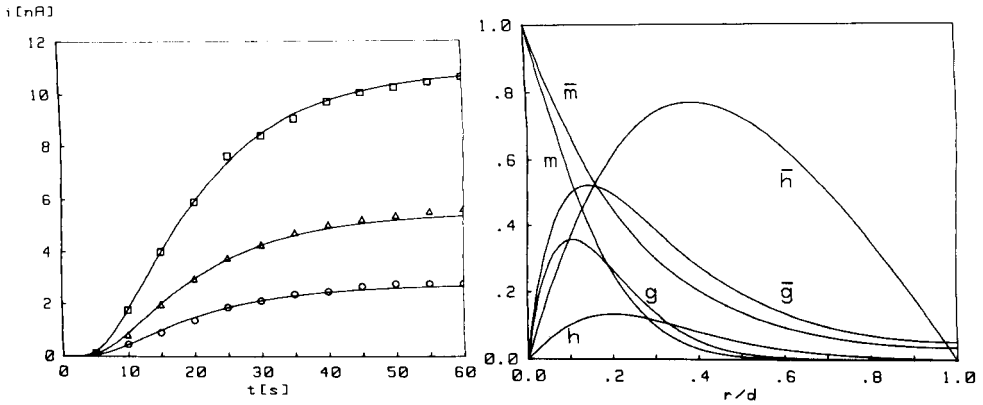

Fig. 1. Transient behaviour of the maltose electrode as least-squares fits of the data in Table 1. The parameter values are given in the text: (○) S^{10} = 0.071 mM; (△) S^{10} = 0.142 mM; (□) S^{10} = 0.285 mM.

Fig. 2. Concentration profiles of the maltose electrode. Profiles are given for t = 5 s and the stationary case (with bar). Maltose (m), glucose (g) and hydrogen peroxide (h) are rendered dimensionless with S^{10}, $S^{10}/10$ and $S^{10}/5$, respectively.

two-enzyme electrodes which can be investigated by the above approach, e.g., an intermediate product-sensitive enzyme sequence electrode [21] and an enzyme-sensitive sequence electrode [24], both of which operate with stationary initial conditions of the first reaction to measure an added substrate. The formulae may be extended to multi-enzyme electrodes.

The authors thank D. C. Litschko for his experimental work.

REFERENCES

1 L. C. Clark and C. Lyons, Ann. N. Y. Acad. Sci., 102 (1962) 29.
2 S. J. Updike and G. P. Hicks, Nature, 214 (1967) 986.
3 G. G. Guilbault and G. Nagy, Anal. Chem., 45 (1973) 417.
4 L. D. Mell and J. T. Maloy, Anal. Chem., 47 (1975) 299.
5 C. Tran-Minh and G. Broun, Anal. Chem., 47 (1975) 1359.
6 F. R. Shu and G. S. Wilson, Anal. Chem., 48 (1976) 1679.
7 P. W. Carr, Anal. Chem., 49 (1977) 799.
8 J. E. Brady and P. W. Carr, Anal. Chem., 52 (1980) 977.
9 W. J. Blaedel, T. R. Kissel and R. C. Boguslaski, Anal. Chem., 44 (1972) 2030.
10 P. W. Carr and L. D. Bowers, Immobilized Enzymes in Analytical and Clinical Chemistry, Wiley, New York, 1980.
11 M. A. Arnold and G. A. Rechnitz, Anal. Chem., 52 (1980) 977.
12 Th. Schulmeister and F. Scheller, Anal. Chim. Acta, 170 (1985) 279.
13 M. Cordonnier, F. Lawny, D. Chapot and D. Thomas, FEBS Lett., 49 (1975) 263.
14 P. R. Coulet and C. Bertrand, Anal. Lett., 12 (1979) 581.
15 D. Pfeiffer, F. Scheller, M. Jänchen, K. Bertermann and H. Weise, Anal. Lett., 13 (1980) 1179.

16 F. Scheller and D. Pfeiffer, Anal. Chim. Acta, 117 (1980) 383.
17 C. Bertrand, P. R. Coulet and D. C. Gautheron, Anal. Chim. Acta, 126 (1981) 23.
18 J. J. Kulys, M. V. Pesliakiene and A. S. Samalius, Bioelectrochem. Bioenerg., 8 (1981) 81.
19 J. J. Kulys and W. V. Pesliakiene, Zh. Anal. Khim., 36 (1981) 752.
20 J. J. Kulys, Enzyme Microb. Technol., 3 (1981) 344.
21 R. Renneberg, D. Pfeiffer and F. Scheller, Anal. Chim. Acta, 134 (1982) 359.
22 F. Scheller and R. Renneberg, Anal. Chim. Acta, 316 (1983) 877.
23 R. Renneberg and F. Scheller, Proc. Int. Meet. Chemical Sensors, Fukuoka, Japan, 1983, p. 711.
24 F. Mizutani, K. Sasaki and Y. Shimura, Anal. Chem., 55 (1983) 35.
25 E. Kamke, Differentialgleichungen, 1. Band, Akademische Verlagsgesellschaft, Leipzig, 1956, Ch. C2.36.
26 J. Crank, The Mathematics of Diffusion, 2nd edn., Clarendon Press, Oxford, 1956, Ch. 8.
27 M. N. Özisik, Heat Conduction, Wiley, New York, 1980, Ch. 6.

Analytica Chimica Acta, 171 (1985) 119—129
Elsevier Science Publishers B.V., Amsterdam — Printed in The Netherlands

LIPOPHILIC SALTS AS MEMBRANE ADDITIVES AND THEIR INFLUENCE ON THE PROPERTIES OF MACRO- AND MICRO-ELECTRODES BASED ON NEUTRAL CARRIERS

D. AMMANN, E. PRETSCH and W. SIMON*

Swiss Federal Institute of Technology (ETH), Department of Organic Chemistry, CH-8092 Zürich (Switzerland)

E. LINDNER, A. BEZEGH and E. PUNGOR

Institute for General and Analytical Chemistry, Technical University, H-1502 Budapest (Hungary)

(Received 21st October 1984)

SUMMARY

The influence of salts containing lipophilic cations and anions on the electrical resistance of the membranes of calcium ion-selective macro- and micro-electrodes based on a neutral carrier is described. The resistance of macroelectrodes was decreased by a factor of about 50 or of about 3 compared to membranes without and with potassium tetrakis-(*p*-chlorophenyl)borate, respectively. No significant reduction of the membrane resistance was achieved for microelectrodes. The lower detection limit and the Ca^{2+}/K^+ selectivity factor were improved for both types of electrode.

The presence of salts consisting of a hydrophilic cation and a lipophilic anion [e.g., sodium tetraphenylborate (NaTPB) or potassium tetrakis(*p*-chlorophenyl)borate (KT*p*ClPB)] in cation-selective membranes based on neutral carriers has proved to be beneficial in many respects. The additives reduce interferences by lipophilic anions in the sample, give rise to significant changes in selectivity, are able to boost cation sensitivity in the case of carriers with poor extraction capability, and lower the electrical membrane resistance considerably [1, 2]. However, the amount of added salt must be strictly limited because excessive concentrations lead to drastic changes in the membrane selectivity [3]. Depending on the stoichiometry of the complex, an increase over a given molar ratio of lipophilic salt/carrier yields a membrane with the properties of a classical cation-exchanger [3]. It has been shown that this drawback can be avoided if both the cations and the anions incorporated into the membrane are lipophilic [4]. Consequently, it can be expected that increasing amounts of these salts will further decrease membrane resistances without changing the membrane selectivity. This can be important for electrokinetic studies (e.g., the evaluation of exchange current densities [5]) on ion-selective macroelectrodes where several difficulties can arise from high membrane resistances [6, 7].

0003-2670/85/$03.30

The reduction of membrane resistances would be most attractive for microelectrodes to be used in physiological studies. Reduction of the electrical resistance of such electrodes should overcome problems related to shielding and to response times limited by electronic instrumentation. Several other advantages would accrue from a general recipe for lowering the resistances of neutral carrier-based microelectrodes. For example, the tip diameters could be reduced, and shunts through the glass wall, that may disturb sodium ion [8] and calcium ion measurements [9], could be eliminated. It should be possible to use non-polar membrane solvents for microelectrodes with selectivity for monovalent cations; at present, polar membrane solvents are used unavoidably, although they reduce the monovalent/divalent cation selectivity, because they decrease the membrane resistance [10, 11]. Lower membrane resistance would also encourage the more widespread use of highly selective carrier microelectrodes instead of the ion-exchanger microelectrodes which have modest selectivity but low resistance (e.g., valinomycin-based membranes instead of the Corning 477317 ion-exchanger [12]). Some neutral carriers have proved valuable in macroelectrode systems but are not appropriate as membrane components in microelectrodes because, when current membrane technology is applied, the membrane resistances are extremely high [13]. Finally, lower membrane resistances should permit a reduction in the amount of the neutral carrier needed in the membrane solution; in almost all solutions for membrane preparation, the carrier content is at least 10% (w/w) [14].

In the microelectrode technique, the performance and the microelectrode membrane resistance depend on many parameters such as the tip diameter, the filling height, the taper angle, the thickness of the glass wall at the extreme tip, etc., and the preparation of electrodes is intricate and time-consuming. Accordingly, preliminary experiments were done with macroelectrodes and with simple conductivity measurements on ion-selective membrane solutions. Because of the severe demands placed on and the great interest in calcium ion-selective microelectrodes, membranes based on a calcium carrier (ETH 1001) were used throughout.

EXPERIMENTAL

Preparation of membranes

To prepare the solvent polymeric membranes, 0.5—1.0% (w/w) Ca^{2+}-carrier (ETH 1001; Fluka, cat. no. 21192, CH-9470 Buchs, Switzerland), ca. 65% (w/w) *o*-nitrophenyl-n-octyl ether (Fluka), ca. 35% (w/w) poly(vinyl chloride) (Fluka), and various amounts of additives (see Table 1 and Fig. 1) were dissolved in about 2 ml of freshly distilled tetrahydrofuran (Fluka; puriss.) and poured into a glass ring with an inner diameter of 23 mm resting on a glass plate (for details, see [15]).

The potassium tetrakis(*p*-chlorophenyl)borate and tetrabutylammonium tetraphenylborate (TBATPB) used as additives were from Fluka. The other

TABLE 1

Composition of membranes as % (w/w)[a] and their properties in macroelectrodes

Membrane components	Membrane																
	1	2	3	4	5	6	7	8	9	10	11	12	13	14	15	16	17
ETH 1001	0.55	0.55	0.55	0.54	1.0	1.0	1.0	1.0	1.0	1.0	0.9	0.92	0 94	0.94	0.93	0.95	0.94
o-NPOE	66.3	66.1	65.6	64.8	64.9	63.8	65.5	65.4	64.3	64.3	62.4	59.8	61.7	62.5	62.9	63.3	62.7
PVC	33.15	33.1	32.8	32.4	34.1	34.8	32.5	31.6	32.2	32.1	33.0	31.5	32.8	33.3	33.5	33.8	32.1
KTpClPB	—	0.25 (67)	0.25 (67)	0.26 (68)	—	0.4	—	—	—	0.1 (10)	0.45 (67)	0.44 (67)	0.46 (67)	0.46 (67)	0.47 (67)	0.45 (67)	0.46 (67)
ETH 500	—	—	0.8 (86)	2.0 (215)	—	—	1.0 (67)	1.9 (120)	2.4 (150)	2.4 (150)	3.25 (202)	7.34 (494)	—	—	—	—	—
ETH 2035	—	—	—	—	—	—	—	—	—	—	—	—	4.1 (199)	—	—	—	—
ETH 2039	—	—	—	—	—	—	—	—	—	—	—	—	—	2.8 (203)	—	—	—
ETH 2037	—	—	—	—	—	—	—	—	—	—	—	—	—	—	2.2 (203)	—	—
TBATPB	—	—	—	—	—	—	—	—	—	—	—	—	—	—	—	1.5 (200)	3.8 (500)
R(kΩ)	2000	132	50	32	700	63	82	50	50	30	35	24	28	28	26	31	24
Detection limit (log a)[b]	−7.1	−8.6	−8.9	−9.0	−7.6	−8.9					−8.8	−9.2	−8.5	−8.9	−7.9		
Slope (10^{-7}–10^{-3} M) (mV/decade)	24.0	28.3	27.9	27.9	26.4	28.5					27.6	28.5	26.9	28.3	25.8	~16	~15

[a]Mol-% relative to ETH 1001 are given in parentheses. [b]a is the single ion activity of Ca^{2+}.

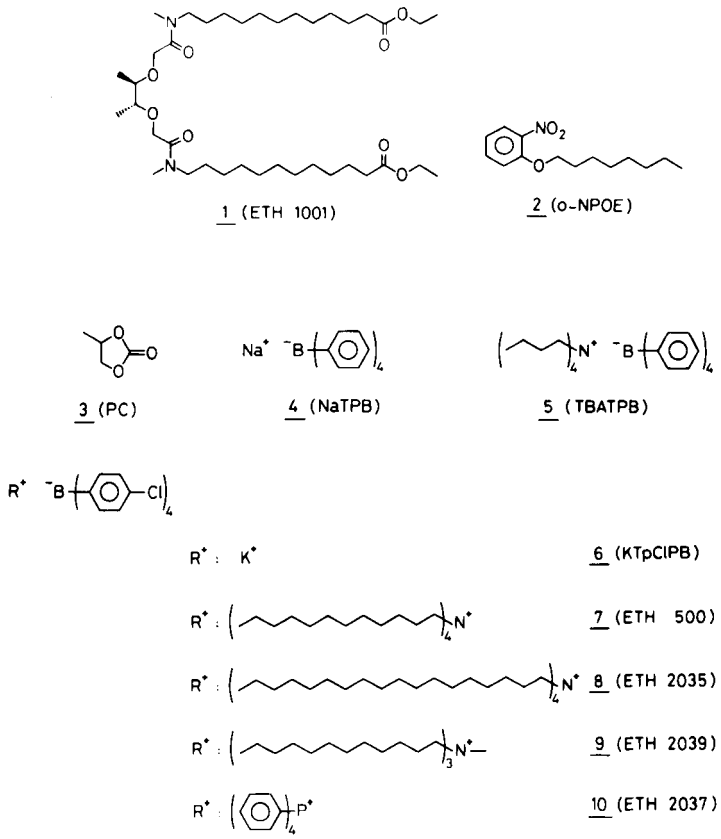

Fig. 1. Constitutions of the membrane components used.

salts (Fig. 1) were isolated in the following manner: NaTPB or KT*p*ClPB was dissolved or suspended in water and the bromide or the iodide salts of the onium ions were dissolved in chloroform. The two phases were vigorously shaken, the chloroform phase was separated and the solvent was evaporated to yield the lipophilic salts. The ^{1}H-n.m.r. spectra were in accordance with the expected structure of the salts. The elemental analysis results obtained (Mikroelementaranalytisches Laboratorium, ETH Zürich) were as follows. For tetradodecylammonium tetrakis(*p*-chlorophenyl)borate (ETH 500): calculated 75.3% C, 10.2% H, 1.2% N, 12.4% Cl; found 75.4% C, 10.2% H, 1.3% N, 12.2% Cl. For tetraoctadecylammonium tetrakis(*p*-chlorophenyl)-borate (ETH 2035): calculated 77.7% C, 11.1% H, 0.9% N; found 77.9% C, 11.3% H, 0.9% N. For methyltridodecylammonium tetrakis(*p*-chlorophenyl)borate (ETH 2039): calculated 73.7% C, 9.5% H, 1.4% N; found 73.3% C, 9.3% H, 1.4% N. For tetraphenylphosphonium tetrakis(*p*-chlorophenyl)borate (ETH 2037): calculated 72.4% C, 4.6% H; found 72.2% C, 4.6% H.

TABLE 2

Properties of microelectrodes based on different membrane solutions

Composition of membrane solution (% w/w)		Membrane resistance [GΩ]	Selectivity factors log K^{pot}_{CaK}	Detection limit (log a)
10	ETH 1001	32.3 ± 5.8	−5.5	−(7.6 ± 0.8)
1	NaTPB	(n = 10)		(n = 5)
89	o-NPOE			
	[12]			
7.4	ETH 1001	32.6 ± 5.9	−5.7	−(7.8 ± 0.3)
1.1	KTpClPB	(n = 5)		(n = 3)
24.8	ETH 500			
66.7	o-NPOE			
9	ETH 1001	5.8 ± 3.9	−4.7	−(6.8 ± 0.4)
1	KTpClPB	(n = 9)		(n = 7)
90	PC			

The compositions of the membrane solutions for Ca^{2+}-selective microelectrodes are listed in Table 2. Propylene carbonate (PC; purum) was obtained from Fluka.

Preparation of ion-selective electrodes

The solvent polymeric membranes prepared as described above were incorporated into Philips IS 561 electrode bodies [16]. Cell assemblies of the type Hg, Hg_2Cl_2, KCl(satd.)/3 M KCl/ sample solution //membrane// internal filling solution, AgCl, Ag were used. The internal filling solution was 0.1 M calcium chloride for macroelectrodes or a pCa 7 buffer solution [9] for the microelectrodes. The external macro reference electrode was a double-junction calomel electrode (Philips R44/2-SD/1).

The preparation of the microelectrodes was as described earlier [17]. Briefly, glass micropipettes were pulled from single-barrelled pyrex capillaries (GC 150 T-15; Clark) by using a Kopf vertical puller (Model 700). The micropipettes, covered with a glass beaker, were placed in an oven and predried at 150°C for 30 min. Then a small amount (about 0.1 ml) of *N*-trimethylsilyldimethylamine (Fluka, purum) was injected into the beaker. The glass surface was allowed to react for 30 min at 200°C with the vapour of the silanization reagent. The micropipettes were filled by means of a syringe and a fine plastic capillary. A small volume of the ion-selective membrane solution was back-filled into the shank of the microelectrode. The membrane solution moved spontaneously or was pushed by use of pressure into the very fine tip. The micropipette was then back-filled with the internal filling solution and a chlorinated silver wire was introduced to complete the microelectrode. For reference microelectrodes, unsilanized micropipettes were filled with 3 M potassium chloride by using a syringe with a small injection needle.

Examination of the membranes

Measurements of e.m.f. The e.m.f. measurements with macroelectrodes were done at 22 ± 1°C by using a 16-channel electrode monitor; each channel was equipped with a FET operational amplifier (AD-515-KH; Analog Devices, Norwood, MA; input impedance, $10^{13}\Omega$/2 pF; bias current, <150 fA; capacity neutralization). Data were acquired with an Intel Data System (Intel Corp., Santa Clara, CA) in combination with a display terminal, ADDS Regent 20 (Applied Digital Data Systems, Hauppauge, NY), a Wenger Print Swiss matrix printer (Wenger Datentechnik, Basel, Switzerland), and our own software.

The e.m.f. measurements with microelectrodes were made at 22 ± 1°C with a FET operational amplifier (AD 515 L, Analog Devices; input impedance $10^{13}\Omega$/1.6 pF differential, $10^{15}\Omega$/0.8 pF common mode; input bias current <75 fA; capacity neutralization). The amplifier was mounted on top of the electrode. The electrode assembly and other high-impedance components were located inside a Faraday cage.

Selectivity factors. Selectivity factors, log K^{pot}_{CaK}, were obtained by the fixed interference method [18]. The activity coefficients used have been described in detail [19]. To obtain the e.m.f. response curves (e.m.f. vs. log a_{Ca}), the experimental e.m.f. values were corrected for changes in the liquid junction potential by using the Henderson formula [19]. The calcium ion-electrode functions were measured from low to high calcium ion activities. The calcium ion buffer solutions containing a constant background of potassium ions (0.125 M) were prepared as described by Tsien and Rink [9]. All solutions were made with salts of high purity (Fluka or Merck) and water doubly-distilled from quartz apparatus.

Determination of membrane resistances. The membrane resistances of macro- and micro-electrodes were evaluated by the voltage divider method [20]. The method relies on recording of the voltage attenuation caused by a reference resistor in parallel with the electrode (Fig. 2). Depending on the polarization of the membrane during the resistance measurement, the response is changed drastically (Fig. 2) [21]. Therefore, only the ohmic potential drop (ΔE_{ohm} in Fig. 2) was taken for evaluation of the membrane resistances.

In some cases, the conductivity of the membrane solution was also measured by using a Philips PW-9501 conductivity meter and a specially designed micro conductivity cell (cell volume ca. 200 µl, cell constant 1.75 cm^{-1}; W. Möller, Glasbläserei, Zurich).

Scanning electron microscopy. Electron micrographs were run on a field-emission scanning electron microscope (Hitachi S-700). The micropipettes were coated with a 5-nm layer of Pt/C by rotational shadowing.

RESULTS AND DISCUSSION

The measured resistances of the solvent polymeric membranes with different compositions clearly indicate that the reduction of the membrane resis-

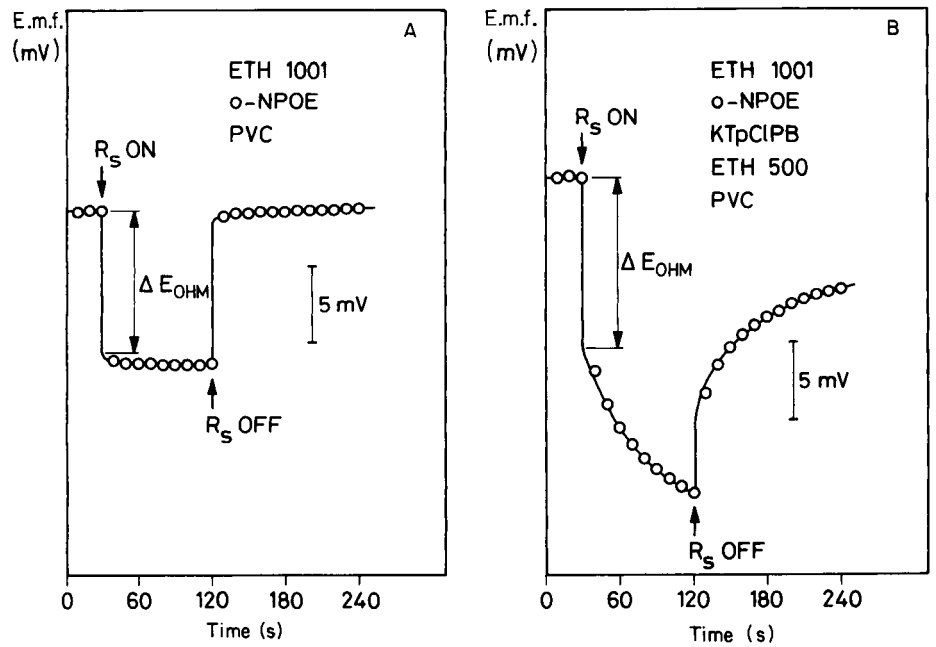

Fig. 2. Potential as a function of time during the determination of the membrane resistances by the voltage divider method: (A) membrane 5 in Table 1 and $R_s = 10^6$ Ω; (B) membrane 12 in Table 1 and $R_s = 10^5$ Ω. The arrows indicate the time when the resistor (R_s) in parallel was switched on or off.

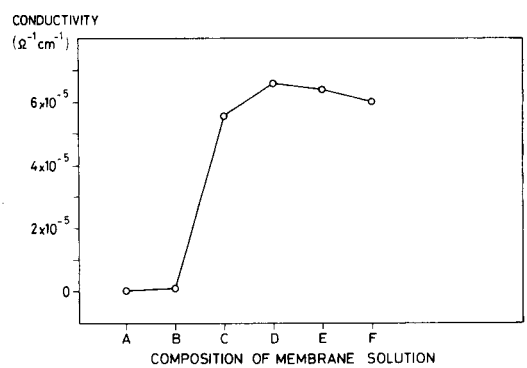

Fig. 3. Conductivity measurements on different membrane solutions: (A) *o*-NPOE; (B) A + ETH 1001 (10% w/w); (C) B + KT*p*ClPB (71% mol/mol); (D) C + ETH 500 (55% mol/mol); (E) D + ETH 500 (140% mol/mol); (F) E + ETH 500 (390% mol/mol). Solution B contained 10% (w/w) of the neutral carrier ETH 1001. The additions of salts in solutions C—F are given in % (mol/mol) relative to the carrier content.

tance by the addition of lipophilic salts into the membrane is limited (e.g., membranes 7—12, Table 1). The same conclusion has to be drawn from conductometric measurements on various membrane solutions (Fig. 3). This might be explained by the limited dissociation of these salts in *o*-NPOE. No further decrease of the resistance could be achieved by the use of different lipophilic salts (membranes 13—16 compared to membrane 11, Table 1). An almost complete loss of the electrode performance occurred when the cation of the salt was rather hydrophilic. For example, membranes with a content of more than 100% (mol/mol) KT*p*ClPB or TBATPB (Fig. 1) yield cation-exchanger properties or deteriorated response, respectively (membranes 16, 17 compared to membrane 2). Further, the membrane electrodes containing TBATPB suffered from a drastic change in the reference potential (E_0) and the slope as a function of time, and the measured potential was heavily dependent on the stirring rate. This might indicate that the poorly lipophilic tetrabutylammonium ions are replaced in the membranes by the more lipophilic calcium complexes of the neutral carrier.

The carrier concentration of the membrane has a significant effect on the membrane resistance only in the absence of lipophilic salts (membrane 1 compared to membrane 5). However, in the presence of lipophilic salts (e.g., ETH 500), the membrane resistance is almost independent of the carrier concentration (membrane 4 compared to membrane 11).

With respect to resistivity, membrane 2 remains the most attractive neutral carrier-based calcium-selective membrane. By using highly lipophilic salts as additives, the membrane resistance can be reduced further by a factor of 2—3 (membrane 4 compared to membrane 2 or membrane 12 compared to membrane 6). The lowest resistances finally obtained are only slightly higher than those of typical macro reference electrodes. A further advantage becomes obvious by comparing the electrode response functions (Fig. 4A and Table 1). The detection limit is shifted in the direction of lower calcium activities, being near $\log a_{Ca} = -7.1$ without additive (membrane 1, Table 1), −8.6 with KT*p*ClPB added (membrane 2), and −9.2 with KT*p*ClPB and ETH 500 added (membrane 12).

The same trend was observed for microelectrodes (Fig. 4B, Table 2), although they exhibited poorer detection limits than the corresponding macroelectrodes. Unfortunately, the membrane resistance of the membrane solution used previously [12] could not be decreased by the addition of large amounts of the lipophilic salt ETH 500 (Table 2). The additive has a beneficial effect on the resistivity only if the polarity of the membrane solvent is simultaneously increased drastically (propylene carbonate has a dielectric constant of 64.9 at 25°C [22]). However, other electrode characteristics were clearly worse than in the case of membrane electrodes containing *o*-NPOE (Table 2).

The deviations of the measured resistances of individual microelectrodes containing the same membrane solution (Table 2) are probably caused by the poor reproducibility of the microelectrode geometry. In order to

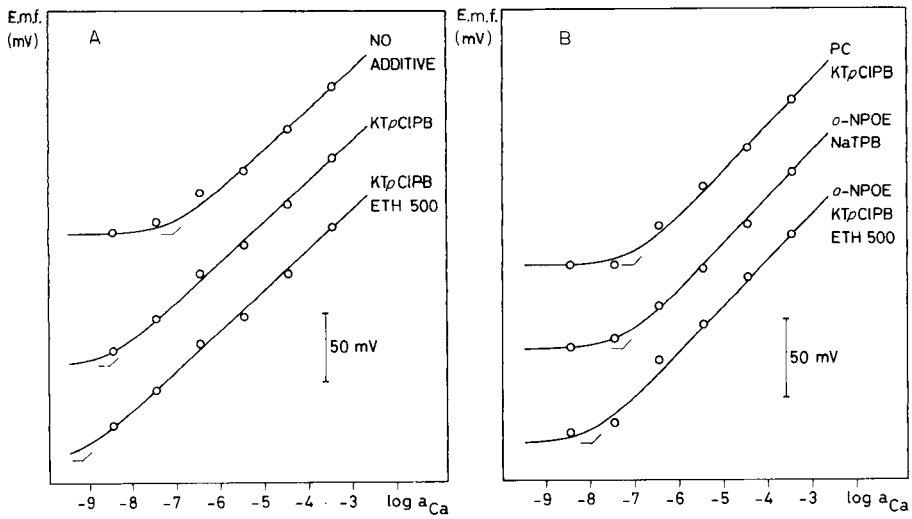

Fig. 4. Electrode functions in Ca^{2+}-buffered solutions with a constant background of 125 mM K^+: (A) macroelectrodes; (B) microelectrodes. The detection limits indicated depend on the composition of the membrane solutions (see text). —7.0 log a_{Ca} (PC/KT*p*ClPB, Table 2), —7.2 log a_{Ca} (*o*-NPOE/NaTPB, Table 2), and —8.0 log a_{Ca} units (*o*-NPOE/KT*p*ClPB/ETH 500, Table 2).

estimate the uncertainty of the microelectrode preparation technique, several reference microelectrodes were prepared and their membrane resistances were measured (3.5 M KCl reference electrolyte, saturated with silver chloride). The resistances were in the range of 10 MΩ and the day-to-day reproducibility of the mean was about 15%. Scanning electron micrographs of several micropipettes proved that the tip diameters of the microelectrodes used in this study were 0.3—0.5 μm (Fig. 5).

In conclusion, the addition of large amounts of highly lipophilic salts to the membrane phase somewhat lowers the electrical membrane resistance of macroelectrodes for calcium ion but has no effect in the case of the corresponding microelectrodes. The detection limits are slightly improved for both the macro- and micro-electrodes. It seems that the addition of these salts enables the content of the neutral carrier in membrane solutions to be reduced drastically for microelectrodes.

We thank Dr. E. Wehrli, Department of Cell Biology, Swiss Federal Institute of Technology, Zurich, for making the electron micrographs. This work was partly supported by the Swiss National Science Foundation.

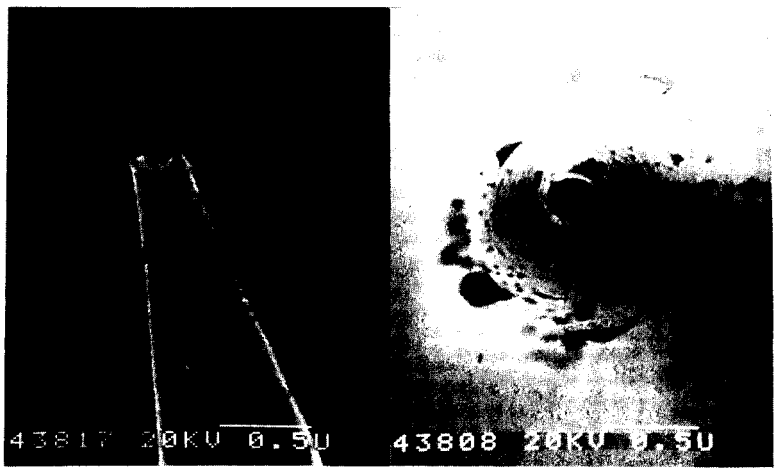

Fig. 5. Scanning electron micrographs of a typical single-barrelled microelectrode used in this work. The micropipette is coated with a ca. 5.0-nm Pt/C layer. The estimated tip diameter is 0.28 μm (scale 0.5 μm; magnification ca. 50 000).

REFERENCES

1 W. E. Morf, The Principle of Ion-Selective Electrodes and of Membrane Transport, Akadémiai Kiadó, Budapest, 1981.
2 D. Ammann, W. E. Morf, P. Anker, P. C. Meier, E. Pretsch and W. Simon, Ion-Selective Electrode Rev., 5 (1983) 3.
3 P. C. Meier, W. E. Morf, M. Läubli and W. Simon, Anal. Chim. Acta, 156 (1984) 1.
4 E. Pretsch, D. Wegmann, D. Ammann, A. Bezegh, O. Dinten, M. W. Läubli, W. E. Morf, U. Oesch, K. Sugahara, H. Weiss and W. Simon, in M. Kessler, D. K. Harrison and J. Höper (Eds.), Recent Advances in the Theory and Application of Ion-Selective Electrodes in Physiology and Medicine, Springer-Verlag, Berlin, 1985.
5 K. Cammann and G. A. Rechnitz, Anal. Chem., 48 (1976) 856.
6 M. Koebel, N. Ibl and A. M. Frei, Electrochim. Acta, 19 (1974) 287.
7 G. Horvai, T. A. Nieman and E. Pungor, Fourth Scientific Session on Ion-Selective Electrodes, October, Matrafüred, Hungary, 1984.
8 S. A. Lewis and N. K. Wills, Biophys. J., 31 (1980) 127.
9 R. Y. Tsien and T. J. Rink, J. Neurosci. Methods, 4 (1981) 73.
10 R. A. Steiner, M. Oehme, D. Ammann and W. Simon, Anal. Chem., 51 (1979) 351.
11 P. Wuhrmann, H. Ineichen, U. Riesen-Willi and M. Lezzi, Proc. Natl. Acad. Sci., 76 (1979) 806.
12 M. Oehme, M. Kessler and W. Simon, Chimia, 30 (1976) 204.
13 D. Ammann, in D. W. Lübbers, H. Acker, R. P. Buck, G. Eisenman, M. Kessler and W. Simon (Eds.), Progress in Enzyme and Ion-Selective Electrodes, Springer-Verlag, Berlin, 1981, p. 194.
14 D. Ammann, F. Lanter, R. Steiner, D. Erne and W. Simon, in E. Syková, O. Hník and L. Vyklický (Eds.), Ion-Selective Microelectrodes and Their Use in Excitable Tissue, Plenum Press, New York, 1981, p. 13.
15 P. Anker, E. Wieland, D. Ammann, R. E. Dohner, R. Asper and W. Simon, Anal. Chem., 53 (1981) 1970.
16 W. Simon, D. Ammann, M. Oehme and W. E. Morf, Ann. N.Y. Acad. Sci., 307 (1978) 52.

17 F. Lanter, R. A. Steiner, D. Ammann and W. Simon, Anal. Chim. Acta, 135 (1982) 51.
18 G. G. Guilbault, R. A. Durst, M. S. Frant, H. Freiser, E. H. Hansen, T. S. Light, E. Pungor, G. Rechnitz, N. M. Rice, T. J. Rohm, W. Simon and J. D. R. Thomas, Pure Appl. Chem., 48 (1976) 127.
19 P. C. Meier, D. Ammann, W. E. Morf and W. Simon, in J. Koryta (Ed.), Medical and Biological Applications of Electrochemical Devices, Wiley, Chichester, 1980, p. 13.
20 R. D. Purves, Microelectrode Methods for Intracellular Recording and Ionophoresis, Biological Technique Series, Vol. 6, Academic Press, London, 1981.
21 K. J. Vetter, Elektrochemische Kinetik, Springer-Verlag, Berlin, 1961.
22 W. H. Lee, in The Chemistry of Nonaqueous Solvents, J. J. Lagowski (Ed.), Academic Press, New York, 1976.

Analytica Chimica Acta, 171 (1985) 131—139
Elsevier Science Publishers B.V., Amsterdam — Printed in The Netherlands

POTENTIOMETRIC MONITORING OF PROTEINS
Part 1. Introduction and Theory for a Silver Electrode

MICHAEL L. HITCHMAN[a]

Department of Chemistry and Applied Chemistry and Thin Film and Surface Research Centre, University of Salford, Salford M5 4WT (Great Britain)

(Received 24th August 1984)

SUMMARY

A brief survey of methods for monitoring of proteins is given, and the relative advantages and disadvantages of potentiometry are considered. A theoretical model is presented for direct potentiometric monitoring of a thiol-containing protein with a silver electrode. The model is used to indicate ways of improving the reproducibility and response of the electrode.

Protein determinations are of great interest in diverse fields, and many methods have been developed, particularly with a view to routine, automated procedures [1]. Spectrophotometry in the near u.v. region (260—280 nm) is extensively used for the assay of protein in solution [2, 3], but the method suffers from the drawbacks of not being reliable for small-scale operations and of not having adequate sensitivity for protein concentrations of $<100\,\mu g\,ml^{-1}$. The turbidimetric method [4—6] overcomes some of these disadvantages but is prone to interferences and is destructive. The Kjeldahl method was the first well known, routine method for protein determination [5] but, of course, it gives positive results for many nitrogen-containing compounds. The use of pulsed n.m.r. [7] is more selective for proteins but n.m.r. requires relatively large samples as well as expensive equipment. The classical biuret method [5, 8, 9], the Lowry method [10, 11] and other colour-producing techniques [12] are widely used and can be automated [13], but they are all destructive methods and are subject to various interferences [12]. Obviously, there is scope for exploring new methods of monitoring proteins. In particular, there is a need for simple, reliable, rapid and inexpensive methods capable of application to small volumes, e.g., for monitoring proteins eluting from h.p.l.c. columns.

Electrochemical methods have long been established for routine monitoring; in particular, significant recent interest has been shown in such methods for use with liquid chromatography [14]. The feasibility of using electrochemi-

[a]Present address: Department of Pure and Applied Chemistry, University of Strathclyde, Thomas Graham Building, 295 Cathedral Street, Glasgow G11XL, Great Britain.

0003-2670/85/$03.30

cal methods for monitoring proteins would therefore seem to be worthwhile examining further. Numerous reports of protein monitoring by polarography have been published. Two types of polarographic wave can be distinguished depending on the kind of solution used, but in both cases the waves correspond to a catalytic process. In buffered solutions, proteins show a distinct wave at a potential just anodic of that expected for the electrolytic reduction of alkali metal cations; even for very dilute protein solutions, the wave height is related almost linearly to the protein concentration [15—17]. The second type of wave is observed when the supporting electrolyte contains a cobalt or nickel salt (the Brdicka reaction) [18—21]; the relationship between wave (or peak) height and protein concentration is less simple in this case and the method is unsuitable for routine work.

Direct amperometry with solid electrodes does not appear to have been studied for protein solutions, but indirect amperometry has been reported. For example, amperometric titrations have been done with silver(I), mercury(II) and organomercury compounds as titrants [22], and with coulometric generation of silver(I) [23], or hypobromite or bromine [24]. The coulometric generation of hypobromite has been extended to titrations of proteins at ring-disc and double-tubular electrodes [25]. Amperometric methods are relatively simple, are capable of high precision and can be readily automated. When coupled with coulometric generation, they offer an interesting possibility for monitoring proteins in h.p.l.c., particularly if a double tubular electrode is used [25].

Potentiometry is even simpler and is the most extensively reported electrochemical method for protein monitoring. Toribara and Koval [26] showed that a silver wire immersed in a solution of a thiol, such as albumin, produced a Nernstian dependence of potential on concentration. Tseng and Gutknecht [27] also obtained a Nernstian response for a silver sulphide membrane electrode in various thiol solutions, and D'Orazio and Rechnitz [28] showed that such an electrode could be used selectively for monitoring thiol-containing proteins, although the response was not always Nernstian. Alexander and Rechnitz [29] used a silver sulphide electrode for direct monitoring of the free silver ion concentration after a known excess of silver(I) had been added to solutions of thiol-containing proteins; the potential was then related to the protein concentration. In principle, direct potentiometry would appear to be a very simple method for protein monitoring, but the method suffers from the problems of very sluggish response to changes in protein concentration, poor reproducibility, and a marked dependence of potentials on the history and pretreatment of the electrodes.

The problem of poor reproducibility of potentials can be overcome by titrating the protein and monitoring the end-point with an electrode sensitive to the titrant [30]. Thus, Toribara and Koval [26] reported direct potentiometry of proteins with a silver wire, but preferred to use indirect potentiometric monitoring. Gruen and Harrap [31] used a silver sulphide membrane electrode with silver(I) as the titrant for thiols; Selig [32] used a halide-selective electrode and mercury(II) as titrant. The problem of slow response

of indicator electrodes in the presence of proteins still remains in potentiometric titrations.

For both direct and indirect potentiometry, electrodes with a faster response to changes in protein concentration are required. For direct potentiometry, which would be preferred for small volumes, better reproducibility is needed. A study of direct potentiometry for protein determinations is reported in this series of papers. The present paper is concerned with a theoretical model for the potential behaviour of a silver electrode in contact with a thiol-containing protein. On the basis of this model, ways are suggested for improving the reproducibility and response of the electrode. Some preliminary results have already been reported [33].

THEORY

Steady-state potential and its attainment

When a silver wire is immersed in a thiol solution, its potential depends on the thiol concentration [26]. The response of the electrode arises from two reactions

$$RSH(aq) \overset{K}{\rightleftharpoons} RS^-(aq) + H^+(aq); \quad Ag(s) + RS^-(aq) \rightleftharpoons AgSR(s) + e^-$$

The coating of insoluble silver-thiol complex on the silver surface provides an electrode of the second kind, the relevant form of the Nernst equation being [26]

$$E = E^0 + 0.059\ pK - 0.059\ pH - RTF^{-1} \ln [RSH] \qquad (1)$$

This equation predicts a gradient of −59 mV per decade change in thiol concentration at 25°C for a simple thiol (e.g., L-cysteine) at constant pH and a shift of −59 mV per pH unit at constant thiol concentration. If the silver acts as an electrode of the first kind [34] then the equation will include the solubility product of the silver-thiol complex, but the overall behaviour of the equilibrium potential will remain the same.

D'Orazio and Rechnitz [28] showed unequivocally that a silver sulphide membrane electrode responded to thiol-containing proteins, and one would expect similar behaviour for a silver wire. The reactions for proteins can be considered as

$$R(SH)_x(aq) \overset{K'}{\rightleftharpoons} R(S^-)_x(aq) + xH^+(aq);$$

$$xAg(s) + R(S^-)_x(aq) \rightleftharpoons (AgS)_xR(s) + xe^-$$

where x is the number of thiol groups in one molecule of protein. The equation analogous to Eqn. 1 will be

$$E = E^0 + (0.059/x)pK' - 0.059\ pH - (RT/xF)\ln [R(SH)_x] \qquad (2)$$

At constant thiol concentration, the potential will still shift to more negative values by −59 mV per pH unit as before, but the slope of the potential vs. log [protein] plot will depend on the number of thiol groups in the protein.

Numerous publications have dealt with the theory of the dynamic response of ion-selective electrodes to step changes in concentration [34—40]. All these models are, however, for membrane electrodes in which ionic species have to enter the membrane so that a diffusion layer is formed at the membrane surface. Transport through such a layer can be the rate-limiting step when the concentration of the active ion changes, and long times may be needed to achieve steady-state concentration profiles and interfacial potentials. In the case of a solid metal electrode, if the electron transfer is rapid enough to cause depletion in the solution adjacent to the interface, then equilibrium will be rapidly established and relaxation of the solution concentration gradients by diffusion will also occur rapidly, especially in stirred solutions. This would be the case if the silver acted as an electrode of the first kind, because the Ag^+/Ag equilibrium is very readily reversible [41]. If, in contrast, the electron transfer were slow then there would be no depletion and no boundary layer close to the electrode surface. It is therefore unlikely that there would be any transport limitation on the attainment of a steady-state potential for a solid electrode. The reactions outlined above both require the adsorption of an aqueous thiol anion onto the solid silver surface, and this could well be a slow step.

For convenience in considering such a slow adsorption, a simple thiol is taken as an example

$$Ag(s) + RS^-(aq) \underset{k_{dT}}{\overset{k_{aT}}{\rightleftharpoons}} AgSR(s) + e^-$$

where k_{aT} ($cm^3\ s^{-1}$) is the adsorption rate constant for the thiol anion, k_{dT} (s^{-1}) is the desorption rate constant. In the following theoretical development, θ_{Tt} is defined as the fraction of surface sites covered by adsorbed thiol anions at time t, $(1 - \theta_{Tt})$ is the fraction of sites not covered, and n_T is the concentration of thiol anions in solution. The anion concentration, n_T, is assumed to remain constant; this is a justifiable assumption provided that the ratio of the electrode surface to the solution volume is not too large, even if the surface becomes completely covered with a monolayer. The net rate of adsorption (s^{-1}) of thiol anion at time t is then given by

$$d\theta_{Tt}/dt = k_{aT}n_T - \theta_{Tt}\,(k_{aT}n_T + k_{dT}) \tag{3}$$

This equation as it stands represents a simple adsorption/desorption process. The equilibrium is complicated, however, by the fact that there will be an interfacial potential difference ($\Delta\phi$) between the electrode surface and the solution and that a charged species will be crossing the electrical double layer associated with this potential difference. Thus there will be an effect of the electric field at the interface on the rate of adsorption and desorption. This effect can be considered, as in electrode kinetics, by writing the rate constants as potential-dependent [42]

$$d\theta_{Tt}/dt = n_T k^0_{aT}\exp[(1-\beta)F\Delta\phi_t/RT] - \theta_{Tt}\{n_T k^0_{aT}\exp[(1-\beta)F\Delta\phi_t/RT] + k^0_{dT}\exp[-\beta F\Delta\phi_t/RT]\} \tag{4}$$

where β is the symmetry factor [34] with a value in the range 0—1 and which represents the fraction of the interfacial potential difference, $\Delta\phi$, that is involved in taking the reduction process (i.e., desorption) from the initial state to the transition state. The pre-exponential terms k^0_{aT} and k^0_{dT} are ordinary chemical rate constants corresponding to zero field ($\Delta\phi = 0$) conditions. The subscript t on $\Delta\phi$ indicates that the interfacial potential is time-dependent.

When equilibrium is achieved, the net rate of change of surface coverage is zero and θ_T and $\Delta\phi$ will have equilibrium values represented by θ_{Te} and $\Delta\phi_e$, respectively. Under these conditions, Eqn. 4 can be written as

$$\Delta\phi_e = (RT/F)\ln(1/K_T)[\theta_{Te}/(1-\theta_{Te})] + (RT/F)\ln(1/n_T) \tag{5}$$

where $K_T = k^0_{aT}/k^0_{dT}$ and is the chemical equilibrium constant for the adsorption/desorption process. Equation 5 in terms of the equilibrium interfacial potential difference, derived on a kinetic basis, has the same form as Eqn. 1 derived on a thermodynamic basis, for the potential dependence on thiol concentration.

As the coverage of the surface by thiol anion changes, the interfacial potential difference will obviously also change. If the double-layer capacitance (C_{DL}) is assumed to remain constant, and this is likely in the presence of background electrolyte, then adsorption of the anion can be described by

$$I_{DL} = -C_{DL}\mathrm{d}\Delta\phi_t/\mathrm{d}t \tag{6}$$

where I_{DL} is the double-layer charging current. The total charge (Q_t) flowing during the double-layer charging will be

$$Q_t = \int_0^t I_{DL}\mathrm{d}\tau = C_{DL}(\Delta\phi_0 - \Delta\phi_t) \tag{7}$$

Further, Q_t can be related to the amount of thiol adsorbed:

$$Q_t = (FAn/L)(\theta_{Tt} - \theta_{T0}) \tag{8}$$

where subscript 0 refers to zero time and L is Avogadro's number.

Rearrangement of Eqns. 4, 7 and 8 yields

$$\begin{aligned}\mathrm{d}\Delta\phi_t/\mathrm{d}t = &-(FAn/LC_{DL})\{n_T k^0_{aT}\exp[(1-\beta)F\Delta\phi_t/RT] \\ &- [(LC_{DL}/FAn)(\Delta\phi_0 - \Delta\phi_t) + \theta_{T0}][n_T k^0_{aT}\exp[(1-\beta)F\Delta\phi_t/RT] \\ &+ k^0_{dT}\exp[-\beta F\Delta\phi_t/RT]]\}\end{aligned} \tag{9}$$

The overpotential, defined as $\eta = \Delta\phi_t - \Delta\phi_e$, is a measure of how far the interfacial potential is from the equilibrium value. With introduction of this parameter, Eqn. 9 becomes

$$\begin{aligned}\mathrm{d}\eta/\mathrm{d}t = &-(FAn/LC_{DL})\{n_T k^0_{aT}[(1-\theta_{Te}) + (LC_{DL}/FAn)\eta] \\ &\times \exp[(1-\beta)F\Delta\phi_e/RT]\exp[(1-\beta)F\eta/RT] - k^0_{dT}[\theta_{Te} - (LC_{DL}/FAn)\eta] \\ &\times \exp[-\beta F\Delta\phi_e/RT]\exp[-\beta F\eta/RT]\}\end{aligned} \tag{10}$$

where $\theta_{Te} = \theta_{T0} + (LC_{DL}/FAn)(\Delta\phi_0 - \Delta\phi_e)$. Equation 10 cannot readily be integrated, but as equilibrium is approached, $\Delta\phi_t/\Delta\phi_e \to 1$ or $\eta \to 0$ and the exponential terms containing η can be expanded

$$(d\eta/dt)_{\eta\to 0} \cong -(FAn/LC_{DL})\{n_T k^0_{aT}[(1-\theta_{Te}) + \eta((1-\beta)(1-\theta_{Te})F/RT + LC_{DL}/FAn)]\exp[(1-\beta)F\Delta\phi_e/RT] - k^0_{dT}[\theta_{Te} - \eta(\beta F\theta_{Te}/RT + LC_{DL}/FAn)]\exp[-\beta F\Delta\phi_e/RT]\} \quad (11)$$

The terms in η^2 have been omitted from this equation because $\eta \to 0$. It has been found in practice [33] that the electrode potential approaches the equilibrium value asymptotically, i.e., as $t \to \infty$ and $\eta \to 0$, $d\eta/dt \to 0$. Thus

$$n_T k^0_{aT}(1-\theta_{Te})\exp[(1-\beta)F\Delta\phi_e/RT] = k^0_{dT}\theta_{Te}\exp[-\beta F\Delta\phi_e/RT] \quad (12)$$

The two terms in this equation have units of s^{-1} and they represent the equal and opposite frequencies at which adsorption and desorption occur at equilibrium. They are equivalent to the standard rate constant associated with the exchange current density of electrode kinetics, and can be called the exchange frequency, k^0. Equation 11 becomes on using k^0

$$(d\eta/dt)_{\eta\to 0} \cong -(FAn/LC_{DL})k^0[F/RT + LC_{DL}/FAn\theta_{Te}(1-\theta_{Te})]\eta \quad (13)$$

Integration with the boundary condition of $t = 0$, $\eta = \eta_0$ gives

$$\ln(\eta/\eta_0) \cong -(FAn/LC_{DL})k^0[F/RT + LC_{DL}/FAn\theta_{Te}(1-\theta_{Te})]t$$

or

$$\eta/\eta_0 \cong \exp\{-(FAn/LC_{DL})k^0[F/RT + LC_{DL}/FAn\theta_{Te}(1-\theta_{Te})]t\} \quad (14)$$

This equation has the form of a first-order rate equation and is valid for the reaction at a pure silver electrode; clearly, the larger the exchange frequency (i.e., the more reversible the system) the more rapid will be the attainment of equilibrium, as would be expected. The exchange frequency will depend on the nature of the surface and will be diminished by poisoning of the surface. Cleaning of the surface before a measurement would be expected to activate the surface sites and therefore to lead to more reproducible and rapidly attained equilibrium potentials. Precleaning of the surface could also improve the electrode response in other ways.

Surface with two types of active site

Toribara and Koval [26] mentioned that chemical cleaning with ammonia solution (1 + 3) of a silver wire used for monitoring the end-point in potentiometric titrations of thiols improved the response of the electrode. This cleaning would remove a surface film (silver adsorbate) as the soluble silver diammine complex. Such a silver adsorbate should be equally well removed by cathodic reduction to silver metal. Whatever method of cleaning is used, there may still be some sites covered with AgX, and the potential-determining equilibrium, $Ag + RS^- \rightleftharpoons AgSR + e^-$, could be considered as occurring on a silver site surrounded by other silver sites or on a silver site with AgX

nearby. The true situation must be complicated but there will obviously be different sites with different activities, though the product of the reaction, a silver thiolate, is the same in all cases. The rate of attainment of the potential-determining equilibrium will depend on the type of site at which it occurs, but the final fraction of equilibrium sites will not be changed. The situation for a virgin silver site is explained by Eqn. 14. For a silver site affected by AgX, this equation can be rewritten as

$$\eta/\eta_0 \cong \exp\{-(FAn/LC_{DL})k^0_X[F/RT + LC_{DL}/FAn\theta_{TXe}(1-\theta_{TXe})]t\} \qquad (15)$$

where the X subscript indicates an adulterated site. Because the final equilibrium, reached by parallel processes, will be identical for both sorts of site, Eqns. 14 and 15 differ only in the exchange frequencies. By analogy with the treatment of two independent parallel first-order reactions with a common product [43], it should be possible to describe the variation of potential with time by a linear combination of Eqns. 14 and 15.

$$\eta/\eta_0 \cong p\exp(-ak^0_S t) + q\exp(-ak^0_X t) \qquad (16)$$

where a has the form $a = (FAn/LC_{DL})[F/RT + LC_{DL}/FAn\theta_e(1-\theta_e)]$, and p and q are coefficients to be evaluated. When $t = 0$, $\eta/\eta_0 = 1$ and so $p + q = 1$. For the case of parallel first-order processes, the coefficients in the linear combination of the equations for the two separate reactions are the initial concentrations of the different reactants [43]. Continuing the use of this analogy suggests that $p = \theta_{S0} + \theta_{T0}$ and $q = \theta_{SX0} + \theta_{TX0}$, where θ_{S0} and θ_{T0} are the fractions of unreacted and reacted pure silver sites at zero time and subscript X indicates an affected site. Thus Eqn. 16 becomes

$$\eta/\eta_0 \cong (\theta_{S0} + \theta_{T0})\exp(-ak^0_S t) + [1-(\theta_{S0} + \theta_{T0})]\exp(-ak^0_X t) \qquad (17)$$

Inspection of this equation shows it to have the correct form within the limits when the surface is either free from Ag/AgX sites or is completely dominated by them. Because cleaning the surface of the electrodes improves its rate of response [26, 33], this indicates that the rate is faster on Ag/Ag sites than on Ag/AgX sites. This is as would be expected, as steric hindrance, for example, could inhibit the formation of a silver-thiol complex in the vicinity of AgX. Figure 1 shows the effect of cleaning on the approach of the electrode potential to equilibrium for given site activities, and Fig. 2 shows the effect of a higher exchange frequency for a clean surface with only Ag/Ag sites.

Effects of pre-anodisation

The general potential-determining equilibrium is similar to that for a reference electrode, such as a silver/silver chloride electrode: $AgCl(s) + e^- \rightleftharpoons Ag(s) + Cl^-(aq)$. Such electrodes are usually prepared by anodising a silver electrode in a chloride solution to form a coating of silver chloride. It would seem reasonable, therefore, to anodise the silver in the thiol solution rather than just rely on direct interaction between the thiol anion and the silver. Making a Ag/AgSR electrode, however, would be less easy than making a Ag/AgCl

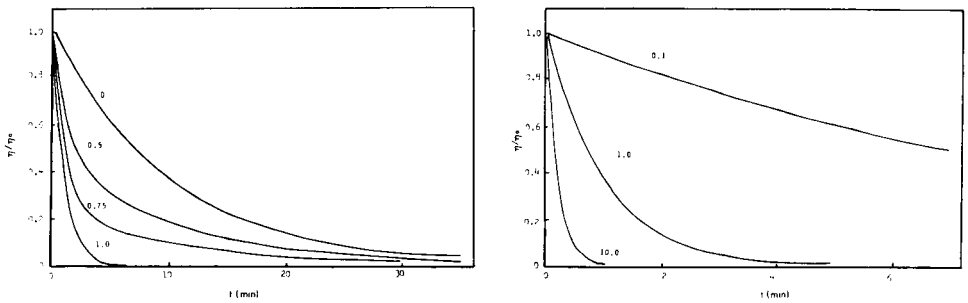

Fig. 1. Effect of cleaning on the approach of electrode potential to equilibrium. The curves were calculated by using Eqn. 17 with $ak_S^0 = 1\ min^{-1}$, $ak_X^0 = 0.1\ min^{-1}$ and for various fractional coverages of the surface. The fractional coverages ($\theta_{S_0} + \theta_{T_0}$) are given on the curves.

Fig. 2. Effect of exchange flux on the approach of electrode potential to equilibrium. The curves were calculated by using Eqn. 17 with ($\theta_{S_0} + \theta_{T_0}$) = 1. The numbers on the curves are values of k_S^0.

electrode, because other anions present (e.g., from a buffer) could compete with the RS^- ions for silver sites during anodisation. Even if such an electrode were prepared, inspection of Eqn. 17 shows that the rate of attainment of equilibrium will not necessarily be changed. Anodisation will increase the fraction (θ_{T0}) of thiol sites at the expense of the fraction (θ_{S0}) of silver sites, but the sum ($\theta_{S0} + \theta_{T0}$) remains constant. However, if anodisation is preceded by cleaning, the potential stabilization time should be further reduced because formation of a silver thiolate on a silver site directly after cleaning will reduce the changes of reformation of AgX and ($\Theta_{S0} + \Theta_{T0}$) will increase towards unity.

Practical application of these considerations are discussed in a subsequent paper [44].

REFERENCES

1 R. G. Martinek, J. Am. Med. Technol., 32 (1977) 177.
2 E. Layne, in S. P. Colowick and N. O. Kaplan (Eds.), Methods in Enzymology, Vol. III, Academic Press, New York, 1957, p. 417.
3 J. B. Murphy and M. W. Kies, Biochem. Biophys. Acta, 45 (1960) 382.
4 O. Folin and W. Dewnis, J. Biol. Chem., 18 (1914) 273.
5 J. M. Clark, Experimental Biochemistry, W. H. Freeman, San Francisco, 1964, p. 75.
6 D. V. Tappan, Anal. Biochem., 14 (1966) 171.
7 B. A. Coles, J. Am. Oil Chem. Soc., 57 (1980) 202.
8 T. E. Weichselbaum, Am. J. Chim. Pathol., 16 (1946) 40.
9 R. H. Haschemeyer and A. E. V. Haschemeyer, Proteins: A Guide to Study by Physical and Chemical Methods, Wiley-Interscience, New York, 1973.
10 O. H. Lowry, N. J. Roseborough, A. L. Farr and R. J. Randall, J. Biol. Chem., 193 (1951) 265.
11 M. R. V. Murphy and T. Leroux, Anal. Biochem., 64 (1975) 18.
12 W. T. Caraway and C. W. Kammeyer, Clin. Chim. Acta, 41 (1972) 395.

13 K. Doetsch, Clin. Chem., 18 (1972) 296.
14 R. J. Rucki, Talanta, 27 (1980) 147.
15 R. Brdicka, M. Brezina and V. Kalous, Talanta, 12 (1965) 1149.
16 R. Brdicka, Collect. Czech. Chem. Commun., 8 (1936) 366.
17 M. Brezina and P. Zuman, Polarography in Medicine, Biochemistry and Pharmacy, Interscience, New York, 1958.
18 R. Brdicka, Collect. Czech. Chem. Commun., 5 (1933) 112.
19 O. H. Muller, in D. Glick (Ed.), Methods of Biochemical Analysis, Vol. 11, Interscience, New York, 1963, p. 329.
20 J. Homolka, in D. Glick (Ed.), Methods of Biochemical Analysis, Vol. 19, Interscience, New York, 1971, p. 435.
21 E. Palecek and Z. Pechan, Anal. Biochem., 42 (1971) 59.
22 R. Benesch and R. E. Benesch, in D. Glick (Ed.), Methods of Biochemical Analysis, Vol. 10, Interscience, New York, 1962, p. 43.
23 J. H. Ladenson and W. C. Purdy, Anal. Chim. Acta, 57 (1971) 365; 64 (1973) 259.
24 G. D. Christian, Anal. Biochem., 14 (1966) 183.
25 W. J. Albery, R. Svanberg and P. Wood, J. Electroanal. Chem., 162 (1984) 29, 45.
26 T. Y. Toribara and L. Koval, Talanta, 17 (1970) 1003.
27 P. K. C. Tseng and W. F. Gutknecht, Anal. Chem., 47 (1975) 2316.
28 P. D'Orazio and G. A. Rechnitz, Anal. Chem., 49 (1977) 41.
29 P. W. Alexander and G. A. Rechnitz, Anal. Chem., 46 (1974) 250, 860.
30 R. Cecil and J. R. McPhee, in C. B. Anfinsen, M. L. Anson, K. Bailey and J. T. Edsall (Eds.), Advances in Protein Chemistry, 14 (1959) 255.
31 L. C. Gruen and B. S. Harrap, Anal. Biochem., 42 (1971) 377.
32 W. Selig, Mikrochim. Acta, 3 (1973) 453.
33 M. L. Hitchman, F. W. M. Nyasulu, A. Aziz and D. D. K. Chingakule, Anal. Chim. Acta, 155 (1983) 219.
34 R. P. Buck, in H. Freiser (Ed.), Ion Selective Electrodes in Analytical Chemistry, Vol. 1, Plenum Press, New York, 1978, pp. 37, 117.
35 G. A. Rechnitz and H. F. Hameka, Z. Anal. Chem., 214 (1965) 252.
36 G. Johansson and K. Norberg, J. Electroanal. Chem., 18 (1968) 239.
37 K. Toth and E. Pungor, Anal. Chim. Acta, 64 (1973) 417.
38 W. E. Morf, E. Lindner and W. Simon, Anal. Chem., 47 (1975) 1596.
39 A. Shatkay, Anal. Chem., 48 (1976) 1039.
40 W. E. Morf and W. Simon, in H. Freiser (Ed.), Ion Selective Electrodes in Analytical Chemistry, Vol. 1, Plenum Press, New York, 1978, p. 246.
41 K. J. Vetter, Electrochemical Kinetics, Academic Press, New York, 1967, p. 668.
42 J. O'M. Bockris and A. K. N. Reddy, Modern Electrochemistry, Vol. 2, Plenum, New York, 1970, Ch. 8.
43 A. A. Frost and R. G. Pearson, Kinetics and Mechanism, Wiley, New York, 1961.
44 M. L. Hitchman, A. Aziz, D. D. Chingakule and F. W. M. Nyasulu, Anal. Chim. Acta, 171 (1985) 141.

Analytica Chimica Acta, 171 (1985) 141—150
Elsevier Science Publishers B.V., Amsterdam — Printed in The Netherlands

POTENTIOMETRIC MONITORING OF PROTEINS
Part 2. Results with Electrochemical Cleaning of a Silver Electrode

M. L. HITCHMAN*[a], A. AZIZ, D. D. K. CHINGAKULE and F. W. M. NYASULU

Department of Chemistry and Applied Chemistry and Thin Film and Surface Research Centre, University of Salford, Salford M5 4WT (Great Britain)

(Received 24th August 1984)

SUMMARY

Results are presented for the direct potentiometric determination of L-cysteine and several proteins with silver electrodes which are electrochemically treated before measurements. Comparisons are made with untreated and chemically cleaned electrodes in terms of Nernstian behaviour and equilibration times. The improved behaviour of the electrochemically treated electrodes is discussed in terms of a theoretical model.

In this paper, results obtained for direct potentiometry of proteins with precleaned silver electrodes are reported and comparisons are made with the theory presented in Part 1 [1].

EXPERIMENTAL

Equipment and materials

All potentiometric measurements were made with conventional instrumentation. Variations of potentials with time were recorded with the aid of a high-impedance voltmeter so that negligible current flowed through the indicator electrode. Indicator electrodes were high-purity (99.99%) silver wires (diameter 1—2 mm). Reference electrodes used were a saturated calomel electrode with a salt bridge and a Ag/AgCl double-junction electrode. The cell was a small beaker with a magnetic stirrer.

L-Cysteine (free base) and the following proteins (all from Sigma Chemical Company) were used as received: human albumin (Cohn fraction V), bovine albumin (Cohn fraction V), human globulin (Cohn fraction II), bovine globulin (Cohn fraction II), human globulin (Cohn fraction IV), ribonuclease A (5× crystallised, from bovine pancreas), lysozyme grade 1 (3× crystallised from egg white). Standard solutions were prepared immediately before use by direct weighing and dissolution in the appropriate buffer with gentle stirring. Solutions with concentrations in the range 10—0.01 mg ml^{-1} were

[a]Present address: Department of Pure and Applied Chemistry, University of Strathclyde, Thomas Graham Building, 295 Cathedral Street, Glasgow G1 1XL, Great Britain.

0003-2670/85/$03.30

generally used, the upper limit being established by the solubility limit of the protein and the lower limit by the detection limit. All buffers were prepared from analytical-grade reagents with the compositions given in standard tables [2].

Procedures

In the chemical cleaning procedure used [3], the electrode was immersed in ammonia solution (1 + 3) for 1—5 min, depending on the thiol, and then washed with distilled water. Further improvement in the cleaning was achieved by immersion in dilute nitric acid (1 + 3) followed by rinsing with methanol and water.

Electrochemical cleaning was done by placing the silver electrode and a platinum foil electrode in either a buffer solution or a buffered thiol solution and making the silver cathodic with respect to the platinum. Cathodic cleaning was also tried in dilute ammonia solution or dilute nitric acid. The simple d.c. circuit consisted of two 1.5-V batteries, a switch and a resistor in series. An elementary estimate of the number of coulombs required to remove a monolayer of adsorbed impurity on a surface with 10^{14}—10^{15} sites cm^{-2} indicates a charge density of 10^{-5}—10^{-4} C cm^{-2} which corresponds to ca. 50 μC for the area of the silver electrode used. Various combinations of currents and cleaning times were tried; a 1-MΩ resistor providing a current ca. 3 μA was most suitable. Cleaning times were in the range 10—90 s but were usually 15 s. The elementary estimate of charge required for cleaning seemed reasonable, as charge densities $<10^{-5}$ C cm^{-2} were not very effective while prolonged cleaning at charge densities $>10^{-4}$ C cm^{-2} did not improve matters.

After the silver electrode had been cleaned, either chemically or electrochemically, it was briefly rinsed with distilled water and then introduced into the test solution. The potential variation with time was monitored until a stable potential was obtained, i.e., a drift of <1 mV in 5 min. The time dependences of the potential and steady-state value were used for comparison with the theoretical equations [1]. When electrochemical cleaning was done in the test solution, switches in the cleaning circuit allowed direct changeover to the measurement of electrode potential after the cathodic treatment.

In order to minimise washing and rinsing procedures, solutions were usually investigated in the order of increasing concentrations, but some experiments were done with the reverse order. No significant differences were found between the two sets of results. In some cases, a random order was chosen to test the reproducibility of the results. All measurements were made at 23 ± 1°C.

RESULTS AND DISCUSSION

Results with standard silver solutions

The silver wire electrodes were first tested in standard silver solutions. Linear Nernstian plots with slopes of 58—59 mV/decade change in silver ion

concentration were obtained in the range 10^{-6}—10^{-3} M. The lower limit is similar to that found for many potentiometric electrodes. In these tests, the steady-state potential was always attained in <30 s.

Results with L-cysteine

L-Cysteine is the amino acid component of thiol-containing proteins. The behaviour of this substance was therefore checked thoroughly under different operating conditions, in order to avoid the possible complications arising from the more complex structures of the proteins. For example, the native structures of proteins (e.g., albumins, globulins) may not allow ready access to the thiol group [4] and so proteins are likely to show more complex behaviour at the silver electrode (see below).

Figure 1 compares the times needed to reach steady-state potentials (stabilisation time) on introducing the electrode into a solution of L-cysteine (1 mg ml^{-1}) at pH 4.5 after chemical cleaning and after cathodic cleaning in the buffer solution. The significant improvement in the stabilisation time with cathodic pretreatment is evident. Similar plots were obtained with other cysteine concentrations and at various pH values in the range 4.5—9.5.

Figure 2 shows the Nernst plots for the final equilibrium potential obtained with chemical and electrochemical cleaning before each measurement. The least-squares slopes of the two plots are —65.3 and —61.0 mV/decade, respectively, with corresponding standard errors of ±3.0 and ±1.8 mV. Both slopes are in reasonable accord with theory, but the improved behaviour of the electrochemically pretreated electrode is again apparent. Results with other buffer solutions showed similar improvements for cathodic cleaning.

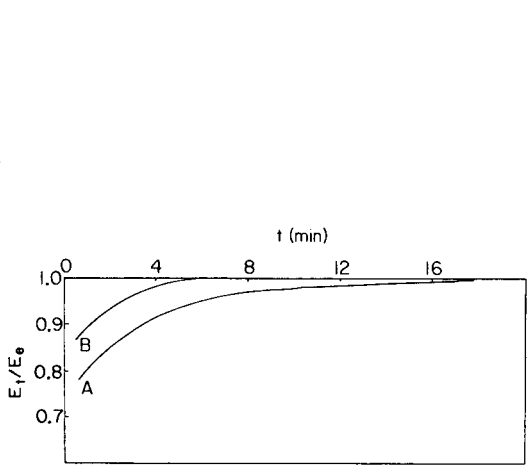

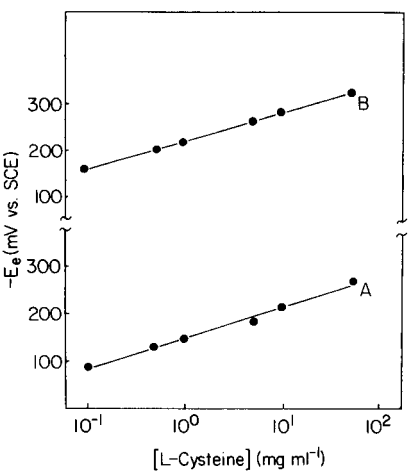

Fig. 1. Stabilisation curves for electrode potentials with L-cysteine (1 mg ml^{-1}; pH 4.5): (A) after chemical cleaning; (B) after electrochemical cleaning. The ratio of the potential (E_t) at time t to the final equilibrium potential (E_e) is plotted.

Fig. 2. Nernst plots for L-cysteine (pH 4.5): (A, B) as in Fig. 1.

The variation of the electrode potential with pH for a constant thiol concentration (1 mg ml^{-1}) was tested over the pH range 4—10. In the pH range 5—9, the slope of the plot of E_e vs. pH was —(60.7 ± 0.7) mV/pH unit, which is in good agreement with the value of —59 mV/pH unit for a simple thiol [1]. The plot levelled off at pH > 9.5, which is consistent with the reported value [6] of 8.5 for the pK_a of the thiol group in cysteine.

From the previous theoretical analysis [1], the variation of the electrode potential with time is expected to have the form

$$(E_t - E_e)/(E_0 - E_e) \approx (\theta_{S0} + \theta_{T0}) \exp(-ak_S^0 t) + [1 - (\theta_{S0} + \theta_{T0})] \exp(-ak_X^0 t) \quad (1)$$

where E_0, E_e and E_t are the potentials initially, finally and at time t, respectively; θ_{S0} and θ_{T0} are the initial surface fractions of silver and thiol-covered sites, a is a system parameter (see Eqn. 16 [1]), and k_S^0 and k_X^0 are the exchange frequencies on clean silver sites and on silver sites adjacent to sites covered with an adsorbed impurity X. The curves of Fig. 1 can be compared with this equation by plotting ln $(1 - E_t/E_e)$ vs. t, as is done in Fig. 3. For chemical cleaning (Fig.3a), there are clearly two sections to the plot which, on the basis of Eqn. 1, would correspond to reactions on two types of sites. With this interpretation, the slope of —0.282 min^{-1} for the region marked S and of —0.132 min^{-1} for X would indicate a ratio of activities for the two sites of about 2:1. With electrochemical cleaning, only one type of site is indicated (Fig. 3b) and the slope of —0.552 min^{-1} suggests that this site is more active than either of the sites available after chemical cleaning. This is consistent with the observation already made that electrochemical cleaning is more effective than chemical cleaning, and also with the fact that electrochemical pretreatment can activate an electrode surface either by removing adsorbed materials which inhibit electron transfer or by altering the microstructure of the electrode surface [7].

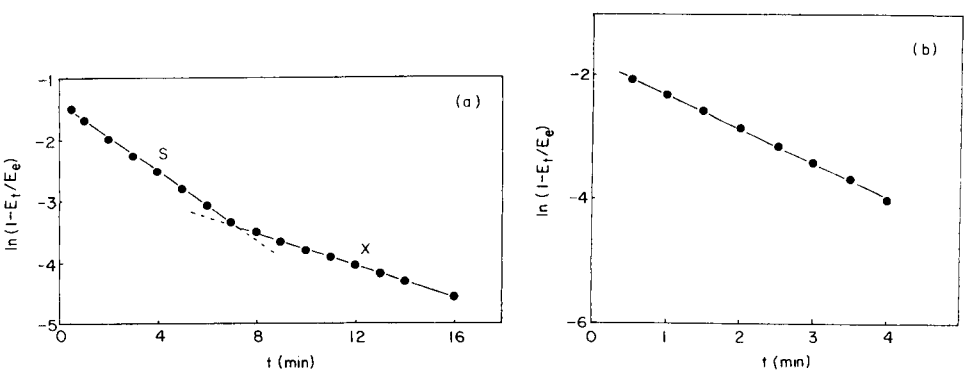

Fig. 3. Test of Eqn. 1 for the variation of potential with time for L-cysteine: (a) with chemical cleaning; (b) with electrochemical cleaning.

Results with lysozyme and ribonuclease A

Figure 4 shows the potential response of a silver electrode to varying concentrations of two proteins without thiol groups. The virtual independence of potential on concentration confirms that the predominant reaction is with the thiol group. The small potential changes at high concentrations are probably due to weak complexing with amino groups; it has been shown that the amino groups of lysine, arginine and methionine can react with silver [5]. With ribonuclease A, the potentials stabilised within 1 min, which is considerably faster than with cysteine (cf. Fig. 1) or with any thiol-containing protein (see below). This is consistent with the suggestion that it is the adsorption of the thiol onto the silver surface which is the slow step [1].

Results with albumins

The results shown in Fig. 5 for potential stabilisation with bovine serum albumin are similar to those of Fig. 1 for L-cysteine. The improvement achieved with electrochemical cleaning is apparent. The stabilisation times are longer than those found for L-cysteine, which is not unexpected for the more complex molecule. For human serum albumin very similar results were obtained, typical stabilisation times for electrochemical and chemical cleaning being about 16 min and 36 min, respectively. For both albumins, faster stabilization times (ca. 10 min) were obtained by prior electrochemical cleaning in both dilute ammonia and nitric acid solutions. However, the improvement was slight; as the aim was to develop the technique for flowing systems, e.g., h.p.l.c., studies of electrode pretreatment were restricted to using buffer and test solutions.

Typical Nernst plots for bovine serum albumin were given previously [8]. The least-squares slopes were (—46.0 ± 11.9) mV/decade, (—68.0 ± 8.8) mV/decade and (—58.6 ± 2.3) mV/decade for no cleaning, chemical cleaning and

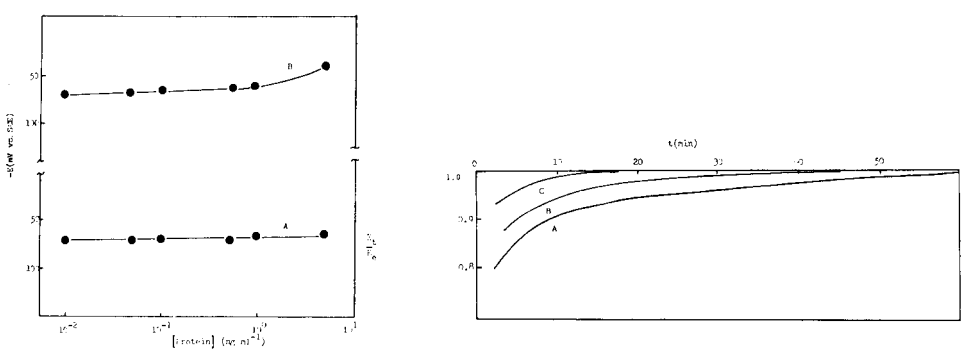

Fig. 4. Potential response to varying concentrations of lyzozyme (A) and ribonuclease A (B) at pH 8.4.

Fig. 5. Potential stabilisation curves with bovine serum albumin (0.5 mg ml^{-1}; pH 8.4): (A) no cleaning; (B) chemical cleaning; (C) electrochemical cleaning.

electrochemical cleaning, respectively. The relative standard deviation is greatly improved by the electrochemical cleaning. Similar results were obtained with human serum albumin with the corresponding slopes being (−70.5 ± 12.2) mV/decade, (−46.3 ± 3.5) mV/decade and (−50.0 ± 0.1) mV/decade.

The number of thiol groups per albumin molecule was determined by the method of Chinard and Hellerman [9]. The values found were 0.66 and 0.70 for bovine albumin at pH 4.5 and 9.0, respectively, and 0.68 and 0.72 for human albumin at pH 4.5 and 9.0, respectively. These values agree with previously reported values [10], and indicate that if the proteins contain one L-cysteine unit, then only two thirds of the thiol group present in the protein molecule is active; although in the presence of urea, the remaining third becomes active [11]. The exact reason for two types of reactivity of the thiol group in albumin has been the subject of some debate. It has been claimed [12] that serum albumins contain two fractions, one fraction (about 70%) being the mercaptalbumin containing one SH/protein molecule and the other fraction (about 30%) having lost the thiol group through formation of a mixed disulphide with cysteine or glutathione [13]. If this were the case, then although the effective concentration of the thiol group would be less than the protein concentration, there would still be one thiol group for reaction with silver and one would expect a Nernstian slope of −59 mV/decade. Alternatively, the thiol group may be "masked" by a rigid iceberg structure of water in the neighbourhood of the protein [14]. With this type of model, there would be an average of only 0.7 thiol group available for reaction and a Nernstian slope of about −84 mV/decade would be expected. The results obtained for determination of the albumin are in closer agreement with the −59 mV slope than with the −84 mV slope, especially for electrochemical cleaning, thus supporting the two fraction hypothesis. Under different conditions, however, slopes in the range of (−80 to −95) mV/decade have been found [8], which would tend to support the "masked" thiol model. This will be discussed subsequently.

For the monitoring of proteins in a flowing system, e.g., in a chromatographic eluate, it would be useful to quantify as well as detect the protein. Typical values for the reproducibility of potentials with electrochemical cleaning were given previously [8]. The reproducibility of the actual potentials from one run to another is not very good, but if the difference (ΔE) between a potential measured in the presence of protein and that measured in the buffer solution alone is taken then the reproducibility is sufficiently improved for quantitative assays.

The potential stabilisation curves can be compared with those expected on the basis of the theoretical model, as in the case of cysteine, by plotting $\ln (1 - E_t/E_e)$ vs. time. Figure 6 shows the plots for bovine albumin without cleaning of the electrode, and with chemical and electrochemical cleaning. Without cleaning and with chemical cleaning, two types of reaction site are again indicated; the corresponding least-squares slopes are given in Table 1.

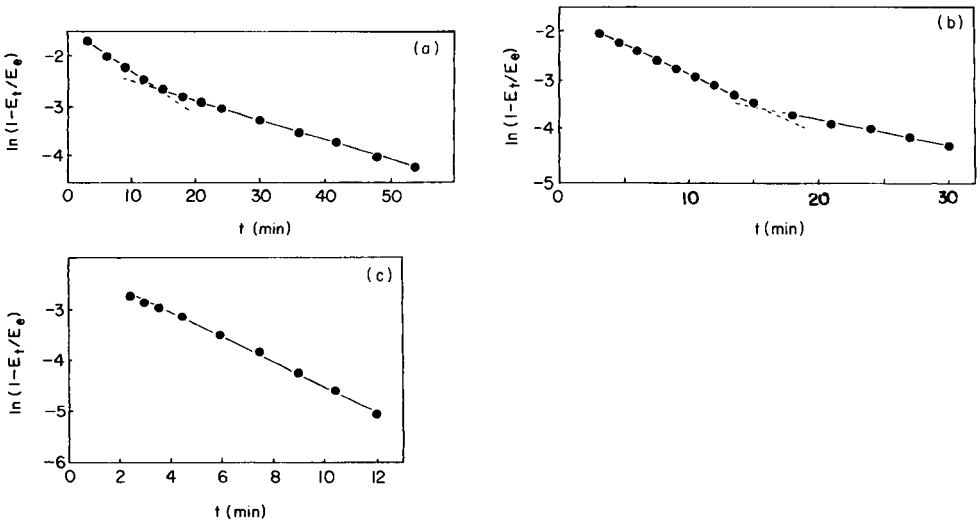

Fig. 6. Test of Eqn. 1 for the variation of potential with time for bovine albumin: (a) no cleaning; (b) chemical cleaning; (c) electrochemical cleaning.

TABLE 1

Slopes of ln $(1 - E_t/E_e)$ vs. time plots for albumins, L-cysteine and albumins

Protein	Cleaning procedure	Initial slope (min^{-1})	Final slope (min^{-1})
Bovine albumin	None	−0.085	−0.039
	Chemical	−0.111	−0.053
	Electrochemical	−0.245	—
Human albumin	None	−0.114	−0.038
	Chemical	−0.195	−0.085
	Electrochemical	−0.236	—
L-Cysteine	Chemical	−0.282	−0.132
	Electrochemical	−0.552	—
Bovine γ-globulin	Chemical	−0.240	—
	Electrochemical	−0.682	—
Human γ-globulin	Chemical	−0.475	—
	Electrochemical	−0.785	—
Human α-globulin	Chemical	−0.196	—
	Electrochemical	−0.603	—

The increasing slopes obtained for cleaned electrodes show the increased surface activity produced by cleaning. For electrochemical cleaning, only one type of reaction site is indicated, as in the case of cysteine. However, in all cases, the slopes are less than the corresponding slopes for L-cysteine (see above), suggesting that the silver/protein equilibrium is less reversible than the silver/cysteine equilibrium, which is not unexpected.

For human albumin, plots similar to those given in Fig. 6 for bovine albumin were obtained; the least-squares slopes are summarised in Table 1. The same features are observed as for bovine albumin, the only notable difference being that chemical cleaning appears to be more effective for human albumin. However, chemical pretreatment of electrode surfaces is less effective at giving reproducible surfaces than electrochemical pretreatment, thus the difference should not be regarded as of great significance. The important point is that electrochemical cleaning is again the best method of activating the silver surface.

Results with globulins

Figure 7 shows the stabilisation of the potential for bovine γ-globulin, human γ-globulin, and human α-globulin with chemical and electrochemical pretreatment of the electrode; measurements without cleaning again showed longer stabilisation times, and again electrochemical cleaning led to more rapid potential stabilisation. The slopes of the Nernst plots for the steady-state potentials obtained for protein concentrations in the range 10^{-2}—5 mg ml^{-1} are summarised in Table 2. The benefits of the electrochemical pretreatment are again apparent.

Values of 0.5 to 1 thiol group/mole of protein have been reported for globulins [15]. Titration with *o*-iodobenzoic acid [9] for the γ-globulins used here gave an average value of (0.82 ± 0.03) SH/mole. If this value can be ascribed to "masking" of the thiol group, one would expect a slope of —72 mV/decade. The slope of —70 mV/decade obtained with electrochemical cleaning for human γ-globulin would support the idea of a "masked" thiol group. The —64 mV/decade slope obtained under similar conditions for bovine γ-globulin, however, is more in line with a two-fraction model as in

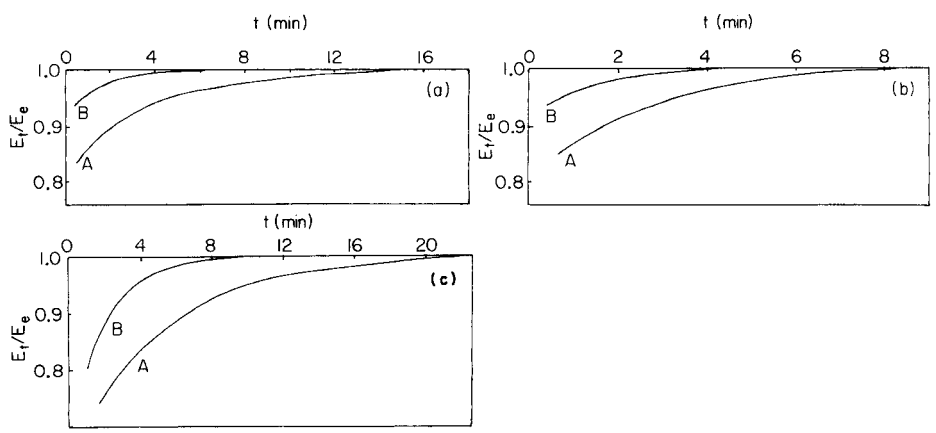

Fig. 7. Potential stabilisation curves with globulins (0.5 mg ml^{-1}; pH 8.4): (a) bovine γ-globulin; (b) human γ-globulin; (c) human α-globulin. Curves: (A) chemical cleaning; (B) electrochemical cleaning.

TABLE 2

Slopes of the Nernst plots for globulins

Protein	Cleaning procedure	Slope (mV/decade)
Bovine γ-globulin	Chemical	−95.3 ± 13.4
	Electrochemical	−63.9 ± 6.6
Human γ-globulin	Chemical	−46.9 ± 4.6
	Electrochemical	−70.2 ± 2.4
Human α-globulin	Chemical	−47.4 ± 2.3
	Electrochemical	−50.0 ± 0.1

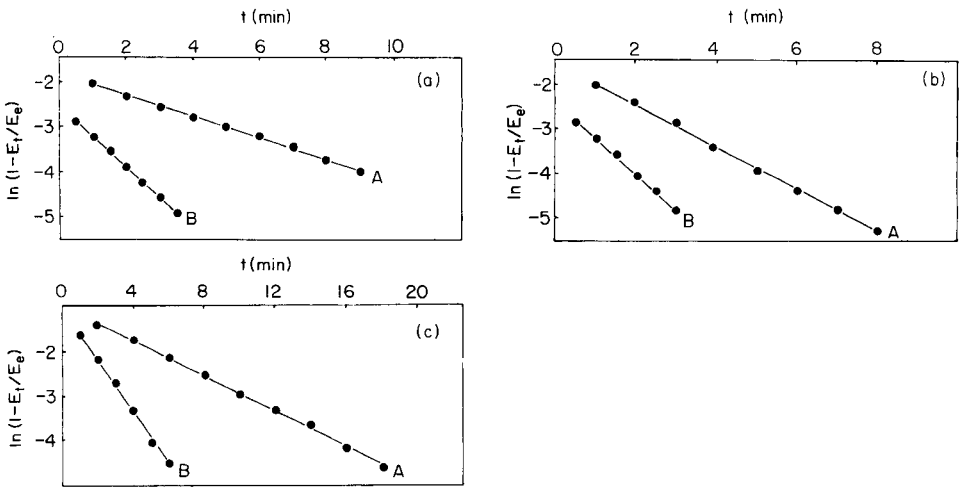

Fig. 8. Test of Eqn. 1 for the variation of potential with time for globulins; (a—c) and A, B as in Fig. 7.

the case of the albumins. The results for human α-globulin do not seem to fit either model. This diversity and complexity of behaviour for the globulins is not surprising because they are a very heterogeneous class of proteins, especially with regard to their binding processes [16]. Therefore, their reactions with a silver electrode will not be simple.

The peculiarities of the globulins are also apparent from their potential stabilisation curves. Figure 8 shows the plots based on Eqn. 1. In contrast to those for L-cysteine and the albumins, the plots are all straight lines whether chemical or electrochemical cleaning is used; this suggests that the formation of the silver-thiol complex is less susceptible to surface impurities in the case of globulins. A comparison of the slopes of these plots with those for L-cysteine and the albumins (Table 1) lends support to this suggestion. With electrochemical cleaning, the slopes are higher for all the globulins than that

for L-cysteine, indicating a higher exchange flux. For chemical cleaning, there is more scatter in the values for the globulins, probably because of the less reproducible surface activation. The apparent relatively high level of reactivity with silver is surprising for such large and complex molecules as the globulins. This probably reflects their heterogeneous nature and wide-ranging functions as efficient binding agents.

We thank the Malaysian Government and the University Sains Malaysia for sponsorship of A. Aziz, the Malawi Government for a scholarship to D. D. K. Chingakule, the British Council for a training award to F. W. M. Nyasulu, and Pharmacia Fine Chemicals AB, Uppsala, for the provision of materials and equipment.

REFERENCES

1 M. L. Hitchman, Anal. Chim. Acta, 171 (1985) 131.
2 R. C. Weast (Ed.), Handbook of Chemistry and Physics, The Chemical Rubber Co., Cleveland, OH, 1970, p. D102.
3 T. Y. Toribara and L. Koval, Talanta, 17 (1970) 1003.
4 J. H. Ladenson and W. C. Purdy, Anal. Chim. Acta, 64 (1973) 259.
5 L. C. Gruen, Biochim. Biophys. Acta, 386 (1975) 270.
6 T. Y. Lin, in H. Neurath (Ed.), The Proteins, Vol. III, 3rd edn., Academic Press, New York, 1977, p. 245.
7 J. O'M. Bockris and A. K. N. Reddy, Modern Electrochemistry, Vol. 2, Plenum, New York, 1970, p. 1170.
8 M. L. Hitchman, F. W. M. Nyasulu, A. Aziz and D. D. K. Chingakule, Anal. Chim. Acta, 155 (1983) 219.
9 F. P. Chinard and L. Hellerman, in D. Glick (Ed.), Methods of Biochemical Analysis, 10 (1962) 1.
10 R. Cecil and J. R. McPhee, Adv. Protein Chem., 14 (1959) 255.
11 R. Benesch and R. E. Benesch, in D. Glick (Ed.), Methods of Biochemical Analysis, 10 (1962) 43.
12 W. L. Hughes, J. Am. Chem. Soc., 69 (1947) 1836.
13 T. P. King, J. Biol. Chem., 236 (1961) PC5.
14 I. M. Klotz and J. Ayers, J. Am. Chem. Soc., 79 (1957) 4078.
15 R. Cecil, in H. Neurath (Ed.), The Proteins, Vol. I, 2nd edn, Academic Press, New York, 1963, p. 388.
16 J. A. Steinhardt and J. A. Reynolds, Multiple Equilibria in Proteins, Academic Press, New York, 1969, p. 149.

Analytica Chimica Acta, 171 (1985) 151—163
Elsevier Science Publishers B.V., Amsterdam — Printed in The Netherlands

POTENTIOMETRIC FLOW-INJECTION DETERMINATION OF COPPER-COMPLEXING ORGANIC LIGANDS WITH A COPPER-WIRE INDICATING ELECTRODE

PETER W. ALEXANDER*, PAUL R. HADDAD and MAREK TROJANOWICZ[a]

Department of Analytical Chemistry, University of New South Wales, P.O. Box 1, Kensington, NSW 2033 (Australia)

(Received 2nd October 1984)

SUMMARY

The potentiometric response of a copper-wire indicator electrode in a flow-injection system with a phosphate-buffered carrier stream can be used to determine copper-complexing ligands; glycine, histidine, L-cysteine, EDTA, ethylenediamine, triethylenetetramine, dopamine and imidazole are discussed. The electrode response is shown to give peak potentials with a Nernstian relationship to total injected ligand concentration over limited ranges, depending on the stoichiometry, stability, and oxidation state of the copper complexes formed. Galvanostatic measurements showed that complex formation with Cu^{2+} or Cu^{+} or mixed species can be responsible for the response characteristics. The effects of adding 0.1 M sodium chloride to the carrier stream are generally beneficial, particularly in obtaining sharper responses. Detection limits can be improved to about 10^{-5} M by adding about 10^{-5} M Cu^{2+} to the carrier stream, but the linear range of Nernstian response is then narrow.

The potentiometric detection of organic ligands can be based on the response of a copper-sensitive membrane electrode or a copper metal indicator electrode. The relationship between the potential of a copper-sensitive solid-state membrane electrode and the concentration of copper-complexing ligands has been reported in several papers [1—6], and the response at copper metal electrodes has been utilized for the detection of amino acids in flow analysis [7] and in high-performance liquid chromatography (h.p.l.c.) [8]. Comparison of the response of these membrane and metal electrodes for continuous flow determination of amino acids in a segmented stream has shown that the latter sensor has some advantages in terms of lower detection limits and faster response in phosphate-buffered medium [7]. Detection with the copper metal electrode has also been applied successfully to the indirect flow-injection determination of metal ions [9] and to the h.p.l.c. determination of alkaline earth metal ions [10]. In flow-injection determinations of several inorganic anions, good agreement was achieved between experimental results and predictions based on the assumption of

[a]Permanent address: Department of Chemistry, University of Warsaw (Poland).

0003-2670/85/$03.30

Nernstian electrode functioning and calculations based on known stability constants of the expected copper complexes with the anions [11].

In the present paper, potentiometric detection with the copper metal electrode is applied in flow-injection determinations of several copper-complexing organic ligands under typical zero-current conditions. The electrode response mechanism is examined and the possibility of improvement in the sensitivity of response by anodic polarization of the copper electrode is also studied. The organic ligands used comprised several amino acids and amines varying in complexing strength towards copper ions.

EXPERIMENTAL

Reagents and solutions

Buffer solutions were prepared from analytical reagent-grade potassium dihydrogenphosphate, sodium hydroxide and sodium chloride (Ajax Chemicals, Australia). Volucon standard buffers (May and Baker) were used for standardization of pH measurements. The ligands examined were: glycine and L-cysteine (BDH Biochemical), DL-histidine (Light and Co.), ethylenediamine and EDTA, disodium salt (May and Baker), triethylenetetramine (trien) (BDH), 3-hydroxytyramine (dopamine) hydrochloride (Sigma Chemical Co.) and imidazole (Merck). All these reagents except trien were used without further purification; trien was purified by four recrystallizations from ethanol as a dinitrate salt. Stock standard solutions (0.01 M) were prepared freshly just prior to use by direct weighing and dissolution in degassed distilled water when a two-line manifold was used or in buffer solution when a single-line manifold was used. The stock solutions were serially diluted with distilled water or the buffer solution as appropriate. All solutions were carefully degassed before measurements.

Instrumentation

Potentiometric data were recorded with a Radiometer PHM 62 digital mV/pH meter coupled to a Houston Omniscribe strip-chart recorder (type EB 5117-5-S). For galvanostatic measurements, a PAR galvanostat (potentiostat model 363) was used. Hydrodynamic voltammograms were recorded with a PAR polarograph type 174A coupled to the Omniscribe recorder.

The flow cell was made of perspex (Fig. 1) and was equipped with a copper wire electrode (0.8 mm diameter), a counter platinum wire electrode and a Ag/AgCl reference electrode placed in a compartment with agar gel containing 0.1 M KCl. The internal diameter of the channels in the block was 1.2 mm. The flow system consisted of a peristaltic pump (Desaga, type 131900) fitted with Elkay PVC tubing connected to a home-made rotary injection valve based on a design by Růžička and Hansen [12]. The outlet of the injection valve was connected to the flow cell via teflon tubing (0.5 mm internal diameter). The wires and tubing in the flow cell and injection valve were mounted with Omnifit connectors. Solution pH readings were measured

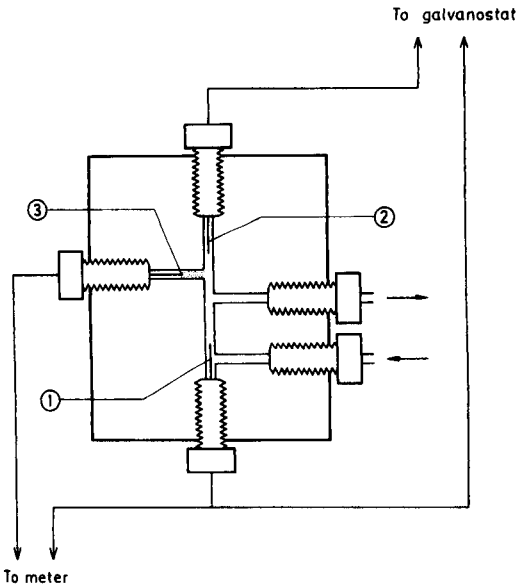

Fig. 1. Schematic diagram of the flow-through cell: (1) copper-wire indicating electrode; (2) auxiliary platinum-wire electrode; (3) reference Ag/AgCl electrode in compartment filled with agar gel containing 0.1 M KCl.

with an Orion model 701A digital mV/pH meter fitted with a combination pH glass electrode.

RESULTS AND DISCUSSION

The response of the copper electrode was monitored after the injection of organic ligands into a phosphate-buffered carrier stream at pH 6.8. The peak-height data were then used to obtain calibration plots of peak-height potentials as a function of total ligand concentration. Nernstian electrode response would be expected from earlier studies on inorganic ligands [11], provided that the organic ligand formed a single predominant complex species with copper ions in a given concentration range. The electrode response to injected ligand also has the limitation that the maximum peak height is observed when hydrogen is evolved:

$$Cu^0 + 2H_2O + L^{2-} \rightleftharpoons CuL + 2OH^- + H_2$$

This occurs when the potential of the half-cell consisting of copper/complexed Cu^{2+} ions is lower than the potential of hydrogen evolution at the free ligand concentration and pH existing in the solution. The limit in peak height depends on the stability of the copper complex formed.

In this study, the organic ligands chosen are known to give a wide variety of stoichiometries and stabilities of complexes with both copper(II) and

copper(I) ions. The flow-injection data obtained here were used in an attempt to explain the response characteristics of the copper metal electrode to injected organic ligands.

Complexation of copper by the selected ligands

The organic ligands chosen for flow-injection studies were glycine, DL-histidine, L-cysteine, EDTA, ethylenediamine (en), triethylenetetramine (trien), dopamine and imidazole. In previous continuous-flow determinations of a large group of α-amino acids with the copper indicator electrode, higher sensitivity for histidine compared to other amino acids and poisoning of the copper electrode by cysteine were observed [7]. Different stoichiometries and complex oxidation states with copper are known; for example, glycine and histidine form 1:1 and 1:2 complexes with copper(II) ions [13], but under the present conditions the 1:2 complex with histidine predominates and much larger potential changes for histidine should be expected. Both glycine [14] and histidine [15] form only very weak complexes with copper(I) ions, whereas the stability constants for complexes of cysteine with copper(II) [16] and copper(I) [17] ions indicate extremely stable copper(I) complexes. In the case of EDTA, the 1:1 complex with copper(II) ions is known to predominate, although a weak 1:1 complex with copper(I) ions has been detected polarographically [18].

Ethylenediamine and imidazole form complexes with both copper oxidation states. For ethylenediamine the stability constants indicate the predominance of the 1:2 complex with copper(II) ions and much weaker binding of copper(I) ions [13]. Imidazole forms a very stable 1:2 complex with copper(I) ions [19]. For dopamine [20] and trien [13], only copper(II) complexes have been reported. In the case of trien, the 1:1 complex predominates. For dopamine at high ligand concentration at pH 6.8, Grgas-Kužnar et al. [20] reported the formation of an extremely stable complex, $Cu(HL)_2$, but at lower concentrations, the CuHL complex was formed.

Flow-injection response in phosphate buffer

Because of the protolytic equilibria of the organic ligands concerned, flow-injection determinations must be done in buffered media. High pH values are advantageous because of the increased fraction of unprotonated species forming complexes. Increased pH also shifts the electrode potential for hydrogen evolution towards more negative values. A buffer of 0.05 M orthophosphate at pH 6.8 was chosen as the most suitable carrier solution to provide sufficient buffering capacity and low complexation of copper ions. For measurements in a single-line manifold with short tubing between the injection valve and flow cell, solutions of the organic ligands were prepared in the same buffer as used for the carrier. When a two-line manifold was used, solutions of each ligand were prepared in water, and then injected into a water stream, which was merged with the stream of buffer solution before reaching the indicator electrode. In this way, constant buffer concentration was maintained in the stream reaching the detector.

The calibration plots for several compounds are shown in Fig. 2. The results obtained for glycine and histidine were similar to those reported previously for a continuous-flow system [7]. The monovalent Nernstian slope observed for histidine agrees with the stability constant data showing formation of the 1:2 complex. For glycine, the curvature of the plot and the low slope of the linear part may be explained by the studies of Keenan et al. [21] who observed adsorption of free ligand on the electrode surface and formation of complexes of lower stoichiometry than expected. In the case of EDTA, the formation of stable Cu-EDTA complexes suggests that large peak heights would be expected; in practice, small peak heights were observed, possibly because of significant adsorption of ligand on the electrode surface, leading to the creation of conditions in the diffusion layer which are quite different from those in the bulk solution. The observed divalent Nernstian slope for the short linear part of the EDTA calibration plot in Fig. 2(a) corresponds to the formation of a 1:1 complex. Despite the shortness of the linear range of this response, it was utilized successfully for indirect determinations of metal ions down to 10^{-5} M level by flow injection [9]. As for previous studies with a continuous-flow system [8], the flow-injection determinations of cysteine were unsatisfactory. Large potential changes were observed but linear calibration with monovalent Nernstian slope was obtained only for total concentrations for cysteine in the injected samples higher than 10^{-3} M (Fig. 2b), corresponding to the

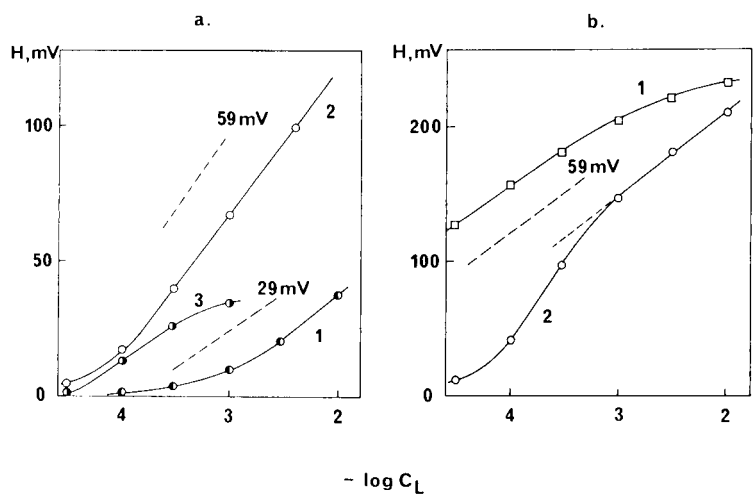

Fig. 2. Experimental calibration plots. (a) Flow-injection measurements for glycine (1), histidine (2) and EDTA (3) in a single-line manifold with L = 15 cm and a flow rate of 4.0 ml min^{-1}. (b) Cysteine measured in: (1) continuous-flow steady-state conditions at a flow rate of 4.2 ml min^{-1}; (2) in flow-injection determinations in a single-line manifold with L = 15 cm and a flow rate of 4.2 ml min^{-1}, using 0.05 M phosphate buffer, pH 6.8, as carrier.

formation of a very stable 1:1 copper(I) complex. At lower total cysteine concentrations in the injected samples, the slow electrode response interfered with flow-injection measurements, but steady-state measurements under the same conditions gave linear calibration with monovalent slope (Fig. 2b).

Other ligands studied gave the response slopes expected for the most stable complex species formed. For ethylenediamine, the calibration plot showed monovalent slope, corresponding to the formation of the 1:2 complex with copper(II) ions (Fig. 3). For dopamine, the slope of the linear part of the calibration plot obtained corresponds to the formation of Cu(II)HL. The equilibrium occurring in the diffusion layer determining the potential of the electrode therefore differs significantly from those in the bulk solution, interpreted using thermodynamic equilibrium constants. Linear calibration with divalent slope for dopamine was obtained only for total dopamine concentrations above 10^{-3} M.

The adsorptive properties of polyamines are commonly known, and are often used to inhibit corrosion. Adsorption was also observed in the electrochemical reduction of copper(II) complexes with polyamines [22]. It seems that the anomalies observed in the flow-injection determination of trien can be attributed to the adsorptive properties of trien. In the measurements made in phosphate-buffered medium, whether in the flow-injection (Fig. 3) or steady-state mode, a curved calibration plot was obtained with a very low slope at higher concentrations. Recorded peaks obtained under these conditions are given in Fig. 4(a).

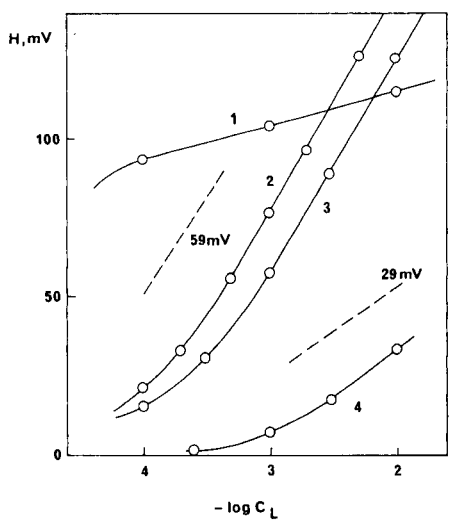

Fig. 3. Experimental calibration plots: (1) trien; (2) imidazole; (3) ethylenediamine; (4) dopamine. Conditions: flow-injection determination with 0.05 M phosphate buffer, pH 6.8, as carrier in a single-line manifold with L = 15 cm and a flow rate of 4.0 ml min^{-1}.

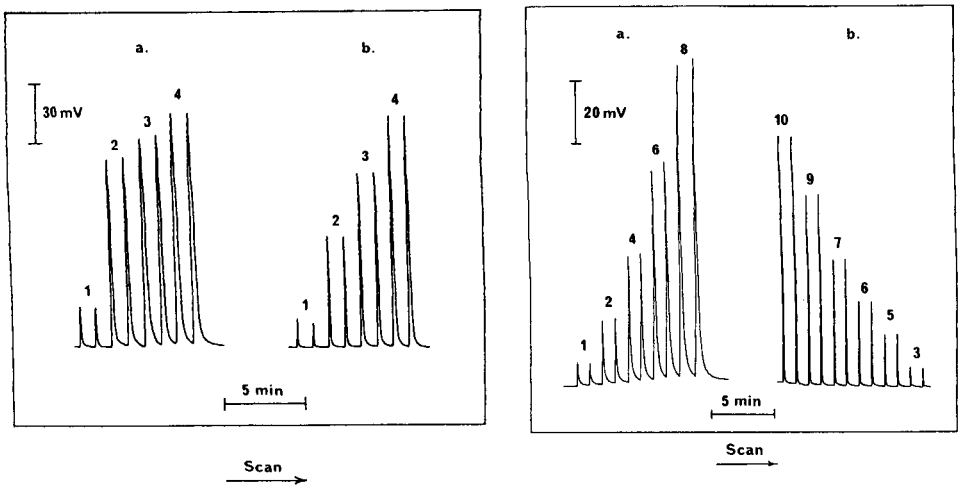

Fig. 4. Recording of peaks obtained for 75-μl injections of trien into: (a) 0.05 M phosphate buffer carrier stream at pH 6.8; (b) into the same buffer containing 0.1 M NaCl in a single-line manifold with L = 25 cm and a flow rate of 3.4 ml min^{-1}. Concentration of injected samples: (1) 0.01, (2) 0.1, (3) 1.0, (4) 10 mM.

Fig. 5. Recording of peaks obtained for 75-μl injections of histidine into: (a) 0.05 M phosphate buffer carrier stream at pH 6.8; (b) the same buffer containing 0.1 M NaCl in a single-line manifold with L = 25 cm and a flow rate of 4.2 ml min^{-1}. Concentration of injected samples: (1) 0.03, (2) 0.1, (3) 0.2, (4) 0.3, (5) 0.5, (6) 1.0, (7) 2.0, (8) 4.0, (9) 5.0, (10) 10.0 mM.

For imidazole, well shaped, regular peaks were obtained; the calibration plot had a slope close to the monovalent Nernstian value (Fig. 3) expected for the copper(I) complex known to predominate [19].

Effect of chloride on flow-injection response

Both in earlier continuous-flow measurements of amino acids with the copper electrode [7] and in the present flow-injection measurements, a fast potential decrease (the rising part of peak) was followed by a much slower return to the initial value. This effect is illustrated for trien (Fig. 4) and histidine (Fig. 5); similar response characteristics were observed for all the ligands investigated, corresponding to fast formation of the complex followed by slower return to the initial equilibrium state because of generation of copper ions in the diffusion layer. Obviously, the slow return to baseline is unfavourable in flow measurements.

The exchange between Cu^{2+} and Cu^0 has been investigated by many authors [23]. It is known that the Cu^{2+}/Cu^+ reduction process is slow, whereas the Cu^+/Cu^0 reduction is fast. In most cases, copper(I) is only an intermediate. However, when the electrolyte interfacing the electrode surface contains a ligand stabilizing Cu^+ in solution, the Cu^+/Cu^0 reduction is fast and the slow total Cu^{2+}/Cu^0 reaction is avoided.

This behaviour was exploited by flow-injection measurements by introduction of chloride into the carrier solution. Chloride caused a decrease in the potential reading of the copper electrode and simultaneously significantly improved the dynamic characteristics of the detector signal, as shown by the peaks recorded for trien and histidine (Figs. 4 and 5). Stabilization of copper(I) in the carrier caused, however, a decrease in peak height for histidine (Fig. 5). It seems to be quite probable that, in such conditions, the source of the electrode potential change is the formation of a 1:1 complex with copper(I). With chloride in the carrier, the peak shapes for trien were sharper and the calibration plot had a slope corresponding to a divalent ion for concentrations above 10^{-4} M trien. That chloride affects adsorption was reported [22] in studies on electrodeposition of copper from solutions containing polyamines and was explained by displacement of the adsorbed species by chloride.

For cysteine, the use of chloride in the carrier also significantly improved the flow-injection response, giving linear calibration with monovalent Nernstian slope for concentrations down to 10^{-4} M cysteine. For ethylenediamine, as for histidine, a marked decrease in signal magnitude was observed, and for glycine the peaks disappeared almost completely. In these cases, the decreased peak heights in chloride solutions may be attributed to the formation of much weaker copper(I) complexes. The equilibrium $CuCl_3^{2-} + 2L^- \rightleftharpoons CuL_2 + 3\ Cl^- + e^-$ is therefore rendered unfavourable for these ligands.

Electrode response in galvanostatic conditions

Anodic polarization of the indicator electrode was examined under flow-injection conditions. Depending on the difference in reversibility and number of electrons involved in the electrode process occurring in the carrier solution and in injected sample zone, increases in the magnitude of potential changes were achieved in some cases. Figure 6 shows hydrodynamic voltammograms recorded for the copper-wire electrode. The application of anodic polarizing currents up to 4 μA caused increased potential changes, but these were accompanied by slower return to base-line because of the increased thickness of the oxide layer formed on the electrode surface [24]. This effect is illustrated by the results for glycine at increasing polarizing current (Fig. 7). Similar results were obtained for histidine, but for trien, irregular non-linear calibration was obtained.

In the presence of chloride, a similar effect, although of smaller magnitude, was observed when a small anodic current was applied. Approximately 30% increased signals were found for histidine by application of a 2-μA polarization. Further increase of current did not change the signal magnitude for higher concentrations of histidine, in agreement with the recorded voltammograms. However, the slope of the calibration corresponded to twice the monovalent Nernstian response when the polarizing current was $\geqslant$10 μA, probably because of the formation of Cu_2L complexes.

In the case of glycine, small sharp peaks corresponding to the formation

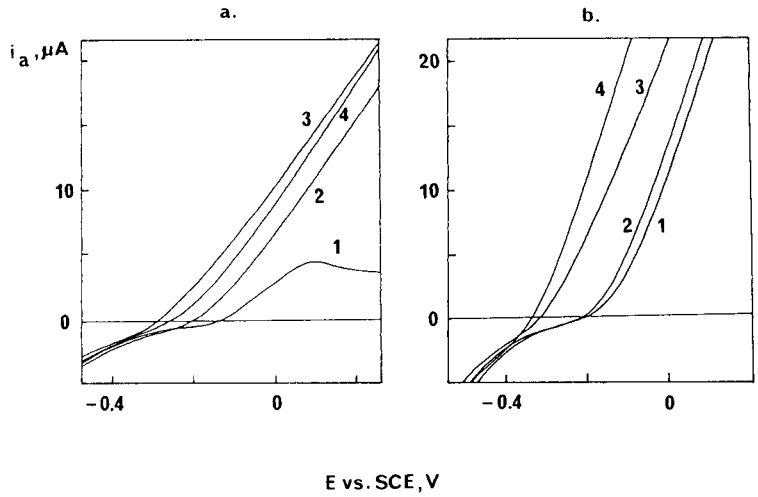

Fig. 6. Hydrodynamic voltammograms obtained with the copper-wire electrode at a potential scan rate of 2 mV s^{-1} in different solutions: (a) 0.05 M phosphate buffer at pH 6.8; (b) 0.05 M phosphate buffer at pH 6.8 containing 0.1 M NaCl. Curves: (1) buffer alone; (2) 0.01 M glycine solution in buffer; (3) 0.01 M histidine solution in buffer; (4) 0.005 M trien solution in buffer. Flow rate, 3.0 ml min^{-1}.

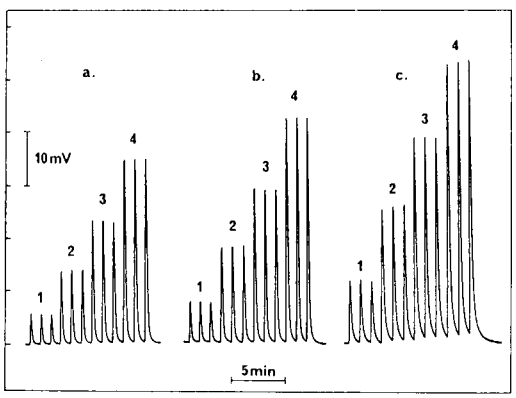

Fig. 7. Recording of peaks obtained for 75-μl injections of glycine into 0.05 M phosphate-buffered carrier, pH 6.8, with the following galvanostatic conditions: (a) at zero current; (b) at an anodic polarization of 2 μA; (c) 4-μA current. Two-line manifold with L = 50 cm and a flow rate of 5 ml min^{-1}. Concentrations of injected samples: (1) 1.0, (2) 2.5, (3) 5.0, (4) 10 mM.

of copper(I) complexes appeared. For ethylenediamine, increasing the polarizing current increased the slope of the linear part of the calibration curve in the high concentration range to twice the value of the monovalent Nernstian slope (Fig. 8a). The slope corresponds to the formation of a 1:2 ethylenediamine/copper(I) complex. Similar explanations can be provided for the

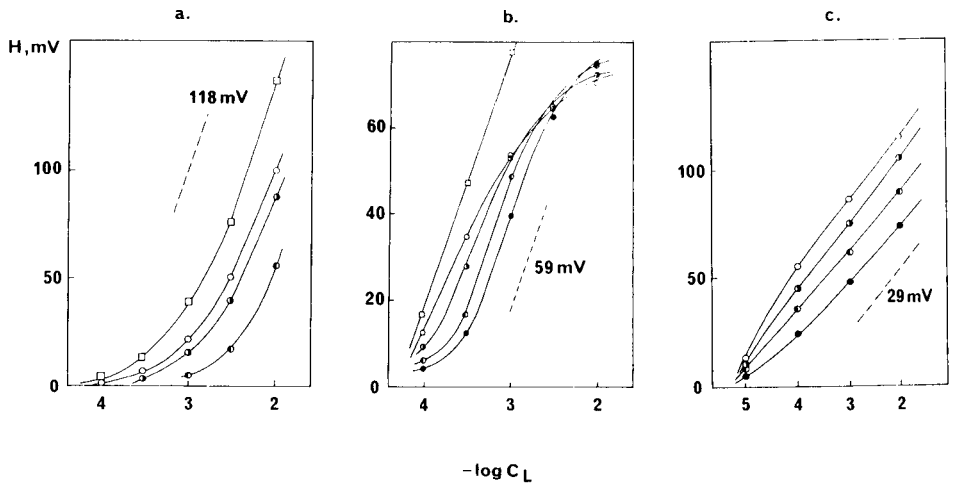

Fig. 8. Effect of anodic polarization of the copper electrode on flow-injection calibration plots for the following ligands. (a) Ethylenediamine: (◦) with zero current; (◑) 2 μA current; (○) 10 μA current; (□) steady-state readings with 10 μA current (anodic polarization). (b) EDTA: (●) 4 μA current; (◐) 6 μA current; (◑) 10 μA current; (○) 15 μA current; (□) steady-state readings with 10 μA current (anodic polarization). (c) Trien: (○) zero current; (◑) 0.1 μA current; (◐) 0.2 μA current; (●) 0.3 μA current (cathodic polarization).

monovalent Nernstian slope of the calibration obtained for EDTA with chloride in the carrier at strong anodic polarization (Fig. 8b). In such conditions, the formation of Cu(I)-EDTA is responsible for the electrode potential changes.

According to the observed voltammogram for trien, the flow-injection response under galvanostatic conditions should also provide peaks of larger magnitude. In fact, non-linear calibration response was obtained with peaks smaller than expected below 10^{-4} M trien. Improved linearity for trien calibration was obtained by applying a small cathodic polarizing current. As shown in Fig. 8(c), cathodic polarization with a 0.2-μA current gave satisfactory calibration with divalent Nernstian slope down to 10^{-5} M trien. Further increases in polarizing cathodic current decreased the peak heights.

Flow-injection determination in the presence of copper(II) ions in the carrier solution

As shown above, the direct response of the copper-wire electrode is often limited to relatively high ligand concentrations in the injected samples. In such cases, it can be advantageous to determine low ligand concentrations in the presence of copper(II) ions in the carrier, where partial binding of copper by the injected ligand can occur.

In the presence of copper(II) ions of concentration C^0_{Cu} in the carrier, the potential of the copper electrode is given by

$$E_1 = \text{const.} + S\log\,(C^0_{Cu}/\alpha_{Cu(B,OH)}) \quad (1)$$

where $\alpha_{Cu(B,OH)}$ is the side-reaction coefficient of copper(II) ions complexed by the components of the carrier solution. In a single-line manifold after the injection of sample containing ligand L of concentration C_L, the potential value at the peak maximum is given by a similar expression

$$E_2 = \text{const.} + S\log\,(C_{Cu}/\alpha_{Cu(B,OH)}) \quad (2)$$

where $C_{Cu} = C^0_{Cu}(1 - D^{-1}) - nC_LD^{-1}$, D being the dilution ratio of the injected sample in the carrier stream (or dispersion coefficient as defined by Růžička and Hansen [12]) and n the number of ligand molecules bound by copper(II) ion in the complex species predominating in the injected zone. From the measured peak height, $H = E_2 - E_1$, the following relationship can be derived

$$1 - 10^{H/S} = D^{-1} + nC_L/C^0_{Cu}D \quad (3)$$

where the term $(1 - 10^{H/S})$ is a linear function of the total ligand concentration, C_L, in the injected samples. In a two-line manifold, where the concentration of copper(I) ions can be kept constant in the stream approaching the detector, Eqn. 3 can be simplified to $1 - 10^{H/S} = nC_L/C^0_{Cu}D$. In both cases, the slope of the relationship between the term $(1 - 10^{H/S})$ and C_L depends on the stoichiometry of the complex formed, the concentration of copper(II) ions in the carrier, and the dispersion D.

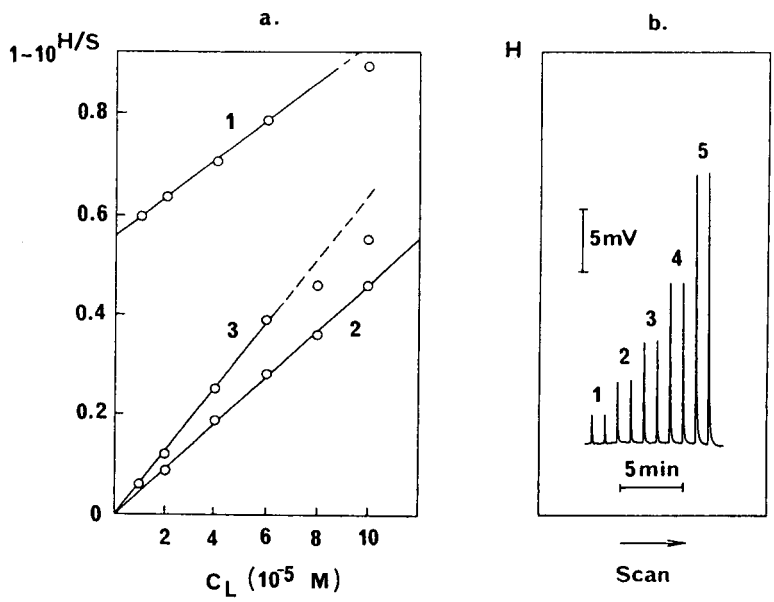

Fig. 9. Flow-injection determination of cysteine with 0.05 M phosphate buffer, pH 6.8, containing copper(II) ions as the carrier solution. (a) Calibration plots obtained after injection into the following copper(II) sulphate concentrations: (1) 1.0×10^{-4} M, (2) 4×10^{-5} M, (3) 8×10^{-6} M; a single-line manifold was used for (1) and a two-line manifold was used for (2) and (3). (b) Recorded peaks for different cysteine concentrations injected: (1) 0.02, (2) 0.04, (3) 0.06, (4) 0.1, (5) 0.2 mM.

As an example of such flow-injection determinations, cysteine was examined; the response peaks are shown in Fig. 9(b). Direct flow-injection determination of cysteine was shown above (Fig. 2b) to be limited to high concentrations. Concentrations between 10^{-5} and 10^{-4} M were processed in a single-line manifold (curve 1, Fig. 9a) and in a two-line manifold at two different concentrations of copper(II) ion in the stream reaching the flow cell (curve 2 and 3). The recorded peaks show good reproducibility and fast return of the potential to base-line. Similar linear calibration plots for such measurements at the same range of ligand concentrations were obtained for EDTA, glycine and trien.

Conclusions

The potentiometric response with the copper-wire electrode in flow-injection determinations of copper-complexing ligands depends on the valency and stoichiometry of the copper ion in the predominating complex. The magnitude of the observed peak height depends on the stability of the complex species.

In flow-injection determinations in phosphate buffer, slow return to base-line was observed, and detection limits in most cases were no better than approximately 10^{-4} M. The addition of chloride to the carrier solution significantly improved the dynamic response characteristics of the detector but favoured the formation of copper(I) complexes. Although this leads to decreased sensitivity for the copper(II)-complexing ligands, the presence of chloride improved the electrode response to cysteine and trien.

Increased peak magnitude in most cases, both in phosphate buffer and in the presence of chloride, was obtained by anodic polarization of the indicating copper electrode, because of generation of copper ions at the electrode surface. Low concentrations of ligand, down to 10^{-5} M, were most successfully determined by adding copper(II) ions to the carrier solution, but linear calibration for such measurements was limited to one order of magnitude of ligand concentration.

The authors express their thanks to Dr. I. Hamilton (Footscray Institute of Technology, Melbourne) for valuable comments and discussions. Financial support from the Australian Research Grants Scheme is also gratefully acknowledged. This paper was presented in part at the 6th Australian Electrochemistry Conference, Deakin University, February, 1984.

REFERENCES

1 M. F. El-Taraz, E. Pungor and G. Nagy, Anal. Chim. Acta, 82 (1976) 285.
2 A. Hulanicki, M. Trojanowicz and M. Cichy, Talanta, 23 (1976) 47.
3 D. S. Nikolelis, D. S. Papastathopoulos and T. P. Hadjiioannou, Anal. Chim. Acta, 78 (1978) 227.
4 G. J. M. Heijne and W. E. van der Linden, Anal. Chim. Acta, 96 (1978) 13.
5 C. R. Loscombe, G. B. Cox and J. A. W. Dalziel, J. Chromatogr., 166 (1978) 403.

6 A. Hulanicki, T. Krawczynski vel Krawczyk and A. Lewenstam, Anal. Chim. Acta, 158 (1984) 343.
7 P. W. Alexander and C. Maitra, Anal. Chem., 53 (1981) 1590.
8 P. W. Alexander, P. R. Haddad, G. K. Low and C. Maitra, J. Chromatogr., 209 (1981) 29.
9 P. W. Alexander, M. Trojanowicz and P. R. Haddad, Anal. Lett., 17(A4) (1984) 309.
10 P. R. Haddad, M. Trojanowicz and P. W. Alexander, J. Chromatogr., 294 (1984) 397.
11 P. W. Alexander, M. Trojanowicz and P. R. Haddad, Anal. Chem., 56 (1984) 2417.
12 J. Růžička and E. H. Hansen, Flow Injection Analysis, Wiley, New York, 1981.
13 A. E. Martell and R. M. Smith, Critical Stability Constants, Vol. 1: Amino Acids, Vol. 2: Amines, Plenum Press, New York, 1974.
14 B. R. James and R. J. Williams, J. Chem. Soc., (1961) 2007.
15 A. Zuberbuhler, Helv. Chim. Acta, 53 (1970) 669.
16 E. C. Knoblock and W. C. Purdy, J. Electroanal. Chem., 2 (1961) 493.
17 W. Stricks and I. M. Kolthoff, J. Am. Chem. Soc., 73 (1951) 1723.
18 K. Srinivasan and R. S. Subrahmanya, J. Electroanal. Chem., 31 (1971) 257.
19 C. J. Hawkins and D. D. Perrin, J. Chem. Soc., (1962) 1231.
20 B. Grgas-Kužnar, Vl. Simeon and O. A. Weber, J. Inorg. Nucl. Chem., 36 (1974) 2151.
21 A. G. Keenan, Ch. A. Webb, D. A. Kramer and K. G. Compton, J. Electrochem. Soc., 123 (1976) 179.
22 M. S. Shapnik, E. M. Gamburg, K. A. Zinkicheva and G. S. Vozdvizhenski, Chem. Abstr., 82 (1975) 23662z.
23 See, e.g., H. P. Agarwal and S. Qureshi, Electrochim. Acta, 19 (1974) 349.
24 H.-H. Strehblow and B. Titze, Electrochim. Acta, 25 (1980) 839.

Analytica Chimica Acta, 171 (1985) 165—174
Elsevier Science Publishers B.V., Amsterdam — Printed in The Netherlands

CONSTRUCTION, ASSESSMENT AND APPLICATIONS OF A DICHROMATE-SELECTIVE LIQUID MEMBRANE ELECTRODE BASED ON TETRAPENTYLAMMONIUM DICHROMATE

P. C. GRITZAPIS, C. E. EFSTATHIOU and T. P. HADJIIOANNOU*

Laboratory of Analytical Chemistry, University of Athens, 104 Solonos Str., Athens 106 80 (Greece)

(Received 9th December 1983)

SUMMARY

A dichromate-selective liquid-membrane electrode based on tetrapentylammonium dichromate dissolved in 2-nitrotoluene is described. The electrode exhibits rapid and linear response to the activity of Cr(VI) anions in the range 5×10^{-4}—2×10^{-2} M dichromate; the slopes of the calibration graphs depend on the acidity. The electrode is useful for end-point indication in titrations of iron(II), arsenic(III), ascorbic acid, thiobarbituric acid, thiourea, and cysteine with dichromate. The electrode is also used as indicator electrode in a potentiometric reaction-rate method for the determination of hydroxyl-containing organic compounds, based on their oxidation by dichromate in acidic solution; ethanol, isopropanol, ethylene glycol, propylene glycol, butylene glycol, and several carbohydrates were determined with a mean error of 1%. The method is applied to determine the ethanol content of alcoholic beverages. Kinetic data are given for the dichromate/ethanol reaction.

Potassium dichromate has long been used in titrations of organic hydroxyl compounds [1—3]. Kinetic studies of these reactions have been done by spectrophotometric methods [4, 5]. In recent years, ion-selective electrodes have been extensively used in kinetic studies and kinetic analysis [6]. Dichromate-selective electrodes have been constructed by Urusov et al. [7] and Iimori et al. [8]; the latter was based on benzyldimethyltetradecylammonium hydrogenchromate in PVC. Dosch [9] found that dichromate gives an orange precipitate with tetrapentylammonium ions in neutral or slightly acidic solutions.

In this paper, a new dichromate-selective electrode with a liquid membrane of tetrapentylammonium dichromate dissolved in 2-nitrotoluene is described. The electrode exhibits rapid and linear response to the activity of Cr(VI) anions in the range 5×10^{-4}—2×10^{-2} M dichromate, and is used here in titrations of various inorganic and organic substances. It is also useful in kinetic studies to monitor the reactions of potassium dichromate with several organic substances and in kinetic analysis.

0003-2670/85/$03.30

EXPERIMENTAL

Apparatus and reagents

The dichromate-selective electrode was used with a single-junction silver/silver chloride reference electrode (Orion, model 90-02-00). Potentials were measured with a Corning Ionanalyzer (Model 12 pH/pIon meter) and recorded with a Heath—Schlumberger system (Model SR-204). The titrant was added with a multispeed constant-rate burette (Radiometer, Model ABU-12). Test solutions were placed in a thermostated double-walled 50-ml cell. All measurements were taken under constant magnetic stirring.

All solutions were prepared with deionized-distilled water and reagent-grade materials.

Stock dichromate, iron(II) and arsenic(III) solutions (0.1000 M) were prepared by dissolving the appropriate amount of potassium dichromate in water, or iron(II) ammonium sulfate in 0.9 M sulfuric acid, and of arsenic(III) oxide in the minimum amount of sodium hydroxide solution with dilution to a final sulfuric acid concentration of 0.9 M, respectively. Stock ascorbic acid (0.1000 M), thiobarbituric acid (0.0200 M), cysteine (0.0200 M), and thiourea (0.1000 M) solutions were prepared in water. Stock 0.500 M solutions of ethanol, isopropanol, ethylene glycol, propylene glycol, butylene glycol (a mixture of the meso and racemic form of 2,3-butanediol), glucose, fructose, galactose, sorbose, lactose, and of sucrose were prepared in water. Working standard solutions were prepared by dilution.

Preparation of the liquid ion-exchanger and electrode construction

Tetrapentylammonium dichromate was precipitated by mixing 20.0 ml of 0.01 M potassium dichromate solution with 20.0 ml of 0.02 M tetrapentylammonium bromide solution. The precipitate was extracted into 20.0 ml of 2-nitrotoluene. The extract was washed twice with distilled water to remove any traces of bromide and dried thoroughly with anhydrous sodium sulfate.

The body of an Orion 92 electrode equipped with a teflon membrane (Millipore LCWPO-1300) was used. The electrode was assembled as recommended by the manufacturer, and the internal reference solution (0.01 M $K_2Cr_2O_7$/0.1 M NaCl) and the liquid ion-exchanger solution (0.01 M tetrapentylammonium dichromate in 2-nitrotoluene) were injected through the appropriate ports of the electrode body.

The dichromate electrode was conditioned by soaking in a 0.01 M dichromate solution for 24 h before use, and was stored in this solution when not in use.

Procedures

Titrimetric determinations. Use a 0.005 M (for the titration of iron(II) and arsenic(III)) or a 0.01 M (for the titration of the organic reductants) dichromate solution in 1.8 M sulfuric acid as titrant.

Pipet into the reaction cell a 20.00-ml aliquot containing 0.07—0.4 mmol of iron(II), or 0.05—0.4 mmol of arsenic(III), or 0.05—0.5 mmol of thiobarbituric acid or thiourea, or 0.02—0.1 mmol of cysteine, or a 15.00-ml aliquot containing 0.03—0.25 mmol of ascorbic acid. All aliquots are adjusted to 1.8 M in sulfuric acid. Start the stirrer and, after the potential has stabilized (about 1 min), start the burette and the recorder simultaneously to obtain the titration curve.

For the determination of ascorbic acid in tablets, weigh twenty tables of each sample, dissolve them in freshly boiled water and dilute to 1 l. Filter if necessary to remove any residue. Dilute further and add sulfuric acid to obtain a solution with the aforementioned ascorbic acid and sulfuric acid concentrations.

Kinetic measurements for the reaction of dichromate with hydroxyl-containing substances. Pipet into the thermostated reaction cell 15.00 ml of 5×10^{-3} M dichromate adjusted to 0.90—3.63 M in sulfuric acid, start the stirrer and, after the potential has stabilized and the solution temperature has reached the desired value within ±0.1° C, start the recorder, pipet quickly 3.00 ml of ethanol solution (0.17—0.85 M) into the cell, and record a large portion of the linear part of the reaction curve. The measured quantity is the slope, $\Delta E/\Delta t$, expressed in mV s^{-1}.

The procedure for the kinetic study of the reactions of dichromate with other organic substances (alcohols, diols, carbohydrates) is the same except that 20.00 ml of 5.0×10^{-3} M dichromate adjusted to 3.6 or 4.5 M in sulfuric acid and a 1 M solution of the organic compound are used.

Kinetic determination of alcohols and diols. Pipet into the reaction cell, thermostated at 26.0° C, 20.00 ml of the appropriate dichromate/sulfuric acid solution (see Table 3), start the stirrer and, after the potential and temperature have stabilized, start the recorder, pipet quickly 2.00 ml of standard or sample solution into the cell, and record the reaction curve.

Kinetic determination of carbohydrates. Pipet into the reaction cell, thermostated at 60° C, 15.00 ml of 5×10^{-3} M dichromate in 4.59 M sulfuric acid and continue as in the determination of alcohols.

Kinetic determination of ethanol in alcoholic beverages. Distil 10.00 ml of spirits down to about 2 ml and dilute the collected distilate to 50.00 ml with water (solution S). For the determination, use 20.00 ml of 0.01 M dichromate in 2.3 M sulfuric acid and 2.00 ml of ethanol working solutions (1—5%, v/v) or solution S.

RESULTS AND DISCUSSION

Characteristics of the electrode

Typical calibration graphs for the dichromate-selective electrode showed a linear response in the 5×10^{-4}—2×10^{-2} M dichromate range. The slope of the calibration graph is linearly dependent on pH in the pH range 0.5—5.5 (Fig. 1). Because almost all dichromate redox reactions take place in strongly

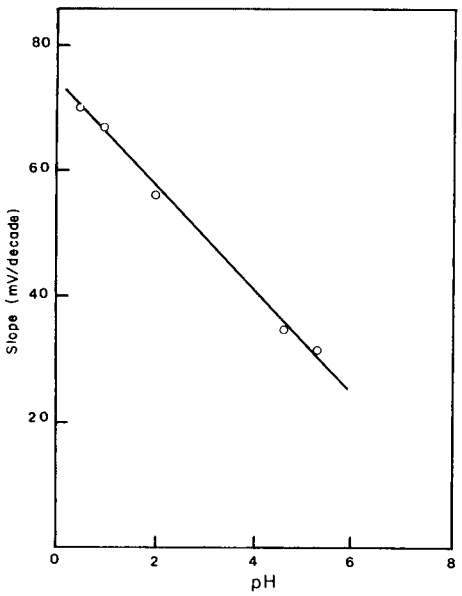

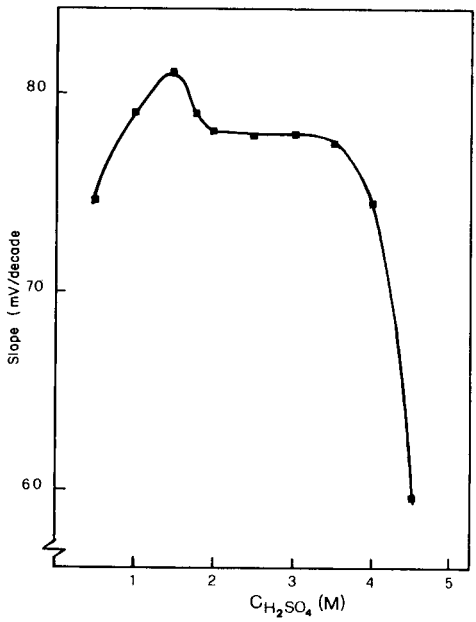

Fig. 1. The pH dependence of the slopes of the calibration graphs for the dichromate-selective electrode.

Fig. 2. Effect of the concentration of sulfuric acid on the calibration slope for the dichromate-selective electrode.

acidic solutions, it was deemed necessary to extend the study of the slope of the calibration graph to more concentrated sulfuric acid solutions. Figure 2, in which the acidity is expressed in terms of molarity of sulfuric acid in the test solution, shows a peculiar dependence of the slope of the calibration graph on the concentration of sulfuric acid, mostly denoting a super-Nernstian response.

The super-Nernstian response can be explained by considering the dimerization of Cr(VI) species at high hydrogen ion concentrations. In the pH range 0.5—5.5, the predominant species is $HCrO_4^-$, but at higher acidities $HCr_2O_7^-$ is formed

$$2HCrO_4^- + H^+ \overset{K}{\rightleftharpoons} HCr_2O_7^- + H_2O$$

Considering that the equilibrium constants for the reactions $2HCrO_4^- \rightleftharpoons Cr_2O_7^{2-} + H_2O$ and $HCr_2O_7^- \rightleftharpoons Cr_2O_7^{2-} + H^+$ are $K_1 = 34$ and $K_2 = 0.85$, respectively [10], then $K = K_1/K_2 = 40.5$. At high acidities (pH < 0), all Cr(VI) species except $HCrO_4^-$ and $HCr_2O_7^-$ can be neglected. If C is the analytical concentration of $Cr_2O_7^{2-}$ used, then from mass-balance considerations $2[HCr_2O_7^-] + [HCrO_4^-] = 2C$. From the above equilibrium reaction, $[HCr_2O_7^-]/[HCrO_4^-]^2 = K[H^+]$. Solving this system of equations yields

$$[HCrO_4^-] = \{-1 + (1 + 16KC[H^+])^{1/2}\}/4K[H^+]$$

$$[HCr_2O_7^-] = C - \{-1 + (1 + 16KC[H^+])^{1/2}\}/8K[H^+]$$

These equations show that, for example, a 10-fold decrease in the concentration of potassium dichromate added does not produce a symmetrical decrease of the two predominant Cr(VI) species. For example, at $[H^+] = 2$ M, a decrease of C from 10^{-2} M to 10^{-3} M produces a 5.3-fold decrease of $[HCrO_4^-]$ and a 28-fold decrease of $[HCr_2O_7^-]$. If the electrode responds to $HCr_2O_7^-$ species then, from a normal slope of about 59 mV per 10-fold decrease of $[HCr_2O_7^-]$, an approximate slope of $59 \times \log(28) = 85$ mV per 10-fold decrease of C, is expected. If, however, the electrode responds to $HCrO_4^-$, a slope of $59 \times \log(5.3) = 43$ mV per 10-fold decrease of C is expected. Apparently, the electrode responds to both $HCrO_4^-$ and $HCr_2O_7^-$, resulting in the peculiar slope dependence shown in Fig. 2 and a potentiometric selectivity coefficient K_{ij}^{pot} of about 0.05 is estimated ($i = HCr_2O_7^-$, $j = HCrO_4^-$). Further increase in the concentration of sulfuric acid (>3.5 M) degrades the electrode response, probably because of full protonation of $HCr_2O_7^-$ and formation of sulfonated Cr(VI) species. Obviously, this strong dependence of the slope of calibration graphs on the sulfuric acid concentration has to be taken into consideration when kinetic data are calculated from electrode potentials.

To check further the pH dependence of the potential of the dichromate-selective electrode, potential/pH curves were constructed. The pH values of the initial solutions were altered by addition of small volumes of concentrated sodium hydroxide or sulfuric acid solutions. The plots (Fig. 3) show that between pH 4 and 5.5, the potential was relatively independent of pH. In this region, $HCrO_4^-$ and $Cr_2O_7^{2-}$ are the predominant ions in the solutions [10]. Presumably $HCrO_4^-$ is the ion sensed by the electrode because at higher pH values there was an increase in potential which corresponded to the decrease in the $HCrO_4^-$ concentration.

The dynamic response was tested for 5×10^{-4}—10^{-2} M dichromate solutions in the presence of various sulfuric acid concentrations (0—4.5 M); the sequence of measurements was from low concentration to high concentration and back. The response times were always quite short (less than 3 s, including mixing). It was therefore possible to use the electrode in titrations with continuous addition of titrant and for kinetic studies.

The interference of perchlorate and nitrate was studied in strongly acidic solutions (0.1 M and 1 M sulfuric acid) by the mixed solution method [11]. Perchlorate interferes strongly ($K^{pot} > 1$) which is not surprising because tetrapentylammonium ion was originally proposed [9] as a precipitant for perchlorate, whereas the interference of nitrate is small ($K^{pot} = 8 \times 10^{-3}$).

Analytical applications

Titrimetric analysis. The dichromate-selective electrode was used as indicator electrode in potentiometric redox titrations of inorganic ions and organic compounds. Iron(II) (0.05—0.4 mmol) and arsenic(III) (0.07—

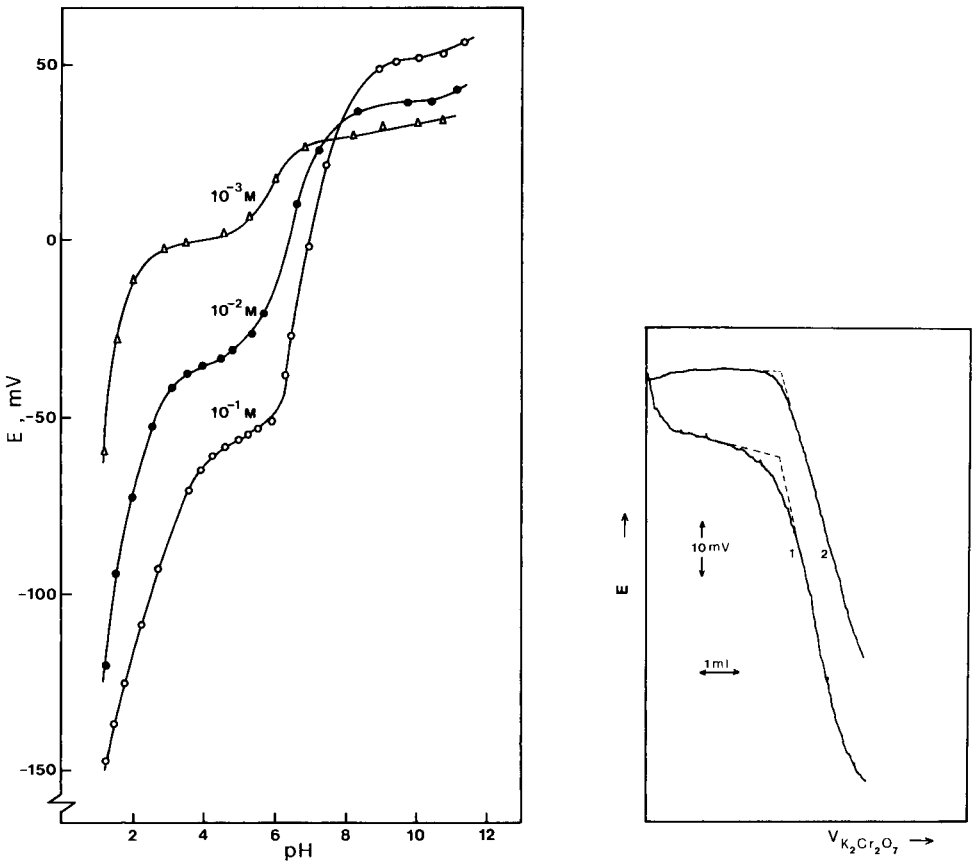

Fig. 3. Effect of pH on the potential of the dichromate-selective electrode at the different concentrations of potassium dichromate.

Fig. 4. Recorded titration curves for 0.1 mmol of arsenic(III), (curve 1), and 0.200 mmol of iron(II) (curve 2) with 0.005 M dichromate in 1.8 M sulfuric acid.

0.4 mmol) were titrated with average errors of 1.3% and 0.8%, respectively. Typical recordings for these titrations are shown in Fig. 4.

Ascorbic acid, thiourea, thiobarbituric acid, and cysteine were oxidized by dichromate in acidic solution rapidly enough for titration purposes but non-stoichiometric molecular ratios were found (Table 1). Similar relationships have been reported for ascorbic acid [12] and thiourea [13—15]. The experimental value of 2.40 moles of ascorbic acid per mole of dichromate was used for the determination of ascorbic acid in pharmaceutical tablets. The results obtained compared favorably (within ±0.8%) with those obtained by the iodate method [16]. Higher results than expected were obtained for ascorbic acid when the tablet also contained other reducing agents (e.g., galactogluconates).

TABLE 1

Mole ratio for the titration of organic reductants with dichromate in 1.8 M sulfuric acid

Reductant	Amount (mmol)	Mole ratio reductant/dichromate with standard deviation
Ascorbic acid	0.030—0.250	2.40 ± 0.013
Thiobarbituric acid	0.050—0.500	2.48 ± 0.100
Cysteine	0.020—0.100	2.51 ± 0.050
Thiourea	0.050—0.500	6.04 ± 0.060

Kinetics of the reactions of dichromate with hydroxyl compounds. The purpose of the kinetic study was to find suitable conditions for possible kinetic determination and to establish the relative reactivity of hydroxyl compounds. The rate of such reactions depends on the temperature and on the concentrations of dichromate, hydroxyl compound (reductant) and sulfuric acid. By keeping the reductant in excess, the reaction becomes pseudo-first order with respect to dichromate. The initial reaction rate can be expressed by the relation $R_0 = k\, C^a_{H_2SO_4}[\text{reductant}]^b[Cr_2O_7^{2-}]$. At constant temperature and for constant acid and reductant concentrations (both in large excess over dichromate), $R_0 = -dC_{Cr_2O_7^{2-}}/dt = k_{obs}C_{Cr_2O_7^{2-}}$, where k_{obs} = 2.303 [slope of potential/time curve (mV s^{-1})]/experimental slope of electrode (mV per conc. decade). The k_{obs} value depends on the nature of the hydroxyl compound (Table 2). The values of a and b can be calculated from $k_{obs} = k_1 C^a_{H_2SO_4}$ and $k_{obs} = k_2[\text{reductant}]^b$ and evaluated experimentally from the slope of the log k_{obs} vs. log (concentration) graph; b ranged between 0.8 and 1.2 for all organic compounds, denoting a practically first-order dependence of the overall reaction rate on their concentration, whereas the a values were more inconsistent, being in the range 0.7—1.7 for alcohols and glycols measured at 26°C and in the range 2.2—3.4 for carbohydrates measured at 60°C. The values of a for the dichromate/ethanol reaction were temperature-dependent, the values being 1.64, 1.68, 1.72, and 1.73 at 22.0, 26.0, 30.0, and 35.0°C, respectively. From Arrhenius plots of ln k vs. K^{-1} (the absolute temperature), the activation energy was calculated to be (10.5 ± 1.2) kcal mol^{-1} for the dichromate/ethanol reaction.

Determination of alcohols and diols. Kinetic determinations of several alcohols and diols in solutions of known concentration gave the results shown in Table 3. The kinetic method was also used to determine the ethanol content in wines and alcoholic beverages. The recorded reaction curves for standard ethanol solutions (1—5% v/v) and the corresponding calibration curve are shown in Fig. 5. A slight induction period was noted for all primary alcohols because of the formation of an intermediate aldehyde which was finally oxidized to organic acid. No induction period was observed with aldehydes and secondary alcohols because the final product is formed practically in one step. Because wines contain many reducing agents besides

TABLE 2

Values of k_{obs} for the dichromate/organic reductant reaction at 25° C

Reductant[a]	$k_{obs} \times 10^4$ (s^{-1})	Reductant[a]	$k_{obs} \times 10^4$ (s^{-1})
Methanol	3.50	Propylene glycol	118
Ethanol	49.0	Butylene glycol	453
Isopropanol	59.0	Formaldehyde	532
Ethylene glycol	19.8	Glucose	24.5

[a]Initial concentrations: $C_{K_2Cr_2O_7} = 4.37 \times 10^{-3}$ M, [Reductant] = 0.130 M, $C_{H_2SO_4}$ = 3.13 M.

TABLE 3

Results for the kinetic determination of alcohols and diols

Substance	Conc. range of sample (M)	Error[a] (%)	Initial concentrations (M)	
			$K_2Cr_2O_7$	H_2SO_4
Ethanol	0.035—0.14	0.7	4.5×10^{-3}	4.18
	0.17—1.21	1.2	4.5×10^{-3}	2.78
Isopropanol	0.26—1.31	0.4	9.1×10^{-3}	2.78
Ethylene glycol	0.36—1.80	1.3	9.1×10^{-3}	2.78
Propylene glycol	0.018—0.091	1.1	4.5×10^{-3}	2.78
	0.018—0.091	0.5	4.5×10^{-3}	3.47
Butylene glycol	0.018—0.182	0.8	4.5×10^{-3}	2.78

[a]Average error of five determinations with synthetic samples covering the stated concentration range.

ethanol which may react with dichromate and cause positive errors, the ethanol was distilled first and quantified in the distillate. It was found that distillation could be omitted for alcoholic beverages if an accuracy of 4% was acceptable. Results obtained by the proposed method were in accord with those obtained by measuring the specific gravity of the distillate. The correlation coefficient r for the two methods was 0.9997 and the equation of the regression line was (% ethanol, kinetic method) = 0.979 (% ethanol, s.g. method) + 0.245 (n = 25).

Determination of carbohydrates. Glucose, fructose, galactose, and sorbose (0.01—0.1 M) in aqueous solutions were determined by the proposed method with an average error of 1%. The reaction rate was the same for equimolar sucrose and invert sugar solutions which proves that sucrose was hydrolyzed quantitatively under the experimental conditions. This was not the case for equimolar lactose and glucose/galactose solutions; the reaction rate was smaller for the former because of incomplete hydrolysis of lactose under the experimental conditions.

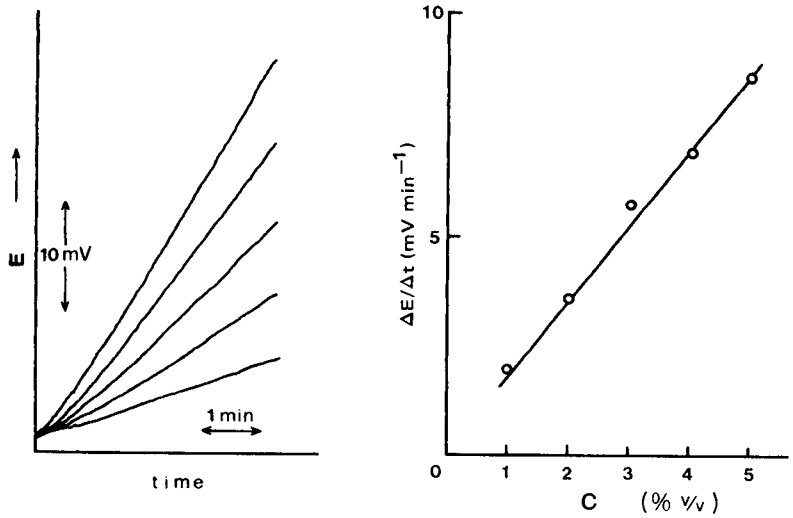

Fig. 5. Recorded curves of cell voltage vs. time for the dichromate/ethanol reaction and the corresponding calibration curve for the determination of ethanol in wines and spirits.

Conclusions

Hitherto, dichromate reactions have commonly been monitored by spectrophotometric means. Potentiometric monitoring based on the Cr(VI)/Cr(III) redox couple is feasible though not practical for monitoring only Cr(VI) species, and has mostly been used for end-point detection in titrations with dichromate.

The membrane electrode proposed above can be used for monitoring only Cr(VI) species and is advantageous for obtaining kinetic data from relatively slow oxidation reactions with dichromate. The kinetic determinations of ethanol and other hydroxyl-containing organic compounds do not offer significant advantages over other more conventional instrumental techniques but are much faster than the corresponding equilibrium (titrimetric) methods and provide another example of the application of ion-selective electrodes in the field of kinetic analysis.

The authors thank E. P. Diamandis for stimulating discussions and E. Holiastou for technical assistance. The research was supported in part by a grant from the Greek National Institute of Research.

REFERENCES

1 Reischamer, Dinglers Polytech. J., 185 (1862) 451.
2 O. Henner, Analyst (London), 12 (1887) 44; J. Soc. Chem. Ind., 8 (1889) 44.
3 M. J. Gardone and J. W. Compton, Anal. Chem., 25 (1953) 1869; Cf 24 (1952) 1903.
4 F. Hasan and J. Roček, J. Am. Chem. Soc., 94 (1972) 3181.

5 G. F. Vandergrift and J. Roček, J. Am. Chem. Soc., 98 (1976) 1371.
6 G. J. Moody and J. D. R. Thomas, in H. Freiser (Ed.), Ion-Selective Electrodes in Analytical Chemistry, Vol. 1, Plenum Press, New York, 1978, p. 346.
7 Yu. I. Urusov, V. V. Sergievskii, A. E. Zhukov and A. V. Gordievskii, Zh. Anal. Khim., 34 (1978) 156.
8 T. Iimori, M. Sugawara and T. Kambara, Denki Kagaku Oyobi Kogyo Butsuri Kagaku, 47(9) (1979) 599; Anal. Abstr., 40 (1981) 2J131.
9 R. G. Dosch, Anal. Chem., 40 (1968) 829.
10 J. N. Butler, Ionic Equilibrium, Addison-Wesley, Reading, MA, 1964, p. 360.
11 G. J. Moody and J. D. R. Thomas, Selective Ion-Sensitive Electrodes, Merrow, Watford, 1971, p. 14.
12 L. Erdey and G. Svehla, Ascorbinometric Titrations, Akadémiai Kiadó, Budapest, 1973, p. 119.
13 A. Kurian and C. V. Suryanarayana, Analyst (London), 97 (1972) 576.
14 K. E. Reid, Organic Chemistry of Bivalent Sulfur, Vol. 5, Chemical Publishing Co., New York, 1963, p. 38.
15 J. Kirchnerová and W. C. Purdy, Anal. Chim. Acta, 123 (1981) 83.
16 G. S. Deshmukh and M. G. Barrat, Z. Anal. Chem., 145 (1955) 254.

Analytica Chimica Acta, 171 (1985) 175—184
Elsevier Science Publishers B.V., Amsterdam — Printed in The Netherlands

AMMONIA ABATEMENT IN AN ENZYMATIC FLOW SYSTEM FOR THE DETERMINATION OF CREATININE IN BLOOD SERA AND URINE

M. MASCINI*, S. FORTUNATI, D. MOSCONE and G. PALLESCHI

Department of Chemical and Technological Sciences, II University of Rome, Tor Vergata, 00173 Rome (Italy)

(Received 25th October 1984)

SUMMARY

The abatement of ammonia in standard solutions, and in human blood and urine samples is achieved by adding suitable amounts of NADPH and α-ketoglutarate to the sample and passing it through a 2-m nylon tube with glutamate dehydrogenase immobilized on the inner wall. The procedure provides removal of 98% of the ammonia ($1—5 \times 10^{-4}$ M) in the original sample in 50 s. The abatement of ammonia permits the use of an ammonia probe coupled with an immobilized degradative enzyme for the determination of creatinine. Creatinine was determined in clinical blood and urine samples by first removing the ammonia from the sample and then cleaving the creatinine to *N*-methylhydantoin and ammonia with immobilized creatininase. Only 200 μl of sample is needed and the entire process is conducted in a single flow stream.

The potentiometric ammonia sensor is a valuable detector for monitoring substrates of biological and clinical interest when coupled with a suitable biological mediator [1—7] or when used as a monitor for enzyme activities in the presence of a suitable substrate [8—10]. The biological mediator (a suitable enzyme, bacteria or whole tissue) selectively converts substrates to ammonia which is rapidly detected by the potentiometric probe. Flow systems are used in most studies when the optimum conditions needed for the biocatalytic activity do not match the pH requirements of the sample for the ammonia probe.

In all cases, the amount of ammonia produced is related to the substrate concentration or to the enzyme activity when the reaction time is fixed. Therefore, the major interference with these sensors arises from the endogenous ammonia of the sample which severely limits the sensitivity. Often, the metabolites of interest (amino acids or similar) are at the same level of concentration as the endogenous ammonia so that useful determinations cannot be achieved. Sometimes, subtraction can be used for correction, but the logarithmic response of the ammonia probe limits such operations to selected cases; if the ammonia concentration is far higher than the metabolite of interest, the error in the subtraction procedure offsets the selectivity of the determination.

0003-2670/85/$03.30

In a recent paper [11], the determination of creatinine in blood and urine samples was reported; the automated system was based on an immobilized creatininase reactor and an ammonia gas sensor. In order to obtain an accurate value for the creatinine when this system was used, the blood samples had to be analyzed as soon as they were taken from the patients; the ammonia had to be determined first and the value subtracted from the final response. The ammonia in urine samples had to be removed by a cation-exchange method before the determination of creatinine.

More recently, Fraticelli and Meyerhoff [12] reported a partial solution to the problem by dialyzing the sample through a teflon gas-permeable tubing (4.2 m long, 1 mm i.d.) which was coiled and placed in a 1-l acid reservoir. Although the coil proved to be quite efficient (>95%) in removing ammonia from aqueous samples ranging between 10^{-5} and 10^{-3} mol l^{-1} ammonia, when real samples (e.g., serum) were assayed the efficiency of ammonia removal decreased to about 80% because the high viscosity of serum or plasma interfered with the diffusion rate of ammonia from the sample.

In the method proposed here, an enzyme immobilized on a nylon coil decreases the amount of ammonia to trace values and virtually eliminates the interference. The enzyme employed is glutamate dehydrogenase (GLDH) which catalyses the reaction

$$NH_4^+ + \alpha\text{-ketoglutarate} \xrightarrow[NADPH/NADP^+]{GLDH} \text{L-glutamate} + H_2O \qquad (1)$$

The enzyme must be immobilized because only the endogenous ammonia should be eliminated and not the ammonia subsequently liberated by the metabolite of interest (amino acid or similar or in the enzymatic reaction). Immobilization of the enzyme on a nylon coil enables a flow system to be used, so that the time needed for a determination is reduced. In this study, two enzymes of different nature were examined, one obtained from beef liver and the other from *Proteus* sp., both immobilized on nylon tubes. The ammonia abatement from aqueous standard solutions was evaluated in the range commonly found for clinical endogenous ammonia (i.e., 5×10^{-4}–10^{-5} M). The system was then applied to the measurement of creatinine in blood and urine after the abatement of ammonia and subsequently through the use of a creatininase reaction [11].

EXPERIMENTAL

Equipment and reagents

An ammonia electrode (Instrumentation Laboratory) was assembled in a flow-through cell with polypropylene microporous membranes (Celanese Plastic Company) in a thermostatted chamber (25 ± 0.1°C); the dead volume was 40 μl. Potentials were measured with an AMEL potentiometric recorder (Model 866).

Nylon tubes (1 mm i.d.) were obtained from Portex (Hythe, Kent,

England). The creatininase nylon coil (1 mm i.d., 1 m long; Clinibond) was provided by Farmitalia Carlo Erba (Milano); the immobilized enzyme is the creatinine iminohydrolase, E.C.3.5.4.27 [11].

Glutamate dehydrogenase (E.C.1.4.1.3, from beef liver) was obtained lyophilized (15 U mg^{-1}) from Boehringher-Mannheim. Glutamate dehydrogenase E.C.1.4.1.4, from *Proteus* sp.) was obtained (Toyobo Enzymes, Tokyo, Japan) as a suspension in 50% (v/v) glycerol buffered with 0.025 M Tris (8000 U ml^{-1}). This enzyme solution was dialyzed against 0.025 M phosphate buffer, pH 7.5, and then diluted with 0.1 M phosphate buffer to obtain a final 2500 U ml^{-1} solution.

The NADH (disodium salt) and NADPH (tetrasodium salt) were obtained from Boehringher-Mannheim. All other reagents were of analytical grade.

Procedure for immobilizing enzymes

The chemical procedure for immobilizing the enzymes on the inner wall of the nylon tube is derived from the work of Hornby and Morris [13]. The nylon tube is washed with a 18% (w/v) calcium chloride solution in methanol/water (1:4) at 60°C for 30 min. This treatment removes the chemicals used in the final manufacturing treatment. The tube is then dried with compressed air, filled with dimethyl sulfate, sealed carefully and immersed in boiling water for 15 min; the reaction is then quenched by immersion in ice water and the tube is washed with methanol. Next, the tube is filled with 18% (w/v) 1,6-diaminohexane in methanol and left for 3 h at room temperature. The tube is then washed with 1 M sodium chloride, filled with a 12.5% (w/v) glutaraldehyde solution in 0.1 M borax buffer (pH 7.5) and left for 15 min at a flow rate of 1 ml min^{-1}. The tube is washed with a 0.1 M phosphate buffer (pH 7.5) and finally filled with the enzyme solution in 0.1 M phosphate buffer (pH 7.5) and left overnight at 4°C.

Before use, the tube is washed with the phosphate buffer and with 1 M sodium chloride to eliminate any unbound enzyme.

Flow system used for ammonia abatement studies

The manifold used to study the ammonia abatement efficiency is shown in Fig. 1. Ammonia standard solutions and biological samples, with α-keto-

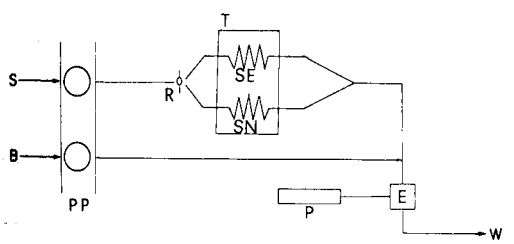

Fig. 1. Manifold for evaluation of the ammonia abatement efficiency: S, sample stream at 1 ml min^{-1}; B, 0.1 M sodium hydroxide at 0.15 ml min^{-1}; PP, peristaltic pump; R, three-way stopcock; T, thermostat at 25 ± 0.1°C; SE, coil with immobilized enzyme; SN, empty nylon coil; E, ammonia probe; P, potentiometer recorder; W, waste.

glutarate and NADH (or NADHP) added at various concentrations, are pumped through the immobilized enzyme coil (SE). The stopcock and the empty coil are provided to minimize variations in flow dispersions during the evaluation of the efficiency of the system. The ammonia electrode is used for evaluating the amount of ammonia left in the flowing sample.

Ammonia standard solutions in a suitable buffer and with α-ketoglutarate and NADH (or NADPH) added were pumped through the empty coil (SN) to calibrate the ammonia electrode in the range 5×10^{-7}—10^{-4} mol l^{-1}. Response times in this range were less than 60 s, as previously reported [11]. Thereafter the standard solutions were pumped through the coil with immobilized enzyme (SE). By using the calibration graph, the residual ammonia concentrations were calculated.

Flow system recommended for creatinine determination with preliminary ammonia abatement

The manifold used for the analysis of sera and urine is shown in Fig. 2. Reactor coil SE (2 m long, 1 mm i.d.) has the immobilized GLDH from *Proteus* sp. (E.C.1.4.1.4). Reactor soil SC is the creatininase nylon coil (see above). The sample stream (S) is 0.1 M Tris buffer, pH 8.5, pumped continuously at 1 ml min^{-1}. Stream B is 0.1 M sodium hydroxide pumped at 0.15 ml min^{-1}.

The procedure is simple. Portions (200 μl) of standard solutions or serum samples are diluted to 1 ml with Tris buffer, pH 8.5, containing the coenzyme NADPH (0.6 mg ml^{-1}) and α-ketoglutarate (1 mg ml^{-1}). While the Tris buffer pH 8.5 is pumped continuously, the potential of the ammonia electrode is recorded; then the sample is pumped for 1 min (the flow rate remains 1 ml min^{-1}), after which the Tris buffer is pumped again. The system is maintained at 25 ± 1°C.

RESULTS AND DISCUSSION

Optimization of the ammonia abatement procedure

The reaction for ammonia abatement depends on the source of the enzyme used (cf. reaction 1). For GLDH from beef liver (E.C.1.4.1.4) the

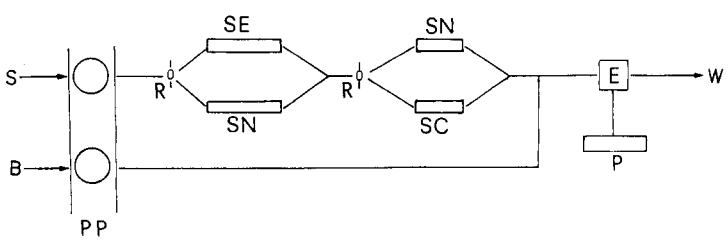

Fig. 2. Manifold for creatinine determination with preliminary ammonia abatement: S, B, PP, R, E, P and W as in Fig. 1; SE, coil with GLDH 1.4.1.4 immobilized; SN, empty nylon coil; SC, coil with immobilized creatininase.

TABLE 1

Ammonia abatement with the two different enzymes for various concentrations of ammonia (immobilized conditions); enzyme immobilized in 2-m tube (1 mm i.d.); 0.1 M Tris buffer, pH 8.5; 6.8×10^{-3} M α-ketoglutarate; with enzyme 1.4.1.3, [NADH] = 1.4×10^{-3} M and with enzyme 1.4.1.4, [NADPH] = 6.0×10^{-4} M

NH_4^+ before reaction (M)	NH_4^+ after reaction (M)	Abatement (%)	NH_4^+ before reaction (M)	NH_4^+ after reaction (M)	Abatement (%)
Enzyme E.C.1.4.1.3			*Enzyme E.C.1.4.1.4*		
1×10^{-5}	6×10^{-7}	94	8×10^{-5}	1.6×10^{-6}	98
2×10^{-5}	8×10^{-7}	96	1×10^{-4}	2×10^{-6}	98
5×10^{-5}	1.4×10^{-6}	97	1.4×10^{-4}	2.8×10^{-6}	98
8×10^{-5}	4.0×10^{-6}	95	2×10^{-4}	3×10^{-6}	98
1×10^{-4}	2×10^{-5}	80	2.7×10^{-4}	7×10^{-6}	97
2×10^{-4}	3.5×10^{-5}	82			

coenzyme is NADPH, whereas for GLDH from *Proteus* sp. (E.C.1.4.1.3) the coenzyme is NADH.

Table 1 lists the abatement of standard solutions of ammonia obtained with the two enzymes immobilized on nylon coils in the manifold outlined in Fig. 1. The more effective nature of the enzyme obtained from *Proteus* sp. (E.C.1.4.1.4.) is evident, the abatement being about 98% even at a level of 10^{-4} M ammonium). Similar results were obtained with a coil only 1 m long with this enzyme. The effects of varying the concentration of the coenzyme were evaluated. Results are collected in Fig. 3 in terms of ammonia abate-

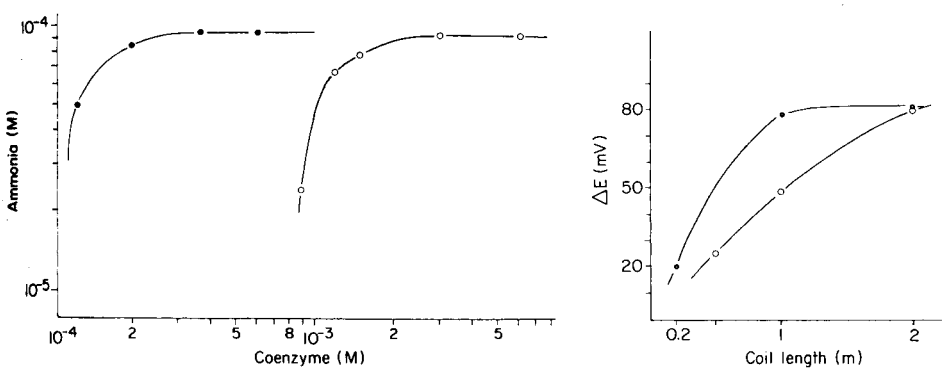

Fig. 3. Ammonia abatement vs. coenzyme concentration for 10^{-4} M ammonium ion. Conditions: Tris buffer pH 8.5; 6.8×10^{-3} M α-ketoglutarate; 2-m coil with immobilized enzyme. Coenzyme: (•) NADPH for GLDH 1.4.1.4; (○) NADH for GLDH 1.4.1.3.

Fig. 4. Effect of coil length on the abatement efficiency for 10^{-4} M ammonium ion: (○) 2.8×10^{-3} M NADH for GLDH 1.4.1.3; (•) 6.8×10^{-4} M NADPH for GLDH 1.4.1.4. Other conditions as for Fig. 3 (except coil length).

ment vs. coenzyme concentration. The superior behaviour of the GLDH from *Proteus* sp. is again evident. It is interesting to note that the enzymatic reaction consumes 1 mol of NADH or NADPH per mole of ammonium ion, while under the conditions used for Fig. 3, the amount of coenzyme necessary to obtain complete abatement of ammonia is far higher than the ammonia concentration and depends on the source of the enzyme.

The effect of the coil length is shown in Fig. 4 for 10^{-4} M ammonia in Tris buffer pH 8.5 at 1 ml min^{-1}. Both enzymes reach 98% removal of ammonia (80 mV change in e.m.f.) with 2 m of coil. Again the E.C.1.4.1.4 enzyme is favoured. The pH and buffer effects with Tris and phosphate buffers are depicted in Fig. 5. The ordinate corresponds to the ammonia abatement (expressed as the change in potential of the ammonia probe on passing standard ammonia solution (10^{-4} M) into the coil at 1 ml min^{-1}). The optimum pH for the 1.4.1.3 enzyme in solution was found to be 7.6 whereas in the immobilized form, the optimum pH value is in the range 8.0—8.5. Temperature in the range 23—35°C caused only a slight increase (10—20%) in the reaction rate, but thermostatting is obviously necessary.

The lifetime of the immobilized enzymes is one of the more delicate parameters to evaluate; it generally depends on the number of analyses and on the temperature of storage. Over a six-month period, during which the coil (when not in use) was stored at 4°C, the efficiency was evaluated for the coil with the GlDH from *Proteus* sp. (E.C.1.4.1.4) which was the more promising from the analytical point of view. There was only a slight decrease in the abatement efficiency (Fig. 6). All samples analyzed (more than 500) contained ammonia in the range of 1—6 × 10^{-4} M, which is the normal concentration of endogenous ammonia in biological samples.

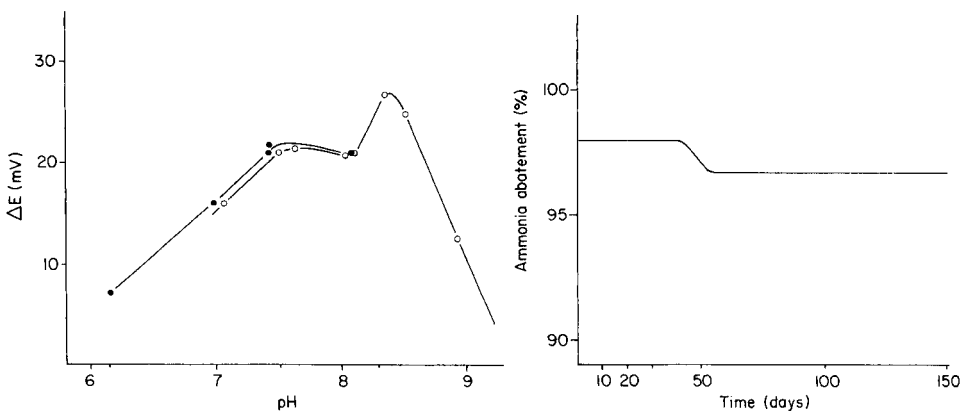

Fig. 5. Buffer and pH effect on GLDH 1.4.1.3 for the abatement of 10^{-4} M ammonium ion: (○) 0.1 M Tris buffer; (●) 0.1 M phosphate buffer. Conditions: 1-m coil; 1.4 × 10^{-3} M NADH; 6.8 × 10^{-3} M α-ketoglutarate.

Fig. 6. Lifetime of the GLDH E.C.1.4.1.4. Conditions: 6.8 × 10^{-3} M α-ketoglutarate, 6 × 10^{-4} M NADPH, 0.1 M Tris buffer pH 8.5; 25°C; 2-m coil; flow rate 1 ml min^{-1}. The ammonia concentrations were in the range 1—6 × 10^{-4} M.

On the basis of all the above results, the recommended conditions for the abatement of up to 2×10^{-4} M ammonia in 100 s to trace levels are as follows: a 2-m coil (1 mm i.d.) of immobilized GLDH from *Proteus* sp. (E.C.1.4.1.4); addition of α-ketoglutarate and coenzyme (NADPH) to the samples to give concentrations of 6.8×10^{-3} M and 6×10^{-4}—1.2×10^{-3} M, respectively; Tris buffer at pH 8.5 with a flow rate of 1 ml min^{-1}; and thermostatting at 25 ± 0.1°C.

Specific activity of immobilized enzymes

The integrated form of the Michaelis—Menten equation for all open tube with an immobilized enzyme can be written as follows [6]

$$FS - K_M \ln (1 - F) = K_T L Q^{-1}$$

where F is the fraction of substrate converted, S the initial concentration of substrate (mM), K_M the substrate concentration needed to obtain half the maximum rate (mM), L the length of the tube (cm), Q the flow rate (ml min^{-1}), and K_T the specific activity of the tube (μmol min^{-1} cm^{-1}). Plots of FS against ln $(1 - F)$ were found to be straight lines with both enzymes when the coil used was either a 50-cm tube with GLDH E.C.1.4.1.3 or a 20-cm tube with GLDH E.C.1.4.1.4. Extrapolation of the straight lines to the ordinate enabled K_T to be calculated. The value found for the enzyme from beef liver (E.C.1.4.1.3) was 9×10^{-3} μmol cm^{-1} min^{-1} and that for the enzyme from *Proteus* sp. (E.C.1.4.1.4) was 1.5×10^{-2} μmol cm^{-1} min^{-1}. The K_M values obtained by computation of the slope were, respectively, 4×10^{-4} M and 3×10^{-4} M for the two enzymes.

Determination of creatinine

By placing a creatininase reactor coil in series after the ammonia abatement stage, it was possible to determine creatinine in clinical samples as previously described [11]. The calibration curve shown in Fig. 7 was obtained by pumping a series of creatinine standards in the Tris buffer. The creatininase cleaves the creatinine to ammonia and *N*-methylhydantoin.

To evaluate the overall system, the manifold in Fig. 2 was assembled; this system could be switched as required to determine the initial ammonia concentration, the abatement percentage, the ammonia left in the flowing solution and the creatinine content of the clinical sample. The two empty coils were also useful in minimizing variations in flow rate and analyte dispersion. Reconstituted sera, human sera, and human urine were analyzed in this manifold with the aid of the calibration curve in Fig. 7.

Table 2 shows a comparison of the creatinine values in reconstituted and human sera obtained by a reference method and by the proposed method described under Experimental. The ammonia concentration after the abatement with the immobilized enzyme was negligible and the ammonia obtained after the enzymatic degradation of creatinine was evaluated directly from the calibration curve. The linear regression for the results (Table 2) obtained

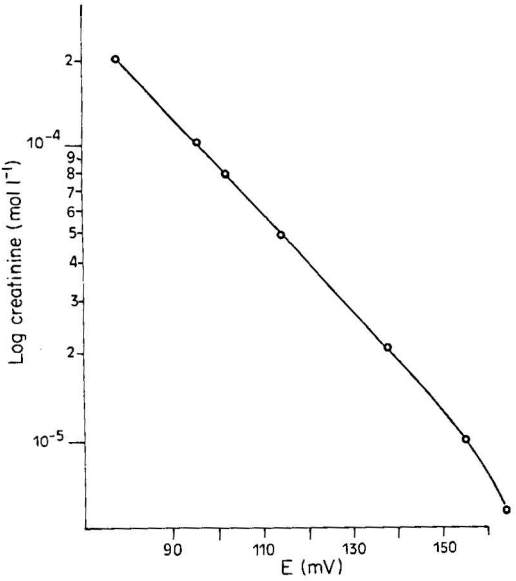

Fig. 7. Calibration curve for creatinine. Conditions: 0.1 M Tris buffer, pH 8.5, 25° C, flow rate 1 ml min^{-1}, 2 m nylon tube with immobilized GLDH, 1-m nylon tube with immobilized creatininase.

TABLE 2

Comparison of results obtained for creatinine in reconstituted sera and human sera received from a local hospital

Serum	Creatinine found (10^{-4} M)		Difference (%)	NH_4^+ found in serum[b] (10^{-4} M)
	Reference method[a]	Proposed method		
Reconstituted				
Precipath U 1-522	3.26	3.15	3	2.5
Precipath U 1-522	3.26	3.25	0.3	5
Precinorm	1.68	1.70	1.2	
Precilip	0.902	0.900	0.2	2
Clinical				
1	2.30	2.10	8.7	0.5
2	0.80	0.79	1.2	1
3	0.53	0.50	5.6	2
4	0.71	0.71	—	2
5	0.80	0.85	6.25	1
6	0.88	0.95	7.9	3
7	0.97	0.95	2	3
8	0.80	0.80	—	3
9	4.0	4.0	—	0.5
10	1.24	1.23	0.8	4
11	0.37	0.38	2.7	—
12	1.10	1.10	—	—

[a]The reference method was spectrophotometric (Beckman Astra 8). [b]Without the abatement procedure.

by the reference method (x) and by the proposed method (y) was $y = 1.0064x - 0.0178$ ($r = 0.9989$; $n = 15$).

With urine samples (Table 3), the dilution was 1:500 because of the high concentrations of ammonia and creatinine. However, the abatement of ammonia still left a measurable ammonia content which was corrected for by subtraction from the ammonia value obtained from the degradation of creatinine. Comparison of the values for creatinine shows a clear difference in some cases. This is probably due in part to the high sensitivity of the spectrophotometric procedure to interference and partly to errors arising from the subtraction in the potentiometric method. Table 4 summarizes the results of recovery experiments in which creatinine was added to urine samples and determined by the proposed method including the ammonia abatement. These results suggest a high level of accuracy for the proposed method.

TABLE 3

Comparison of results obtained for creatinine in urine samples received from a local hospital

Sample	Creatinine found (10^{-2} M)		Difference (%)	Ammonium (10^{-2} M)	
	Reference method	Proposed method		In sample	After abatement
1	0.57	0.56	2	2.1	0.1
2	2.16	2.5	14	6.3	0.25
3	3.23	4.4	36	8.75	0.36
4	1.1	1.4	27	4.4	0.18
5	1.4	1.2	14	3.7	0.15
6	6.3	7.5	16	2.0	0.083
7	1.9	1.8	5	5.4	0.21
8	1.3	1.8	38	5.5	0.22

TABLE 4

Recovery of creatinine added to urine samples

Creatinine (10^{-2} M)		Recovery (%)	Ammonium (10^{-2} M)	
Added	Found		In sample	After abatement
0	2.5	—	4.3	0.12
2.0	4.5	100	4.3	0.12
2.0	6.5	100	4.3	0.12
0	2.6	—	5.0	0.2
1.0	3.5	97	5.0	0.2
1.0	4.4	96	5.0	0.2
2.0	6.5	98	5.0	0.2

Conclusion

The proposed method for abatement of endogenous ammonia proved to be valid when synthetic samples as well as clinical samples, like serum and urine were tested. The measurement of creatinine after the abatement of ammonia becomes easy. The pH and buffer suitable for the enzymatic degradation of creatinine with creatininase are the same as the conditions needed for the enzymatic abatement stage. The determinations of other metabolites (e.g., asparagine or leucine), or of enzyme activities, which are based on specific degradation to ammonia and which suffer interference from endogenous ammonia, could be simplified and made more practical by similar arrangements. Work on these aspects is in progress.

REFERENCES

1 G. G. Guilbault, S. P. Chen and S. S. Kuan, Anal. Lett., 13 (1980) 1607.
2 G. A. Rechnitz, M. A. Arnold and M. E. Meyerhoff, Nature, 278 (1979) 446.
3 M. A. Arnold and G. A. Rechnitz, Anal. Chim. Acta, 113 (1980) 351.
4 S. Kuriyama and G. A. Rechnitz, Anal. Chim. Acta, 131 (1981) 91.
5 C. L. DiPaoloantonio, M. A. Arnold and G. A. Rechnitz, Anal. Chim. Acta, 128 (1981) 121.
6 M. Mascini and G. A. Rechnitz, Anal. Chim. Acta, 116 (1980) 169.
7 D. P. Nikolelis and T. P. Hadjiioannou, Anal. Chim. Acta, 147 (1983) 33.
8 P. Seegopaul and G. A. Rechnitz, Anal. Chim. Acta, 151 (1983) 91.
9 C. R. Gebauer, M. E. Meyerhoff and G. A. Rechnitz, Anal. Biochem., 45 (1979) 479.
10 M. Hato, H. Nakayama and Y. Shimura, Anal. Chim. Acta, 149 (1983) 203.
11 M. Mascini and G. Palleschi, Anal. Chim. Acta, 136 (1982) 169.
12 Y. M. Fraticelli and M. E. Meyerhoff, Anal. Chem., 55 (1983) 359.
13 W. E. Hornby and D. L. Morris, in H. H. Weetall (Ed.), Immobilized Enzymes, Antigens, Antibodies and Peptides, M. Dekker, New York, 1975, p. 141.

Analytica Chimica Acta, 171 (1985) 185—194
Elsevier Science Publishers B.V., Amsterdam — Printed in The Netherlands

SIMULTANEOUS DETERMINATION OF SUCROSE AND GLUCOSE IN MIXTURES BY FLOW INJECTION ANALYSIS WITH IMMOBILIZED ENZYMES

M. MASOOM and ALAN TOWNSHEND*
Chemistry Department, University of Hull, Hull HU6 7RX (Great Britain)
(Received 25th October 1984)

SUMMARY

Sucrose is determined in a flow-injection system by using a manifold comprising columns of invertase/mutarotase and glucose (immobilized on controlled-pore glass) in sequence, and amperometric detection of the hydrogen peroxide produced. The system can be modified to allow the sequential determination of sucrose and glucose (10^{-4}—10^{-2} M) by incorporating a controlled bypass around the invertase column, thus allowing one sample to traverse both columns (giving a response from glucose and sucrose) and the next to pass through only the glucose oxidase column (glucose response only). Further modification allows a single sample to be split between the two flow paths, so that two peaks are obtained in sequence (sucrose/glucose, and glucose). Both procedures are rapid and precise.

Enzyme electrodes have been applied not only to the determination of glucose [1—3] but enzyme sequence electrodes based on glucose oxidase have been developed for the determination of disaccharides, such as sucrose [4—7], lactose [5] and maltose [7]. The disaccharide-hydrolyzing enzyme (e.g., invertase for sucrose) is co-immobilized with glucose oxidase and fixed over an oxygen electrode [4]. These enzyme sequence electrodes can be used for the determination of disaccharides only in the absence of glucose because the electrode also responds to glucose. In many foods and beverages, however, combinations of sugars (e.g., glucose and sucrose) are common and the measurement of both components is necessary for effective process and product control.

Measurements of glucose and disaccharides have been achieved by two differently constituted enzyme electrodes [8]. For example, maltose in the presence of glucose has been determined by using a measuring cell with two electrodes containing glucose oxidase and glucose oxidase/glucoamylase, respectively. The first electrode measures glucose only, while the enzyme sequence electrode measures the sum of glucose and maltose. A multilayer enzyme electrode has been used for direct determination of sucrose in glucose-containing samples [9] where the glucose is eliminated by an outer layer containing glucose oxidase and catalase whilst the sucrose reaches the

0003-2670/85/$03.30

glucose oxidase/invertase layer which is in contact with the indicating electrode for hydrogen peroxide. Successive measurements of glucose and sucrose have also been achieved by using a measuring cell reactor containing a glucose oxidase membrane electrode, and inverting sucrose in the measuring cell by means of soluble invertase [10]. Immobilized invertase was later applied to the same system [11]. All these methods suffer from the disadvantages of long times, high reagent consumption and poor reproducibility.

In an earlier paper [12], glucose was determined by flow injection analysis with immobilized glucose oxidase. The method was rapid (300 samples h^{-1}), economical and was used to determine glucose in blood. This paper extends this procedure to the simultaneous determination of sucrose and glucose in mixtures by using the appropriate immobilized enzymes in packed columns. The method is again simple, rapid and sensitive and has been applied to standard mixtures of sucrose and glucose as well as to soft drinks.

EXPERIMENTAL

Reagents

Glucose oxidase (Glucose:oxygen oxidoreductase, EC.1.1.3.4., ex. *Aspergillus niger*, 250 U mg^{-1}), invertase (β-D-fructofuranoside fructohydrolase, EC.3.2.1.26., ex. bakers yeast, 100 U mg^{-1}) and mutarotase (aldose mutarotase; aldose L-epimerase, EC.5.1.3.3., ex. pig liver, 5000 U mg^{-1}) were obtained from Sigma Chemical Co. Glucose and sucrose were AnalaR grade (BDH Chemicals). Their solutions were freshly prepared in 0.1 M phosphate buffer. Other chemicals were as described earlier [12].

Enzyme-immobilization procedures

Immobilized glucose oxidase was prepared as reported earlier [12]. Invertase was immobilized on controlled pore glass (CPG) following the procedure adopted for glucose oxidase. The amount of enzyme taken for immobilization was 15 mg g^{-1} CPG (ca. 1500 U). The stock immobilized enzyme in phosphate buffer (pH 7.0) was stored at 4° C. Bacterial growth occurred in the stock insoluble enzyme after 3 months, therefore it is recommended that a drop of toluene be added to the buffer in the tube or the stock enzyme should be stored below 0° C.

For mutarotase two methods were investigated. The first involved cross-linking with glutaraldehyde, using the method described above for glucose oxidase and invertase; 0.5 mg (ca. 2500 U) of enzyme per g of CPG was used. The second method involved the preparation of arylamino CPG followed by coupling of the enzyme by diazotization of the amino group or by cross-linking with glutaraldehyde. A 10-g amount of CPG-240 was boiled in 100 ml of 5% (v/v) nitric acid for 30 min. The CPG was filtered on a glass filter, washed with deionized water and dried in an oven at 95° C. To 45 ml of water was added 5 ml of γ-aminopropyltriethoxysilane and the pH was carefully adjusted to 3.45 with 5 M hydrochloric acid. The nitric acid-treated CPG was

added. The pH was checked and adjusted if necessary to 3.45. The mixture was kept at 75° C on a water bath for 150 min, swirling the flask every 15 min. The alkylamino CPG was filtered off, washed with deionized water and dried in an oven as before. The silanization process was repeated to ensure maximum activation of the glass. A 1-g batch of the alkylamino CPG was refluxed overnight (with mechanical stirring) in a 10% (w/v) solution of *p*-nitrobenzoyl chloride in chloroform (20 ml), filtered off and dried in an oven at 50° C and in a vacuum desiccator. The nitro group was reduced to an amino group by treatment with a 10% (w/v) sodium dithionite solution in boiling deionized water for 30 min. The resulting arylamino CPG was washed with water and dried in an oven at 50° C and in a vacuum desiccator.

Two methods were used to couple the enzyme to the arylaminated glass. In the diazotization method, 1 g of arylamino CPG was stirred with 5 ml of ice-cold 2 M hydrochloric acid at 0° C for 5 min, and 4 ml of ice-cold aqueous 2% (w/v) sodium nitrite solution was added dropwise. Stirring was continued for another 15 min. The diazotized derivative of CPG was washed several times with 15-ml amounts of ice-cold 0.1 M phosphate buffer (pH 6.0). After each washing the contents were centrifuged and the washings decanted. Four washings were enough to free the support from excess of acid, as confirmed by pH paper. After the final washing, 0.5 ml of the ice-cold phosphate buffer containing 0.5 mg (2500 U) of mutarotase was added and the coupling was allowed to take place for 48 h at 0—5° C with continuous moderate stirring. A 10-ml portion of ice-cold phenol (0.01% in aqueous 10% sodium acetate solution) was added to the mixture and the reaction was allowed to continue for 15 min at 0° C. (This was necessary to deactivate untreated diazo groups on the support.) The contents were centrifuged and the supernatant liquid was discarded. The insoluble enzyme derivative was washed well with the ice-cold phosphate buffer and stored moist in a stoppered tube until needed. The reactions involved are

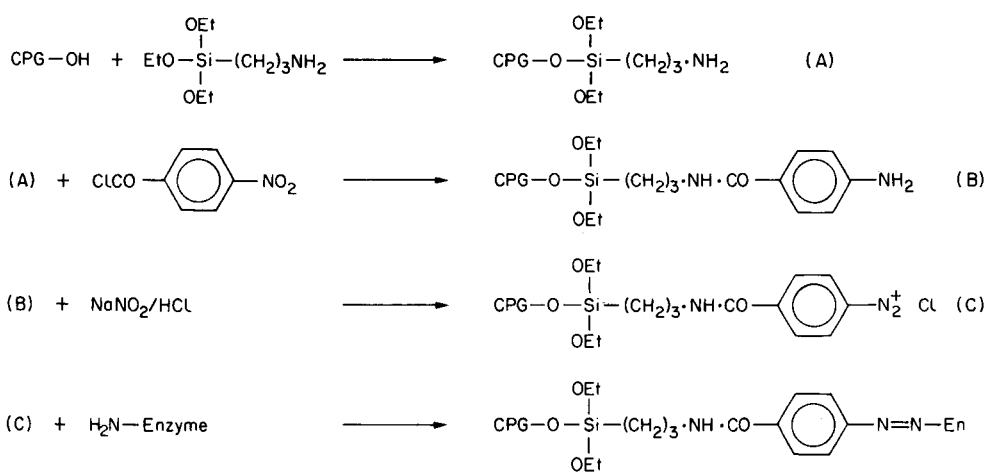

In the second method, mutarotase was immobilized by cross-linking of the arylamino CPG with glutaraldehyde which was done was described above for glucose oxidase and invertase.

Co-immobilization of invertase and mutarotase

A mixture of invertase (ca. 1500 U) and mutarotase (ca. 2500 U) was co-immobilized on arylaminated CPG by cross-linking with glutaraldehyde. The method is as described above, and the reactions involved are

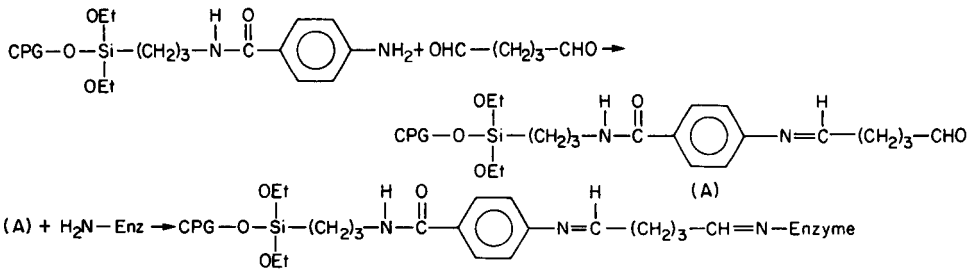

Apparatus

The basic flow-injection manifold equipped with a flow-through amperometric detector was the same as that used for the determination of glucose [12]. Initially, for sucrose determination an immobilized invertase column (25 × 2.5 mm, unless otherwise stated) was inserted prior to the glucose oxidase column. The manifolds for sucrose and glucose determination are described later in the text.

RESULTS AND DISCUSSION

Determination of sucrose

As reported earlier [12], the optimum pH for glucose determination was 4.5. The same system was used initially for sucrose determination by incorporating an invertase column prior to the glucose oxidase column. The effect of pH on sucrose determination was investigated by using various 0.1 M phosphate buffers as the carrier stream. The greatest response for sucrose was obtained at pH 7.0, as shown in Fig. 1. Invertase immobilized on CPG has a very similar pH optimum to that reported for the soluble enzyme [13]. Therefore pH 7.0 was used for the sucrose determination when only the invertase and glucose oxidase columns were used. Greatest peak height sensitivity was obtained at a flow rate of 2.0 ml min^{-1}, which is recommended for achieving good sensitivity and a reasonable sample throughput.

The activity of the immobilized invertase was investigated by injecting sucrose solutions into the above manifold. The calibration graph is shown in Fig. 2. It is evident that the use of the invertase column provided only limited sensitivity to sucrose. The sensitivity was not improved by increasing the amount of immobilized invertase by using a longer column (50 × 2.5 mm). The main reason is that sucrose is hydrolyzed to D-fructose and α-D-glucose,

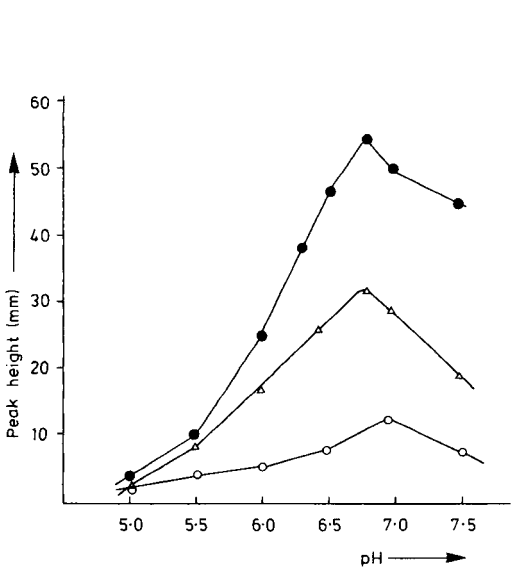

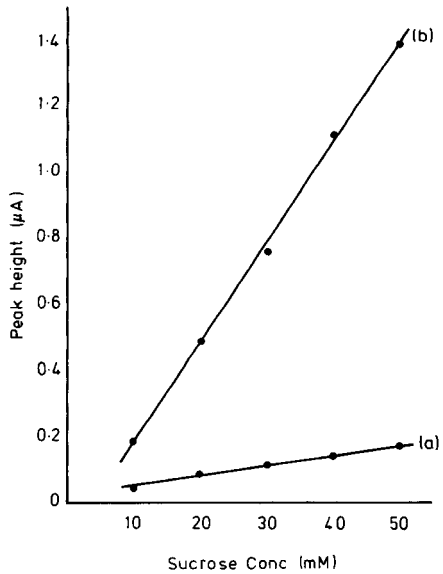

Fig. 1. Effect of pH on activity of enzymes: (○) invertase; (△) immobilized invertase, mutarotase and glucose oxidase in separate minicolumns; (●) co-immobilized invertase and mutarotase, and glucose oxidase. Sample injected: 20 μl of 10 mM sucrose.

Fig. 2. Calibration graphs for sucrose at pH 7.0: (a) without an immobilized mutarotase minicolumn; (b) with a column of mutarotase immobilized on arylaminated CPG with glutaraldehyde.

whereas the substrate for glucose oxidase is β-D-glucose. α-D-Glucose does mutarotate slowly and spontaneously to β-D-glucose, and the rate of mutarotation was measured by using the flow injection procedure to determine the concentration of β-D-glucose formed. A fresh solution of α-D-glucose was prepared in pH 7.0 phosphate buffer, and 20-μl aliquots were injected into the flow system after various times. Figure 3 shows that mutarotation at 25° C ceased after 40 min.

In the present flow system, α-D-glucose formed in the invertase column took only a few seconds to reach the glucose oxidase column, so during this short time very little mutarotation could occur. It was therefore essential to speed up production of β-D-glucose. This was done initially by adding a column of mutarotase immobilized on CPG between the invertase and glucose oxidase columns. The enzyme rapidly promotes the isomerization of α-D-glucose to the β-anomer and freshly prepared α-D-glucose. At this stage, the enzyme columns were thermostated at 25° C, by water passing through water jackets surrounding the columns. The pH for mutarotase was optimized as for invertase by using various 0.1 M phosphate buffers as the carrier stream. The highest sensitivity was obtained at pH 6.8 (Fig. 1). Therefore pH 6.8 was used for sucrose determination when invertase, mutarotase and glucose oxidase were used in the system.

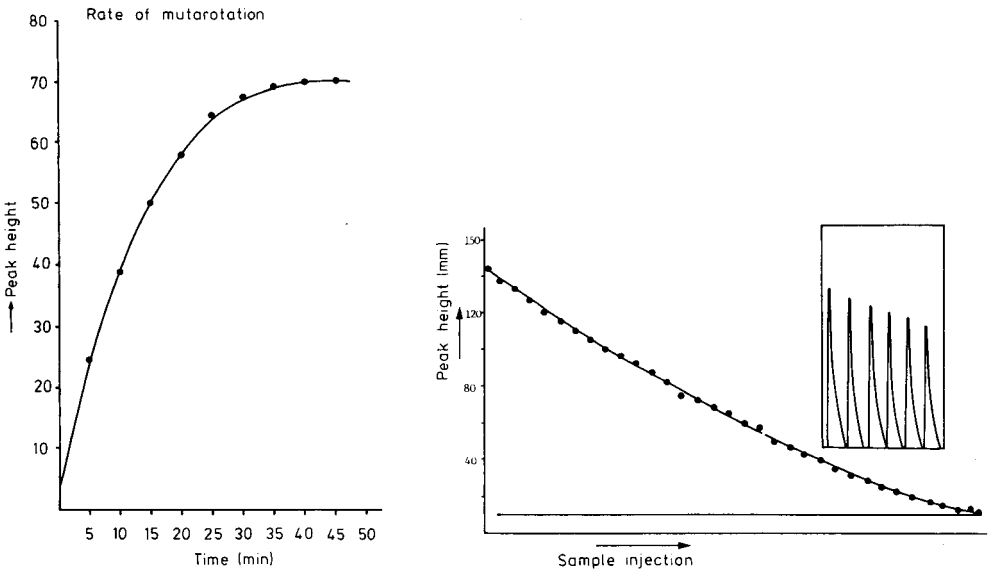

Fig. 3. Mutarotation of 0.1% (w/v) α-D-glucose solution (pH 7.0, 25°C) monitored by f.i.a. with the immobilized glucose oxidase column.

Fig. 4. Decreasing peak heights for 10 mM sucrose with successive sample injections, when the separate immobilized mutarotase minicolumn was used. The insert shows a typical sequence of peaks obtained during this experiment.

This system was initially successful, in that there was a considerable increase in response to sucrose, but the signal continually decreased with successive injections of 10×10^{-3} M sucrose (Fig. 4) until it reached the level achieved in the absence of a mutarotase column. It was concluded that the immobilization of mutarotase was unsatisfactory and the enzyme was gradually being removed from the column. Other immobilization procedures were attempted. Mutarotase immobilized on CPG by diazotization gave a column that packed so compactly that no solution could flow through it. When viewed under a microscope, the CPG was seen to be broken into extremely small particles. For comparison, microscope pictures of free CPG and enzymes immobilized on CPG by other procedures are shown in Fig. 5.

Coupling of the enzyme to arylaminated CPG by cross-linking with glutaraldehyde was more successful. When $1-5 \times 10^{-2}$ M sucrose solutions were injected into the system incorporating mutarotase immobilized in this way, good sensitivity for sucrose was achieved. The calibration graph obtained for sucrose is shown in Fig. 2. The immobilized mutarotase was much more stable, but there was still a slight loss of activity with time (ca. 10% decrease in peak height after 100 injections).

Co-immobilization of enzymes can be an effective means of increasing the efficiency and speed of sequential enzyme reactions [14, 15]. It seemed

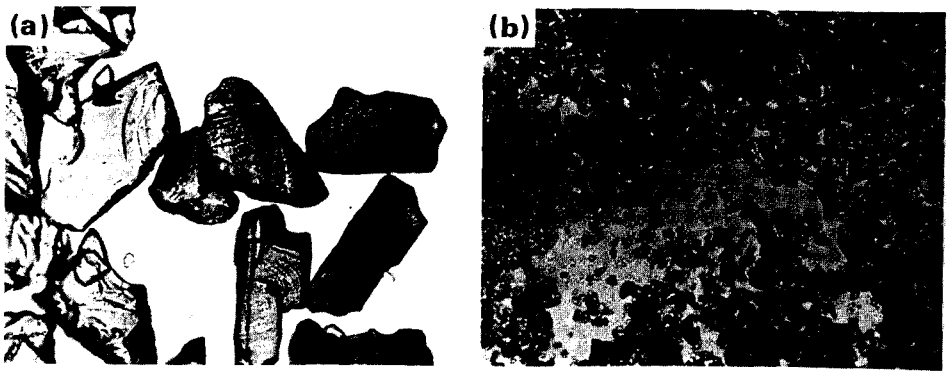

Fig. 5. Pictures taken under a microscope: (a) CPG with immobilized glucose oxidase; (b) CPG after immobilization of mutarotase by the diazo method.

sensible, therefore, to attempt to co-immobilize invertase and mutarotase on CPG. This was achieved as described above, and the co-immobilized enzyme was packed in a column (2.5 × 25 mm) ahead of a glucose oxidase column. When sucrose samples were injected into this system, the sensitivity was increased by nearly an order of magnitude as shown by comparing the calibration graph in Fig. 6 to that in Fig. 2. The graph is slightly curved but the co-immobilized enzyme preparation was very stable and had lost no activity after ca. 12 weeks. The limit of detection was ca. 1×10^{-5} M sucrose.

Sequential determination of sucrose and glucose

The system used for the determination of sucrose can be modified to allow the sequential determination of sucrose and glucose in samples containing both compounds. As shown in Fig. 7, a bypass around the invertase/mutarotase column controlled by two 2-way keys enables the flow to pass either through both columns (for determination of sucrose plus glucose) or through only the glucose oxidase column (for determination of glucose only). Thus two sequential sample injections, with the bypass first in and then out of circuit, allows both components to be determined.

The two sugars were determined in standard mixtures (Table 1) within 25 s. The results are accurate and the method is very simple and reliable.

A non-alcoholic beverage (Coca-Cola) was analysed for the two sugars. A 0.5% (v/v) solution was prepared in pH 6.8 phosphate buffer, without any pretreatment or colour removal. A standard addition procedure and direct calibration were applied. The calibration graph showed a 33% decrease in slope compared to pure solutions. The results obtained by the standard addition method were 1.32 g of glucose per 100 ml and 7.2 g of sucrose per 100 ml with relative standard deviations of 1.5% (n = 3). Thus soft drinks, juices, etc., can be analysed directly without pretreatment. The method was also applied to sugar beet, after crushing and extraction with phosphate buffer (0.1 M, pH 6.8), with satisfactory results.

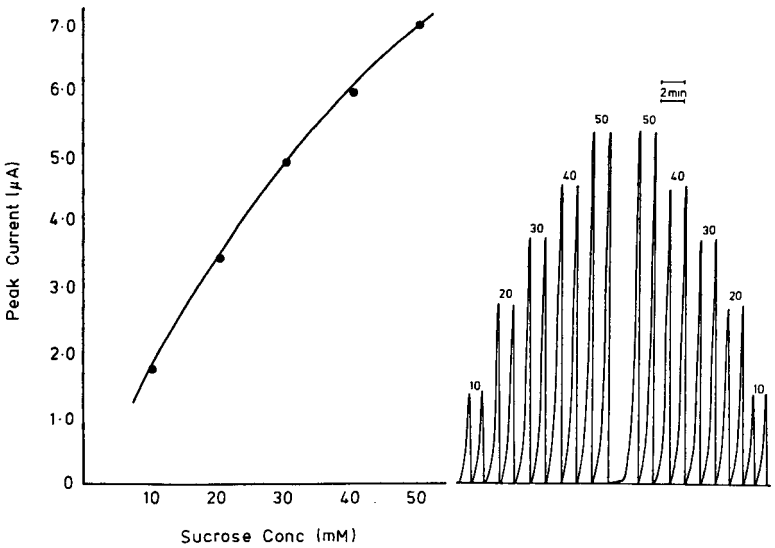

Fig. 6. Calibration graph and peaks for sucrose obtained with a co-immobilized invertase/mutarotase column in the system. The numbers on the peaks indicate mM sucrose.

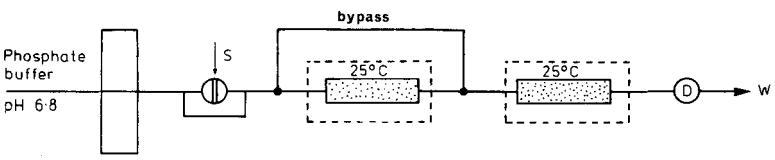

Fig. 7. Manifold for sequential determination of sucrose and glucose. The first column contains immobilized invertase and mutarotase and the second glucose oxidase. Both columns are thermostatted at 25° C.

Simultaneous determination of sucrose and glucose

The sequential system can be refined to determine sucrose and glucose in a single injection by splitting the sample so that one portion flows through the invertase and glucose oxidase columns, and the other only through the glucose oxidase column. This was achieved in the manifold shown in Fig. 8. The portion bypassing the invertase column is delayed in a coil, so that it reaches the glucose oxidase column after the other portion. Thus two signals are obtained in succession from the detector. The first from sucrose plus glucose, the second from glucose only. The signals were recorded by means of an electronic integrator (Fig. 9). The relative standard deviations (n = 5) for the peak areas in Fig. 9 are 1.8% for the combined peak and 2.9% for the glucose peak. Each combined determination takes 2 min.

The determination of sucrose and glucose in this way illustrates one principle of simultaneous determination by f.i.a. [16], in this case with immobilized enzymes. There are many other systems which can be amenable

TABLE 1

Sequential determination of sucrose and glucose

Glucose ($\times 10^{-3}$ M)	Sucrose ($\times 10^{-3}$ M)	Combined signal (μA)	Glucose signal (μA)	Sucrose signal in mixture (μA)	Pure sucrose signal (μA)
0.5	0.0	0.44	0.44	0.00	0.00
	1.0	0.89	0.44	0.44	0.420
	2.0	0.98	0.42	0.56	0.56
	3.0	1.26	0.42	0.84	0.79
	4.0	1.401	0.42	0.98	0.98
	5.0	1.59	0.42	1.17	1.12
1.0	0.0	0.84	0.84	0.00	0.00
	10	2.62	0.84	1.77	1.77
	20	4.25	0.79	3.45	3.41
	30	5.65	0.84	4.81	4.81
	40	6.82	0.84	5.98	5.93
	50	7.85	0.84	7.00	7.00

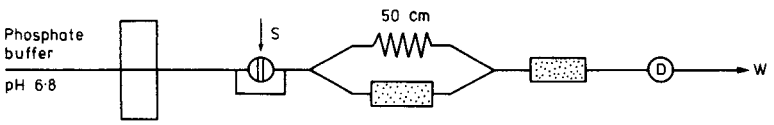

Fig. 8. Manifold for simultaneous determination of sucrose and glucose. Columns as for Fig. 7.

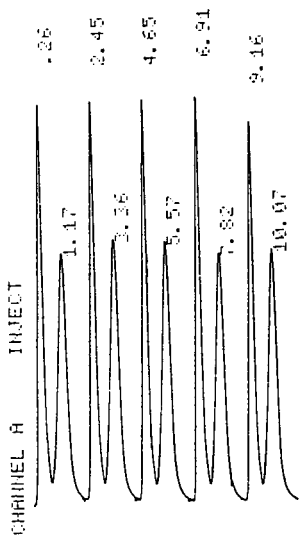

Fig. 9. Responses obtained from replicate measurements of sucrose and glucose in soft drink. Manifold as in Fig. 8 (numbers indicate time at which peaks appear, in min).

to similar treatment, and the principle can be extended to the determination of more than two substances, as is often needed in clinical laboratories.

M. Masoom thanks the Ministry of Education, Government of Pakistan, for a research grant, and the University of Baluchistan for study leave.

REFERENCES

1 L. Clark and C. Lyons, Ann. N.Y. Acad. Sci., 102 (1962) 29.
2 G. Guilbault and G. Lubrano, Anal. Chim. Acta, 64 (1973) 439.
3 D. Pfeiffer, F. Scheller, M. Janchen, K. Bertermann and H. Weise, Anal. Lett., 13B (1979) 96.
4 I. Satoh, I. Karube and S. Suzuki, Biotechnol. Bioeng., 18 (1976) 269.
5 C. Bertrand, P. Coulet and D. Gautheron, Anal. Chim. Acta, 126 (1981) 23.
6 J. J. Kulys, Anal. Lett., 14B (1981) 377.
7 P. Coulet and C. Bertrand, Anal. Lett., 12B (1979) 581.
8 D. Pfeiffer, F. Scheller, M. Jänchem, K. Bertermann and H. Weise, Anal. Lett., 13B (1980) 1179.
9 F. Scheller and R. Renneberg, Anal. Chim. Acta, 152 (1983) 265.
10 H. Weise, F. Scheller, G. Kreibich and D. Pfeiffer, Lebensmitteland, 28 (1981) 401.
11 F. Scheller and C. Karsten, Anal. Chim. Acta, 155 (1983) 29.
12 M. Masoom and A. Townshend, Anal. Chim. Acta, 166 (1984) 111.
13 D. P. Nikolelis and H. A. Mottola, Anal. Chem., 50 (1978) 1665.
14 M. Shana'a, M. Sc. Dissertation, Chemistry Department, University of Hull, 1984.
15 M. Tabata, J. Endo and T. Murachi, J. Appl. Biochem., 3 (1981) 84.
16 M. D. Luque de Castro and M. Valcarcel, Analyst (London), 109 (1984) 413.

Analytica Chimica Acta, 171 (1985) 195—204
Elsevier Science Publishers B.V., Amsterdam — Printed in The Netherlands

ADSORPTIVE STRIPPING VOLTAMMETRY OF SEX HORMONES AT THE STATIC MERCURY DROP ELECTRODE

JOSEPH WANG*, PERCIO A. M. FARIAS[a] and JAWAD S. MAHMOUD
Department of Chemistry, New Mexico State University, Las Cruces, NM 88003 (U.S.A.)
(Received 1st October 1984)

SUMMARY

Controlled adsorptive accumulation of testosterone, methyltestosterone and progesterone on the static mercury drop electrode provides the basis for direct stripping measurement of these compounds at nanomolar concentrations. The adsorptive stripping behavior is evaluated with respect to preconcentration time and potential, stripping mode, concentration dependence, drop size and other variables. With 5-min accumulation, peak current enhancements of 45, 18 and 12 are observed for 5×10^{-8} M testosterone, progesterone and methyltestosterone, respectively, relative to direct pulse voltammetry. Detection limits are 1.6×10^{-10} M for testosterone, 2×10^{-10} M for progesterone and 3.3×10^{-10} M for methyltestosterone with 15-min preconcentration. The relative standard deviation for 8×10^{-8} M progesterone is 3.4% (n = 8). Applicability to direct measurements of methyltestosterone in pharmaceutical formulations is assessed.

The sex hormones are steroids responsible for the sex characteristics of male and female mammals. A sensitive method is required for routine determination of these compounds in various matrices, including physiological fluids. The polarographic behavior of several ketosteroids such as testosterone, methyltestosterone, and progesterone has been previously studied by several authors [1—4], and it is generally agreed that the mechanism involves reduction of the double bond conjugated to the carbonyl moiety. The detection limit for a.c. and d.c. polarography is about 3×10^{-5} M, and for second-harmonic a.c. polarography about 5×10^{-6} M [3]. Similar detection limits are obtained with differential pulse polarography [4].

This work describes an extremely sensitive electroanalytical procedure for trace measurements of ketosteroids based on adsorptive stripping voltammetry. Adsorptive stripping voltammetry has been demonstrated to be a sensitive analytical method for a wide range of electroactive compounds adsorbing onto the electrode surface. Work to date has been summarized recently [5]. Such adsorptive stripping measurements exhibit a sensitivity that is 10^3—10^4 times greater than that of conventional (solution-phase) pulse voltammetry. For example, controlled adsorptive accumulation of

[a]Present address: Department of Chemistry, Pontificia Universidade Catolica do Rio de Janeiro, Rio de Janeiro, Brazil.

0003-2670/85/$03.30

riboflavin onto the static mercury drop electrode gives a detection limit of 2.5×10^{-11} [6]. It was demonstrated recently that cardiac glycosides, possessing the same steroidal nucleus as the sex hormones, strongly adsorbed onto the static mercury drop electrode to yield a well defined adsorptive stripping response [7]. As the adsorptive behavior is postulated to involve a planar orientation of this ring system and the electrode surface, it seems highly likely that other important steroids can be quantified by using a similar stripping methodology. The present study tests the adsorptive stripping behavior of sex hormones at the static mercury drop electrode. The effects of various operational parameters on the response are examined.

EXPERIMENTAL

Apparatus and reagents

Stripping and cyclic voltammograms were obtained with an EG & G Princeton Applied Research Corp. (PAR) Model 264A stripping analyzer. The working electrode was a PAR Model 303A static mercury drop electrode. The sample cell (PAR Model 0057) was fitted with a Ag/AgCl (satd. KCl) reference electrode and a platinum wire auxiliary electrode. The cell was covered with aluminum foil. A magnetic stirrer (Troemner Model 500) and a stirring bar (1-cm long, 2-mm thick) provided the convective transport during the preconcentration step. A PAR Model 0073 X-Y recorder was used for the collection of experimental data.

Stock solutions (2×10^{-4} M) of the different steroids (Sigma) were prepared daily by dissolving the compounds in 10—20 ml ethanol and making up to 100 ml with deionized water. The solutions were stored in the dark at 4° C. All solutions were prepared from deionized water and analytical-grade reagents. For tablets, one tablet (containing 10 mg of hormone) was dissolved in 100 ml of chloroform, and then diluted (5 + 45) with 25 ml of ethanol and 20 ml of 0.005 M sodium hydroxide. A 20-μl aliquot of this solution was added to the blank solution in the cell.

Procedure

A known volume (10 ml) of the supporting electrolyte solution (usually 0.005 M sodium hydroxide) was added to the cell and degassed with nitrogen for 8 min (and for 30 s before each adsorptive stripping cycle). The preconcentration potential (usually −0.8 V) was applied to the electrode for a selected time, while the solution was stirred at 400 rpm. The stirring was then stopped, and after 15 s the voltammogram was recorded by applying a negative-going potential scan. The scan was terminated at −1.7 V, and the adsorptive stripping cycle was repeated with a new mercury drop. After the background stripping voltammograms had been obtained, aliquots of the steroid standards were introduced. The entire procedure was automated, as controlled by the PAR 264A stripping analyzer. Throughout this operation, nitrogen was passed over the solution surface. All data were obtained at ambient temperature.

RESULTS AND DISCUSSION

Effect of operational parameters

Figure 1 compares differential-pulse and linear-scan adsorptive stripping voltammograms for 2×10^{-7} M testosterone, progesterone and methyltestosterone after 1 min preconcentration. The corresponding direct response (no accumulation) is also shown. For the short preconcentration period used, significant improvement in the sensitivity is obtained. For example, the linear-scan mode yields well-defined peaks after the accumulation, while the quantitation is not feasible in the direct mode. Similarly, peak potential enhancements of 6—8 are observed in the differential-pulse stripping mode (with further enhancements obtained by using longer preconcentration periods). Overall, the latter stripping mode offers improved sensitivity, as it corrects for the charging background current, and was used throughout the further study. The stripping peak characteristics (potential, E_p and half-width, $b_{1/2}$) of both stripping modes are summarized in Table 1.

Figure 2 shows the dependence of the adsorptive stripping peak current on the preconcentration time for 2×10^{-7} M methyltestosterone, testosterone and progesterone. The peak increases linearly with time at first and then levels off. Such time-dependent profiles represent the corresponding absorption isotherms (because the peak current depends on the amount adsorbed). Obviously, full surface coverage is approached for preconcentration times

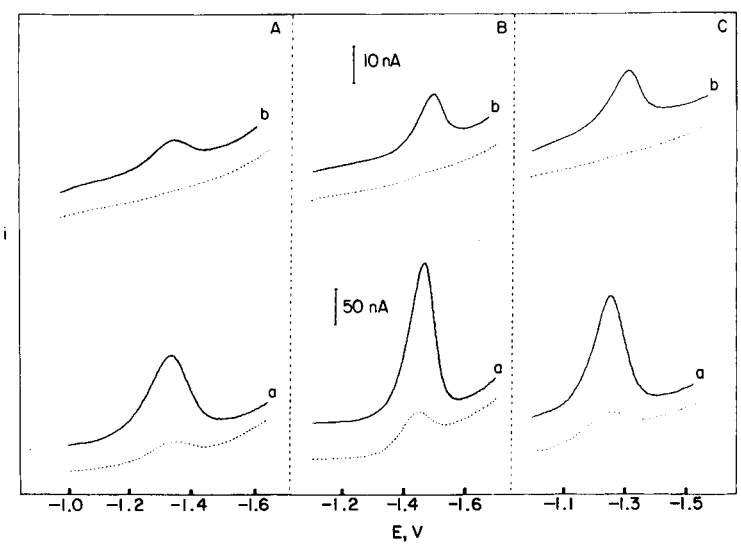

Fig. 1. Differential-pulse (a) and linear-scan (b) stripping voltammograms for 2×10^{-7} M testosterone (A), progesterone (B) and methyltestosterone (C). Preconcentration at −0.8 V for 1 min. Differential pulse conditions: 5-mV s^{-1} scan rate, 50-mV amplitude and 0.5-s repetition time. Linear scan rate, 50 mV s^{-1}. Large drop size. The dotted lines represent the corresponding responses without preconcentration.

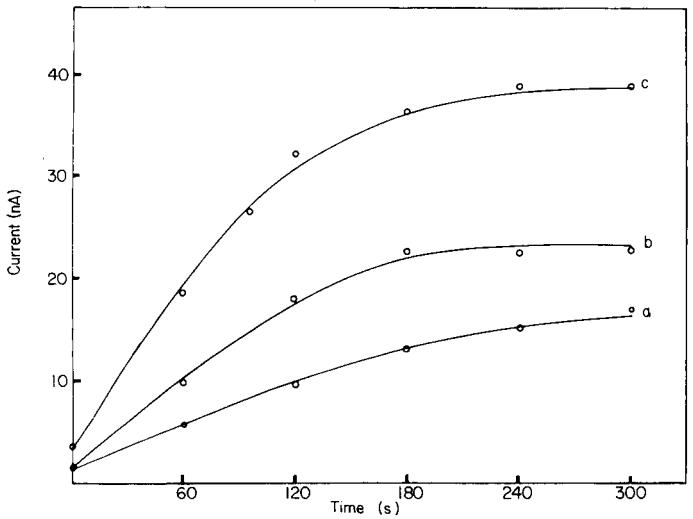

Fig. 2. Dependence of the stripping peak current on the preconcentration time for 2×10^{-7} M methyltestosterone (a), testosterone (b) and progesterone (c). Differential pulse waveform with 5-mV s^{-1} scan rate, 50-mV amplitude and 0.5-s pulse repetition. Medium drop size. Preconcentration potential, —0.8 V.

TABLE 1

Characteristics of the stripping peak currents[a]

Compound	Linear scan		Differential pulse	
	E_p (V)	$b_{1/2}$ (mV)	E_p (V)	$b_{1/2}$ (mV)
Testosterone	—1.36	113	—1.35	136
Methyltestosterone	—1.30	107	—1.27	111
Progesterone	—1.47	82	—1.46	87

[a]Conditions as in Fig. 1.

longer than 3 min. At this point, the peak current enhancement relative to direct measurements ranges from 10 to 17. Non-linearity is obtained for the corresponding plots of peak current vs. the square root of the preconcentration time (in contrast to what is expected for diffusion-controlled absorption). Because the amount adsorbed is a function of many variables such as bulk concentration, mass transport or drop size, different time profiles are obtained under different conditions. For example, similar experiments with 5×10^{-8} M solutions yield linear peak current vs. time plots for methyltestosterone and progesterone (slopes: 0.75 and 3.65 nA min^{-1}; correlation coefficients, 0.994 and 0.995, respectively); the corresponding testosterone response exhibits linearity over the first 4 min. At this concentration, peak current enhance-

ments of 45, 18 and 12 are obtained for testosterone, progesterone and methyltestosterone, respectively (for 5 min preconcentration). These values represent the relative extent of adsorption of the different steroids. The reasons for this trend are not completely clear from the molecular structures.

Cyclic voltammograms show well-defined cathodic peaks ($E_{p,c}$ = −1.41 V for testosterone, −1.52 V for progesterone and −1.47 V for methyltestosterone) and poorly-defined anodic peaks ($E_{p,a}$ = −1.37 V for testosterone, −1.45 V for progesterone and −1.27 V for methyltestosterone). Repetitive scans show only a slight increase of the cathodic peak, while the anodic peak remains essentially the same. However, if the potential is held at −0.8 V for a given period of time (with stirring), a substantial increase of the peaks is observed; the subsequent scan produces smaller peaks. These data indicate that while the reactant strongly adsorbed at potentials more positive than $E_{p,c}$, the product rapidly desorbed from the surface.

The solution conditions affect the size and shape of the stripping peak response. Various basic electrolytes such as borate buffer, ammonium acetate, and sodium hydroxide were examined. (Acidic solutions cannot be used because the hydrogen background current masks the peaks of interest.) Best results were obtained with a 0.005 M sodium hydroxide solution; this electrolyte was used throughout this study.

Figure 3 shows the effects of the drop size (A) and differential pulse scan rate (B) on the stripping peak current. A tenfold increase in the peak current

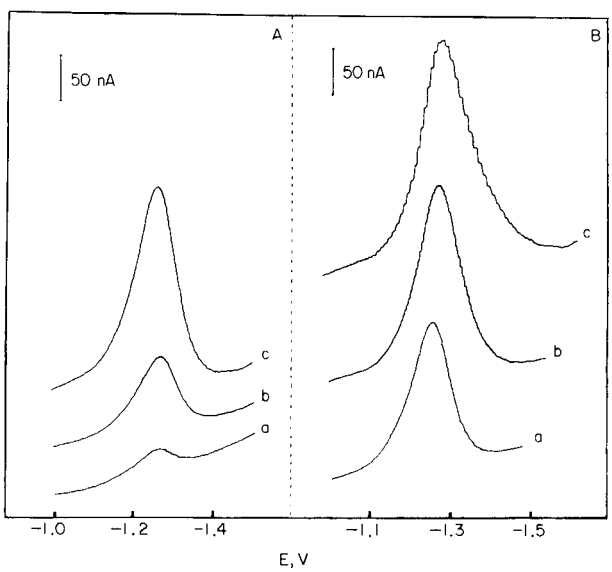

Fig. 3. Effects of drop size (A) and scan rate (B) on the differential-pulse stripping peak for 2 × 10^{-7} M methyltestosterone. (A) Preconcentration time, 90 s; drop size, small (a), medium (b), large (c); scan rate, 5 mV s^{-1}. (B) Preconcentration time, 60 s; drop size, large; scan rate, 5 (a), 10 (b), 20 (c) mV s^{-1}. Other conditions as in Fig. 2.

is observed on changing the drop size from small to large; these drop sizes correspond to surface area ratio of 1:2.5. As the background current remains essentially the same, the large drop size is recommended when maximum sensitivity is required. Unlike anodic stripping measurements of trace metals for which higher sensitivity is obtained for lower electrode volumes, the adsorptive stripping response increases with the electrode area because it depends on the amount adsorbed on the surface. Scan rates of 10 and 20 mV s^{-1} offer 30% and 50% enhancements, respectively, of the peak current over that obtained at 5 mV s^{-1}. However, this gain in sensitivity is accompanied by peak broadening (ca. 30% increase in $b_{1/2}$). Overall, a scan rate of 10 mV s^{-1} would be the best compromise when considering the sensitivity, resolution and speed requirements.

Figure 4 shows the dependence of the stripping peak currents on the preconcentration potential. A gradual decrease in the current is observed as the preconcentration potential is changed from —0.2 to —1.0 V. Part of this profile may be attributed to continued accumulation during the additional time (from E_{acc} to E_p). A potential of —0.8 V was used throughout as a compromise between sensitivity and speed. Mass transport during preconcentration affects the amount of analyte adsorbed, i.e., the sensitivity. For example, 400 rpm stirring produces a fourfold enhancement in peak current over that obtained in a quiescent solution (1×10^{-7} M testosterone, 3-min preconcentration). Such stirring was used throughout.

Quantitative utility

The effective preconcentration associated with the adsorption process lowers the detection limits by 2—3 orders of magnitude compared to the corresponding direct measurements. Figure 5 shows differential pulse voltammograms for 5×10^{-9} M progesterone after different preconcentration times. While quantitation is not feasible by direct voltammetry, well-defined stripping peaks are obtained after preconcentration for 10 and 20 min. Detection limits near 1.4×10^{-10} M and 3.3×10^{-10} M are estimated based on the signal-to-noise characteristics (S/N = 2) of the data for 20 and 10 min, respectively. For testosterone and methyltestosterone, the detection limits are 1.6×10^{-10} M and 3.3×10^{-10} M, respectively, after preconcentration for 15 min and 3×10^{-10} M and 4.2×10^{-10} M, respectively, after preconcentration for 5 min. Thus, 400—900 pg can be detected in the 10 ml of solution used, i.e., 40—90 pg ml^{-1}. Such detection limits are comparable with those obtained for measurements of trace metals by anodic stripping voltammetry.

At 10^{-7}—10^{-8} M concentrations, significantly shorter preconcentration times suffice. Figure 6 illustrates the response for successive standard additions of 2.5×10^{-8} M progesterone using 2-min preconcentration. The corresponding direct response (dotted lines) allows convenient quantitation only at concentrations higher than 1×10^{-7} M. The stripping peak current increases linearly with the concentration, yielding the equation: i(nA) = $(1.82 \pm 0.04)(10^{-8}\ \text{M}) - (0.56 \pm 0.32)$nA, $r = 0.999$. Least-squares analyses

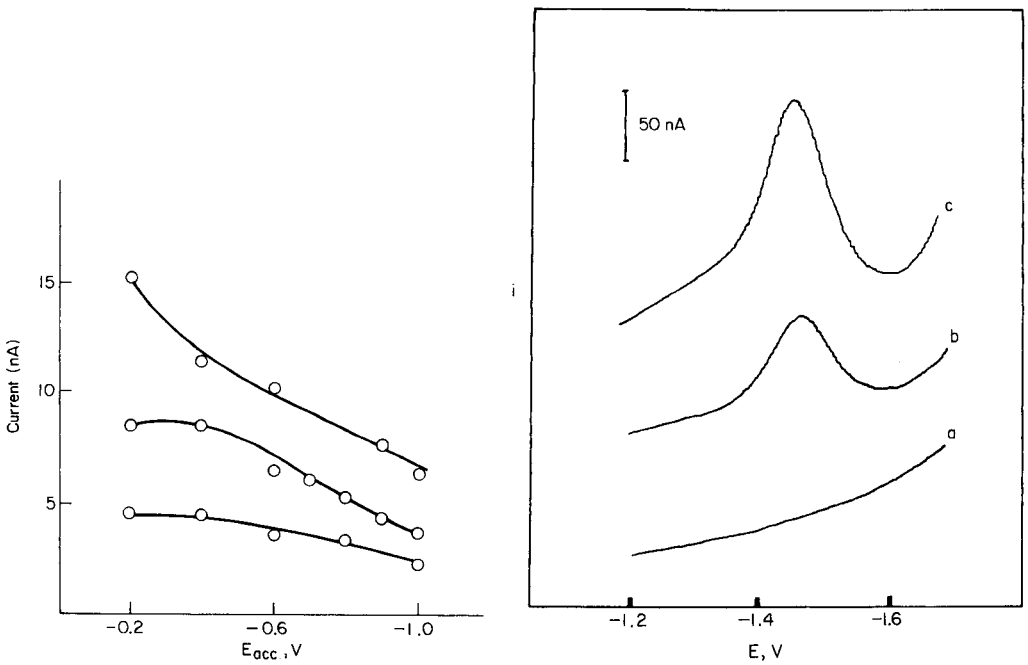

Fig. 4. Effect of preconcentration potential on the differential-pulse peak currents for 1×10^{-7} M methyltestosterone (a), testosterone (b) and progesterone (c). Preconcentration time, 1 min; other conditions as in Fig. 2.

Fig. 5. Differential-pulse voltammograms for 5×10^{-9} M progesterone with preconcentration for 0 (a), 10 (b) and 20 (c) min. Scan rate, 10 mV s^{-1}; other conditions as in Fig. 1(a).

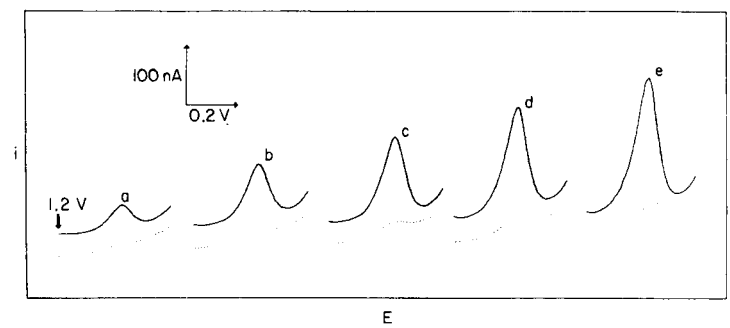

Fig. 6. Stripping voltammograms obtained for increasing progesterone concentrations in 2.5×10^{-8} M steps (a—e). Preconcentration for 2 min. Other conditions as in Fig. 2. The dotted line represents the direct (0 min) response.

of calibration plots for the three sex hormones, over the 5×10^{-8}—4×10^{-7} M range, are summarized in Table 2. While the progesterone response exhibits linearity over the entire range, the plots for testosterone and methyltestosterone level off at concentrations higher than 3×10^{-7} M. The curvature of the calibration plots is consistent with a process that is limited by adsorption of the analyte; above a certain level, the surface becomes saturated with the adsorbed compound. At lower concentrations, linear isotherm conditions exist. Similarly, nonlinearity is obtained when these data are replotted as $1/i$ vs. $1/c$. The linear range is particularly important when standard addition methods are considered. It is stressed here that this linear range is a function of the preconcentration conditions and so can be extended by using shorter preconcentration times or unstirred solutions. However, this is not essential as direct differential-pulse voltammetry can be used at concentrations higher than 10^{-7} M. For convenient quantitation of the hormones at 10^{-7} M, 10^{-8} M and 10^{-9} M levels, 0.5-, 3- and 10-min preconcentrations are sufficient.

In order to evaluate the precision of stripping peak currents, eight repetitive measurements of 8×10^{-8} M progesterone were done (conditions, as in Fig. 2 except that 1-min preconcentration was used). The mean peak current was 64 nA with a range of 61—67 nA and a relative standard deviation of 3.4%.

Figure 7 demonstrates the applicability of adsorptive stripping voltammetry to measurement of sex hormones in pharmaceutical tablets. Commercial tablets (Metandren, Ciba Pharmaceutical Co.), nominally containing 10 mg of methyltestosterone, were assayed. Quantitation was based on standard additions. The average of five individual tablets was 8.9 mg with a relative standard deviation of 7%. The relative standard deviation for repeated voltammograms using the same tablet solution was 5%. The high sensitivity of adsorptive stripping voltammetry permits significant dilution of the tablet solution, thus potentially minimizing possible interferences from tablet excipients. While optical measurements may be suitable for quantifying ketosteroids in tablets, such measurements do not possess sufficient sensitivity when biological samples are concerned. Stripping measurements in biological

TABLE 2

Dependence of peak current on bulk concentration of sex hormones[a]

Compound	Slope (nA/10^{-8} M)	σ_s[b] (nA/10^{-8} M)	Intercept (nA)	σ_I[c] (nA)	Correlation coefficient
Progesterone	1.02	0.03	−0.71	1.05	0.997
Testosterone	0.90[d]	0.06	−2.2	0.91	0.994
Methyltestosterone	0.52[d]	0.02	−0.62	0.40	0.998

[a]Conditions, as in Fig. 2, except that the preconcentration time was 90 s. [b]Standard deviation of the slope. [c]Standard deviation of the intercept. [d]Slope of initial linear portion (5×10^{-8}—3×10^{-7} M).

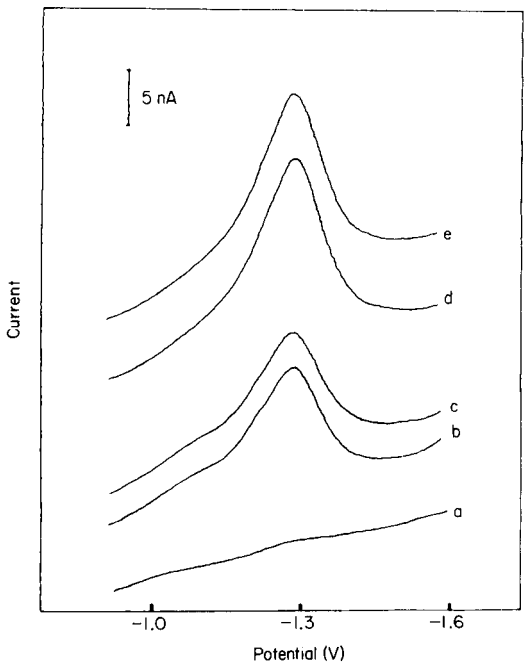

Fig. 7. Determination of methyltestosterone in a pharmaceutical tablet by differential-pulse stripping voltammetry in aliquots of a sample solution (1:500 dilution): (a) without preconcentration; (b, c) after 7-min preconcentration; (e, d) after standard addition of 5×10^{-8} M methyltestosterone and 7-min preconcentration. Other conditions as in Fig. 2.

fluids would require separation of potential interferences, mainly proteins, that compete for the surface sites.

In conclusion, the three steroids investigated here all exhibit similar adsorptive stripping behavior. Careful choice of operational parameters provides extremely low detection limits (40—90 pg ml^{-1}). It is probable that other steroidal hormones will also be suitable for adsorptive stripping measurements. Based on the similarities in the redox and adsorption behavior, differentiation between closely related compounds may be difficult and would require prior separation.

This work was supported by the National Institutes of Health under Grant No. GM30913-01A1. P. A. M. Farias acknowledges the financial support of the National Council for Scientific Development (CNPq) of the Brazilian government.

REFERENCES

1 J. L. Spahr and A. M. Knevel, J. Pharm. Sci., 55 (1966) 1020.
2 J. T. Stewart and W. P. Mason, Am. J. Pharm. Educ., 37 (1973) 619.

3 A. L. Woodson and D. E. Smith, Anal. Chem., 42 (1970) 242.
4 L. G. Chatten, R. N. Yadav and D. K. Madan, Pharm. Acta, Helv., 51 (1976) 381.
5 J. Wang, Stripping Analysis: Principles, Instrumentation and Applications, Verlag Chemie International, Deerfield Beach, FL, 1985.
6 J. Wang, D. B. Luo, P. A. M. Farias and J. S. Mahmoud, Anal. Chem., 57 (1985) 158.
7 J. Wang, J. S. Mahmoud and F. A. M. Farias, Analyst, in press.

Analytica Chimica Acta, 171 (1985) 205—213
Elsevier Science Publishers B.V., Amsterdam — Printed in The Netherlands

THE CATHODIC STRIPPING VOLTAMMETRIC DETERMINATION OF TRACES OF IODIDE WITH A HANGING COPPER AMALGAM DROP ELECTRODE

RENATA BILEWICZ and ZENON KUBLIK*

Department of Chemistry, University of Warsaw, Pasteura 1, Warsaw 02093 (Poland)

(Received 28th September 1984)

SUMMARY

A hanging copper amalgam drop electrode (HCADE) is used for the determination of traces of iodide by cathodic stripping voltammetry. The cathodic stripping peak of copper(I) iodide from the HCADE is better defined than that of mercury(I) iodide from a hanging mercury drop electrode. Optimum conditions and interferences are reported. With a 3-min deposition time at —0.1 V vs. SCE, the calibration plot is linear up to 2×10^{-6} mol dm^{-3} iodide. The detection limit for iodide with the HCADE under voltammetric conditions is 4×10^{-8} mol dm^{-3}; this is lowered to 8×10^{-9} mol dm^{-3} by using the differential pulse stripping technique.

Several attempts have recently been made to replace the deposition of slightly soluble mercury compounds by the appropriate copper compounds in cathodic stripping voltammetry. The copper(I) compounds have been deposited on the electrode surface either by electro-oxidation of copper from the copper amalgam electrode [1], or by electroreduction of copper(II) ions added to the solution [1, 2].

The aim of the present work was to check the potentialities of the hanging copper amalgam drop electrode (HCADE) for the determination of traces of iodides by cathodic stripping voltammetry. The value of the solubility product for copper(I) iodide is 1×10^{-12} [3] or 5×10^{-12} [4], i.e., it is sufficiently low to obtain the copper(I) iodide deposit on the electrode surface. Iodides have been determined by cathodic stripping techniques previously but silver [5] or mercury [6] electrodes were used. However, the proper preparation of the surface of the silver electrode is time-consuming and long times are needed for the deposition of silver iodide. The determination of iodides at the HMDE is not simple. According to Boult and Thirsk [7], the anodic deposit on the mercury electrode in the presence of iodides is a mixture of Hg_2I_2, HgI_2 and HgO. Under such conditions, multiple peaks are easily formed on the stripping voltammograms even when the amount of deposit is insufficient to form a monolayer. Propst [8] observed such splitting on the cathodic stripping voltammograms obtained at the HMDE in the presence of traces of iodides.

0003-2670/85/$03.30

EXPERIMENTAL

Voltammograms were recorded with a Radelkis OH-105 polarograph and the pulse voltammograms with a Unitra PPO4 pulse polarograph connected with a Kabid-Press 6801 X-Y recorder. The reference electrode was a saturated calomel electrode and a platinum foil with a surface area of 1 cm^2 served as the counter electrode. The indicating electrode was either a conventional HMDE of the type described by Kemula and Kublik [9] or the same arrangement filled with copper amalgam (HCADE); the surface area of these electrodes was 0.024 cm^2. Copper amalgam was prepared by dissolving an appropriate amount of copper in mercury. Because the copper amalgam is not stable [10], the concentration of copper in the amalgam was checked on the basis of the equation of Nicholson and Shain [11] from the height of the copper dissolution peak recorded in 0.1 mol dm^{-3} sodium perchlorate solution. The value used for the diffusion coefficient of copper in mercury was 1.06×10^{-5} cm^2 s^{-1} [12].

All supporting electrolytes were prepared from reagent-grade chemicals and distilled water. The stock solutions of sodium iodide were stored for not longer than three days. The dilute solutions of iodides were prepared daily and were kept under argon. As a rule, the samples of iodide solutions were added to the deaerated supporting electrolytes. High-purity argon was used to remove other gases from solutions. During the deposition step, the solutions were stirred magnetically. All experiments were done in a cell with a water jacket, the water being thermostated at 25 ± 0.2°C.

RESULTS

Preliminary experiments

Figure 1 shows a comparison of two cathodic stripping curves obtained for iodides at the HCADE and at the HMDE in the same solution containing a low concentration of iodides. It is evident that the cathodic stripping peak obtained with the HCADE is markedly better developed than the peak obtained with the HMDE. In addition, the peak obtained with the HCADE occurs at more negative potentials.

The cathodic stripping peaks obtained for iodides under conditions where the copper(I) ions were generated either from the copper amalgam (case A) or from copper(II) ions (case B) are compared in Fig. 2. The method of generating copper(I) affects the shape of the background current curves. At the HCADE, the background current attains a flat plateau very quickly after the stirring has stopped (curve 1); in the presence of copper(II) ions in solution, this current is not only significant but its height depends markedly on time (curves 1′ and 1″). It is evident that in case B, precise measurement of the peak height can pose serious difficulties. An increase in the copper concentration in the amalgam has, in practice, no significant influence on the shape and height of the background current curve, whereas an increase in the

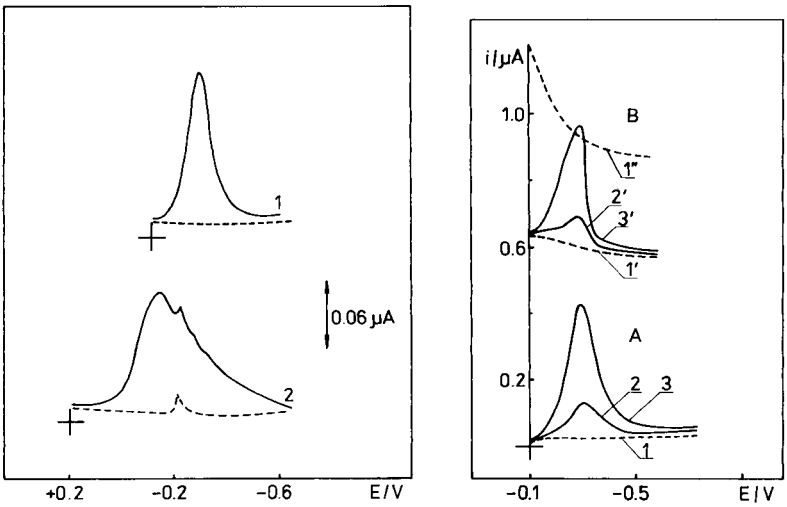

Fig. 1. Cathodic stripping voltammetric curves: (1) for copper(I) iodide at the HCADE; (2) for mercury(I) iodide at the HMDE. Conditions: 2×10^{-7} mol dm^{-3} sodium iodide in 0.1 mol dm^{-3} perchloric acid; 3 min deposition time (at −0.12 V for curve 1 and +0.2 V for curve 2); 3.2×10^{-3} mol dm^{-3} copper in the amalgam; voltage scan rate 2 V min^{-1}. (---) Background currents.

Fig. 2. Comparison of the cathodic stripping curves of copper(I) iodide obtained in 0.1 mol dm^{-3} perchloric acid solution: (A) at HCADE with 5×10^{-4} mol dm^{-3} copper in the amalgam; (B) at HMDE with 5×10^{-4} mol dm^{-3} Cu(II) in the solution. Concentration of sodium iodide: (1, 1', 1") 0; (2, 2') 2×10^{-7}; (3, 3') 5×10^{-7} mol dm^{-3}. Deposition for 3 min at −0.1 V with stirring. Waiting time after stirring stopped: (1, 2, 3) 20 s; (1") 40 s; (1', 2', 3') 90 s. Voltage scan rate 2 V min^{-1}.

copper(II) concentration in solution leads to further increase of the background current.

Effects of varying solution conditions and instrumental parameters

The supporting electrolyte and pH. For this series of experiments, the solutions contained 1×10^{-7} mol dm^{-3} iodide. For 0.1 mol dm^{-3} solutions of acetate buffer, sodium perchlorate, sodium nitrate (all over the pH range 2—5) and perchloric acid, the shape and height of the cathodic stripping peak of copper(I) iodide were unaltered. In contrast, when the pH of the solutions exceeded 5, the results became irreproducible. Thus, in further experiments, the pH of solutions was kept below 5.

The optimum potential and time of deposition of copper(I) iodide. The results presented in curve 2 (Fig. 3) show that the optimum range of potentials for the deposition of copper(I) iodide is −0.1 to −0.15 V. The accumulation of copper(I) iodide at slightly more positive potentials leads to a decrease in the height of the stripping peak. At still more positive potentials, there is competition between the formation of CuI and Hg_2I_2 and the curves

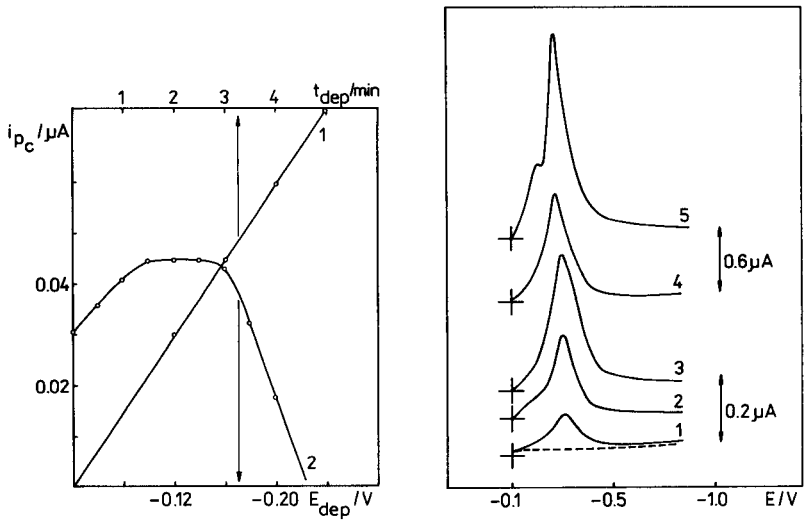

Fig. 3. Dependence of the height of the copper(I) iodide stripping peak: (1) on deposition time for deposition at —0.1 V with stirring; (2) on deposition potential for a 3-min deposition under stirring. Solution: 1×10^{-7} mol dm^{-3} sodium iodide in 0.1 mol dm^{-3} sodium perchlorate, pH 2. HCADE and scan rate as for Fig. 1.

Fig. 4. Cathodic stripping voltammograms obtained at the HCADE for increasing concentrations of sodium iodide: (1) 2×10^{-7}; (2) 5×10^{-7}; (3) 8×10^{-7}; (4) 2×10^{-6}; (5) 2×10^{-5} mol dm^{-3}. Conditions: 3×10^{-3} mol dm^{-3} copper in the HCADE; 0.1 mol dm^{-3} sodium perchlorate, pH 2; deposition for 3 min at —0.1 V with stirring; scan rate 2 V min^{-1}.

become complex. As curve 1 in Fig. 3 shows, the height of the stripping peak is proportional to the deposition time over the range 1—5 min. At longer deposition times, the reproducibility of the results deteriorated.

The voltage scan rate. Variations in the voltage scan rate, v, affect both the peak height and the peak potential. These dependences were studied after deposition of copper(I) iodide for 3 min from a solution with an iodide concentration of 1×10^{-6} mol dm^{-3}. The range of scan rates tested was 0.25—4 V min^{-1}; the plot i_p vs. v was rectilinear with a slope of 0.22 μA min V^{-1}. The peak potential, E_p, shifts towards more negative potentials when v is increased. The plot of E_p vs. log v was rectilinear with slope 0.38. This value is slightly higher than the value of 0.3 predicted theoretically by Brainina [13] for the reversible reduction of a solid substance from a submonolayer of deposit.

Calibration range and limits of detection for iodide

The stripping peaks obtained at the HCADE for increasing concentrations of iodide (Fig. 4) prove that only one well-developed peak appears over a large range of iodide concentration. Figure 5 shows the calibration plots obtained

for two different deposition limits. With deposition for 3 min, the detection limit is 4×10^{-8} mol dm^{-3} and the plot is linear up to 2×10^{-6} mol dm^{-3} iodide. Above this range, the slope of the plot decreases and the stripping peak splits when the iodide concentration exceeds 1.4×10^{-5} mol dm^{-3} (curve 5, Fig. 4). The relative standard deviation for 5 measurements was 4.9% when the concentration of iodide was 6×10^{-8} mol dm^{-3}, and 3.2% for 6×10^{-7} mol dm^{-3} iodide. For deposition times of 1 min, the detection limit is 1×10^{-7} mol dm^{-3} and the calibration plot is linear up to 6×10^{-6} mol dm^{-3}.

If it is assumed that the occurrence of the deviation from the rectilinear behaviour of the i_p vs. C_{I^-} plot corresponds to coverage of the electrode surface by a compact monolayer of the deposit, it is possible to calculate the surface area covered by one molecule of copper(I) iodide. The quantity of electricity consumed for the appropriate peak at its limiting height was 113 μC cm^{-2} and the surface area of CuI, calculated from this value, was 0.141 nm^2. The surface area of the copper(I) iodide molecule, calculated on the basis of crystallographic data [14], is 0.145 nm^2. The accordance bet-

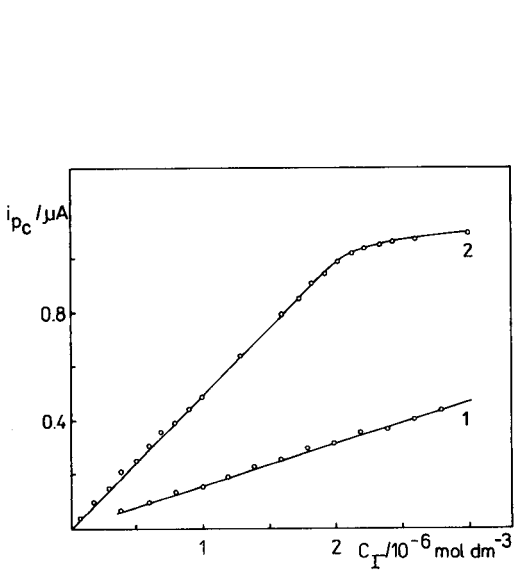

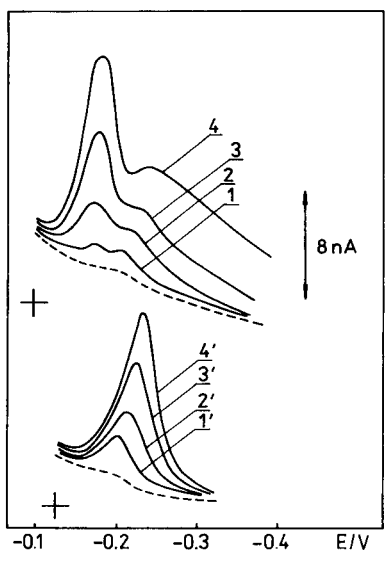

Fig. 5. Dependence of the height of the copper(I) iodide stripping peak on the concentration of iodide in solution. Deposition time: (1) 1 min; (2) 3 min. Other conditions as in Fig. 4.

Fig. 6. Comparison of the cathodic stripping pulse voltammograms: (1—4) mercury(I) iodide at the HMDE; (1'—4') copper(I) iodide at the HCADE (3×10^{-3} mol dm^{-3} copper in amalgam). Sodium iodide concentration: (1,1') 8×10^{-9}; (2,2') 1.2×10^{-8}; (3,3') 2×10^{-8}; (4,4') 3×10^{-8} mol dm^{-3}. (---) Background currents. Deposition for 200 s at: (1—4) +0.15 V; (1'—4') —0.12 V. Other conditions: pulse amplitude 20 mV; waiting time 20 ms; sampling time 20 ms; 0.1 mol dm^{-3} perchloric acid.

ween these two values is very good, which indicates that the formation of the monolayer of copper(I) iodide is in fact responsible for the deviation from linearity of the calibration plot.

The influence of variations in the concentration of copper in the HCADE or copper(II) ion in aqueous solution

An increase in the concentration of copper in the HCADE leads initially to increased stripping peak heights but when the concentration exceeds 1×10^{-3} mol dm^{-3}, the peak height becomes independent of further increases in the copper concentration. For analytical purposes, it is obviously better to use amalgams containing more than 1×10^{-3} mol dm^{-3} copper; slight variations in the amalgam concentration will not then affect the reproducibility of the results.

If, instead of the HCADE, copper(II) ions are added to solution, an increase in their concentration also leads to increasing stripping peak heights. However, under these conditions, higher copper(II) concentrations in solution produce significantly higher background currents, which have unfavourable effects on reproducibility (see Fig. 2).

Variations in the concentrations of either the copper in the HCADE or the copper(II) ions in aqueous solution affect the range of optimum potentials for the deposition step and also the iodide detection limits. Data illustrating the latter dependence are presented in Table 1. It is evident that the variant based on the HCADE offers much lower detection limits.

Use of differential pulse voltammetry

Cathodic stripping differential-pulse voltammetry was used for the determination of iodides by Propst [8], who preconcentrated iodide on the HMDE as mercury(I) iodide. Several cathodic stripping differential-pulse curves obtained for iodide at the HMDE and at the HCADE are compared in Fig. 6. The significant advantages of using the HCADE are again demonstrated. All the curves presented were recorded under conditions for which

TABLE 1

Dependence of the detection limit for iodide on the concentration of copper in the HCADE or copper(II) ion in solution[a]

Cu(II) conc. (mol dm^{-3})	Detection limit (mol dm^{-3})	Cu in amalgam (mol dm^{-3})	Detection limit (mol dm^{-3})
1×10^{-5}	1×10^{-6}	6×10^{-5}	6×10^{-7}
1×10^{-4}	1×10^{-7}	5×10^{-4}	8×10^{-8}
1×10^{-3}	—[b]	3×10^{-3}	3×10^{-8}

[a] Deposition for 3 min at —0.1 V in stirred 0.1 mol dm^{-3} perchloric acid.
[b] High and time-dependent background current makes it impossible to measure the peak height precisely.

only the submonolayer of the deposit should be formed. In spite of this, the peaks obtained at the HMDE show a marked split. The single peaks obtained with the HCADE by the pulse technique are narrower ($b_{1/2}$ = 55 mV) than the peaks obtained with the HMDE ($b_{1/2}$ = 98 mV).

For the peaks obtained by the pulse technique, the plot of i_p vs. C_{I^-} was rectilinear over a wide iodide concentration range and the detection limit attained after 200-s preconcentration was lower (8×10^{-9} mol dm^{-3}) than those attained by the d.c. stripping technique.

Interferences

Figure 7 shows the positions of the cathodic stripping peaks of several substances that may affect the stripping peak of copper(I) iodide. It is evident that possible interferences caused by the formation of Hg_2I_2 and Hg_2Br_2 may easily be eliminated by the appropriate choice of deposition potential. Interference from even low concentrations of thiocyanate, however, may be significant. The reduction peaks of lead(II) and thallium(I) ions occur at potentials more negative than the stripping peak of copper(I) iodide, but an excess of these ions decreases the height of the stripping peak for copper(I) iodide.

In Table 2, the concentrations of interfering substances are given that cause a 10% change in the stripping peak height for copper(I) iodide. The interfering action of comparatively high concentrations of lead(II) and thallium(I) ions cannot stem from simple peak overlap, which would lead to enhanced copper(I) iodide peaks. The decreased peak heights observed

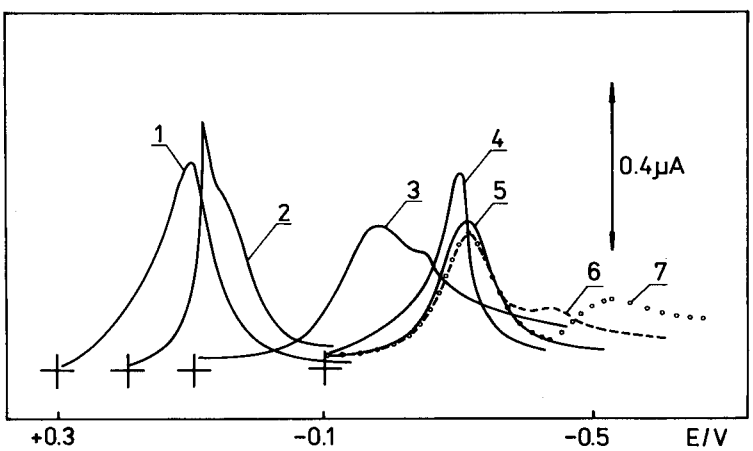

Fig. 7. Comparison of the locations of the cathodic stripping peaks of several interfering substances. Electrodes: (1—3) HMDE; (4—7) HCADE (3×10^{-3} mol dm^{-3} copper). Ion added: (1) Cl^-, 2×10^{-5}; (2) Br^-, 3×10^{-6}; (3 and 5) I^-, 5×10^{-7}; (4) SCN^-, 5×10^{-7}; (6) I^-, 5×10^{-7} and Pb^{2+}, 5×10^{-6}; (7) I^-, 5×10^{-7} and Tl^+, 1×10^{-5} mol dm^{-3}. Deposition for 2 min at: (1) 0.3 V; (2) 0.2 V; (3) 0.1 V; (4—7) - 0.1 V. Voltage scan rate, 2 V min^{-1}; supporting electrolyte, 0.1 mol dm^{-3} perchloric acid.

TABLE 2

Interferences[a] of some common ions on the cathodic stripping peak of copper(I) iodide

Interfering ion	Concentration (mol dm^{-3})	Comments
Iron(III)	1×10^{-4}	Increased background current; decrease in i_p
Thallium(I)	1×10^{-5}	Decrease in i_p; additional peak at −0.55 V
Lead(II)	5×10^{-6}	Decrease in i_p; additional peak at −0.4 V
Cl^-	5×10^{-3}	Distortion and decrease of the peak; increased background current
Br^-	1×10^{-4}	Distortion and decrease of the peak; increased background current
SCN^-	1×10^{-7}	Severe overlap of the CuI and CuSCN peaks

[a]10% change in the peak height. [b]Conditions: 1×10^{-7} mol dm^{-3} sodium iodide in 0.1 mol dm^{-3} perchloric acid; 3×10^{-3} mol dm^{-3} copper in amalgam

are probably caused by the coprecipitation of TlI and PbI_2. The harmful action of high concentrations of chloride and bromide is probably caused by precipitation of their copper(I) salts; the solubility products of these salts [4] are $10^{-7.4}$ and $10^{-8.3}$, respectively. Interference caused by the formation of copper(I) chloride was observed by Lundquist and Cox [15] during the cathodic stripping determination of phosphate at a copper electrode. It should be stressed, however, that high concentrations of chloride affect the Hg_2I_2 stripping peak far more than the CuI peak. For example, it was found that 1×10^{-3} mol dm^{-3} chloride interfered markedly with the Hg_2I_2 stripping peak but had no significant effect on the CuI stripping peak. Severe interferences would be caused by hydrogen sulphide or hydrocyanic acid but traces of these substances can easily be expelled from the cell by passing a fast flow of an inert gas through the solution acidified to pH 1.

DISCUSSION

Cathodic stripping voltammetry is firmly established in trace analysis. However, until recently, only a limited number of electrodes have given satisfactory results, and the great majority of cathodic stripping determinations is done with mercury electrodes. The application of new convenient electrodes should contribute to the further development of this technique.

The advantages of using the copper amalgam electrode come from several features. First, copper will form less soluble compounds with various substances than will mercury. Such an effect was exploited by Bilewicz and Kublik [1] for the determination of thiocyanate. Secondly, the standard potentials of various copper compounds are, as a rule, more negative than the potentials of the corresponding mercury compounds. This effect was observed above for iodides. The more negative standard potentials can facilitate the separation of the required stripping peak from interfering peaks or

from the anodic oxidation current of mercury itself. Further, the more negative the deposition potential, the fewer contaminants should be deposited on the electrode surface simultaneously with the deposit studied. For instance, the Hg_2I_2 stripping peak is more affected by moderate (10^{-3} mol dm^{-3}) concentrations of chloride, than the CuI stripping peak. Thirdly, supporting electrolytes are often contaminated by traces of copper(II) ions. In solutions which contain contaminants at the 10^{-7} mol dm^{-3} level, the HMDE may give two stripping peaks, the first corresponding to the mercury compound, and the second (usually unexpected) corresponding to the analogous copper compound.

As shown above, it is more convenient to use the copper amalgam electrode for the formation of the slightly soluble copper(I) deposits than to add copper(II) to the solution. The addition of copper(II) produces a significant, time-dependent background current which makes measurements of the stripping peak difficult; and the detection limit is poorer than that obtained for the HCADE. The addition of copper(II) ions to the bulk iodide solution could lead to the reaction: $2\ Cu^{2+} + 4\ I^- = 2\ CuI + I_2$, which is well known in titrimetric analysis [16]. Under the experimental conditions used here, this side-reaction proceeded slowly but when the experiments lasted several hours, a marked decrease in the height of the iodide stripping peak was observed.

This work was done as part of Project MR I 32.

REFERENCES

1 R. Bilewicz and Z. Kublik, Anal. Chim. Acta, 123 (1981) 201.
2 U. Forsman, J. Electroanal. Chem., 111 (1980) 325; 122 (1981) 215; Anal. Chim. Acta, 146 (1983) 71.
3 A. Ringbom, Complexation in Analytical Chemistry, Interscience, New York, 1963.
4 R. M. Smith and A. E. Martell, Critical Stability Constants, Vol. IV, Plenum Press, New York, 1976.
5 I. Shain and S. Perone, Anal. Chem., 33 (1961) 325.
6 W. Kemula, Z. Kublik and J. Taraszewska, Chem. Anal. (Warsaw), 8 (1963) 171; and in N. D. Cheronis (Ed.), Proc. Int. Symp. Microchem. Techn., Interscience, New York, 1963, p. 865.
7 E. H. Boult and H. R. Thirsk, Trans. Faraday Soc., 50 (1954) 404.
8 R. C. Propst, Anal. Chem., 49 (1977) 1199.
9 W. Kemula and Z. Kublik, Anal. Chim. Acta, 18 (1958) 104.
10 S. Głodowski and Z. Kublik, Anal. Chim. Acta, 149 (1983) 137.
11 R. S. Nicholson and I. Shain, Anal. Chem., 36 (1964) 706.
12 Z. Galus, CRC Crit. Rev. Anal. Chem., (1975) 370.
13 Kh. Z. Brainina, Inversionnaya Voltamperometria Twierdykh Phaz, Khimya, Moskow, 1972.
14 Handbook of Chemistry and Physics, 58th edn., CRC Press, West Palm Beach, FL, 1978/79.
15 G. L. Lundquist and J. A. Cox, Anal. Chem., 46 (1974) 360.
16 H. A. Laitinen and W. E. Harris, Chemical Analysis, McGraw-Hill, New York, 1975.

Analytica Chimica Acta, 171 (1985) 215—223
Elsevier Science Publishers B.V., Amsterdam — Printed in The Netherlands

TRACE DETERMINATION OF LANTHANUM, CERIUM, AND PRASEODYMIUM BASED ON ADSORPTIVE STRIPPING VOLTAMMETRY

JOSEPH WANG*, PERCIO A. M. FARIAS[a] and JAWAD S. MAHMOUD
Department of Chemistry, New Mexico State University, Las Cruces, NM 88003 (U.S.A.)
(Received 19th November 1984)

SUMMARY

A sensitive stripping procedure is described for quantifying lanthanum, cerium and praseodymium ions, based on the controlled adsorptive accumulation of the lanthanide/*o*-cresolphthalexon complex onto the static mercury drop electrode. The effect of various operational parameters on the stripping response is discussed. A 20-min accumulation period coupled with differential pulse measurement of the current resulting from the adsorbed complex permits quantitation down to the 1×10^{-10} M level. For concentrations ranging from 2.5×10^{-8} M to 2.5×10^{-9} M, a 0.5- to 4-min accumulation period is sufficient. The relative standard deviation at the 7×10^{-8} M level ranges from 1 to 6%.

The electrochemical behavior of lanthanides makes their voltammetric determination very difficult. On mercury electrodes, poorly defined waves are obtained at extremely negative potentials [1]. Various workers [2, 3] have used reducible organic dyes, capable of complexing lanthanide ions, for the polarographic determination of these metals. The resulting complexes produce discrete reduction waves which are separated from the free-dye wave by a potential difference which depends on the atomic number of the lanthanide. By using the adsorptive complex wave with *o*-cresolphthalexon (OCP), the polarographic procedure yielded a detection limit of 1×10^{-7} M lanthanum [3].

For the above reasons, trace determination of lanthanides by the most sensitive electroanalytical technique, stripping voltammetry, has rarely been attempted. An indirect stripping procedure for lanthanides, based on the displacement reaction between these metal ions and the EDTA chelate of zinc was described by Berge and Drescher [4]; this procedure allows quantitation down to the 5×10^{-7} M level. The only lanthanide determined directly by stripping voltammetry is cerium [5]; cathodic stripping voltammetry at a graphite electrode yielded a detection limit of 6×10^{-7} M. Micromolar levels of cerium can be quantified by potentiometric stripping, by depositing known amounts of silver onto the working electrode and using

[a]Present address: Department of Chemistry, Pontificia Universidade Catolica de Janeiro, Rio de Janeiro, Brazil.

0003-2670/85/$03.30

the cerium(IV) as oxidizing agent [6]. Stripping measurements of lanthanides at the nanomolar level have not been attempted previously.

This paper describes a very sensitive stripping procedure for quantifying various lanthanides based on the adsorptive accumulation of the lanthanide/*o*-cresolphthalexon complex on the static mercury drop electrode followed by reduction of the adsorbed complex. Adsorptive stripping voltammetry is known to be useful for many analytes that cannot be accumulated electrolytically [7]. With the static mercury drop electrode, reproducible results are obtainable at the submicromolar and nanomolar concentration levels, with detection limits as low as 2.5×10^{-11} M [8]. While most applications of absorptive stripping voltammetry have been concerned with organic analytes, it is possible also to determine metal ions based on the absorptive accumulation of their complexes with various organic ligands. For example, nickel [9] and uranium [10] can be quantified after adsorptive accumulation of their dimethylglyoxime and pyrocatechol complexes, respectively, onto mercury electrodes. Similar behavior is obtained in the present study for the lanthanide/*o*-cresolphthale (OCP) complexes. The adsorbed OCP complexes of lanthanum, cerium and praseodymium yield stripping peaks distinctly different from that of the organic dye. Hence, the detection limits for these lanthanides can be improved by several orders of magnitude.

EXPERIMENTAL

Apparatus and reagents

Voltammograms were obtained with an EG & G Princeton Applied Research Corp. (PAR) Model 264A stripping analyzer. The working electrode was a PAR Model 303A static mercury drop electrode. The sample cell (PAR Model 0057) was fitted with a Ag/AgCl (satd. KCl) reference electrode and a platinum wire auxiliary electrode. The cell was covered with aluminum foil. A magnetic stirrer (Troemner Model 500) and a stirring bar (1-cm long, 2-mm thick) provided the convective transport during the preconcentration step. A PAR Model 0073 X-Y recorder was used for the collection of experimental data.

A 1000 mg l^{-1} lanthanum stock solution (atomic absorption standard, Aldrich) was used, and diluted as required for standard additions. Similar stock solutions of praseodymium, cerium and europium were prepared by dissolving the pure metal, its salt or its oxide, respectively. A portion (6.4 mg) of *o*-cresolphthalein complexone (Sigma Chemical Co.) was dissolved with several drops of 1 M sodium hydroxide and the reddish solution was diluted to give a 10^{-4} M stock solution. All solutions were prepared from deionized water and analytical-grade reagents.

Procedure

The supporting electrolyte solution (10 ml), 0.1 M NH_3/NH_4Cl (pH 9.4) containing 5×10^{-7} M OCP, was added to the cell and degassed with

nitrogen for 8 min (and for 30 s before each adsorptive stripping cycle). The preconcentration potential (usually −0.4 V) was applied to the electrode for a selected time while the solution was stirred at 400 rpm. The stirring was then stopped, and after 15 s the voltammogram was recorded by applying a cathodic differential pulse scan. The scan was terminated at −1.3 V, and the adsorptive stripping cycle was repeated using a new mercury drop. After the background stripping voltammogram was obtained, aliquots of the lanthanide standards were introduced. The entire procedure was automated, as controlled by the PAR 264A Stripping Analyzer. Throughout this operation, nitrogen was passed over the solution surface. All data were obtained at room temperature.

RESULTS AND DISCUSSION

Response characteristics

Figure 1 shows differential pulse voltammograms obtained for 3.2×10^{-8} M (4.5 μg l^{-1}) lanthanum, cerium and praseodymium, in the presence of 5×10^{-7} M OCP, after different accumulation times. The lanthanide/OCP complex yields a well-defined reduction peak at −1.1 V, which is separated from the free-dye reduction peak (at −0.94 V). The peak height for the complex increases rapidly with increasing preconcentration time, indicating an enhancement of the complex concentration on the mercury surface. Some enhancement of the OCP peak height is also observed at 1-min accumulation. This is in agreement with the chronocoulometric study of

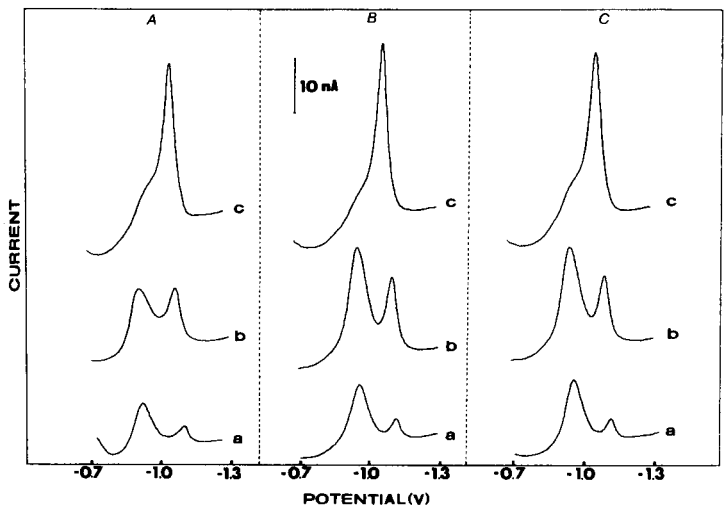

Fig. 1. Differential pulse voltammograms for 7.2×10^{-8} M La (A), Ce (B), and Pr (C), after different preconcentration times: (a) 0; (b) 1; (c) 5 min. Preconcentration at −0.4 V with 400 rpm stirring. Differential pulse waveform with 5 mV s^{-1} rate and 50-mV amplitude; medium drop size; solution, 0.1 M NH_3/NH_4Cl (pH 9.4) containing 5×10^{-7} M OCP.

Gao and Zhang [3], in which it was found that the complex adsorbs more strongly than OCP does. Possibly, at longer accumulation periods (5 min), the complex displaces the OCP from the surface. The peak widths at half peak height were 80 mV (OCP) and 50 mV (complex). The 1- and 5-min accumulation periods result in approximately 4- and 8-fold peak current enhancements, respectively, over those attained by conventional solution-phase pulse voltammetry (no accumulation). Obviously, longer preconcentration periods would yield further peak current enhancements (see below). As a result of this adsorptive accumulation, nanomolar levels of these lanthanide ions can easily be quantified. Because the potential difference between the peaks of the complex and free ligand decreases with increasing atomic number of the lanthanide, heavy lanthanide ions cannot be measured conveniently.

Plots of peak current vs. accumulation time were linear with the 1—5 min accumulation periods. Least-squares fits of these data yielded slopes of 4.71 (La, Ce), and 4.86 (Pr) nA min^{-1}, with intercepts of 5.8 (La), 9.55 (Ce), and 8.32 (Pr) nA, and standard errors of estimates of 0.06 (La), 1.04 (Ce) and 0.72 (Pr). The nonzero intercepts are attributed to the response obtained without accumulation (Fig. 1a). Deviations from linearity may result at higher concentrations or with use of longer accumulation times, as full surface coverage is approached (see below). The similarity of the time-dependent response profiles, and of other response characteristics, indicates that the adsorption behavior of the three complexes is similar. To optimize the accumulation time, there would be a trade-off between sensitivity and speed. Accumulation times of 0.5 and 4 min provide such compromise for measuring lanthanide ions at the 2.5×10^{-8} M and 2.5×10^{-9} M levels, respectively.

Measurements of the dependence of the complex stripping peak current on the OCP concentration indicated that the peak current rises rapidly when the concentration ratio, [OCP]/[M], is less than 5, and then more slowly when the ratio is higher. The free OCP peak increases linearly with the dye concentration. Accordingly, a 5×10^{-7} M OCP level was chosen as a compromise for lanthanide measurements over the 10^{-7}—10^{-9} M range, and used throughout. (A 1:1 stoichiometry has been suggested for the lanthanide/OCP complexes [3]).

The effect of the accumulation potential was examined over the —0.2 to —0.9 V range. Both the complex and OCP peaks remained unchanged when the potential was varied from —0.2 V to —0.6 V, and decreased (up to 50%) at more negative potential values. A potential of —0.4 V was used throughout. Mass transport during the accumulation step also affected the lanthanide/OCP stripping peak. At a stirring rate of 400 rpm, a 4-fold enhancement of the response was obtained compared to the response in a quiescent solution (6×10^{-8} M lanthanum, 2-min accumulation). Such mass-transport control indicates fast rates of adsorption.

The differential pulse stripping response was compared to that obtained

in corresponding linear-scan stripping measurements. Although significant peak-current enhancement was obtained in both stripping modes, compared to the response without accumulation, the differential pulse mode offers improved performance in terms of sensitivity and resolution from the OCP peak. This is attributed to its ability to compensate for the charging background current and the sharpness of the stripping peaks. Among the parameters of the differential pulse waveform, the use of a 50-mV amplitude and 5 mV s^{-1} scan rate provided the best compromise between sensitivity, resolution and speed. These parameters were used throughout.

Quantitative utility

Quantitative evaluation was based on the linear correlation between the peak current and the lanthanide ion concentration. Figs. 2 and 3 present the adsorptive stripping response to standard additions over different concentration ranges, 3.5×10^{-9}—3.5×10^{-8} M (0.5—5 $\mu g\ l^{-1}$) praseodymium and 3.5×10^{-8}—1.75×10^{-7} M (5—25 $\mu g\ l^{-1}$) lanthanum, respectively. Accumulation for 4 min and 1 min, respectively, are sufficient to obtain well-defined voltammetric peaks at these concentration levels. In contrast, the conventional voltammetric response, without accumulation, does not permit

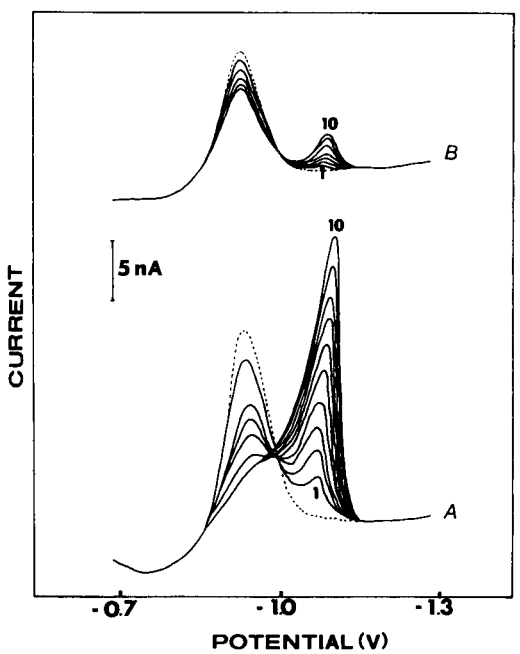

Fig. 2. Differential pulse voltammograms obtained after successive concentration increments of 3.5×10^{-9} M (0.5 $\mu g\ l^{-1}$) praseodymium after preconcentration for 4 (A) and 0 (B) min. Other conditions as in Fig. 1. The numbers 1 and 10 designate the response for the lowest and highest concentrations, respectively. Dotted lines represent the response before addition of the metal ion.

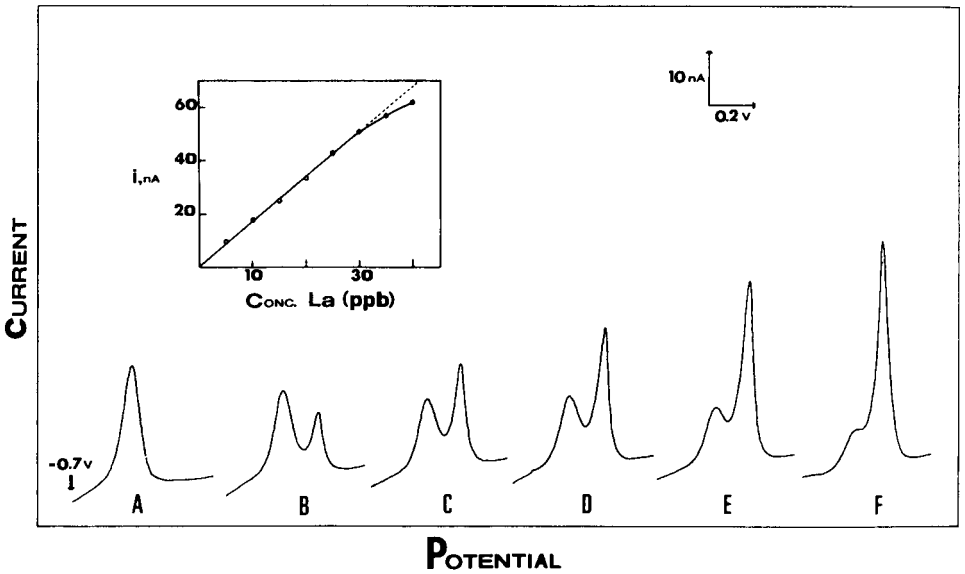

Fig. 3. Differential pulse voltammograms obtained after successive concentration increments of 3.5×10^{-8} M lanthanum after 1-min preconcentration. Other conditions as in Fig. 1. Also shown is the resulting calibration plot.

convenient quantitation at the nanomolar level (Fig. 2B). There is a gradual decrease of the OCP peak associated with increasing lanthanide concentration. This decrease is attributed to the lower level of the free ligand and to its displacement from the surface by the strongly adsorbed complex. The change in the OCP peak on increasing the lanthanide concentration is nonlinear and cannot be used for quantitation. The complex peak increases linearly with the lanthanide concentration (slopes, 4.35 nA l μg^{-1} (Pr), 1.65 nA l μg^{-1} (La); intercepts, 0.98 nA (Pr), 1.05 nA (La); standard errors of estimate, 0.63 (La), 0.17 (Pr) nA). The five measurements shown in Fig. 3 are a part of eight concentration increments summarized in the calibration plot (also shown). Deviations from linearity are observed for lanthanum concentrations higher than 2.1×10^{-7} M (30 $\mu g\ l^{-1}$). Similar standard additions for praseodymium and cerium exhibited similar behavior. For these ions, least-squares treatment of the initial linear portion (5—30 $\mu g\ l^{-1}$) yielded slopes of 1.99 nA l μg^{-1} (Pr) and 1.88 nA l μg^{-1} (Ce), intercepts of 3.39 nA (Pr) and 2.46 (Ce) with standard errors of estimate of 1.95 nA (Pr) and 0.77 nA (Ce) (conditions, as in Fig. 3). The curvature of the calibration plots is consistent with a process that is limited by adsorption of the analyte, i.e., deviations from linearity as full surface coverage is approached. The linear range depends on the operational parameters (e.g., accumulation time or stirring rate) that affect the surface coverage. For example, standard additions, with 30- and 90-s accumulation, yielded linear response up to 35 and 25 $\mu g\ l^{-1}$ praseodymium, respectively, with slopes of

1.31 and 2.31 nA l μg^{-1} (other conditions as in Fig. 3). At higher concentrations, solution-phase voltammetry can be used. In contrast, for trace measurements of lanthanide ions, only adsorptive stripping voltammetry offers the desired sensitivity, as is evident from the present data. When the method of standard additions is used, three additions are necessary to ensure that the measured current corresponds to the linear portion.

The effective preconcentration, obtained by the adsorption of the lanthanide/OCP complexes, results in extremely low detection limits (Table 1). For a 20-min accumulation, similar detection limits, ranging from 1.2×10^{-10} M to 1.7×10^{-10} M, were obtained for the three lanthanides examined. These concentrations correspond to 170—250 pg in the 10-ml samples used. With 5-min accumulation, the detection limits range from 2.9×10^{-10} M to 3.8×10^{-10} M. These values are comparable to those obtained in anodic stripping measurements of electrolytically plated metals. Compared to previous voltammetric procedures for lanthanide ions [2—6], the adsorptive stripping procedure lowers the detection limits by 3—4 orders of magnitude. The adsorptive stripping detection limits are below the detection limits of techniques currently available for trace lanthanide determinations, e.g., neutron activation, atomic absorption and inductively-coupled plasma spectroscopy [11]. Only selective excited probe ion luminescence offers detection limits comparable to those obtained here [11]. The above data illustrate again the similar extent of adsorption of the different lanthanide/OCP complexes.

Also shown in Table 1 is the precision obtained for eight successive measurements of 7×10^{-8} M (10 $\mu g\ l^{-1}$) of each lanthanide ion. The relative standard deviations range from 1.1% to 6.4%.

Interferences would be likely to occur primarily via two modes of action, namely, competition on the surface sites by surfactants present in the sample and competition for the OCP by other metal ions. Gelatin, albumin, cholesterol, and chloride were used as model surface-active species. A 10^3-fold excess of chloride did not affect the response. In contrast, excess of the organic surfactants affected (in different degrees) the ligand and complex peaks. Low levels (sub-mg l^{-1}) of gelatin and albumin affected only the OCP

TABLE 1

Reproducibility and detection limits[a]

Element	Detection limit[b] (M)	Relative standard deviation[c] (%)
La	1.2×10^{-10}	1.1
Ce	1.7×10^{-10}	6.4
Pr	1.4×10^{-10}	5.9

[a]Conditions as in Fig. 1. [b]Based on measurements of 3.5×10^{-9} M of the lanthanides, after 20-min accumulation, and S/N = 2. [c]Eight successive measurements of 7×10^{-8} M of the lanthanides, after 1-min accumulation.

peak. Under these conditions, the surfactant preferentially displaced the weakly adsorbed OCP from the surface, while the strong adsorption of the complex was not affected. As a result, the voltammogram may exhibit only the complex peak of interest (Fig. 4), and quantitation is improved. This is especially advantageous in measurements of heavier lanthanides which exhibit larger degrees of peak overlap. For example, in stripping measurements of europium, the ligand and complex peaks are separated by 80 mV and quantitation is not convenient (Fig. 4A, curve a). However, with the addition of 0.6 mg l^{-1} gelatin, the OCP peak disappears, and the complex is measured without interference (Fig. 4A, curves b, c). The quantitative utility of this effect requires re-examination of the linear range, as the extent of surface coverage is changed. At higher concentrations of gelatin and albumin (>4 mg l^{-1}), the quantitation of μg l^{-1} levels of lanthanides suffers from significant depressions of the complex peak of interest. Under these conditions, the surfactant preferentially displaces both the ligand and complex from the surface. The addition of a 10^3-fold amount of cholesterol results in an enhancement (300%) of the complex stripping peak. However, the quantitative utility of this unusual enhancement effect is restricted because of limited linear range. Overall, solutions containing a large amount (>10^3 fold) of interfering surfactants may require a separation step prior to adsorptive stripping.

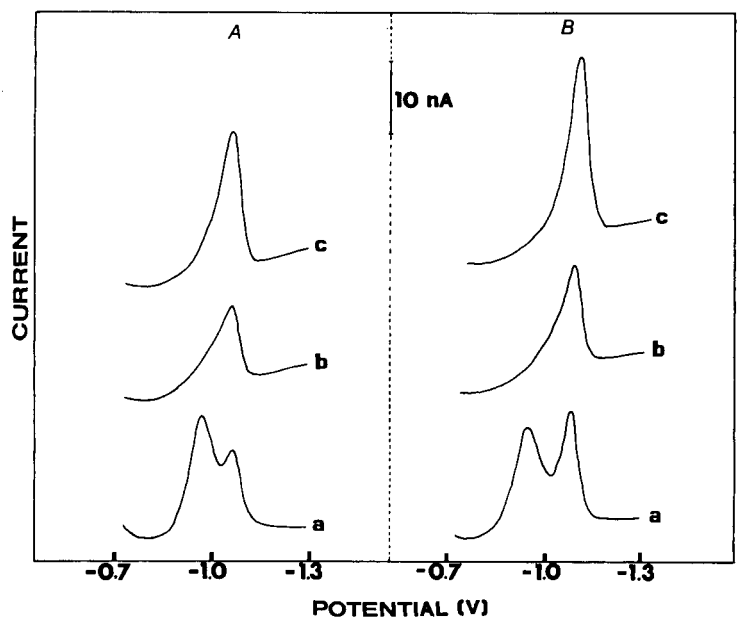

Fig. 4. Determination of europium (A) and cerium (B) in the presence of gelatin: (a) 5 × 10^{-7} M OCP and 3 × 10^{-8} M of the lanthanide; (b) same as (a), but after addition of 0.6 mg l^{-1} gelatin; (c) same as (b) but after addition of 3 × 10^{-8} M of the lanthanide. Accumulation for 2 min; other conditions as in Fig. 1.

As most metal ions do not form complexes with OCP [3], their presence does not affect the lanthanide determination. Concentrations of 10^{-6} M Ca^{2+}, Mg^{2+}, Al^{3+}, Cu^{2+}, Cd^{2+}, Hg^{2+} and Zn^{2+} did not interfere with the determination of 7×10^{-8} M La^{3+}. The presence of some of these metal ions (e.g., Cd^{2+}, Ca^{2+} and Mg^{2+}) enhanced the OCP peak. In contrast, mixtures of lanthanide ions would require prior separation because of the similarity in the peak potentials of the complexes. Because of the similar responses obtained for La, Pr and Ce, stripping measurements of their mixtures would correspond to the total light lanthanide content.

In conclusion, it is shown that the spontaneous adsorptive accumulation of the lanthanide/OCP complexes offers several advantages in the voltammetric measurement of lanthanide ions. The method allows quantitation of nanomolar levels of cerium, lanthanum and praseodymium, using relatively short accumulation times and inexpensive instrumentation. The use of other organic dyes, e.g., eriochrome violet B, may be useful for adsorptive stripping measurements of other lanthanides. Similar methodology may be applied for trace measurements of other metal ions which are difficult to quantify with conventional stripping methods. Work in this laboratory is continuing in this direction.

This work was supported by the National Institutes of Health under Grant No. GM30913-01A1. P. A. M. Farias acknowledges the financial support of the National Council for Scientific Development (CNPq) of the Brazilian government.

REFERENCES

1 W. Noddack and A. Bruckl, Angew. Chem., 50 (1937) 362.
2 T. M. Florence and G. H. Aylward, Aust. J. Chem., 15 (1962) 65.
3 X. Gao and M. Zhang, Anal. Chem., 56 (1984) 1912.
4 H. Berge and A. Drescher, Anal. Chim. Acta, 52 (1970) 363.
5 Kh. Z. Brainina, Zh. Anal. Khim., 19 (1964) 810.
6 S. Bruckenstein and J. W. Bixler, Anal. Chem., 37 (1965) 786.
7 J. Wang, Stripping Analysis: Principles, Instrumentation and Applications, VCH Publishers, Deerfield Beach, FL, 1985.
8 J. Wang, D. B. Luo, P. A. M. Farias and J. S. Mahmoud, Anal. Chem., 57 (1985) 158.
9 H. Braun and M. Metzger, Z. Anal. Chem., 318 (1984) 321.
10 N. K. Lam, R. Kalvoda and M. Kopanica, Anal. Chim. Acta, 154 (1983) 79.
11 F. J. Gustafson and J. C. Wright, Anal. Chem., 51 (1979) 1762.

Analytica Chimica Acta, 171 (1985) 225—231
Elsevier Science Publishers B.V., Amsterdam — Printed in The Netherlands

SIMULTANEOUS ASSAY OF ORGANIC FLUORINE COMPOUNDS IN BIOLOGICAL FLUIDS BY FLUORINE-19 NUCLEAR MAGNETIC RESONANCE SPECTROMETRY OVER A LARGE SPECTRAL WIDTH
Application to Fluoropyrimidines

J. P. BETEILLE, A. LOPEZ, M. BON, M. C. MALET-MARTINO and R. MARTINO*

Laboratoire des IMRCP, UA CNRS 04-470, Université Paul Sabatier, 118, route de Narbonne, 31062 Toulouse Cédex (France)

(Received 21st August 1984)

SUMMARY

^{19}F-n.m.r. spectrometry is used as a direct method to assay simultaneously in body fluids (urine, plasma) all the fluorinated metabolites of a new antineoplastic drug fluoropyrimidine, 5′-deoxy-5-fluorouridine. The resonances of these metabolites are spread over a large spectral width (about 100 ppm). The calibration graphs for 5′-deoxy-5-fluorouridine and its major metabolite, α-fluoro-β-alanine, are linear over the range 10^{-5}—10^{-1} M; the accuracy is 3—5% for urine samples and 5—7% for plasma samples. The method is applied to the determination of all the metabolites in urine from a patient.

Nuclear magnetic resonance spectrometry (n.m.r.) is a useful technique in the study of drug metabolism, as it is non-invasive and it allows both a direct analysis of the biological fluids without a need for extraction, and a simultaneous detection of all the metabolites. Among the nuclei commonly studied by n.m.r., fluorine-19 has many inherent advantages for biological studies. It is an excellent n.m.r. probe (spin 1/2, relative sensitivity 0.833 that of proton, 100% natural abundance) and its biological level is very low (the total fluorine content in human serum is generally in the range 5×10^{-6}—1.5×10^{-5} M whereas ionic fluoride lies in the range 10^{-6}—3×10^{-6} M [1]) making it undetectable by n.m.r. This avoids the problem of interference between the signals of the fluorinated drug (and/or those of its fluorinated metabolites) and those of the biological components. This is not the case for proton, carbon-13 or phosphorus-31 n.m.r.

In a previous work [2], a qualitative description was presented for the metabolic pathway of a new antineoplastic fluoropyrimidine drug (5′-deoxy-5-fluorouridine, 5′-DFU) in human biological fluids (blood, plasma, urine) by using ^{19}F-n.m.r. In addition to the known metabolites 5-fluorouracil (5-FU) and 5,6-dihydro-5-fluorouracil (5-FUH_2) [3], two catabolites were found that had not previously been reported for 5′-DFU, α-fluoro-β-alanine (FBAL) and α-fluoro-β-ureidopropionic acid (FUPA) (Fig. 1). The resonances of the different fluorinated metabolites of 5′-DFU are spread over a large

0003-2670/85/$03.30

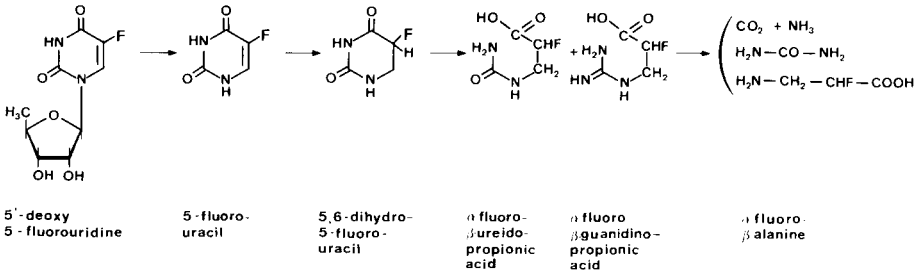

Fig. 1. Catabolic pathway of 5'-deoxy-5-fluorouridine (5'-DFU).

chemical shift range (about 100 ppm) (Fig. 2) and with some Fourier-transform (FT) n.m.r. standard spectrometers (particularly the Cameca 250 FT instrument used in this study), it is not possible to obtain a quantitative response of ^{19}F-n.m.r. signals over such a wide spectral width.

^{19}F-n.m.r. methodology was therefore developed for the assay of 5'-DFU and its metabolites in human body fluids. This procedure may be also useful in the determination of any fluorinated compound found at low levels in biological fluids (10^{-5}—10^{-3} M) and giving ^{19}F signals over a spectral width of about 120 ppm. It required some modification of the spectrometer, a selection of specific references and knowledge of the spin-lattice relaxation times (T_1) of the different fluorine nuclei.

EXPERIMENTAL

Reagents

The 5'-DFU was a gift from Hoffmann-La Roche (Bâle, Switzerland); FBAL was obtained from Koch-Light and sodium monofluoroacetate (FAC) from Fluka. Sodium 4-fluorobenzoate (FBEN) was prepared by titrating 4-fluorobenzoic acid (Fluka) with sodium hydroxide solution. Chromium(III) acetylacetonate [Cr(acac)$_3$] was a product from Spectrométrie Spin Techniques. Standard solutions of 5'-DFU, FBAL, FAC and FBEN, for calibration purposes, and Cr(acac)$_3$ solution were prepared in deionized water.

Instrumentation

For calibration and assay, ^{19}F-n.m.r. spectra were recorded at 250 MHz on a Cameca 250 FT spectrometer interfaced with a 16K memory Nicolet 80 computer. Spectra were run without proton decoupling and with no frequency field lock, in 5-mm diameter n.m.r. tubes. The resonance positions were measured from the H_2O proton signal which was always positioned arbitrarily for any sample at the same frequency and referenced to the resonance peak of an external standard trifluoroacetic acid (0.5% w/v aqueous solution). The instrumental settings for quantitative work were as follows: probe temperature 20°C; spectral width 29 411 Hz; pulse width 2.6 μs ($\alpha \cong 75°$); recycling time 2 s; number of scans 400—78 000; computer resolution 3.6 Hz/point (each

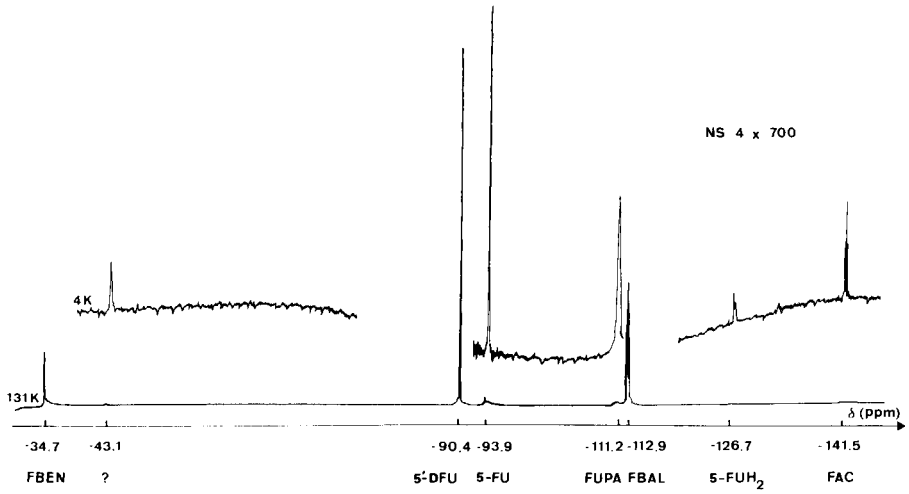

Fig. 2. ^{19}F-n.m.r. spectrum of a urine sample of a patient treated with 5'-DFU. 5'-DFU, 5-FU, FUPA, FBAL and 5-FUH$_2$ are 5'-DFU metabolites; ? is an unknown metabolite; FBEN and FAC are internal references. Number of scans (NS), 2800.

peak being described by at least 9 points); line broadening caused by exponential multiplication was 5 Hz for urine samples and 20 Hz for plasma samples. The magnetic field was shimmed by using the ^{1}H-n.m.r. resonance of water observed in the continuous wave (c.w.) mode.

Fluorine-19 spin-lattice relaxation times were measured by the inversion-recovery method at 188.3 MHz on a Bruker AM-200 instrument equipped with quadrature phase detection (Bruker Spectrospin Application Laboratory, Wissembourg, France). The probe temperature was 23°C; 5-mm tubes were used. The spectra were recorded with no field frequency lock and with proton decoupling. The instrumental settings were: pulse width 6.5 μs (90° pulse); the recycling time was 22.5 s when no Cr(acac)$_3$ was added to the solutions and 9.3 s when Cr(acac)$_3$ (concentration $>4.1 \times 10^{-4}$ M) was added. For the evaluation of T_1, the different media were spiked with the four fluorinated compounds, FBEN, 5'-DFU, FAC and FBAL, at concentrations of 2×10^{-2}—3×10^{-2} M. To bypass the problem of finite pulse excitation power over the large spectral width of 25 kHz, the T_1 measurements of the FBEN signal and of the other signals were made in two separate experiments. The spectra covering a spectral width of 5000 Hz in the first experiment and 13 000 Hz in the second one were accumulated into 16K and 64K channels, respectively. Values of T_1 were calculated by a non-linear least-squares fit to the function $I(\tau) = A - B \exp(-\tau/T_1)$ with 15 different τ values. It was verified that the T_1 value of each fluorinated compound in water did not increase when the concentrations were $<4 \times 10^{-2}$ M.

Calibration by "spiking" urine and plasma

Aliquots of the biological medium (600 μl) were placed into a n.m.r. tube. Final concentrations of 1.48×10^{-5}—1.44×10^{-1} M 5'-DFU, 2.6×10^{-5}—1.03×10^{-1} M FBAL, 4.53×10^{-5}—9.01×10^{-2} M FBEN, and 5.36×10^{-5}—1.06×10^{-1} M FAC were obtained by adding various quantities of solutions of these different compounds; in order to avoid an exaggerated disproportion of the peak areas, samples containing similar concentrations of these compounds were analyzed. A $Cr(acac)_3$ solution was then added so that the final concentration was 2.2×10^{-4} M; it was verified that such a concentration did not modify the spectra. The total volume of aqueous standard and $Cr(acac)_3$ solutions added never exceeded 10% of the biological fluid volume used. The ^{19}F-n.m.r. spectra were recorded as described above. The concentrations of the different compounds were evaluated from the intensities of their respective n.m.r. signals. These intensities were estimated by comparing the areas of the n.m.r. signals areas with that of FAC. The comparison was made after cutting and weighing the different signals which had first been enlarged (20 Hz cm^{-1} for urine, and 60 Hz cm^{-1} for plasma).

Procedure for intravenous perfusion, sampling and ^{19}F-n.m.r. assay

The patient evaluated in this study was randomly recruited from a group of patients treated in a phase-II trial run by the EORTC Clinical Screening Group. According to the trial protocol, 5'-DFU (10 g m^{-2} = 22.5 g) was dissolved in 500 ml of 5% glucose isotonic solution and infused over 6 h. Urines were collected after each spontaneous micturition over 21 h and an aliquot was frozen and stored at −20° C until analysis. After thawing, the urine sample (600—800 μl) was placed in a n.m.r. tube. Internal reference (FAC and FBEN) solutions were added so that the final concentrations of FAC and FBEN were close to the concentrations of the 5'-DFU metabolites. The solution of $Cr(acac)_3$ was then added. The ^{19}F-n.m.r. spectra were recorded as described above. The 5'-DFU and FBAL concentrations were evaluated by comparing their n.m.r. signals (as expanded areas) with that of FBEN; the 5-FU, 5-FUH_2 and FUPA concentrations were obtained by comparing their n.m.r. signals (expanded areas) with that of FAC.

RESULTS AND DISCUSSION

Modifications of the spectrometer

Modifications were necessary because of the insufficient spectral density of the radiofrequency (r.f.) pulse and because of the weak receiver bandwidth. The first difficulty was solved by improving the high-frequency (h.f.) amplifier power by 3 dB (i.e., 150 W). When equipment thus modified was tested on biological samples, it was verified that a tipping angle α of 90° was obtained for a pulse width of 3.5 μs. With the simple phase-detection spectrometer used, the spectral density of a 2.6-μs pulse (i.e., $\alpha \cong 75°$) allows the study of a 30-kHz spectral width with an amplitude error of <1%. For the

receiver, a decrease of about 6 dB at 30 kHz was blamed on the low-frequency (l.f.) amplifier. In preference to modifying the structure of this system, a new system was constructed which had better characteristics with regard to the bandwidth and signal/noise ratio. This amplifier consisted of two identical units, each of which had two differential amplifiers followed by a low-impedance stage, as shown in Fig. 3. This set-up demonstrated a maximum gain of 60 dB and a bandwidth at −3 dB ranging from d.c. to 100 kHz.

Choice of references and recycling times

As small 5-mm tubes were used, only internal references were possible. They had to be soluble in the aqueous biological media and their n.m.r. signals had to fall within the spectral scale studied. For all these reasons, sodium 4-fluorobenzoate (FBEN) and sodium fluoroacetate (FAC) were chosen; these compounds give peaks at each end of the chemical shift range studied (Fig. 2) which, additionally, simplified the phase-correction.

To choose the recycling time, the spin-lattice relaxation times (T_1) of both the internal references and the different types of 5′-DFU metabolites were evaluated in various media (Table 1). As the T_1 values in plasma and urine were too high to allow quantification in a reasonable period of time, a relaxation reagent was added (blood showed an acceptable T_1 value); chromium acetylacetonate, $Cr(acac)_3$, was chosen as it has the advantage of being sufficiently soluble in aqueous medium at biological pH (the limit of solubility is 2.9×10^{-3} M). The recycling time used was therefore 2 s and it was verified that a value of >2 s did not modify the signal intensities.

Verification of the validity of the method

Blank human urine was spiked with known amounts of 5′-DFU, FBAL, FBEN and FAC. The peak areas of 5′-DFU, FBAL and FBEN were compared

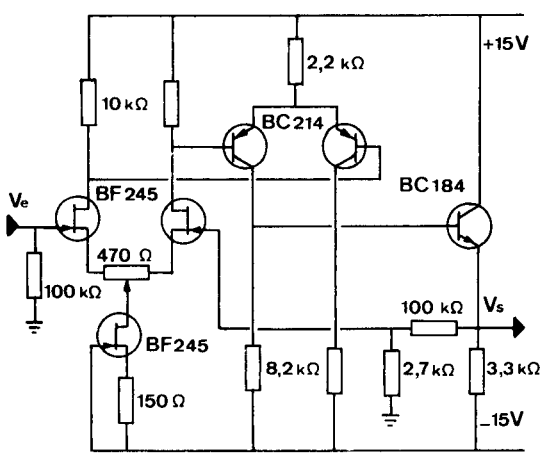

Fig. 3. Schematic diagram of one unit of the low-frequency amplifier constructed.

TABLE 1

Fluorine-19 relaxation times, T_1, of internal references (FBEN, FAC), 5'-DFU and a metabolite (FBAL) in biological media

Biological medium	T_1 (s)			
	FBEN	5'-DFU	FBAL	FAC
Plasma	1.50 ± 0.11	1.82 ± 0.56	2.04 ± 0.30	2.70 ± 0.33
Plasma + $Cr(acac)_3$	0.94 ± 0.06	0.78 ± 0.05	1.46 ± 0.15	1.58 ± 0.20
Blood		0.97 ± 0.30	1.59 ± 0.09	1.64 ± 0.26
Urine		1.84 ± 0.11	1.88 ± 0.30	2.87 ± 0.36
Urine + $Cr(acac)_3$		0.85 ± 0.09	1.48 ± 0.12	1.71 ± 0.18

with that of FAC, which was the most precise because it is located near the r.f. carrier. The calibration graphs, constructed by plotting the added concentration of each compound (x) and the measured signal concentration of the same compound (y), were linear in the concentration ranges 1.48×10^{-5}—1.44×10^{-1} M for 5'-DFU, 2.6×10^{-5}—1.03×10^{-1} M for FBAL and 4.53×10^{-5}—9.01×10^{-2} M for FBEN. From the linear regressions thus derived, the following equations were obtained

FBEN $y = 0.976\,x + 0.502 \times 10^{-4}$ ($n = 21$, $r = 0.998$, r.s.d. = 5.4)
FBAL $y = 1.081\,x + 5.121 \times 10^{-4}$ ($n = 20$, $r = 0.999$, r.s.d. = 3.1)
5'-DFU $y = 1.063\,x + 4.287 \times 10^{-4}$ ($n = 21$, $r = 0.999$, r.s.d. = 4.0)

where n is the number of measurements, r the correlation coefficient and r.s.d. is the relative standard deviation (%). These results demonstrate that the recommended experimental conditions provide a good quantification of signals from fluorinated compounds located over a spectral range of 120 ppm.

The limit of sensitivity of the ^{19}F-n.m.r. method was 10^{-5} M. Its reproducibility was tested by analyzing ten separate urine samples spiked with known and nearly equal concentrations of the different compounds. For a signal-to-noise ratio (S/N) $\geqslant$ 30, the reproducibility was 3%; for S/N = 15, the reproducibility was 5%.

Several assays of spiked plasma samples indicated that this method is also applicable to body fluids containing proteins. The accuracy in this case was less than in urine samples, but still acceptable (5—7% r.s.d.). This deterioration was due to signal broadening, a consequence of the fluorinated compounds binding to plasma proteins.

Application of the procedure to the determination of 5'-DFU metabolites in human urine after 5'-DFU IV perfusion

For a patient who had received 22.5 g of 5'-DFU during a 6-h continuous perfusion, 67% of the dose was eliminated in 21 h (Fig. 4). The two main compounds found were unmetabolized 5'-DFU and the metabolite FBAL. The sum of these two compounds represented 64.1% of the dose. The 5'-DFU

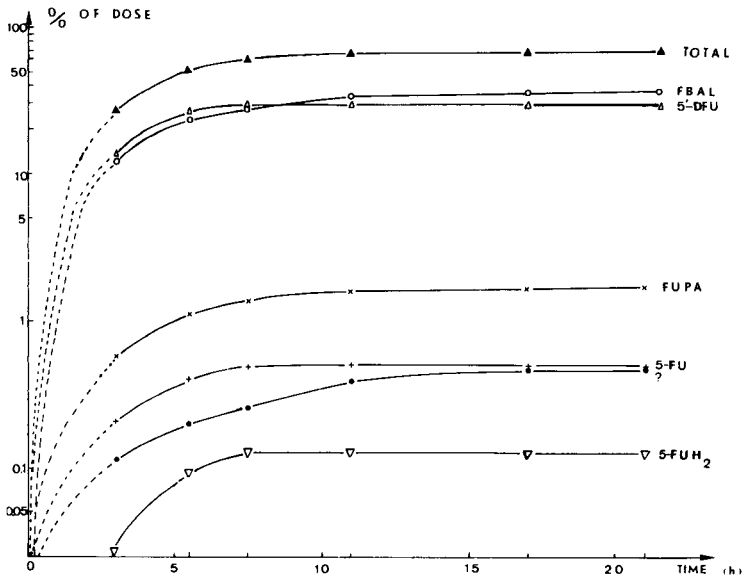

Fig. 4. Cumulative urinary excretion of 5'-DFU and metabolites after perfusion of 5'-DFU; ? is an unknown metabolite.

was especially excreted during the first 8 h. Cumulative excretion of FBAL was about 25% during the first 7 h and reached 35.7% after 21 h. Among the other metabolites (5-FU, 5-FUH_2, FUPA and an unknown metabolite), FUPA was the major compound; 5-FUH_2 and 5-FU were especially detected at the beginning of the perfusion whereas the unknown metabolite increased gradually up to 21 h.

In conclusion, the ^{19}F-n.m.r. method allows a direct, simultaneous and accurate determination of the various fluorinated metabolites, found at low concentrations in any biological fluid, which give fluorine-19 n.m.r. signals on a spectral width as large as about 120 ppm.

The authors are greatly indebted to Drs. C. Brevard and A. Pagelot (Bruker Spectrospin, Wissembourg, France) for their kind hospitality and their technical assistance. They also acknowledge the financial support of Université Paul Sabatier (Toulouse, France) for this work.

REFERENCES

1 J. Alary, P. Bourbon and C. Balsa, Anal. Chim. Acta, 148 (1983) 311.
2 M. C. Malet-Martino, R. Martino, A. Lopez, J. P. Béteille, M. Bon, J. Bernadou and J. P. Armand, Cancer Chemother. Pharmacol., 13 (1984) 31.
3 J. P. Sommadossi, C. Aubert, J. P. Cano, J. Gouveia, P. Ribaud and G. Mathé, Cancer Res., 43 (1983) 930.

Analytica Chimica Acta, 171 (1985) 233—239
Elsevier Science Publishers B.V., Amsterdam — Printed in The Netherlands

CHARGE-TRANSFER DERIVATIZATION IN FAST-ATOM-BOMBARDMENT MASS SPECTROMETRY

G. C. DIDONATO and K. L. BUSCH*
Department of Chemistry, Indiana University, Bloomington, IN 47405 (U.S.A.)
(Received 31st August 1984)

SUMMARY

The formation of charge-transfer complexes as derivatization reactions for fast-atom-bombardment (f.a.b.) mass spectrometry has been investigated. The donor *N,N,N',N'*-tetramethyl-1,4-phenylenediamine (TMPD) and the acceptor 2,3-dichloro-5,6-dicyanobenzoquinone (DDQ) were studied. The f.a.b. spectrum of this complex in glycerol first yielded the cation radical, $TMPD^+$ at *m/z* 164. However, with time the dominant ion becomes $(TMPD+H)^+$. Results suggest that although a strong charge-transfer complex is formed, protonation of the donor molecule occurs whenever possible. In dimethylsulfoxide, initial f.a.b. spectra contain $(TMPD+H)^+$, but as solvent evaporates, this ion is supplanted by the cation radical. Increased abundances of the cation radicals for charge-transfer complexes are observed in the absence of solvent or with the use of aprotic solvents. Characteristic ultraviolet/visible spectra of charge-transfer complexes clarify the competing processes of electron and proton transfer, and their time dependence. Charge-transfer derivatization is used to increase signals for the donor cation radicals of anthracene/picric acid, pyrene/picric acid, and indole/trinitrofluorenone.

Charge-transfer derivatization is one of several types of derivatization reactions developed for fast-atom-bombardment mass spectrometry (f.a.b.m.s.) [1]. The goal of these reactions is to create preformed ions in the glycerol matrix, which usually appear as abundant ions in the f.a.b. spectrum. Many reactions are based on formation of ions via protonation, or the formation of new bonds with polyatomic charged species. These reactions can lead to increased sensitivity [2] or functional group specificity [3]. Charge-transfer reactions are particularly attractive in that the ion formed directly indicates the molecular weight of the sample, and further in that many classes of compounds react uniquely via charge-transfer complex formation. Advantages of photoirradiation of the complex in order to increase dissociation have been mentioned by De Pauw [1].

When placed in a polar solvent, charge-transfer complexes consisting of electron donors (D) and electron acceptors (A) undergo dissociation into ions according to the reaction [4]

$$D + A \rightarrow (D^+ \cdot A^- \cdot) \rightarrow D^+ \cdot + A^- \cdot$$

0003-2670/85/$03.30

Thus charge-transfer complexes should yield the radical species, $D^{+}\cdot$ and $A^{-}\cdot$ in the f.a.b. spectrum in the absence of other factors. De Pauw has studied the complex formed between *N,N,N',N'*-tetramethyl-1,4-phenylenediamine (TMPD) and certain substituted benzoquinones. This donor-acceptor pair is among the strongest of the charge-transfer complexes [4].

In order to understand more fully the precise behavior of charge-transfer complexes, the complex formed between TMPD and 2,3-dichloro-5,6-dicyanobenzoquinone (DDQ) was studied in detail in this work. It was possible to monitor the formation of this complex spectrophotometrically because the formation of $TMPD^{+}\cdot$ gives rise to distinct bands in the ultraviolet/visible spectrum. In the case of the TMPD/DDQ complex, absorption at 580 and 620 nm indicates formation of the $TMPD^{+}\cdot$ cation radical. The compounds used as liquid matrices in f.a.b. mass spectrometry were used as solvents, and the positive ion f.a.b. spectra of each of the solutions were obtained. Comparisons between mass spectra and u.v./visible spectra are therefore possible.

EXPERIMENTAL

Reagents and apparatus

N,N,N',N'-tetramethyl-1,4-phenylenediamine (TMPD), 1,2,4-butanetriol, and 3-mercapto-1,2-propanediol (thioglycerol) were used as obtained from Aldrich. 2,3-Dichloro-5,6-dicyanobenzoquinone (DDQ; Alfa Chemical), glycerol, methanol, and dimethylsulfoxide (Mallinkrodt) were used as received.

All spectra were obtained on a Kratos MS80RFAQ mass spectrometer of EBQQ geometry using the intermediate detector located after the magnetic sector but before the quadrupoles. A resolution of 1000 was used to record all spectra. Argon gas was fed into an Iontech gun which produced a beam of mixed ions and neutral molecules of 5-keV energy. The sample mixture (1 μl) was loaded onto a copper platform which intercepts the primary beam at an angle of 45°. Optical spectra were obtained with a Hewlett-Packard 8450A photodiode-array spectrophotometer. A 1-cm quartz cell was used to contain about 3 ml of solution.

Procedures

The TMPD and DDQ were mixed together in a 1:1 stoichiometric ratio at a concentration of 0.1 mg ml^{-1} for u.v./visible absorption measurements. Solvents used were glycerol, dimethylsulfoxide, methanol, 1,2,4-butanetriol and thioglycerol. For time-resolved spectra, an initial spectrum of a stirred solution was obtained in about 2 s. Stirring continued as consecutive spectra were obtained every 3 min in glycerol and dimethylsulfoxide (DMSO).

The same solutions monitored by u.v./visible spectrophotometry were also monitored by f.a.b.m.s. Because glycerol has a vapor pressure of about 10^{-3} torr at room temperature, 1 μl loaded onto the f.a.b. probe will evaporate within about 20 min. Most f.a.b. spectra are reported not to vary during

that time, but spectral changes can occur with solvent evaporation [5]. DMSO is significantly more volatile than the glycerol matrix and evaporates during the course of a 5-min monitoring period, leading to significant changes in the f.a.b. spectrum (vide infra).

RESULTS AND DISCUSSION

An advantage in studying charge-transfer derivatization is the large body of literature detailing the behavior of charge-transfer complexes [4]. The complexes of TMPD with several electron acceptors have been studied by u.v./visible spectrophotometry. The $TMPD^{+\cdot}$ radical has a characteristic absorption doublet at 580 and 620 nm. The behavior of the complex in a number of solvents had been studied [6—8], although not in any of the matrices used for f.a.b. mass spectrometry. Spectrophotometry thus offers a means of following the formation of the radical ions independently of mass spectrometry.

Figure 1 shows the u.v./visible absorption spectrum of the 0.1 mg ml^{-1} TMPD/DDQ complex in glycerol and its changes with time. Spectra were recorded at 3-min intervals; spectra (a) and (j) correspond to times of 0 and 27 min, respectively. An increasing absorbance at both 580 and 620 nm indicates an increased amount of the $TMPD^{+\cdot}$ cation radical. The color of the solution changes from a light blue to a dark purple during this time. Maximum absorbance for the charge-transfer bands is reached after about 1 h.

Although the u.v./visible absorption data indicate the presence of the TMPD cation radical, the f.a.b. mass spectrum of a freshly prepared TMPD/

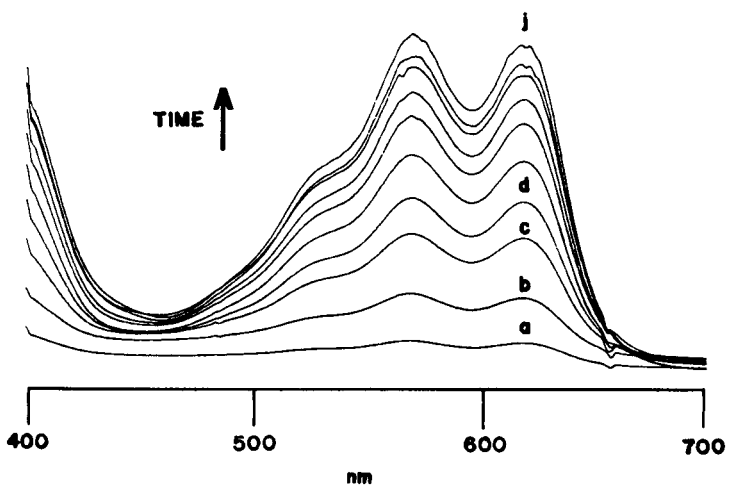

Fig. 1. Time-dependent u.v./visible absorption spectrum of the TMPD/DDQ complex in glycerol. Spectra were obtained at 3-min intervals. Trace (a) is the initial spectrum and trace (j) is the spectrum after 27 min.

DDQ solution contains the $(TMPD+H)^+$ ion in an abundance equal to that of the expected $TMPD^{+\cdot}$. As the solution ages, the f.a.b. spectra show increasing abundances of $(TMPD+H)^+$ relative to $TMPD^{+\cdot}$ until finally all of the ion current is found in the protonated ion. Paradoxically, then, for TMPD/DDQ in glycerol, u.v./visible spectrophotometry indicates increasing $TMPD^{+\cdot}$ while f.a.b. mass spectrometry provides evidence for decreasing $TMPD^{+\cdot}$. Even for this strong charge-transfer complex, competition between charge transfer and acid-base chemistry is evident.

The effect of pH on the u.v./visible spectra of the TMPD/DDQ complex was therefore investigated further by the addition of small amounts of acid and base to glycerol solutions of the sample (1:1 at 0.1 mg ml^{-1}). The addition of 50 μl of 0.5 M sodium hydroxide to a fresh solution transforms it from purple to yellow, and the absorption band caused by the TMPD cation radical disappears. The addition of 50 μl of 1.0 M hydrochloric acid to the alkaline mixture resulted, after several minutes, in the reappearance of the purple color, and the absorption doublet at 580 and 620 nm. Addition of acid (50 μl of 0.5 M hydrochloric acid) to the glycerol solution of the complex also results in a disappearance of the characteristic absorption bands.

The complex chemistry of the TMPD/DDQ system is evident from these experiments. That the absorption doublet is in fact due to the radical cation $TMPD^{+\cdot}$ is proven by the absence of these bands in the spectra of either TMPD alone or acidified (HCl) TMPD. A scheme must thus be devised to explain the disappearance of the $TMPD^{+\cdot}$ absorption bands with addition of either acid or base. The addition of base must reversibly decrease the amount of $TMPD^{+\cdot}$ in solution. Neutral TMPD is reformed as a result of the interaction of the electron acceptor DDQ with the hydroxide ion

$$DDQ + OH^- \leftrightharpoons DDQ^{-\cdot} + OH\cdot$$

Subsequent addition of acid removes the hydroxide ion, and DDQ then reacts with TMPD to form $TMPD^{+\cdot}$ and the characteristic absorption bands reappear. If an excess of acid is added to the alkaline solution, or if acid is added to the dissolved complex directly, TMPD is protonated to form $(TMPD+H)^+$, and the absorption bands decrease in intensity.

Next, the f.a.b. spectra of glycerol solutions of TMPD and the TMPD/DDQ complex were obtained with analogous addition of acid and alkali. The positive-ion f.a.b. spectrum of TMPD alone in glycerol does not contain an ion at either *m/z* 164 ($TMPD^{+\cdot}$) or 165 $(TMPD+H)^+$ above the background level. Addition of hydrochloric acid to the solution increases the abundance of the $(TMPD+H)^+$ ion, as expected. The addition of acid to the TMPD/DDQ complex in glycerol also produces an enhancement of the protonated form at the expense of the radical cation. The equal relative abundances of $TMPD^{+\cdot}$ and $(TMPD+H)^+$ observed in the spectrum of the complex are replaced by a total concentration of ion current in the latter species. Addition of alkali to the solution of the complex in glycerol and study by f.a.b. produces only background signals in the molecular ion region, consistent with the species thought to be present (vide infra).

To summarize, TMPD/DDQ in glycerol is a complex system participating in both charge-transfer and acid/base processes. Although glycerol is a slightly acidic solvent, it does not transform $TMPD^{+\cdot}$ to $(TMPD+H)^{+}$, as shown by u.v./visible spectrophotometry. Bombardment of the mixture catalyzes the protonation of TMPD, with glycerol serving as the hydrogen source.

These experiments underscore the importance of the solvent in f.a.b. and in the use of charge-transfer chemistry for derivatization. Behavior of the TMPD/DDQ complex was therefore investigated in other solvents which are used in f.a.b. mass spectrometry. In 1,2,4-butanetriol, both u.v./visible absorption and mass spectral data paralleled that of the complex in glycerol, with slowly increasing u.v./visible absorption caused by the formation of the cation radical, but an abundant ion signal for $(TMPD+H)^{+}$ in the f.a.b. spectrum. In contrast, TMPD and DDQ do not form the charge-transfer complex in thioglycerol, as deduced from the absence of absorption bands in the u.v./visible spectrum. A transient purple color was noted upon initial mixing of TMPD and DDQ, but it disappeared within 2—4 s. The f.a.b. mass spectrum of the complex in thioglycerol contained an abundant $(TMPD+H)^{+}$. Because thioglycerol is a more acidic matrix than glycerol, any radical cation formed is transformed very quickly into $(TMPD+H)^{+}$. Charge-transfer chemistry evident in glycerol and 1,2,4-butanetriol cannot be observed in thioglycerol.

De Pauw noted an increase in the abundance of $TMPD^{+\cdot}$ compared to $(TMPD+H)^{+}$ when the TMPD/DDQ complex was dissolved in DMSO [1]. Because there is no significant difference in solvent polarity, this effect was explained as being due both to the lack of protons in DMSO, as well as precipitation of the complex upon evaporation of the more volatile solvent in the mass spectrometer source. The present experiments showed that when equimolar amounts of TMPD and DDQ were mixed in DMSO, the complex formed a deep purple solution, which faded to green within 20 min. Optical absorption by the TMPD cation radical decreased steadily over a 30-min period (Fig. 2). The f.a.b. mass spectrum of the complex in DMSO contained

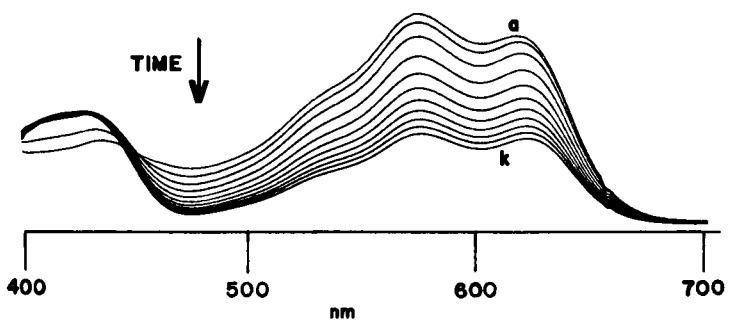

Fig. 2. Time-dependent u.v./visible absorption spectrum of the TMPD/DDQ complex in dimethylsulfoxide. Spectra were obtained at 3-min intervals. Trace (a) is the initial spectrum and trace (k) is the spectrum after 30 min. While the absorption of $TMPD^{+\cdot}$ increases with time in glycerol, the opposite behavior is observed in dimethylsulfoxide.

an abundant $(TMPD+H)^+$ ion during the first 2 min of bombardment by the argon beam, despite the "nonacidity" of this solvent. However, after two additional minutes (4 min total bombardment), the cation radical, $TMPD^{+\cdot}$, became the dominant ion in the spectrum. Immediate removal and examination of the f.a.b. probe revealed a dry surface.

The data for TMPD/DDQ in DMSO also present a paradox, although in a direction opposite to the trends observed with a glycerol solvent. While the u.v./visible spectra show a decrease in $TMPD^{+\cdot}$ with time, the f.a.b. spectra show an increase which persists until the DMSO solvent disappears and no further spectra can be obtained. The source of protons for formation of $(TMPD+H)^+$ is probably the DMSO solvent; this suggestion is consistent with decrease in intensity of this ion as the solvent disappears. As postulated for glycerol, irradiation of the matrix by the primary atom beam seems to catalyze the acid-base reaction. Because f.a.b. matrices almost always contain hydrogen, such acid-base reactions which mask charge-transfer processes may be a general phenomenon. The increase in abundance of the cation radical in the f.a.b. spectrum can thus be attributed solely to precipitation. Thus, the effect of using charge-transfer agents for derivatization will be more pronounced with the solid complex. An alternative may be the use of aprotic solvents such as Fomblin or other perfluorinated compounds. Accordingly, the f.a.b. mass spectrum of a solution of TMPD/DDQ in Fomblin yields a signal at *m/z* 164 three to four times that of TMPD in Fomblin alone at the same concentration. There is no ion at *m/z* 165, reflecting the lack of available protons.

The appearance of $M^{+\cdot}$ upon evaporation of the solvent led to a reinvestigation of several charge-transfer complexes studied previously in this laboratory, such as the complex formed between 2,4,6-trinitrophenol (picric acid) and polynuclear aromatic hydrocarbons [9], specifically anthracene. A portion (2 μg) of the charge-transfer complex of picric acid and anthracene was placed directly on the copper probe tip for study by f.a.b. The spectrum contained an abundant ion at *m/z* 178, for the radical cation of the anthracene donor. This signal was a factor of 10 greater than that given by the same amount of underivatized anthracene. The f.a.b. spectrum of anthracene in glycerol did not give an ion at *m/z* 178 above the background signal at that mass, and furthermore the preformed complex would not dissolve in glycerol alone. When methanol was added to the glycerol to aid dissolution, the complex dissolved but an accompanying color change indicated that the complex had reverted into the uncharged donor and acceptor molecules. A 7-fold increase in the cation radical was also noted for the complex formed between pyrene and picric acid, compared to an equivalent amount of underivatized compound, and a similar enhancement occurred for a complex formed between indole and trinitrofluorenone. These spectra and the use of charge-transfer derivatization in quantifying polynuclear aromatic hydrocarbons have been studied more completely and the results are being prepared for publication.

CONCLUSIONS

The use of charge-transfer derivatization in f.a.b. mass spectrometry can lead to an increase in the abundance of radical cations, but the spectra can be complicated by dominant effects of acid-base interaction between sample and solvent. The reaction of TMPD and DDQ produces a strong charge-transfer complex, but the TMPD is preferentially protonated during f.a.b. in most solvents and $(TMPD+H)^+$ rather than $TMPD^{+\cdot}$ is observed in the spectra. When charge-transfer complexes are studied as solids, the radical cation appears with a signal significantly increased over that of the uncomplexed form. The use of aprotic solvents provides an opportunity for charge-transfer derivatization chemistry to be observed in solution.

Molecular absorption spectrophotometry provides a valuable adjunct to mass spectrometry in establishing the time-dependent behavior of these complexes in solvents used for f.a.b. studies, especially as the solution pH is varied. The present results suggest that careful study of solvent effects on the formation and subsequent reaction of charge-transfer complexes will be necessary fully to exploit the utility of these derivatization reactions in fast-atom-bombardment mass spectrometry.

We thank Prof. L. K. Montgomery for helpful discussions.

REFERENCES

1 E. De Pauw, Anal. Chem., 55 (1983) 2195.
2 K. L. Busch, S. E. Unger, A. Vincze, R. G. Cooks and T. Keough, J. Am. Chem. Soc., 104 (1982) 1507.
3 K. L. Busch, B.-H. Hsu, K. V. Wood, R. G. Cooks, C. G. Schwarz and A. R. Katritzky, J. Org. Chem., 49 (1984) 764.
4 R. Foster, Organic Charge-Transfer Complexes, Academic Press, New York, 1969.
5 D. J. Barofsky, Int. J. Mass Spectrom. Ion Phys., 53 (1983) 319.
6 K. Kalnins, N. G. Antonov and N. G. Koton, Dokl. Akad. Nauk SSSR Phys. Chem., 246 (1979) 641.
7 K. Kalnins, M. M. Koton, N. G. Antonov, V. M. Svetlichnyi, V. V. Kudryavtsev, G. V. Lyubimova and V. I. Blinova, Dokl. Akad. Nauk SSSR Phys. Chem., 244 (1979) 400.
8 N. H. Kolodny and K. Bowers, J. Am. Chem. Soc., 94 (1972) 1113.
9 L. O. Fitton and J. H. Hill, Selected Derivatives of Organic Compounds, Chapman and Hall, London, 1970, p. 37.

Analytica Chimica Acta, 171 (1985) 241—249
Elsevier Science Publishers B.V., Amsterdam — Printed in The Netherlands

COMPARISON OF THE HELIUM/OXYGEN/ACETYLENE AND AIR/ACETYLENE FLAMES AS ATOM SOURCES FOR CONTINUUM-SOURCE ATOMIC FLUORESCENCE SPECTROMETRY

DANIEL A. WILSON, ANNA M. YUEN and GARY M. HIEFTJE*
Department of Chemistry, Indiana University, Bloomington, IN 47405 (U.S.A.)
(Received 3rd December 1984)

SUMMARY

The helium/oxygen/acetylene flame is compared to the more widely used air/acetylene flame for its utility as an atom cell for atomic fluorescence spectrometry. Nearly identical experimental arrangements were used for both flames in order to make the comparison valid. With a continuum source used for excitation, fluorescence detection limits in the helium/oxygen/acetylene flame were between 13 and 60 times better (lower) than those determined for the same eight elements in the air/acetylene flame. The improved detection limits are attributable mainly to the higher temperature, increased thermal conductivity and lower quenching in the helium flame. Fluorescence background spectra were obtained for both flames over the wavelength range 185—650 nm, and showed the helium flame to have slightly smaller background fluctuations, but a much larger background because of the more favorable fluorescence conditions in the flame.

Many different types of flames have been used for atomic fluorescence spectrometry (a.f.s.). The most popular flames have been those used in commercial atomic absorption instruments, namely air/acetylene for most elements and nitrous oxide/acetylene for elements which are more difficult to atomize [1, 2]. Other flames which have been suggested as possible atom sources for atomic fluorescence include the argon/oxygen/acetylene [3] and helium/oxygen/acetylene [4—6] mixtures. These latter flames use an inert gas/oxygen mixture having approximately the same concentration of oxygen as air.

Both of the inert gas/oxygen/acetylene flames which have been suggested for flame a.f.s. should be useful as atom cells for atomic fluorescence because the inert support gas should provide a lower quenching cross-section than the nitrogen present in air- or nitrous oxide-supported flames. Quenching occurs when an excited atom collides with another species in the flame (such as nitrogen) which carries away its energy before it can fluoresce. Other advantages suggested for the helium/oxygen/acetylene flame arise from its greater thermal conductivity. The increased thermal conductivity should reduce the temperature gradient in the flame and provide a greater available region for atomization of the element of interest. Increased thermal conductivity should also enhance atom-formation efficiency of solutes for which vaporization is controlled by heat transfer.

0003-2670/85/$03.30

The helium/oxygen/acetylene flame has a maximum temperature of approximately 2800 K [5], intermediate between those of the air/acetylene (2500 K) and nitrous oxide/acetylene (2990 K) mixtures [7]. Such a higher temperature aids in the desolvation of the droplets of solution introduced into the flame and in the atomization of the element to be studied by a.f.s.

Another important characteristic of a flame as a source for atomic spectroscopy is its background spectrum. The emission background of the helium/oxygen/acetylene flame contains the spectral features found in the air/acetylene flame, although at slightly higher intensity [5]. The background of both flames is much less structured and much less intense than the background of the nitrous oxide/acetylene flame.

In the present study, an air/acetylene flame and a helium/oxygen/acetylene flame were compared as atom reservoirs for continuum-source atomic fluorescence spectrometry. Detection limits were determined for eight elements and the fluorescence background spectra were obtained for both flames over the wavelength range of common interest in a.f.s. The experimental configurations used for both flames were kept as similar as possible in order to permit a valid comparison.

EXPERIMENTAL

Apparatus

The experimental arrangement used with both flames was the same except for the burner design. A block diagram of the optical and electronic components of the system is shown in Fig. 1. The components and measurements are described in detail below.

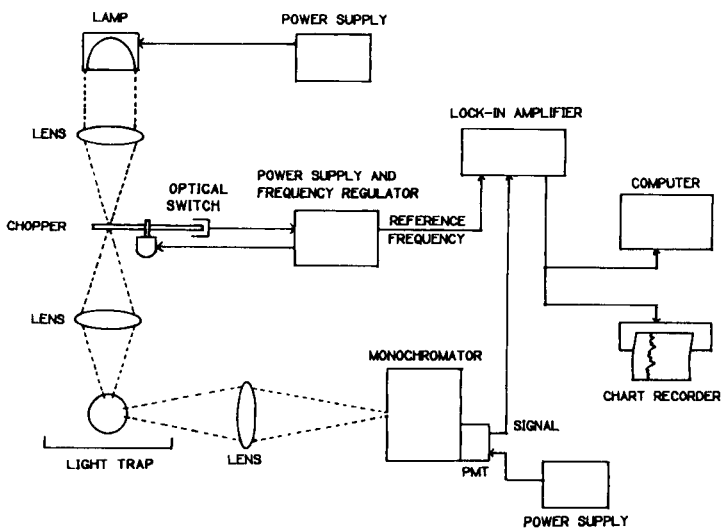

Fig. 1. Block diagram of the optical and electronic components used for both flames.

Sample introduction system. An ultrasonic nebulizer was used so that the nebulization rate and efficiency were not dependent on either the gas flow rate or composition. In the present work, a peristaltic pump (Minipuls 2; Gilson Medical Electronics, Middleton, WI) was used to deliver a constant flow (0.5 ml min^{-1}) of either sample solution or distilled, deionized water to a Meinhard-type glass concentric pneumatic nebulizer. This nebulizer was then used to spray the sample as a fine mist onto an ultrasonic nebulization transducer crystal (Model CPMT; Channel Products, Chesterland, OH) (see Fig. 2). The nebulizing gas in the concentric nebulizer was oxygen when the helium-diluted flame was used; oxygen has approximately the same density as nitrogen. Only a low gas flow was required for this nebulizer and the oxygen was sufficient, even though it was less than 18.5% of the total gas flow. Because the concentric nebulizer was being used only to spray solution onto the ultrasonic nebulizer crystal (located about 1 cm from the tip of the concentric nebulizer), the efficiency of the nebulization process was not crucial as long as all of the solution reached the crystal.

The crystal holder (designed and built in-house) clamped the crystal at its edges and the high-frequency voltage used to vibrate the piezoelectric material within the transducer was applied to the rear of the crystal. The chamber behind the crystal was cooled by circulated distilled water. The power supply used for the ultrasonic nebulizer was also built in-house.

The mist produced by the ultrasonic nebulizer was swept by the gas flow from the pneumatic nebulizer into a 150-ml chamber where the flame gases were mixed. The mixed flame gases and sample aerosol then passed through a series of baffles to remove large droplets prior to their entry into the burner chamber.

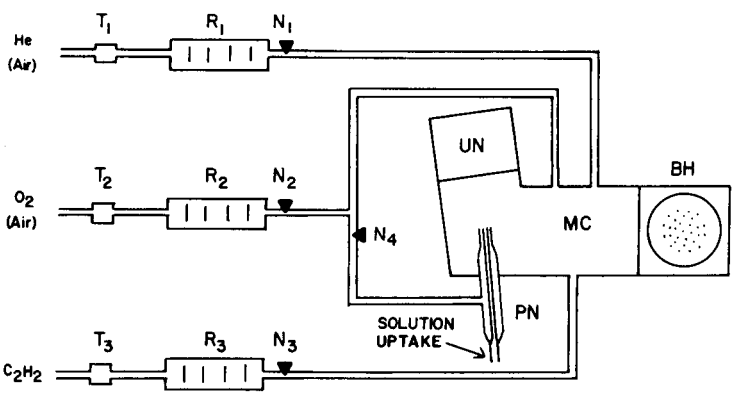

Fig. 2. Gas-handling system used for both flames. For the air/acetylene flame, the helium and oxygen lines were both used for air. T_1, T_2, T_3, Toggle shut-off valve for each gas flow; R_1, R_2, R_3, rotameter for each gas flow; N_1, N_2, N_3, needle valve for controlling each gas flow; N_4, needle valve for controlling the split ratio for O_2 (air) to the pneumatic nebulizer; PN, pneumatic nebulizer; UN, ultrasonic nebulizer; MC, mixing chamber; BH, burner head.

Flame arrangement. The gas-handling system used for both flames is shown in Fig. 2. For the helium/oxygen/acetylene flame, each gas was metered through a different rotameter (Model 4; Dwyer Instruments, Michigan City, IN). The helium and acetylene went directly to the mixing chamber while the oxygen flow was split, with part directed to the concentric pneumatic nebulizer and the balance going directly to the mixing chamber. For the air/acetylene flame, one rotameter was used for the acetylene while the other two were both used for air, because the air flow was too high for a single rotameter and it was desired to use the same equipment for both flames. Part of the air flow was used in the pneumatic nebulizer and the rest was directed to the mixing chamber. All cited gas flows have been corrected to standard temperature and pressure.

The biggest difference between the experimental arrangements for the two flames was the burner head. Both flames used a modified Meker-type burner head. However, because the helium/oxygen/acetylene flame has a much greater burning velocity than the air/acetylene flame (336 cm s^{-1} for the helium-diluted flame compared to 158 cm s^{-1} for the air/acetylene flame) [7], and because the total gas flow was the same for both flames, it was necessary to use a burner head with much smaller gas-outlet ports for the helium/oxygen/acetylene flame [8]. These ports matched the flame gas rise velocity to its burning velocity and prevented flashback. The burner head used for the helium/oxygen/acetylene flame had 169 ports of 0.45-mm diameter arranged in concentric circles. The burner head was constructed of nickel-plated brass and had a coil of 1/8-in. (3.2-mm) copper tubing silver-soldered around it. The coil was used to cool the burner head with a flow of tap water at approximately 3 l min^{-1}, in order to prevent deformation of the brass burner head. When an attempt was made to use the same burner head for the air/acetylene flame, the flame became unstable and lifted off the top of the burner head. Therefore, it was necessary to use a burner head with 29 ports of 1-mm diameter. The larger holes better matched the slower rise velocity of the air/acetylene flame and provided a more stable flame.

Excitation source. A 300-W Xenon arc lamp (Model No. VIX-300UV; Varian Eimac Division, San Carlos, CA) was used as a continuum source to excite the atomic fluorescence of the sample atoms (see Fig. 1). The radiation from the lamp was focused to a spot of approximately 1-cm diameter where it was modulated at 75 Hz by a rotating mechanical chopper. The chopped radiation was then focused to a spot slightly smaller than the diameter of the flame at a point 1 cm above the burner head. This height was chosen by optimizing for signal-to-noise ratio for zinc atomic fluorescence at 213.9 nm.

Detection system. The fluorescence radiation from the flame was focused by a quartz lens onto the entrance slit of a 0.35-m monochromator (Model EU 700; Heath Co., Benton Harbor, MI) (see Fig. 1). The monochromator slit widths were set at 50 μm. Two different photomultiplier tubes (PMT) were used in this study. For elements with resonance fluorescence wavelengths below 320 nm, an R166 solar-blind PMT (Hamamatsu, Middlesex, NJ;

wavelength range 185—320 nm) was used. For the other elements and for the measurement of fluorescence background spectra, a 1P28 PMT (Hamamatsu, Middlesex, NJ; range 185—650 nm) was used. Both tubes were supplied with —800 V from a high-voltage power supply (Model HVS-1, Princeton Applied Research, Princeton, NJ).

The current from the anode of the PMT was directed to a lock-in amplifier (Model 8440; Keithley Instruments, Cleveland, OH) which derived its reference signal from a light-emitting diode/photodiode combination attached to the chopper. The frequency-selected signal from the lock-in amplifier was sent to both a strip-chart recorder (Heath Co., Benton Harbor, MI) for real-time monitoring and a MINC-11 computer (Digital Equipment Corporation, Maynard, MA) for data collection and signal-to-noise calculations.

Calculations of detection limit

Signal-to-noise ratios were evaluated for at least five solution concentrations up to approximately two orders of magnitude above the detection limit for each element. The time constant of the lock-in amplifier was 1 s. The average voltage obtained for a blank (distilled water) run over a recorded period of 100 s was subtracted from the average voltage for the sample, to give the corrected signal. This value was then divided by the standard deviation of the blank signal (1000 points) to give the signal-to-noise ratio. Three ratios were determined for each solution and averaged. A regression line was then fitted to the plot of S/N vs. sample concentration and detection limits were obtained from it at a S/N of 2. Sample solutions were made from stock solutions prepared according to Dean and Rains [9].

RESULTS AND DISCUSSION

Gas-flow optimization

In order to make the comparison between the two flames as fair as possible, all flame-gas flow rates were optimized with respect to S/N ratio for atomic fluorescence from a 10 μg ml^{-1} zinc solution. For the helium/oxygen/acetylene flame, the three gas flow rates were optimized by using the simplex method of Deming and Morgan [10, 11]. The total gas flow was held constant at 10.57 l min^{-1}, and the fuel/oxidant ratio and percent helium within the flame were varied. The constant total flow rate assures that the dilution factor of the analyte in both flames will be constant. Both fuel-to-oxidant ratio and percent helium were found by Saturday [8] to be important in governing the stability and temperature of the flame. Each vertex obtained from the simplex program was compared to the safe operating limits defined earlier by Saturday [8], and was discarded (given a negative response) if it exceeded the safe conditions.

Because only two gases are used in the air/acetylene flame, the only parameter to be optimized is the fuel-to-oxidant ratio, calculated using the 21% of oxygen in air as the oxidant. The optimal ratios for the two flames

were found to be different because the S/N ratio for zinc depends on several factors besides the fuel-to-oxidant ratio, most notably the temperature of the flame.

The gas flow rates and fuel-to-oxidant ratios that were shown to be optimal for both flames are summarized in Table 1. Fuel-to-oxidant ratio is defined as the flow rate of acetylene divided by the flow rate of oxygen into the flame.

Detection limits

The detection limits evaluated in this work are compiled in Table 2. It can be seen that the helium/oxygen/acetylene flame gives detection limits for all elements studied that are a factor of 13—60 better (lower) than those found with the air/acetylene flame. Several factors are responsible for the respective detection limits. One is the hotter temperature of the helium/oxygen/acetylene flame, which should lead to faster and more complete desolvation, vaporization and atomization of the analytes. For the flame conditions found to be optimal, the temperature of the helium flame should be approximately

TABLE 1

Optimal flow rates for the flame gases

Air/acetylene flame		Helium/oxygen/acetylene flame	
Gas	Flow (l min^{-1})	Gas	Flow (l min^{-1})
C_2H_2	1.75	C_2H_2	1.60
Air	8.82	He	7.02
Total	10.57	O_2	1.95
Fuel-to-oxidant ratio = 0.95		Total	10.57
		Fuel-to-oxidant ratio = 0.82	
		He in the He/O_2 mixture = 78%	
		He in the flame = 66%	

TABLE 2

Comparison of detection limits for the two flames

Element	Wavelength (nm)	Detection limit (μg ml^{-1})	
		$He/O_2/C_2H_2$ flame	Air/C_2H_2 flame
Zn	213.856	0.3	4
Cd	228.802	0.05	3
Fe	248.327	1	20
Mg	285.213	0.03	1
Cu	324.754	0.3	9
Ag	328.069	0.2	10
Cr	357.869	2	60
Sr	460.733	0.08	3

2650 K [8], whereas the temperature of the air/acetylene flame should be about 2400 K [12]. Also, the greater thermal conductivity of the helium/oxygen/acetylene flame should produce a larger and more uniform region of high temperature than will be present in the air/acetylene flame. In the study by Clampitt and Hieftje [4], it was found that the increased thermal conductivity of the helium/oxygen/acetylene flame leads also to an increase in desolvation and vaporization efficiency. Similarly, Saturday and Hieftje [6] showed that the relative free atom fractions for all of the elements they studied in the helium/oxygen/acetylene flame were roughly the same as or up to three times better than the relative free atom fractions in the air/acetylene flame.

Another important factor in determining the utility of a flame for atomic fluorescence is the quantum efficiency (or atomic fluorescence power efficiency) of each element in the flame. Fluorescence power efficiencies for atoms in flames are equal to the ratio of the fluorescence intensity to the intensity of radiation absorbed from the excitation source [13—15]. Saturday et al. [15] determined the fluorescence power efficiencies for five elements in both of the flames studied here and found the helium/oxygen/acetylene flame to have efficiencies ranging from 2.3 to 5.7 times better than those in an air/acetylene flame.

These increases in atom-formation and fluorescence power efficiencies do not account completely for the improvements in detection limits found in this study. Only three elements, iron, copper and chromium, were used in all three studies. For all three elements, the improvement in detection limits is between three and ten times better than would be expected from the improvements in free atom fraction and power efficiencies. One major reason for this difference is that the relative free atom fractions [6] were evaluated by using a conventional pneumatic nebulizer, which would be much less efficient for the helium flame. The ultrasonic nebulizer used in the present work should assure that the same nebulization and transport efficiencies exist in both flames and lead to a more valid comparison.

Fluorescence background of the flames

The fluorescence from intrinsic flame-gas species was compared for the two flames. Both flames displayed small fluorescence signals between about 280 and 320 nm corresponding to OH fluorescence. There was also fluorescence from both flames in the region from 380 to 600 nm, attributable to fluorescence from C—H and C_2 species. This band fluorescence produced a slight rise above the baseline for the air/acetylene flame but was about 6 times more intense in the helium/oxygen/acetylene flame.

Molecular band fluorescence is much more pronounced in the helium/oxygen/acetylene flame because of the smaller quenching cross-section of helium compared to nitrogen. This same process is partly responsible for the improved detection limits in the flame. Strontium was the only element studied which had its resonance fluorescence signal in the wavelength region of

the strong band fluorescence. Interestingly, its signal-to-noise ratio was not degraded appreciably, probably because the background signal is fairly constant and does not add greatly to the noise.

CONCLUSION

The helium/oxygen/acetylene flame provides detection limits for atomic fluorescence spectrometry which are between 13 and 60 times better than those found for the same elements in an air/acetylene flame when nearly identical instrumentation and conditions are used. The improved detection limits are due to the helium/oxygen/acetylene flame having a higher temperature, better thermal conductivity and a smaller quenching cross-section than the air/acetylene flame. The noise on the background is less in the helium/oxygen/acetylene flame than in the air/acetylene flame, but the helium flame also has a larger fluorescence background.

Although the detection limits for a.f.s. are better in the helium/oxygen/acetylene flame, there are several disadvantages to its use. These disadvantages include the high cost of the helium and oxygen used in place of the air and the relatively low pneumatic nebulization efficiency of helium, the most abundant gas in the flame. The decreased nebulization efficiency argues for the use of a nebulizer which is not sensitive to the mass or flow of any gas, such as the ultrasonic nebulizer used in the present study.

The absolute values of the detection limits found in this study are not impressive because the instrument was not fully optimized. Several things could be done to improve the detection limits in the helium/oxygen/acetylene flame, including sheathing the flame with an inert gas or using an optical system in which the exciting radiation is passed through the flame several times and in which a greater solid angle of fluorescence is viewed.

This work was supported in part by the National Science Foundation through grants CHE 82-14121 and CHE 83-20053 and by the Office of Naval Research.

REFERENCES

1 A. H. Ullman, B. D. Pollard, G. D. Boutilier, R. P. Batch, P. Hanley and J. D. Winefordner, Anal. Chem., 51 (1979) 2382.
2 R. F. Browner and D. C. Manning, Anal. Chem., 44 (1972) 843.
3 D. J. Johnson and J. D. Winefordner, Anal. Chem., 48 (1976) 341.
4 N. C. Clampitt and G. M. Hieftje, Anal. Chem., 46 (1974) 382.
5 K. A. Saturday and G. M. Hieftje, Anal. Chem., 49 (1977) 2013.
6 K. A. Saturday and G. M. Hieftje, Anal. Chem., 52 (1980) 786.
7 G. F. Kirkbright and M. Sargent, Atomic Absorption and Fluorescence Spectrometry, Academic Press, New York, 1974, p. 204.
8 K. A. Saturday, Ph.D. Thesis, Indiana University, Bloomington, IN, 1979.
9 J. A. Dean and T. C. Rains in J. A. Dean and T. C. Rains (Eds.), Flame Emission and Atomic Absorption Spectrometry, Vol. 2, M. Dekker, New York, 1971.

10 S. N. Deming and S. L. Morgan, Anal. Chem., 45 (1973) 278A.
11 S. L. Morgan and S. N. Deming, Anal. Chem., 46 (1974) 1170.
12 R. Mavrodineanu and H. Boiteux, Flame Spectroscopy, Wiley, New York, 1965.
13 D. R. Jenkins, Proc. R. Soc., Ser. A, 293 (1966) 493.
14 S. J. Pearce, L. de Galan and J. D. Winefordner, Spectrochim. Acta, 23B (1968) 793.
15 K. A. Saturday, A. Yuen and G. M. Hieftje, Anal. Chim. Acta, 164 (1984) 51.

Analytica Chimica Acta, 171 (1985) 251—258
Elsevier Science Publishers B.V., Amsterdam — Printed in The Netherlands

A FLUORESCENT SENSOR FOR ALUMINUM(III), MAGNESIUM(II), ZINC(II) AND CADMIUM(II) BASED ON ELECTROSTATICALLY IMMOBILIZED QUINOLIN-8-OL SULFONATE

ZHANG ZHUJUN[a] and W. RUDOLF SEITZ*
Department of Chemistry, University of New Hampshire, Durham, NH 03824 (U.S.A.)
(Received 11th March 1984)

SUMMARY

An optical sensor responding to Al(III), Mg(II), Zn(II) and Cd(II) is prepared by immobilizing quinolin-8-ol-5-sulfonate (QS) on an ion-exchange resin and attaching the resin to the end of a trifurcated fiber-optic bundle. Immobilization leads to weak fluorescence from QS and causes shifts in the fluorescence spectra of the QS/metal complexes. Detection limits for the metal ions studied are all below 1×10^{-6} M. Response to metal ion concentration is nonlinear. The shape of the response fits a model that assumes a 1:1 metal/QS chelate is formed. Formation constants for immobilized QS complexes calculated from the model are similar to those observed for dissolved QS. Immobilized and dissolved QS behave similarly with respect to pH and interferences.

The development of fiber-optic sensors for metal ions based on immobilized ligands with fluorescent characteristics that change on complexation is of interest. Previous reports have described sensors for aluminium(III) and beryllium(II) based on fluorescence from immobilized morin [1]. The potential of immobilized calcein has also been investigated [2]. These sensors may be used to study metal ion equilibria or for continuous sensing.

A study of a sensor based on immobilized quinolin-8-ol-5-sulfonate (QS) is described here. Quinolin-8-ol and its derivatives have been widely used as fluorimetric reagents for the determination of metal ions [3—5]. The ligand does not fluoresce significantly itself but forms strongly fluorescent complexes with several metal ions including Al(III), Cd(II), Zn(II), Ca(II), Mg(II), Be(II) and Sr(II) [6]. Quinolin-8-ol has been covalently attached to solid supports and used to preconcentrate metal ions [7]. However, the preferred immobilization method involves the formation of an azo link which renders all complexes nonfluorescent. Accordingly, it was decided to immobilize the 5-sulfonate of quinolin-8-ol electrostatically on an ion-exchange resin. This is convenient and makes it possible to vary the relative amounts of ligand and substrate. Electrostatic immobilization has previously been used to prepare a quinolin-8-ol-treated stationary phase for the chromatographic separation of metal ions [8].

---

*Present address: Department of Chemistry, Shaansi Normal University, Sian, Shaansi, People's Republic of China.

0003-2670/85/$03.30

EXPERIMENTAL

Apparatus

The instrumentation was a modified version of an arrangement used earlier [9]. It consisted of a QH-150 tungsten-halogen source (Labsource), an RCA-1P21 photomultiplier detector, filters for wavelength selection and a trifurcated fiber-optic bundle (Maxlight, Phoenix, AZ). The trifurcated fiber-optic bundle has one branch of fused silica fibers through which fluorescence is excited. Fluorescence was observed through a branch of glass optical fibers while the third branch was capped off and not used. Each branch was one foot long. The diameter of the common end of the fiber bundle was 4.0 mm.

The excitation filter used was a bandpass filter with maximum transmittance of 57% at 363 nm and a bandwidth of 53 nm at half maximum transmittance. The emission wavelength was selected by a dielectric interference filter (1 in. × 0.5 in.), with peak transmittance at 520 nm and a bandwidth of 8.2 nm at half maximum transmittance. The signals from the photomultiplier module were recorded on a Heath SR-255B strip-chart recorder.

A Perkin-Elmer Model MPF-44E fluorescence spectrophotometer equipped with a xenon arc lamp and 1.00-cm quartz cells was used to record the excitation and emission spectra of both dissolved and immobilized metal/QS complexes. An Orion Digital Ionalyzer/501 equipped with an Orion combination pH glass electrode was used to measure pH.

Reagents

Quinolin-8-ol-5-sulfonic acid (QS) dihydrate (Aldrich Chemical Company) was recrystallized several times from water and dried at 110°C before use. The anion-exchange resin was Amberlite CG-400 (100—200 mesh, chromatographic grade; Mallinckrodt).

Acetate buffers were prepared by dissolving 20 g of sodium acetate in 100 ml of water and adjusting to pH 4.50 with 6 M acetic acid. Ammonia/ammonium chloride buffers were prepared by dissolving 20 g of ammonium chloride in 100 ml of water and adjusting to pH 8.00 with 6 M ammonia.

A 0.0100 M aluminum stock solution was prepared by dissolving 2.372 g of $KAl(SO_4)_2 \cdot 0.5\ H_2O$ in water. After addition of 5 ml of concentrated hydrochloric acid, the solution was transferred to a 500-ml volumetric flask and diluted to the mark with water. A 0.0100 M magnesium stock solution was prepared by dissolving 1.204 g of anhydrous magnesium sulfate in water and diluting to 1.000 l with water. A 0.01000 M zinc stock solution was prepared by dissolving 0.6537 g of zinc metal in a minimum amount of dilute hydrochloric acid and diluting to 1.000 l with water. A 0.0100 M cadmium stock solution was prepared by dissolving 1.124 g of pure cadmium metal in a minimum amount of dilute nitric acid and diluting to 1.000 l with water. Other metal ion standard solutions were prepared by dilution from these stock solutions.

A 0.0100 M QS stock solution was prepared by dissolving 2.613 g of recrystallized QS in a minimum amount of sodium hydroxide solution and diluting to 1.000 l with water. This solution was diluted to prepare various standards.

All chemicals used were of analytical-reagent grade. Deionized distilled water was used throughout.

Procedures

The QS was immobilized by adding 2.0 g of Amberlite CG-400 resin to 100 ml of QS solution in a 100-ml beaker and stirring. After 12 h, the resin with immobilized QS was filtered through a Buechner funnel with S & S 589 filter paper, washed with water, dried at 50°C, ground in an agate mortar to 400-mesh size and stored in a glass bottle. The amount of QS bound to the resin was controlled by appropriately choosing the concentration of the QS solution. In all cases, the amount of added QS was well below the capacity of the anion-exchange resin (3.3 meq g^{-1}). In no case was there detectable QS remaining in the supernatant solution after the immobilization procedure was complete (determined by adding metal ion and looking for fluorescence). Resins with QS loadings from 0.10 mmol to 0.50 mmol per gram of resin were prepared by this procedure. Unless otherwise noted, all experiments were done with resin containing 0.50 mmol QS g^{-1} resin.

Spectra of immobilized complexes were measured by using a thin layer of resin coated on a piece of cellophane tape. The immobilized reagent was left in a solution containing 8.0×10^{-5} M metal ion at the pH of interest for at least 10 min to allow time for the complex to form.

Response to metal ions. A thin layer of the resin with immobilized QS was spread on a piece of cellophane tape by placing the tape over a vial containing the resin. The vial was shaken until a uniform layer formed. The tape was held in place on the end of the fiber optic by a piece of tygon tubing. The end of the fiber optic was immersed into 10.0 ml of a stirred buffer solution. After the background had stabilized, microliter amounts of metal ion standard solutions were added through the injection port from a syringe, and the response to metal ion was recorded.

RESULTS AND DISCUSSION

Spectra

Figure 1 shows the fluorescence spectra of immobilized QS and its complexes with zinc(II) and cadmium(II). Although dissolved QS does not fluoresce significantly at any pH, the immobilized QS does fluoresce with maximum intensity at 439 nm. This emission is the main source of background when the response of immobilized QS to added metal ion is measured.

Immobilization broadens the spectra of metal/QS complexes. This is generally accompanied by a shift of a few nanometers in the wavelength of the

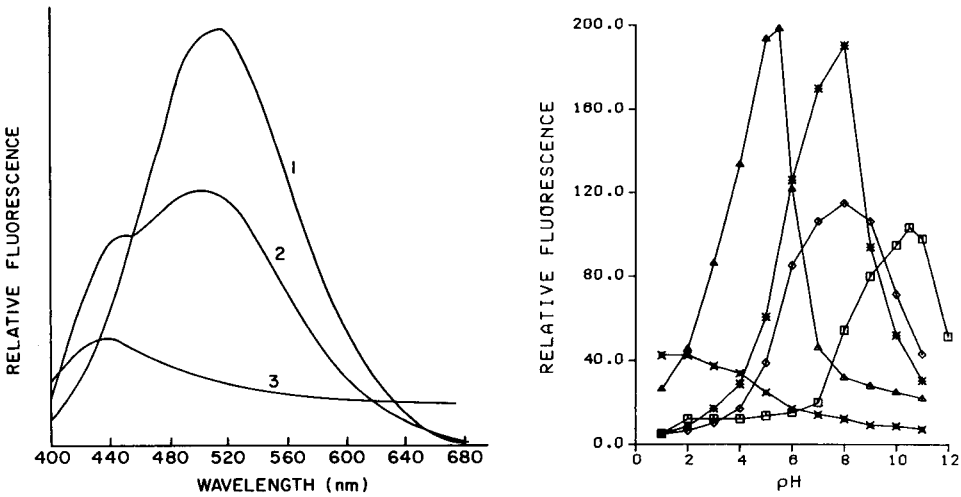

Fig. 1. Fluorescence spectra (uncorrected): (1) immobilized Zn/QS; (2) immobilized Cd/QS; (3) immobilized uncomplexed QS.

Fig. 2. Variation of fluorescence with pH: (×) immobilized QS; (△) Al(III) complex; (□) Mg(II) complex; (★) Zn(II) complex; (◇) Cd(II) complex.

maximum emission. For example, in the case of zinc(II), the maximum shifts from 525 nm to 515 nm on immobilization and the width at half maximum emission increases from 90 to 105 nm.

In the case of cadmium(II), immobilization leads to a new band in the spectrum with a maximum at 448 nm. This band could be useful in distinguishing cadmium from other metals that form fluorescent complexes with QS.

In this study, response to metal ions was measured as the fluorescence intensity at the wavelength of maximum emission for the immobilized metal/QS complex. In practice, a superior alternative might be to relate metal concentration to the ratio of intensity at the wavelength of maximum complex emission to the intensity at 439 nm where the uncomplexed QS emits most strongly. The ratio would be less sensitive to instrumental drift and to slow processes affecting the amount of QS.

Effect of pH

Figure 2 shows the effect of pH on the fluorescence from immobilized QS and its metal complexes. The immobilized reagent itself is most fluorescent at low values of pH. For the immobilized metal complexes, fluorescence intensity as a function of pH is similar to data for complexes in solution. At low values of pH, fluorescence decreases because the conditional formation constant for complex formation is too small. At high pH, the decrease in fluorescence occurs because of the tendency of the metal to form

hydroxide complexes. At all pH values for all complexes, there is an observable signal; however, this can be attributed to background from scattering plus fluorescence from uncomplexed QS. As is evident from Fig. 2, pH control provides a valuable means of achieving selectivity.

Response to metal ions

The response of immobilized QS to added metal ion is shown in Fig. 3. The response is nonlinear, levelling off at high concentrations because of saturation of the immobilized QS with metal ion. The smallest amounts measured were 3×10^{-7} M for Al(III) and Zn(II) and 5×10^{-7} M for Mg(II) and Cd(II). The response to metal ions varies with pH because it depends on the conditional equilibrium constant for complex formation.

As discussed previously [1], if the stoichiometry of the reaction is 1:1 and if the amount of metal combining with the immobilized reagent phase is small relative to the amount in solution, then the following equation applies:

$$C_M/I_F = C_M/kC + 1/kCK \quad (1)$$

where I_F is the fluorescence intensity, k is a proportionality constant relating fluorescence intensity to the amount of complex, C_M is the concentration of metal ion, C is the amount of immobilized ligand and K is the conditional equilibrium constant for complex formation. As predicted by Eqn. 1, plots of C_M/I_F vs. I_F are linear, confirming a 1:1 stoichiometry and that the amount of bound metal is small relative to the amount in solution. Conditional binding constants determined from the slopes and intercepts of

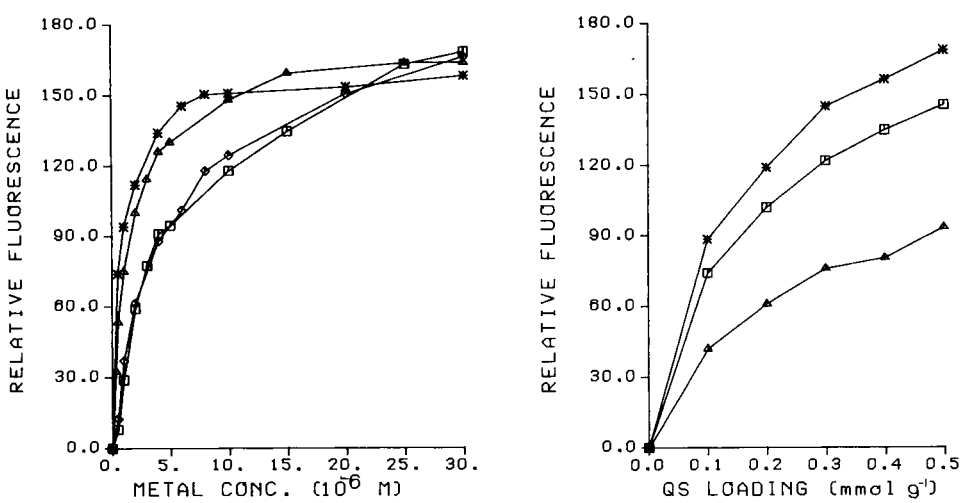

Fig. 3. Fluorescence as a function of added metal ion concentration: (△) Al(III) at pH 5; (□) Mg(II) at pH 10; (*) Zn(II) and (◇) Cd(II) at pH 6.

Fig. 4. Fluorescence as a function of the loading of immobilized QS at pH 10.00 in the presence of different amounts of Mg(II): (△) 0.010 mM; (□) 0.050 mM; (★) 0.10 mM.

TABLE 1

Logarithms of conditional formation constants for metal complexes with immobilized QS at various pH values

M/QS	Formation constant			
	pH 5.00	pH 6.00	pH 8.00	pH 10.0
Mg(II)	—	2.5	4.1(3.9)[a]	4.9
Al(III)	5.5	6.5	—	—
Zn(II)	5.2(4.3)[a]	6.1	8.0	—
Cd(II)	4.3	5.3	7.1	

[a]The values in parentheses are calculated for dissolved 1:1 metal/QS from formation constants at an ionic strength of 0.1 [10].

these plots are listed in Table 1. The values vary as expected with pH and are close to those observed for 1:1 metal/QS complexes in solution.

Increasing temperature causes the fluorescence intensity to decrease. In the temperature range 20—40°C, the temperature coefficients are 1.3, 1.4, 2.4, and 1.6%/°C for the Zn(II), Al(III), Cd(II) and Mg(II) complexes, respectively. These are typical values for fluorescence and are generally attributed to increases in the rate of internal conversion at higher temperatures.

Addition of sodium chloride also causes a reduction in fluorescence intensity. The coefficients range from 30%/M for the Zn(II) complex to 21%/M for the Mg(II) complex. This is attributed to the effect of chloride and/or ionic strength on the fluorescence quantum efficiency. There is no evidence that the sodium chloride displaces the complexes from the resin.

Response time

Steady-state intensity is reached in 1.5—2.5 min when metal ion is added to QS immobilized on Amberlite CG-400 which has 4% crosslinking. When Dowex 1-X2-400 anion-exchange resin with 2% crosslinking was used instead, the response time was reduced to about 1 min. This is consistent with the idea that internal diffusion of metal in the pores of the resin is the factor limiting the rate of response. However, the Dowex 1-X2-400 was not used in other experiments because it did not adhere well to the cellophane tape.

Loading of QS

Increasing the amount of immobilized QS causes an increase in fluorescence intensity as shown in Fig. 4. At high coverages, intensities approach a limiting value. At a typical coverage of 0.6 mg of resin per cm^2, the absorbance of resin containing 0.1 mmol QS g^{-1} is about 0.2 (as calculated from the molar absorptivity of the QS/Mg^{2+} complex). At these levels, the inner-filter effect caused by absorption of the excitation radiation by the immobilized reagent is quite significant and is the main effect causing the curvature in the data of Fig. 4.

If significant concentration quenching were occurring, one would expect a decrease in fluorescence intensity with increased loadings of QS. This is not the case, indicating that concentration quenching does not occur. This is not unexpected because there is very little overlap between the excitation and emission spectra of QS complexes.

Interferences

The sensor is subject to three types of interferences. Metal ions which form fluorescent complexes interfere positively in the determination of other metal ions. Metal ions which form nonfluorescent complexes interfere negatively by combining with immobilized QS and reducing the amount available to form complexes. (The second type of interference would be reduced if one measured the ratio of the fluorescence intensity of the metal complex to the intensity at 439 nm where immobilized QS emits most strongly.)

The third type of interference is due to the presence of ligands which combine with the analyte and render it unavailable to immobilized QS. As with potentiometric metal ion sensors, the measured parameter is the "free" rather than the "total" metal ion concentration.

Because the formation constants for immobilized metal/QS complexes are similar to those for dissolved 1:1 metal/QS complexes, published solution equilibrium constants can be used to predict whether a particular interference is likely to occur and at what level.

Stability of QS

In the chromatographic study of QS immobilized on an ion-exchange resin, leaching of QS from the resin was cited as a problem [8]. In the present work, no loss of QS was observed even in the presence of 2.0 M sodium chloride. Because of strong hydrophobic interactions with QS, the resin is highly selective for QS. In addition, the resin used in this study is significantly undersaturated with respect to QS. There is a large excess of ionic sites to capture any QS that momentarily becomes free in solution. The only way to displace QS is to add an excess of an organic anion that, like QS, can interact hydrophobically as well as electrostatically with the resin.

In the course of a day, there was no observable photodegradation of immobilized QS or its complexes. Long-term stability is unknown because a fresh layer of immobilized QS was used each day.

Partial support for this research was provided by NSF CHE 82-06131.

REFERENCES

1 L. A. Saari and W. R. Seitz, Anal. Chem., 55 (1983) 667; Analyst (London), 109 (1984) 655.
2 L. A. Saari and W. R. Seitz, Anal. Chem., 56 (1984) 810.

3 W. E. Ohnesorge and L. B. Rogers, Spectrochim. Acta, 15 (1959) 27, 41.
4 F. E. Lytle, D. R. Storey and M. E. Juricich, Spectrochim. Acta, 29A (1973) 1357.
5 J. A. Bishop, Anal. Chim. Acta, 87 (1976) 255.
6 W. R. Seitz, CRC Crit. Rev. Anal. Chem., 8 (1980) 367.
7 S. N. Willie, R. E. Sturgeon and S. S. Berman, Anal. Chim. Acta, 149 (1983) 59.
8 K. S. Lee, W. Lee and D. W. Lee, Anal. Chem., 50 (1978) 255.
9 L. A. Saari and W. R. Seitz, Anal. Chem., 54 (1982) 821.
10 R. M. Smith and A. E. Martell, Critical Stability Constants, Vol. 2, Plenum Press, New York, 1975.

Analytica Chimica Acta, 171 (1985) 259—267
Elsevier Science Publishers B.V., Amsterdam — Printed in The Netherlands

FEASIBILITY OF LOW-VOLTAGE CATHODIC ELECTROLUMINESCENCE AT OXIDE-COVERED ALUMINUM ELECTRODES FOR TRACE METAL DETERMINATIONS IN AQUEOUS SOLUTIONS

KEIJO HAAPAKKA*, JOUKO KANKARE and SAKARI KULMALA
Department of Chemistry, University of Turku, SF-20500 Turku 50 (Finland)
(Received 1st October 1984)

SUMMARY

Metal-catalyzed electroluminescence is generated at an oxide-covered aluminum electrode during the reduction of oxygen, potassium peroxodisulfate, and especially hydrogen peroxide in aqueous solutions. The feasibility of this electroluminescence for the determination of copper (5×10^{-9} M) and thallium ($>10^{-10}$ M) is demonstrated.

Light emission is generated during the anodization of an aluminum electrode at relatively high voltages (>30 V) in aqueous electrolytes. This anodic electroluminescence was first observed by Braun in 1898 in anodizing an aluminum electrode in dilute sulfuric acid [1]. Since then, the electroluminescence has been the subject of many studies, and two reviews on its mechanism have been published [2, 3].

Light is also emitted at semiconductor and oxide-covered valve-metal electrodes during the reduction of hydrogen peroxide, oxygen and potassium peroxodisulfate in aqueous solutions at low electrode voltages. This cathodic electroluminescence has been studied by using CdS, GaAs, GaP, SnO_2, ZnO, Al_2O_3, Ta_2O_5, TiO_2, CdSe and ZnS electrodes in different experimental conditions [4—13] and according to these studies, the electroluminescence is due to the electron—hole recombination connected with hole injection by hydroxyl, peroxide or sulfate radicals.

From the analytical viewpoint, the electroluminescence at an oxide-covered electrode may open new possibilities for the determination of trace metals, because metal ions are readily adsorbed and enriched on an oxide surface in aqueous electrolytes [14—20]. Furthermore, the chelation of metal ions alters, in some cases drastically, their adsorption properties [21, 22] thus creating an interesting basis for the development of selective trace metal analysis. However, the effect of adsorbed species on electroluminescence has not been extensively studied earlier.

Some preliminary results have been reported concerning the catalytic effects of adsorbed metal ions on the hydrogen peroxide-induced electro-

0003-2670/85/$03.30

luminescence at an oxide-covered aluminum electrode [8, 23]. The present work demonstrates the feasibility of this low-voltage cathodic electroluminescence for trace metal determinations in aqueous solution.

EXPERIMENTAL

Apparatus

The apparatus has been described in detail elsewhere [24]. In the present work, the four-electrode potentiostat was replaced by a conventional three-electrode potentiostat and the oscilloscope by a digital storage oscilloscope (Gould OS1420). A disc electrode was made by imbedding a 9.5-mm diameter aluminum rod (Alfa, 99.999%) in PTFE and polishing the end, first mechanically with 1-μm diamond paste and then electrochemically at 1 A cm^{-2} for 5 s in a (1 + 3) mixture of perchloric acid (60%) and ethanol. In order to obtain a non-porous oxide film having a thickness proportional to the formation voltage, the aluminum electrode was anodized in aqueous 2.5% (w/v) boric acid solution (Suprapur) adjusted to pH 6 with 0.1 M ammonia first galvanostatically at 1 mA cm^{-2} to the required voltage and then potentiostatically until the current had reached 10 μA cm^{-2} [25].

Reagents

All water used was quartz-distilled, prepared and stored as described previously [24]. Unless specified otherwise, all reagents were of pro analysi grade (Merck). Sodium acetate, acetic acid and sodium hydroxide (all Suprapur) were used as received. Hydrogen peroxide (30%) and potassium peroxodisulfate were used as received. The hydrogen peroxide stock solution (ca. 0.1 M) was standardized weekly by iodimetric titration [26]. Copper(II) nitrate was used (as received) to prepare a 0.01 M stock solution. The other metal salts and organic ligands were of analytical grade from various manufacturers and were also used as received, excluding tetraethylenepentamine (tetren) which was first precipitated as its sulfate [27] and determined by the method of Hulanicki et al. [28].

Nitrogen and oxygen were of the purest grade available and were passed into the test solution through a soda lime tube and through a wash bottle filled with water.

Procedure

In order to avoid memory effect, the surface of the oxide-covered aluminum electrode was electrolytically pretreated before each measurement. The pretreatment was done in aqueous 0.1 M acetic acid, 6×10^{-4} M in hydrogen peroxide, by scanning the pulse amplitude of the s.d.s. potential (see below) between 0 V and 10 V until the cathodic electroluminescence intensity became constant. Usually this was achieved within 5 runs.

A 50-ml aliquot of the sample solution with appropriate amounts of sodium acetate was adjusted to the desired pH, hydrogen peroxide was

pipetted into the electroluminescence cell and the solution was deaerated with nitrogen for 10 min. A suitable amount of copper(II) was added and the rotation of the electrode and the scanning of the pulse amplitude were started. The electroluminescence pulses were recorded on the digital storage oscilloscope and the average electroluminescence intensity vs. pulse amplitude on the x-y recorder.

RESULTS AND DISCUSSION

Preliminary measurements of electroluminescence

The low-voltage cathodic electroluminescence obtained in the presence of hydrogen peroxide at the oxide-covered aluminum electrode was excited by using the symmetric double-step (s.d.s.) potential shown in Fig. 1A. The electroluminescence generated under these conditions and the effects of traces of copper(II) on the anodic and cathodic electroluminescence are presented in Fig. 1B and 1C, respectively. According to these figures, copper(II) has no effect on the anodic electroluminescence. The positive pulse was found to be necessary for the generation of copper(II)-enhanced electroluminescence. The time average of the anodic and cathodic electroluminescence as a function of the pulse amplitude is presented in Fig. 2, under the conditions stated in Fig. 1B. (The corresponding cathodic electroluminescence curve with 1×10^{-6} M copper present is shown later in Fig. 4F.) The recorder response of the anodic electroluminescence is the time average of the difference between the anodic light pulse and the light output during the preceding zero potential level. The corresponding cathodic electroluminescence is analogous. The recorder response is hereafter referred for simplicity to as the electroluminescence intensity and is given in arbitrary units.

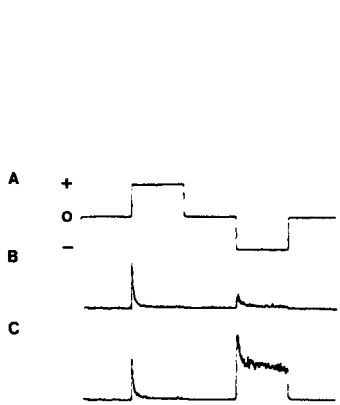

Fig. 1. (A) The symmetric double step potential; (B) the corresponding electroluminescence in the presence of hydrogen peroxide at the oxide-covered aluminum electrode without added copper(II); (C) as (B) but with 1×10^{-7} M copper(II). (Conditions as in Fig. 5.)

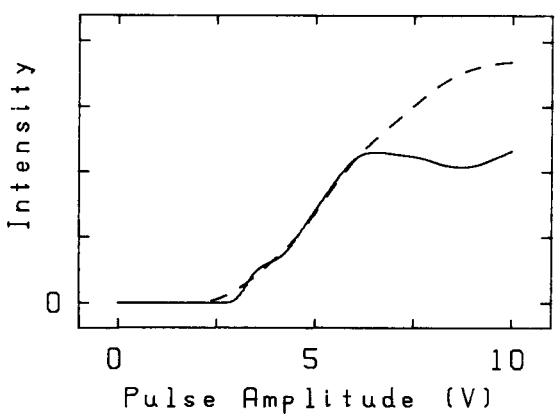

Fig. 2. Effect of pulse amplitude: (---) on the anodic electroluminescence, (—) on the cathodic electroluminescence, without added copper(II). (Conditions as in Fig. 5.)

The anodic and cathodic electroluminescence pulses were also generated during the reduction of oxygen and potassium peroxodisulfate under the conditions presented in Fig. 1, and the anodic electroluminescence was in both cases similar to that shown above. Copper(II) enhanced the cathodic electroluminescence reactions but the enhancing effect was quite small compared to that obtained by using hydrogen peroxide.

On the basis of these results, low-voltage cathodic electroluminescence based on the reduction of hydrogen peroxide was selected for further study.

Effect of oxide layer thickness

Under the anodization conditions used, the thickness of the oxide layer formed on the aluminum electrode is proportional to the anodization voltage, and is given by 1.3 nm V^{-1} [29]. In order to study the effect of the thickness of the oxide layer, the aluminum electrode was anodized at 20, 40 and 60 V, which correspond to oxide layer thicknesses of 28, 56 and 84 nm, respectively. In addition, an aluminum electrode which was polished as described above but not anodized at all was also tested. Unfortunately, the thickness of the oxide layer cannot be estimated accurately in this case but is obviously a few nanometers. The electroluminescence measurements were made under the conditions stated in Fig. 1 and the results, for the fifth electroluminescence measurement after anodization, are shown in Fig. 3.

The most intense cathodic electroluminescence signal was obtained at the aluminum electrode which was not anodized, while the electrodes with thick oxide layers gave only weak electroluminescence signals during the first measurements. However, the cathodic electroluminescence intensity at the electrodes anodized at 20, 40 and 60 V continuously increased with successive scans of the s.d.s. pulse train from 0 V to 10 V in such a way that ca. 30, 80 and 130 scans, respectively, were needed in order to reach the electroluminescence intensity level obtained at the unanodized electrode. Consequently, it seems evident that the oxide layer anodized on the aluminum electrode is gradually removed from the electrode surface during the electroluminescence

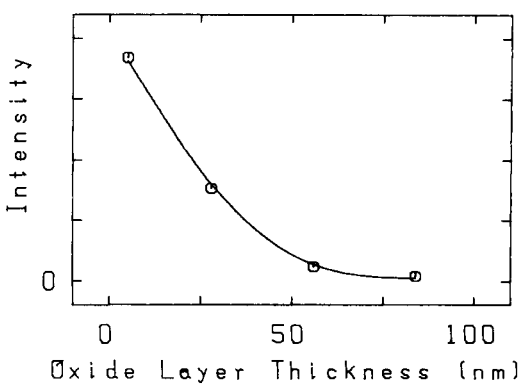

Fig. 3. Effect of oxide layer thickness on the cathodic electroluminescence from 1 × 10^{-6} M copper(II). (Conditions as in Fig. 5.)

measurements. Therefore, further electroluminescence measurements were made with the unanodized electrode.

Effect of other experimental variables

In order to have optimum conditions for the determination of copper(II), the cathodic electroluminescence intensity was recorded as a function of pH, hydrogen peroxide concentration, electrode rotation rate, scan rate, and pulse length and pulse amplitude of the s.d.s. potential. Figure 4 shows the effect of these experimental variables. The corresponding blank measurements, i.e., measurements without any added copper(II), gave similar electroluminescence intensity profiles as those shown in Fig. 4. The effect of pulse amplitude was estimated both by scanning at 260 mV s^{-1} up to the predetermined potential, and by an abrupt change of the potential, as shown in Fig. 4F. No marked difference in the electroluminescence sensitivity was observed between these methods and consequently scanning of pulse amplitude was used in later measurements because more reproducible results were obtained in this way. On the basis of these experiments, the values of the experimental variables presented in Fig. 5 were selected for the copper(II) determination.

Calibration graph, limit of detection and precision

The log-log plot of electroluminescence intensity vs. copper(II) concentration is shown in Fig. 5. This graph is linear from 1×10^{-6} M down to at least 5×10^{-9} M and its slope is 0.5 showing that the response is proportional to $[Cu^{2+}]^{1/2}$.

The limit of detection for copper(II) was evaluated, as recommended by I.U.P.A.C. [30], to be 5×10^{-9} M copper(II). Twenty successive measurements of 1×10^{-7} M copper(II) over two days gave a relative standard deviation of 12%.

Effect of complexation of copper(II)

The effect of complexation of copper(II) on the cathodic electroluminescence intensity was evaluated by using some amines and aminocarboxylic acids as complexing agents. The experiments were done under the conditions stated in Fig. 5, and the results are presented in Table 1. Of these complexing agents, the aminocarboxylic acids form stable complexes with copper(II) and aluminum(III) and the amines only with copper(II). The plots of electroluminescence intensity vs. log complexing agent concentration were obtained for all these complexing agents; those of tetren, dien, EDTA and gly are shown in Fig. 6. Similar profiles were obtained with the other complexing agents. Fluoride, which forms stable complexes only with aluminum(III), inhibited the cathodic electroluminescence by ca. 30% under these conditions.

As can be concluded from Table 1, the complexation of copper(II) by an organic compound inhibits the cathodic electroluminescence intensity.

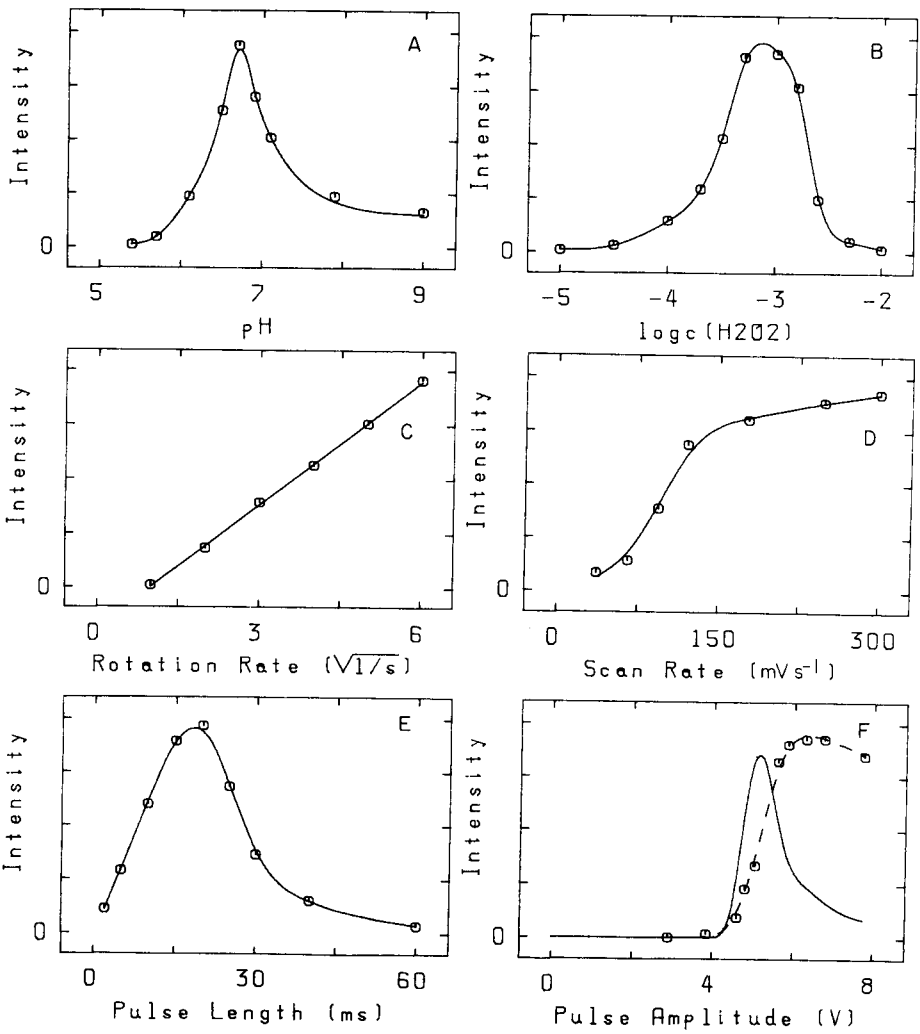

Fig. 4. Effects of experimental variables on the cathodic electroluminescence from 1×10^{-6} M copper(II): (A) pH; (B) hydrogen peroxide concentration; (C) rotation rate; (D) scan rate; (E) pulse length, (F) pulse amplitude, (—) by scanning and (---) by an abrupt change in potential. Except for the variable under investigation, the conditions were: 0.100 M sodium acetate, pH 6.7, 4×10^{-4} M hydrogen peroxide, rotation rate 25 rps, scan rate 130 mV s^{-1}, pulse length 16 ms, pulse amplitude 5 V; all solutions were deaerated with nitrogen.

However, severe interference on the copper(II) determination was obtained only with tetren and trien (which form only 1:1 complexes with copper(II)) and dien which also forms a 1:2 complex ($p\beta_2^* = 15.6$ at pH 7).

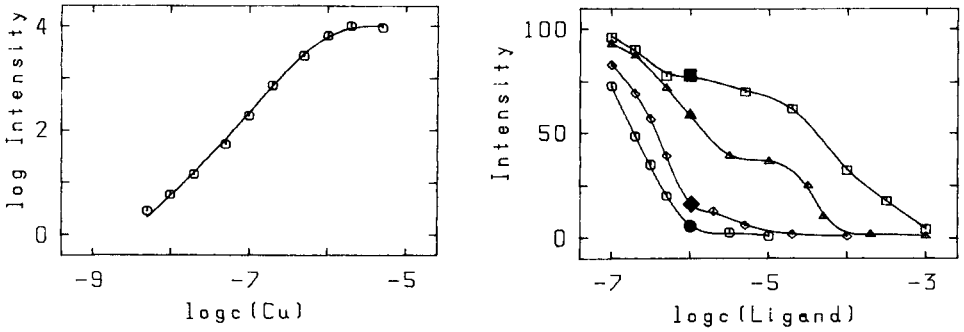

Fig. 5. Calibration graph for copper(II). Conditions: 0.100 M sodium acetate, pH 6.7, 6×10^{-4} M hydrogen peroxide, rotation rate 25 rps, scan rate 260 mV s^{-1}, pulse length 17 ms, pulse amplitude 5 V; solutions deaerated with nitrogen.

Fig. 6. Inhibition effects on cathodic electroluminescence with 1×10^{-6} M copper(II): (○) tetren; (◇) dien; (△) EDTA; (□) glycine. (●, ◆, ▲, ■) are the points where the concentrations of copper(II) and ligand are equal. (Conditions as in Fig. 5.)

Effect of other metal ions

In addition to copper(II), the catalytic effect of 26 metal ions on the low-voltage cathodic electroluminescence was tested under the conditions shown in Fig. 5. The measurements were made with 1×10^{-6} M metal ion solutions. The results, compared to the intensity obtained with copper(II), are summarized in Table 2. From these results, only silver(I), mercury(I, II), lead(II) and thallium(I) have a marked catalytic effect on the cathodic electroluminescence, thus being potential interferents in the copper(II) determination. All these metal ions were irreversibly adsorbed on the oxide surface of the electrode, so in order to avoid memory effect, the electrode surface had to be cleaned before the next measurement, as described above.

TABLE 1

Inhibition by amines and aminocarboxylic acids of the cathodic electroluminescence intensity (1×10^{-6} M copper(II) and 1×10^{-6} M ligand)

Amine[a]	Inhibition (%)	pK_1^{*b}	Acid[c]	Inhibition (%)	pK_1^{*b}
en	30	5.1	gly	25	5.6
dien	85	10.7	IDA	35	8.2
trien	95	14.7	NTA	20	10.6
tetren	95	16.3	EDTA	40	13.4

[a]en = ethylenediamine; dien = diethylenetriamine; trien = triethylenetetramine; tetren = tetraethylenepentamine. [b]Values for copper(II) calculated at pH 7 from literature stability constants [31]. [c]gly = aminoacetic acid; IDA = iminodiacetic acid; NTA = nitrilotriacetic acid; EDTA = ethylenediaminetetraacetic acid.

TABLE 2

Effects of metal ions on the relative cathodic electroluminescence intensity (I) at the oxide-covered aluminum electrode

Metal ion[a]	Source	I_{Me}/I_{Cu}[b]	Metal ion[a]	Source	I_{Me}/I_{Cu}[b]
Blank		0.002	Hg(II)	$Hg(C_2H_3O_2)_2$	3
Cu(II)	$Cu(NO_3)_2$	1.00	In(III)	$InCl_3$	0.07
Ag(I)	$AgC_2H_3O_2$	0.3	Mg(II)	$MgCl_2$	0.002
Al(III)	$Al(NO_3)_3$	0.002	Mn(II)	$MnCl_2$	0.02
Bi(III)	$Bi(NO_3)_3$	0.002	Ni(II)	$NiCl_2$	0.002
Ca(II)	$CaCl_2$	0.002	Pb(II)	$Pb(NO_3)_2$	0.7
Cd(II)	$CdSO_4$	0.04	Rh(II)	$Rh(C_2H_3O_2)_2$	0.002
Ce(IV)	$Ce(SO_4)_2$	0.002	Sb(III)	$SbCl_3$	0.002
Co(II)	$Co(NO_3)_2$	0.002	Sn(II)	$SnCl_2$	0.002
Cr(III)	$CrCl_3$	0.001	Tb(III)	$Tb(ClO_4)_3$	0.006
Cr(VI)	Na_2CrO_4	0.001	Tl(I)	TlCl	30
Eu(III)	Eu_2O_3/HCl	0.001	U(VI)	$UO_2(NO_3)_2$	0.002
Fe(III)	$FeCl_3$	0.002	V(V)	$NaVO_3$	0.002
Hg(I)	$Hg_2(C_2H_3O_2)_2$	3	Zn(II)	$Zn(C_2H_3O_2)_2$	0.002

[a] 1×10^{-6} M (other conditions as in Fig. 5). [b] I_{Me}/I_{Cu} is the peak cathodic intensity compared to that for 1×10^{-6} M copper(II).

Thallium(I) gave 30 times more intense cathodic electroluminescence than copper(II) under the conditions optimized for the copper(II) determination. Consequently, it seems probable that a selective determination of thallium(I) at levels well below 10^{-10} M could be developed by optimizing the experimental variables for this determination.

Conclusions

The main purpose of the present paper is to show that the low-voltage cathodic electroluminescence generated at the oxide-covered aluminum electrode during hydrogen peroxide reduction can be utilized for the determination of traces of metal ions in aqueous solution. The equilibrium system under these experimental conditions is very complicated and at present it is not possible to give any detailed reaction scheme for the cathodic electroluminescence. A study on the mechanism of this low-voltage cathodic electroluminescence is in progress.

Adsorption of metal ions on the aluminum oxide surface can easily be changed by complexation. Work along these lines is also in progress in order to achieve further selectivity for the trace determination of metal ions.

Financial aid from the Academy of Finland is gratefully acknowledged.

REFERENCES

1 F. Braun, Ann. Phys. Chem., 65 (1898) 361.
2 S. Ikonopisov, Electrochim. Acta, 20 (1975) 783.
3 S. Tajima, Electrochim. Acta, 22 (1977) 995.
4 B. Pettinger, H.-R. Schöppel and H. Gerischer, Ber. Bunsenges. Phys. Chem., 80 (1976) 849.
5 F. Decker, B. Pettinger and H. Gerischer, J. Electrochem. Soc., 130 (1983) 1335.
6 Y. Nakato, A. Tsumura and H. Tsubomura, Bull. Chem. Soc. Jpn., 55 (1982) 3390.
7 T. Yamase and H. Gerischer, Ber. Bunsenges. Phys. Chem., 87 (1983) 349.
8 J. Kankare, D. Ryan and B. Furst, Can. J. Chem., 55 (1977) 1193.
9 R. Noufi, P. Kohl, S. Frank and A. Bard, J. Electrochem. Soc., 125 (1978) 246.
10 Y. Nakato, A. Tsumura and H. Tsubomura, J. Phys. Chem., 87 (1983) 2402.
11 H. Streckert and A. Ellis, J. Phys. Chem., 86 (1982) 4921.
12 H. Streckert, J.-R. Tong and A. Ellis, J. Am. Chem. Soc., 104 (1982) 581.
13 F.-R. Fan, P. Leempoel and A. Bard, J. Electrochem. Soc., 130 (1983) 1866.
14 R. James and T. Healy, J. Colloid Interface Sci., 40 (1972) 42.
15 C.-P. Huang and W. Stumm, J. Colloid Interface Sci., 43 (1973) 409.
16 F. Dalang and W. Stumm, in M. Kerker (Ed.), Colloid and Interface Science, Vol. 4, Academic Press, New York, 1976, p. 157.
17 P. Schindler, B. Furst, R. Dick and P. Wolf, J. Colloid Interface Sci., 55 (1976) 469.
18 M. Benjamin and J. Leckie, J. Colloid Interface Sci., 83 (1981) 410.
19 K. Hachiya, M. Sasaki, Y. Saruta, N. Mikami and T. Yasunaga, J. Phys. Chem., 88 (1984) 23.
20 K. Hachiya, M. Sasaki, T. Ikeda, N. Mikami and T. Yasunaga, J. Phys. Chem., 88 (1984) 27.
21 H. Elliot and C.-P. Huang, J. Colloid Interface Sci., 70 (1979) 29.
22 A. von Zelewsky and J.-M. Bemtgen, Inorg. Chem., 21 (1982) 1771.
23 K. Haapakka, J. Kankare and S. Kulmala, J. Lumin., 31/32 (1984) 966.
24 K. Haapakka and J. Kankare, Anal. Chim. Acta, 138 (1982) 253.
25 S. Ikonopisov, Electrochim. Acta, 14 (1969) 761.
26 I. Vogel, Textbook of Quantitative Inorganic Analysis, 4th edn., Longman, London, 1981, p. 381.
27 C. Reilley and A. Vavoulis, Anal. Chem., 31 (1959) 243.
28 A. Hulanicki, M. Trojanowicz and J. Domanska, Talanta, 20 (1973) 1117.
29 J. Diggle, T. Downie and C. Goulding, Chem. Rev., 69 (1969) 365.
30 I.U.P.A.C., H. Irving, H. Freiser and T. West (Eds.), Compendium of Analytical Nomenclature, Pergamon Press, Oxford, 1978, p. 117.
31 I.U.P.A.C., D. Perrin (Ed.), Stability Constants of Metal-ion Complexes: Part B, Organic Ligands, Pergamon Press, Oxford, 1979.

Analytica Chimica Acta, 171 (1985) 269—277
Elsevier Science Publishers B.V., Amsterdam — Printed in The Netherlands

DETERMINATION OF INDIUM IN MINERALS, RIVER SEDIMENTS AND COAL FLY ASH BY ELECTROTHERMAL ATOMIC ABSORPTION SPECTROMETRY WITH PALLADIUM AS A MATRIX MODIFIER

SHAN XIAO-QUAN, NI ZHE-MING* and YUAN ZHI-NENG

Institute of Environmental Chemistry, Academia Sinica, P.O. Box 934, Beijing (People's Republic of China)

(Received 29th April 1984)

SUMMARY

A method is described for the determination of indium (10—40 $\mu g\ g^{-1}$) in lead-zinc ores and magnetic pyrites. Graphite furnace atomic absorption spectrometry is used with palladium as a matrix modifier. Indium (down to 0.085 $\mu g\ g^{-1}$) in river sediments and coal fly ash can be determined after pre-extraction with ammonium iodide into 4-methyl-2-pentanone. In the presence of palladium, the maximum tolerable ashing temperatures for indium in aqueous solution or organic extract can be raised to 1200°C or 1000°C, respectively, and the sensitivity is greatly improved.

Indium is a rare element in the sense that no part of the world is especially rich in indium minerals; even in sphalerite and chalcopyrite, which are the principal sources of indium, its content ranges from less than 1 to 1000 $\mu g\ g^{-1}$. As a typically dispersed element, it enters into the composition of many rock-forming minerals and its over-all abundance in the earth's crust has been estimated as 0.11 $\mu g\ g^{-1}$ [1]. Therefore, analyses have depended on neutron activation and spark-source mass spectrometry because the sensitivities of these methods are normally sufficient to determine indium in minerals and rocks at such low levels. Smales and coworkers [2, 3] applied neutron activation analysis to the determination of traces of indium in standard rock samples G-1 and W-1, using the radionuclides indium-114 and indium-116. The radiochemical separations after the addition of carrier were based primarily on precipitation of indium as its hydroxide and sulphide, together with liquid-liquid extraction. Radiochemically pure indium was finally precipitated and counted as the tris-(8-quinolinol) complex. Taylor [4] reported a method of spark-source mass spectrometry for this purpose and satisfactory agreement was achieved with the other values. Recently, Eskenazy and Mincheva [5] used a chemical concentration procedure followed by emission spectrography to determine indium contents of $\leqslant 1\ \mu g\ g^{-1}$ in geochemical samples. Spitzer and Tesik [6] described a method for determining 2—10 $\mu g\ g^{-1}$ indium in pyrites, pyrites ashes, and intermediate products of chlorination roasting, by using flame atomic absorption spectrometry after extraction and back-extraction.

0003-2670/85/$03.30

The present study describes a direct method for the determination of indium in lead-zinc ores and magnetic pyrites ranging from 10 to 36 $\mu g\ g^{-1}$, by graphite-furnace atomic absorption spectrometry with μg-amounts of palladium added as a matrix modifier (as used in previous determinations [7—9]). A liquid-liquid extraction procedure is also recommended for the determination of indium ($<0.1\ \mu g\ g^{-1}$) in river sediments and coal fly ash.

EXPERIMENTAL

Apparatus

The Perkin-Elmer model 4000 atomic absorption spectrometer used was equipped with a model HGA-400 graphite furnace atomizer. Signals obtained with argon in the stopped flow and maximum power modes were recorded on a Perkin-Elmer model 056 chart recorder. The spectral bandwidth was set at 0.7 nm. A hollow-cathode lamp (Shanghai Electro-Optic Instruments Works) was operated at 10 mA. Deuterium arc background correction was used throughout. A 10- or 20-μl Eppendorf pipette fitted with disposable polypropylene tips was used to introduce sample solution into the graphite tube.

Reagents

An indium stock solution (1000 $\mu g\ ml^{-1}$) was prepared by dissolving 0.1209 g of Specpure In_2O_3 (Johnson Matthey, London) in an adequate volume of dilute nitric acid and diluting to 100 ml with demineralized water. All other working standards were prepared from this stock solution by serial dilution with demineralized water.

A palladium solution was prepared by dissolving a suitable amount of palladium chloride in sufficient aqua regia, with gentle heating, and adding several milliliters of concentrated nitric acid, after which the solution was evaporated nearly to dryness. This operation was repeated and the residue was dissolved in dilute nitric acid.

Ammonium iodide (8 M) and ascorbic acid (10%) solutions were freshly prepared from analytical-reagent materials just before use. All other chemicals were of analytical-reagent grade.

Procedures

Dissolution of lead-zinc ore. Accurately weigh 100 mg of sample into a 30-ml teflon crucible (from a pressure decomposition vessel), add 0.5 ml of 0.01 M nitric acid to moisten the sample thoroughly, followed by 1 ml each of 72% perchloric acid, 68% nitric acid and 35% hydrofluoric acid. Follow the procedure reported previously [10] but use a sample dissolution time of 7 h. Transfer the final contents of the pressure vessel to a 50-ml volumetric flask and dilute to the mark with 0.1 M nitric acid.

Dissolution of magnetic pyrites. Use the above procedure, but add 1—2 ml of concentrated hydrochloric acid and heat to remove sulphur from the residue in the vessel.

Dissolution of river sediments and coal fly ash. Use the first procedure, and add 6 ml of 4 M hydrochloric acid to dissolve the residue in the vessel. Transfer all the contents to a 50-ml separatory funnel, add 6.2 ml of 10% (w/v) ascorbic acid solution and the same volume of 8 M ammonium iodide and dilute to 25 ml with demineralized water. Add 2.0 ml of 4-methyl-2-pentanone (MIBK), shake the contents for 2 min, and allow to stand for a few minutes for phase separation. Discard the aqueous phase and transfer the organic phase to a pre-dried quartz centrifuge tube. Centrifuge at 2000 rpm for 5 min and determine the indium in the organic extract as described below.

Determination of indium in lead-zinc ores and magnetic pyrites. After appropriate dilution of the aqueous sample solution, add sufficient 5% (w/v) ascorbic acid solution to give a concentration in the final solution of 1 mg ml^{-1} for lead-zinc ores or 0.4 mg ml^{-1} for magnetic pyrites. Inject 20 μl of the sample solution and the same volume of aqueous 100 $\mu g\ ml^{-1}$ palladium solution into the graphite furnace. After drying at 110°C, char at 1100°C for 30 s using a ramp time of 1 s, and atomize at 2000°C using maximum power and the internal argon flow interrupted mode. Measure indium absorbance at the 303.9-nm resonance line. Finally, clean the tube at 2650°C for 5 s.

Use a similar procedure for indium in the organic extract, but dry at 200°C for 30 s using a ramp time of 5 s and char at 1000°C for 30 s using a ramp time of 1 s. Do not add ascorbic acid.

Measurement of InO absorbance. The experimental procedures and the operating conditions of the graphite furnace were as follows: a deuterium arc lamp was used as the light source, and the spectral bandwidth was 0.07 nm. A 10-μl aliquot of 0.10 mg ml^{-1} indium solution and 10 μl of 0.5 mg ml^{-1} palladium solution were injected into the graphite tube. After drying, the residue was vaporized at various temperatures under conditions of gas stop and maximum power heating. The peak absorbances were measured at 273.0 nm [11] in the absence or presence of palladium.

RESULTS AND DISCUSSION

Stabilizing effect of palladium on indium

Optimal conditions for the determination of indium in aqueous solutions of various acids and in organic extracts have been investigated with the Perkin-Elmer HGA-74 atomizer [12]. Best sensitivity was obtained in 0.1 M nitric or sulphuric acid. The presence of halogen acids causes a significant decrease in atomic absorption signals which are dependent on the halide ions and their concentrations. In order to improve the sensitivity for indium in both aqueous solutions and organic extracts and to eliminate chemical interferences, the platform technique has been adopted in combination with the addition of ascorbic acid [13]. In the present study, the above findings were confirmed yet it was found that the sensitivity was still not sufficient

for the analysis of real samples. Furthermore, serious matrix interference remained.

The low sensitivity for indium was assumed to be due to the vaporization of molecular species of indium during the pre-atomization stages, and many efforts were made to find suitable matrix modifiers which might prevent such a vaporization loss. In this report, several metal salts were tested for this purpose. The indium absorbance in the absence of matrix modifier obtained after ashing at 600°C was used as a baseline, against which the enhancement properties were measured. The results, listed in Table 1, show that palladium was the best modifier, although all metals tested at least doubled the sensitivity. The stabilizing effects of palladium on indium in aqueous solution and an organic extract are shown in Figs. 1 and 2, respectively. There are two branches to each curve. The left-hand branch refers to the signals obtained at various ashing temperatures and an optimal atomization temperature; the right-hand branch refers to signals obtained by varying the atomization temperatures for an optimal ashing temperature. The results show that the presence of microgram amounts of palladium allows the tolerable ashing temperature for indium to be raised up to 1200°C for aqueous solution, and the sensitivity is improved by a factor of three compared to that obtained for pure aqueous indium solutions. The sensitivity for organic extracts is increased 11-fold in the presence of 2 μg of palladium, and the maximum tolerable ashing temperature is raised to 1000°C. The indium absorbance depends on the amount of palladium added (Fig. 3); it increases with increase in palladium concentration from 10 to 80 μg ml^{-1}, and highest absorbances are obtained over the range 80—150 μg ml^{-1}. Therefore 20 μl of a 100 μg ml^{-1} palladium solution was used in the remainder of the study.

TABLE 1

Comparison of various matrix modifiers for indium (20 μl of 50 ng ml^{-1} indium solution)

Matrix modifier	Added as	Metal conc. (mg ml^{-1})	Tolerable ashing temp. (°C)	Relative absorbance
—	—	—	800	1.0
Ni	$Ni(NO_3)_2 \cdot 6H_2O$	1.0	1000	2.0
Ir	$(NH_4)_2IrCl_6$	0.1	1200	2.2
Ca	$Ca(NO_3)_2$	1.0	1000	2.3
W	$Na_2WO_4 \cdot 2H_2O$	Coating[a]	1000	2.4
Co	$Co(NO_3)_2 \cdot 6H_2O$	1.0	1000	2.5
V	NH_4VO_3	1.0	800	2.5
Mo	$(NH_4)_6Mo_7O_{24} \cdot 4H_2O$	1.0	800	2.6
Al	$Al(NO_3)_3$	1.0	900	2.7
Cr	$K_2Cr_2O_7$	1.0	900	2.7
Ta	Ta_2O_5	Coating[a]	800	2.8
Pt	$PtCl_2$	0.1	1200	3.0
Pd	$PdCl_2$	0.1	1200	3.1

[a]On tube wall.

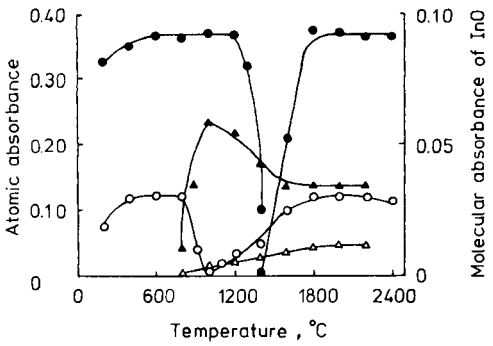

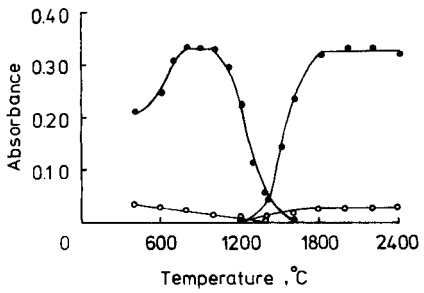

Fig. 1. Effect of ashing and atomization temperature on the atomic absorbance of indium and the InO molecular absorption from aqueous solution. Atomic absorption: (○) 1 ng In; (●) 1 ng In + 2 μg Pd. Molecular absorption: (▲) 1 μg In; (△) 1 μg In + 5 μg Pd.

Fig. 2. Effect of ashing and atomization temperature on the atomic absorbance of indium from an organic extract: (○) 0.8 ng In; (●) 0.8 ng In + 2 μg Pd.

A method similar to that of Campbell and Ottaway [14] was applied for measurements of appearance temperatures. The instrument was set to give an absorbance of 1.0 at the optimum atomization temperature for indium in the absence or presence of palladium. The atomization temperature was then decreased until the signal just disappeared. The atomization temperature was increased until a small absorbance (0.01) appeared and the corresponding temperature under this condition was defined as the appearance temperature. The appearance temperatures for indium in the absence and presence of palladium were found to be 920°C and 1340°C, respectively. Obviously, the stabilizing effect of palladium on indium caused the upward shift of the appearance temperature for indium.

In order to elucidate the reason for the sensitivity enhancement with palladium, molecular absorption spectra of InO were investigated. Because an aqueous nitric acid solution of indium was used for constructing the ashing and atomization curves shown in Fig. 1, and palladium was added as its nitrate, no indium halides were likely to be formed in the graphite furnace. The effects of furnace operating conditions on InO absorbance are shown in Fig. 1. With no palladium added, the InO absorbance increased with increase in atomization temperature from 800°C to 1000°C; above 1000°C, the absorbance decreased, then levelled off. However, the InO absorbance was decreased in the presence of palladium. Therefore it may be assumed that the addition of palladium stabilizes indium by forming more thermostable compounds or alloys [15] and decreases the formation of volatile species such as InO, thus enhancing the atomic absorbance, as observed above.

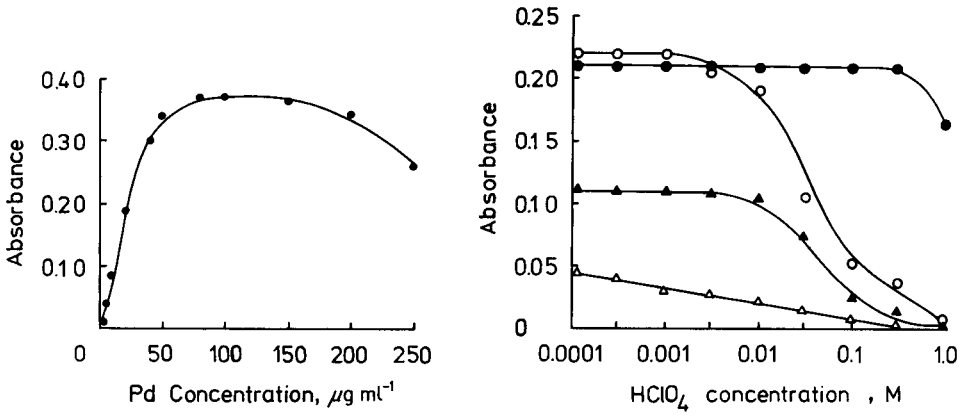

Fig. 3. Dependence of absorbance of 1.0 ng of indium on the concentration of the palladium solution added (20 μl).

Fig. 4. Effectiveness of matrix modifiers in decreasing the interference from perchloric acid: (○) 0.6 ng In + 2 μg Pd + 20 μl $HClO_4$; (●) 0.6 ng In + 2 μg Pd + 20 μl of 5% ascorbic acid + 20 μl $HClO_4$; (△) 0.6 ng In + 20 μl $HClO_4$; (▲) 0.6 ng In + 20 μl of 5% ascorbic acid + 20 μl $HClO_4$.

Effect of foreign ions

The interferences caused by major components of the samples were examined. A 20-μl aliquot of indium solution (30 ng ml^{-1}) containing 100 μg ml^{-1} palladium and the same volume of foreign ion solution was injected into the graphite furnace. The recommended temperature program described for aqueous solutions was run, and the absorbance obtained in the presence of the concomitants was compared to that obtained in their absence. It was found that there were no significant interferences from the following species: 1.0 mg ml^{-1} K^+, Li^+, Ca^{2+}, Sr^{2+}, Co^{2+}, Al^{3+}, V(V), fluoride or sulphate; 0.5 mg ml^{-1} Na^+, Ni^{2+}, silicate or borate; 0.2 mg ml^{-1} Mg^{2+} or Zn^{2+}; 0.1 mg ml^{-1} Cd^{2+}, Fe^{3+} or Nb(V); and 50 μg ml^{-1} Ag^+, Ba^{2+}, Pb^{2+}, As^{3+}, Ga^{3+}, Mn(VII), Cr(VI) or Te(VI).

Because the addition of perchloric acid and nitric acid as well as hydrofluoric acid is necessary to destroy organic substances in the samples, which otherwise interfere with the determinations, the effects of perchloric acid and perchlorate were studied in detail. The results are shown in Figs. 4 and 5, respectively. The absorbance of 0.6 ng of indium was seriously suppressed by 0.003 M perchloric acid when no matrix modifiers were used. However, such effects were negligible if palladium or ascorbic acid was present. Furthermore, there was no interference from 0.3 M perchloric acid when both palladium and ascorbic acid were added. As far as the interference of magnesium perchlorate was concerned, the situation was less severe and there was no pronounced interference from 2.0 mg ml^{-1} magnesium perchlorate on the determination of 0.6 ng of indium, in the presence of palladium and ascorbic acid.

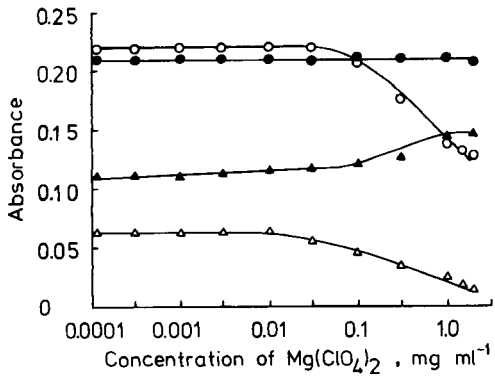

Fig. 5. Effectiveness of matrix modifiers in decreasing the interference from magnesium perchlorate: (○) 0.6 ng In + 2 μg Pd + 20 μl $Mg(ClO_4)_2$; (●) 0.6 ng In + 2 μg Pd + 20 μl of 5% ascorbic acid + 20 μl $Mg(ClO_4)_2$; (△) 0.6 ng In + 20 μl $Mg(ClO_4)_2$; (▲) 0.6 ng In + 20 μl of 5% ascorbic acid + 20 μl $Mg(ClO_4)_2$.

Extraction of indium

Because the indium content of geochemical samples is below 1 μg g^{-1}, preconcentration is necessary for the determination of indium in river sediments and coal fly ash. Various liquid-liquid extraction methods have been reported and briefly reviewed [16]. In this study, an ammonium iodide/MIBK system was applied for extracting 80 ng of indium; the optimal concentrations were established to be 0.5—7 M ammonium iodide and 0.1—3 M hydrochloric acid, respectively. In order to avoid liberation of iodine, which influences the extraction efficiency of indium from hydrochloric acid, ascorbic acid was added at a concentration of 2.5%.

Recovery study and analysis of real samples

Although no severe interferences were encountered in the direct determination of indium by the proposed method, a recovery study was undertaken to test for synergic effects of various sample components. The results are shown in Table 2.

Because the recoveries were in the range 88—105%, a standard addition method was adopted for the analysis of samples. The results obtained by the direct method and after extraction are summarized in Table 3. The relative standard deviation was found to be 3.1% for 11 replicate determinations of the 81-101 river sediment containing 0.18 μg g^{-1} indium. It can be expected, therefore, that the recommended method is applicable to the determination of indium at levels below 1 μg g^{-1} in geochemical samples.

TABLE 2

Recovery of indium from various samples

Sample	Sample weight (mg)	Indium in sample (ng)	Indium added (ng)	Total indium found (ng)	Recovery (%)	
					Direct method	After extraction
Lead-zinc ore	100	1000	1000	1900	90	—
			2000	3050	105	—
River sediment	200	45	20	64	—	95
			40	83	—	95
Coal fly ash	200	32	20	50	—	90
			40	67	—	88
			60	93	—	102

TABLE 3

Determination of indium in samples

Sample	Sample weight (mg)	Indium content ($\mu g\ g^{-1}$)		
		Direct method	After extraction	Reference value[a]
Lead-zinc ore	100	10.5	10.0	10
	(1 mg ml^{-1})[b]	11.0		11
		11.0		
Magnetic pyrites	100	38.0	37.5	36
	(0.4 mg ml^{-1})[b]	38.0		
NIES No. 2 pond sediment (Japan)	200		0.10	
			0.085	
			0.085	
	100		0.095	
81-101 River sediment (China)	200		0.18	
			0.17	
			0.19	
NBS SRM 1633a Coal fly ash	200		0.17	
			0.16	
			0.15	
	100		0.17	

[a]Obtained by anodic stripping voltammetry after extraction. [b]Ascorbic acid added.

REFERENCES

1 D. M. Shaw, Geochim. Cosmochim. Acta, 2 (1952) 185.
2 A. A. Smales, J. van R. Smit and H. Irving, Analyst (London), 82 (1957) 539.
3 K. F. Fouche and A. A. Smales, Chem. Geol., 2 (1967) 5.
4 S. R. Taylor, Geochim. Cosmochim. Acta, 29 (1965) 1243.
5 G. M. Eskenazy and E. I. Mincheva, Analyst (London), 103 (1978) 1179.

6 H. Spitzer and G. Tesik, Z. Anal. Chem., 241 (1968) 218.
7 Jin Long-zhu and Ni Zhe-ming, Can. J. Spectrosc., 26 (1981) 219.
8 Shan Xiao-quan and Ni Zhe-ming, Can. J. Spectrosc., 27 (1982) 75.
9 Shan Xiao-quan, Ni Zhe-ming and Zhang Li, Anal. Chim. Acta, 151 (1983) 179.
10 Shan Xiao-quan, Ni Zhe-ming and Zhang Li, At. Spectrosc., 5 (1984) 1.
11 H. Haraguchi and K. Fuwa, Spectrochim. Acta, Part B, 30 (1975) 535.
12 B. Ya. Spivakov, L. N. Sukhoveeva, K. Dittrich, A. V. Karyakin and Yu. A. Zolotov, Zh. Anal. Khim., 34 (1979) 1947.
13 L. N. Sukhoveeva, G. G. Butrimenko and B. Ya. Spivakov, Zh. Anal. Khim., 35 (1980) 649.
14 W. C. Campbell and J. M. Ottaway, Talanta, 21 (1974) 837.
15 K. Wade and A. J. Banister, Aluminium, Gallium, Indium and Thallium in J. C. Bailar Jr., H. J. Emeleus, R. Nyholm and A. F. Trotman-Dickenson (Eds.), Comprehensive Inorganic Chemistry, Vol. 1, Pergamon Press, Oxford, 1973, p. 1074.
16 S. D. Shets and V. M. Shinde, Analyst (London), 107 (1982) 225.

Analytica Chimica Acta, 171 (1985) 279—284
Elsevier Science Publishers B.V., Amsterdam — Printed in The Netherlands

SENSITIVITY ENHANCEMENT BY PALLADIUM ADDITION IN THE ELECTROTHERMAL ATOMIC ABSORPTION SPECTROMETRY OF MERCURY

LIU PING and KEIICHIRO FUWA

Department of Chemistry, Faculty of Science, University of Tokyo, Hongo, Bunkyo-ku, Tokyo 113 (Japan)

KAZUKO MATSUMOTO*

Department of Chemistry, School of Science and Technology, Waseda University, Okubo, Shinjuku-ku, Tokyo 160 (Japan)

(Received 31st July 1984)

SUMMARY

In graphite-furnace atomic absorption spectrometry of mercury, addition of 50 μg ml^{-1} palladium improves the peak height for 5 μg Hg ml^{-1} 50 times. Further addition of 20 μg ml^{-1} platinum doubles the enhanced peak height. The effect is due to amalgam formation. The best sensitivity is 0.3 ng (1% absorption) and the detection limit is 0.1 ng. The method allows higher ashing temperatures than for solutions without noble metal addition and can be applied to solutions containing substantial amount of organic matter.

Although graphite-furnace atomic absorption spectrometry (a.a.s.) provides convenient and highly sensitive detection for most metals, this is not the case for mercury. Owing to the volatile nature of the element, the sensitivity is not sufficiently high and cold-vapor a.a.s. is normally used for trace determinations [1—4]. Although the latter method has a very low detection limit (ca. 50 pg Hg), the procedure requires a long time per sample compared with the conventional graphite furnace a.a.s. and applications to real samples require conversion to solutions containing a limited range of inorganic substances, because of interference of organic and some inorganic species in the samples. In order to improve the sensitivity for mercury in a.a.s., oxidants such as hydrogen peroxide or potassium permanganate have been added to retain mercury in the furnace up to as high a temperature as possible; this enhances the sensitivity 2—10 times [5, 6]. However, this technique also cannot be applied to solutions containing organic compounds, because the reagent is consumed by the organic species, and therefore is less effective for retaining mercury in the furnace.

As an alternative method of retaining mercury in the furnace, amalgam formation with gold has been studied; the sample, either as the original solid or after dissolution, is heated and mercury is expelled into a gold-plated carbon furnace. After all the mercury has been trapped in the furnace, the

0003-2670/85/$03.30

atomic absorption signal is measured with the tube heated in the normal fashion [7].

In this study, possible enhancement effects were investigated for those elements (Au, Ag, Pt, Pd, Se) which would readily form amalgams or precipitate with mercury. These elements were added in solution to the sample solution before measurement and the graphite furnace was operated normally.

EXPERIMENTAL

Apparatus and materials

A Shimadzu AA-640-13 atomic absorption spectrometer equipped with a Shimadzu GFA-4 graphite-furnace atomizer was used for the measurements. A 30-μl sample was injected into the furnace by an Eppendorf micropipette. The solutions of Hg, Pd, Pt, Au, Ag and Se were 1000 μg ml^{-1} certified standard solutions for atomic absorption spectrometry (Wako Chemicals Co.).

Procedure

Each Au, Ag, Pt, Pd or Se solution was added to the mercury solution prior to injection. The treated sample solution (30 μl) was injected into the furnace, and then dried for 60 s, ashed for 60 s and atomized for 6 s at various temperatures. The furnace was protected from air with an argon flow of 2 l min^{-1}. The mercury atom line at 253.7 nm was used for atomic absorbance measurements.

RESULTS AND DISCUSSION

Effects of Au, Ag, Pt, Pd and Se

In the attempt to minimize the vaporization loss of mercury during ashing, various elements were added at 5—50 μg ml^{-1} concentrations to a mercury solution, and the sensitivities were compared. The results are shown in Fig. 1 for ashing temperatures of 200 and 400°C. Silver and gold enhance the sensitivity when the ashing temperature is 200°C, but at 400°C, no enhancement is observed, which indicates that amalgams of these elements exist only at relatively low temperatures, and are decomposed or vaporized at 400°C. Platinum and selenium further increase the sensitivity. The effect of selenium is probably due to formation of mercury(II) selenide. Palladium showed by far the greatest enhancement effect, about 50-fold, for 50 μg ml^{-1} palladium; this can be further increased to about 100 times by the addition of both 50 μg ml^{-1} palladium and 20 μg ml^{-1} platinum with ashing temperatures of $<$500°C (Fig. 1). Above this temperature, the sensitivity decreases.

Effect of experimental variables

The effect on the sensitivity of the amount of palladium added was studied at 2 μg Hg ml^{-1}, which is around the maximum of the calibration range. The result is shown in Fig. 2. As the palladium increased from 1 $\times$ 10^{-4}% to

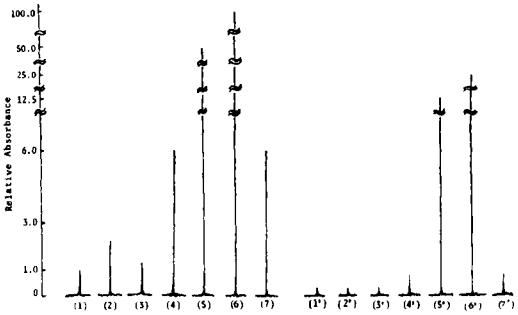

Fig. 1. Effects of Au, Ag, Pd, Pt and Se on the mercury signal obtained by graphite-furnace a.a.s.: (1) 5 μg Hg ml^{-1}; (2) 5 μg Hg ml^{-1} + 50 μg Au ml^{-1}; (3) 5 μg Hg ml^{-1} + 50 μg Ag ml^{-1}; (4) 5 μg Hg ml^{-1} + 50 μg Pt ml^{-1}; (5) 5 μg Hg ml^{-1} + 50 μg Pd ml^{-1}; (6) 5 μg Hg ml^{-1} + 50 μg Pd ml^{-1} + 20 μg Pt ml^{-1}; (7) 5 μg Hg ml^{-1} + 50 μg Se ml^{-1}. Conditions: drying, 150°C for 40 s; ashing, 200°C for 60 s; atomizing, 1400°C for 6 s, for absorption profiles (1)—(7); ashing, 400°C, otherwise as above, for (1')—(7').

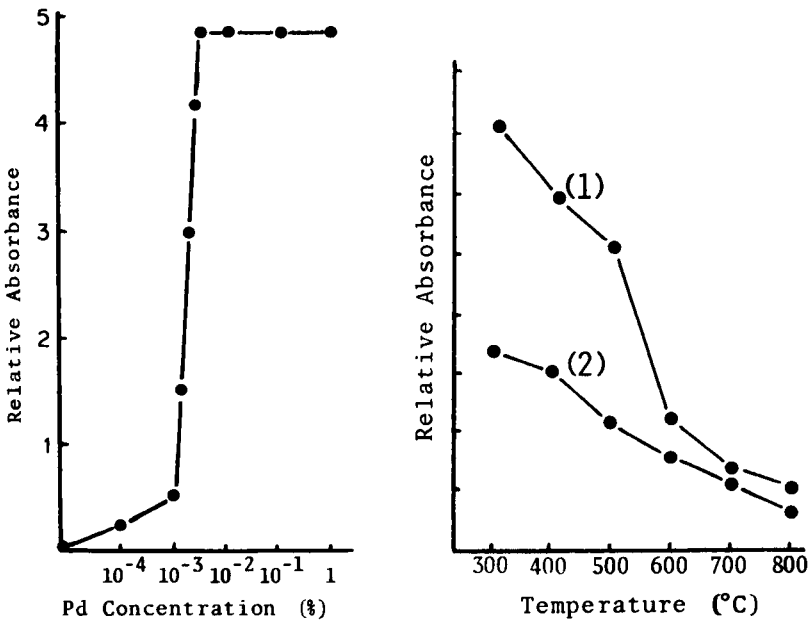

Fig. 2. The effect of palladium concentration on mercury peak height. Conditions: drying, 150°C for 40 s; ashing 450°C for 60 s; atomizing, 1800°C for 6 s; 2 μg Hg ml^{-1}.

Fig. 3. Effect of ashing temperature on mercury peak height: (1) 5 μg Hg ml^{-1}, 100 μg Pd ml^{-1} + 20 μg Pt ml^{-1}; (2) 5 μg Hg ml^{-1} + 100 μg Pd ml^{-1}. Conditions: drying, 150°C for 40 s; ashing, 60 s; atomizing, 2000°C for 6 s.

5×10^{-3}%, the sensitivity increased in proportion; above this level no further increase was observed. Therefore, in the following experiments, the palladium concentration was always adjusted to 1×10^{-2}%.

In Fig. 3, the effect of ashing temperature on the sensitivity is shown for 5 μg Hg ml^{-1}; one solution also contained palladium and the other contained palladium and platinum. It seems that the mercury loss increases with increase in temperature in both cases. The effect of atomizing temperature on mercury sensitivity was investigated for 20 μg Hg ml^{-1} solutions without palladium addition and for 2 μg Hg ml^{-1} solution with 100 μg Pd ml^{-1}. When no palladium was added, an increase in sensitivity was observed only up to 1600°C, whereas in the presence of palladium, maximum sensitivity was at 1800°C, and the sensitivity was 3.5 times greater when palladium was added. This is due to the formation of palladium amalgam, which has an atomizing temperature higher than that of mercury and, therefore, retains mercury in the furnace up to higher temperatures.

Calibration and detection limit

Calibration graphs for mercury in the presence of platinum and palladium, are shown in Fig. 4. The sensitivity in the presence of both noble metals is 0.3 ng (1% absorption). As expected from the study of the effect of ashing temperature, the detection limit is a sensitive function of ashing temperature (Fig. 5). It increases with increasing temperature; a typical value is 10 ng ml^{-1} or 0.1 ng when the ashing temperature is 250°C. The detection limit is defined as the concentration corresponding to twice the relative standard deviation of the background. In the application of the present method to real

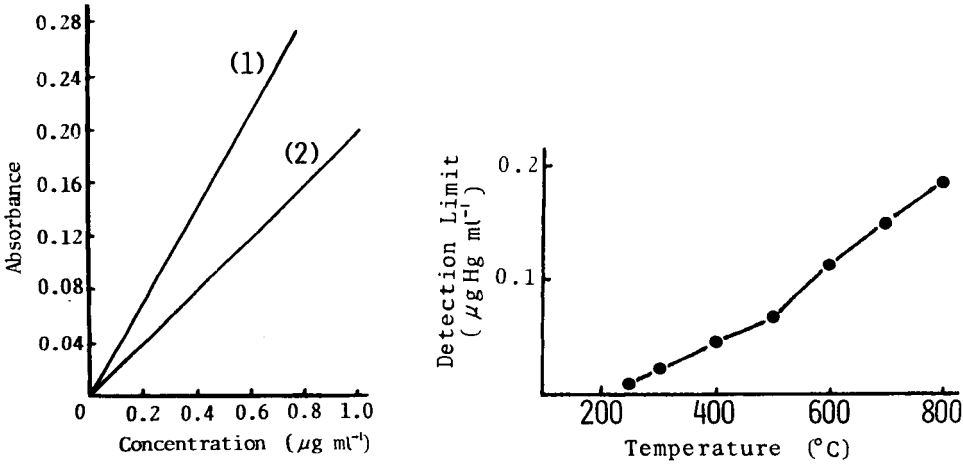

Fig. 4. Calibration graphs for mercury: (1) 100 μg Pd ml^{-1} + 20 μg Pt ml^{-1} added; (2) 100 μg Pd ml^{-1} added. Conditions: 150°C for 40 s; ashing, 250°C for 60 s; atomizing at 2000°C for 6 s.

Fig. 5. Dependence of detection limit on ashing temperature.

samples, therefore, the ashing temperature should be chosen by balancing the necessity to achieve a low detection limit against the temperature needed to remove any organic materials by ashing.

Interference of organic matter

Because the present method enables higher ashing temperatures to be employed, compared to the previous hydrogen peroxide or permanganate addition methods, it was expected that the method could be applied to samples which contain organic substances, unlike the alternative procedures, as explained above. As a typical example, albumin was selected and added to mercury solution. Several solutions were prepared which contained 2 μg Hg ml^{-1}, 100 μg Pd ml^{-1}, 20 μg Pt ml^{-1} and several concentrations of albumin up to 440 μg ml^{-1}. In order to distinguish the mercury atomic absorption from the molecular absorption caused by organic materials, absorptions were measured both with a hollow-cathode lamp and a deuterium lamp. It was found that, up to 40 μg ml^{-1} albumin, no background absorption was observed. Although at higher albumin concentrations, background absorption was observed, this could be subtracted from the total absorption by using the background correction mode. Taking into consideration the background absorbance range which can accurately be corrected in the background correction mode, the experiment showed that the method can be applied to a solution containing albumin or equivalent organic materials up to concentrations of about 0.2%. Although the method can be applied to solutions containing such high concentrations of organic materials, some mercury is lost as the albumin concentration increases and, accordingly, the sensitivity is decreased.

As a typical example of the application of the proposed method, an extract of dolphin liver containing mercury and selenium at high concentrations (ca. 80 μg ml^{-1} on a wet basis) was studied. The liver was extracted with 0.1 M ammonium acetate (pH 7), and chromatographed on an anion-exchange resin. The effect of palladium addition was investigated on the

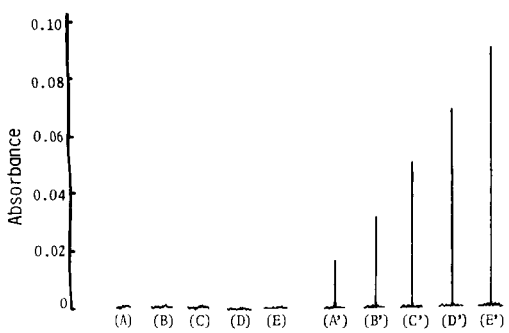

Fig. 6. Mercury responses obtained for a standard addition method with and without palladium addition to a chromatographic eluate from an extract of dolphin liver: (A) no addition; (B) +0.25; (C) +0.50; (D) +0.75; (E) +1.0 μg Hg ml^{-1}. (A'—E') are the same as (A—E) but with 100 μg Pd ml^{-1} added.

eluate, with the results shown in Fig. 6. When palladium was not added, no mercury signal was observed. On addition of 100 μg Pd ml^{-1}, mercury signals were obtained, which increased with increasing mercury concentration.

REFERENCES

1 N. S. Poluektov, R. A. Vitkum and Y. V. Zelyukova, Zh. Anal. Khim., 19 (1964) 937.
2 H. Agemian and A. S. Y. Cau, Anal. Chem., 50 (1978) 13.
3 S.-L. Tong and W.-K. Leow, Anal. Chem., 52 (1980) 581.
4 R. F. Suddendorf, Anal. Chem., 53 (1981) 2234.
5 H. J. Issaq and W. L. Zielinski Jr., Anal. Chem., 46 (1974) 1436.
6 K. Fujiwara, K. Sato and K. Fuwa, Bunseki Kagaku, 26 (1977) 773.
7 D. Siemer and R. Woodriff, Anal. Chem., 46 (1974) 597.

Analytica Chimica Acta, 171 (1985) 285—291
Elsevier Science Publishers B.V., Amsterdam — Printed in The Netherlands

COMPARISON OF TEN DIGESTION PROCEDURES FOR THE DETERMINATION OF ARSENIC IN SOILS BY HYDRIDE-GENERATION ATOMIC ABSORPTION SPECTROMETRY

N. G. VAN DER VEEN, H. J. KEUKENS and G. VOS*

State Institute for Quality Control of Agricultural Products, P.O. Box 230, 6700 AE Wageningen (The Netherlands)

(Received 31st July 1984)

SUMMARY

Ten different digestion methods were investigated for the determination of arsenic in soils by hydride-generation atomic absorption spectrometry. These methods included a dry ashing/digestion, several acid-leaching procedures, and digestions in a pressure decomposition vessel or a Kjeldahl apparatus. A certified reference sample was analysed and the results obtained for five other soil samples were compared with the data obtained by spectrophotometry. A nitric/sulphuric acid digestion was the most suitable. A brief interference study is reported.

The presence of arsenic in food products may cause health problems [1, 2]. In order to locate the origin of arsenic present in vegetables, it is important to know the arsenic content of the soils on which these vegetables are grown. Numerous procedures for the determination of arsenic in a variety of matrices have been described [3—12]. Spectrophotometric methods based on molybdenum blue or silver diethyl dithiocarbamate have been recommended [3, 4]. More recently, methods have been described which are based on the generation of arsenic hydride [5—10]. The arsine is swept into an electrically heated cuvette, in which it is decomposed. Arsenic is usually measured by atomic absorption spectrometry (a.a.s.). This method was found to have considerable advantages in speed, sensitivity and accuracy over the spectrophotometric methods.

For both types of procedure, digestion of soil samples is necessary prior to the measurement. Many decomposition procedures have been described [5—12]. Several acid mixtures have been applied for wet ashing [5—8, 11, 12]. The presence of hydrogen fluoride in acid mixtures, which is necessary to decompose the silicate matrix completely, appeared to cause losses of arsenic by volatilization [6, 11, 12]. A nitric/perchloric acid mixture has been applied successfully by several authors [5—7]. The use of perchloric acid at elevated temperatures, however, requires a specific fume hood for safety precautions, which is not available in many laboratories. Thompson and Thoresby [8] obtained reliable results using a leaching procedure with a

0003-2670/85/$03.30

nitric/sulphuric acid mixture. Alternative methods, often applied to plant materials and foods, are dry ashing with magnesium nitrate [9] and acid digestion under pressure [10].

In the present investigation, ten digestion procedures are compared for the determination of arsenic in soils by a.a.s. with the hydride-generation technique.

EXPERIMENTAL

Apparatus

Arsenic was measured with a Perkin-Elmer Model 300 atomic absorption spectrometer. An arsenic electrodeless discharge lamp was operated according to the manufacturer's instructions. An electrically heated quartz tube was used for atomising arsenic. Arsine generation was done with a Perkin-Elmer MHS-1 system.

For digestions under pressure, Uniseal decomposition vessels were used. The automatic wet digestion device of Budna and Knapp [13] was obtained from Hans Kürner, Neuberg, D.D.R. Muffle furnaces model MI 254-X (Wild Barfield Ltd.) were used for dry ashing.

Before use, all glassware was soaked in (1 + 1) nitric acid (v/v) and rinsed several times with redistilled water.

Reagents

Chemicals of the highest purity available were used throughout. Arsenic(III) standard solutions were prepared from a Merck Titrisol solution by dilution. The potassium iodide solution was prepared by dissolving 4 g of potassium iodide in 25 ml of water. The sodium tetrahydroborate solution was prepared by dissolving first 1.5 g of sodium hydroxide and then 16 g of sodium tetrahydroborate in 250 ml of water. The solution was stirred for 10 min and filtered before use. This solution was prepared daily.

Soil digestion methods

The soil samples were dried at 105°C before the decomposition procedure. The quantities of soil mentioned below in the experimental and results sections refer to dry material, and were accurately weighed.

Method A. A 0.2-g portion of soil was transferred to a teflon pressure decomposition vessel and 1.5 ml of concentrated nitric acid was added. The vessel was closed with its screw cover and heated for 3 h at 140°C in an oven. After cooling to ambient temperature, the digestate was transferred to a 50-ml volumetric flask and diluted to the mark with water.

Method B. A 0.2-g portion of soil was transferred to a test tube, and 7 ml of concentrated nitric acid was added. After standing overnight at room temperature, the solution was transferred to a 50-ml volumetric flask and diluted to the mark with water. (A similar procedure had been found satisfactory for the determination of mercury in soils.)

Method C. A 0.2-g portion of soil was weighed into a test tube. After the addition of 7 ml of concentrated nitric acid, the tube was heated for 3 h on a boiling water bath. After cooling, the digestate was transferred to a 50-ml volumetric flask and diluted to the mark with water.

Method D. A 0.5-g portion of soil was transferred to a 40-ml tube suitable for digestion in the automatic Knapp decomposition device [13]. After addition of 5 ml of concentrated nitric acid, the sample was heated for 3 h at 150°C in the device. After cooling to ambient temperature, the digestate was diluted to the mark on the tube (i.e., to 40 ml) with water.

Method E. A 1-g portion of soil and 4 g of magnesium nitrate were weighed into a beaker. After addition of 5 ml of concentrated nitric acid, the solution was evaporated to dryness on a hot-plate. The beaker was placed in a muffle furnace and the temperature was increased slowly (50°C h^{-1}) to 450°C. This temperature was maintained for 8 h. After the beaker had cooled, 5 ml of concentrated nitric acid was added and evaporated nearly to dryness. The beaker was then placed in the furnace at 450°C for 30 min. The last nitric acid addition and furnace heating was repeated once. The cooled digestate was dissolved in 7.5% hydrochloric acid, transferred to a 100-ml volumetric flask and diluted to the mark with 7.5% hydrochloric acid.

Method F. A 0.2-g portion of soil was weighed into a test tube. After addition of 7 ml of a concentrated nitric acid/hydrochloric acid mixture (3:1) the tube was allowed to stand overnight at room temperature. The sample was diluted with water to 50 ml in a volumetric flask.

Method G. In a test tube, 7 ml of a concentrated nitric acid/perchloric acid mixture (2:1) was added to 0.2 g of soil. After standing overnight at ambient temperature, the digestate was transferred to a 50-ml volumetric flask and diluted to the mark with water.

Method H. A 0.5-g portion of soil was transferred to a 250-ml conical flask, and 20 ml of concentrated nitric acid, 10 ml of (1 + 1) sulphuric acid and a few glass boiling beads were added. The solution was evaporated to fumes of sulphur trioxide over a flame. A few drops of nitric acid were added and evaporation was repeated. This procedure was repeated until a colourless digestate was obtained. The cooled solution was diluted cautiously with about 35 ml of water, transferred to a 100-ml volumetric flask and diluted to the mark with water. A similar procedure has been described by Thompson and Thoresby [8].

Method J. A 6-ml aliquot of concentrated hydrochloric acid and 2 ml of water were added to 0.2 g of soil in a test tube. After heating for 3 h on a boiling water bath, the cooled solution was diluted with water to 50 ml in a volumetric flask.

Method K. A 0.5-g portion of soil was transferred to a 100-ml Kjeldahl digestion flask. After the addition of 5 ml of 30 vol. hydrogen peroxide and a few glass boiling beads, 2.5 ml of concentrated sulphuric acid was added cautiously. The flask was heated gently over a flame. Hydrogen peroxide was added dropwise until a colourless digestate was obtained. After cooling, 5 ml

of water was added and the solution was evaporated until fumes were evolved. After cooling, the digestate was transferred with water to a 100-ml volumetric flask and diluted to the mark with water.

Arsenic measurement

The spectrometer, including the cuvette heater, was switched on and allowed to stabilize for 30 min before use. A 0.2-ml aliquot of digestate was transferred to a reaction vessel of the MHS-1 system, 5 ml of 7.5% hydrochloric acid and 0.25 ml of the potassium iodide solution were added and the vessel was connected to the MHS-1 system. A 2.5-ml aliquot of the sodium tetrahydroborate solution was added and the arsine formed was swept with nitrogen into the quartz cuvette at 1000°C. The arsenic signal was measured at 193.7 nm. Every measurement was made at least in duplicate. The method of standard additions was used. No background correction was applied. The data presented were corrected for blank values, which were usually very low for all the methods studied.

Spectrophotometric determinations of arsenic were done by Rijksdienst IJsselmeer Polders, Lelystad, The Netherlands. After digestion with a mixture containing nitric, sulphuric and perchloric acids and hydrogen peroxide, the silver diethyldithiocarbamate method was applied.

Samples

The certified reference sample (soil 5) was obtained from the International Atomic Energy Agency (IAEA). The remaining samples were obtained from Rijksdienst IJsselmeer Polders. The samples were collected at different sites in the Netherlands and were selected for their range of compositions. Some relevant data on these soil samples are listed in Table 1.

RESULTS AND DISCUSSION

The certified reference sample soil 5 was analysed by use of all ten digestion procedures described above. The results are listed in Table 2. The

TABLE 1

Data on the soil samples investigated

Sample code	$CaCO_3$ (%)	Humus (%)	Slime (%)	Lutum (%)	Arsenic (mg kg^{-1})
Soil 5[a]	—	—	—	—	93.9 ± 7.5
1	<0.5	9.7	61.7	39.4	20.5[b]
2	10.2	3.2	49.2	29.7	14.8[b]
3	8.6	4.3	35.1	19.4	16.3[b]
4	6.4	1.6	16.5	9.1	17.1[b]
5	<0.5	7.9	5.5	2.9	3.2[b]

[a]Certified reference sample from IAEA. [b]Obtained by spectrophotometry.

TABLE 2

The results obtained for the analysis of certified soil 5 (93.9 ± 7.5 mg As kg^{-1}) using 10 different digestion methods

Digestion method	No. of determinations	Mean As conc. found (mg kg^{-1})	R.s.d. (%)	Mean recovery (%)
A	9	106.0	9.8	112.9
B	10	56.5	8.3	60.2
C	22	100.0	11.9	106.5
D	14	93.4	11.9	99.5
E	6	62.3	10.3	66.3
F	12	96.9	12.6	103.1
G	10	50.4	7.8	53.7
H	7	92.7	10.6	98.7
J	4	92.4	14.1	98.4
K	2	107.0	10.7	114.0

acid-leaching procedures with nitric acid (method B) and nitric/perchloric acid mixture (method G), both at room temperature gave incomplete recoveries of arsenic. The low recovery obtained in the dry ashing/digestion procedure (method E) might be partly due to the high magnesium content of the analyte solutions. The effect of high concentrations of magnesium on the recovery of arsenic has been reported previously [14]. Because of the poor results obtained, these three digestion methods were not investigated further. For the remaining seven decomposition procedures, the arsenic concentrations found were in good agreement (i.e., 98—114% recovery) with the certified concentration of 93.9 ± 7.5 mg kg^{-1}.

Owing to the absence of additional certified reference samples, five other soil samples were analysed and the results were compared with those obtained by use of the silver diethyldithiocarbamate method. The recoveries of arsenic obtained by the different digestion procedures are listed in Table 3. The best results were obtained by using the acid-leaching procedure with a nitric/sulphuric acid mixture (method H). Application of this digestion method resulted in satisfactory recoveries for all soils investigated. Thompson and Thoresby [8], who used a similar digestion procedure in combination with hydride generation a.a.s., compared their results with the data obtained by a molybdenum blue spectrophotometric method. They found ca. 20% higher arsenic concentrations by a.a.s., which was believed to reflect the greater inherent accuracy of a.a.s. procedure. The present a.a.s. data are in excellent agreement with the results obtained by the silver diethyldithiocarbamate method. The sulphuric acid/hydrogen peroxide digestion (method K) yielded satisfactory results for all soils except sample 5. This procedure, however, has to be followed very cautiously, which is a major disadvantage.

Based on the data in Table 3 the acid-leaching procedure with the nitric/sulphuric acid mixture was selected for further study. The accuracy of this

TABLE 3

Arsenic recoveries (%) obtained in the analysis of six soil samples by applying seven digestion procedures

Soil sample	Arsenic recoveries (%)[a] from different digestions						
	A	C	D	F	H	J	K
Soil 5	112.9(9)	106.5(22)	99.5(14)	103.1(12)	98.7(7)	98.4(4)	114.0(2)
1	96.1(3)	69.3(5)	70.2(1)	92.4(1)	107.3(10)	100.0(1)	107.3(3)
2	87.2(3)	60.8(4)	86.5(1)	80.3(1)	103.4(8)	62.8(1)	102.0(3)
3	92.0(3)	74.8(4)	77.3(1)	79.8(1)	107.4(7)	87.7(1)	100.6(3)
4	110.5(3)	82.5(4)	100.6(1)	95.9(1)	103.5(6)	100.0(1)	111.1(3)
5	71.9(3)	65.6(4)	81.2(1)	46.9(1)	100.0(7)	75.0(1)	71.9(3)
R.s.d.[b]	19.9	24.6	15.6	19.5	11.6	16.5	17.4

[a]Recoveries with respect to the arsenic values in Table 1; the number of replicate determinations is given in parentheses. [b]Relative standard deviation (%) for all samples.

method was tested further on the basis of recovery experiments, the results of which are listed in Table 4. An average recovery of 102 ± 11% was obtained. These results confirm the conclusion that this digestion procedure is suitable for the determination of total arsenic in soils.

The occurrence of interference effects on the generation of the arsine was investigated by making standard additions of arsenic(III) to several solutions containing possible interfering metal ions. The presence of 40 mg l^{-1} selenium did not suppress the arsenic signal. It may be assumed that, upon addition of potassium iodide, selenium(IV) is reduced to elemental selenium, thereby eliminating possible interference by this element. A cation solution containing 20 mg l^{-1} zinc, 5 mg l^{-1} each of Cr, Cu, Fe and Pb, 2 mg l^{-1} nickel and 0.1 mg l^{-1} each of Cd, Co and Hg did not interfere. In the presence of 200 mg l^{-1} zinc, 50 mg l^{-1} each of Cr, Cu, Fe and Pb, 20 mg l^{-1} nickel, and 1 mg l^{-1} each

TABLE 4

Recoveries obtained with nitric/sulphuric acid digestion (method H) after standard additions

Soil sample	Mean recovery (%)[a]		
	1 ng As[b]	10 ng As[b]	20 ng As[b]
Soil 5	—	99(1)[a]	105(2)
1	—	110(2)	—
2	—	101(5)	102(2)
3	—	96(2)	—
4	—	111(3)	—
5	89(2)	—	—

[a]No. of results in parentheses. [b]Amount of arsenic added to 0.5 g of sample.

of Cd, Co and Hg, 20% suppression of the signal was observed. These data indicate that no significant metal interferences are normally to be expected in the determination of arsenic in soils, when the procedure recommended in this paper is applied. Furthermore, small signal suppressions can usually be corrected for by applying the method of standard additions. Interferences in the determination of arsenic by hydride-generation a.a.s. have been studied extensively by Pierce and Brown [15].

Conclusions

In the present paper, ten different digestion procedures for the determination of arsenic in soils by a.a.s. have been compared. Eight digestion methods, including a digestion in a pressure decomposition device, proved to be inadequate. A procedure with sulphuric acid and hydrogen peroxide yielded acceptable results for all samples except one. This method, however, needs careful handling. The best results were obtained with a nitric/sulphuric acid leaching procedure. Although testing was not exhaustive, the data show that this method is capable of yielding reasonably accurate and precise results. Serious interference effects caused by metal ions are not likely, but it is advisable to quantify the data by applying the method of standard additions. Although the proposed digestion method is probably applicable to all kinds of soil sample, it is recommended that the performance of the procedure be checked before the analysis of samples with a composition considerably different from the soils listed in Table 1.

The authors thank Mrs. A. C. H. Driessen and Mr. J. C. Moraal for doing some of the experiments.

REFERENCES

1 H. W. Lakin, Adv. Chem. Ser., 123 (1973) 96.
2 A. Pelfrene, J. Toxicol. Environ. Health, 1 (1976) 1003.
3 Official Methods of Analysis, 12th edn., AOAC, Washington, DC, Sect. 25.006—25.019, 1975.
4 Analytical Methods Committee, Analyst (London), 100 (1975) 54.
5 K. S. Subramanian, Fresenius, Z. Anal. Chem., 305 (1981) 382.
6 S. Bajo, Anal. Chem., 50 (1978) 649.
7 B. Pahlavanpour, J. H. Pullen and M. Thompson, Analyst (London), 105 (1980) 274.
8 A. J. Thompson and P. A. Thoresby, Analyst (London), 102 (1977) 9.
9 G. K. H. Tam and G. Lacroix, J. Assoc. Off. Anal. Chem., 65(3) (1982) 647.
10 M. Stoeppler and F. Backhaus, Fresenius Z. Anal. Chem., 291 (1978) 116.
11 Z. Sulsek, P. Povondra and J. Dolezal, CRC Crit. Rev. Anal. Chem., 6 (1977) 255.
12 S. Terashima, Anal. Chim. Acta, 86 (1976) 46.
13 K. W. Budna and G. Knapp, Fresenius Z. Anal. Chem., 294 (1979) 122.
14 G. K. H. Tam and G. Lacroix, Int. J. Environ. Anal. Chem., 8 (1980) 283.
15 F. D. Pierce and H. R. Brown, Anal. Chem., 48 (1976) 693; 49 (1977) 1417.

Analytica Chimica Acta, 171 (1985) 293—301
Elsevier Science Publishers B.V., Amsterdam — Printed in The Netherlands

EFFECT OF MATRIX MODIFIER AND FURNACE MATERIAL ON THE DETERMINATION OF TRACES OF FLUORIDE BY ELECTROTHERMAL MOLECULAR ABSORPTION SPECTROMETRY OF ALUMINUM MONOFLUORIDE

KAZUYOSHI ITAI* and HUMIO TSUNODA

Department of Hygiene and Public Health, School of Medicine, Iwate Medical University, 19-1 Uchimaru, Morioka 020 (Japan)

MASAHIKO IKEDA

Nippon Jarrel-Ash Co. Ltd., Shimotoba, Fushimi-ku, Kyoto 612 (Japan)

(Received 20th February 1984)

SUMMARY

In the determination of fluoride by AlF absorbance measurements, the interference from strontium nitrate is avoided by using magnesium nitrate or barium nitrate added to aluminum solution as the matrix modifier. The effects of the graphite-furnace material on AlF absorbance are investigated. Glassy carbon and synthetic carbon gave longer furnace lifetimes and better sensitivity than the other materials tested. The maximum sensitivity (4.2 μg ml^{-1} fluoride for 0.0044 absorbance with a 10-μl injection) was obtained with synthetic carbon. The r.s.d. was $<5\%$ for 0.1 μg ml^{-1} fluoride (n = 10). Na^+, K^+, Pb^{2+}, Zn^{2+}, Cu^{2+} and Ag^+ did not affect the measurements up to 500 μg ml^{-1}, but Ni^{2+}, Co^{2+}, Fe^{2+}, Sr^{2+} and especially Ca^{2+} depressed the absorbance.

A fluoride ion-selective electrode method [1] is generally used for the determination of fluoride. This method has a better detection limit than spectrophotometric determinations such as the lanthanum/alizarin fluoride blue method [2, 3]. Molecular absorption spectrometry based on aluminum monofluoride has been reported for the determination of ultra-traces of fluoride [4, 5]. This method has some advantages; the sample volume is very small (5—20 μl) and the sensitivity is high enough for fluoride to be determined at the μg l^{-1} level [6, 7]. However, this method requires strontium nitrate as a matrix modifier [4, 6, 7], and the sensitivity for low concentrations of fluoride gradually decreases for each firing of the graphite furnace used for generating the aluminum monofluoride vapor. Also, the graphite furnace rapidly deteriorates because the vapor generation stage requires a very high temperature (2700—2900°C), and the previous stage, which converts fluoride in the sample solution to a relatively refractory compound (e.g., magnesium fluoride), requires a relatively high temperature (700—800°C) for a long time [7]. Therefore, the sensitivity of the AlF absorbance may be changed greatly and the precision will decrease, because of ageing of the graphite furnace.

0003-2670/85/$03.30

This paper reports a matrix modifier which is free from interference with co-existent ions, and a graphite furnace material which gives continuing high sensitivity and precision.

EXPERIMENTAL

Apparatus, reagents and materials

A Nippon Jarrell-Ash atomic absorption spectrometer (Model AA-855) equipped with a deuterium simultaneous background correction system and a graphite-furnace atomizer (Model FLA-100) were used. A Hitachi HLA-4S platinum hollow-cathode lamp was used as the radiation source for measuring the AlF absorbance. A Nippon Jarrell-Ash Model MC-100 microprocessor readout system was used to give the peak height of the AlF signal.

A standard fluoride solution was prepared by dissolving analytical-grade sodium fluoride (Wako Pure Chemicals) in distilled water. A 1.0 M aluminum solution was prepared by dissolving 0.745 g of aluminum metal powder (99.5%, Wako) in 40—50 ml of concentrated nitric acid and diluting to 250 ml with distilled water.

All metal salts used in the interference study were nitrates. Titanium chloride and tantalum chloride were dissolved in ethanol, and niobium chloride, sodium tungstate, sodium molybdate and zirconyl nitrate were dissolved in distilled water. They were used as soaking solutions (ca. 1.0 M) to form metal carbides on the graphite furnace surface by Zatka's method [8].

Ringsdorf RW003 (Bonn, Bad Godesberg, West Germany), National Carbon S-6 (New York) and Mitsubishi pencil F-15 and C-51 (Takeishi Fujioka, Gunma) were used in this study. The RW003 is rich in natural crystal graphite (NCG); it was treated to form metal carbides (NCG/MeC) for some experiments. Carbon S-6 is relatively porous graphite which is rich in natural amorphous graphite; it was also treated with metal carbides (NAG/MeC) for some experiments. The F-15 is glassy carbon (GC) and C-51 is synthetic carbon (SC); these materials are made mainly from artificial graphite.

Argon used as the purge gas required purification as it contained fluorine as an impurity. An argon flow for 5 min at 2 l min^{-1} gave an AlF signal equivalent to an 0.1 μg ml^{-1} fluoride solution. Therefore, the argon was passed through 0.5 M sodium hydroxide and a column filled with active charcoal to eliminate fluorine before passing to the graphite furnace.

Procedure

The instrumental conditions used were as follows. The wavelength was 227.5 nm, with a spectral bandwidth of 0.34 or 0.68 nm. The argon flow was 2.0 l min^{-1}. A 10-μl aliquot of 0.05 M aluminum solution was injected into the furnace, and dried for 20 s at 150° C. After the furnace had cooled, 10 μl of sample solution was added, dried for 30 s at 150° C and ashed at 710° C for 30 s. Vapor generation was done at 2800° C for 7 s. A step mode was used for the last two stages. Matrix modifiers (magnesium nitrate or barium nitrate) were added in the aluminum solution (see below).

RESULTS AND DISCUSSION

Effect of matrix modifier

Although an increase in fluoride sensitivity is achieved by addition of strontium, iron or nickel as nitrates to the aluminum solution [4, 6], AlF absorption signals cannot be detected at low concentrations of fluoride (10 ng ml^{-1}), and the sensitivity for up to 50 ng ml^{-1} fluoride gradually decreases with each firing when 0.02 M strontium nitrate is added to 0.02 M aluminum solution. Generally, metal ions such as magnesium and calcium react readily with fluoride, and this is often utilized in metal refining by distillation [9]. The compounds formed have low vapor pressures, so that a high ashing temperature can be applied to segregate fluoride from an organic matrix or metals with high vapor pressures.

The effect of alkaline earth metals on AlF absorption was studied. Aluminum powder (99.5%) was dissolved in nitric acid (the commercially available aluminum nitrate from Wako was found to contain traces of fluoride) and diluted to give a 0.05 M aluminum solution; enough magnesium nitrate, calcium nitrate, strontium nitrate or barium nitrate to give a 0.05 M solution was added. Figure 1 shows calibration graphs for 5—200 ng ml^{-1} fluoride. When calcium or strontium nitrate was added to the aluminum solution, the calibration graphs were not linear below 50 ng ml^{-1} fluoride, especially for

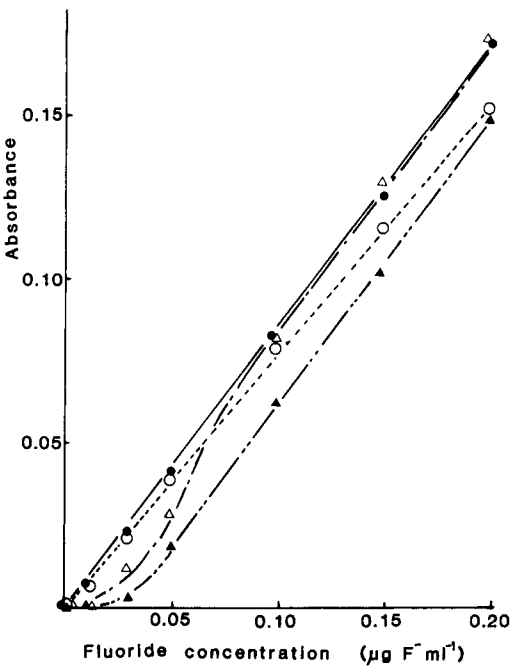

Fig. 1. Fluoride calibration graphs obtained by use of 0.05 M metal nitrate/0.05 M aluminum solution: (●) Ba^{2+}; (○) Mg^{2+}; (△) Sr^{2+}; (▲) Ca^{2+}.

calcium nitrate. The magnesium or barium salts did not cause non-linearity, and barium nitrate gave the higher sensitivity. Dittrich and Meister [10] reported an improvement in the detection limit by addition of barium. They concluded that the reason for this improvement was that the barium species not only evaporated later than other metal species, as they partly reacted with the carbon of the furnace, but also they led to a more coincident evaporation of the aluminum. Consequently, the maximum fluoride concentration in the vapor occurred at the same time as the maximum aluminum concentration [10, 11]. Magnesium can also react with the carbon, but less extensively than barium. Because the boiling temperature of magnesium oxide is higher than that of barium oxide, when magnesium nitrate is used as a matrix modifier, aluminum evaporates later than the fluoride [12]. This produces a time difference between the appearances of maximum fluoride concentration and maximum aluminum concentration in the vapor when magnesium nitrate serves as matrix modifier. The time difference is highly critical. It can easily be influenced by graphite furnace materials and sample matrix.

The AlF absorption spectra obtained from 0.1 μg ml^{-1} fluoride, 0.01 M aluminum and 0.01 M magnesium nitrate, calcium nitrate, strontium nitrate or barium nitrate are shown in Fig. 2. Figure 2(b) shows some calcium atomic absorption, and Fig. 2(c) some strontium atomic absorption of the deuterium radiation. Because AlF absorption is measured only a little more quickly than calcium or strontium atomic absorption, they overlap. Therefore, background over-correction seems to occur when calcium nitrate or strontium nitrate serves as matrix modifier. The effect is greater at lower fluoride concentrations, as can be seen in Fig. 1. The differences in the calibration graphs below 50 ng ml^{-1} fluoride when calcium or strontium nitrate is used can be ascribed to the difference between the calcium and strontium atomic absorbances. Magnesium and barium nitrate do not show an atomic absorption signal near 227.5 nm, so that the calibration graphs show good linearity between 10 and 50 ng ml^{-1} fluoride.

The dependence of AlF absorbance on the spectral bandwidth is very small. There is no difference in the absorbance for bandwidths between 0.34 and 0.68 nm, but the intensity decreases slightly by 1.37 nm. At 1.37 nm, the strong aluminum atomic absorption at 226.93 nm is measured by the deuterium lamp, so background over-correction seems to occur. Therefore, the spectral bandwidth of the spectrometer was set at 0.68 nm.

Effect of graphite-furnace materials

The graphite furnace may wear appreciably, forming aluminum carbide. Therefore the AlF absorption signal may also change, because the atomization temperature is so high (2700—2900° C) and the concentration of the aluminum solution is also high in this method. The properties required of the material used for the graphite furnace are to give high sensitivity and long-term stability.

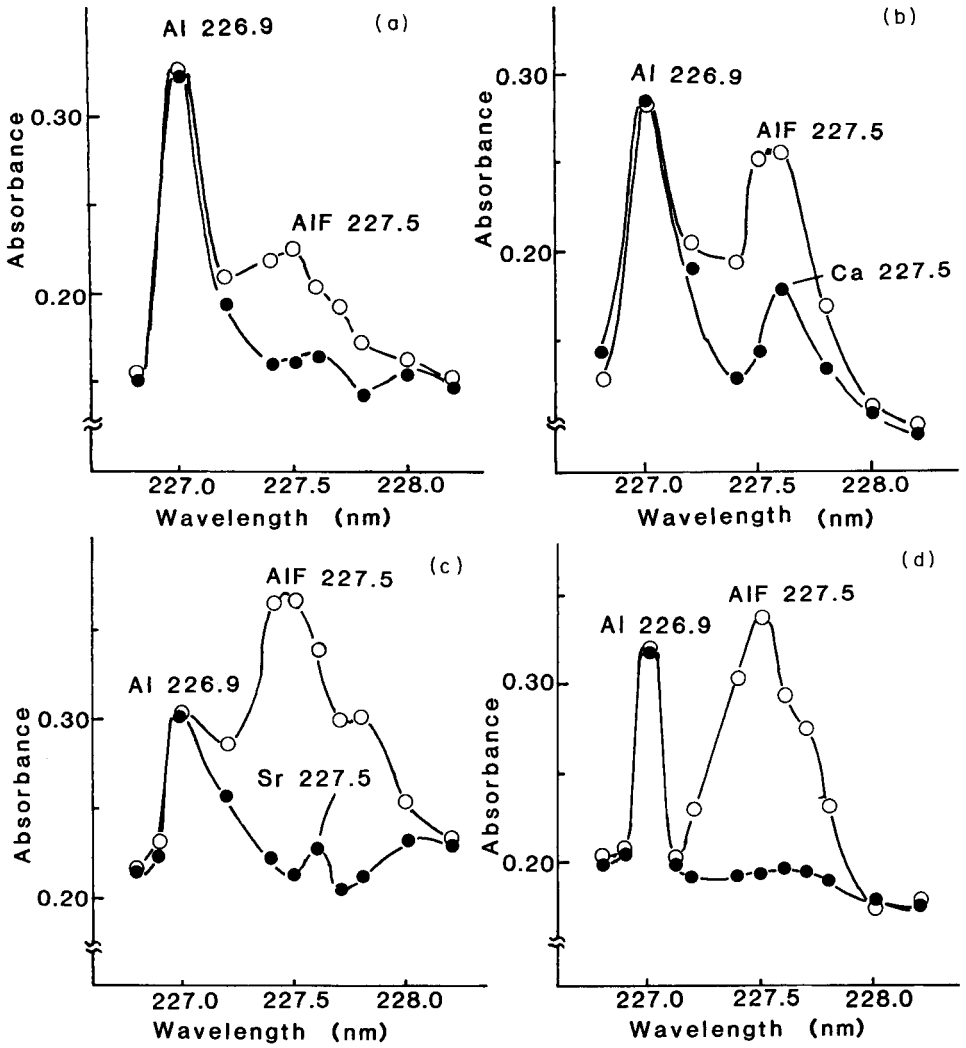

Fig. 2. Absorption spectra obtained from: (•) 0.01 M Al^{3+}; (○) 0.01 M Al^{3+} + 0.20 μg ml^{-1} fluoride. Salt added: (a) $Mg(NO_3)_2$; (b) $Ca(NO_3)_2$; (c) $Sr(NO_3)_2$; (d) $Ba(NO_3)_2$ (all 0.01 M).

Table 1 shows the results obtained for four kinds of furnace materials. For each, magnesium nitrate or barium nitrate was added to 0.05 M aluminum solution as the matrix modifier. As shown in Table 1, the absorbance of AlF absorption depends on both the furnace material and the matrix modifier. Molybdenum, niobium, tungsten, titanium, tantalum and zirconium were used to form refractory metal carbides over the entire inner surface of the furnace by Zatka's method [8]. Generally, these metal carbides have high melting points and are chemically inert. But the relative absorbances obtained

TABLE 1

Relative absorbance for 0.10 $\mu g\ ml^{-1}$ fluoride with different furnace materials

Furnace material	Relative absorbance			
	$Ba(NO_3)_2$ (M)[a]		$Mg(NO_3)_2$ (M)[a]	
	0.015	0.05	0.015	0.05
NCG[b]	1.00	0.81	0.70	0.70
NAG[c]				
—MoC	0.66	0.61	0.67	0.54
—NbC	0.66	0.60	0.71	0.60
—WC	0.68	0.51	0.78	0.61
—TiC	0.72	0.51	0.59	0.47
—TaC	0.49	0.49	0.61	0.53
—ZrC	0.60	0.46	0.61	0.49
NCG				
—NbC	0.81	0.87	0.87	0.91
—WC	0.51	0.76	0.52	0.86
GC[d]	0.79	1.09	0.77	0.70
SC[e]	1.20	1.04	0.94	0.81

[a]Each reagent was added to 0.05 M aluminum solution. [b]Natural crystal graphite. [c]Natural amorphous graphite. [d]Glassy carbon. [e]Synthetic carbon.

with these carbides were less than that with NCG. When these metal carbides are used for the furnace, barium or magnesium fluoride may vaporize at relatively low temperatures, so that fluoride evaporation is faster than that of aluminum. In the GC and SC furnaces, slightly higher absorbances were obtained than with NCG. In the GC, SC and NCG furnaces, slightly higher relative absorbances were obtained when barium nitrate rather than magnesium nitrate was the matrix modifier.

The effects of the concentrations of matrix modifiers for the NCG, NCG/NbC, GC and SC furnaces were studied. The results are shown in Fig. 3. Barium nitrate was used as the matrix modifier for the NCG, GC and SC furnaces, and magnesium nitrate for the NCG/NbC furnace. With all furnaces, the changes of AlF absorbance were not great for 0.01—0.1 M barium or magnesium nitrate, but the absorbances decreased slightly as the concentration of barium or magnesium nitrate increased. When large amounts of barium or magnesium were added, the aluminum and fluoride evaporated more slowly.

The effects of aluminum concentration were examined. The results are shown in Fig. 4. In NCG and GC furnaces, the AlF absorbance is constant for 0.01—0.06 M aluminum, but is slightly decreased above 0.07 M. In NCG/NbC and SC furnaces, the absorbance is constant for 0.01—0.10 M aluminum. Tsunoda et al. [4] studied the effect of the amount of aluminum on AlF absorbance. They reported that the absorbance became constant above 0.01 M aluminum. Dittrich [5] also reported that the absorbance was constant above

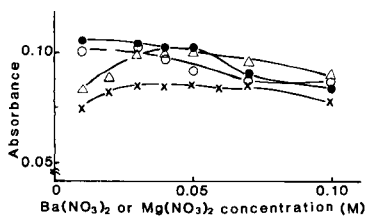

Fig. 3. Effect of concentration of barium or magnesium nitrate added to 0.05 M aluminum solution on the absorbance from 0.10 μg ml^{-1} fluoride in different furnaces: (○) NCG; (×) NCG/NbC; (△) GC; (●) SC. Magnesium nitrate was used for NCG/NbC, and barium nitrate for the other furnaces.

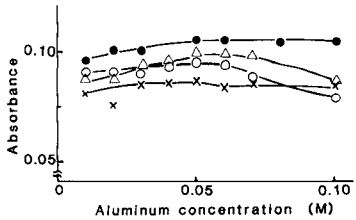

Fig. 4. Effect of concentration of aluminum on absorbance from 0.10 μg ml^{-1} fluoride. Other conditions as in Fig. 3.

1 μg Al^{3+} in 10 μl when 100 μg of sodium nitrate was added. The effect of aluminum concentration on AlF absorbance may be influenced by the sample matrix [7].

The effects of ashing temperature were studied as shown in Fig. 5. With all the graphite furnace materials, the AlF absorbance was not changed between 400 and 900°C, but above 1000°C, the absorbance was greatly decreased. Barium or magnesium fluoride are converted to barium or magnesium oxide above this temperature. Therefore, an ashing temperature of 710°C is recommended.

Figure 6 shows the effects of atomizing temperature on AlF absorbance. For all the graphite furnace materials used, the absorbance gradually increased as the atomizing temperature increased between 2500 and 3100°C. But, as the atomizing temperature is increased, the lifetime of the furnace decreases, so the recommended atomizing temperature is 2800°C.

The maximum sensitivity is obtained with the synthetic carbon furnace; 4.2 μg ml^{-1} fluoride (10-μl injection) is the concentration that shows an absorbance of 0.0044. The sensitivities in the GC, NCG and NCG/NbC furnaces are 4.5, 5.0 and 5.2 μg ml^{-1} fluoride, respectively. Calibration is linear up to 0.2 μg ml^{-1} fluoride in all furnaces, and the relative standard deviation for the use of each graphite furnace material is <5% (0.1 μg ml^{-1} fluoride; n = 10).

Table 2 shows the effects of various cations in the fluoride solution on AlF absorbance, under the recommended conditions. Even if 500 μg ml^{-1} Na^+, K^+, Zn^{2+}, Pb^{2+}, Cu^{2+} or Ag^+ were present, no effect was observed for any of the graphite furnace materials. But when Ni^{2+}, Co^{2+}, Fe^{2+}, Sr^{2+} and especially Ca^{2+} were present, the absorbance was decreased. Accurate background correction was not achieved, because background correction was increased by atomic absorption of these metals near 227.5 nm [13], which overlapped the AlF absorption.

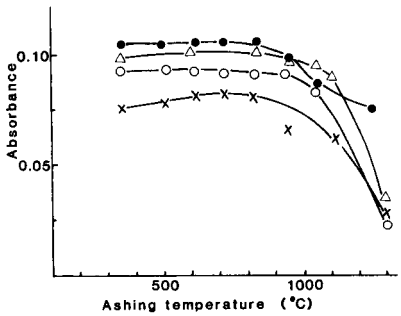

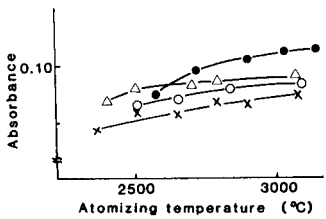

Fig. 5. Effect of ashing temperature on absorbance from 0.10 μg ml^{-1} fluoride, with 0.05 M aluminum. Conditions otherwise as in Fig. 3.

Fig. 6. Effect of atomizing temperature. Conditions otherwise as in Fig. 5.

TABLE 2

Effect of various cations on the recovery of 0.10 μg ml^{-1} fluoride with different furnace materials

Cation[a]	Fluoride recovery (%)							
	500 mg l^{-1}				1000 mg l^{-1}			
	NCG	NCG/NbC	GC	SC	NCG	NCG/NbC	GC	SC
None	100	100	100	100	100	100	100	100
Na^+	104	110	98	103	102	100	97	99
K^+	102	111	100	101	101	97	97	95
Zn^{2+}	100	105	100	103	88	92	100	94
Pb^{2+}	99	104	99	108	100	93	102	93
Cu^{2+}	92	104	99	102	88	93	96	98
Ag^+	101	99	98	100	93	81	95	90
Ni^{2+}	88	100	95	99	61	73	93	89
Co^{2+}	82	101	92	85	73	81	90	87
Fe^{2+}	91	87	91	93	74	65	83	87
Sr^{2+}	83	93	92	89	85	94	88	78
Mg^{2+}	84	—	82	83	79	—	82	90
Ca^{2+}	74	89	78	71	53	84	68	49

[a]Added as nitrate.

The lifetimes of the NCG/NbC, GC and SC furnaces were twice as long as that of NCG. The sensitivities in the GC and SC furnaces were higher than that in NCG/NbC. Therefore, it is concluded that glassy and synthetic carbon are superior to the other materials as the furnace material for the determination of fluoride by measurement of AlF absorbance.

REFERENCES

1 M. S. Frant and J. W. Ross, Science, 154 (1966) 1553.
2 R. Belcher, M. A. Leonard and T. S. West, Talanta, 2 (1959) 92.
3 R. J. Hall, Analyst (London), 88 (1963) 76.
4 K. Tsunoda, K. Fujiwara and K. Fuwa, Anal. Chem., 49 (1977) 2035.
5 K. Dittrich, Anal. Chim. Acta, 111 (1979) 123.
6 K. Tsunoda, K. Chiba, H. Haraguchi and K. Fuwa, Anal. Chem., 51 (1979) 2059.
7 S. Fujimori, K. Itai and H. Tsunoda, Fluoride, 17 (1984) 27.
8 V. J. Zatka, Anal. Chem., 50 (1978) 538.
9 C. Hayashi and K. Muramatsu, Vacuum Metallurgy, Nikkan Kogyo Shinbun, Tokyo, 1965, p. 206.
10 K. Dittrich and P. Meister, Anal. Chim. Acta, 121 (1980) 205.
11 K. Dittrich, Prog. Anal. At. Spectrosc., 3 (1980) 209.
12 W. Slavin, G. R. Carnrick and D. C. Manning, Anal. Chem., 54 (1982) 621.
13 G. R. Harrison (Ed.), Wavelength Tables, The MIT Press, Cambridge, MA, 1969.

Analytica Chimica Acta, 171 (1985) 303—312
Elsevier Science Publishers B.V., Amsterdam — Printed in The Netherlands

SPECTROPHOTOMETRIC DETERMINATION OF ACIDITY-CONSTANTS OF UNSTABLE COMPOUNDS BY FLOW INJECTION ANALYSIS

A. RÍOS, M. D. LUQUE DE CASTRO and M. VALCÁRCEL*

Department of Analytical Chemistry, Faculty of Sciences, University of Córdoba, Córdoba (Spain)

(Received 6th April 1984)

SUMMARY

Spectrophotometric methods of determining acidity constants of ligands in solution can be used satisfactorily for the determination of such constants of unstable ligands by flow injection analysis. The technique can also be used in the stopped-flow mode, to allow the extent of the reaction causing the instability to be established. The procedures are applied to glyoxal bis(2-hydroxyanil), 6-methylpicolinaldehyde azine, 2-hydroxybenzaldehyde hydrazone and benzoylpyridine oxime.

When new analytical methods are developed, the physicochemical features of a reagent or ligand are studied, but it is very common not to take into account the possibility of the compound undergoing irreversible changes under the working conditions, with total or partial transformations that hinder its activity [1, 2]. When the acid-base behaviour of a reagent is studied, the presence of hydrogen ions or hydroxide ions can be a cause of instability of the compound, owing to their high concentration (extreme pH values) or because they catalyze a side-reaction of the reagent, thus diminishing its concentration. Sometimes the reagent can react with itself under the experimental conditions. Causes of instability such as the presence of oxidizing or reducing substances are easily detected, but others such as atmospheric oxidation or photochemical decomposition may go unnoticed. Many of these reactions take place so quickly that by the time the measurements by conventional methods have been made, the reaction causing the instability, has reached equilibrium. Therefore, many analytical methods involve the use of a large excess of reagent or make measurements once stable conditions have been attained. Flow injection analysis (f.i.a.) can avoid or diminish the extent of undesirable reactions by considerably decreasing the interval between the mixing of the reagents and detection of the product.

On this basis, f.i.a. is used here for the spectrophotometric determination of the acidity constants of unstable compounds, and previous values are shown to be erroneous. By using f.i.a. in the stopped-flow mode, the extent of the instability is measured, and, by comparing the measurements made before and after equilibrium has been reached, conclusions about the nature

0003-2670/85/$03.30

of the reactions involved can be drawn. Ramsing et al. [3] reported a manifold for determining pK_a values with no injection system; it consisted of a gradient vessel, the pH of which was changed at a fixed rate and recorded against the absorbance of the continuously circulating solution on an x-y recorder. This manifold is not suitable for unstable compounds.

EXPERIMENTAL

Reagents

All reagents were of analytical-reagent grade and solutions were prepared with distilled water. Glyoxal bis(2-hydroxyanil) solutions were 0.05% (w/v) in methanol, or 0.025% in 1:1 methanol/water. 6-Methylpicolinaldehyde azine and 2-hydroxybenzaldehyde hydrazone solutions were 0.05% in ethanol, or 0.025% in 1:1 ethanol/water. The former reagent was synthesized from stoichiometric amounts of 6-methylpicolinaldehyde and hydrazine [4, 5], and the latter by adding an excess of hydrazine hydrate to 2-hydroxybenzaldehyde [6]. Benzoylpiridine oxime solutions were 0.05% (w/v) in ethanol, or 0.025% in 1:1 ethanol/water. The reagent was synthesized by refluxing a stoichiometric mixture of benzoylpyridine and hydroxylammonium chloride neutralized with sodium carbonate [7].

Apparatus and procedures

A Pye-Unicam SP6-500 spectrophotometer connected to a Radiometer REC 80 recorder was used. A FIAtron 721 cell was connected to a Beckman 3500 pH meter for continuous pH control. The glass/calomel combined microelectrode was calibrated by circulating buffer solutions (Merck) through the flow cell at the working flow rate. A Tecator 5020 analyzer with a microprocessor was used for stopped-flow measurements. A Tecator L-100-1 injection valve and a Tecator TM-II "Chemifold" were also used.

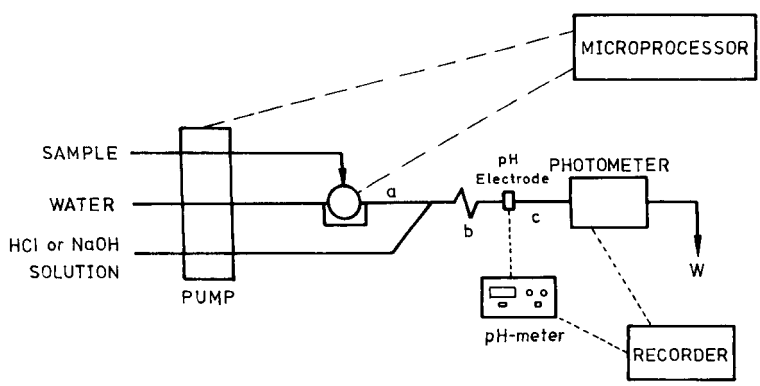

Fig. 1. Manifold used to provide data for the calculation of the pK_a values of unstable compounds: (a) 15 cm; (b) 35 cm; (c) 15 cm; overall flow rate, 1.40 ml min^{-1}; volume injected, 44.2 μl; inner diameter of tubing, 0.5 mm.

Flow-injection system. A schematic diagram of the manifold is shown in Fig. 1. The reagent is injected into a distilled water stream which later merges with a hydrochloric acid or sodium hydroxide stream, thus allowing the pH of the sample to be changed, and continuously monitored by the electrode placed immediately before the spectrophotometric detector. In this way, the combination of absorbance and pH values needed to calculate the pK_a values of the reagents studied is obtained and the conventional method of Stenstrom and Goldsmith [8] can be applied.

Given the instability of the reagents studied, the variables in the manifold were optimized in order to minimize the time interval between injection and detection. Nevertheless, this interval must be long enough to ensure perfect mixing between the sample and the acidic or basic solution. The optimal values found for these variables are shown in Fig. 1. The delay time was 30 s; the residence time was 26 s.

RESULTS AND DISCUSSION

In the study reported, measurements of the absorbance were made at the peak maxima recorded at different pH values, and absorbance/time plots were recorded in the stopped-flow mode, which permits the instability of the reagent to be quantified at each pH value. When changes in absorbance are due only to acid-base equilibria, they can be detected by the absorbance at the peak maximum as well as by the final absorbance of the stopped-flow curves, which are comparable to the absorbances obtained by conventional spectrophotometric techniques. The variations of absorbance caused by reagent instability under given working conditions can be shown by stopped-flow measurements, whereas they will not be shown significantly in normal recordings in a flow-injection system.

Determination of acidity constants in a flow-injection system

Glyoxal bis(2-hydroxyanil) (GBHA). This reagent has often been used for the spectrophotometric determination of calcium [9, 10]. The well-known instability of its aqueous solutions has been studied by Lindstrom and Milligan [11]. The absorption spectra of GBHA show a band (λ_{max} = 295 nm) at all pH values and another (λ_{max} = 450 nm) at strongly alkaline pH. These wavelengths were chosen to study the influence of pH on GBHA by both flow-injection procedures. Figure 2(a) shows the results found by normal f.i.a. at the two wavelengths and various pH values. Increases in absorbance are found above pH 11.5, small for the u.v. band and larger for the visible band. Both may be attributed to deprotonation of the hydroxyl group:

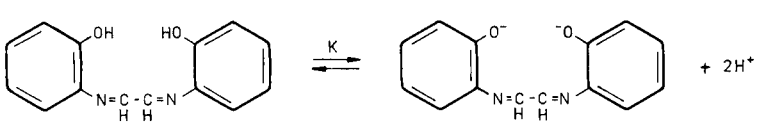

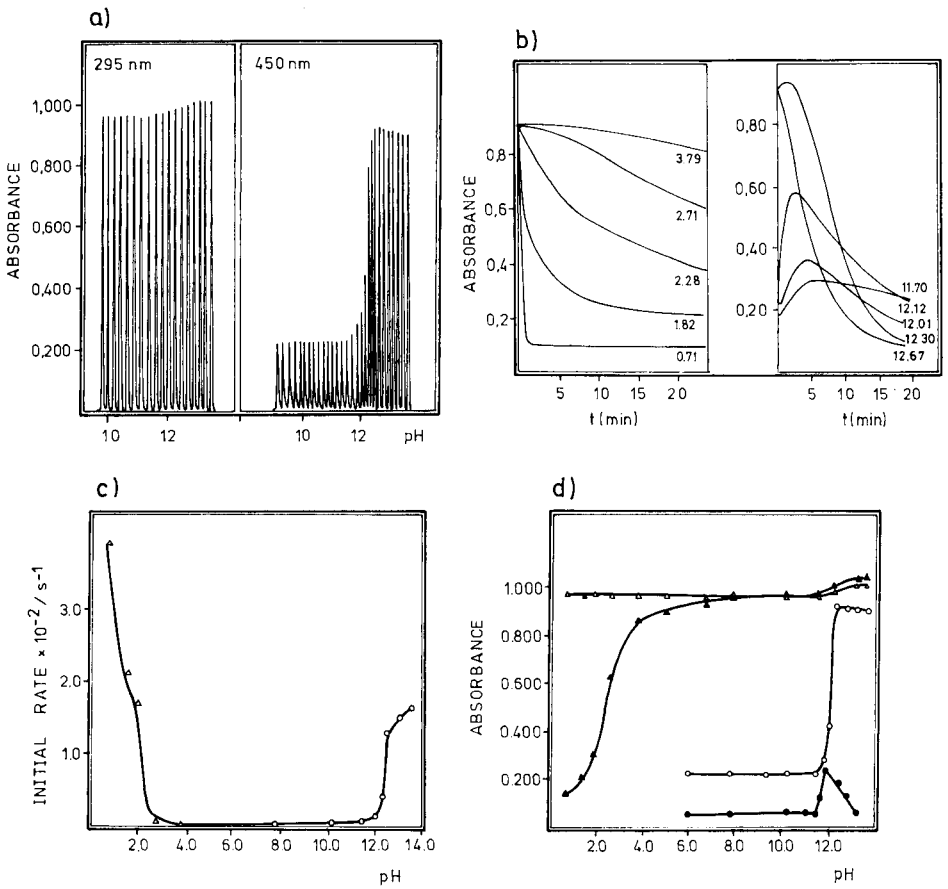

Fig. 2. Acid-base behaviour of GBHA (0.05% w/v). (a) Absorbances obtained at various pH values at two characteristic wavelengths. (b) Absorbance/time curves at the pH values indicated on the curves. (c) Hydrolysis rate vs. pH. (d) Absorbance/pH dependences measured by normal f.i.a. at (△) 295 nm and (○) 450 nm, and in the stopped-flow mode at (▲) 295 nm and (●) 450 nm.

The stopped-flow recordings (Fig. 2b) show the instability of aqueous solutions of GBHA in acidic solutions, as well as in moderately or strongly alkaline conditions, owing to the hydrolysis of GBHA to 2-hydroxyaniline and glyoxal. The absorbance/time curves are very different in acidic and basic media. In acidic solutions, the shape of these curves is typical of a hydrolytic degradation, whereas at alkaline pH an initial increase in absorbance occurs when the pump stops, followed by the expected decrease resulting from hydrolysis. This can be explained as follows. The maximum corresponds to the concentration of the dianion of GBHA when the sample plug reaches the flow cell; the increasing absorbance is due to the gradual formation of this form from the protonated form (this process accelerates

as the pH increases, and occurs within the residence time at pH $\geqslant$12.7). The portion of decreasing absorbance corresponds to the alkaline hydrolysis of GBHA, the extent of which increases with the pH. The extent of these hydrolytic processes (both acidic and alkaline) is shown in Fig. 2(c), which is a plot of pH against the disappearance rate of the reagent, measured by the tangent method applied to the absorbance/time curves obtained from the stopped-flow experiments. The acidic hydrolysis is the more important; alkaline hydrolysis is only significant above pH 12, whereas acidic hydrolysis takes place below pH 4 and is particularly important below pH 2. As a consequence of these processes, there is no agreement between the absorbance/time curves obtained by normal f.i.a. and those obtained from the final absorbances of the stopped-flow kinetic curves (chemical equilibrium). The final absorbance provides a fictitious value for pK_a in the acidic zone, which is only the manifestation of the acidic hydrolysis of this reagent. The single pK_a value of GBHA (deprotonation of the hydroxyl groups) appears, logically, in the alkaline zone, as is shown in the four curves in Fig. 2(d). It should be noted that the absorbance increase with pH is more important in normal f.i.a., and that the absorbances are constant at pH 12.5. This is not so with the equilibrium measurements, which are affected by alkaline hydrolysis to a different extent, so that more accurate values for pK_a are obtained by normal flow-injection method. The pK_a values for GBHA obtained from the different curves in Fig. 2 are summarized in Table 1.

6-Methylpicolinaldehyde azine (6-MePAA). This compound, bearing the cuproine group, has been used for the spectrophotometric determination of copper [12]. Its instability under given working conditions has been demonstrated, and used for analytical purposes [13].

TABLE 1

The pK_a values of unstable compounds obtained by different techniques

Compound	Wavelength (nm)	pK_a values obtained			Instabilities observed
		Normal f.i.a.[a]	Stopped-flow[a,b]	Usual method[c]	
GBHA	295	12.25 ± 0.01	12.20 ± 0.01	—[d]	Acidic (pH < 4) and alkaline (pH > 12) hydrolysis
	450	12.05 ± 0.05	11.70 ± 0.05		
6-MePAA	295	4.50 ± 0.01	5.50 ± 0.02	5.30[5]	Acidic (pH < 6) and alkaline (pH > 10) hydrolysis
	350	4.80 ± 0.01	4.85 ± 0.02	5.25[5]	
2-OH-BAH	300	9.65 ± 0.02	9.55 ± 0.03	9.80[6]	Acidic hydrolysis (pH < 2); autotransformation to azine (2 < pH < 6); alkaline hydrolysis (pH > 11.5)
	350	9.85 ± 0.01	9.50 ± 0.02	10.10[6]	
BPO	310 pK_{a1}	3.55 ± 0.01	3.45 ± 0.02	4.55[7]	Slight acidic (pH < 1.5) and appreciable alkaline (pH > 12) hydrolysis
	310 pK_{a2}	10.30 ± 0.01	9.95 ± 0.01	10.10[7]	

[a]Mean and standard deviation of 3—5 determinations. [b]Absorbance values measured when equilibrium was attained. [c]References are given in brackets. [d]Fast hydrolysis at pH > 12 hindered reproducible absorbance measurements.

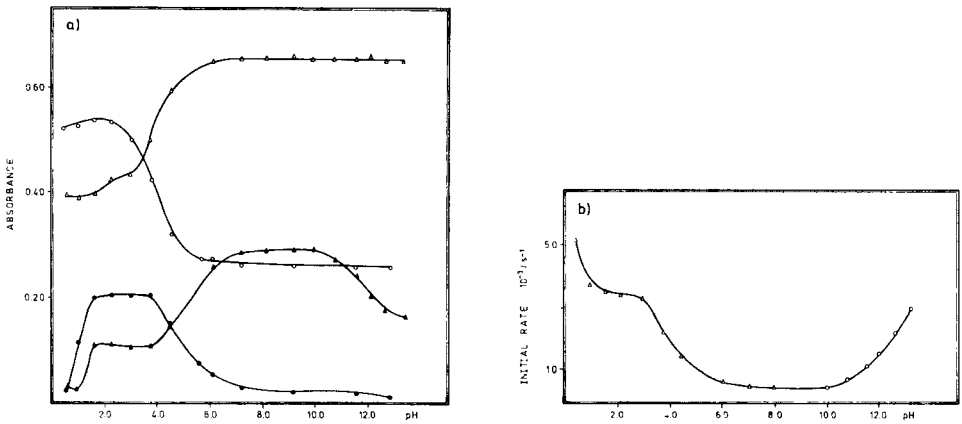

Fig. 3. Acid-base behaviour of 6-MePAA (0.025% w/v). (a) Absorbance dependence measured by normal f.i.a. at (△) 295 nm and (○) 350 nm, and in the stopped-flow mode at (▲) 295 nm and (●) 350 nm. (b) Effect of pH on rate of hydrolysis.

The u.v.-visible absorption spectrum of 6-MePAA has different shapes at pH 0.7, 3.6, 8.3 and 12.4. From these spectra, absorbances at 295 and 350 nm were chosen for the calculation of the acidity constants of this reagent. Figure 3(a) shows the absorbance/pH curves obtained by the normal f.i.a. technique and, under equilibrium conditions, by the stopped-flow mode. The former results show the occurrence of a single pK_a for the 6-MePAA, corresponding to the deprotonation of the pyridine nitrogen

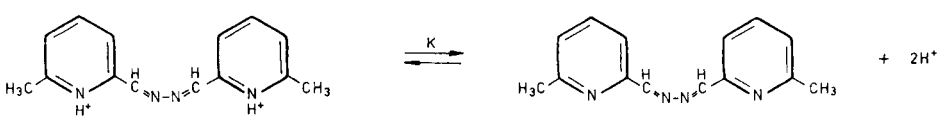

The curves obtained from the absorbance values under equilibrium conditions are different and seem to indicate the existence of three acidity constants. Valcárcel et al. [5] suggested three acidity constants for this reagent; their absorbance/pH graphs coincide with those obtained here on the basis of the final absorbance obtained from the stopped-flow recordings. In fact, the previous absorbance measurements had been made 3 h after preparation of the samples in order to obtain reproducible results. The K_{a_1} and K_{a_3} values obtained under these conditions correspond to changes in absorbance arising from hydrolysis, and only the K_{a_2} value is a real acidity constant. This is clearly demonstrated in Fig. 3(b), in which the rate of disappearance of 6-MePAA vs. pH is plotted. 6-Methylpicolinaldehyde and hydrazine were detected spectrophotometrically as the reaction products; this confirms the hydrolysis of 6-MePAA, which is more significant in acidic than in alkaline conditions. The values found for the constants are listed in Table 1. They show a noteworthy difference between the values obtained

by the normal flow-injection method and the others, which implies that the measurements under equilibrium conditions are affected to various extents by hydrolysis.

2-Hydroxybenzaldehyde hydrazone (2-OH-BAH). This compound has been applied for the spectrophotometric [14] and fluorimetric [15] determination of several metal ions. Its main shortcoming is that it is contaminated by the azine during its synthesis. The u.v.-visible absorption spectra at different pH values show 300 and 350 nm as the optimal wavelengths for the determination of acidity constants. Figure 4 shows the absorbance/pH plots obtained from the heights of the peaks in the normal flow-injection technique as well as from the final absorbance values from the stopped-flow kinetic curves. Best agreement between these curves occurs at moderately alkaline pH. The behaviour is attributed to the deprotonation of the hydroxyl groups of 2-OH-BAH

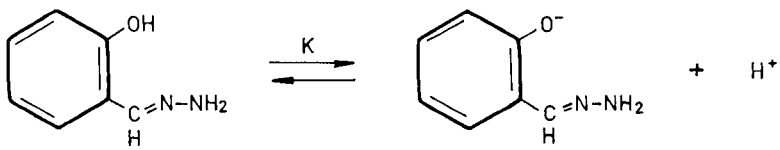

The decrease in the absorbance (equilibrium value) at pH > 12 can be accounted for by alkaline hydrolysis, which does not affect the normal flow-injection measurements. The behaviour in acidic media is more complicated. The normal flow-injection recordings, and the equilibrium measurements made by the stopped-flow mode, yield absorbance/pH curves which are hardly reliable for giving information about the acidic or basic forms of

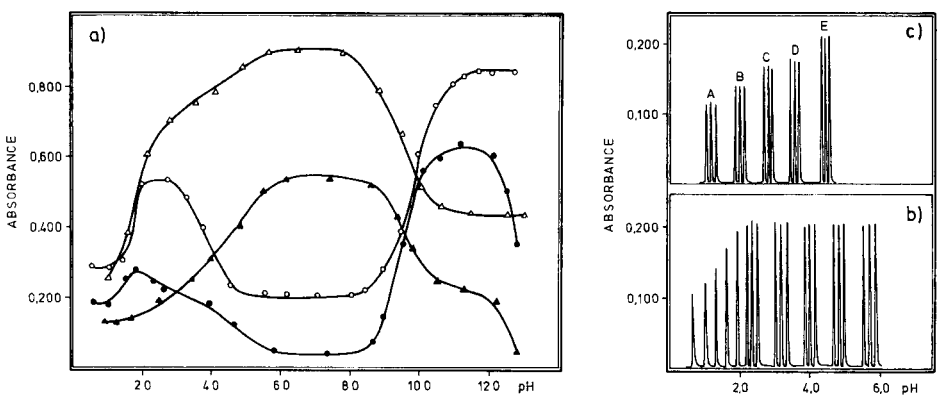

Fig. 4. Acid-base behaviour of 2-OH-BAH (0.025% w/v). (a) Absorbance/pH dependence measured by normal f.i.a. at (△) 300 nm and (○) 350 nm, and in the stopped-flow mode. (b) Influence of hydrazine on the peak height at 350 nm. (c) Influence of hydrazine concentration on the peak height of 2-OH-BAH at pH 1.0 measured at 350 nm: hydrazine concs, (A) 1 × 10^{-2} M (B) 0.10 M; (C) 1.0 M; (D) 2.5 M; and (E) 1 × 10^{-2} M at pH 2.5, at which pH there is no hydrolysis.

2-OH-BAH, because an autotransformation process has occurred, by which the hydrazone is converted to the azine. This behaviour has been described by Szmant and McGinnis [16] and can be regarded as a variant of the interchange of C=N groups [17] in which the amine is substituted by another azomethine. It is noteworthy that this process is much faster than the hydrolysis, and so is also liable to be detected in normal recordings in f.i.a. This transformation can be inhibited by adding hydrazine to the aqueous carrier into which the sample is injected (Fig. 1). Thus, by using a 1×10^{-2} M hydrazine solution, the absorbance of the flow-injection peaks is kept constant over the pH range 2—8 (Fig. 4b). The inhibiting effect of hydrazine on the autotransformation of the hydrazone into the azine is due to the conversion of the azine to the hydrazone by an interchange of C=N groups. A decrease in absorbance occurs below pH 2, because of the hydrolysis of 2-OH-BAH, in this case to yield salicylaldehyde and hydrazine. This reaction is also partially inhibited by hydrazine, as is shown in the following scheme

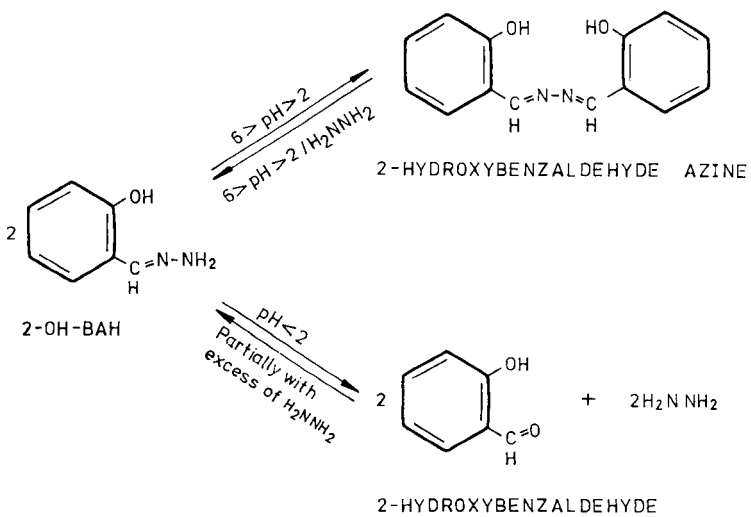

The values of the single pK_a found for 2-OH-BAH are summarized in Table 1.

2-Benzoylpyridine oxime. Since its synthesis in 1948 [18], 2-benzoylpyridine oxime (BPO) has been used for the spectrophotometric determination of metal ions and their mixtures [19] and for polarographic applications [20]. The absorption spectra of BPO at different pH values are very similar, hence a single wavelength (310 nm) was chosen to study its acid-base behaviour.

From the curves shown in Fig. 5, two acidity constants may be attributed to this oxime, corresponding to the deprotonation of the pyridine nitrogen (K_{a1}) at moderately acidic pH and to the ionization of the oxime group (K_{a2})

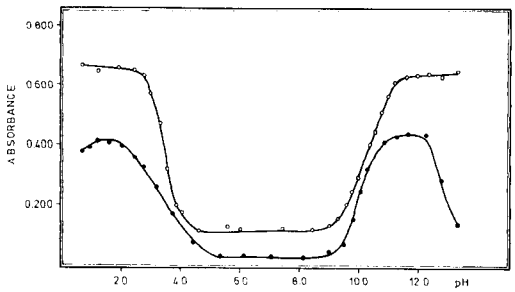

Fig. 5. Absorbance changes for BPO (0.025% w/v) vs. pH at 310 nm: (○) normal f.i.a.; (●) stopped-flow mode.

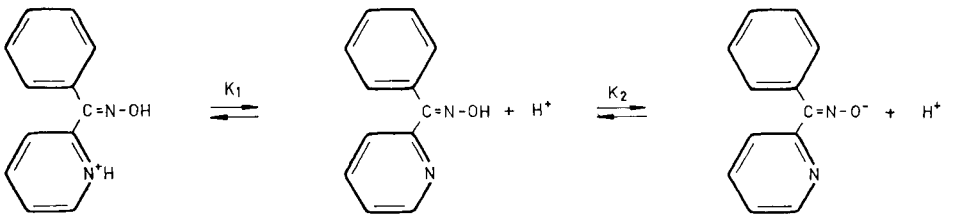

The curves obtained from the final absorbance obtained in stopped-flow studies show, in addition to the two changes associated with the acid-base behaviour of the oxime, instability in the extreme pH regions caused by hydrolysis. The alkaline hydrolysis (pH > 12) is especially important, whereas in acidic media, it is only slight, possibly because of the formation of intramolecular hydrogen bonds, which protect the C=N bond by forming a stable five-member ring.

The values of the constants obtained by the different techniques are listed in Table 1.

Advantages provided by the flow-injection technique for these calculations

From the results summarized in Table 1 for the different reagents by the normal and stopped-flow techniques for f.i.a., it can be concluded that the spectrophotometric determination of acidity constants by the proposed methods has important advantages compared to traditional methods. The flow-injection techniques avoid the inclusion of errors caused by changes in absorbance resulting from the instability of the reagent. Also, when acid-base equilibrium is reached, the pK_a values obtained by f.i.a. are probably more accurate because the absorbance measurements are not affected by side-reactions, which develop only to a minimal (or negligible) extent during the short interval that elapses between mixing the reagents and making the measurements. Finally, the stopped-flow mode allows the extent of the reaction causing the instability of the reagent to be estimated.

REFERENCES

1 M. D. Luque de Castro, M. Silva and M. Valcárcel, Analyst (London), 109 (1984) 1375.
2 M. D. Luque de Castro, M. Silva and M. Valcárcel, Analyst (London), 109 (1984) 1383.
3 A. Ramsing, J. Růžička and E. H. Hansen, Anal. Chim. Acta, 114 (1980) 165.
4 F. I. Allan and G. G. Allan, J. Org. Chem., 23 (1958) 639.
5 M. Valcárcel, D. Pérez-Bendito and F. Pino, Inf. Quím. Anal., 25 (1971) 1.
6 R. Alarcón, Thesis, University of Córdoba, Spain, 1982.
7 M. A. Gómez-Nieto, M. D. Luque de Castro and M. Valcárcel, Electrochim. Acta, 28 (1983) 325.
8 W. Stenstrom and N. Goldsmith, J. Phys. Chem., 30 (1926) 1683.
9 J. R. W. Kerr, Analyst (London), 85 (1960) 867.
10 K. T. Williams and J. R. Wilson, Anal. Chem., 33 (1961) 224.
11 F. Lindstrom and C. W. Milligan, Anal. Chem., 39 (1967) 132.
12 M. Valcárcel, D. Pérez-Bendito and F. Pino, Inform. Quím. Anal., 25 (1971) 39.
13 A. Ríos and M. Valcárcel, Quím. Anal., 1 (1983) 227; Talanta, in press; Analyst, 109 (1984) 1147.
14 H. Ray, B. S. Gard and R. P. Singh, J. Curr. Sci., 48 (1979) 346; J. Am. Chem. Soc., 23 (1976) 346; J. Indian Chem. Soc., 56 (1979) 975.
15 Z. Holzbecher, Konf. Anal. Chemiku, 166 (1952) 9.
16 H. H. Szmant and C. McGinnis, J. Am. Chem. Soc., 72 (1950) 2890.
17 S. Patai, The Chemistry of the Carbon-Nitrogen Double Bond, Interscience, New York, 1970, p. 81.
18 E. H. Huntress and H. C. Walter, J. Am. Chem. Soc., 70 (1948) 3702.
19 R. B. Singh, B. S. Gard and R. P. Singh, Talanta, 26 (1979) 425.
20 M. A. Gómez-Nieto, M. D. Luque de Castro and M. Valcárcel, J. Electroanal. Chem., 153 (1983) 201; Electrochim. Acta, 29 (1984) 611.

Analytica Chimica Acta, 171 (1985) 313—323
Elsevier Science Publishers B.V., Amsterdam — Printed in The Netherlands

SIMULTANEOUS SPECTROPHOTOMETRIC DETERMINATION OF BINARY MIXTURES OF NICKEL, COBALT AND VANADIUM WITH 3-(PICOLYDENE)BENZENESULPHONIC ACID 2-HYDROXYBENZOYLHYDRAZONE

M. GARCIA-VARGAS, M. MILLA, I. ANTEQUERA and J. A. PÉREZ-BUSTAMANTE*
Department of Analytical Chemistry, Faculty of Sciences, University of Cádiz, Cádiz (Spain)

(Received 26th April 1984)

SUMMARY

The synthesis and characterization of a water-soluble reagent, 3-(picolydene)benzenesulphonic acid 2-hydroxybenzoylhydrazone, is described. The reagent is stable in aqueous media. The colour reactions with nickel(II), cobalt(III) and vanadium(V) ions in slightly acidic solutions have molar absorptivities in the range 1.4—3.6 × 10^4 l mol^{-1} cm^{-1}. Simultaneous determinations of Ni, Co and V in binary mixtures are possible. Interference data are reported.

Aroylhydrazones can be regarded as carbonyl azomethines characterized by the grouping C=N—NH—CO—; they are easily prepared from the aroylhydrazide and a carbonyl derivative dissolved in a suitable solvent. Such compounds may possess tuberculostatic activity [1], attributed to the formation of stable chelates with transition metals present in the cell. The functional grouping causes these reagents to behave as bidentate ligands for metal ions, a five-membered ring being formed; coordination occurs by bonding from the first two nitrogen atoms and from the oxygen atom. Because of keto-enol tautomerism, coordination may occur through the oxygen of the keto form [2] or, more probably, of the enol form [3—9]. Chelates involving the azine grouping tend to give stable strongly coloured metal complexes [10, 11], whereas a pyridinic nitrogen in the carbonyl derivative improves the solubility and stability of aroylhydrazones. A common drawback of most of these reagents is their poor solubility in water.

Aroylhydrazones have been applied in the detection, determination and isolation of compounds containing the carbonyl group [1]. They have also been used in the detection and determination of various metals. Isonicotinoylhydrazones have probably been most studied but salicyloylhydrazones have been proposed for the determination of zinc or nickel [12], vanadium [13], iron [14] and some other metals [15].

In the present paper, the synthesis and properties of 3-(picolydene)benzenesulphonic acid 2-hydroxybenzoylhydrazone (PBSHB) are described.

0003-2670/85/$03.30

Optimum conditions for the separate spectrophotometric determination of nickel, cobalt or vanadium are reported, as well as for simultaneous determinations of binary mixtures of these metal ions.

EXPERIMENTAL

Reagents and equipment

Synthesis of PBSHB. First, 3-(picolinoyl)benzenesulphonic acid (PBS) was prepared as described by Bradsher et al. [16]. The product was recrystallized from 1:1 ethanol/water. To synthesize PBSHB, ethanolic solutions of PBS (1 g in 50 ml) and salicyloylhydrazide (0.64 g in 10 ml) were mixed and a few drops of concentrated hydrochloric acid were added. The precipitate was filtered off and crystallized from 3:2 ethanol/water. The results of analysis for C, H, N and sulphur were in good agreement with the empirical formula $C_{19}H_{15}N_3SO_5 \cdot 2H_2O$.

Solutions. The PBSHB is moderately soluble (1 g l^{-1}) in most common organic solvents, but is more soluble (>10 g l^{-1}) in dimethylformamide or water. Reagent solutions (0.1 and 1% w/v) in dimethylformamide or water were prepared by dissolving appropriate amounts of PBSHB dried at 110°C; aqueous solutions were prepared in dilute sodium hydroxide and then neutralized.

Standard solutions of nickel(II) (2.090 g l^{-1}) and cobalt(II) (2.054 g l^{-1}) were prepared by dissolving the pure metal in nitric and hydrochloric acid, respectively, neutralizing, and standardizing with EDTA (murexide and xylenol orange, respectively) in the usual manner. The vanadium(V) solution was prepared from sodium vanadate; it was standardized gravimetrically with silver nitrate.

Buffer solutions (chloroacetate for pH 3.7, acetate for pH 4.7, ammonia for pH 9.3, and borate for pH 9.2) and solutions of cations and anions of different concentration were prepared with distilled water from analytical-grade chemicals.

Equipment. Pye-Unicam SP8-200 and Perkin-Elmer Coleman 575 spectrophotometers were used with 1-cm glass or quartz cells. A Pye-Unicam SP3-300 infrared spectrophotometer (KBr discs) and a Metrohm Herisau E-516 Titriskop pH meter were also used.

Procedures

Acidity constants. To determine pK_{a2} and pK_{a3}, enough reagent solution was added to 10-ml volumetric flasks to give a final concentration of 2.52×10^{-5} M. The pH was adjusted with dilute hydrochloric acid or sodium hydroxide solutions and the absorbances were measured at 295, 305, 330 and 360 nm against an appropriate blank. The sulphonic acid group was examined similarly in solutions containing varying amounts of 70% (d = 1.67 g ml^{-1}) perchloric acid.

Spectrophotometric determination of nickel, cobalt or vanadium. To a solution containing up to 20 μg of Ni(II) or Co(II) or up to 50 μg of V(V),

were added 1 ml of aqueous 0.1% (w/v) PBSHB solution, 0.5 ml of 1% hydrogen peroxide in the case of cobalt, and 4 ml of 0.5 M acetate buffer (Ni, Co or V) or 2 ml of 0.3 M chloroacetate buffer (V). The solution was diluted to the mark in 10-ml volumetric flasks. The absorbance was measured at 375 and 385 nm for nickel, 400 and 415 nm for cobalt and 395 nm for vanadium, against the appropriate blank solution.

Simultaneous determination of binary mixtures. To solutions containing up to 20 μg of Ni and Co, Ni and V, or Co and V, 1 ml of 0.1% (w/v) reagent solution, 5 ml of acetate buffer, and 0.5 ml of 1% hydrogen peroxide for mixtures of Co and Ni were added and the solution was diluted to the mark in 10-ml volumetric flasks. Absorbances were measured at 370 and 415 nm (Ni + Co), 370 and 420 nm (Ni + V), or 395 and 415 nm, 2 h after preparation of the sample for Co + V mixtures, against the appropriate blanks in all cases. The concentration of each ion in the mixture was calculated by solving simultaneous equations.

RESULTS AND DISCUSSION

Infrared spectra and thermogravimetric analysis of the reagent

The infrared spectrum of PBSHB was recorded between 200 and 4000 cm^{-1}. Comparison with the spectra obtained from the parent compounds and with the spectral data given by Domiano et al. [3] and Pelizzi et al. [8, 9] for related aroylhydrazones permitted assignment of the vibrational characteristics (Table 1).

The PBS spectrum shows two intense absorption bands in the 1150—1250 cm^{-1} region that can be attributed to symmetrical and antisymmetrical stretching of the SO_2 group (cf. [17—19]). Similar bands (1170—1235 cm^{-1}) are observed in the PBSHB spectrum. For both PBS and PBSHB, the strong band located at 3500—3400 cm^{-1} caused by OH stretching is noteworthy. The phenolic hydroxyl of the reagent is strongly associated (band at 2800—2550 cm^{-1}); this band disappears from the spectrum of PBS heated at 200°C, but is still observed for PBSHB heated at 200° C. Thermogravimetric analysis of PBSHB showed a constant weight between 100 and 200° C; a weight loss corresponding to two water molecules was observed between 200 and 250° C, indicating the presence of chemically bonded water molecules in PBSHB.

Ultraviolet-visible spectra of the reagent and dissociation constants

The spectral characteristics of PBSHB (2.52×10^{-5} M) were studied by recording its u.v.-visible spectra in several solvents (Fig. 1). It can be seen that the absorption maximum is shifted to higher wavelengths as the solvent polarity decreases, although polar solvents usually cause bathochromic shifts when $n \rightarrow \pi^*$ transitions are involved [3]. In aqueous solutions (Fig. 2), the maximum is around 325 nm in acidic solution (pH 2.6), whereas in alkaline media a new band appears at 365 nm. The corresponding pK_a values associated with these absorbing species, calculated by the Stenström-Goldsmith

TABLE 1

Infrared spectra of 2-benzoylpyridine (BP) and salicyloylhydrazide (SH) and their derivatives

Assignment	BP	PBS	SH	PBSHB
ν_{OH} (water)		3410		3490
ν_{NH}			3320 s	
			3280 s	3260 w
			3140 w	
$\nu_{(=CH)}$	3080 w	3110 w	3060	3100
	3060 w	3090 w	3010	
	3010 w			
ν_{OH}		2900—2500 w	2850—2500	2800—2550 m
ν_{CO}	1670 vs	1660 s		
δ_{NH_2}			1640 sh	
Amide I			1625 s	1660 s
Aromatic ring	1600 w			1600 m
	1580 m	1585 s	1575 m	1570 w
Amide II			1560 s	1530 m
		1540 m	1510 m	1500 m
Aromatic ring	1460 w	1470 ms	1480 m	1460 m
	1440 ms		1440 m	
	1430 w	1430 m		
		1410 w		
ν_{SO_2}		1150—1250 vs		1235—1170 s
δ_{CH}[a]		820 m		810 w
	785 s	790 m	760 m	780 m
δ_{CH}[b]	750 s	755 vs		750 m
δ_{CH}[a]	700 vs	710 s		710 s
		700 vs		700 sh

[a]Out of plane (phenyl). [b]Out of plane (pyridine).

[20] and Sommer [21] methods, are $pK_{a2} = 3.5 \pm 0.2$ (protonation of the pyridine N atom) and $pK_{a3} = 6.7 \pm 0.2$ (deprotonation of the hydroxyl group). In perchloric acid media, the absorption band at 365 nm reappears. The pK_a corresponding to deprotonation of the sulphonic group, was found to be -1.81 ± 0.07, which was evaluated by the method of Yates and Wai [22], the absorbance being measured at 320 and 380 nm and the weight percentage of perchloric acid in the sample being converted to the equivalent Hammett acidity function.

Stability of the PBSHB solutions

The reagent is remarkably stable (>40 days) in ethanol, anhydrous acetic acid, chloroform and isoamyl alcohol, but less stable (about 15 days) in dimethylformamide. In aqueous buffered solution, the stability depends on pH: 15 days at pH 2.6, 20 days at pH 4.7 and >30 days at pH 9.3. In strongly acidic solution (2 M), the reagent is stable for only about 2 h, being decom-

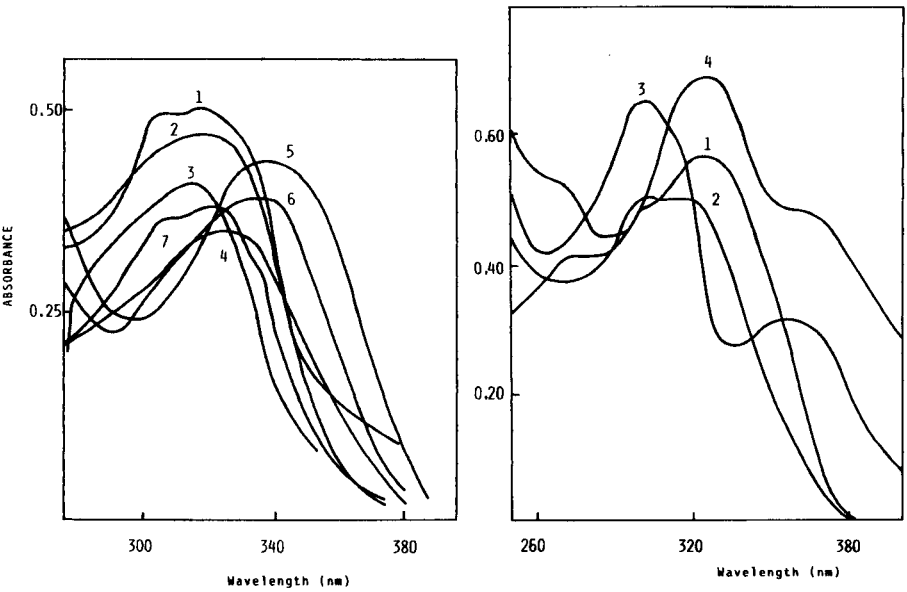

Fig. 1. Absorption spectra of PBSHB (2.5×10^{-5} M) in various solvents: (1) benzene; (2) chloroform; (3) anhydrous acetic acid; (4) isoamyl alcohol; (5) ethanol; (6) dimethylformamide; (7) water.

Fig. 2. Absorption spectra of aqueous PBSHB solutions (2.52×10^{-5} M) at different pH values: (1) pH 2.6; (2) pH 4.7; (3) pH 9.2; (4) 39.1% (w/w) perchloric acid.

posed completely after several weeks. The stability in 4 M or 2 M sodium hydroxide is only a little longer than in acidic medium of equal concentration. The stability of PBSHB in aqueous solutions is good in comparison with that of related aroylhydrazones. This can be attributed to the presence of the sulphonic group in the benzene ring which favours the formation of a ring by intramolecular bonds involving the —C=N— group.

Reducing agents (hydrazine, hydroxylamine, sulphite, ascorbic acid) and peroxydisulphate at moderate concentrations do not alter the absorption spectra of the aqueous reagent solution over a wide range of pH. However, hydroxylamine affects substantially the absorption spectra of PBSHB at pH 2.6, probably because of an exchange of C=N groups. Hydrogen peroxide slowly decomposes the reagent in all media tested.

Reactions with metal ions

Among the 42 ions tested in aqueous media, a coloured reaction was observed with Pb, Cu, Cd, Pt(IV), Fe(III), V(V), rare earths, Co, Ni, Zn, Fe(II), Mn(II) and Ca. Of these ions, the most interesting are the reactions with Ni(II), Co(II) and V(V), because of their sensitivity, stability and colour contrast. None of the metal complexes of PBSHB can be extracted into methyl isobutyl ketone, iso-amyl alcohol or benzene.

Study of the reactions with nickel, cobalt and vanadium

Aqueous solutions of PBSHB react quickly with Ni(II), Co(II) and V(V) to give yellow chelates with absorption maxima located at 375 nm (Ni), 370 nm (Co) and 395 nm (V). The absorption maximum of the cobalt(II) chelate at pH 4.7 shifts slowly to 415 nm. The relative facility with which Co(II) is oxidized when it is bonded to ligands containing nitrogen donor atoms is well known. Thus, an attempt was made to evaluate the oxidation state of cobalt in the complex. When the spectrum was recorded after deaerated solutions (nitrogen stream) of reagent and cobalt(II) had been mixed, the absorption maximum (370 nm) remained unchanged for a day at least. Without these precautions, the shift to 415 nm was complete in 2 h and occurred even in the presence of ascorbic acid. In contrast, only the maximum at 415 was observed when hydrogen peroxide was added. It seems, therefore, that PBSHB reacts initially with cobalt(II) to yield a complex with maximum absorbance at 370 nm, which evolves to a cobalt(III) complex with maximum absorbance at 415 nm.

The metal-to-ligand stoichiometric ratios of the metal chelates, investigated by the continuous variations method, were found to be 1:2 for nickel and cobalt(III) and 1:1 for vanadium(V). In order to investigate the charge of the metal complexes, they were percolated through cationic (Dowex 50-X8, sodium form) and anionic (Dowex 1-X8, chloride form) exchange columns. All the metal complexes were retained on the anion-exchange resin, indicating that they are negatively charged. The Co(III) and V(V) complexes were partially retained on the cation-exchange resin, but the Ni(II) complex was not. It is apparent that PBSHB acts as a tridentate ligand in the nickel chelate, forming an octahedral complex with four five-membered rings. The exact configuration is similar to that previously established for other metal/aroylhydrazone complexes [3, 5, 8, 9].

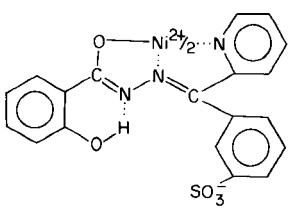

The conditions for metal/PBSHB chelate formation were optimized for the three systems by studying all the variables affecting the complexation reactions. Optimum conditions are listed in Table 2. The cobalt/PBSHB system shows two distinct pH zones (3.7—4.0 and 5.5—6.7) of different absorbance when the pH is adjusted with dilute hydrochloric acid or sodium hydroxide solutions; the optimum pH range is 3.7—5.8 if acetate buffer is used. The optimum pH range for the vanadium chelate increased from 3.0—4.5 to 3.0—5.5 when acetate-buffered solutions were used.

Of the three chelates, only that of vanadium(V) is affected by the order of reagent addition, so that the most favourable order of addition for the

TABLE 2

Optimum conditions of formation and spectrophotometric characteristics of the chelates of Ni(II), Co(III) and V(V)

Characteristic	Ni/PBSHB	Co/PBSHB	V/PBSHB
λ_{max} (nm)	375	415	395
pH range	4.0—5.3	3.7—4.0 and 5.5—6.7(3.7—5.8)[a]	3.0—4.5(3.0—5.5)[a]
Buffer solution (ml)	Acetate (1—6)	Acetate (1—5)	Acetate (1—4) Chloroacetate (1—3)
Volume of reagent (ml)[b]	0.5—5	0.75—4	1—3
Order of addition	Immaterial	Immaterial	Metal/reagent/buffer
Ionic strength (KCl, KNO_3)	$\leqslant 0.8$	$\leqslant 0.6$	$\leqslant 0.6$
Temperature (°C)	15—50	15—25	15—50
Stability (days)	1	1	1 (pH 4.7); some h (pH 3.7)
Molar absorptivity (l mol^{-1} cm^{-1})	3.6×10^4	2.7×10^4	1.4×10^4 (pH 4.7); 1.3×10^4 (pH 3.7)
Sandell sensitivity (μg cm^{-2})	1.6×10^{-3}	2.2×10^{-3}	3.7×10^{-3}
Beer's law (mg l^{-1})	0.05—2.0	0.05—1.75	0.25—5.0 (pH 4.7); 0.25—3.7 (pH 3.7)
Minimum error zone	0.32—1.26	0.5—1.5	0.7—2.7 (pH 4.7); 0.3—2.5 (pH 3.7)
Relative standard deviation	0.4	0.3	0.9 (pH 4.7); 0.7 (pH 3.7)
Hydrogen peroxide (ml)[c]	Unaffected (up to 3)	0.5—3	Affected

[a]In acetate-buffered solution. [b]Aqueous 0.1% (w/v) solution. [c]Aqueous 1% (w/v) solution.

vanadium complex was chosen for the simultaneous determination of binary mixtures of the ions. The presence of hydrogen peroxide, needed to oxidize Co(II) to Co(III), affected the formation of the vanadium complex, and had to be avoided in the case of simultaneous determination of cobalt and vanadium.

A systematic study of the interfering effects of foreign ions on the determination of 1 mg l^{-1} nickel or cobalt and 2 mg l^{-1} vanadium in acetate buffer was conducted (Table 3). The maximum metal ion/foreign ion ratio considered was 1:1000; the absorbances were measured at 375 and 385 nm for Ni, at 400 and 415 for Co, and at 395 for V. There were no appreciable differences in the perturbing effects of a given ion at either wavelengths used for nickel and cobalt and at both pH values (3.7 and 4.7) used in the determination of vanadium. At the same concentration level as the analyte, the following ions did not interfere: Hg(I), Hg(II) and Pd(II) (nickel determination); these ions plus Pt(IV), Cr(III), Sn(II) and citrate (vanadium

TABLE 3

Tolerance limits towards foreign ions in the separate determinations of nickel (1 mg l^{-1}), cobalt (1 mg l^{-1}) and vanadium (2 mg l^{-1})

Metal determined	Ions tested	Concentration tolerated (mg l^{-1})
Ni	Alkali metals, alkaline earths, Tl(I), Mg, As(III), As(V), Mo(VI), W(VI), halides, NO_3^-, ClO_4^-, SCN^-, CO_3^{2-}, SO_4^{2-}, $S_2O_3^{2-}$, PO_4^{3-}, borate, oxalate, tartrate, citrate	1000
Co	Alkali metals, NH_4^+, F^-, Cl^-, ClO_4^-, NO_3^-, SO_4^{2-}, PO_4^{3-}	
V	Alkali metals, Ba, As(V), Cl^-, Br^-, I^-, NO_3^-, NO_2^-, CN^-, ClO_4^-, borate, CO_3^{2-}, SO_4^{2-}, $S_2O_3^{2-}$	
Ni	La	500
Co	CO_3^{2-}, $S_2O_3^{2-}$, NO_2^-[a], tartrate, citrate[a]	
V	SCN^-	
Ni	Ba, Mn(II), NO_2^-	250
Co	Mg, As(III), As(V)[a], borate[a]	
V	PO_4^{3-}	
Ni	Ca[a], Br^-	100
Co	As(III), Mo(VI), Tl(I)	
Ni	Cr(III)[a], Al, Au(III), Pt(IV)	50
Co	Be[a], Sr[a], Mn(II), La, Nd, I^-, SCN^-[a], oxalate	
V	Pr, U(VI), F^-	
Co	Al[a], Pr, Rh(III), U(VI)[a], Mo(VI)[a], W(VI)[a]	25
V	Sr[a], Cd, Mn(II), Sb(III)[a], Al[a], La, tartrate	
Ni	Pb, Pr[a], Er[a], Sm[a], Sb(III)[a], Th(IV), U(VI), CN^-	10
Co	Ba[a], Cd[a], Eu[a], Sm[a], Th(IV)[a], CN^-, S^{2-}	
V	NH_4^+, Mg, Ca[a], Pb[a], Cd, Eu	
Ni	Cd, Sn(II)	5
Co	Pb[a], Tl(I)[a], Sb(III), Au(III), Pt(IV), Hg(II)	
V	Be, Th(IV), W(VI), Au(III)	

[a]Maximum concentration investigated.

determination); and Pd(II), Cr(III) and Sn(II) (cobalt determination). The ions of Zn, Bi, Cu(II), Fe, In, Ti and S^{2-} interfered at the same concentration level of Ni, Co or V. The interfering effects of these ions could be reduced for simultaneous determinations of binary mixtures of Ni, Co and V, by appropriate masking reactions with phosphate, sulphate, thiosulphate, chloride, thiocyanate or cyanide; oxalate, tartrate and citrate could be used for simultaneous determinations of cobalt and nickel.

Simultaneous determinations of binary mixtures of nickel, cobalt and vanadium

The characteristics of the Ni, Co and V systems investigated as described above permit the simultaneous evaluation of binary mixtures of these ions. Thus, the differences in the maximum absorption wavelengths of the three chelates could be utilized for the simultaneous determination of mixtures of Ni and Co, Ni and V and Co and V.

The absorption spectra of the acetate-buffered solutions, prepared as described under Experimental, with 1 mg l^{-1} nickel, 1 mg l^{-1} cobalt and 3 mg l^{-1} vanadium, in different binary combinations, are shown in Fig. 3. In all instances, the absorption spectra of the mixed complexes are the sum of the two separated complexes.

Two wavelengths of measurement were selected for each mixture: 370 and 415 nm for Ni and Co, 370 and 420 nm for Ni and V, and 395 and 415 nm for Co and V. To evaluate the molar absorptivities of the complexes at these wavelengths, calibration graphs were used, as shown at the top right corners of A, B and C in Fig. 3.

To determine traces of binary mixtures of metal ions, a single solution is processed as described under Experimental and the results are evaluated by solving sets of simultaneous equations.

For the Ni/Co system: $A_{370} = 3.6 \times 10^4\ C_{Ni} + 9.7 \times 10^3\ C_{Co}$

$$A_{415} = 2.7 \times 10^4\ C_{Co} + 2.9 \times 10^3\ C_{Ni}$$

For the Ni/V system: $A_{370} = 3.6 \times 10^4\ C_{Ni} + 5.6 \times 10^3\ C_{V}$

$$A_{420} = 6.3 \times 10^3\ C_{V}$$

For the Co/V system: $A_{395} = 1.4 \times 10^4\ C_{Co} + 1.4 \times 10^4\ C_{V}$

$$A_{415} = 2.7 \times 10^4\ C_{Co} + 7.0 \times 10^3\ C_{V}$$

where C_i is the unknown concentration of the pertinent metal ion. The molar absorptivities used will obviously have to be adjusted for local conditions.

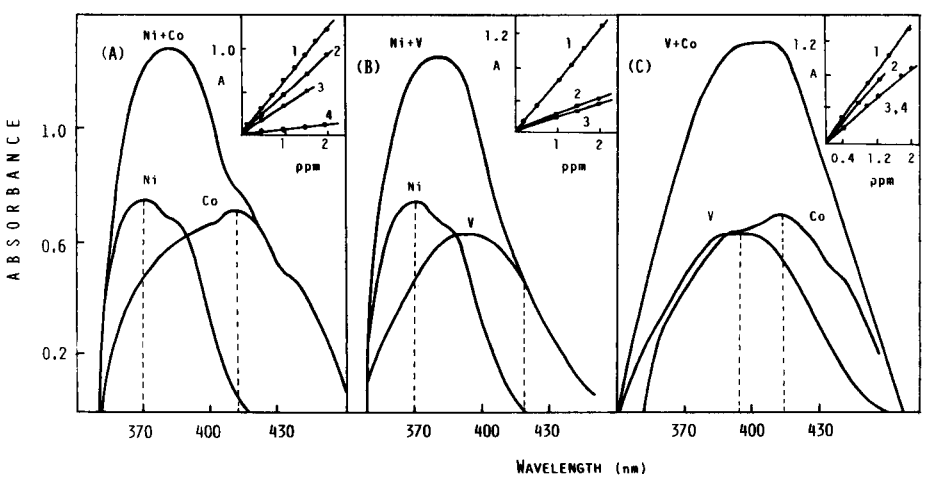

Fig. 3. Evaluation of binary mixtures of Ni, Co and V. Absorption spectra: (A) Ni, Co and Ni + Co; (B) Ni, V and Ni + V; (C) Co, V and Co + V. Calibration graphs (right top corners) for each mixture: (A) lines 1 (Ni) and 3 (Co) at 370 nm, and lines 2 (Co) and 4 (Ni) at 415 nm; (B) lines 1 (Ni) and 3 (V) at 370 nm, and line 2 (V) at 420 nm; (C) lines 1 (V) and 3 (Co) at 395 nm, and lines 2 (V) and 4 (Co) at 415 nm. Metal ion concentrations: 1 mg l^{-1} (ppm) for Ni or Co and 3 mg l^{-1} for V. Dashed lines indicate the wavelengths used for simultaneous determinations.

The results obtained in the determination of each pair of metal ions, for different metal/metal ratios, are shown in Table 4. Mixtures of Ni and Co or Ni and V can be resolved without great error for nickel/metal mass ratios ranging between 0.05 and 3—4. For the Co/V system, Co/V mass ratios must be from 0.33 to 19. It can be seen that the reported methods give satisfactory results for analyzing the binary mixtures outlined.

Conclusions

Aroylhydrazones suffer from two serious drawbacks in their use as analytical reagents. The first derives from their poor solubility in water and ethanol, which necessitates the use of large amounts of water-miscible organic solvent to prevent precipitation of the reagent in the reaction medium. The presence of the pyridine-nitrogen atom in the reagent molecule produces an insufficient

TABLE 4

Simultaneous determinations of Ni, Co and V in binary mixtures[a]

Amount taken (mg l^{-1})			Amount found (mg l^{-1})			Difference		
Ni	Co	V	Ni	Co	V	Ni	Co	V
0.10	1.90	—	0.11	2.05	—	+0.01	+0.15	—
0.20	1.80	—	0.25	1.93	—	+0.05	+0.13	—
0.40	1.60	—	0.43	1.69	—	+0.03	+0.09	—
0.50	1.50	—	0.57	1.64	—	+0.07	+0.14	—
1.00	1.00	—	1.10	0.99	—	+0.10	—0.01	—
1.30	0.70	—	1.35	0.82	—	+0.05	+0.12	—
1.50	0.50	—	1.50	0.60	—	0.0	+0.10	—
1.60	0.40	—	1.67	0.52	—	+0.07	+0.12	—
1.80	0.20	—	1.78	0.35	—	—0.02	+0.15	—
0.10	—	1.90	0.06	—	1.84	—0.04	—	—0.06
0.20	—	1.80	0.16	—	1.74	—0.04	—	—0.06
0.40	—	1.60	0.38	—	1.54	—0.02	—	—0.06
0.50	—	1.50	0.47	—	1.40	—0.03	—	—0.10
1.00	—	1.00	0.92	—	0.98	—0.08	—	—0.02
1.30	—	0.70	1.19	—	0.68	—0.11	—	—0.02
1.50	—	0.50	1.41	—	0.38	—0.09	—	—0.12
1.60	—	0.40	1.48	—	0.26	—0.12	—	—0.14
1.80	—	0.20	1.64	—	0.06	—0.16	—	—0.14
1.90	—	0.10	1.62	—	0.38	—0.28	—	—0.28
—	0.20	1.80	—	0.55	1.55	—	+0.35	—0.25
—	0.50	1.50	—	0.42	1.30	—	—0.08	—0.20
—	1.00	1.00	—	1.13	0.90	—	+0.13	—0.10
—	1.30	0.70	—	1.34	0.73	—	+0.04	+0.03
—	1.50	0.50	—	1.44	0.42	—	—0.06	—0.08
—	1.60	0.40	—	1.66	0.37	—	+0.06	—0.03
—	1.80	0.20	—	1.84	0.13	—	+0.04	—0.07
—	1.90	0.10	—	1.86	0.06	—	—0.04	—0.04

[a]Each result is the mean of three separate determinations.

increase in solubility; sulphonation of the reagent helps to solve the problem, as it has done for many other reagents. The second drawback stems from the hydrolytic reactions that these reagents undergo in acidic aqueous solutions which implies decomposition of the reagent and, in some cases, formation of metal chelates of low stability. This can be avoided by making the —C=N— group participate in a ring, as happens when pyridoxal or a sulphonated derivative is used for the synthesis of the aroylhydrazone compounds.

Despite these drawbacks, the colour reactions of aroylhydrazones with various cations present attractive sensitivities and therefore the attainment of a degree of selectivity is of interest. The new salicyloylhydrazone derived from 3-picolinoylbenzenesulphonic acid produces anionic metal complexes, which circumvent the solubility problems arising from the use of analogous reagents. Although the extensive complexing ability of the =N—C—C=N—NH—CO— grouping for metal ions still imposes some limitations on the use of these reagents, the new reagent described above yields metal chelates that can be differentiated in suitable cases. This feature has been utilized to establish spectrophotometric procedures for the simultaneous determination of binary mixtures of nickel, cobalt and vanadium that are more sensitive and selective than other methods previously reported for related compounds [23—25].

REFERENCES

1 M. Katyal and Y. Dutt, Talanta, 22 (1975) 151.
2 R. C. Aggarwal and B. Singh, Transition Met. Chem., 1(6) (1976) 275.
3 P. Domiano, A. Musatti, M. Nardelli and C. Pelizzi, J. Chem. Soc. Dalton Trans., 295 (1975).
4 M. Lever, N. Z. J. Med. Lab. Technol., 27(1) (1973) 15.
5 P. Domiano, A. Musatti and G. Predieri, Crystallogr. Struct. Commun., 3(4) (1974) 717.
6 N. S. Biradar, R. H. Raythatha and V. B. Mahale, Curr. Sci., 45(4) (1976) 124.
7 N. S. Biradar and B. R. Havinale, Inorg. Chim. Acta, 17(1) (1976) 157.
8 C. Pelizzi, G. and G. Pelizzi, J. Chem. Soc. Dalton Trans., 1970 (1980).
9 C. Pelizzi, G. Pelizzi, G. Predieri and S. Resola, J. Chem. Soc. Dalton Trans., 1349 (1982).
10 M. Garcia-Vargas, M. Gallego and M. de la Guardia, Analyst (London), 105 (1980) 965.
11 M. Garcia-Vargas, J. M. Bautista, S. Avila Novas and R. Coy-Yll, Microchem. J., 27 (1982) 519.
12 M. Gallego, M. Garcia-Vargas, F. Pino and M. Valcárcel, Microchem. J., 23 (1978) 353.
13 M. Gallego and M. Garcia-Vargas, Microchem. J., 24 (1979) 143.
14 M. Gallego, M. Garcia-Vargas and M. Valcárcel, Analyst (London), 104 (1979) 613.
15 M. Gallego, M. Valcárcel and M. Garcia-Vargas, Anal. Chim. Acta, 138 (1982) 311; Analyst (London), 108 (1983) 92; Mikrochim. Acta, 289 (1983).
16 C. K. Bradsher, J. C. Parhan and J. D. Turner, J. Heterocyclic Chem., 2 (1965) 228.
17 N. B. Colthup, J. Opt. Soc. Am., 40 (1950) 397.
18 L. J. Bellamy, The Infrared Spectra of Complex Molecules, Methuen, London, 1958.
19 R. J. Timpson, J. Am. Chem. Soc., 74 (1952) 1354.
20 W. Stenström and N. J. Goldsmith, Phys. Chem., 30 (1926) 1683.
21 L. Sommer, Folia Fac. Sci. Nat. Univ. Purkynianae, Brno, 5 (1965) 1.
22 K. Yates and H. Wai, J. Am. Chem. Soc., 86 (1964) 5408.
23 J. L. Gómez Ariza and J. M. Cano Pavón, Anal. Lett., 9(7) (1976) 677.
24 A. Garcia de Torres, M. Valcárcel and F. Pino, Anal. Chim. Acta, 79 (1975) 257.
25 J. L. Bahamonde, D. Bendito and F. Pino, Analyst (London), 99 (1974) 355.

Analytica Chimica Acta, 171 (1985) 325—332
Elsevier Science Publishers B.V., Amsterdam — Printed in The Netherlands

HIGHLY SENSITIVE SPECTROPHOTOMETRIC KINETIC DETERMINATION OF VANADIUM BY CATALYSIS OF THE GALLIC ACID-BROMATE REACTION

TSUTOMU FUKASAWA*, SUSUMU KAWAKUBO and TATSUO YAMANOUCHI

Department of Applied Chemistry, Faculty of Engineering, Yamanashi University, Takeda-4, Kofu-shi 400 (Japan)

(Received 30th September 1983)

SUMMARY

Conditions are described for improving the speed and sensitivity of this catalytic determination of vanadium. The reaction of 0.018 M gallic acid with 0.96 M sodium bromate at pH 3.8 and double-beam spectrophotometric measurement at 380 nm are recommended. The calibration curves are obtained by the tangent (2-point) and fixed-time (single-point) method. The highest practical sensitivity at 22—30° C was ca. 40 pg for an absorbance change of 0.0005, 50 times better than previously. The detection limit was ca. 0.5 ng of vanadium. Reaction at 50° C gave even better sensitivity.

Traces of vanadium have been determined spectrophotometrically by measuring the rate of a vanadium-catalyzed gallic acid/bromate redox reaction [1]. The method was applied successfully to the determination of vanadium in various samples [2—4]. However, it required measurement of the absorbance change over a period as long as 40 min, which would be a particularly severe disadvantage if the procedure were to be used in flow injection analysis (f.i.a.) because of the large dispersion which would result from a residence time of 40 min in a flow system. This paper describes a method, based on the above reaction, which is much faster than that described previously. Reagent concentrations as high as possible, reaction temperature, and pH were especially studied in order to achieve this improvement. The highest sensitivity was about 50 times that achieved in the previous papers [1—4].

EXPERIMENTAL

Reagents and apparatus

All chemicals were of analytical grade. Deionized-distilled water was used throughout. A standard vanadium solution (400 μg ml^{-1}) was prepared by dissolving ammonium metavanadate in water. More dilute solutions were prepared from this by appropriate dilution with water, immediately before use. Gallic acid (0.060 M) and 2.4 M sodium bromate were prepared by dissolving the chemicals in water. These solutions were used within two days.

0003-2670/85/$03.30

Acetate buffer solution was prepared by mixing 10 M acetic acid and 2 M sodium acetate solution. All working solutions were kept in a thermostatted water bath (Model CTE-20, Komatsu Electronics, Japan) before use.

All spectrophotometric measurements were done with a double-beam spectrophotometer (Shimadzu Model UV-200S) equipped with a scale expander, a strip-chart recorder (Shimadzu Model U-125MU) and 10-mm quartz cells. The full-scale absorbance was changed to 2, 1, or 0.1 by the scale expander depending on the absorbance of the sample to be measured. The cell chamber was maintained at a given temperature within ±0.5°C by circulating water from the thermostatted water bath. A Hitachi-Horiba model M-5 pH meter was used to measure pH.

Recommended procedure

Add a sample solution of less than 2.5 ml containing less than 60 ng of vanadium to a 20-ml test tube with a ground-glass stopper. Add 0.49 ml of buffer solution (10 M acetic acid/2 M sodium acetate = 22:27, pH 4.1) to adjust the pH of the final solution to 3.8. Add 3 ml of 0.060 M gallic acid and dilute to exactly 6 ml with water. Keep the tube in the thermostatted water bath for 10 min to bring the solution to the required reaction temperature (depending on the required sensitivity and determination range, Tables 1—3). Add 4 ml of 2.4 M bromate previously brought to this temperature, and mix well to initiate the reaction. Immediately transfer an appropriate quantity of the reacting solution to the spectrophotometric cell, place the cell in the cell chamber at the appropriate temperature and record the absorbance change against an appropriate reference (water or methyl orange solution) at 380 nm for 12 min after initiation of the reaction, using appropriate conditions (Tables 1—3). Calculate the change in absorbance from 4 to 12 min (2-point method) or merely record the absorbance after 12 min (single-point method). Repeat the measurement in the absence of added vanadium to obtain the values for the uncatalyzed reaction, and subtract this blank value from the previous value. From the net values obtained from standard vanadium solution, construct a calibration graph of change of absorbance per min vs. vanadium concentration.

TABLE 1

Experimental conditions for determination of vanadium

Experiment	1	1′	2	2′	3	4
Reaction temperature (°C)	22	22	30	30	50	30
Elapsed times (min)	4, 12	4, 12	4, 12	4, 7.2	4, 12	20, 40
Full scale absorbance	1.0, 2.0	0.1	2.0	0.1	2.0	2.0
Reference	H_2O	M.O.[a] (0.03 Abs.)	H_2O	M.O.[a] (0.043 Abs.)	H_2O	H_2O
Max. abs. measured	0.56	0.09	0.36	0.10	1.55	1.62
Linear calibration range (ng V)	0—50	0—5	0—10	0—5	0—60	0—25

[a]Methyl orange (abs. measured against water).

TABLE 2

Sensitivity and precision of determination at different temperatures (an abundance of 2.00 gave full scale deflection)

Temp. (°C)	22	30	50	30
Times (min)	4, 12	4, 12	4, 12	20, 40
Sensitivity (ng)[a]				
2-point method	1.6	0.82	0.32	1.0
1-point method	1.6	0.84	0.34	0.30
Standard deviation[b]				
2-point method	—	1.20	0.52	1.10
1-point method	—	0.95	1.60	0.93

[a]Quantity of vanadium that gave 0.5% f.s.d. [b]For 5 determinations of 10 ng V.

TABLE 3

Sensitivity and precision of determination of various scale expansions

Temp. (°C)	22	22	22	30	30
Abs. full scale	2.00	1.00	0.100	2.00	0.100
Sensitivity (ng)[a]					
2-point method	1.6	0.78	0.096	0.82	0.041
1-point method	1.6	0.80	0.12	0.84	0.042
Standard deviation					
2-point method	—	0.83[b]	0.24[c]	1.2[b]	0.28[b]
1-point method	—	1.1[b]	0.39[c]	0.95[b]	0.49[b]

[a]As in Table 2. [b]5 determinations of 10 ng V. [c]5 determinations of 5 ng V.

RESULTS AND DISCUSSION

Absorption spectra and absorbance/time dependence

Figure 1 shows the absorption spectra, accompanied by an elapsed time scale, for a gallic acid solution and for reacting sample solutions with or without vanadium. Although the reaction is proceeding during the spectral measurements, the absorbance change during the 0.8 min required for measuring each spectrum was less than 10% at 380 nm, and so had little significant effect on the spectra. The figure shows that measurements at 380 nm are more sensitive than measurements at 420 nm, used previously [1], so that 380 nm was used in the work described here.

Figure 2 shows examples of absorbance/time plots at 22°C and 50°C. Between 3 and 12 min, every plot was approximately linear, indicating a zero-order reaction in gallic acid. This is similar to the results in the previous paper, except for the time scale. A rate coefficient (k) was evaluated as the absorbance change per min between 4 and 12 min, i.e., $(A_{12} - A_4)/8$; this is used as a measure of reaction rate.

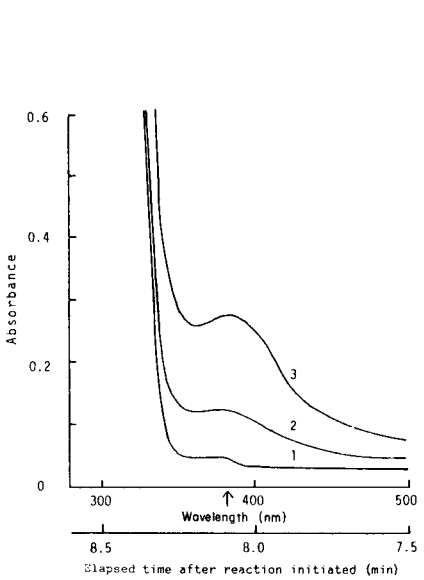

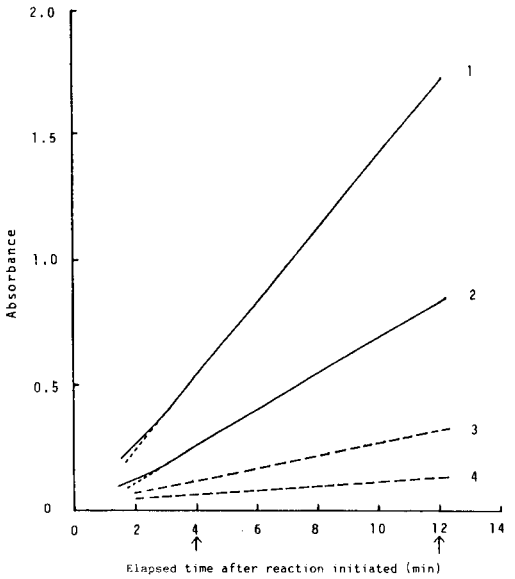

Fig. 1. Absorption spectra: (1) 0.018 M gallic acid; (2) 4 ml of 2.4 M bromate and 3 ml of 0.06 M gallic acid, pH 3.8, 22°C, without vanadium; (3) as (2) with 25 ng of vanadium, water as reference. The recommended wavelength is indicated by an arrow.

Fig. 2. Absorbance/time plots (0.96 M bromate, 0.018 M gallic acid, pH 3.8, 380 nm) in the presence of: (1) 25 ng V, 50°C; (2) no vanadium, 50°C; (3) 25 ng V, 22°C; (4) no vanadium, 22°C. The arrows indicate the times used for rate measurements.

Effect of pH

Figure 3 shows the effect of pH on the uncatalyzed and catalyzed reactions at 22°C, which were studied with solutions containing no added vanadium (blank) or 25 ng of vanadium. The pH was adjusted by adding buffer solutions prepared from 0.27 ml of 2 M acetate and 0.12—1.17 ml of 10 M acetic acid. The rate coefficient of the catalyzed reaction was obtained as the difference ($k_o - k_u$) between the rate coefficients for the overall and uncatalyzed reactions. The rate coefficient of the catalyzed reaction, increased slightly with decrease of pH, but that for the uncatalyzed reaction showed an undesirably large increase with decrease in pH, especially at pH <3.5. The relative standard deviation (r.s.d.) of the values was 63% at pH 3.1 and 8.3% at pH 3.8 for five analyses of solutions each containing 10 ng of vanadium. Therefore, pH 3.8 is recommended, for the same reason as in the previous paper [1], although the sensitivity at pH 3.8 was slightly lower than that at pH 3.1.

The slightly increased rate of the catalyzed reaction and the greatly increased rate of the uncatalyzed reaction at pH <3.5 were found when the reactants were used at high concentrations, as in the present study. In the previous paper [1], the rate of the catalyzed reaction increased significantly with decrease of pH from 5.0 to 3.5, whereas the rate of the uncatalyzed reaction was negligible throughout the pH range.

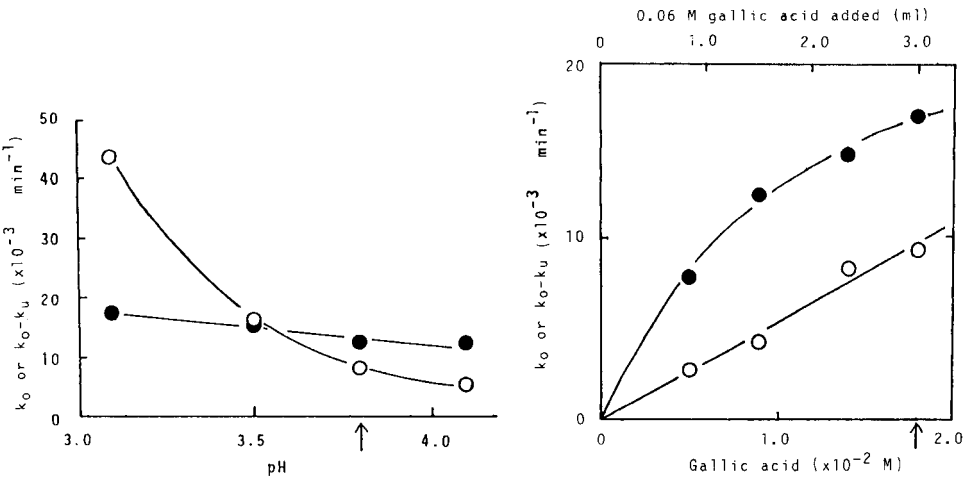

Fig. 3. Effect of pH on the rate coefficients at 22° C: (○) uncatalyzed reaction; (●) reaction catalyzed by 25 ng of V (4 ml of 2.4 M bromate, 3 ml of 0.060 M gallic acid). The arrow indicates the recommended pH.

Fig. 4. Effect of gallic acid concentration on the rate coefficients at 22° C: (○) uncatalyzed reaction; (●) reaction catalyzed by 25 ng V (4 ml of 2.4 M bromate pH 3.8). The recommended concentration is arrowed.

Effects of concentrations of gallic acid and bromate and of temperature

Gallic acid (0.053 M) and 0.12 M potassium bromate, were used previously [1—4]. The kinetics suggest that higher concentrations of reactants give faster reactions. Therefore, the use of concentrations of gallic acid and bromate as high as possible was desirable to find the greatest practical sensitivity for the catalytic method. The solubility of gallic acid is about 0.07 M in water of 25° C. the solubilities of potassium bromate (used in the previous papers) and sodium bromate at 20° C are about 0.4 M and 2.4 M in water, respectively. Thus, 0.060 M gallic acid and 2.4 M sodium bromate were selected as the working solutions. Compared with the solutions used previously [1], the concentration of gallic acid was only slightly higher but the bromate concentration was about 20 times higher.

The effects of the concentrations of these reagents on k_u and $k_o - k_u$ are shown in Figs. 4 and 5. Increasing the concentrations of each reagent in the range shown significantly increased the rate of both the uncatalyzed and catalyzed reactions, though in the previous study [1] the rate coefficient of the uncatalyzed reaction was negligible regardless of the concentrations of the reagents. Thus, 3 ml of 6×10^{-2} M gallic acid solution and 4 ml of 2.4 M sodium bromate solution are recommended here; these amounts gave the fastest catalyzed reaction, which was essentially zero order in bromate and gallic acid, although such concentrations give a relatively rapid uncatalyzed reaction, as shown in both figures. Thus, the initial concentrations of gallic

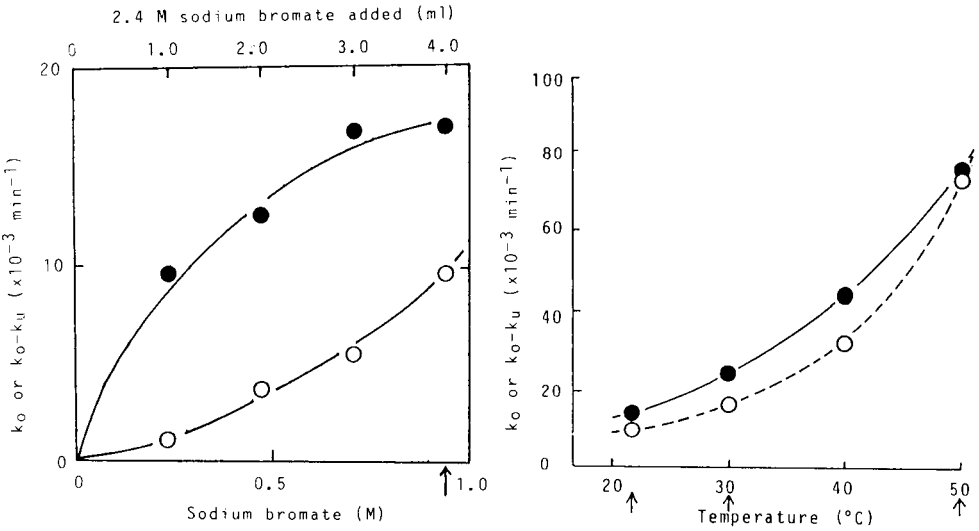

Fig. 5. Effect of sodium bromate concentration on the rate coefficients at 22° C: (○, ●) as in Fig. 4 (3 ml of 0.06 M gallic acid, pH 3.8). The recommended concentration is arrowed.

Fig. 6. Effect of temperature on the rate coefficients: (○, ●) as in Fig. 4. (Recommended concentrations of gallic acid and bromate, pH 3.8.)

acid and bromate in the reacting solution are 0.018 M and 0.96 M, respectively, which are twice and 80 times, respectively, those used previously.

The effect of temperature was studied for the catalyzed, as well as the now important uncatalyzed reaction. Figure 6 shows that both reactions are affected by temperature in a similar manner. The plot of log k_u or log ($k_o - k_u$) vs. the reciprocal of the absolute temperature gave linear Arrhenius plot; 22, 30 and 50° C were later investigated for the determination of vanadium.

Determination of vanadium

Table 1 shows the experimental conditions, maximum absorbances measured, and the linear calibration ranges that were used for determination of vanadium. In some experiments, a methyl orange solution was used in the spectrophotometer reference cell to balance a major part of the absorbance caused by the uncatalyzed reaction, so as to measure more effectively the absorbance change caused only by the vanadium-catalyzed reaction at the greatest scale expansion. The calibration graph for solutions at 30° C was approximated by two straight lines which intersected at ca. 10 ng of vanadium, although the determination of vanadium up to at least 25 ng was possible.

The precision of spectrophotometric measurements in kinetic methods is poorer than in the conventional equilibrium methods because the absorbance is continuously changing during the measurement. Nevertheless, the relative standard deviations of 10% obtained for 10 ng of vanadium was considered

to be reasonable. The sensitivities obtained under the various conditions can be compared by measuring the vanadium concentrations which give rise to an absorbance change of 0.5% of full scale, under the same scale expansion. Table 2 shows that the sensitivity increases with increasing temperature, and that the sensitivities are very similar for the single- and two-point measurement methods. If the reaction time was extended to measure the change in absorbance between 20 and 40 min, or merely at 40 min, the single-point measurement had a similar sensitivity to measurement at 50° C, and the two-point method was less sensitive. The precision was unaffected.

Table 3 shows the sensitivities and precisions obtained at greater scale expansion. The sensitivity improved in proportion to the expansion and the precision was also improved. The highest sensitivity achieved was around 40 pg of vanadium. The lower limit of detection (2σ) was ca. 0.5 ng at 22 and 30° C. The sensitivity and detection limit were improved 50 times and 4 times, respectively, over those reported previously [1]. Because measurements are made within 12 min, it seems likely that the catalyzed reaction could be adapted to f.i.a.

Effect of diverse ions

Several ions were found previously [1] to cause significant errors. Table 4 shows the effects of these ions on the determination of 5 ng of vanadium by the two-point method at 22° C (Expt. 1′, Table 1). The following ions did not interfere: Al^{3+} (500 ng), Fe^{3+} (5 ng), Mo(VI) (500 ng), Cu^{2+} (1 μg), Br^- (10 μg) and I^- (250 ng). Allowable ratios of these foreign ions to vanadium were similar to those obtained previously. The presence of up to 10 μg of Ca^{2+}, Mn^{2+}, Ni^{2+}, Zn^{2+} or Pb^{2+} did not cause interference.

TABLE 4

Effect of foreign ions on the determination of 5 ng of vanadium

Ion	Amount (ng)	Added as	V found (ng)	Relative error (%)
Al^{3+}	5000	$AlK(SO_4)_2 \cdot 12H_2O$	5.7	14
	1000		5.5	10
	500		5.2	4
Fe^{3+}	1000	$FeNH_4(SO_4)_2 \cdot 12H_2O$	9.9	98
	25		5.5	10
	5		5.1	2
MoO_4^{2-}	2500	$(NH_4)_6(Mo_7O_{24}) \cdot 4H_2O$	5.7	11
	500		4.9	−2
Cu^{2+}	1000	$CuSO_4 \cdot 5H_2O$	5.0	0
Br^-	10000	KBr	4.8	−4
I^-	500	KI	6.0	20
	250		5.2	4

REFERENCES

1 T. Yamane and T. Fukasawa, Bunseki Kagaku, 25 (1976) 454.
2 T. Yamane and T. Fukasawa, Bunseki Kagaku, 26 (1977) 692.
3 T. Fukasawa and T. Yamane, Anal. Chim. Acta, 88 (1977) 147.
4 T. Fukasawa and T. Yamane, Anal. Chim. Acta, 113 (1980) 123.

Analytica Chimica Acta, 171 (1985) 333—336
Elsevier Science Publishers B.V., Amsterdam — Printed in The Netherlands

Short Communication

THE BIOLUMINESCENT DETERMINATION OF ADENOSINE TRIPHOSPHATE WITH A FLOW-INJECTION SYSTEM

P. J. WORSFOLD* and A. NABI
Department of Chemistry, University of Hull, Hull, HU6 7RX (Great Britain)

(Received 5th October 1984)

Summary. A procedure is described, for the bioluminescent determination of adenosine-5'-triphosphate (ATP), based on firefly luciferin and luciferase and a purpose-built flow-through detector. The limit of detection is 10^{-14} mol and the sample throughput is 200 h^{-1}. The useful response range for a 30-μl sample was 10^{-8}—10^{-4} M ATP and the correlation coefficient (r) for a log-log plot over this range was 0.9991.

The attraction of using flow injection analysis (f.i.a.) to monitor transient chemiluminescent reactions in solution is that sample and reagent can be mixed rapidly and reproducibly in front of a photomultiplier [1, 2]. This approach results in improved precision, higher sample throughput and increased sensitivity compared with conventional discrete systems. The use of bioluminescent reactions in conjunction with f.i.a. offers a twofold advantage over most chemiluminescent systems; sensitivity is enhanced by the higher quantum yields and selectivity is increased because of the enzymes involved.

The two commonest bioluminescent systems are those derived from fireflies (*Photinus pyralis*) and from bacteria (*Photobacterium fischeri*), which require ATP and NAD(P)H, respectively, as co-factors. The firefly system can be used to monitor ATP directly, as an indicator for an ATP-producing reaction or as an immunoassay label [3]. This communication describes a flow-injection system with merging zones for the determination of ATP via a bioluminescent reaction with firefly luciferin/luciferase. The effects of various system parameters are discussed and the system is optimized.

Experimental

Reagents. An aqueous Tris buffer solution containing tris(hydroxymethyl)-aminomethane (0.1 M) and EDTA (1 mM) was adjusted to pH 7.75. Glycylglycine (0.1 M), glycine (50 mM)/arsenate (10 mM) and phosphate (0.1 M) buffers containing EDTA (1 mM) at pH 7.5 were prepared in a similar way. Sodium hydroxide (1 M) or hydrochloric acid (2 M) was used for pH adjustment. An aqueous stock solution of 0.1 mM ATP (Sigma) was prepared and stored at 4°C. Standards were prepared by serial dilution of the stock solution

0003-2670/85/$03.30

with Tris buffer. Luciferin and luciferase were obtained as desiccated firefly tails (Sigma) and stored at 0°C in the dark. All other reagents were of analytical grade, and deionized water was used throughout.

Extraction and purification of luciferin and luciferase. For the extraction, an aqueous glycylglycine buffer solution (0.1 M) containing EDTA (1 mM), magnesium sulphate (10 mM) and bovine serum albumin (1 g l^{-1}) was prepared and adjusted to pH 7.75. To extract luciferin and luciferase from firefly tails, the method of Rasmussen and Nielsen [4] was followed. Desiccated firefly tails (250 mg) were finely ground with acid-washed sand, glycylglycine buffer (2 ml) was added and the mixture was centrifuged. The supernatant liquid was decanted and made up to 25 ml with glycylglycine buffer. This extract was used in the optimization of the flow-injection system. The extract was purified by elution from a low-porosity Sephadex G-25 column with glycine/arsenate buffer at a flow rate of 5 ml h^{-1}. Fractions (4 ml) were collected and the fluorescence (λ_{ex} = 366 nm; λ_{em} = 535 nm) and u.v. absorbance (280 nm) were monitored. Those fractions containing luciferin and luciferase [5] were pooled and used in the calibration of the flow-injection system. The extraction and purification were done at 4°C.

Instrumentation and procedures. A merging-zones manifold with Tris buffer carrier streams was used. The ATP standards (30 μl) and luciferin/luciferase (30 μl) were simultaneously injected into separate carrier streams, each with a flow rate of 1.1 ml min^{-1}, via a dual-injection rotary valve. If consumption of expensive reagents is not a constraint, the luciferin/luciferase volume can be increased to facilitate complete sample-reagent mixing. The merged zones were passed through a short mixing coil and into a glass coil placed in front of an end window photomultiplier tube (Thorn EMI 9844B). The manifold tubing was polyethylene (0.5 mm i.d.), the total length from the merging point to the entry into the glass coil being 6 mm. The detector was enclosed in a light tight box to minimize stray light [6] and the photomultiplier output was fed to a recorder. The optimized conditions described below were used for calibration.

Results and discussion

Optimization of the flow-injection system. The effect of flow rate on the emission signal was investigated over the range 1.0—3.4 ml min^{-1} by using a 10^{-6} M ATP standard. The signal increased with flow rate up to 2.3 ml min^{-1}, at which point the maximum bioluminescence emission was coincident with the passage of the sample zone through the glass coil. The manifold can therefore be easily modified to study faster chemiluminescent processes by altering either the flow rate or the length of the mixing coil. The relative standard deviation (r.s.d.) for ten replicate injections at each flow rate tested ranged from 1 to 5% with 2.0 ml min^{-1} giving the most precise results. A study of the effect of pH showed that maximum bioluminescence emission occurred at pH 7.5 with 80% of the maximum intensity at pH 7.0 and pH 8.0. The presence of magnesium ions is also required for maximum bioluminescence

TABLE 1

Bioluminescence emission obtained at various ATP concentrations

ATP Conc. (M)	Output voltage (mV)	R.s.d. (%)	ATP Conc. (M)	Output voltage (mV)	R.s.d. (%)
0	0	—	1×10^{-6}	17.5	5.0
1×10^{-9}	0.1	—	1×10^{-5}	120	7.6
1×10^{-8}	0.5	6.0	1×10^{-4}	600	1.4
1×10^{-7}	2.5	4.1			

emission [7] and the signal was greatest at 1×10^{-2} M magnesium. All subsequent experiments were therefore done with Tris buffer containing 1×10^{-1} M magnesium at pH 7.5, pumped at a total flow rate of 2.0 ml min^{-1}.

The composition of the buffer also has a significant effect on bioluminescence emission [8] and under the above conditions glycylglycine buffer gave the best results (100%), with Tris buffer (50%) and phosphate buffer (10%) giving much smaller signals. Therefore glycylglycine was used for the calibration experiments discussed below.

Calibration for ATP. Preliminary experiments with the firefly tail extract showed a high background signal caused by the presence of ATP and other low-molecular-weight substances. Further studies were therefore done with the partially purified extract. The results obtained are shown in Table 1 and indicate a detection limit of 10^{-9} M ATP with a 30-μl sample. The useful response range for ATP is 10^{-8}—10^{-4} M and a log-log plot of the data for this region had a correlation coefficient (r) of 0.9991. Above 10^{-4} M ATP the response levels off because of substrate saturation and product inhibition of the enzyme. The throughput of 200 samples h^{-1} and the precision data show that f.i.a. provides an excellent tool both for the study of bioluminescence reactions and for routine bioluminescence assays. Major modifications to the detector design should also considerably improve the detection limit and decrease the reagent volume per assay. The manifold can also accommodate immobilized reagents in packed reactor columns (e.g., immobilized luciferase [9, 10]) which would decrease costs still further.

REFERENCES

1 G. Rule and W. R. Seitz, Paper No. 18, 11th Annual Symposium on Advanced Analytical Concepts for the Clinical Laboratory, Oak Ridge, TN, April, 1979.
2 J. L. Burguera, A. Townshend and S. Greenfield, Anal. Chim. Acta, 114 (1980) 209.
3 A. Lundin, in M. Serio and M. Pazzagli (Eds.), Luminescent Assays: Perspectives in Endocrinology and Clinical Chemistry, Raven, New York, 1982.
4 H. Rasmussen and R. Nielsen, Acta Chem. Scand., 22 (1968) 1745.
5 R. Nielsen and H. Rasmussen, Acta Chem. Scand., 22 (1968) 1757.
6 A. T. Faizullah and A. Townshend, Anal. Proc., 22 (1985) 15.

7 W. D. McElroy, J. W. Hastings, J. Coulombre and V. Sonnenfeld, Arch. Biochem. Biophys., 46 (1953) 399.
8 J. J. Webster, J. C. Chang, E. R. Manley, H. O. Spivey and F. R. Leach, Anal. Biochem., 106 (1980) 7.
9 J. Ford and M. De Luca, Anal. Biochem., 43 (1981) 110.
10 L. J. Kricka, G. K. Weinhausen, J. E. Hinkley and M. De Luca, Anal. Biochem., 129 (1983) 392.

Analytica Chimica Acta, 171 (1985) 337—343
Elsevier Science Publishers B.V., Amsterdam — Printed in The Netherlands

Short Communication

A FAST PROCEDURE FOR STANDARD ADDITIONS IN FLOW INJECTION ANALYSIS

M. C. U. ARAÚJO, C. PASQUINI and R. E. BRUNS*

Instituto de Química, Universidade Estadual de Campinas, C.P. 1170, 13100 Campinas, S.P. (Brasil)

E. A. G. ZAGATTO

Centro de Energia Nuclear na Agricultura, USP, 13400 Piracicaba, S.P. (Brasil)

(Received 24th October 1984)

Summary. A method based on the concentration/time profile generated by the injection of a single standard solution is described. The method is applied to the determination of sodium, potassium and calcium by flame photometry. Calibration graph errors as high as 60% are reduced to 3% by using the standard addition method.

The standard addition method (s.a.m.) [1], usually employed to overcome sample matrix effects, requires successive additions of known amounts of the analyte to the sample. If linear response of the detection system is assumed, linear regression calculation permits the original concentration to be evaluated regardless of the matrix effect, while also providing information on the magnitude of this effect. However, the manual standard addition procedure is cumbersome and can be wasteful when used with sample-consuming sensors such as the atomic emission spectrometer. The feasibility of using standard additions in flow injection analysis (f.i.a.) has been demonstrated by several workers [2—7] who have pointed out that most of the drawbacks of the manual method are minimized in flow-injection systems, which always yield highly precise measurements after rapid processing of small sample volumes.

In the simplest f.i.a./s.a.m. combination, as devised by Tyson [4] and later applied to the determination of chromium in steels [5], different standard solutions were injected into a continuously moving carrier stream which consisted of the sample placed in an infinite volume situation [8]. As dispersion is very reproducible in f.i.a., different portions of the established zone can be characterized by well defined and previously determined sample-to-standard ratios. Therefore, the standard addition procedure is achieved simply by taking into account different measurements related to selected portions of the dispersed sample zone. To each addition level, however, there corresponds a different degree of sample dilution and, thus a different extent of the matrix effect.

0003-2670/85/$03.30

The merging-zones approach [9] was used to achieve standard additions under constant sample dispersion. In this system, both the sample and the standard solutions were injected into two separate carrier streams, the interaction between the established zones occurring after the merging of these streams. With this system, a generalized standard addition method (g.s.a.m.) [10, 11] was used to overcome spectral interferences and matrix effects in the atomic emission spectrometry of copper, nickel and zinc in alloys [2]. This extended s.a.m. evaluates the complete **K** matrix which contains values for the sensitivities of each sensor for each analyte. This procedure, however, required the preparation of a large set of standard solutions to provide different addition levels and to cover wide concentration ranges. Giné et al. [3] demonstrated that a single standard solution was enough for a f.i.a./s.a.m. combination with the merging-zones approach and the zone-sampling process [12]. In this system, the standard solution was introduced into a first carrier stream and, after a defined time interval, an aliquot of the dispersed zone was resampled and introduced into a second carrier stream, being added to the sample zone via the merging-zones approach. By selecting different time intervals, several standard concentrations could be selected for addition, so that only one standard solution per analyte was required. The procedure, which was successfully applied to the determination of nitrate in plant leaves, required an electronically operated injector and an elaborate flow injection analyzer. Because each standard addition requires a separate injection, the sample volume requirement is relatively high by f.i.a. standards and sample throughput is hindered.

The above procedures can be greatly simplified by using an injection of the standard solution into a carrier stream to be merged with the undispersed sample. As shown below, a single standard injection suffices to achieve the complete standard addition procedure under constant matrix conditions. The efficiency of the method is illustrated by applications of the g.s.a.m. on synthetic samples giving both spectral interferences and matrix effects in atomic emission spectrometry involving sodium, potassium and calcium.

Experimental

Reagents and solutions. All chemicals including the 99% ethanol were of analytical-reagent quality; freshly distilled water was always used. Separate stock standard solutions (1000 mg l^{-1}) of sodium, potassium and calcium were prepared from the chloride salts. The synthetic samples were obtained by dilutions of these stock solutions with water and ethanol in order to achieve final ethanol concentrations in the range 0—10% (v/v).

Apparatus. An Ismatec MP-13-GJ4 peristaltic pump provided with Solvaflex pump tubes was used. Thick-walled polyethylene tubing (1.0 mm i.d.) was used in the manifold. Details of the injector-commutator and connectors were reported earlier [13]. A Micronal B262 two-channel flame photometer, operated with an air/butane (natural gas) flame as specified by

the manufacturer, was connected to an ECB (Equipamentos Científicos do Brasil) RB101 recorder.

Flow diagram. The flow diagram of the proposed system is shown in Fig. 1. Both carrier streams are water. The standard solution to be added is aspirated, filling the sampling loop, the excess going to waste. Movement of the injection commutator to the alternative position places the sample in the infinite volume situation. After steady-state achievement, the injector is displaced to the injection position, introducing the standard solution and initiating chart movement by means of the micro-switch. The standard solution zone undergoes dispersion in the C_1 coil, merging with the sample at point Y. After the C_2 line, the sample reaches the detector and a transient signal is recorded. Thereafter, the injector and the commutator are placed back in the positions specified in Fig. 1, allowing the next sample to be processed.

As sensitivity was not critical, a symmetrical confluence configuration was chosen, the average flow rate reaching the inlet of the nebulizer being higher than the pneumatic aspiration rate of the photometer (5.6 ml min^{-1}). The C_2 (15 cm) line—nebulizer connection used has already been described [13]. The C_1 length (21 cm) was sufficient to permit dispersion of the standard whereas C_2 was as short as possible. It should be stressed that the C_1 length should be increased to allow almost complete dispersion before the confluence point, if the sample matrix affects the dispersion of the standard zone. If sensitivity is a critical factor in the determination, the flows of the sample and carrier streams can be optimized to obtain the desired dilution of the sample.

Procedure. Initially, the standard solution to be added is pumped through the sample line, instead of the sample, to permit the evaluation of H_p (Fig. 2a). Then, the concentration/time profiles (Fig. 2b) are obtained by

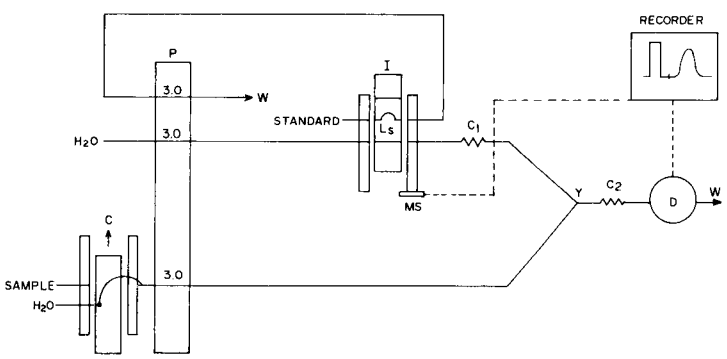

Fig. 1. The flow diagram of the proposed system. P, peristaltic pump, giving flow rates of 3.0 ml min^{-1}; I, the standard solution injector; D, flame photometer; W, waste; Y, confluence point; L_S, standard solution loop; MS, the micro-switch that activates the recorder; C, the commutator for changing samples or for replacing the sample with water; C_1, C_2, mixing coils (see text).

injecting the standard solution; 300-μl injections were used in all cases. The micro-switch provides reproducible timing, matching the moments of injection and chart paper movement. When the commutator is positioned to introduce the sample, the concentration/time profile is recorded above the sample steady-state signal, H_0 (Fig. 2c and d). Only this last step is necessary for subsequent samples.

From the recorded chart profile of Fig. 2(b), the heights H_1, $H_2 \cdots H_n$ associated with appropriate standard addition levels are selected and measured manually, and the corresponding times t_1, $t_2 \cdots t_n$ are noted; n is the number of standard additions used. For all samples, heights H'_1, $H'_2 \cdots H'_n$ are measured at these time intervals (Fig. 2c and d). The analyte concentration in the sample is obtained by linear regression computation from the two sets of time-dependent height measurements, the H values being converted to appropriate concentration units; the cases considered here give linear responses.

For the g.s.a.m. applications, the same procedure for obtaining the H and H' data sets was used for each analyte. In the present applications, six times corresponding to six standard additions were chosen; the heights were measured after the peak maximum because the available times for mixing are then longer and the concentration/time profile is more reproducible.

Results and discussion

The proposed procedure can correct for sudden changes in some operating conditions of the system which may happen between successive samples. For example, variations in the air flow rate caused only slight modifications in the final results (Table 1) in contrast to the results obtained by the usual manual calibration method, which is strongly dependent on this flow rate. Of course, as the sample is very rapidly processed in the proposed f.i.a./

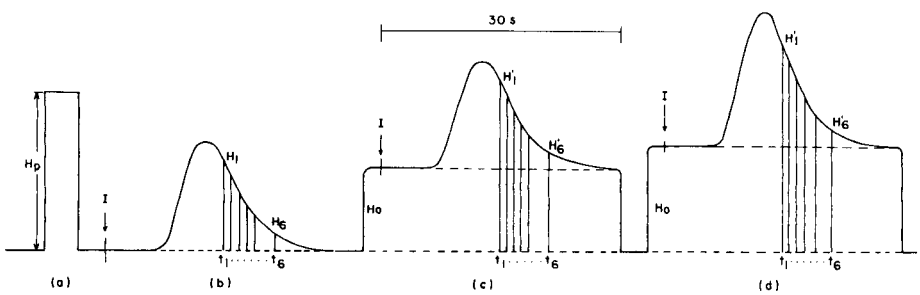

Fig. 2. Measurements obtained with the proposed system: (a) the 20 mg l^{-1} potassium standard solution pumped continuously (steady state) in the sample line; (b) the same potassium standard solution injected into the carrier stream; (c) the same potassium standard solution injected into the carrier stream and merging with a continuous flow of aqueous 10 mg l^{-1} potassium sample solution; (d) identical to (c) except that the 10 mg l^{-1} potassium sample solution contained 10% (v/v) ethanol to simulate a matrix effect.

TABLE 1

Comparison of calcium concentrations obtained from a calibration graph and by the proposed method for varying air flow rates

Variations in air pressure (Psi)	Concentration found (mg l^{-1})[a]	
	Proposed method	Calibration graph
0.80	103	111
0.83[b]	102	102
1.00	99.7	69.7

[a]100 mg l^{-1} calcium solution taken. [b]Pressure specified by the photometer manufacturer.

s.a.m. system, the possibilities of variations in the operating conditions are reduced. The correlation coefficients for all the calibration plots used in this work were 0.9997 or higher.

The calcium, potassium and sodium results found by the proposed standard additions procedure were almost unaffected by modifications in the sample matrix, here exemplified by changes in the ethanol content. Table 2 indicates that the errors are usually less than 3% when the ethanol content in the sample is changed from 0 to 10% (v/v). The errors associated with conventional calibration plots are much larger, because the nebulization efficiency is very dependent on the alcohol content of the samples. These data illustrate the importance of using a method that eliminates any matrix effect

TABLE 2

Comparison of calcium, potassium and sodium concentrations in ethanolic solutions obtained from the standard additions method, the generalized standard additions method and calibration graphs

Ethanol (% v/v)	Concentrations found (mg l^{-1})						Error (%)					
	Standard additions			Calibration graph			Standard additions			Calibration graph		
	Ca	K	Na	Ca	K	Na	Ca	K	Na	Ca	K	Na
Proposed standard additions method[a]												
2	256	9.73	0.98	266	10.6	1.09	+2.4	−2.7	−2.0	+6	+6	+9
4	252	9.90	0.98	283	11.1	1.17	+0.8	−1.0	−2.0	+13	+11	+17
6	254	10.0	0.98	290	11.8	1.26	+1.6	0.0	−2.0	+16	+18	+26
8	250	9.98	1.06	304	12.2	1.38	0.0	−0.2	+6.0	+22	+22	+38
10	258	9.99	1.03	318	12.8	1.42	+3.2	−0.1	+3.0	+27	+28	+42
The generalized standard additions method[b]												
5	204	10.0	2.56	267	12.2	3.66	+2.0	0.0	+2.4	+33	+22	+46
10	204	10.5	2.58	293	13.7	4.19	+2.0	+5.0	+3.2	+46	+37	+68

[a]Concentrations taken were 250 mg l^{-1} Ca, 10.0 mg l^{-1} K and 1.00 mg l^{-1} Na. [b]Concentrations taken were 200 mg l^{-1} Ca, 10.0 mg l^{-1} K and 2.50 mg l^{-1} Na. See text for full explanation.

caused by unknown amounts of alcohol in the samples. In the proposed method, all the H' and H_0 values are measured for a constant degree of sample dilution, so that errors caused by variations in the matrix effect are minimized. Because the angular coefficient of the s.a.m. equation reflects the magnitude of the matrix effect, it might be possible to determine the alcohol content by the proposed single-injection method.

The usefulness of the proposed procedure becomes strikingly evident for multicomponent determinations in which both matrix effects and spectral interferences may affect the accuracy adversely. Table 2 includes results for the joint determinations of sodium, potassium and calcium in ethanolic solutions, obtained by the f.i.a./g.s.a.m. method and from the usual calibration plots. There is little difference in the errors related to the f.i.a./g.s.a.m. and the f.i.a./s.a.m. procedures. The errors associated with the use of calibration graphs for the ethanolic solutions are significantly larger for the multicomponent determinations (Table 2). This illustrates the serious discrepancies that can occur when errors caused by matrix effects are compounded by errors from spectral interferences; e.g., a 68% error in the sodium concentration is caused by the presence of 10% (v/v) ethanol and other species, whereas with the single analyte the error, caused only by the matrix effect, is 42%.

The proposed f.i.a./s.a.m. procedure has several advantages over other f.i.a./s.a.m. procedures. For example, only a simple manifold with a homemade injector and commutator is needed, only one standard solution is used for each analyte, and a single injection provides the number of standard additions deemed necessary for accurate analyte determination. The time necessary to complete the procedure is around 2 min, which gives an appreciable economy in sample consumption compared with other methods [2—7]. As the proposed method is fast, it is less vulnerable to errors from fluctuations in instrumental conditions. A method requiring only one injection per analyte makes the f.i.a./g.s.a.m. much more attractive from the practical point of view.

Current studies include the use of a microcomputer in obtaining and processing the analytical data with the aim of increasing the efficiency and precision of the proposed method while decreasing the time required. Applications in atomic absorption and spectrophotometric measurements are also being pursued.

The authors thank M. F. Giné and F. J. Krug for critical comments. One of us (M.C.U.A.) is grateful to the Universidade Federal da Paraiba for a fellowship (CAPES/PICD).

REFERENCES

1 M. Bader, J. Chem. Educ., 57 (1980) 703.
2 E. A. G. Zagatto, A. O. Jacintho, F. J. Krug, B. F. Reis, R. E. Bruns and M. C U. Araújo, Anal. Chim. Acta, 145 (1983) 169.

3 M. F. Giné, B. F. Reis, E. A. G. Zagatto, F. J. Krug and A. O. Jacintho, Anal. Chim. Acta, 155 (1983) 131.
4 J. F. Tyson, Analyst (London), 106 (1981) 1125.
5 J. F. Tyson and A. B. Idris, Analyst (London), 109 (1984) 23.
6 S. Greenfield, Spectrochim. Acta, Part B, 38B (1983) 93.
7 Y. Israel and R. M. Barnes, Anal. Chem., 56 (1984) 1192.
8 J. Ruzicka and E. H. Hansen, Flow Injection Analysis, Wiley-Interscience, New York 1981.
9 H. Bergamin F.°, E. A. G. Zagatto, B. F. Reis and F. J. Krug, Anal. Chim. Acta, 101 (1978) 17.
10 B. E. H. Saxberg and B. R. Kowalski, Anal. Chem., 51 (1979) 1031.
11 J. H. Kalivas and B. R. Kowalski, Anal. Chem., 53 (1981) 2207.
12 B. F. Reis, A. O. Jacintho, J. Mortatti, F. J. Krug, E. A. G. Zagatto, H. Bergamin F.° and L. C. R. Pessenda, Anal. Chim. Acta, 123 (1981) 221.
13 A. O. Jacintho, E. A. G. Zagatto, H. Bergamin F.°, F. J. Krug, B. F. Reis, R. E. Bruns and B. R. Kowalski, Anal. Chim. Acta, 130 (1981) 243.

Analytica Chimica Acta, 171 (1985) 345—350
Elsevier Science Publishers B.V., Amsterdam — Printed in The Netherlands

Short Communication

ENZYME ELECTRODE FOR UREA WITH AMPEROMETRIC INDICATION
Electrode with Diffusional Limitation

DIETER KIRSTEIN and FRIEDER SCHELLER

Akademie der Wissenschaften der DDR, Zentralinstitut für Molekularbiologie, Bereich Angewandte Enzymologie, 1115 Berlin-Buch (German Democratic Republic)

BO OLSSON and GILLIS JOHANSSON*

Department of Analytical Chemistry, University of Lund, P.O. Box 124, S-221 00 Lund (Sweden)

(Received 22nd November 1984)

Summary. Urea can be determined amperometrically with an enzyme electrode consisting of urease trapped in a poly(vinyl alcohol) gel and confined by a dialysis membrane. A pH-dependent hydrazine oxidation at a platinum anode is used as the detector reaction. The current is a linear function of the urea sample concentration over the range 1—80 mM with 50-μl samples injected into 2 ml of hydrazine buffer in the cell. With enzyme loadings above 20 U cm^{-2}, the current became limited by the rate of mass transfer in the membrane arrangement. Forty samples per hour could be analyzed with negligible carry-over when the time derivative was used for quantitation.

Electrochemical methods for the determination of urea usually combine the selectivity of urease with potentiometric detection methods. The urease-catalyzed reaction produces an increase in ammonium ion concentration and in pH which can be detected by ammonium ion-selective electrodes [1, 2], ammonia gas electrodes [3] or pH electrodes [4]. There is a logarithmic relationship between signal and urea concentration in all cases.

The relation between current and concentration of hydroxyl ions has been reported to be linear in the Tafel region of the anodic oxidation of hydrazine at platinum electrodes in alkaline [5] and acidic [6] solutions. This property can be used to linearize the response of enzymatic urea sensors [7]. The performance of such sensors with high enzyme loading is reported in this communication.

Experimental

Preparation of enzyme electrodes. Urease (E.C.3.5.1.5, from jack beans, type IX; Sigma Chemical Co.) was dissolved in 0.1 ml of double-distilled water and mixed with 0.5 ml of an aqueous 10% poly(vinyl alcohol) solution (PVA; type 55/2, VEB Chemische Werke Buna, G.D.R.). This mixture was

0003-2670/85/$03.30

cast on an acrylic glass plate (10 cm^2) and water was evaporated at 4° C overnight. Membranes with urease contents of 0.1, 8.5, 17, 34, 68, and 136 U cm^{-2} were prepared (1 U will liberate 1 μmol of ammonia under the conditions specified by Sigma). A piece of an enzyme membrane (8 × 8 mm) was mounted with the help of a cellophane dialysis membrane (thickness 0.025 mm) onto the platinum tip (4 mm diameter) of a commercial oxygen electrode (Forschungsinstitut Meinsberg, G.D.R.). The inner volume of the electrode was filled with the background solution and the electrode was mounted in a measuring cell with magnetic stirring.

The thickness and swelling characteristics of the enzyme/PVA membranes were determined by an inductive thickness measuring device. The thickness of the combined membranes increased to 0.5 mm in a few hours. The swelling will be less pronounced when the membrane is mounted in the electrode because of back-pressure by the dialysis membrane.

Background solution. The background solution contained hydrazinium sulphate (11.5 mM), EDTA (1 mM), Tris-citrate buffer (1 mM), and potassium chloride (0.1 M). All chemicals were of reagent grade. The pH was adjusted to 7.0.

Measurements. A potential of +0.1 V was applied between the platinum electrode and the Ag/AgCl reference electrode with a polarograph (type GWP 673, Academy of Sciences, G.D.R.). The current or the time derivative of the current was recorded with a y/t recorder. All solutions and the cell were thermostated at 25 ± 0.5°C. Standard urea solutions were prepared in the background solution. A typical measuring cycle was started by filling the cell with background solution (2 ml), rinsing for 1 min and then refilling; a sample (50 μl) was injected with a syringe after 2 min of equilibration, and the current was recorded until a steady-state signal was reached. Alternatively, in the derivative mode of operation, the signal was followed to the maximum, and the sensor was then ready for a new cycle.

The background current (2—4 μA) was stable for a given electrode and was recorded prior to the injections. The results were normalized by dividing the responses by the background current.

Results

The amperometric response of the hydrazine reaction at the membrane-covered electrode was studied by adding sodium hydroxide to the background solution. The correlations between added base, pH and current were as shown in Fig. 1. The current increased linearly with the amount of added sodium hydroxide between pH 6.0 and 8.0. A plot of the logarithm of the current versus the pH (not shown) gave an apparent reaction order of 0.7 with respect to the hydroxide concentration between pH 7.0 and pH 8.0. Hydroxide reaction orders of 0.8 have been reported previously for the oxidation of hydrazine and dimethylhydrazine at gold electrodes in acidic solutions [8, 9]. The complex changes of pH with added base (Fig. 1) reflects the presence of the buffering components, i.e., hydrazine (pK_a = 8.0) and Tris (pK_a = 8.1). It is

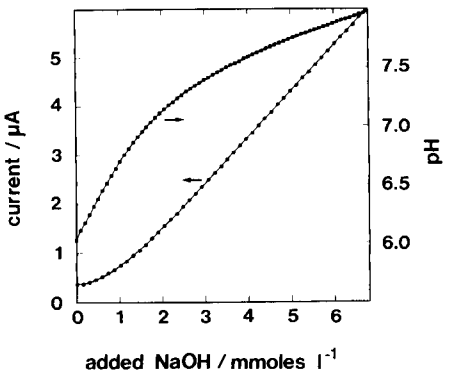

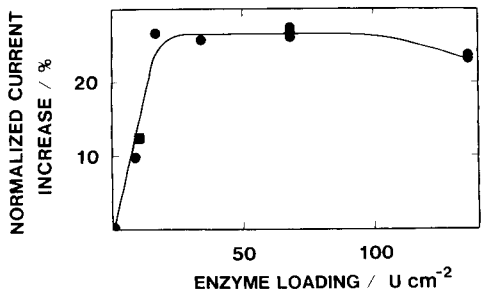

Fig. 1. Current response of the urea sensor (left axis) and pH response of a glass electrode (right axis) on the addition of sodium hydroxide to the background solution.

Fig. 2. The normalized steady-state electrode response in 0.25 mM urea solutions versus the enzyme loading: (•) this work; (▪) with soy bean urease [7].

seen that the buffer capacity of the background solution increases with pH and it was found that the logarithm of the buffer capacity was linearly dependent on pH between pH 6.9 and 7.8. It is essential that the concentration of hydroxide in the background solution increases linearly with the amount of hydrolyzed urea in order to obtain a proportional increase in current. This implies that the buffer capacity should increase with pH, which will be true if the initial pH of the background solution is below the pK_a of the main buffering component. The pH in the used solution, before urea addition, was one unit below the pK_a values.

The buffer capacity of the supporting electrolyte is also an important factor for the sensitivity of the electrode. Both the normalized current increase and the normalized derivative signal decreased six-fold when the concentration of Tris buffer was increased from 1 mM to 10 mM.

The mass-transfer relationships at a rotated electrode were studied in a manner analogous to that of Gough and Leypoldt [10]. The largest mass-transfer resistance for hydrazine was exerted by the dialysis membrane although the PVA membrane was much thicker. A similar relation would also be expected for the substrate, urea. The mass-transfer resistance in the external solution in the measuring cell became negligible because of the high stirring speed.

The response of several electrodes with different enzyme loadings was determined by injection of urea to a concentration of 0.25 mM in the cell (Fig. 2). At sufficiently high loadings, all urea that diffuses inward will be hydrolyzed, so that the concentration at the surface of the platinum electrode approaches zero. The pH and thus the steady-state current should then remain the same even if the enzyme loading is increased. About 20 U cm^{-2} was required to make an electrode with a steady-state response controlled by

TABLE 1

Response times of the urea electrodes

Enzyme loading (U cm^{-2})	8.5	17	34	68	136
Peak time(s)[a]	21	17	11	7	15
Time to reach 95% of steady-state current[b]	70	70	40	20	60

[a]Derivative mode. [b]Current mode.

mass transfer. The responses were similar for electrodes made with soy bean [7] and jack bean urease (Fig. 2).

The response time of the urea electrode was affected by the enzyme loading and thickness of the membrane. The time to reach 95% of the steady-state current, as well as the time to reach the peak in the derivative mode, decreased with increased enzymatic activity (Table 1). The height of the derivative peak consequently increased with the enzyme loading (Fig. 3). It is noteworthy that it continued to increase even in the region where the steady-state current is diffusion-controlled. At very high enzyme loadings (136 U cm^{-2}), there was a decrease in performance, probably because the urease then constituted a large fraction of the solids in the enzyme membrane (2 mg enzyme/5 mg PVA).

With mass transfer-controlled electrodes (Fig. 2), the complete hydrolysis of 0.25 mM urea gives a current increase of 26%. The results shown in Fig. 1

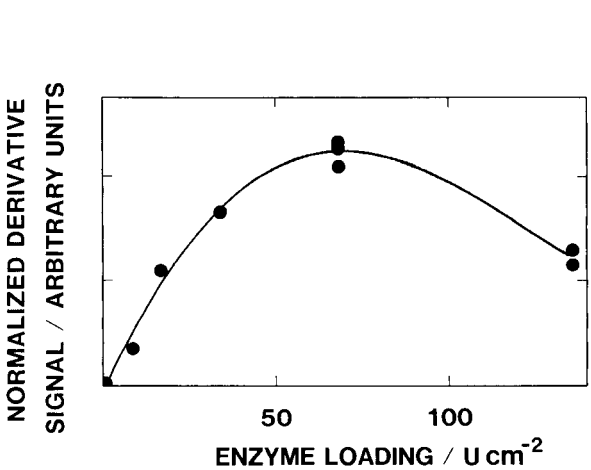

Fig. 3. The normalized derivative response in 0.25 mM urea solutions versus the enzyme loading.

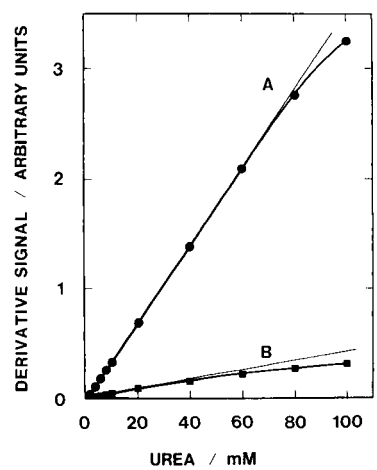

Fig. 4. Calibration curves in the derivative mode for an electrode with a urease loading of 68 U cm^{-2} in background solutions containing (A) 1 mM and (B) 10 mM Tris buffer.

can be used to calculate that the pH at the platinum electrode surface increases from 7.00 to 7.14 under these conditions. Soluble urease was used to hydrolyze 0.25 mM urea in the background solution and it was found that the pH increased 0.11 units from the initial value of 7.0. Evidently, the steady-state response of mass transfer-controlled urease membrane electrodes is similar to, or even better than, the expected equilibrium response after complete hydrolysis of urea. The validity of this conclusion was checked by adding soluble urease to the background solution in the measuring cell before injecting the urea sample. The current decreased with time as the urea in the bulk was decomposed. When the hydrolysis was complete, the response was only 60—70% of the value obtained without soluble urease in the cell. This indicates that the local pH change at the electrode surface is higher than the bulk pH change at complete hydrolysis. The reason may be that there is a favourable partition of urea to the membrane or that urea diffuses more quickly than the charged hydrolysis products in the membrane.

The derivative mode of measurement was evaluated for an electrode with a loading of 68 U cm^{-2}. The response was linear from 0.8 to 80 mM urea in the injected samples (Fig. 4). The linear range and the sensitivity decreased if the Tris concentration was increased. The relative standard deviation for successive injections of 10 mM urea was about 1% in both modes of operation. The inter-electrode variation was larger but most of it is levelled out by dividing the response by the background current of the respective electrode. The sample through-put in the derivative mode was 40 h^{-1} with optimal enzyme loading (68 U cm^{-2}). With a rinse time of 30 s and an equilibration time of 30 s, the carry-over was negligible. The operational stability of an electrode with an enzyme loading of 68 U cm^{-2} was about 20 days, whereafter the sensitivity was rapidly lost.

Discussion

The operational characteristics of the new urea electrode demonstrate the feasibility of coupling an enzyme-catalyzed reaction involving a pH change with a pH-dependent faradaic electrode process. The fast response and linear calibration are important advantages over the potentiometric electrodes for urea.

By analogy with the usual amperometric or potentiometric enzyme electrodes at high enzyme loadings, the overall process is controlled by the substrate diffusion in the membrane arrangement, as is evident from the fact that the enzyme loading above a certain level does not affect the sensitivity. The increased functional stability underlines the existence of an excess of enzyme in the membrane. The transition from the reaction-controlled process to the diffusion-limited steady-state response occurs at considerably higher enzyme loadings than those described for the potentiometric urea electrode [11].

This work was done as part of a cooperation supported by the G.D.R. Academy of Sciences and the Royal Swedish Academy of Sciences.

REFERENCES

1 G. G. Guilbault and E. Hrabankova, Anal. Chim. Acta, 52 (1970) 287.
2 G. G. Guilbault, G. Nagy and S. S. Kuan, Anal. Chim. Acta, 67 (1973) 195.
3 M. Mascini and G. G. Guilbault, Anal. Chem., 49 (1977) 795.
4 H. E. Booker and J. L. Haslam, Anal. Chem., 46 (1974) 1054.
5 J. Heitbaum and W. Vielstich, Electrochim. Acta, 18 (1973) 501, 967.
6 J. A. Harrison and Z. A. Khan, J. Electroanal. Chem., 28 (1970) 131.
7 D. Kirstein, L. Kirstein and F. Scheller, Biosensors, 1 (1985) 117.
8 U. Eisner and E. Gileadi, J. Electroanal. Chem., 28 (1970) 81.
9 U. Eisner and N. Zommer, J. Electroanal. Chem., 30 (1971) 433.
10 D. A. Gough and J. K. Leypoldt, J. Electrochem. Soc., 127 (1980) 1278.
11 G. G. Guilbault and J. G. Montalvo, J. Am. Chem. Soc., 92 (1970) 2533.

Analytica Chimica Acta, 171 (1985) 351—355
Elsevier Science Publishers B.V., Amsterdam — Printed in The Netherlands

Short Communication

EFFECT OF METAL IONS ON THE RESPONSE OF A CYANIDE-SELECTIVE ELECTRODE

AMITABH GUPTA*, ERNEST F. JOHNSON and RICHARD H. SCHLOSSEL[a]
Department of Chemical Engineering, Princeton University, Princeton, NJ 08544 (U.S.A.)
[a]*Consultant, 15 Woodside Avenue, Metuchen NJ 08840 (U.S.A.)*
(Received 19th November 1984)

Summary. An extended model and its experimental verification are presented for the response of a cyanide-selective electrode in the presence of metal ions. The model takes into account the effect of metal-hydroxide complexes at high pH values. The electrode responds to the total cyanide concentration even in the presence of an excess of zinc and cadmium ions. When copper(I) is present, the cyanide complexes must be decomposed before the total cyanide concentration can be measured. The results show the importance of considering both metal-cyanide and the metal-hydroxide complexation.

Cyanide-selective electrodes are useful only at high pH. The effect of pH on the response of the cyanide electrode and the effect of metal ions on the response due to the formation of metal-cyanide complexes have been studied [1, 2]. Mascini and Napoli [2] regulated the pH between 6 and 8; in this range, the electrode response varied significantly. Toth and Pungor [3] studied the effect of metal ions at pH 11.

In this communication, the response is modelled at high pH values, taking account of the effects of metal-hydroxide complexes. The error associated with neglect of these complexes is illustrated and the response predicted by the model is checked experimentally.

Theory

The primary reaction at the electrode membrane with equilibrium constant K_1 is

$$AgI(s) + 2CN^- \rightleftharpoons Ag(CN)_2^- + I^- \quad (1)$$

Other reactions considered are the association of hydrogen and cyanide, $H^+ + CN^- \rightleftharpoons HCN$, with equilibrium constant K_2, the complexation of metal (M) and cyanide, $M^{m+} + iCN^- \rightleftharpoons M(CN)_i^{m-i}$, with overall formation constants β_i, and the complexation of metal and hydroxide, $M^{m+} + jOH^- \rightleftharpoons M(OH)_j^{m-j}$, with overall formation constants γ_j. From eqn. 1, $[I^-] = [Ag(CN)_2^-] = K_1^{1/2} \times [CN^-]$. Manipulation of these equations yields the following expressions for the total cyanide concentration (C_{CN}) and total metal concentration (C_M):

0003-2670/85/$03.30

$$C_{CN} = [CN^-] + 2K_1^{1/2}[CN^-] + K_2[H^+][CN^-] + \sum_{i=1}^{n} i\beta_i[M^{m+}][CN^-]^i \quad (2)$$

$$C_M = [M^{m+}] + \sum_{i=1}^{n} \beta_i[M^{m+}][CN^-]^i + \sum_{j=1}^{p} \gamma_j[M^{m+}][OH^-]^j \quad (3)$$

The electrode response is related to log $[I^-]$ by the Nernst equation. For the model, the values of C_{CN} and pH are fixed at several typical values. The plots of log $[I^-]$ vs. log C_M are derived from Eqns. 2 and 3 by the method of Mascini and Napoli [2].

The values of the equilibrium constants used were log K_1 = 4, log K_2 = 9.484 and pK_w = 14.184 [2, 4, 5]. The values used for the overall formation constants of metal-cyanide complexes were: for zinc ions, log β_1 = 5.34, log β_2 = 11.03, log β_3 = 16.68 and log β_4 = 21.57; for cadmium ions, log β_1 = 5.62, log β_2 = 10.84, log β_3 = 15.72 and log β_4 = 19.20; and for copper(I) ions, log β_2 = 24, log β_3 = 28.59 and log β_4 = 30.30. The values used for the overall formation constants of the metal-hydroxide complexes were; for zinc ions, log γ_1 = 6.31, log γ_2 = 11.19, log γ_3 = 14.31, log γ_4 = 17.70; and for cadmium ions, log γ_1 = 4.3, log γ_2 = 7.7, log γ_3 = 10.3, log γ_4 = 12.0. These are representative values available in the literature [4, 6, 7]. Only mononuclear complexes are considered. No evidence was found for the hydroxide complexes of copper(I).

Experimental

An Orion 94-06 cyanide-selective electrode was used with an Orion 90-02 double-junction reference electrode. Cyanide standards were prepared from reagent-grade sodium cyanide. All cyanide standards and samples were prepared with a background ionic strength of 2 M sodium nitrate. This background eliminates any significant variation in the ionic strength of different samples. The pH was determined with a combination glass electrode and the metals were quantified with a Techtron AA-120 atomic absorption spectrometer. Electrode response was measured at pH 12.5 and at varying concentrations of Zn^{2+}, Cd^{2+} and Cu^+ ions in well stirred solutions. The pH of all samples was maintained within 0.1 pH units of the reported value by adjustment with sodium hydroxide and hydrochloric acid. Zinc and cadmium standards were prepared from zinc oxide and cadmium metal dissolved in dilute nitric acid. Copper(I) standard was made by dissolving copper(I) oxide in a 50-fold molar excess of hydrochloric acid.

Results and discussion

The electrode was calibrated at pH 12.5 with six standards covering the range 2×10^{-5}—10^{-3} M cyanide in 2 M sodium nitrate. The plot of the electrode potential (E) vs. log $[CN^-]$ followed the expected straight line behavior very well.

The calculated and measured electrode responses are shown in Fig. 1 as a

function of varying total zinc concentration. The importance of considering the zinc-hydroxide complexes at a high pH is evident. The response was measured at total cyanide concentrations of 10^{-4} M and 10^{-3} M. Thus the electrode essentially measures the total amount of cyanide in the presence of an excess of zinc ions. Figure 2 shows the results for the electrode response in the presence of cadmium ions. This figure also clearly illustrates the importance of considering the metal-hydroxide complexes.

As shown in Fig. 3, the electrode does not, however, measure the total cyanide in the presence of an excess of copper(I) ions. The predicted response

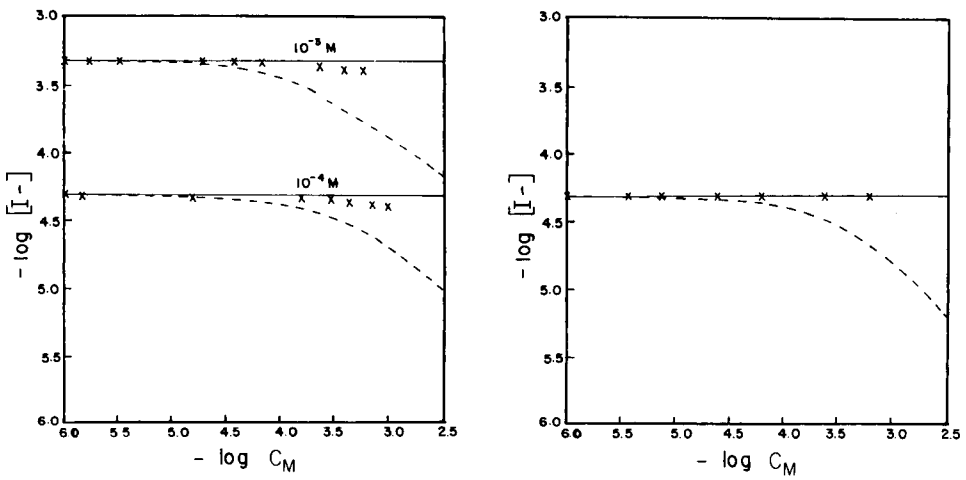

Fig. 1. Model predictions and experimental points (×) for the zinc-cyanide system at pH 12.5 and two total cyanide concentrations. (—) Model including metal-hydroxide complexes; (---) model without metal-hydroxide complexes.

Fig. 2. Model predictions and experimental points for the cadmium-cyanide system at pH 12.5 and a total cyanide concentration of 10^{-4} M. Symbols as for Fig. 1.

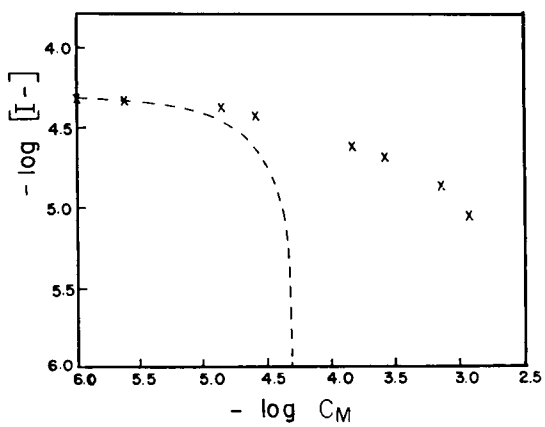

Fig. 3. Model predictions and experimental points for the copper(I)-cyanide system at pH 12.5 and a total cyanide concentration of 10^{-4} M. Symbols as for Fig. 1.

for this system was plotted by considering only the Cu^+—CN^- complexes as no information is available in the literature on copper(I)-hydroxide complexes. For an excess of copper(I) ions, the data do not fit the predicted response very well. It is evident that the electrode can be used to measure total cyanide only if the copper concentration is low. The observed decrease in the electrode response cannot be due to the presence of chloride because for a total cyanide concentration of 10^{-4} M and total copper(I) concentration between 10^{-6} M and 10^{-3} M, the $[Cl^-]/[CN]$ ratio varies from 0.5 to 500. The calculated selectivity ratio for chloride to interfere with cyanide ions is 10^5 [8].

No precipitates were observed in the ranges of pH and metal concentrations considered. The results of Figs. 1—3 were found to be valid at pH values above 11. A computer program was written to calculate the distribution of various species present at various pH and total metal and cyanide concentrations. At pH 11 and $C_{CN} = 10^{-4}$ M the concentration of free cyanide in the bulk varied from 9.47×10^{-5} M to 2.95×10^{-5} M as the total zinc concentration varied from 10^{-6} M to 10^{-3} M. For this range, the complexed cyanide concentration varied from 2.4×10^{-6} M to 7×10^{-5} M. The rest of the cyanide was present as hydrogen cyanide. At pH 12.5 almost all the zinc was complexed with hydroxide ions and all the cyanide was present as free cyanide. So at pH 12.5, the electrode responds to total cyanide because of masking of zinc by hydroxide. However, at pH 11 the electrode membrane responds to total cyanide even though in the bulk a substantial amount of the cyanide is complexed primarily as $Zn(CN)_4^{2-}$ and $Zn(CN)_3^-$. This is because at the electrode membrane reaction 1 also takes place, thereby causing the distribution of the various cyanide species to be different from the bulk. Similar calculations were done for the cadmium system. In the pH and concentration ranges for which the electrode response was measured, a substantial amount of cyanide was complexed with cadmium. It is evident that for both cadmium and zinc systems masking by hydroxide ions is not sufficient to decompose all the metal-cyanide complexes and the electrode responds to total cyanide even in the presence of their metal-cyanide complexes.

Similar modeling was also done in order to predict the electrode response in presence of two metals (M1 and M2). Overall balances similar to Eqns. 2 and 3 were written for C_{CN}, C_{M1} and C_{M2}. These were solved to get plots of $\log [I^-]$ vs. $\log C_{M1}$ using C_{CN}, C_{M2} and pH as parameters. Results obtained for high pH (>11) were similar to those shown in Figs. 1—3. The electrode responded to total cyanide even in presence of an excess of mixed cadmium and zinc ions. However, in the mixed Cd^{2+}—Cu^+ system and the mixed Zn^{2+}—Cu^+ system, the response was dominated by the copper(I) ions because the cyanide complexes of copper(I) are much more stable than those of zinc and cadmium.

Conclusions

At a high pH, the cyanide-selective electrode measures the total cyanide concentration in the presence of an excess of zinc and cadmium ions and

small amounts of copper(I) ions. Copper(I) ions complex very strongly with cyanide and the response falls off at higher copper concentration. To determine total cyanide in the presence of copper(I), the complexes must be decomposed. This can be done by EDTA or by ultraviolet irradiation [9—11]. In the above treatment, diffusion of the ions from the bulk solution to the silver iodide membrane of the electrode and the presence of combined metal-hydroxo-cyano complexes has not been considered. Similar modeling can predict the response of the cyanide-selective electrode in the presence of other metals either separately or mixed.

We gratefully acknowledge the help of M. T. Beck in understanding the cyanide chemistry.

REFERENCES

1 M. Mascini, Anal. Chem., 45 (1973) 614.
2 M. Mascini and A. Napoli, Anal. Chem., 46 (1974) 447.
3 K. Toth and E. Pungor, Anal. Chim. Acta, 51 (1970) 221.
4 H. Persson, Acta Chem. Scand., 25 (1971) 543.
5 J. Vesely, D. Weiss and K. Stulik, Analysis with Ion-Selective Electrodes, Ellis Horwood, Chichester, England, 1978, p. 153.
6 L. G. Sillen and A. E. Martell, Stability Constants, Chem. Soc. Spec. Publ. 17, London, 1964.
7 Lange's Handbook of Chemistry, 12th edn., McGraw-Hill, New York, 1979.
8 I. Sekerka and J. F. Lechner, Water Res., 10 (1976) 479.
9 P. D. Goulden, B. K. Afghan and P. Brooksbank, Anal. Chem., 44 (1972) 1845.
10 M. S. Frant, J. W. Ross Jr. and J. H. Riseman, Anal. Chem., 44 (1972) 2227.
11 B. Fleet and H. von Storp, Anal. Lett., 4 (1971) 425.

Analytica Chimica Acta, 171 (1985) 357—361
Elsevier Science Publishers B.V., Amsterdam — Printed in The Netherlands

Short Communication

BORAZON-GATE pH-SENSITIVE FIELD EFFECT TRANSISTOR

D. SOBCZYŃSKA and W. TORBICZ*

Institute of Biocybernetics and Biomedical Engineering, Polish Academy of Science, 55 Krajowej Rady Narodowej, 00-818 Warszawa (Poland)

A. OLSZYNA and W. WŁOSIŃSKI

Institute of Technology of Electronic Materials, 6 Konstruktorska Street, 02-673 Warszawa (Poland)

(Received 28th January 1984)

Summary. A borazon-gate ISFET is used as a pH sensor. Boron nitride was deposited by the reactive-pulse plasma method and electron diffraction served for membrane identification. The borazon-gate sensors responded linearly to pH in the range 1.8—10; the slope was about 52 mV pH^{-1}. Selectivity for H^+ ions over K^+, Na^+ or Ca^{2+} ions was better than that of silicon nitride-gate ISFETs.

The selectivity of ion-selective field effect transistors (ISFET) is obtained by placing a suitable membrane on top of the gate insulator of the FET. For pH transducers, dielectric or polymeric membranes have been used; FETs with silica [1], silicon nitride [2], alumina [3], and polymeric [4] membranes have been reported.

In the work described here, borazon (boron nitride) membranes were shown to provide competitive, or better, selectivity, reaction time and lifetime.

Experimental

Standard technology was used in preparation of the ISFETs. Construction was based on *p*-silicon of 5—9 Ω cm impedance. The required threshold voltage was obtained by phosphorus implantation in the gate region. The dielectric layer consisting of silica (80-nm thick) and silicon nitride (100-nm thick) was built up in the gate region. A layer of boron nitride (80—100-nm thick) was formed on top of these layers by using the reactive pulse plasma method [5].

Electron diffraction on the membrane (Fig. 1) confirmed the cubic structure of boron nitride (borazon). Secondary-ion mass spectrometry was used to examine the depth structure of the membranes [6]. Experimental $BN/SiO_2/Si$ sandwich samples were tested. The depth concentration profiles for B^+, Na^+, Si_2O^+ and Si^+ ions in the sample indicated that the B^+ ion concentration

0003-2670/85/$03.30

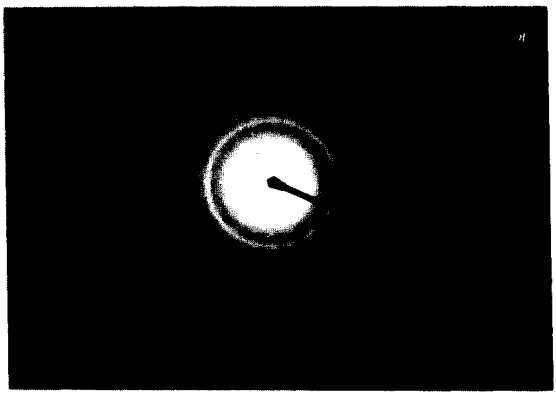

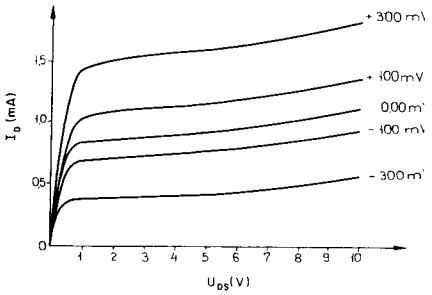

Fig. 1. Electron beam interference rings of boron nitride.

Fig. 2. Output characteristics of the sensor for pH 4.07.

was constant over a large part of the borazon layer with a clear increase near the silica layer; the N^+ ion concentration was smaller in the middle of the borazon layer. Silicon and silicon oxide ions appeared over the entire depth of the borazon layer.

The region around the gate was insulated by a silicon nitride layer (200 nm thick) and by a borazon layer. The ISFET was finally sealed with Dow-Corning R-6101 resin. The leakage current did not exceed 8 nA.

Measurements with the ISFETs were made in the common source configuration. The chemical steady-state responses were measured for a constant value of the drain current [7]. Output and transfer voltage/current curves were recorded on a Bryans XY-29000-A4 recorder. A Radiometer K901 calomel reference electrode was used in all measurements.

The drain current response time, step changes of gate voltage and pH were measured with the use of a Tektronix 7623A storage oscilloscope. The gate-voltage rise time was less than 5 ns. Step changes of pH were obtained by directing a jet of the appropriate solution from a syringe onto the gate window [8]. A 5-ml polyethylene syringe with 1.8 mm tip was used. The pH measurements were checked with a Radiometer PHM-64 research pH meter.

Results

Typical drain current/drain voltage and drain current/gate voltage characteristics for these ISFETs at pH 4.07 are presented in Figs. 2 and 3, respectively. To measure the chemical response of these sensors, a drain current of 1 mA was chosen. This operational point is placed on the nonlinear (saturated) region of the transducer characteristics.

The pH responses of the boron nitride sensor obtained at 21° C in four different tests are shown in Fig. 4. In two tests, citric acid (0.2 mol l^{-1}) was mixed with 0.2 mol l^{-1} ammonia solution to give the required pH; in the other tests, diammonium hydrogencitrate (0.2 mol l^{-1}) was mixed with

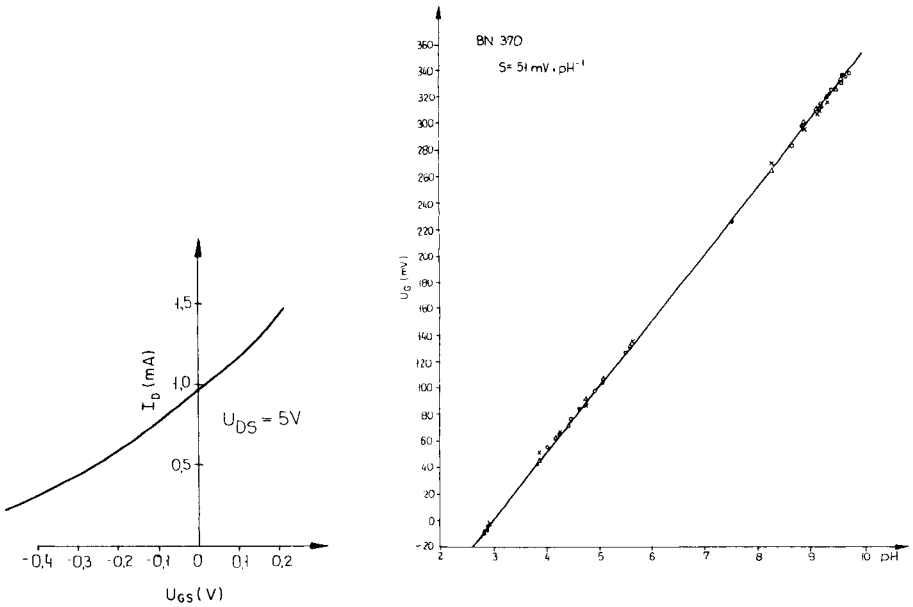

Fig. 3. Transfer characteristics of the sensor for pH 4.07.

Fig. 4. pH response of the sensor. The symbols indicate four different tests: (×) blank; (△) Na^+; (○) K^+; (●) Ca^{2+}.

0.2 mol l^{-1} ammonia solution. Figure 4 shows good linearity with a sensitivity of 52 mV pH^{-1}. The dispersion of the experimental points indicates errors of ±4 mV. The borazon-gate sensors were tested in the pH linear range 1.8—10. The sensitivity varied in the interval 46—59 mV pH^{-1}.

To compare the selectivities of the borazon and the silicon nitride [7] ISFETs, the chemical response of the borazon sensor to potassium, sodium and calcium ions was measured at constant pH. Solutions were prepared by adding separately the required quantities of potassium, sodium or calcium chloride to citric acid/diammonium hydrogencitrate/ammonia buffers (see Table 1). (All chemicals were of analytical grade.) Selectivity coefficients K_i were calculated from the Nikolski equation, which for the buffer solution with one interfering ion is:

$$E = E_0 + 2.303\,RTF^{-1} \log (a_1 + K_i a_i^{1/z_i})$$

where a_i is the activity of the interfering ion, and z_i its ionic charge. The selectivity coefficients found at pH 4.08, 7.15 and 9.2 are presented in Table 1.

The temperature sensitivity of the borazon sensor was monitored over the range 28—41°C in the buffer solution. The temperature coefficient (for the combined sensor, buffer solution and reference electrode) was about 4 mV K^{-1} (K = Kelvin), which corresponds to ca. 0.08 pH K^{-1} without temperature compensation. Temperature compensation may be obtained by placing a MOSFET transistor on the same chip.

TABLE 1

Selectivity coefficients at an interfering ions concentration of 1 mol l^{-1}

pH	4.08	7.15	9.2
K^+	—	3.5×10^{-8}	—
Na^+	8×10^{-5}	6×10^{-8}	2×10^{-9}
Ca^{2+}	—	4×10^{-8}	—

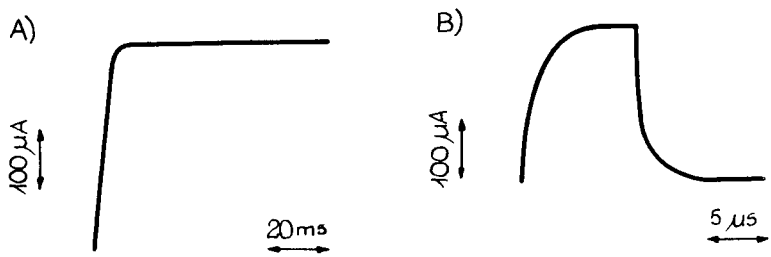

Fig. 5. Chemical (A) and electrical (B) response time of the sensor.

As mentioned above, the chemical response time was measured by means of an injection technique. A citric acid solution of pH 5.6 was injected against the ISFET window to a solution at pH 3.2. Figure 5A, which shows the drain current response to a step change of pH, indicates that the chemical response time is 8 ms. The electrical response time was 3 μs; Fig. 5B shows the drain current response to a square-wave change in gate voltage. In tests of the long-term stability of the borazon-gate ISFETs, the U_g vs. pH function remained linear up to 6 months.

Discussion

The above results indicate that the boron nitride and silicon nitride ISFETs have comparable chemical sensitivities, probably because both nitrides have similar covalent bonds [9]. The selectivity of the borazon gate is better than that of the silicon nitride gate, probably because of the smaller value of the ionic component in the covalent bond. The cubic structure (diamond like) of borazon favours extension of the borazon-gate lifetime. The chemical response times of both the nitride gates are similar [8] though the electrical response time of the borazon ISFET is shorter. The temperature sensitivity of both these sensors is quite high. Apart from the factors mentioned above, this is influenced by the temperature dependence of the n^+ drain and the source resistance of 204Ω, which is connected in series to the load resistance.

The authors express their gratitude to Mr. P. Dumania for making the ISFET chips, to Mrs. H. Gołowacz for the secondary-ion mass spectrometry and to Mr. J. Kruk for technical assistance. This work was supported by Research Program 06.9 of the Polish Academy of Sciences.

REFERENCES

1 P. Bergveld, IEEE Trans. Biomed. Eng., 19 (1972) 342.
2 M. Esashi and T. Matsuo, IEEE Trans. Biomed. Eng., 25 (1978) 184.
3 H. Abe, M. Esashi and T. Matsuo, IEEE Trans. Electron Devices, 26 (1979) 1939.
4 P. T. McBride, J. Janata, P. A. Comte, S. D. Moss and C. C. Johnson, Anal. Chim. Acta, 101 (1978) 239.
5 M. Sokołowski, A. Sokołowska, A. Michalski, Z. Romanowski, A. Rusek-Mazurek and M. Wronikowski, Thin Solid Films, 80 (1981) 249.
6 J. A. McHugh, Methods of Surface Analysis, Elsevier, Amsterdam, 1975, Ch. 6.
7 P. W. Cheung, W. H. Ko, D. J. Fung and S. H. Wong, Theory, Design and Biomedical Application of Solid-State Chemical Sensors, C.R.C. Press, Boca Raton, 1978, pp. 91, 112.
8 J. Janata and R. J. Huber, Ion-Selective Electrode Rev., 1 (1979) 31.
9 V. G. Aleshin, Izv. Akad. Nauk SSSR, Neorg. Mater., 15 (1979) 677.

Analytica Chimica Acta, 171 (1985) 363—367
Elsevier Science Publishers B.V., Amsterdam — Printed in The Netherlands

Short Communication

CATALYTIC-KINETIC POTENTIOMETRIC DETERMINATION OF THYROXINE

M. TIMOTHEOU-POTAMIA*, E. G. SARANTONIS, A. C. CALOKERINOS and T. P. HADJIIOANNOU

Laboratory of Analytical Chemistry, University of Athens, Athens (Greece)

(Received 6th March 1984)

Summary. A kinetic method is described for the determination of thyroxine (0.4—4 μg ml^{-1}), based on its catalytic effect on the reduction of cerium(IV) by arsenic(III). The reaction is monitored potentiometrically; the time required for a 20-mV change in potential is inversely proportional to the thyroxine concentration. The method is applicable to tablets.

Many methods based on the reaction in which a trace of iodide accelerates the reduction of cerium(IV) by arsenic(III) have been developed [1—9]. Iodine-containing organic compounds are usually determined after destruction of the organic matter and isolation of iodide [10, 11] but thyroxine and triiodothyronine [2, 12—16] and substituted iodobenzenes of general formula XC_6H_4I [8] have been found to catalyze the reaction. Because the catalytic effect of iodide on the cerium(IV)/arsenic(III) reaction can be monitored by potentiometry [17, 18], it was decided to extend the method to the determination of thyroxine in tablets. The assay of thyroxine in tablets and bulk material is normally based on measurement of iodide liberated by fusion with potassium carbonate [19, 20] or potassium hydroxide [19], or by oxygen-flask combustion [19].

In this communication, a catalytic-kinetic method for the determination of thyroxine is reported. The thyroxine-catalyzed cerium(IV)/arsenic(III) reaction is monitored with a platinum indicator electrode, and the time required for a fixed change in potential is measured and related to the thyroxine concentration. Thyroxine in the range 0.4—4 μg ml^{-1} is determined with an average error of 1%. The method has been applied successfully for the determination of thyroxine in tablets with 96—108% recoveries.

Experimental

Apparatus. A platinum indicator electrode (Model S-30515, E. H. Sargent Co.) was used in conjunction with a mercury(I) sulphate reference electrode (Model EA-406, Metrohm). The recording system was as previously reported [21]. All measurements were made at ambient temperature in a 50-ml beaker; stirring was done magnetically with a teflon-coated follower.

0003-2670/85/$03.30

Reagents. All solutions were prepared with deionized-distilled water from reagent-grade materials, except where stated. A 3×10^{-4} M cerium(IV) working solution was prepared by dissolving 0.1213 g of cerium(IV) sulphate tetrahydrate (Merck, p.a.) in 1 M sulphuric acid/1 M nitric acid and diluting with the mixed acid solution to exactly 1 l. A 1.000 M arsenic(III) working solution was prepared by dissolving 12.99 g of sodium arsenite (Merck, p.a.) in water and diluting to 100.0 ml. A 1.00×10^{-3} M thyroxine stock solution was prepared by dissolving 0.0889 g of L-thyroxine, sodium salt pentahydrate (Ferak, Berlin) in 0.1 M sodium hydroxide and diluting with 0.1 M sodium hydroxide to 100.0 ml. The solution was stable for at least a month if kept in an amber-coloured bottle in the dark. More dilute solutions were prepared by dilution with 0.1 M sodium hydroxide.

Determination of thyroxine in aqueous solutions. Transfer 20.00 ml of 3×10^{-4} M cerium(IV) and 1.00 ml of 1.000 M arsenic(III) working solutions to the measuring cell and start stirring and recording the potential. Inject 2.00 ml of sample solution and allow the reaction to proceed. Empty the cell and repeat the procedure for each sample solution. Measure the time required for the potential to increase from 5 mV to 25 mV.

Determination of thyroxine in tablets. Weigh at least 20 tablets containing thyroxine, and pulverize them uniformly in a mortar. Weigh an appropriate amount of the pulverized sample, dissolve it in 0.1 M sodium hydroxide, and dilute the solution with 0.1 M sodium hydroxide to 50.00 ml, so that the resulting solution contains 0.4—4 μg ml^{-1} of thyroxine. If the solution is turbid, filter through a Whatman No. 41 filter paper. Proceed as for thyroxine in aqueous solution, using 2.00 ml of the clear filtrate.

Calibration. Introduce 2-ml aliquots of standard thyroxine solution containing 0.4—4.0 μg thyroxine ml^{-1} and measure the change in potential as above. Calculate the time required for the cell potential to increase from 5 mV to 25 mV. Construct a calibration graph by plotting reciprocal time ($1000/t$) vs. thyroxine concentration (μg ml^{-1}), the time being measured in seconds.

Results and discussion

In any kinetic method, the choice of initial reactant concentrations is governed by the reaction rate, the experimental technique and the sensitivity of the measurement system. The rate of the cerium(IV)/arsenic(III) reaction catalyzed by iodide or iodine-containing organic compounds depends on the mole ratio and initial concentration of the reactants and the acidity of the medium. These parameters have often been investigated for the iodide-catalyzed reaction but not for the thyroxine-catalyzed reaction. Therefore, the effects of the various experimental parameters on the rate of the thyroxine-catalyzed reaction were investigated.

The reaction rate increased with initial arsenic(III) concentration and maximum reciprocal times were observed at 4.3×10^{-2} M arsenic(III), which was used for all further measurements. At initial cerium(IV) concentrations of 5.2×10^{-4}, 2.6×10^{-4}, 1.3×10^{-4} and 0.65×10^{-4} M, the reciprocal times

were 9.3×10^{-3}, 14.2×10^{-3}, 10.7×10^{-3} and 7.8×10^{-3} s^{-1}, respectively; 0.65×10^{-4} M cerium(IV) was used in all further work. An increase in sulphuric acid concentration from 0.1 to 3.0 M resulted in a gradual increase in the rate when catalyzed by iodide [1]. In the present studies, an increase in sulphuric acid concentration from 0.5 to 1.0 M in the cerium(IV) working solution increased the reciprocal time for 2.3 μg ml^{-1} thyroxine by ca. 70%. Higher (>1.0 M) or lower (<0.5 M) sulphuric acid concentrations had no effect on the reaction rate. When nitric acid was used instead of sulphuric acid, the catalytic effect of iodide increased 20-fold [14, 15]; the catalytic effect of thyroxine doubled when 1 M nitric acid was used in addition to the optimized sulphuric acid concentration, in accordance with observations of other workers [15]. At >1 M nitric acid, the change in potential with time was not linear and was not reproducible. Thus 1 M nitric acid was used as a compromise between linear, reproducible responses and increased reciprocal times.

Figure 1 shows typical responses for the thyroxine-catalyzed reaction. After initiation of the reaction, a pre-measurement time corresponding to a 5-mV change was chosen to ensure thorough mixing of the reagents. The calibration graph is linear in the range 0.4—4 μg ml^{-1} of thyroxine ($1/\Delta t$ = 0.007[thyroxine]), while, under the same experimental conditions, the calibration graph for iodide is linear in the range 0.2—2 μg ml^{-1} ($1/\Delta t$ = 0.020[I^-]). As expected, the sensitivity of the method for thyroxine is less than that for iodide. Comparative measurements of iodide and thyroxine revealed an apparent 57% activity for the iodine atoms in the organic molecule, compared to iodide, which is very close to the value calculated by Knapp and Leopold [15]. The relative standard deviation was 2.1% (n = 7) for a 2.3 μg ml^{-1} thyroxine sample.

Results for the determination of thyroxine in aqueous solutions are shown in Table 1. They indicate an average error of 1.0%. Ions that interfere with the determination of iodide [2, 22] also interfere with the determination of thyroxine. The effect of the commonest pharmaceutical

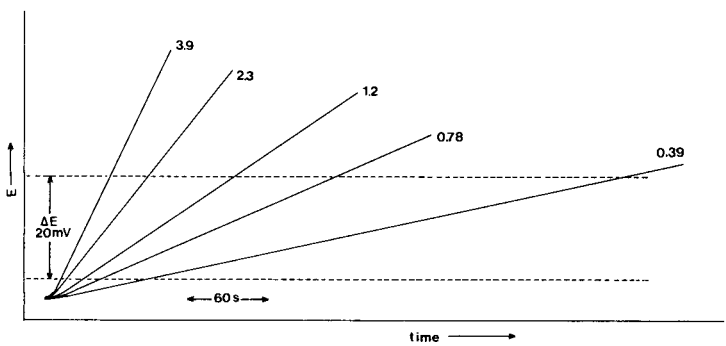

Fig. 1. Recorded changes of cell voltage vs. time for the cerium(IV)/arsenic(III) reaction in the presence of thyroxine at the concentrations (μg ml^{-1}) given on the lines.

TABLE 1

Results for aqueous thyroxine solutions

Thyroxine (μg ml^{-1})		Relative error (%)	Thyroxine (μg ml^{-1})		Relative error (%)	Thyroxine (μg ml^{-1})		Relative error (%)
Taken	Found[a]		Taken	Found[a]		Taken	Found[a]	
0.393	0.385	−2.0	1.02	1.02	0.0	3.15	3.13	−0.6
0.551	0.545	−1.1	1.57	1.58	+0.6	3.54	3.50	−1.1
0.708	0.710	+0.3	2.36	2.40	+1.7	3.94	4.00	+1.8

[a]Mean of 2 measurements, from a calibration graph constructed with 2 standards.

TABLE 2

Recovery of thyroxine from solutions of commercial tablets

Thyroxine (μg ml^{-1})			Recovery (%)
Initially present	Added	Found[a]	
0.598	0.787	1.42	104
	1.57	2.24	105
	2.36	2.93	99
0.488	0.787	1.34	108
	2.36	2.91	103
	3.15	3.74	103
0.419[b]	0.787	1.18	97
	1.57	1.93	96
	3.15	3.54	99

[a]Mean of 2 measurements, from calibration graph constructed with 2 standards. [b]Tablet contained thyroxine and triiodothyronine (4+1).

excipients was investigated by determining 1.6 μg ml^{-1} thyroxine in an aqueous 7% (w/v) solution of the excipient in 0.1 M sodium hydroxide. The reciprocal times were compared with those obtained from an uncontaminated thyroxine solution. No effect was observed from kaolin, Carbowax-4000, magnesium stearate or mannitol. Sodium chloride, glucose and starch increased the reciprocal time by 42.5, 39.3 and 16.6%, respectively, whereas sodium lauryl sulphate and talc decreased the reciprocal time by 69.8 and 7.7%, respectively. In all cases, there was no catalytic effect when the pure excipient solution was injected into the cerium(IV)/arsenic(III) mixture.

The method was used for the determination of thyroxine in solutions of tablets which were spiked with the pure compound (Table 2). Recoveries ranged from 96 to 108% with an average of 101.6%, including one sample which contained triiodothyronine. Two commercial products, stated by the manufacturer to contain 0.1 mg of thyroxine per tablet, were found to contain 0.07 and 0.08 mg by the proposed and standard [19] methods, respectively.

The proposed catalytic-kinetic potentiometric method for thyroxine is simpler than other available methods and can be used for the analysis of pharmaceutical preparations with good accuracy and precision.

The authors thank M. Koupparis for stimulating discussions and M. Milonakis for assistance.

REFERENCES

1 P. A. Rodriguez and H. L. Pardue, Anal. Chem., 41 (1969) 1369; 41 (1969) 1377.
2 P. J. Ke, R. J. Thibert, R. J. Walton and D. K. Soules, Mikrochim. Acta, (1973) 569.
3 T. P. Hadjiioannou, Anal. Chim. Acta, 30 (1964) 488, 537.
4 S. D. Jones, C. P. Spencer and V. W. Truesdale, Analyst (London), 107 (1982) 1417.
5 M. M. Timotheou-Potamia and T. P. Hadjiioannou, Mikrochim. Acta, (1983) 59.
6 H. Weisz and K. Rothmaier, Anal. Chim. Acta, 80 (1975) 351.
7 S. Pantel and H. Weisz, Anal. Chim. Acta, 89 (1977) 47.
8 S. Pantel, Anal. Chim. Acta, 141 (1982) 353.
9 J. M. Elvecrog and P. W. Carr, Anal. Chim. Acta, 121 (1980) 135.
10 H. V. Malmstadt and T. P. Hadjiioannou, Anal. Chem., 35 (1963) 2157.
11 K. Lauber, Anal. Chem., 47 (1975) 769.
12 C. H. Bowden and N. F. Maclagen, Biochem. J., 56 (1954) VII.
13 C. H. Bowden, N. F. Maclagen and J. H. Wilkinson, Biochem. J., 59 (1955) 93.
14 G. Knapp and H. Spitzy, Talanta, 16 (1969) 1353, 1361.
15 G. Knapp and H. Leopold, Anal. Chem., 46 (1974) 719.
16 G. Knapp, H. Spitzy and H. Leopold, Anal. Chem., 46 (1974) 724.
17 T. P. Hadjiioannou and E. A. Piperaki, Anal. Chim. Acta, 90 (1977) 329.
18 M. M. Timotheou-Potamia and T. P. Hadjiioannou, Mikrochim. Acta, (1983) 59.
19 The British Pharmacopoeia, H.M.S.O., London, 1973, pp. 269, 476—477, A93—94.
20 S. L. Richhmeimer and M. S. Schachet, J. Pharm. Sci., 72 (1983) 822.
21 T. P. Hadjiioannou and E. P. Diamandis, Anal. Chim. Acta, 94 (1977) 443.
22 M. Dubravcic, Analyst (London), 80 (1955) 146.

Analytica Chimica Acta, 171 (1985) 369—374
Elsevier Science Publishers B.V., Amsterdam — Printed in The Netherlands

Short Communication

PRECONCENTRATION AND X-RAY SPECTROMETRIC DETERMINATION OF ARSENIC(III/V) AND CHROMIUM(III/VI) IN WATER

D. E. LEYDEN*, K. GOLDBACH and A. T. ELLIS[a]

Department of Chemistry, Colorado State University, Fort Collins, CO 80523 (U.S.A.)

(Received 21st August 1984)

Summary. The speciation of chromium and arsenic in their two common oxidation states is determined by the use of selective preconcentration and energy-dispersive x-ray spectrometry. Chromium(VI) and arsenic(III) are recovered by precipitation with dibenzyldithiocarbamate and filtration. Chromium(III) and arsenic(V) are determined in the filtrate by coprecipitation with hydrated iron(III) oxide. The chromium and arsenic content of each precipitate is determined by use of x-ray spectrometry.

Chromium and arsenic may exist in two different oxidation states in natural and industrial water systems, Cr(III) and Cr(VI), and As(III) and As(V), respectively. Because the toxicity of these elements depends upon the oxidation state, it is of interest to obtain information on the speciation of these elements in environmental waters. There are several methods for determining chromium and arsenic in water without regard to the oxidation state of these elements. Selective preconcentration followed by energy-dispersive x-ray spectrometry allows oxidation state speciation of these potentially harmful pollutants.

Arsenic(III) and Cr(VI) are precipitated, along with many other metal ions, by dibenzyldithiocarbamate (DBDTC) [1]. These elements can be quantified directly by energy-dispersive x-ray spectrometry after collection of the precipitate on a membrane filter [1—4]. To obtain arsenic and chromium speciation data, it is necessary to determine Cr(III) and As(V) in the filtrates. The filtrate may be analyzed by techniques other than x-ray spectrometry, such as inductively-coupled plasma emission spectrometry or atomic absorption spectrometry. Because DBDTC precipitates most of the metal ions in the sample quantitatively, it removes many of the potential chemical and spectroscopic interferences in the filtrate. Therefore, a simple method, such as coprecipitation with hydrated iron(III) oxide, is applicable for recovery of the chromium and arsenic species remaining in the filtrate.

[a]Present address: Link Systems, Halifax Road, High Wycombe, Buckinghamshire, HP12 3SE, Great Britain.

0003-2670/85/$03.30

Iron(III) coprecipitation has been used previously for effective preconcentration of trace metals from aqueous solutions prior to x-ray spectrometry [4, 5].

Experimental

Apparatus. All x-ray measurements were done with a Spectrace 440 energy-dispersive x-ray spectrometer equipped with a TN 2000 analyzer (Tracor Xray, Mountain View, CA). A silver target tube was used with a silver primary filter. The intensities of the K-lines of chromium and arsenic were extracted using the vendor program XML for fitting previously acquired single element spectra of elements which are present in the sample. The x-ray net counts are the integral of peak counts minus background counts for the combined K_α and K_β peaks. These values were converted to net counts per second for preparation of calibration curves. In order to determine chromium and arsenic simultaneously, the tube voltage was 35 kV. The current was adjusted to set the system deadtime near but less than 50%.

Precipitation with DBDTC. Sodium dibenzyldithiocarbamate was prepared as reported previously [1]. A 100-ml aliquot of water sample was placed in a 150-ml beaker and adjusted to pH 2.5 ± 0.05 with 0.1 M hydrochloric acid, and 1.0 ml of a 1.2% (w/v) solution of sodium dibenzyldithiocarbamate in anhydrous methanol was added. The solution was stirred intermittently for 15 min, and then left for 15 min. The sample was filtered through a 25-mm diameter, 0.45-μm pore diameter membrane filter. The filter was allowed to air-dry, and then mounted between 1/4-mil Mylar films on a Chemplex (Eastchester, NY) sample cup.

Single-element calibrations were established for Cr(VI) and As(III) by using DBDTC as a precipitation reagent. The elemental concentration in the standard solutions ranged from 200 to 1000 $\mu g\ l^{-1}$, and duplicates were made for each concentration. The calibration data obtained are shown in Table 1.

Optimization for the hydrated iron(III) oxide coprecipitation. To achieve maximum sensitivity for Cr(III) and As(V) determined simultaneously, three parameters had to be considered: the amount of Fe(III) added for the precipitation; the pH of the solution during precipitation; and the aging time for the precipitate prior to filtration. Figure 1 shows the x-ray intensity vs. the amount of hydrated iron(III) oxide used for the precipitation of 100 μg

TABLE 1

Calibration parameters for the DBDTC and iron(III) coprecipitation methods

	Slope (cps μg^{-1})	Intercept (μg)	Correlation coefficient
Cr(VI) by DBDTC	2.54 ± 0.15	1.70 ± 0.11	0.990
As(III) by DBDTC	13.25 ± 0.66	3.29 ± 0.16	0.997
Cr(III) by Fe(III) coprecipitation	2.47 ± 0.14	0.18 ± 0.02	0.995
As(V) by Fe(III) coprecipitation	11.96 ± 0.60	2.83 ± 0.14	0.995

of As(V). The 100-ml sample contained 100 μg of As(V), the pH was 4.0 and the aging time prior to filtration was 20 min. With increasing Fe(III), the recovery of arsenic increased and became constant between 150 and 250 μg of Fe(III). To investigate the effect of pH, 200 μg of Fe(III) was used to precipitate 100 μg of As(V); an aging time of 20 min was used. As shown in Fig. 2, recovery of the As(V) is good between pH 4 and 7.

The effect of aging time was studied for 100 μg of As(V), coprecipitated with 200 μg of Fe(III) at pH 5.0. At aging times greater than about 10 min, the As(V) recovery slowly decreased. The results of precipitate aging were essentially the same for Cr(III) recovery. For all subsequent determinations, 100-ml samples were used with 200 μg of Fe(III) added as the chloride, pH 5.0 (adjusted with sodium hydroxide), and an aging time of 5 min. The precipitate was filtered and the filter mounted as in the procedures for the DBDTC filters.

The x-ray counts for 100 μg of As(III) on filters bearing the DBDTC precipitate are shown on Figs. 1 and 2 as a point of reference. The intensity of the iron(III)-coprecipitated As(V) is not expected to reach this value because the mass absorption coefficient of the hydrated iron(III) oxide matrix is larger than that for the DBDTC precipitate.

Calibration for coprecipitation with hydrated iron(III) oxide. Calibration was obtained for the coprecipitation method in a manner similar to the DBDTC calibration. Standard solutions with Cr(III) and As(V) concentrations in the range 200—1000 μg l^{-1} in duplicates were used. Table 1 shows the calibration parameters obtained for Cr(III) and As(V). It was found that the ratio of net counts of trace metal to net counts of iron gave better precision than the net counts for the trace metal taken alone.

The sensitivity of this coprecipitation compared to the DBDTC method is somewhat lower for both chromium and arsenic. This is caused primarily by

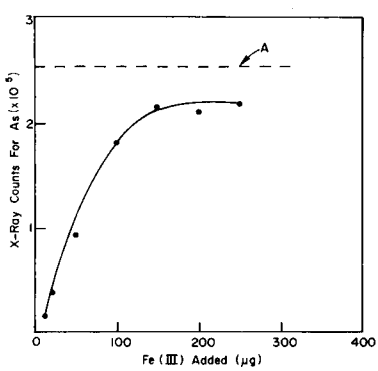

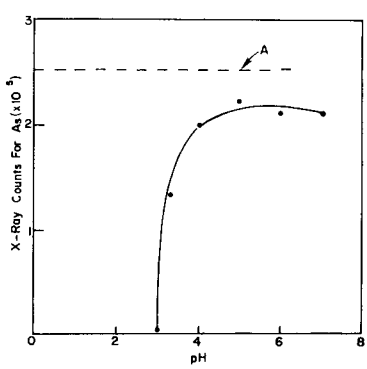

Fig. 1. X-ray counts for 100 μg of As(V) vs. μg of Fe(III) added as coprecipitating reagent. The x-ray counts for 100 μg of As(III) precipitated by DBDTC are shown by line A.

Fig. 2. X-ray counts for 100 μg of As(V) vs. pH of solution during coprecipitation. The x-ray counts for 100 μg of As(III) precipitated by DBDTC are shown by line A.

the larger mass and mass absorption coefficient of the iron-containing matrix in the coprecipitate. The DBDTC precipitates do not contain the heavy carrier so that x-ray matrix effects are minimal. Enhancement of the chromium intensity by the iron fluorescence contributes to its minimal decrease in sensitivity, while absorption of arsenic x-radiation signal by iron significantly decreases its sensitivity.

Results

Determination of chromium and arsenic in standard mixtures. Twelve standard solutions were prepared with mixtures of the oxidation states of chromium and arsenic, including a reagent blank. The total volume of the samples was 500 ml. Two 100-ml aliquots of each sample were processed by DBDTC precipitation, followed by coprecipitation with hydrated iron(III) oxide of the residue in the filtrate. Two other 100-ml portions were processed directly by iron(III) coprecipitation. Table 2 shows the composition of the samples and the mean results from the duplicates for both procedures. Only Cr(III) and As(V) are recovered quantitatively by hydrated iron(III) hydroxide.

Determination of chromium and arsenic in standard mixtures containing other trace elements. The determination of chromium and arsenic species in

TABLE 2

Composition of chromium and arsenic mixtures and results of determination

Sample no.	Composition of mixture (μg/100 ml)				Results (μg/100 ml)		
	As(III)	As(V)	Cr(III)	Cr(VI)	DBDTC precipitate	Fe(III) coprecipitation from filtrate	Direct Fe(III) coprecipitation from sample
1	30	—	—	—	30.2 As	—	14.8 As
2	—	30	—	—	3.5 As	29.3 As	30.5 As
3	—	—	30	—	3.4 Cr	27.9 Cr	30.1 Cr
4	—	—	—	30	33.2 Cr	1.5 Cr	6.7 Cr
5	30	30	—	—	32.7 As	26.9 As	37.5 As
6	—	—	30	30	32.9 Cr	29.5 Cr	36.4 Cr
7	30	30	30	—	8.8 Cr	20.1 Cr	29.3 Cr
					28.9 As	29.7 As	43.2 As
8	30	30	—	30	30.5 Cr	— Cr	1.4 Cr
					29.9 As	27.9 As	38.1 As
9	30	—	30	30	34.0 Cr	27.0 Cr	41.0 Cr
					27.7 As	4.8 As	15.2 As
10	—	30	30	30	40.5 Cr	19.9 Cr	33.0 Cr
					4.7 As	24.7 As	29.2 As
11	20	20	20	20	24.0 Cr	20.1 Cr	23.0 Cr
					18.6 As	24.7 As	30.5 As
12	—	—	—	—	1.5 Cr	0.5 Cr	— Cr
					2.2 As	— As	— As

TABLE 3

Composition of standard mixtures (μg/100 ml)

Sample	Se(VI)	Cu(II)	Fe(III)	Ni(II)	Zn(II)	Co(II)	Cr(III)	Cr(VI)	As(III)	As(V)
1	2.5	40	20	16	30	20	10	20	2	6
2	5	40	80	16	48	34	30	—	—	18
3	2	4	8	10	2	10	—	6	—	6
4	2.5	20	50	8	10	6	20	—	—	10
5	1	1	2	1	0.5	4	4	—	4	—

TABLE 4

Determination of arsenic and chromium in standard mixtures given in Table 3 (μg/100 ml)

Sample	DBDTC precipitate[a]		Iron(III) coprecipitate[b]	
1	17.0 Cr	17.8 Cr	10.5 Cr	9.5 Cr
	— As	— As	8.1 As	7.8 As
2	0.2 Cr	0.3 Cr	29.6 Cr	29.2 Cr
	— As	0.3 As	19.3 As	18.1 As
3	5.4 Cr	5.6 Cr	— Cr	— Cr
	— As	0.3 As	5.5 As	6.1 As
4	0.1 Cr	0.1 Cr	19.3 Cr	19.6 Cr
	0.3 As	— As	9.8 As	10.1 As
5	0.2 Cr	0.2 Cr	3.4 Cr	3.5 Cr
	2.9 As	2.9 As	0.7 As	0.1 As

[a]Cr(VI) and As(III). [b]Cr(III) and As(V) from filtrate.

mixtures containing other elements creates potential chemical and spectroscopic interferences, as well as x-ray absorption/enhancement effects. In order to test these to some degree, synthetic mixtures were prepared which contained Se, Cu, Fe, Ni, Zn, Co, Cr, and As. The DBDTC precipitation recovers many of these elements and it is in this stage that interferences are most severe [1, 2]. Table 3 shows the composition of each of the mixtures tested. The results of the determinations of chromium and arsenic are shown in Table 4. Chromium and arsenic are recovered almost quantitatively in these mixtures. It is likely that disproportionation will occur in these complex mixtures when one oxidation state, such as Cr(VI), is added. For example, if any ligands are present to stabilize Cr(III), and traces of Fe(II) are present, then Cr(VI) may be reduced.

Conclusions

Two precipitation methods have been used successfully to determine chromium and arsenic in their respective oxidation states in water samples. The DBDTC precipitation method recovers Cr(VI) and As(III) selectively over Cr(III) and As(V) as a first precipitation step. The remaining Cr(III) and

As(V) are quantified in a second step by coprecipitation with hydrated iron(III) oxide. Sensitivity is higher for chromium and arsenic by the DBDTC method because of increased matrix absorption for iron(III) in the coprecipitated samples. The method will likely not supplant atomic absorption or inductively-coupled plasma emission spectrometry for accuracy and precision, but it does provide speciation information and a fast economical method. Standards can be stored indefinitely.

This work was supported in part by Cooperative Agreement No. R806520-03 from the Environmental Protection Agency.

REFERENCES

1 H. Linder, H. Seltner and B. Schreiber, Anal. Chem., 50 (1978) 896.
2 A. T. Ellis, D. E. Leyden, W. Wegscheider, B. B. Jablonski and W. B. Bodnar, Anal. Chim. Acta, 142 (1982) 73.
3 A. T. Ellis, D. E. Leyden, W. Wegscheider, B. B. Jablonski and W. B. Bodnar, Anal. Chim. Acta, 142 (1982) 89.
4 K. Goldbach and K. H. Lieser, Fresenius Z. Anal. Chem., 33 (1982) 183.
5 Y. Inore and M. Munemori, Environ. Sci. Technol., 13 (1979) 443.

Analytica Chimica Acta, 171 (1985) 375—379
Elsevier Science Publishers B.V., Amsterdam — Printed in The Netherlands

Short Communication

ULTRAVIOLET-VISIBLE DIODE-ARRAY SPECTROPHOTOMETER AS A DETECTOR FOR GAS CHROMATOGRAPHY

MARK KUBE, MICHAEL TIERNEY and DAVID M. LUBMAN*
Department of Chemistry, The University of Michigan, Ann Arbor, MI 48109 (U.S.A.)
(Received 19th October 1984)

Summary. An ultraviolet-visible diode-array spectrophotometer is used as a detector for gas chromatography. This detector can provide a full u.v.-visible spectrum of each compound as it elutes from the column, thus enhancing discrimination between incompletely separated components. A discrimination of ca. 1:5000 could be achieved for a mixture of toluene and benzene. The detection limit is comparable to that of the thermal conductivity detector, i.e., about 0.5 μg for the various components. The detector is particularly useful when gases other than helium are used because the sensitivity does not depend on the gas used.

Chromatographic techniques serve as powerful means of separating compounds. However, because gas and liquid chromatography are usually limited to the use of retention times for the identification of compounds, identification is often enhanced by interfacing these techniques to detection systems such as mass spectrometry or Fourier transform infrared spectrometry that provide additional qualitative information. In this study, a u.v.-visible diode-array spectrophotometer is used to aid in the identification of components. The advantage is that the diode-array device can provide an almost continuous monitoring of the whole spectrum from 200 to 800 nm. Most large polyatomic molecules have broad spectra at room temperatures; however, the range of molecules that are volatile below 300°C and are easily studied in gas chromatography generally have distinctive features which allow unambiguous identification of molecules. These features may allow not only identification but also enhanced discrimination between molecules by optical means which may not be easily achieved by gas chromatography [1—5]. The sensitivity in this technique depends very strongly on such parameters as the path length and the absorptivity (ϵ).

The sensitivity demonstrated herein may not be better than existing methods of detection, but in many cases the problem is one of rapid identification rather than of sensitivity. This would be especially true in situations involving bulk samples from chemical waste disposal sites. Moreover, in pyrolysis experiments, in which rapid sampling and identification is essential, this technique would be useful. In such problems, the ability to identify each component in a rapid and simple manner is the crucial point.

0003-2670/85/$03.30

Experimental

The experimental system is shown in Fig. 1. A Gow-Mac Model 69-1000 gas chromatograph was used. The column (0.25-in. diameter, 6 ft. long) was packed with a bonded phase of 5% SP-1200 and 1.75% bentone-34. A typical flow rate of 60 ml min^{-1} helium and a column temperature of 90°C were used. This unit contained a thermal conductivity detector which could be used to monitor the effluent independently of the optical experiments. The effluent was connected to the absorption cell. The cell (12.5-cm long and 1.5-cm internal diameter; total volume about 30 ml) was made of glass except for the windows, which were of Suprasil quartz for transmission down to 200 nm. Helium was continuously flushed through the cell at a rate of about 150 ml min^{-1}; this was done to minimize cell dead volume, because otherwise residual material from one peak would remain in the cell for an extended period thus significantly broadening the detected peak width. The flow of gas allowed peak widths almost as sharp as those obtained from the thermal conductivity detector. The cell was heated, usually at about 70°C (chromel-alumel thermocouple), with a heating tape to prevent the components from condensing onto the cell windows.

A Hewlett-Packard 8450A diode-array spectrophotometer was used. This spectrophotometer is microprocessor-controlled and can be programmed to display only a given portion of the spectrum. For most volatile aromatic compounds of interest, the 500—200 nm region is generally most useful.

For sensitivity studies, one of the pure components (e.g., benzene) was diluted with one of the other components (e.g., toluene). The detection limit was defined as the point at which the S/N ratio for the benzene peak was 2. Samples (typically, 0.2—0.5 μl) were injected from a Hamilton 701 microliter syringe. For these measurements, the diode-array spectrophotometer can be programmed to monitor the absorption at one wavelength as a function of time to obtain a chromatogram for each concentration of sample injected. The wavelength for each compound was selected and optimized experimentally by first studying the spectrum of pure components. In addition to obtaining an absorption chromatogram, the detector could be pro-

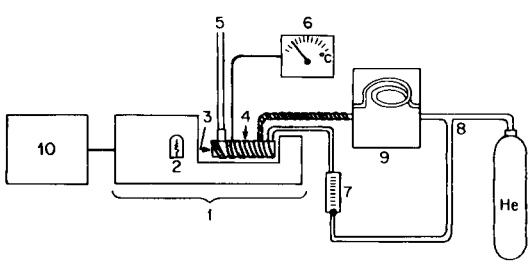

Fig. 1. Experimental set-up of the diode array/gas chromatographic detector: (1) Hewlett-Packard u.v.-visible diode-array spectrophotometer; (2) excitation lamp; (3) optical gas absorption cell; (4) heating tape; (5) gas outlet; (6) thermocouple readout; (7) regulator for helium flow to purge cell; (8) helium tank; (9) gas chromatograph; (10) printer.

grammed to obtain a full spectrum of the contents of the cell as a function of time, e.g., every 3 s. Thus, as each peak eluted from the chromatograph, a spectrum was displayed providing an aid in the identification of each component. In this manner, a three-dimensional plot of wavelength vs. time could be constructed for identification and as a means of discriminating compounds in a mixture.

Results and discussion

One point illustrated by this work is that simple volatile organic compounds can be identified by their u.v.-visible spectra. In Fig. 2 are shown the spectra of five compounds recorded for single-component samples passed through the column; only the portion of the spectra between 226 to 350 nm is displayed because these compounds do not absorb visible radiation. Although the u.v. bands are generally broad because of the Boltzmann population of states at room temperature, the spectra are still different enough that even xylene isomers can be identified. For equal amounts of the five components in a mixture, it was shown that three components are resolved completely and two (*p*- and *m*-xylene) are incompletely resolved with a resolution of 0.7. The u.v. spectra of the eluent can be used to resolve the two components. In Fig. 3, the peaks at 264, 266 and 272 nm in the spectrum taken at 383 s show clearly that it is the spectrum of *p*-xylene. The spectrum taken 24 s later shows that the relative intensities of the peaks at 264 and 266 nm have changed and the peak at 272 nm has been shifted 1 to 2 nm toward shorter wavelengths, thus indicating that the peak is *m*-xylene.

The limits of discrimination obtainable from g.c. alone vs. the combination of g.c. and diode-array detector were further compared for mixtures of

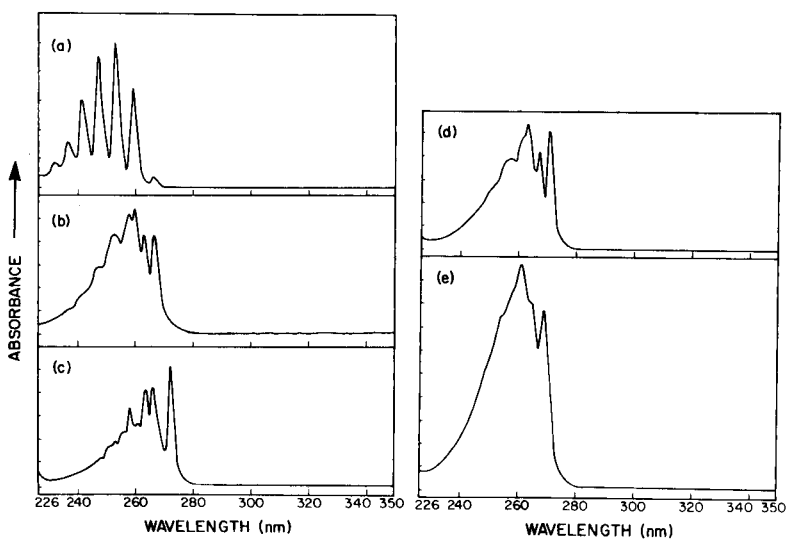

Fig. 2. Absorption spectra of five compounds taken as each eluted from the column: (a) benzene; (b) toluene; (c) *p*-xylene; (d) *m*-xylene; (e) *o*-xylene.

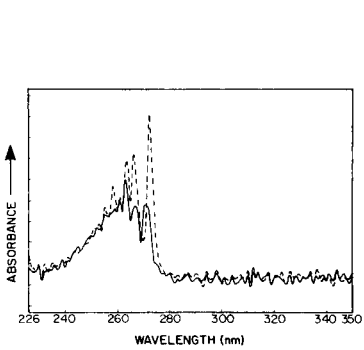

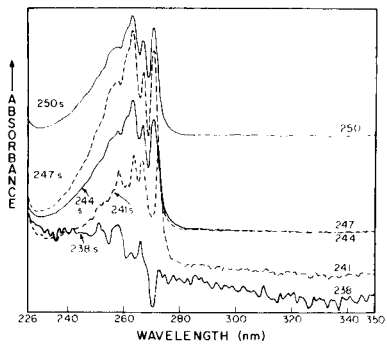

Fig. 3. Ultraviolet absorption spectra of *p*-xylene and *m*-xylene in an unresolved mixture: (- - -) spectrum taken at 383 s; (——) spectrum taken at 407 s.

Fig. 4. Ultraviolet spectra of a 1:50 mixture of *p*- and *m*-xylene eluted from the chromatograph as a function of time.

toluene in benzene and *p*-xylene in *m*-xylene. The thermal conductivity detector could discriminate toluene in a 1:600 toluene/benzene mixture in a 0.4-μl sample; however, it could not discriminate toluene in a 1:1200 mixture. In the second mixture, the injection sample was doubled to 0.8 μl so that the amount of toluene would remain the same because its detection limit in this technique was approached. With the diode-array detector (260 nm), it was possible to discriminate a 1:5000 toluene/benzene mixture but not a 1:10 000 mixture. Further, g.c. alone can barely resolve *p*- and *m*-xylene peaks even in a 1:1 mixture. The diode-array detector, however, can detect *p*-xylene in a 1:50 mixture of *p*- and *m*-xylenes (see Fig. 4). Even though *m*-xylene absorbs in the same wavelength range as *p*-xylene, the shift between the two spectra is sufficient to allow such discrimination. The thermal conductivity detector cannot discriminate the components in this mixture. Of course, there are high-resolution chromatographic techniques that can discriminate between such mixtures, but the advantage herein is the capability for rapid separation and identification of simple mixtures.

The limits of detection were evaluated for the five components of Fig. 1. Table 1 shows the detection limits for both detectors. At the optimum

TABLE 1

Limits of detection for the diode-array and thermal conductivity detectors

Compound	Limit of detection (μg)		Compound	Limit of detection (μg)	
	Diode array	Thermal cond.		Diode array	Thermal cond.
Benzene	0.53	0.53	*o*-Xylene	0.88	0.44
Toluene	0.52	0.31	*m*-Xylene	0.29	0.29
			p-Xylene	0.43	0.43

wavelength for each compound, the detection limits were comparable to the thermal conductivity detector.

Azulene was studied briefly. The molar absorptivity of the s_2 state of azulene is about 100 times that of the s_1 state of benzene and a detection limit in the low nanogram range would be predicted. However, the azulene peak is broadened even under optimum column conditions and thus the relative peak height is lower than if the peak were sharp like that of benzene. A limit of detection of about 100 ng was found for azulene when separated from benzene.

There are many problems associated with the use of different gases with thermal conductivity detectors. The diode-array detector should not be affected by the use of different carrier gases, because most do not absorb in the 200—800 nm region. With the thermal conductivity detector, there are significant differences in the limits of detection of benzene in various carrier gases; the ratio for $He:N_2:Ar:CO_2$ was found to be 1:0.05:0.04:0.04 under useful conditions for each gas. No significant change was observed in sensitivity for the optical detector as a function of carrier gas and the spectra of benzene and toluene were exactly the same when these carrier gases were used.

One problem inherent in the use of the diode-array detector is that small changes in the position of the cell may cause changes in the observed absorbances. Thus, the optical cell must be firmly mounted in position and not changed between experiments. However, in this study, the change in the absorbance of benzene in the detector was less than 25% over an average of many measurements using the same and different carrier gases.

The support of this project by a University of Michigan Rackham Award is acknowledged.

REFERENCES

1 W. Kaye, Anal. Chem., 34 (1962) 287.
2 J. Merritt, F. Comendant, S. T. Abrams and V. N. Smith, Anal. Chem., 35 (1963) 1461.
3 A. Bylina, D. Sybilska, Z. R. Grabowski and J. Koszewski, J. Chromatogr. Sci., 83 (1973) 357.
4 M. S. Denton, T. P. DeAngelis, A. M. Yacynych, W. R. Heineman and T. W. Gilbert, Anal. Chem., 48 (1976) 20.
5 M. Novotny, F. J. Schwende, M. J. Hartigan and J. E. Purcell, Anal. Chem., 52 (1980) 736.

Analytica Chimica Acta, 171 (1985) 381—385
Elsevier Science Publishers B.V., Amsterdam — Printed in The Netherlands

Short Communication

CITRATE COMPLEXES OF TIN(IV) STUDIED BY LIQUID-LIQUID EXTRACTION WITH 5,7-DICHLORO-8-QUINOLINOL

A. M. GUTIERREZ*, C. PEREZ-CONDE and M. P. REBOLLAR

Departamento de Química Analítica, Facultad de Ciencias Químicas, Universidad Complutense, 28040 Madrid (Spain)

(Received 23rd August 1984)

Summary. The tin(IV)/5,7-dichloro-8-quinolinol/chloroform extraction system is used to determine the composition and the stability constants of the aqueous complexes of tin(IV) with citric acid, in the pH range 2.0—3.5. The tin(IV):citric acid ratios found are 1:1 and 1:2, depending on the concentration of the acid. The conditional stability constants are $(5.5 \pm 0.4) \times 10^3$ and $(1.3 \pm 0.3) \times 10^8$ for the 1:1 and 1:2 complexes, respectively. This extraction system is convenient in studies of aqueous tin(IV) complexes that cannot be extracted into chloroform.

Studies of the extraction equilibria of metal chelates provide an interesting method of determining the composition and stability constants of non-extractable aqueous complexes. The presence of complexing species in the aqueous phase is reflected by a decrease in the distribution ratio of the metal into the organic phase [1, 2]. When the availability of data permitted the comparison, good agreement was found between the stability constants obtained by the extraction method and those obtained by other techniques [3]. Recently, tin(IV) was successfully extracted into chloroform by use of 5,7-dichloro-8-quinolinol (HDCQ) [4]. This system can be applied in studies of complexes of tin(IV) in aqueous solutions, for which few data are available [5]. No data on tin(IV) complexes with citric acid seem to have been reported. This communication is concerned with the determination of the composition and the stability constants of aqueous tin(IV)/citrate complexes, by liquid-liquid extraction with HDCQ into chloroform.

Experimental

Reagents and equipment. Standard tin(IV) solutions were prepared by dilution of a stock solution as described earlier [4]. The HDCQ was dissolved in 1.7 M sulphuric acid. All chemicals were of analytical grade. Absorbance measurements were done with a Pye-Unicam Model SP-8-200 spectrophotometer and the pH was measured with a Metrohm pH meter Model E-516. An Instrumentation Laboratory, Model 357 atomic absorption spectrometer, with a nitrous oxide/acetylene flame was used for the determination of tin.

0003-2670/85/$03.30

Extraction procedure and distribution measurement. The HDCQ reagent dissolved in 1.7 M sulphuric acid was added to the tin(IV) solution in a 100-ml separating funnel. Then the citric acid solution was added, the pH was adjusted with 3 M ammonia, and the volume was adjusted to 10 ml, yielding a tin concentration of 4.25×10^{-5} M. Finally, 10 ml of chloroform was added and the extraction was achieved by vigorous manual shaking of the funnel for 4 min. When equilibrium had been reached, the two phases were separated and the concentration of tin in the organic and/or aqueous phase was determined by absorbance measurement of the Sn(IV)/HDCQ complex (at 390 nm) or by a.a.s.

Establishment of formulae. According to the formulation proposed by Rydberg [6] and Sillén [7], which is applicable to liquid-liquid extraction of a hydrolyzable metal M with a chelating agent HA in the presence of another complexing agent H_pL, the general formula of the aqueous complex can be written as $M(HpL)_l(H_{-y})^{N-y}$ and that of the complex extracted into the organic phase as $M(HA)_xH_{-N}$. The expressions that give the variation of the distribution ratio, D, of the metal [2, 8, 9] applied to the present complexes are $\partial \log D/\partial \log [HDCQ]_o = x$, $\partial \log D/\partial pH = N - y$, and $\partial \log D/\partial \log [H_3Cit] = -l$. Here, x, l and y are as defined in the formulae of the complexes, o refers to the organic phase, H_3Cit stands for citric acid, N is the metal charge, and $N - y$ represents the charge of the complexes. The desired values x, $N - y$ and l, were obtained by the slope analysis method [1, 2].

Calculation of stability constants. The distribution ratio of tin(IV), D_o, in the absence of complexing agents can be represented by $D_o = K_{ex}[HDCQ]_o^x/[H]^x$, where K_{ex} is the extraction constant. From published data for distribution constants of HDCQ between water and organic solvents [10] it can safely be assumed that, in the present experimental conditions, $[HDCQ]_o$ was equal to the total added concentrations, C_{HDCQ}.

The value of D in the presence of the complexing agent H_2Cit can be expressed as

$$D = K_{ex}[HDCQ]_o^x/[H]^x \left(1 + \sum_l \beta_l [H_2Cit]^l\right) \quad (1)$$

where β_l are the overall formation constants of the tin(IV) complexes with the ligand H_2Cit (charges on ions are omitted for simplicity). The concentration of H_2Cit at equilibrium was evaluated from the total added concentration of citric acid by using the dissociation constants (corrections were made when the concentration of the complex was not negligible). The concentration of the citric acid in the organic phase was assumed to be negligible.

If $[HDCQ]_{o,1/2}$ and $[\overline{HDCQ}]_{o,1/2}$ are the concentrations for which the distribution ratio of the metal is equal to unity in the presence and absence of citric acid, respectively, it is possible to obtain, with the aid of the above expressions for D_o and D, the relationship

$$A = ([HDCQ]^{x}_{o,1/2}/[\overline{HDCQ}]^{x}_{o,1/2} - 1) = \sum_{l} \beta_l [H_2Cit]^l \quad (2)$$

From the x-axis intercepts in the log D vs. log $[HDCQ]_o$ plot, the $[HDCQ]_{o,1/2}$ and $[\overline{HDCQ}]_{o,1/2}$ can be obtained. A plot of log A vs. log $[H_2Cit]$ will give straight lines with different slopes, l, for each citric complex and the y-axis intercepts will give their respective stability constants.

Results and discussion

The distribution ratio for tin(IV) between the organic and the aqueous phase containing citric acid was examined as a function of the concentrations of HDCQ and citric acid, and of pH. At pH 2.5 in the presence of citric acid in the range 0—1.0 × 10^{-2} M, a set of parallel lines, with a mean slope of 3.0, was obtained in the log D vs. log $[HDCQ]_o$ plot (Fig. 1), indicating a stoichiometric ratio Sn(IV):HDCQ of 1:3. The same ratio was obtained in the absence of citric acid [4] and identical visible absorption spectra of the complexes

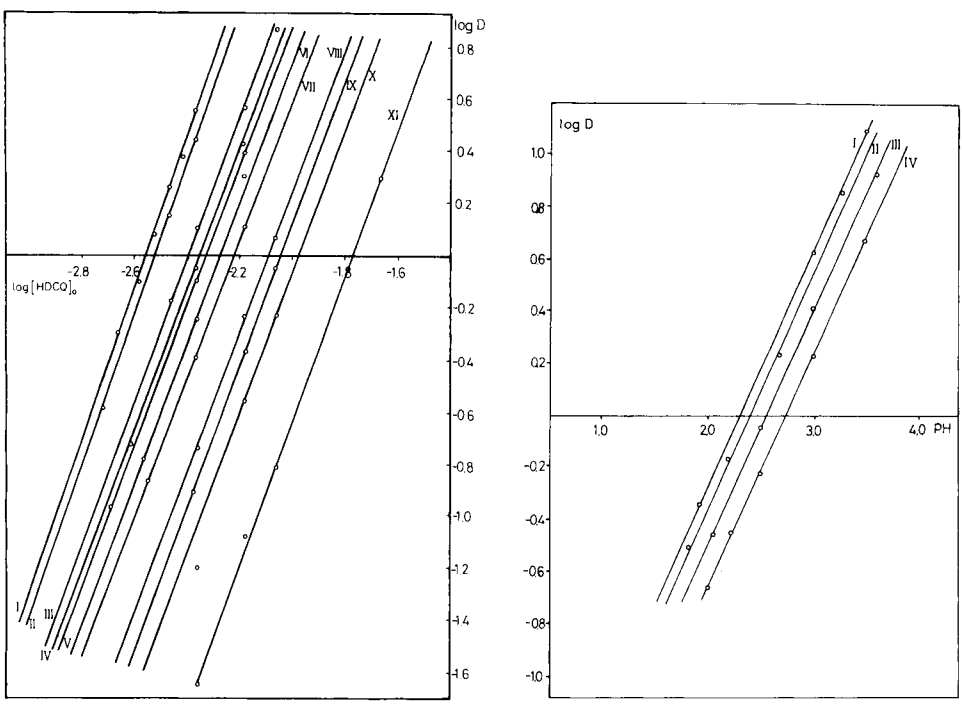

Fig. 1. Dependence of the distribution ratio D on $[HDCQ]_o$. Conditions: 4.25 × 10^{-5} M Sn(IV), pH 2.5; lines I—XI correspond to total citric acid concentrations of 0, 0.075, 0.50, 0.75, 1.0, 1.6, 2.5, 4.0, 5.0, 7.0 and 10 mM, respectively.

Fig. 2. pH dependence of the distribution ratio D. Conditions: 4.25 × 10^{-5} M Sn(IV); 8.5 × 10^{-3} M HDCQ; lines I—IV correspond to total citric acid concentrations of 1.0, 1.6, 5.0 and 7.0 mM, respectively.

were also obtained in the presence and absence of citric acid. The latter two facts preclude any significant formation of other ternary complexes involving citrate ions, extractable to the organic phase.

The log D vs. pH plot (Fig. 2) in the pH range 2.0—3.5 gives straight lines with a mean slope of 0.9, indicating that the charge on the complex formed in the aqueous phase is + 1. Substitution of this value into the equation $\partial \log D/\partial \mathrm{pH} = N - y$ (see above), gives $y = 3$. The plot of log D vs. log [H_3Cit] (Fig. 3) shows two straight sections with mean slopes of —0.72 and —1.9 corresponding to concentrations of H_3Cit less than and greater than 2.5 × 10^{-3} M, respectively. This behaviour suggests that there are two complexes in the aqueous phase depending on the total citric acid concentration. The latter was confirmed in the plot of log A vs. log [H_2Cit] at equilibrium (Fig. 4), in which two straight lines are again obtained. The corresponding slopes are 0.9

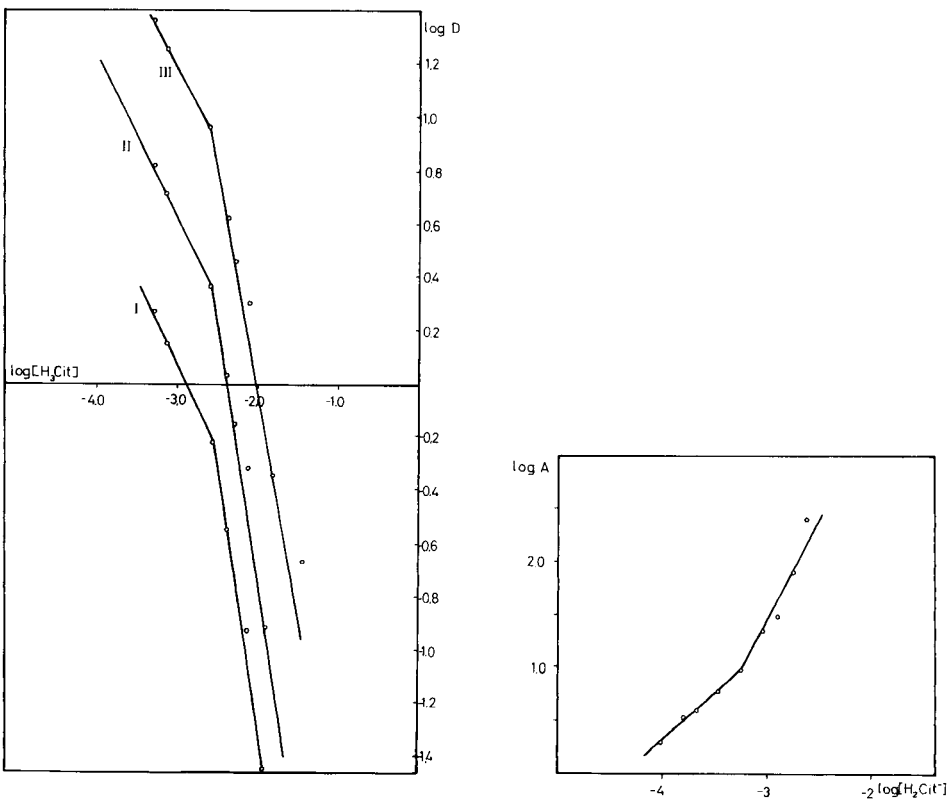

Fig. 3. Dependence of the distribution ratio D on the total concentration of citric acid. Conditions: 4.25 × 10^{-5} M Sn(IV); pH 2.5; lines I—III correspond to total HDCQ concentrations of 5.0, 7.9 and 13 mM, respectively.

Fig. 4. Dependence of $A = ([\mathrm{HDCQ}]^3_{o,1/2}/[\overline{\mathrm{HDCQ}}]^3_{o,1/2}) - 1$ on the concentration of H_2Cit (4.25 × 10^{-5} M Sn(IV), pH 2.5).

and 2.2, which agree well with the values obtained before, so that it can be concluded that the Sn(IV):H_3Cit ratios are 1:1 and 1:2.

With the data obtained from Figs. 2—4 (i.e., $N - y = 1$ and $l = 1$ or $l = 2$), the formulae of the two aqueous complexes written in Rydberg's notation (see above) are $Sn(H_3Cit)(H_{-3})^+$ and $Sn(H_3Cit)_2(H_{-3})^+$. This gives rise to the following set of possible formulae that in principle will justify the data: $Sn(H_3Cit)(OH)_3^+$, $Sn(H_2Cit)(OH)_2^+$ and $Sn(HCit)(OH)^+$ for $l = 1$ and $Sn(H_3Cit)_2(OH)_3^+$ and $Sn(H_2Cit)_2(OH)^+$ for $l = 2$. It is not likely that citric acid could act as a complexing agent without losing a proton; as the working pH range was 2.0—3.5, the most probable formulae that can be proposed for the tin(IV)-citric acid complexes are $Sn(H_2Cit)(OH)_2^+$ and $Sn(H_2Cit)_2(OH)^+$.

The overall conditional stability constants in the pH range considered, obtained from the y-axis intercepts in Fig. 4, were $\beta_1 = (5.5 \pm 0.4) \times 10^3$ and $\beta_2 = (1.3 \pm 0.3) \times 10^8$ for the formation of the complexes $Sn(H_2Cit)(OH)_2^+$ and $Sn(H_2Cit)_2(OH)^+$, respectively. No stability constants of tin(IV)-citric acid complexes obtained by other methods are available at present for comparison. The stability constant of the tin(II)-citric acid 1:1 complex has been reported [11] to be $10^{5.5}$, a value greater than that of the corresponding tin(IV)-citric acid complex given above ($\beta_1 = 10^{3.7}$).

REFERENCES

1 J. Stary, The Solvent Extraction of Metal Chelates, Pergamon, Oxford, 1964, p. 18.
2 R. Guillaumont, R. Muxart and G. Bouissières, Bull. Soc. Chim. Fr., 5 (1968) 1952.
3 Y. Inoue and O. Tochiyama, Polyhedron, 2 (1983) 627.
4 A. M. Gutierrez, R. Gallego and A. Sanz-Medel, Anal. Chim. Acta, 149 (1983) 259.
5 L. G. Sillén and A. E. Martell, Stability Constants of Metal-Ion Complexes, Suppl. No. 1. The Chemical Society, London, 1971.
6 J. Rydberg, Arkiv. Kemi, 8 (1955) 101.
7 L. G. Sillén, Acta Chem. Scand., 10 (1956) 803.
8 R. Guillaumont, Bull. Soc. Chim. Fr., 5 (1968) 1956.
9 A. Moutte and R. Güillaumont, Rev. Chim. Minerale, 6 (1969) 603.
10 J. Stary and H. Freiser, I.U.P.A.C. Equilibrium Constants of Liquid-Liquid Distribution Reactions, Part IV: Chelating Extractants, Pergamon, Oxford, 1978, p. 82.
11 J. Jarosz and C. Sinicki, C.R. Seances Acad. Sci., Ser. 2, 292 (1981) 793.

Analytica Chimica Acta, 171 (1985) 387
Elsevier Science Publishers B.V., Amsterdam — Printed in The Netherlands

Erratum

B. Dinesen and H. D. Anderson, Monitoring the Production of Biosynthetic Human Growth Hormone by MicroEnzyme-linked Immunosorbent Assay.

Anal. Chim. Acta, 163 (1984) 119—125.

p. 123, last line of text should read: "amino terminal part" and not "terminal amino group"; the legend to Fig. 3 should read: "(△) human chorionic gonadotropin" and the legend to Fig. 4 should read "(○) volume fraction data; (●) hGH data."

p. 124, the heading to Table 1 should read: "Reproducibility of the various e.l.i.s.a. modifications".

✓ Ch. S.
31 MA. 28

0003-2670/85/$03.30

ANALYTICA CHIMICA ACTA, VOL. 171 (1985)

AUTHOR INDEX

(Continued from outside back cover)

CONTENTS

(Abstracted, Indexed in: Anal. Abstr.; Biol. Abstr.; Chem. Abstr.; Curr. Contents Phys. Chem. Earth Sci.; Life Sci.; Index Med.; Mass Spectrom. Bull.; Sci. Citation Index; Excerpta Med.)

(Continued on inside back cover)